Progress in Nuclear Magnetic Resonance Spectroscopy 132–133 (2022) 1–112

Contents lists available at ScienceDirect

Progress in Nuclear Magnetic Resonance Spectroscopy

journal homepage: www.elsevier.com/locate/pnmrs

In-cell NMR: Why and how?

Francois-Xavier Theillet [a,*], Enrico Luchinat [b,c]

[a] Université Paris-Saclay, CEA, CNRS, Institute for Integrative Biology of the Cell (I2BC), 91198 Gif-sur-Yvette, France
[b] Dipartimento di Scienze e Tecnologie Agro-Alimentari, Alma Mater Studiorum – Università di Bologna, Piazza Goidanich 60, 47521 Cesena, Italy
[c] CERM – Magnetic Resonance Center, and Neurofarba Department, Università degli Studi di Firenze, 50019 Sesto Fiorentino, Italy

Edited by David Neuhaus and David Gadian

ARTICLE INFO

Article history:
Received 15 September 2021
Accepted 27 April 2022
Available online 04 May 2022

Keywords:
Structural biology
Biophysics
Metabolomics
Drug research
Cellular environment

ABSTRACT

NMR spectroscopy has been applied to cells and tissues analysis since its beginnings, as early as 1950. We have attempted to gather here in a didactic fashion the broad diversity of data and ideas that emerged from NMR investigations on living cells. Covering a large proportion of the periodic table, NMR spectroscopy permits scrutiny of a great variety of atomic nuclei in all living organisms non-invasively. It has thus provided quantitative information on cellular atoms and their chemical environment, dynamics, or interactions. We will show that NMR studies have generated valuable knowledge on a vast array of cellular molecules and events, from water, salts, metabolites, cell walls, proteins, nucleic acids, drugs and drug targets, to pH, redox equilibria and chemical reactions. The characterization of such a multitude of objects at the atomic scale has thus shaped our mental representation of cellular life at multiple levels, together with major techniques like mass-spectrometry or microscopies.

NMR studies on cells has accompanied the developments of MRI and metabolomics, and various subfields have flourished, coined with appealing names: fluxomics, foodomics, MRI and MRS (i.e. imaging and localized spectroscopy of living tissues, respectively), whole-cell NMR, on-cell ligand-based NMR, systems NMR, cellular structural biology, in-cell NMR... All these have not grown separately, but rather by reinforcing each other like a braided trunk. Hence, we try here to provide an analytical account of a large ensemble of intricately linked approaches, whose integration has been and will be key to their success.

We present extensive overviews, firstly on the various types of information provided by NMR in a cellular environment (the "why", oriented towards a broad readership), and secondly on the employed NMR techniques and setups (the "how", where we discuss the past, current and future methods). Each subsection is constructed as a historical anthology, showing how the intrinsic properties of NMR spectroscopy and its developments structured the accessible knowledge on cellular phenomena. Using this systematic approach, we sought i) to make this review accessible to the broadest audience and ii) to highlight some early techniques that may find renewed interest. Finally, we present a brief discussion on what may be potential and desirable developments in the context of integrative studies in biology.

Contents

* Corresponding author at: CEA-Saclay, bât. 144, 91191 Gif-sur-Yvette, France.
E-mail address: francois-xavier.theillet@cnrs.fr (F.-X. Theillet).

https://doi.org/10.1016/j.pnmrs.2022.04.002
0079-6565/

1. Introduction

1.1. Definitions and scope

The initial intention for this review was to focus on the modern concept of in-cell NMR, i.e. NMR studies of macromolecules in cellular milieus, as coined by Dötsch and his coworkers in 2001 [1]. It has been 10 years since the last review on this topic in this journal [2,3]. A significant body of results has been published in the meantime, but also many reviews [4-24] (see also the excellent book recently edited by Ito, Dötsch and Shirakawa [25]). Events in 2020-21 (particularly the COVID-19 pandemic and the "Great Lockdown") gave us time in which to extend background research to include literature in "neighboring" NMR fields, and also publications from the early days of NMR spectroscopy. Hence, we identified consistent themes and patterns running through the very many publications from the overall field of NMR studies on cells. Such a continuity has been stressed in an inspiring fashion by Lippens [15] (and earlier by Szwergold [26] or Dötsch [1], or more recently by Selenko [22]), but has not been explored extensively in a review. We thought it would be a good time to attempt to bring together an account of this long-term body of knowledge: this would help us to propose a perspective after 70 years of works in the broad, integrated field of in-cell NMR spectroscopy, a field encompassing NMR studies using intact cells.

Our aim here is thus to cover NMR studies analyzing cells and, when closely related, "*in situ*" studies on cell extracts, membranes, virus and viral particles, organelles, dissected tissues or small model animals such as flies or worms. NMR spectroscopy permits the analysis of living cells or tissues and their content in a non-invasive fashion. It has applications in a very broad variety of fields, e.g. metabolomics, MRI, cellular biophysics, structural biology, drug development, etc. We will only mention briefly MRI and metabolomics, which represent an immense, independent literature [27] (see [28-32] for a few selected applications in clinics or cognitive science, see [33-35] for MRS metabolic imaging and some future prospects [36,37], see [38-46] for metabolomics and some future NMR metabolomics strategies [47,48]).

Our overall goal was to attempt to integrate and analyze the wide landscape of past and present NMR studies on cells. We have adopted a chronological narrative in most sections to present the progressive technical achievements and the observations they gave access to. We felt such a presentation could be helpful for non-NMR readers and novice NMR students, as well as perhaps for more experienced spectroscopists.

We have attempted to present each section such that it can be read independently. We have deliberately avoided equations, but have tried to provide experimental numerical data wherever possible. We hope that this approach to presentation will be stimulating both for a broad non-expert readership and for NMR spectroscopists.

1.2. The basic principles of in-cell NMR

1.2.1. Observing a broad range of phenomena

The appealing concept of in-cell NMR is to obtain information at the atomic scale on chosen nuclear isotopes in living environments. Indeed, NMR spectroscopy reports on the impact of the local chemical environment, conformation or interaction dynamics on the detected populations of nuclei.

These nuclei can be incorporated in molecules of any size, and can become sensors for more global physical properties like pH or viscosity. NMR spectroscopy can also provide information on local homogeneity and dynamics, from the picosecond to the second timescales by measuring magnetization relaxation times. However, these can be difficult to interpret, because they are dependent on rotational correlation times, conformational dynamics and interaction kinetics at the same time [49].

In addition, because NMR is a non-destructive technique, time series of successive spectra can be recorded over minutes to days on a single sample, provided that conditions to maintain its integrity are met. Chemical reactions or environmental changes can thus be monitored through widely ranging experimental timescales.

Hence, in-cell NMR can provide a broad range of information at multiple scales. Of course, several limitations exist that we will explore later. Still, we can mention the two we see as the most important: i) "NMR-visible" molecular species are limited to those that do not interact or interact very weakly (i.e. rapid exchange below the μs time scale and low populations in the order of magnitude of 1 %) with large macromolecular assemblies (in the case of solution NMR) or those that do not interact with too many cellular binding partners (in the cases of either solution or solid-state NMR); ii) standard NMR techniques cannot determine the spatial localization of the detected molecules at the micrometer scale and below, i.e. the subcellular scale. A subcellular position can thus be inferred only from secondary pieces of evidence, in those cases where organelles/compartments contain markedly distinct chemical environments (e.g. pH, redox potential, presence of binding partners, etc.) that result in well-defined spectral changes.

1.2.2. Achieving selective detection from the cellular background

NMR spectroscopy of cellular species permits the selective observation of specific nuclei (more precisely the precession of their nuclear magnetic moments) in the cellular milieu. Three main factors can make a particular population of nuclei distinguishable from others in the same sample: i) among nuclei, each nuclear species (isotope) generates magnetic resonances in a relatively narrow and precise range of frequencies due to its different gyromagnetic ratio γ (ω_0=-γB_0 [49] defining the precession frequency ω_0 of a nuclear spin having a gyromagnetic ratio γ in a magnetic field B_0); ii) among populations of the same isotope, nuclei having the same chemical environment will contribute signals at a very speci-

Glossary

ADP	Adenosine DiPhosphate
AMP	Adenosine MonoPhosphate
α-Syn	α-Synuclein
ATP	Adenosine TriPhosphate
BIRD	Bi-linear Rotation Decoupling
BOLD	Blood Oxygenation Level Dependent
cAMP	Cyclic Adenosine MonoPhosphate
CEST	Chemical Exchange Saturation Transfer.
CP-MAS	Cross-Polarization Magic Angle Spinning
CPMG	Carr-Purcell-Meiboom-Gill (pulse sequence)
CPP	Cell-Penetrating Peptide
CRINEPT	Cross Relaxation-enhanced INEPT
CSA	Chemical Shift Anisotropy
cryo-EM	Cryogenic Electron Microscopy
cryo-ET	Cryogenic Electron Tomography
DCP	Double Cross-Polarization
dDNP	dissolution Dynamic Nuclear Polarization
DNA	DeoxyriboNucleic Acid
DNP	Dynamic Nuclear Polarization
DOTA	1,4,7,10-tetraazacyclododecane-1,4,7,10-tetraacetic acid
DP	Direct Polarization
DPG	DiPhosphoGlycerate
DQF/TQF	Double quantum filter / Triple quantum Filter
ECM	ExtraCellular Matrix
EDTA	EthyleneDiamineTetraacetic Acid
EPR	Electron Paramagnetic Resonance
FID	Free Induction Decay
FLIM	Fluorescence Lifetime Imaging Microscopy
FRET	Förster or Fluorescence Resonance Eenergy Transfer
FT	Fourier Transform
GFP	Green Fluorescence Protein
GPCR	G-Protein-Coupled Receptor
GSH	Glutathione
HMQC	Heteronuclear Multiple Quantum Coherence
Ht	Haematocrit
HR-MAS	High-Resolution Magic Angle Spinning
HSQC	Heteronuclear Single Quantum Coherence
IDP	Intrinsically Disordered Protein
IDR	Intrinsically Disordered Region (of a protein)
INEPT	Insensitive Nuclei Enhanced by Polarization Transfer
MD	Molecular Dynamics
NAD+	Nicotinamide Adenine Dinucleotide+
NADP+	Nicotinamide Adenine Dinucleotide Phosphate
NMR	Nuclear Magnetic Resonance
MAS	Magic Angle Spinning
MRI	Magnetic Resonance Imaging
mRNA	messenger RiboNucleic Acid
MRS	Magnetic Resonance Spectroscopy (*in vivo*, spatially localized biochemical analysis)
NOE	Nuclear Overhauser Effect
NOESY	Nuclear Overhauser Effect SpectroscopY
NUS	Non-Uniform Sampling
PCS	Pseudo-Contact Shift
PFG	Pulsed Field Gradient
PFT	Pore-Forming Toxin
PG	PeptidoGlycan
PHIP	ParaHydrogen Induced Polarization.
ppm	parts per billion
ppm	parts per million
PRE	Paramagnetic Relaxation Enhancement
PTM	Post-Translational Modification.
RBC	Red Blood Cell
RDC	Residual Dipolar Coupling
REDOR	Rotational-Echo DOuble-Resonance
RNA	RiboNucleic Acid
rRNA	ribosomal RiboNucleic Acid
SLO	Streptolysin O
smFRET	Single-molecule FRET
SOD1	SuperOxide Dismutase 1
SOFAST-HMQC	Selective Optimized Flip-Angle Short-Transient Heteronuclear Multiple Quantum Coherence
SNR	Signal-to-Noise Ratio
ssNMR	solid-state Nuclear Magnetic Resonance
ssRNA	single-strand RiboNucleic Acid
STD	Saturation Transfer Difference
STDD	Saturation Transfer Double Difference
τ_C	Correlation time for overall (isotropic) tumbling of the protein
TANGO	Testing for Adjacent Nuclei with a Gyration Operator
TRNOE	TRansferred NOE
TR-NUS	Time-Resolved Non-Uniform Sampling.
TROSY	Transverse Relaxation-Optimized SpectroscopY.
VAS	Variable Angle Spinning
WATERGATE	Water suppression by Gradient-Tailored Excitation
waterLOGSY	Water-Ligand Observed via Gradient SpectroscopY
WATERGATE	WATER suppression by GrAdient Tailored Excitation
WT	Wild-Type
WTA	Wall Teichoic Acid

fic resonance frequency, the so-called chemical shift ($\delta=(\omega-\omega_0)/\omega_0$); iii) among populations with similar chemical shifts, nuclei with relatively high abundance will stand out. Further distinctions can be exploited that are based on the selective manipulation of nuclei bound to a determined nuclear isotope (e.g. protons covalently bound to ^{15}N or ^{13}C).

NMR signal intensities are proportional to the number of nuclei resonating at the corresponding frequency. However, a large population does not guarantee its detectability: conformational and interaction dynamics, sample homogeneity, and other intrinsic properties of the observed nuclei have consequences on the signal linewidth, all of which are decisive for NMR signal intensity as we will often see below.

1.3. Which nuclei?

We must recall that only nuclei having a non-zero spin magnetic moment can be observed. This excludes, unfortunately, the naturally predominant isotopes ^{12}C, ^{16}O and ^{32}S, which are thus "NMR invisible". Other abundant isotopes like ^{14}N have unfavorable nuclear spin quantum numbers ($I > 1/2$) that generate fast relaxation, hence very broad signals that are impractical to detect (except for very small, symmetric molecules like NH_4^+). NMR spectroscopists have circumvented and even transcended this difficulty by incorporating ^{13}C- or ^{15}N-labeled species in cells and then detecting those in a specific fashion. The stable isotopes ^{13}C and ^{15}N have low natural abundances (1.1% and 0.4%, respectively) and their NMR detection generates thus low background signal intensities from the endogenous material.

Besides null spins, we can classify nuclei in two categories. The most useful isotopes are spin ½ nuclei, like ^{1}H, ^{13}C, ^{15}N, ^{19}F, ^{31}P. These have manageable mono-exponential "transverse" relaxation in solution on timescales of the order of 1 to 100 milliseconds. This holds true for homogeneous pools of molecules tumbling in the 10 nanoseconds range or less, that do not experience interactions in the micro- to milli-second time scale. Indeed, such "intermediate

time scale" binding events can cause line broadening, which makes the signals more difficult to detect. Importantly, in the cellular context, detecting molecules involved in complexes larger than ~30 kDa often necessitates more advanced NMR strategies, whose success is not guaranteed.

Other isotopes are "quadrupolar" nuclei, like ^{2}H, ^{7}Li, ^{14}N, ^{17}O, ^{23}Na, ^{25}Mg, ^{27}Al, ^{39}K, ^{43}Ca and almost all metals with non-zero nuclear spin: their non-spherical distribution of nuclear charges generates a quadrupolar moment interacting with the surrounding electric field, which can cause a strong relaxation of nuclear magnetic resonances in the case of a non-symmetric local environment, as typically occurs when transient binding to macromolecules occurs in cells. There, such quadrupolar nuclei show fast, multi-exponential relaxations, whose rates depend on the quadrupole strengths. This severely limits their detectability. We will show that these quadrupolar nuclei can still be exploited, even though they sometimes gave rise to misinterpretations in early studies.

2. Applications of NMR spectroscopy on living cells.

Anfinsen, who established the deterministic relationship between amino acid sequence and three-dimensional structure (at least for small folded proteins), emphasized that "a protein molecule only makes stable, structural sense when it exists under conditions similar to those for which it was selected" [50]. This thought is clearly at the heart of many biophysicists' concerns: to what extent do molecules behave the same or differently in the test tube and in cells? There is no question about the importance of *in vitro* studies using purified material: they are key to exploring the properties and the manipulation of biological molecules. However, presenting a complete picture in molecular biophysics requires characterizing molecules and their interactions in their native environment. Let's push an open door: To fully understand molecular phenomena occurring in cells, one has to study them in cells. NMR has been instrumental in this task. Here, we discuss the various questions that NMR can tackle.

2.1. Cellular solvent

NMR spectroscopy offers the possibility to manipulate and detect selectively the chosen nuclear spins, because every isotope has a different gyromagnetic ratio (see Section 1.2.2.). A broad spectrum of analysis is thus achievable on the composition of the cellular solvent. NMR is familiar for studies focusing on metabolites and proteins, but it can provide information on more fundamental properties of cells: this starts with water of course, but a number of exotic nuclei can be studied, as well as pH or redox potentials, as we will show in the paragraphs below.

2.1.1. Water: intracellular and transmembrane diffusion, interactions and correlation times

Water combines many advantages where NMR spectroscopy is concerned: it is a fast-tumbling, symmetric, abundant small molecule containing two (equivalent) protons. ^{1}H is the highest gyromagnetic ratio nucleus (except for the radioactive ^{3}H), whose spin ½ is the simplest to manipulate and detect. All these parameters have beneficial consequences for NMR relaxation rates, simplicity of spin manipulation and sensitivity. The T1 and T2 relaxation rates of water are sensitive to the chemical environment, and are sufficiently slow to be measured accurately. They are also slow enough to be affected in a substantial and observable manner by many solutes. Hence, because of its convenient NMR behavior, detection of water signals has been the basis for some of the most successful applications of NMR, water-based MRI being a particularly clear example.

After a slow, error-prone start (see Section 3.1.1.), NMR of cellular water became useful in the following three main categories: measurements of i) transmembrane diffusion, ii) intracellular diffusion, iii) the correlation times of bulk water and of water molecules associated with cellular macromolecules.

The water permeability of erythrocytes has been thoroughly studied since the 1970's. T2 relaxation measurements have been carried out in the absence or presence of extracellular, impermeable paramagnetic agents (notably Mn^{2+}), which greatly enhance the extracellular T2 rate but not the intracellular one (similar to the contrast agents used in MRI). The global T2s of water and their differences in absence/presence of paramagnetic agents give access to transmembrane exchange kinetics (see the previous reviews for the relevant equations [51,52]). This was a good alternative to methods using radioactive tritiated water from the late 1950's. It permitted measurement of transmembrane water exchange of erythrocytes in varying osmolarity, temperature or pH conditions [53-59], upon exposure to chemicals [57,60], from patients with various illnesses [61,62] or from a great number of animals [63]. Hence, by the end of the 1980's, NMR had already made an important contribution to the field [51,64,65]. However, the extracellular paramagnetic species used at that time was mostly Mn^{2+}, which actually penetrates erythrocytes at high concentrations, hence diminishing the apparent water exchange rate and introducing discrepancies among the published reports [51,66]. MRI-related Gd^{3+}-chelators are more reliable in this regard [67].

Another approach was proposed, which did not require use of an external paramagnetic agent. It relied on the possibility to measure diffusion coefficients using Pulsed Field-Gradient (PFG) NMR, a method developed in the 1950-60's. The extensive presentation of its principles is out of our scope; a number of reviews are available [68-72]. Briefly, PFG NMR relies on i) the imposition of a spatial gradient of magnetic field for a short time, which causes a loss of spatial coherence of the NMR signals, ii) waiting for a defined delay, and iii) applying a second gradient pulse of opposite sign: hence, the coherence is fully recovered for immobile species, but only partially recovered for species that diffused in the delay inserted between the two gradient pulses (Fig. 1). The resulting observable NMR intensities are anti-correlated to the diffusion coefficients and to the time between the two gradient pulses. Thus, measuring these intensities gives access to NMR diffusometry. PFG NMR has been successful in measuring molecular displacements from 10 nm to 100 μm in a non-invasive fashion. This concept was used in the early 1970's to measure water diffusion in frog and rat muscles, which was found to be on average about half the rate seen in distilled water [73,74].

Because intracellular water diffusion is restricted by cell walls, long delays between the pulsed gradients cause a progressively attenuated signal decay. This would reach a plateau if the intracellular pool of water was trapped forever, since the cellular dimensions limit how far a water molecule can diffuse, but in reality, transmembrane exchange causes further decay, resulting in a measurable weighted average of the intra- and extra-cellular diffusion coefficients (Fig. 1). Theoretically, this effect allows estimation of intra- and extra-cellular self-diffusion coefficients of water, the cellular size defining the restricted space of diffusion, and the transmembrane water exchange rate [52,69]. It has been used by Andrasko in 1975 to measure simultaneously the transmembrane water exchange rate in erythrocytes and the average intracellular diffusion coefficient of water [82]. These measurements neglected the effects of magnetic susceptibility inhomogeneities in cell samples, which generate intrinsic field gradients and thus additional signal decay during PFG NMR experiments (These can themselves be used to measure intracellular diffusion coefficients of water in live and fixed cells [83,84]); the effects of such inhomogeneities on NMR signals are rather complicated and are treated in

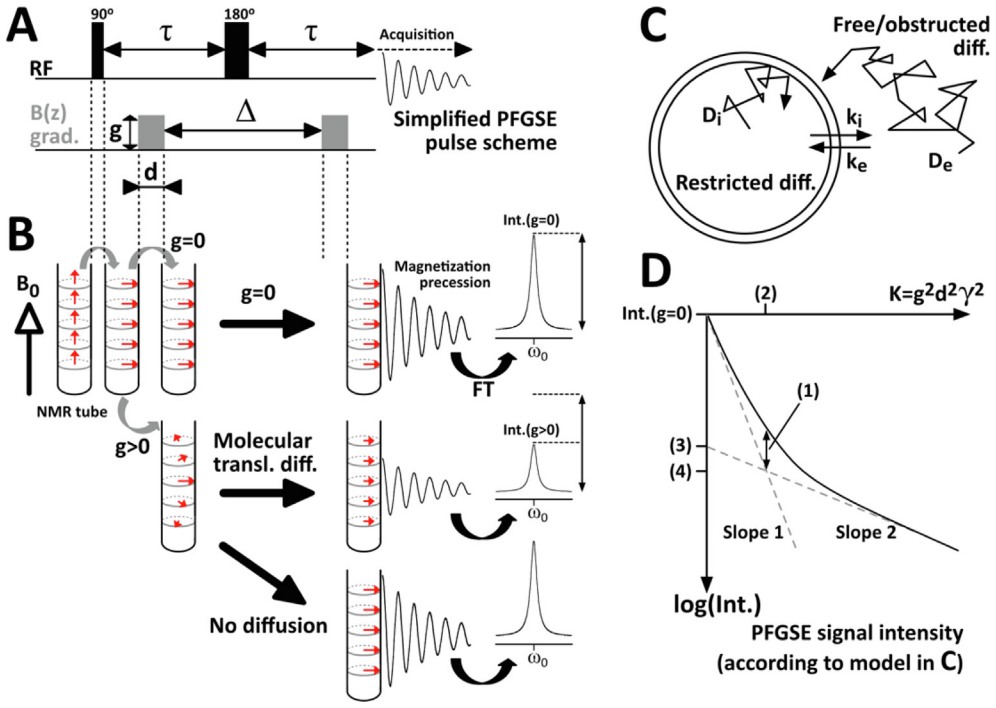

Fig. 1. Measurement of molecular diffusion in presence of intra- and extra-cellular compartments. **A)** Sketch of a simple Pulsed Field Gradients Spin Echo (PFGSE) pulse sequence used to measure molecular translational diffusion by NMR, where the z-gradient pulses have a duration d, a power g and are separated by a delay Δ ; **B)** Brief schematic explanation showing the z-dependent magnetization (red arrows) before and after the first pulsed field gradient, and showing the final magnetization, magnetization precession (free-induction decay, FID) and the signal intensities after Fourier Transform (FT) ; **C)** Scheme introducing the parameters to fit, D_i/D_e the diffusion coefficients, P_i/P_e the molecular populations, τ_i/τ_e the average residency times, k_i/k_e the transmembrane exchanges of intra- and extra- cellular molecules, respectively; In the case of free Brownian motion, the final acquired signal intensity is proportional to $S(2\tau)=M_0\exp(-2\tau/T2)\exp[-D\gamma^2g^2(\Delta-d/3)]$, with M_0 the equilibrium magnetization, T2 the transverse relaxation time, D the diffusion coefficient and τ, Δ and d the PFGSE-defined parameters; a number of improved variants of this pulse sequence have been proposed [75-79], notably the Stimulated Echo sequences, where diffusion is affected by T1 and not T2 (T1 is often much longer and more favorable than T2 in cells and tissues) ; **D)** Theoretical graph of the PFGSE attenuated signal intensity of a solute diffusing in two compartments in exchange, in the model situation corresponding to packed cells or tissues, where $P_i>>P_e$ and $D_e>>D_i$; (1)=$\exp(-\Delta/2\tau_i)$; (2) = $1/(\tau_iP_eD_e)$; (3) = $\exp(-\Delta/\tau_i)$; (4) = $\exp(-\Delta/\tau i(1+D_i/P_eD_e))$; slope1 = $\exp(-\Delta/\tau_i)*\exp(-K\Delta(P_eD_e+D_i)$; slope2 = $\exp(-K\Delta(P_eD_e+D_i)$. Adapted from Waldeck et al. 1997 [69,72,80,81].

Section 3.2. They were also ignored in the later PFG NMR studies on cells published since the 1990's, which aimed at measuring transmembrane water exchange in erythrocytes with varying cholesterol contents [85] and in the Gram positive *Corynebacterium glutamicum* [86], or self-diffusion coefficients of water in cultured mammalian cells through the cell cycle [87] and in camel erythrocytes [88]. PFG NMR experiments have also been used to measure simultaneously both water self-diffusion coefficients and transmembrane exchange in various systems: in yeast at different growth phases [89], in unicellular algae *Chlorella* [90], in erythrocytes [91-94], in cultured mammalian cells [95-97], or in plant systems like banana tissues [98], lupin roots upon exposure to lead [99], in maize roots of different lengths, or upon oxidative stress or at varying CO_2 concentrations [100-102]. Interestingly, MRI contrast agents were shown to inhibit transmembrane water exchange in this latter system [103].

Recent improvements have been proposed to this technique [75-79]. An interesting example takes advantage of the full signal decay of species in the extracellular medium, which experience unrestricted diffusion: a pair of strong pulsed gradients generate a "diffusion-filter" that leaves only the species in the restricted intracellular volume observable [75,76]. Their magnetization can be subsequently manipulated for any purpose, including diffusion measurements. Such a diffusion-filter has also been used for in-cell structural biology: it helped to filter out the leaking population of proteins and thus to observe intracellular proteins selectively [104].

In a rough summary, NMR spectroscopy has helped to evaluate the mean intracellular lifetime of water molecules to be about 10-20 ms in erythrocytes, and about 100 ms in HeLa cells. It also permitted quantification of intracellular water self-diffusion: it is about half as fast in cells as it is in pure aqueous buffers, and this number varies only slightly depending on cell types and conditions.

Concerning water rotational dynamics, NMR spectroscopy -and more specifically water T1 relaxation- has been used to study them, notably in the context of macromolecules hydration since the 1960's [105-109]. Many mechanisms combine to influence ^{1}H T1 relaxation in biological samples: solute-water cross-relaxation, solute-water proton exchange and the broad diversity of water interactions, which provoke many magnetic interactions and relaxation pathways [106,107,110,111]. Hence, interpretation of ^{1}H T1 relaxation often remains ambiguous. Fortunately, water dynamics can be studied using NMR spectroscopy of ^{17}O- and ^{2}H nuclei, whose low gyromagnetic ratios and quadrupolar nature of these nuclei are better adapted to water dynamics studies. The ^{17}O and ^{2}H bulk water relaxation times are largely immune to the phenomena of cross-relaxation and spin-diffusion, and are also only little affected by chemical exchange. These relaxation times are dominated by quadrupolar interactions, which are mostly sensitive to tumbling dynamics. ^{17}O and ^{2}H bulk water relaxation rates are fast enough to allow monitoring of water dynamics from the picosecond to the nano-microsecond timescale. Measuring magnetic relaxation at varying fields provides "relaxation dispersion"

profiles reflecting the exchange rates between "bound" and "free" water molecules.

The most abundant isotope of oxygen, ^{16}O, has a null spin and is thus useless from an NMR standpoint. The only "NMR-visible" isotope of oxygen, ^{17}O, is rare (< 0.04 % natural abundance), but can be enriched and incorporated in biological systems, where it becomes a potent NMR tracer. Although not trivial to manipulate, its spin 5/2 can be fruitfully exploited to delineate water populations that interact with cellular species. Succinctly, the quadrupolar nature of ^{17}O causes faster relaxation of water molecules "bound" to macromolecules. The very large field of ^{17}O-NMR studies is beyond our scope, dedicated reviews are available [112,113]. Early work in the 1970's used ^{17}O relaxation measurements to show that multiple water populations were constantly exchanging in cells, notably a minor fraction bound to nucleic acids or proteins, and a major "free" fraction [55,114-117]. In publications from the 1990's, this helped to estimate that below 1% of the cellular water molecules could be considered as "strongly bound", i.e. hydrogen-bonded, with correlation times of about 5-10 ns [118]. This number could reach 2% in mitochondria, but ^{17}O NMR confirmed that the great majority of cellular water molecules had correlation times in the picosecond timescale [119]. This dismissed the existence of any substantial population of "ordered" water molecules in these highly crowded organelles, although they contain about 400 g/L of macromolecules. In bacteriophage Pf1, 4% of the water molecules are bound to macromolecules according to ^{17}O relaxation measurements, which corresponds to about 4 water molecules per phage nucleotide [120].

In the late 2000's, Halle and colleagues measured ^{2}H and ^{17}O magnetic relaxation dispersion in *E. coli*, in the halophile archae *Haloarcula marismortui* and in *Bacillus subtilis* spores [121-123]. In both *E. coli* and *H. marismortui*, they showed that ~85% of water molecules had correlation times of about 1.5 ps, 15% had correlation times of about 25-30 ps corresponding to the hydration-shells of cellular macromolecules, and only 0.1 % of water molecules were trapped in buried sites on the microsecond time scale. Even in the dense core of *B. subtilis* spores, the hydration water molecules had tumbling times of only 50 ps and buried water represented ~0.15 % of the total. These numbers were in line with those measured on *in vitro* dilute proteins samples.

We stress again the fact that these experiments do not report the *translational* behavior of water molecules, which can be measured by neutron scattering [124-126] and NMR measurements of diffusion (see above). The numbers above are consistent with results from more recent studies using other techniques like time-resolved infrared spectroscopy or dielectric relaxation spectroscopy [127].

Altogether, NMR spectroscopy has thus contributed greatly to the progressive understanding of water dynamics in cells.

2.1.2. Quantification and interactions of metal ions:

Metal ions are key components of cellular life, involved in modulating solvent properties, membrane potentials and thus neuron or muscle excitability, and in enzyme catalytic sites. They find applications in imaging or radiation therapy. They all have one or multiple isotopes with non-zero magnetic moment, but these are not necessarily found at high natural abundance (see [128] or https://www.webelements.com).

$^{6}Li^{+}$ and $^{7}Li^{+}$, $^{23}Na^{+}$, $^{27}Al^{3+}$, $^{39}K^{+}$, $^{85}Rb^{+}$ and $^{87}Rb^{+}$, $^{113}Cd^{2+}$ and $^{133}Cs^{+}$ have all been studied by direct NMR detection in cells. They have also been studied using molecules that change their chemical shifts according to whether they are in extra- or intra-cellular media, the so-called "shift reagents" (Fig. 2). These contain paramagnetic ions that shift the observed NMR frequencies of species in the same sample compartment. Hence, they make it possible to distinguish intra- and extra-cellular species. These shift reagents are similar to contrast agents used for MRI, but induce less NMR relaxation of the solvent signals. Some "smart" contrast agents have been designed more recently by coupling basic contrast agents to metal-ion-chelating scaffolds: upon ion binding of the second moiety, the paramagnetic core of the contrast agent is exposed to the solvent (Fig. 3). These ion-activated contrast agents can thus reveal the presence of free cellular metal ions by enhancing the water NMR relaxation.

Mg^{2+}, Ca^{2+}, Fe^{2+}, Zn^{2+} have active NMR isotopes at very low abundance, which precludes sensitive direct NMR detection. Moreover, paramagnetic states prevent NMR direct detection of Mn(II), Mn(III), Fe(III), Cu(II), Co(II) to name only a few. The abundant and diamagnetic isotopes of metal ions are however not easy to handle either. Their high spin $\geq$ 3/2 causes fast, multi-exponential relaxation, and thus intrinsically weak NMR signals. Their low gyromagnetic ratios can further plague their NMR detectability, which is typically the case for ^{39}K. Hence, reporters have been designed that incorporate sensitive nuclei (e.g. ^{19}F), whose chemical shifts change when chelating the cation of interest. These will be called "labeled chelators/sensors" (Fig. 4).

We describe the strategies used in NMR studies of the main ions in the sections below. Some further pieces of information on these nuclei are given in Section 3.3.1. Other more exotic species have been studied sporadically by NMR in cells, e.g. $^{10}B/^{11}B$ or ^{195}Pt [146-152]. Overall, NMR has been very useful in understanding the dynamics of all these ions in cells. NMR of metal ions is unable to provide spatial information at the (sub)micrometric scale of the subcellular level. However, it is still a very versatile technique that we suggest may find further applications in nutrition or toxicology studies on living microorganisms, plants, small animals or organoids, where it would also offer millimetric imaging capacities. All the studies below may be reinterpreted/readapted with these capabilities in mind.

2.1.3. Li^{+}

Lithium is only found in trace amounts in living organisms, but it is commonly used therapeutically in treatment of bipolar disorders and may be effective against some cancers or neurodegenerative diseases [153-155]. The mechanisms behind its beneficial and adverse effects are still not well defined: they may be related to competition with Mg^{2+} in binding to kinases or phosphatases, competition with Na^{+} in GPCR binding, or membrane binding [156-158]. Both ^{6}Li and ^{7}Li have non-zero spins, but ^{7}Li has been almost the only species used in NMR cellular studies, because it is much more abundant and shows better relaxation properties than ^{6}Li [159]. Important results came from solution NMR investigations using direct ^{7}Li one-dimensional spectroscopy. In a first study in the 1970's, Andrasko used the PFG-NMR strategy (see above in Section 2.1.1.) to reveal the restriction of Li^{+} diffusion in erythrocytes and measure their transmembrane exchange [160]. Then, in the 1980-90's, the use of "shift reagents" and solution ^{7}Li-NMR permitted non-invasive quantification of Li^{+} cellular uptake, and detection of Li^{+} interactions with nucleic acids or phospholipids. Monitoring of Li^{+} cellular uptake was performed in yeast [161] and in erythrocytes [162-164] and astrocytomas [165]. An improved, more membrane-impermeant Tm-DOTP "shift reagent" was used in the 1990's to study Li^{+} cellular uptake of erythrocytes [166] and neuroblastoma cells (Fig. 5) [167,168]. ^{7}Li has also been used as a surrogate for studying Na^{+} efflux in rat hearts [169-171].

Measurements of ^{7}Li NMR relaxation times helped to show that it was binding preferentially to the inner phospholipid layer of erythrocytes (and not to sialic acid, actin or hemoglobin) [172-175]. Li^{+} phospholipid binding was later observed also in neuroblastoma cells [65]. Li^{+} competes with Mg^{2+} for binding to phospholipid in erythrocytes, as shown by fluorescence microscopy and ^{31}P NMR [176] and later by ^{6}Li and ^{7}Li NMR relaxation measurements

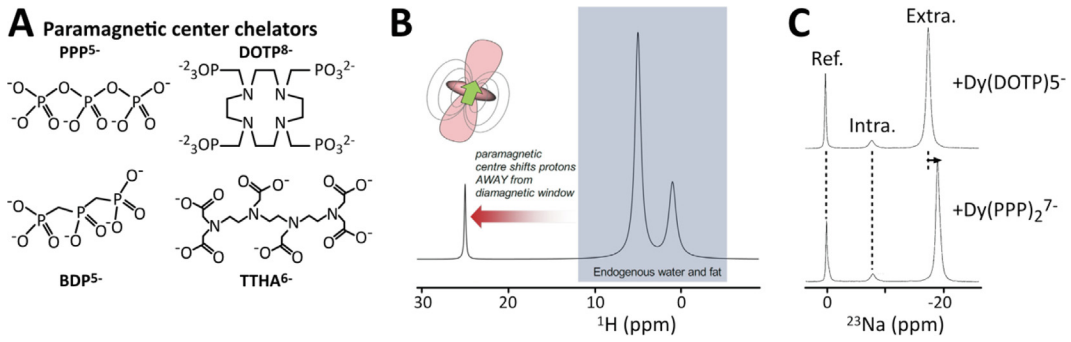

Fig. 2. Operating principle of "shift reagents", **A)** Chemical structures of the main shift reagents used in cellular studies (adapted from Szklaruk et al. 1990 [129]): these chelators are typically loaded with transition metals (most often Mn^{2+}) or lanthanide ions. **B)** Schematic ^{1}H NMR signals from mouse tissue water and fat, adapted from Harnden et al. 2019 [130]: the extracellular chelated paramagnetic center provokes important changes in chemical shifts of extracellular species, here water, or **C)** $^{23}Na^{+}$ NMR signals from human erythrocytes in suspension (the reference signal is generate from a capillary containing a pure aqueous NaCl solution), adapted from Sherry et al. 1988 [131]. Paramagnetic induced chemical shifts are mostly due to the merging effects of hyperfine shifts and bulk magnetic susceptibility (see [130,132,133] for more comprehensive explanations). Shift reagents also accelerate relaxation times and thus signal linewidths of species in the same sample compartment.

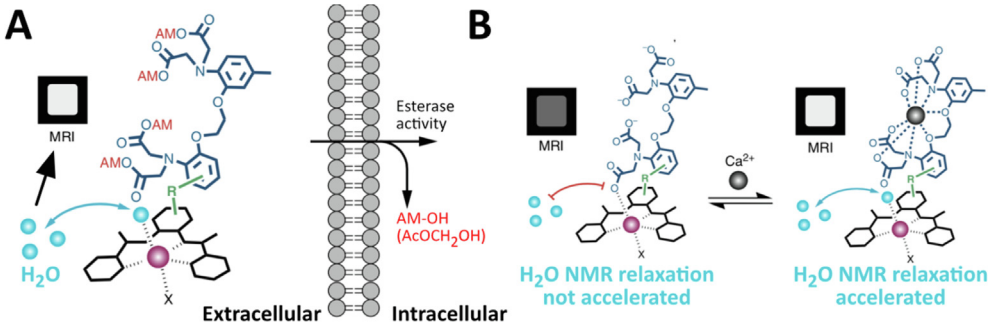

Fig. 3. Operating principle of ion-dependent ("smart") contrast agents, adapted from Barandov et al. 2019 [134]. **A)** Schematic chemical structure of a Ca^{2+}-activated, Mn^{2+}-contrast agent: a Mn^{2+} chelator is linked to an acetomethoxyl-BAPTA moiety; the acetomethoxyl ester groups are removed upon cell internalization by cellular enzymes, which traps the complex in cells. **B)** In presence of free Ca^{2+}, the BAPTA moiety chelates Ca^{2+} preferentially and does not chelate any longer the Mn^{2+} paramagnetic center, which, in turn, is more exposed to solvent; this induces a faster NMR relaxation of solvent signals. The insets show the resulting ^{1}H-water signal observed by MRI. A number of chemical scaffolds have been proposed with the same purpose [135-141]. These can be used for NMR studies on cells; the final goal is often to obtain probes for functional MRI.

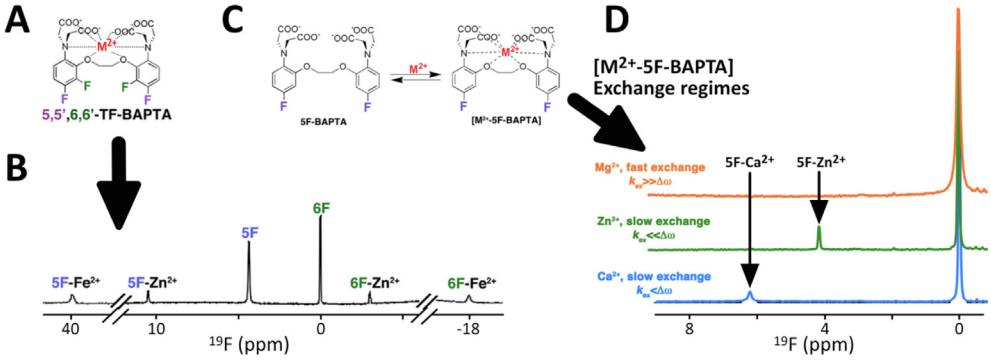

Fig. 4. Operating principle of "labeled chelators/sensors" that report the presence of metal ions in cells, adapted from Bar-shir et al. 2013 and 2015 [142,143]. We show here one of the most commonly used scaffolds in the literature, the cell-penetrant BAPTA chelators. Their acetoxymethyl ester form (nF-BAPTA-AM) freely enters into cells, where it is converted to an impermeable form (devoid of acetoxymethyl ester function, nF-BAPTA) by intracellular esterases [144,145]. Being fluorinated, these molecules are observable by ^{19}F-NMR spectroscopy, which does not suffer any background signal in cells. Different fluorination schemes result in different affinities and exchange rates for every divalent metal ion. **A)** Chemical structure of 5,5',6,6'-TF-BAPTA and **B)** the 1D ^{19}F NMR obtained in presence of Fe^{2+} or Zn^{2+}, showing the 5,5'-^{19}F and 6,6'-^{19}F signals in purple and green, respectively. **C)** Chemical structure of 5F-BAPTA and the exchange between free and chelating situations, whose exchange rates **D)** cause different ^{19}F signal linewidths in 1D ^{19}F NMR spectra (recorded at 11.7 T, k_{ex} is the exchange rate, and $\Delta\omega$ is the difference of NMR frequencies between the signals from the free and chelating forms of nF-BAPTA). Other labeled sensors have been proposed, which can also use ^{13}C- or ^{15}N- labeling. The sensitivity of these sensors can be enhanced by Chemical Exchange Saturation Transfer (CEST) methods, allowing detection levels of metal ion concentration in the submicromolar range [142,143].

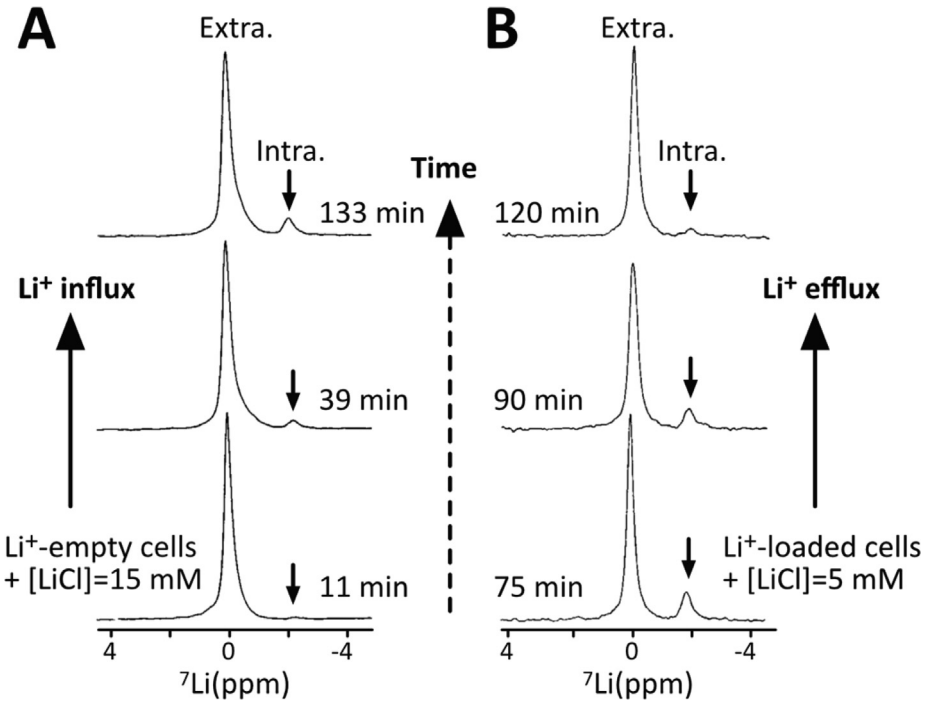

Fig. 5. A) 1D ^{7}Li NMR spectra showing the Li^{+} influx in SH-SY5Y human neuroblastoma cells perfused by a culture medium supplemented with the shift agent $HTmDOTP^{4-}$ and with LiCl at 15 mM after (a) 11 min, (b) 39 min and (c) 133 min; **B)** 1D ^{7}Li NMR spectra showing the Li^{+} efflux from Li^{+}-loaded SH-SY5Y human neuroblastoma cells perfused by a culture medium supplemented with the shift agent $HTmDOTP^{4-}$ and with LiCl at 5 mM after (d) 75 min, (e) 90 min and (f) 120 min. Adapted from Nikolakopoulos et al. [168].

[177]. ^{7}Li relaxation was also used to demonstrate another competition of Li^{+} with Mg^{2+} in chromaffin cells and in lymphoblastoma and neuroblastoma, where faster relaxation was measured than in erythrocytes [178,179]. This was interpreted as being due to supplementary interactions of Li^{+} with unknown targets, or to changes in composition of cellular phospholipids upon exposure to Li^{+} [180,181]. Li^{+} does indeed compete with Mg^{2+} at many levels [156]: it binds to ATP [182], to the kinase Gsk3β, and to the inositol phosphatase [183], provoking an increase of phosphoinositol content. The precise mechanisms of Li^{+} actions are thus not yet elucidated, but in-cell NMR has made important contributions in the field. These studies have moreover paved the way for ^{7}Li-MRI approaches, which have helped improve understanding of the distribution of Li^{+} in brain upon lithium treatments [159,184,185].

2.1.4. Na^{+}

Na^{+} is less abundant in cells (∼10-30 mM) than in extracellular fluids (∼100-150 mM). The mechanisms ensuring low Na^{+} intracellular concentrations are of great importance, notably because they are essential to the proper functioning of excitable cells and of Na^{+}-dependent membrane proteins [186]. Because ^{23}Na represents 100% of sodium and has a relatively favorable gyromagnetic ratio (about ¼ of ^{1}H), ^{23}Na NMR has long been attractive for NMR studies.

Early $^{23}Na^{+}$ NMR measurements by Cope in the 1960's reported large NMR-invisible populations, representing about 60% of intracellular $^{23}Na^{+}$ [187,188], similar to the situation for $^{39}K^{+}$ that we will describe later (see below and Section 3.1.2.). The "invisibility" of this fraction of the intracellular $^{23}Na^{+}$ population was interpreted by some authors as indicating that it was bound or immobilized [187-193]. An exception was found in the very "watery" plant vacuoles, where few interactions with macromolecules exist [194]. However, Civan and Shporer showed in the 1970's that these early measurements had to be re-interpreted using an appropriate theory of quadrupolar nuclei relaxation, which led to the conclusion that actually less than 1% of $^{23}Na^{+}$ was bound and immobilized in cells [195-197]. Parallel investigations on ^{39}K reinforced this theoretical framework (see below). T2 relaxation of cellular $^{23}Na^{+}$ has two components, one fast (∼0.5-2.5 ms) and one slow (∼10-50 ms) corresponding to 60% and 40% of the total signals, respectively. In the early times, the experimental set up was not likely to permit detection of the fastest relaxation components of quadrupolar ions in cells – hence the invisibility of 60% of the signal.

Improved equipment such as faster electronic systems and higher field spectrometers (>5 T) paved the way to studies focusing on Na^{+} transmembrane exchange in the 1980's. In 1982, Springer, Gupta and their coworkers proposed independently the use of extracellular shift reagents, i.e. dysprosium and thulium complexes, to distinguish NMR signals from intra- and extra-cellular $^{23}Na^{+}$ (Fig. 6) [161,198,199]. Recording a time series of simple 1D ^{23}Na NMR spectra was thus sufficient to monitor the influx and efflux of Na^{+} in a non-invasive fashion, in real-time with a timeframe of one minute. At that time, other methods were used for such measurements, such as atomic absorption spectrometry, flame-emission photometry, radioisotope tracing and ion-selective microelectrodes. These were destructive, time consuming methods, which did not come to consistent conclusions on cation transport and dynamic equilibria [200-204]. ^{23}Na NMR was thus seen as an interesting opportunity in the field, not requiring prior separation of the cells or their culture medium. This strategy using shift reagents was adopted by many groups in the 1980's to monitor intracellular levels of $^{23}Na^{+}$ in yeast [161,200], in bacteria [205-214], in frog oocytes [215], in amoeba [216], in erythrocytes [203,217-222], in animal tissues and organs such as perfused hearts [223-230] and in living rats or rabbits [231-235]. These NMR experiments were combined with ^{31}P-NMR to measure intracellular pH in parallel, and sometimes also with ^{39}K NMR. Among others things, this permitted studies of the regulation of Na^{+} levels in microorganisms submitted to osmotic shocks

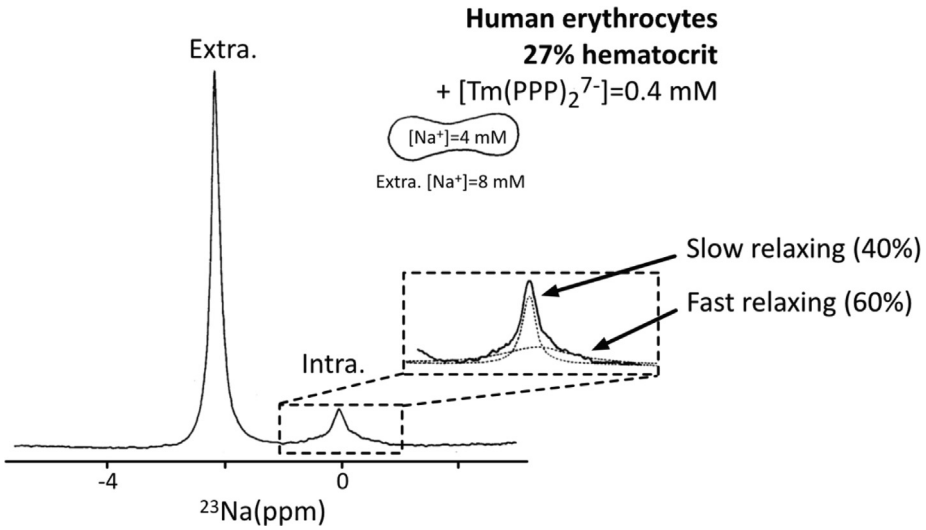

Fig. 6. 1D ^{23}Na NMR spectrum of human erythrocytes (27% hematocrit) resuspended in a medium containing the shift agents $Tm(PPP)_2$ necessary to separate intra- (at 0 ppm) and extra- (at ∼-2 ppm) cellular $^{23}Na^+$ NMR signals. The dashed lines in the inset show the two fitted Lorentzian lines of the intracellular $^{23}Na^+$ signal, with a fast and a slow relaxing component representing 40% and 60% of the integrated intensity, respectively. The spectrum was recorded at 8.46 T (frequency of ^{23}Na: 95.245 MHz) in ∼ 9 minutes in 1984. Adapted from Pike et al. 1984 [242].

[200,205,206,211,213], evaluation of the selectivity of cation-carrying chemicals penetrating Gram positive bacteria [209,221,222,236], and measurement of the activity of the Na^+/K^+ ATPase pump *in situ* [224,228,229,237]. The assumed stability and inertness of the shift reagents used was however disproved in the late 1980's [238-241].

Another approach has been adopted to observe the signal from intracellular $^{23}Na^+$ selectively: selecting the double-quantum transitions of ^{23}Na has a filtering effect, which permits observation of only those $^{23}Na^+$ ions that experience the bi-exponential relaxation caused by interactions with macromolecules [243-245]. Even though much attenuated, the extracellular $^{23}Na^+$ signal can also immediately be recognized in such Double-Quantum filtered (DQF) spectra, because of interactions with exterior cellular membranes or proteins in the extracellular medium [246,247]. Addition of a low concentration of extracellular paramagnetic Gd^{3+} was necessary to quench this remaining signal. Triple-Quantum filtering (TQF) was shown to perform slightly better in isolating the intracellular $^{23}Na^+$ signal [248,249], but was also not capable of cancelling the extracellular $^{23}Na^+$ signal completely (Fig. 7) [250-252]. In the mid 1990's, these DQF or TQF methods were still proposed to monitor intracellular Na^+ levels upon ischemia in cultured cells [253,254] or in perfused rat heart [255], because the DQF/TQF $^{23}Na^+$ signal variations were only due to changes in intracellular Na^+ levels. TQF ^{23}Na NMR has been applied to study the intracellular sodium levels in tumors implanted in mice or rats [256,256-259], and even to map intracellular sodium in human brain [260,261]. TQF suffers from significant signal-to-noise losses as compared to Single-Quantum ^{23}Na NMR, and other ^{23}Na MRI strategies have been developed, which we can only mention here (see [262-265]). Recent improvements in pulse sequences permitted detection of TQ and SQ signals simultaneously with improved sensitivity, and reporting of the minute-timescale evolution of intracellular $^{23}Na^+$ levels in just ∼15 million cells [266-268].

2.1.5. K^+, and Rb^+ as a surrogate

Potassium is the least receptive of the alkali metals in NMR studies. Indeed, although found in high natural abundance (93.3%), ^{39}K suffers from its low gyromagnetic ratio and its quadrupolar nature, yielding 180-fold lower *in vivo* sensitivity than ^{23}Na. ^{39}K was first observed in cells in 1970 using halobacteria that contain intracellular K^+ concentrations as high as 4-5 mol/L [269]. Importantly, ^{39}K NMR has also helped in understanding cellular ion mobility. Similar to water proton and ^{23}Na NMR studies (see above), erroneous conclusions were drawn in the late 1960's from data obtained with early spectrometers and incorrect interpretations, namely that the weak 30-40% NMR visibility of cellular ^{39}K was due to the remaining K^+ being immobilized in a semi-crystalline cellular milieu [269]. Very soon afterwards, in the 1970's, studies using more advanced equipment and NMR theory showed that only at most a few percent of $^{39}K^+$ were actually transiently interacting with cellular molecules [270-273]. We give more details on this controversy in Section 3.1.2. Starting from the early 1980's, shift reagents permitted distinction of extra- and intra-cellular ^{39}K, and thus allowed them to be quantified [274], to monitor transmembrane ion transport in erythrocytes [218], in halobacteria [275], in yeast [200], in *E. coli* [276], and later in frog [277], rat [225,278] or guinea pig hearts [279], and rat salivary glands [280]. Because potassium homeostasis is linked to heart injuries or cellular membrane potential in brain, ^{39}K MRI studies were attempted from the late 1990's [281]. Use of higher magnetic fields [282,283] and more sensitive spectrometer probes [284] progressively pushed the sensitivity limits of this approach.

Rubidium has for long been established as a good surrogate for cellular potassium uptake [285], and used in quantitative studies primarily in its radioactive form ^{86}Rb [286]. Its stable isotope ^{87}Rb was considered in the late 1980's for achieving NMR studies of potassium uptake in intact rat kidney and heart [287-289], in mammalian cultured cells [290], in erythrocytes [291,292], in rat salivary glands [293] and in skeletal muscles of living rats [294]. Sensitivity assessment in erythrocytes indeed showed that direct ^{87}Rb NMR detection was likely to provide about 19 times more signal than ^{39}K [291]. However, as with ^{23}Na or ^{39}K, the quadrupolar nature of ^{87}Rb causes fast, bi-exponential relaxation in cells [295,296]. This was initially used to distinguish two overlapped ^{87}Rb peaks, one broad signal that would correspond to intra-kidney $^{87}Rb^+$, and one narrow revealing the extracellular signal [287,288]. Fitting to the sum of these Lorentzian signals helped to quantify ^{87}Rb uptake in perfused organs, where the ^{87}Rb signal was so broad that shift agents in the extracellular milieu could

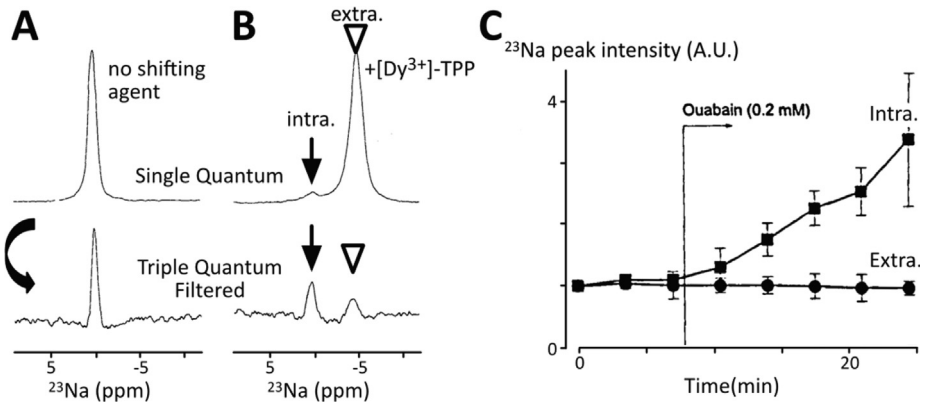

Fig. 7. A) 1D ^{23}Na NMR spectra of a perfused rat heart: One pulse SQ NMR (upper spectrum, 24 scans, t_{acq}~5 s) and TQF (lower spectrum, 960 scans, t_{acq}~200 s) spectra; **B)** 1D ^{23}Na NMR spectra of a perfused rat heart in a medium containing the shift reagent [Dy^{3+}]-(tripolyphosphate)$_2$: One pulse SQ NMR (upper spectrum) and TQF (lower spectrum) spectra, showing intra- (peak at the left) and extra- (peak at the right) cellular $^{23}Na^+$ signals; **C)** Plotted intensities of signals from intra- (square) and extra-cellular (circles) $^{23}Na^+$ in 1D ^{23}Na TQF NMR spectra of perfused (triplicates) rat hearts in a medium containing $Tm(DOTP)^{5-}$ as a shift reagent, before and after exposure to the inhibitor of the Na^+/K^+-ATPase pump ouabain, leading to an increase of intracellular Na^+. A) and B) are adapted from Jelicks et al. 1993 [250], the spectra were recorded at 9.4 T in 1993; C) is adapted from Dizon et al. 1996 [255].

not separate extra- and intra-cellular peaks [297]. A strategy was proposed to cancel the extracellular ^{87}Rb signal using lanthanide contrast reagents [298]. In later studies on animal tissues, an internal reference was used to quantify $^{87}Rb^+$ concentration, which consists of a capillary containing ^{87}Rb in a KI saturated solution, generating a ^{87}Rb signal shifted by 55 ppm [294]. ^{87}Rb NMR spectroscopy evolved towards functional studies on Na^+/K^+ ATPase activity in injured hearts [299] and brain potassium imaging [300,301]. We have not found any study using ^{87}Rb NMR published in the last ten years. The limited sensitivity and natural abundance of ^{87}Rb requires high concentrations of Rb^+ for measurement, resulting in partial replacement of K^+ in cells, with reported cardiac consequences [299].

2.1.6. Mg^{2+}

With an intracellular concentration in the range of 10 mM, Mg^{2+} is the second most abundant cation in cells after K^+ [302]. It is essential in many regards, notably for the proper functioning of many enzymes and channel proteins [303]. It can be considered an integral part of many RNA and DNA structures [304-306]. Understanding the impact of intra- and extra-cellular Mg^{2+} levels in many pathologies has been a longstanding aim. The only NMR visible isotope is ^{25}Mg, which has a very low intrinsic sensitivity because of its poor natural abundance (~10 %), its low gyromagnetic ratio and its spin 5/2. It has thus been studied mostly via its chelating partners and their chemical shift changes upon Mg^{2+} binding.

The main example of this is ATP, whose ^{31}P NMR chemical shifts follow the Mg^{2+} binding equilibrium [202,307,308]. ATP proton chemical shifts of the ribose also depend on Mg^{2+} chelation [309,310]. As we will see in Section 2.3.2. on metabolites, ^{31}P NMR is convenient in cells because of its relatively good sensitivity when present in small molecules and the small number of observable signals. Hence, ^{31}P NMR and the survey of ATP chemical shifts has been used since the late 1970's [311,312] to measure the intracellular free Mg^{2+} and the ATP:Mg^{2+} population in erythrocytes [202,312-317], lymphocytes [318], Ehrlich ascites tumor cells [319], cultured mammalian cells [320,321], animal tissues [322-327], in worms, amoebae or sea snail [328-330], and more recently in MRI/MRS studies [331-335]. These ^{31}P NMR studies have regularly reported that the concentration of free intracellular Mg^{2+} is only ~0.3-0.6 mM in mammalian cells, while the total concentration of 10-20 mM in most cells [336] (with an exception: only ~2 mM in erythrocytes that contain low quantities of nucleic acids). They also revealed that more than 90% of the cellular ATP (intracellular concentrations between 2 and 10 mM) is found in a Mg^{2+} bound form. These measurements could be ambiguous, because of the uncertain amount of invisible ATP that would bind cellular macromolecules, because of the possible compartmentalization of ATP:Mg^{2+}, because of the salt and pH dependency of ATP:Mg^{2+} association constant, and because the ATP ^{31}P chemical shifts are themselves strongly dependent on pH and temperature, all of which aspects were progressively taken into account as models developed [202,307,308,326,337-343]. Diphosphoglycerate ^{31}P chemical shifts are also dependent on pH and Mg^{2+} chelation, and it was thus used with ATP in a complementary fashion to measure free Mg^{2+} and pH in erythrocytes (Fig. 8) [344]. The ^{31}P peak linewidths of ATP have also been proposed for quantification of Mg^{2+} binding [345,346], although this type of analysis may be affected by field homogeneity [347]. In any case, these measurements were non-invasive and extremely useful, by making it possible to study the evolution of ATP:Mg^{2+} and cellular free Mg^{2+} levels under different stresses. They provided a complementary method to the early fluorescence measurements, which tended to overestimate the free Mg^{2+} levels. The studies based on fluorescence spectroscopy used reporters that had their flaws in terms of selectivity (notably towards Ca^{2+}) and leakage, in addition to the potential that they might compete with endogenous binders of Mg^{2+} [202,307,348]. Improved fluorescence sensors have since been tailored, although the perfect sensor is still elusive [349,350].

To complete this section, we present a few direct detection NMR studies that use ^{25}Mg : by measuring the ^{25}Mg NMR peak linewidth at increasing concentrations of ATP, ADP, DPG, or in presence of actin filaments, these studies have provided direct proof of the formation of ATP:Mg^{2+} and $(ATP)_2$:Mg^{2+} (Fig. 9) [351] and of the very loose binding of Mg^{2+} to actin filaments acting only like polyelectrolytes and not as a cognate partner [352]. The chelated Mg^{2+} is in fast exchange with free Mg^{2+} and is never trapped in these complexes unless actin filament bundles form. $^{25}Mg^{2+}$ has also been shown to have weak affinities for a number of proteins [351,353-355]. An interesting feature is its regular competition with Ca^{2+} and not with other cations [353,354]. All these ^{25}Mg NMR *in vitro* studies most probably recapitulate some cellular aspects. We did not find any published in-cell ^{25}Mg studies. Still, these studies show how much information NMR has yielded that shaped understanding of cellular Mg^{2+}.

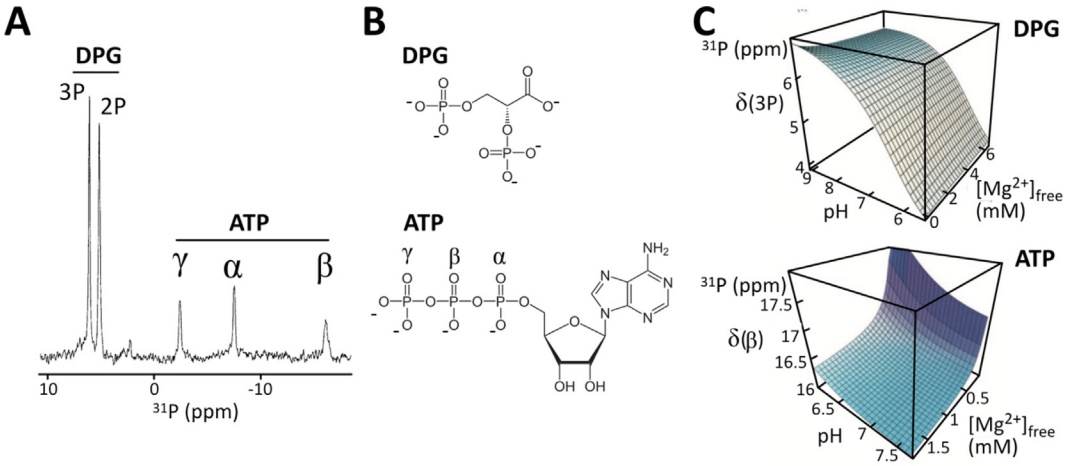

Fig. 8. A) 1D ^{31}P NMR spectrum of human erythrocytes (~35-50% hematocrit, recorded at 310K and 9.4 T in 2002, 2048 scans, t_{acq}~30 min), showing the ^{31}P signals from the two main species diphosphoglycerate (or 2,3-bisphosphoglycerate) and ATP; **B)** Chemical structures of DPG and ATP; **C)** *Up:* Plot of the chemical shift (absolute values) of the β phosphate of ATP in function of pH and of $[Mg]^{2+}_{free}$; *Bottom:* Plot of the chemical shift of the 3-phosphate of DPG in function of pH and of $[Mg]^{2+}_{free}$. Adapted from Willcocks et al. 2002 [344].

2.1.7. Ca^{2+}

Ca^{2+} is involved in an very wide variety of cell signaling pathways, from cell proliferation to apoptosis, thymocytes activation or synaptic transmission and cell contraction in metazoans [356], and in many adaptative reactions in plants [357]. These all rely on spatiotemporal variations of cellular concentrations of Ca^{2+}. Resting cells keep their cytosolic Ca^{2+} at about 100 nM and store Ca^{2+} in the Golgi apparatus, endoplasmic reticulum (ER) and sarcoplasmic reticulum of muscle cells at 0.5-1 mM. These organelles eventually trigger calcium signaling upon stimulation via Ca^{2+} release that enhances its cytosolic concentration to 200-500 nM (extracellular Ca^{2+} is at 2 mM) [356,358]. Direct NMR detection of calcium in solution is impractical: the only detectable isotope ^{43}Ca is present at very low natural abundance (0.14%) and yields low and broad signals because of its quadrupolar nature [359]. Very few solution ^{43}Ca NMR studies have been published, to the best of our knowledge, and ^{43}Ca NMR is probably more of interest for solid-state applications [360].

This limitation has motivated NMR spectroscopists to test calcium detection via calcium-sensitive probes in the early 1980's: inspired by existing fluorescent probes, Ca^{2+} chelators were designed to integrate ^{19}F atoms in their chemical structures, which permitted ^{19}F-NMR detection and quantification of cytosolic Ca^{2+} in thymocytes [144]. The free and chelating forms of these ^{19}F-labeled sensors indeed do show two different chemical shifts, and the area of the two peaks are proportional to the corresponding populations (Fig. 4). This principle has been very widely exploited. It has been applied to Ca^{2+} measurement in aging or sickle erythrocytes [145,361-363], platelets [364], synaptosomes [365], leukemic cells [366], osteoblasts [367,368], hear cells [369], kidneys [370], perfused hearts [371-373] and brain [374-376] in the native ~50-100 nM range. The initial sensors have moreover been modified for tuning cell delivery and for quantifying other metals: ^{19}F-containing chelators have different affinities and ligation kinetics for every metal, and are also associated with different specific chemical shifts [137]. The initial advance was the use of acetoxymethyl ester 5F-BAPTA-AM, which freely enters cells and is converted to the cell-impermeant 5F-BAPTA by intracellular esterases [144,145]. The 5F-BAPTA sensor was actually able to report simultaneously cellular Ca^{2+} and Zn^{2+} concentrations [365,377,378] or Ca^{2+} and Pb^{2+} [367], and later Ca^{2+}, Cd^{2+} and Zn^{2+} [379]. It has for example been used recently to monitor Ca^{2+} uptake in erythrocytes upon mechanical distortion [380]. Other sensors for transition metals quantification or pH measurement were developed (see below). Moreover, because 5F-BAPTA ^{19}F resonances were also recognized to be pH-sensitive, pH sensors were designed in a similar way (see below).

In a series of derivatives, the ~500 nM Ca^{2+} affinity of 5F-BAPTA was modified down to ~50 nM for DiMe-5F-BAPTA, which permitted lower sensor load, hence less perturbation of Ca^{2+} pulses in perfused beating hearts [381,382]. These improvements were of course motivated by the opportunity to carry out *in vivo* Ca^{2+} studies, which started in the 1990's [383]. It was however hampered by the low sensitivity of 5F-BAPTA ^{19}F-NMR spectroscopy, estimated to be 10^5 fold less than standard proton MRI [384].

Chemical Exchange Saturation Transfer (CEST) approaches (Fig. 4, Fig. 14) have been proposed that enhance 5F-BAPTA-mediated Ca^{2+} detection by a factor 100 [142,143]. To further increase sensitivity, sensors incorporating multiple equivalent ^{19}F nuclei were designed and combined with the use of CEST; similarly, ^{15}N- or ^{13}C- containing sensors were hyperpolarized and used in CEST strategies as well; Ca^{2+} sensors coupled to cryptophane cages recognizing hyperpolarized ^{129}Xe were also proposed in combination with CEST. None of these methods have been tested yet in cells to the best of our knowledge [137,385].

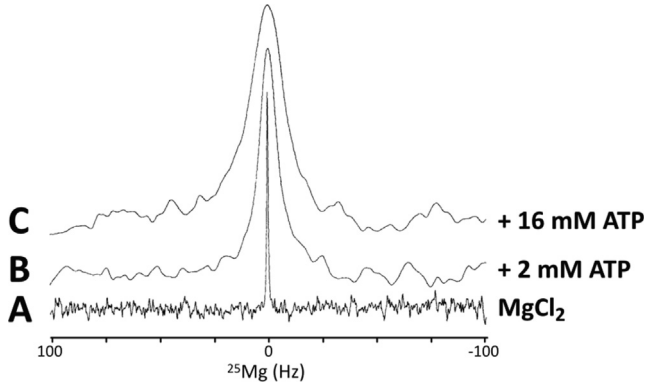

Fig. 9. 1D ^{25}Mg NMR spectra of samples containing **A)** 2 mM $^{25}MgCl_2$, 100 mM KCl, 20 mM Tris-HCl, 20% ^2H_2O at pH7.2, **B)** supplemented with2 mM ATP and **C)** 16 mM ATP. Spectra were obtained from A) 256 scans (t_{acq}~100 s), B) 4096 scans (t_{acq}~1600 s) and C) 29109 scans (t_{acq}~11600 s) at 9.4 T (^{25}Mg frequency of 24.485 MHz) in 1991. (Adapted from Bock et al. [351])

Another approach was developed, which takes advantage of molecules combining a Ca^{2+} chelator fragment that modulates the relaxivity of a paramagnetic fragment (Fig. 3): the first of these "smart contrast agents" was designed in the late 1990's, and exposed the paramagnetic Gd^{3+} to the solvent in presence of Ca^{2+} [386]. This strategy adopts the common MRI strategy of contrast agents, which accelerates water ^{1}H resonance relaxation, revealed by lower signal intensities. It was progressively improved by a number of groups, tested in cells [136,387], and recently used in MRI studies of extracellular Ca^{2+} dynamics in the brain interstitial space [388] and during cerebral ischemia [389]. Cell-permeable Ca^{2+}-sensor contrast agents were also designed, which have shown MRI compatible sensitivity in cultured cells [138] and even in living rats [134]. However, none of these developments circumvent the inability of NMR to assess the functional inhomogeneity of intracellular Ca^{2+}, which are accessible by fluorescent probes for example [358,390].

2.1.8. Transition metal ions Mn^{2+}, Fe^{2+}/Fe^{3+}, Co^{2+}, Ni^{2+}, Cu^{+}/Cu^{2+} and Zn^{2+}, Pb^{2+}

Because of their paramagnetic properties, transition metal ions Mn^{2+}, Fe^{2+}/Fe^{3+}, Co^{2+}, Ni^{2+}, Cu^{2+} are not directly observed by NMR. They are mostly chelated and involved in enzymatic catalytic sites, and their concentration as free ions is very low in living organisms. Copper is present in cells in its diamagnetic ionic form Cu^{+}, but it is also completely coordinated in proteins or by glutathione in prokaryotic and eukaryotic cells, resulting in sub-femtomolar concentrations of free Cu^{+} [391-395]. The quadrupolar ^{63}Cu and ^{65}Cu would be expected to provide very broad NMR signals and poor sensitivity. In-cell NMR spectroscopy is thus not very well adapted to probing the intracellular behavior and exchange of transition metals. However, they all bind the ^{19}F-labeled Ca^{2+}-sensor 5F-BAPTA and its derivatives with submicromolar affinities [382], with which they each show different chemical shifts, allowing them to be detected and identified simultaneously. Hence, using ^{19}F NMR spectroscopy, authors have reported the parallel monitoring of Ca^{2+} and Pb^{2+} [367] or Ca^{2+}, Cd^{2+} and Zn^{2+} in cultured cells [379]. However, we found only a limited body of literature on NMR studies in cells focusing on these ions. Other sensors have been suggested, and Ca^{2+} sensors or fluorescence reporters may be redesigned for NMR studies of these metals. Paramagnetic metal ions may help to accelerate T1 relaxation and S/N per experimental time in the future, as shown *in vitro* [396-401]. Gd^{3+} or V^{3+} complexes may be more suitable because they would avoid binding competition from endogenous divalent metal ions. Transition metal ions are also useful to establish MRI contrast agents in association with chelator molecules to induce faster water relaxation, or in combination with fluorinated sensors also for use in MRI [137]. Re-designing such agents to create cell-permeable forms, or adapting Ca^{2+}-sensors, should be feasible in some cases [134].

Zn^{2+} is an integral structural component of about 3000 human proteins, among which are included many enzymes or small protein domains, notably the well-known family of zinc-fingers [402]. In total, cells contain Zn^{2+} at hundreds of micromolar concentrations, but only pico- to nano-molar concentrations of free Zn^{2+}. However, zinc may also have signaling functions and "Zn^{2+} waves" occur [403]. Zn^{2+} is not paramagnetic but its only NMR-observable isotope ^{67}Zn is quadrupolar, has a low gyromagnetic ratio and is present at low natural abundance (~4%). Given also its low concentration, it is overall poorly amenable to NMR studies via direct detection, and consistent with this, it has not been much studied in cells using ^{67}Zn NMR, to the best of our knowledge. Like other divalent ions, Zn^{2+} can still be detected through the NMR signals of chelating agents. Zn^{2+} has been recognized to bind the Ca^{2+} chelator 5F-BAPTA since the very first use of this reporter in the early 1980's [144]. Zn^{2+} had actually a much better affinity than Ca^{2+} for 5F-BAPTA, i.e. 1 versus 500 nM, respectively [382]. Fortunately, Ca^{2+} and Zn^{2+} binding result in different ^{19}F chemical shifts of 5F-BAPTA, and the two ions have been detected in parallel in Ehrlich ascite tumor cells [378], in perfused ferret hearts [377], in guinea-pig cortical slices [376,404], and in cultured neuroblastoma cells [379]. Another BAPTA derivative, 5,5',6,6'-tetrafluoro-BAPTA (TF-BAPTA) has been to shown to chelate Ca^{2+} poorly, and thus it is potentially a good sensor of intracellular Zn^{2+}/Fe^{2+} [405]. Other ^{19}F-labeled, ^{11}B-labeled or hyperpolarized ^{13}C-labeled or ^{129}Xe-cage ion sensors have been designed that can report and distinguish the presence of Zn^{2+} and Ca^{2+} by NMR, but with few applications in cells up to now [137]. We can also mention that many groups have recently proposed Zn^{2+}-activated MRI contrast agents to probe extracellular Zn^{2+} in brain or prostate, where it may have amyloidogenic properties or diagnostic potential, respectively [140,141,406,407]. Upon Zn^{2+} chelation, these molecules either expose a paramagnetic center or exchangeable protons to the solvent, or show altered chemical shifts of ^{19}F moieties.

Hence, NMR spectroscopy can report on the presence of free divalent metal ions in cells, using cell-permeable sensors and their chemical shift variations upon chelation. The subcellular localization information is lost most of the time, but the chemical shift variations are metal dependent. This ability to monitor and distinguish simultaneously multiple metal ions is not always perfectly executed by fluorescence probes.

2.1.9. More highly toxic species: Al^{3+}, Cd^{2+} and Cs^{+}

NMR spectroscopy can help in studies focusing on toxic metal species: the tissues or cells of interest can be characterized without organelle separation and without solute extraction by hydrophobic/hydrophilic solvents. Moreover, they do not require radioactive isotopes. Chemical shifts can reveal the type of chelation or the storage organelle. Hence, NMR spectroscopy of species like Al^{3+}, Cd^{2+} and Cs^{+} can be highly complementary to other techniques.

Several ^{27}Al-NMR studies have been carried out on plants. Tea, buckwheat, hydrangea or eucalyptus can accumulate high aluminum concentrations despite its usual toxicity. Detoxification mechanisms have been characterized using solution ^{27}Al-NMR of intact plant leaves. Direct one-dimensional ^{27}Al-NMR experiments provided spectra of Al^{3+} stored in leaves of the organisms studied, revealing chemical shifts identical to those of Al:citrate and Al:oxalate complexes [408-416]. This led to the conclusion that these plants stored aluminum under these forms. In rape plant, Al:malate complex was also detected [417]. Hence, NMR was instrumental in describing these non-covalent storage strategies adopted by plants.

Like ^{27}Al, ^{113}Cd has permitted NMR studies of cadmium detoxification in plants, more specifically in the cadmium-accumulator plant *Thlaspi caerulescens*. After growth in a $^{113}Cd(NO_3)_2$ enriched nutrient medium, one-dimensional solution NMR of leaves using direct ^{113}Cd-detection revealed a ^{113}Cd chemical shift identical to that of the Cd:malate complex [418]. ^{113}Cd NMR sensitivity is poor though, so a ^{19}F-labeled chelator probe has been used to report simultaneously Cd^{2+} and Zn^{2+} uptakes and to measure their effects on cellular Ca^{2+} concentration [379]. Cd^{2+} interaction with diphosphoglycerate (DPG) also gives rise to shifts of diphosphoglycerate (DPG) ^{31}P NMR signals, but these could not be detected in erythrocytes [419].

Living cells assimilate cesium primarily through potassium transport systems [420]. The stable isotope ^{133}Cs has been exploited as an NMR-practical ^{39}K congener to study potassium cellular influx and efflux and intracellular distribution. Moreover, cesium has a mild toxicity in regular circumstances, but is very deleterious in the form of the radioactive isotope ^{137}Cs, which is produced and released by military and civil nuclear activities. It

would thus be of interest to understand the toxicity mechanism of ^{133}Cs, and to characterize cesium integration in the food chain by plants [421]. ^{133}Cs has much better NMR characteristics than ^{39}K and ^{87}Rb: i) it represents 100% of stable cesium; ii) it has a small quadrupole moment yielding moderately fast relaxation, hence reasonably high and sharp NMR signals; iii) it shows a large chemical shift range and a high sensitivity to its chemical environment, especially to its counter anions [422]. Hence, two separated peaks from intracellular and extracellular media were early observed in halobacteria using one-dimensional direct ^{133}Cs NMR detection [423], which occurs through an active translocation mechanism resulting in cesium accumulation [424]. Several NMR studies on erythrocytes provided similar spectra showing two resonances from intra- and extracellular ^{133}Cs without the need of adding extracellular shift reagents. Cesium ions were shown to compete with potassium ions in the cellular uptake process, cesium rates being one third of that of potassium [425,426]. $^{133}Cs^+$ was thus used to study K^+ transport in cultured cells of perfused rat hearts [427-430]. Magnetic susceptibility effects were shown to be only a minor cause of intracellular chemical shifts, while non-ideal water solvation and interactions with phospho-anions, notably diphosphoglycerate (DPG), had larger contributions [431-433]. This interaction with DPG appears to displace the DPG:deoxyhemoglobin interaction. Consistently, various ^{133}Cs chemical shifts were observed in various rat tissues organs [434,435], but the measured relaxation rates argued for a common Cs^+-free state in fast exchange with anion-binding Cs^+ [436]. Even more interesting, ^{133}Cs proved to be a good subcellular probe: two intracellular ^{133}Cs NMR peaks were detected in maize root tissue, corresponding to cytosolic and vacuolar compartmentation [437], and two peaks also appeared from cytoplasmic and mitochondrial ^{133}Cs internalized in hepatocytes [438]. Because the ^{133}Cs resonance is also very sensitive to nitrate concentration, the two subcellular ^{133}Cs reporter peaks permitted monitoring of *in vivo* nitrate incorporation into maize root compartments [439], and cesium/potassium exchange in *Arabidopsis* [440]. To the best of our knowledge, this interesting ^{133}Cs sensing of the chemical environment has been only sparsely used in the last 15 years. Because of its preference for the intracellular space, it has been less popular than ^{87}Rb in K^+ translocation studies [300], although Rb^+ has also been shown to be a better congener of K^+ for influx than for efflux studies [291]. Moreover, the rather low sensitivity of ^{133}Cs NMR ($\gamma(^{133}Cs)\sim\gamma(^{1}H)/8$) requires too high intracellular concentrations given its intrinsic toxicity. Using DNP-sensitivity enhancement, recent studies achieving ^{133}Cs hyperpolarization followed by dissolution and mixing with live cells have reported cesium translocation rates measurements in yeast [441] and erythrocytes [442]. This strategy necessitates measuring the NMR signal before ^{133}Cs polarization relaxes: ^{133}Cs fast T1 relaxation (< 10 s) may limit the number of applications of ^{133}Cs hyperpolarization.

2.1.10. Common anions

Phosphate ions are treated in Section 2.3.2.

NH_4^+ and NO_3^- are treated in the Section 2.3.3.

Cl^- is an abundant anion in cells, but its concentration can vary significantly depending on the culture medium, the cell type, the growth phase or the organelle: it can reach concentrations between 10 and 100 mM in bacterial and animal cells [443-447]. ^{35}Cl is the most abundant isotope of chlorine, and also the best adapted to NMR studies. It is however a spin 3/2 nucleus, whose quadrupolar nature has hindered cellular investigations, similar to what we have seen with ^{17}O (Section 2.1.1.), ^{23}Na and ^{39}K (Sections 2.1.4. and 3.1.2). Since the 1970's, publications have shown that the ^{35}Cl signal is considerably broadened by its transient interactions with proteins [448,449]. A mean binding lifetime between 10 and 1000 nanoseconds had been calculated for Cl^- interacting with hemoglobin. In these conditions, the electric field gradients felt by $^{35}Cl^-$ contacting proteins, combined with the slow protein tumbling, lead to T1 and T2 values of about 10 ms at only 4 g/L of BSA or hemoglobin. In cells, the NMR signal of $^{35}Cl^-$ was so broad that it was undetectable in early studies [450,451], while the extracellular $^{35}Cl^-$ generated sharp signals. Hence, ^{35}Cl NMR was used in the 1980's to measure cellular volumes as inferred from the intensity of the extracellular peak of $^{35}Cl^-$ [451-454]. In the early 1990's, $^{35}Cl^-$ NMR detection was reported from algae and tobacco suspension cells, probably from the watery vacuoles, and in erythrocyte ghosts (i.e. emptied cells) [455]. $^{35}Cl^-$ ions were finally observed in erythrocytes in the mid-1990's and a double exponential relaxation was measured ($T2_{slow}$=1.2 ms, $T2_{fast}$=0.09ms) [444], in agreement with the theoretical behavior of spins 3/2 interacting transiently with macromolecules. Using Co^{2+}-chelating shift agents, the peak from extracellular $^{35}Cl^-$ was shifted sufficiently to be distinguished from the intracellular peaks in erythrocytes and fibroblasts, and the exchange of intracellular Cl^- with extracellular $H_2PO_2^-$ could be observed by ^{35}Cl NMR in erythrocytes [456,457]. The sensitivity was poor according to the authors and we have not found any other attempts to study intracellular Cl^- using ^{35}Cl NMR in the literature since the early 2000's. $^{35}Cl^-$ NMR has been explored for use in MRI in the 2010's: because it is very sensitive to the protein concentration, it could be useful to localize liquid accumulation upon strokes or edema [445,458-460]. The bi-exponential T2 rates of ^{35}C are in the millisecond range in these extracellular environments, and are still not very sensitive.

Altogether, the contribution of NMR spectroscopy to characterizing the intracellular behavior of Cl^- was not substantial up to now.

2.1.11. Viscosity, pH, redox potential

Intracellular viscosity is a complex, multifaceted property, and its measurement by NMR spectroscopy is treated separately in Section 3.2.1. Viscosity can be derived from two types of molecular mobilities, namely molecular tumbling and translational diffusion. These can both be determined by NMR, but they should be interpreted carefully: i) interactions with intracellular species can affect both tumbling and translation; ii) organelles, cytoskeleton, and cellular compartments cause restricted diffusion; iii) the apparent cellular viscosity is size-dependent, small and large molecules being differently retarded by the cellular meshwork.

In contrast, pH is a physical parameter that is usually very accessible by NMR spectroscopy: it needs a protonatable molecule carrying an "NMR-visible" isotope, whose chemical shift is intrinsically dependent on the protonation state [461]. Studies reporting intracellular pH values from an observed metabolite are too numerous to list. We mention a few below. ^{31}P-NMR has been used to measure intracellular pH since the early 1970's [462]: it does not require any isotopic enrichment, and biological phosphate-containing molecules are numerous, commonly with pKa values around 6.5-7, so that their ^{31}P chemical shifts are good pH sensors. Inorganic phosphate, DPG, ATP, etc. have thus been used regularly to monitor intracellular pH in animal, plant or microbial cells [463-465]. A few lines on this topic appear in Section 2.3.2, focusing on ^{31}P-NMR monitoring of cellular metabolism. The recent commercial multi-channel probes designed for high-sensitivity ^{1}H and ^{31}P detection are certainly interesting in this regard [465,466]. In addition, ^{1}H-, ^{13}C-, ^{15}N-NMR or $^{13}C/^{15}N$-edited/^{1}H-detected NMR can faithfully report on pH through observation of metabolites that show pH-dependent protonation states with pKa close to 7. Notable examples include histidine (or imidazole-containing molecules), citrate, carnitine and bicarbonate [461,467-470]. However, ^{1}H-NMR pH-dependent chemical shifts are often problematic for real-time monitoring of cellular metabolism, because a number of peaks can shift over time and possibly cross or overlap (see

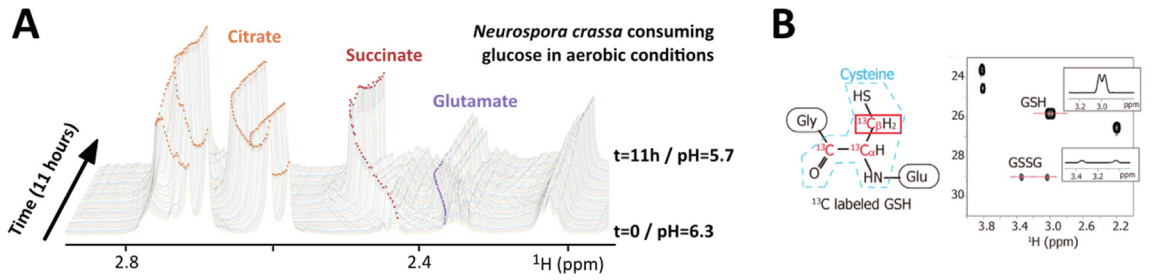

Fig. 10. A) Time series of ^{1}H HR-MAS NMR spectra (restricted spectral window) of *N. crassa* showing the variations of chemical shifts of citrate, succinate and glutamate, consistent with pH changing from 6.3 to 5.7 (adapted from Judge et al. 2019 [474]; **B)** NMR peak separation of GSH and GSSG at the position Cβ, ^{13}C-labeling originates from ^{13}C-cysteine supplementation in the growth medium of cultured mammalian cells (adapted from Mochizuki et al. [475]).

Fig. 10). ^{19}F-labeled probes have also been designed for intracellular pH measurements [461,471-473]. These can be convenient, notably because of the absence of ^{19}F-background in cells.

Redox potential is measurable via the thermodynamic equilibria of the main cellular redox couples NAD+/NADH, NADP+/NADH and GSSG/GSH (GSH= reduced glutathione). ^{13}C-labeled NAD+/NADH, NADP+/NADPH have been observed in *E. coli* and yeast upon incorporation of ^{13}C-labeled nicotinate [476,477]. The redox reaction of the nicotinamide moiety generates two sets of chemical shifts. Unfortunately, the chemical shifts are very similar in the NAD+/NADP+ (or NADH/NADPH) forms [477], so that monitoring the two couples correctly by NMR is not generally possible. The glutathione redox equilibrium has been monitored by ^{1}H-^{15}N or ^{1}H-^{13}C NMR after supplementing the culture medium with ^{15}N-glycine [478] or ^{13}C-cysteine [475,479], respectively: these two amino acids can enter cells and are incorporated in cellular glutathione. GSH and GSSG ^{1}H-chemical shifts overlap, therefore ^{15}N or ^{13}C-labeling is necessary to distinguish these two forms [475,478-480]. The ratio [GSSG]/[GSH]^{2} enables measurement of a redox potential between ∼-250 and -100 mV, which corresponds to the intracellular variations between proliferative and apoptotic cells (∼-270 to -170 mV, respectively) [481]. However, these values should be interpreted cautiously: i) because the reaction occurs between GSSG and 2*GSH, the equivalence in terms of redox potential is GSH concentration-dependent [481,482]; ii) intracellular concentrations of GSH vary between different organelles (concentration ranges from 1 to 15 mM, and redox potential down to -340 mV in mitochondrial matrix) [483,484]; iii) like all other redox couples in cells (measured by NMR or any other technique), the GSSG/2*GSH ratio does not necessarily exactly reflect the real cellular redox potential, because spontaneous redox reactions are much slower than enzyme-catalyzed reactions in cells, hence the measured ratio may not correspond to a redox equilibrium [483,485]. The redox ratios of ^{13}C-labeled ascorbic acid and dehydroascorbic acid have also been measured, but these compounds are constantly exchanged between the intra- and extra-cellular media [486-488].

NMR spectroscopy can thus provide information on a range of intracellular biophysical parameters. It reports averaged information on observable metabolites, with no subcellular details. Hence, it does not compete with up-to-date fluorescence microscopy approaches for functional investigations. However, NMR measurements of viscosity, pH and redox potential can be very valuable to monitor cell viability or overall populations of metabolites in real-time, possibly in parallel with other NMR characterizations.

2.2. Cell wall composition and dynamics

Plant, algae and microorganisms often establish dense polymeric layers surrounding their lipid membranes: these are carbohydrate-rich networks, which help in shaping cells, in adapting them to environmental variations, and in escaping host immune defenses or pathogen attacks. The detailed characterization of biological carbohydrate-containing polymers can help for example in designing vaccines [489,490], in understanding pathological microorganisms features and capacities [491-496], or in exploiting their potential for medical and industrial purposes [497-499]. In most cases, the chemical composition of these polymers has been established since a long time, but the knowledge obtained from chemical extraction, purification and degrading chemical analysis has of course severe limitations. Supplementary techniques such as *in situ* NMR spectroscopy were necessary to learn about their three-dimensional structure, dynamics, packing, grafting ratios, degradation mechanisms and kinetics, interactions with antibiotics etc. We discuss below the contributions made by NMR spectroscopy of intact cells in understanding these coating polymers.

We will only briefly mention here the existence of NMR studies on biofilms [500-503]: although they are closely related to live-cell material and not truly inert, we classified biofilms as being out of the scope of this review.

2.2.1. Plant cell walls

Somewhat similar arguments could be given about the inert nature of plant cell walls, but we have included a more extensive discussion for them: solid-state NMR spectroscopy has made highly valuable contributions over the last 40 years in characterizing plant cell walls, using progressively more native material, including intact plant stems, in recent years.

Related studies also represented important steps in the development of NMR methods: it was with the aim of characterizing wood (together with polysulfone and ivory) that Stejskal and Schaefer reported the first use of Cross-Polarization Magic Angle Spinning (CP-MAS), a technique that has since had enormous importance for solid-state NMR [504,505]. This is a point not only of intense interest to spectroscopists: solid-state NMR spectroscopy revealed the different conformations of cellulose [506-514] and lignin [511,515-517] and how the crystalline and amorphous ratios were correlated to soft- and hard-woods [518,519]; it also helped in monitoring their evolution through rot, drying/rewetting and industrial processes [516,520-529].

The more mobile pectin polymers were also characterized from the mid-1990's in non-dried samples using various NMR strategies, either taking advantage of variable cross-polarization efficiency or ^{1}H relaxation times associated with different mobilities and hydration regimes [530-532], or using direct polarization (DP) MAS [533]. Solid-state NMR approaches progressively showed that pectins i) were distributed among different pools showing different mobilities, more or less associated to cellulose [534-539], and ii) became more mobile upon ripening of fruits while cellulose did not [540-543]. CP and DP are now regularly combined to achieve

a more integrated description of both rigid and mobile fractions of plant cell walls, respectively [544-546].

NMR studies on plant cell walls were carried out mostly on natural abundance samples until 2010. In the last 10 years, uniform ^{13}C-labeling permitted comprehensive NMR signal assignments of plant cell wall polymers, notably by Mei Hong and her coworkers [547-550], and Kikuchi and his coworkers [551]. This led to renewed studies of the intermolecular contacts between cellulose, lignin and the complex hemicellulose and pectin heteropolysaccharides: indeed, it permitted detection of interatomic spatial contacts as revealed by magnetization transfer [552,553].

Very recently, this research became more "in-cell related" NMR spectroscopy with the analysis of intact material: using fresh ^{13}C-labeled *Arabidopsis* stems, Dupree and his coworkers have shown that a specific, twofold helical population of hemicellulosic xylan binds to cellulose fibrils [554-556]; they observed the same xylan-cellulose interaction in spruce wood, showing also an additional binding of hemicellulosic galactoglucomannan to cellulose [557]. In a complementary fashion, using DNP-enhancement on intact ^{13}C-labeled maize, rice, switchgrass and *Arabidopsis* stems, Wang and his coworkers showed in 2019 that lignin binds to the various populations of xylan through electrostatic interactions [558]. This last remarkable study also identified an impressive number of contacts between the different polymers and their level of interpenetration, which completely changed the accepted structural model of lignocellulose: lignin forms nanoaggregates and xylan bridges them with cellulose microfibrils.

Wang and Hong had also used DNP previously to characterize the trace occurrences of interactions between the lysis protein expansins and cellulose [559]. ^{1}H-detected fast MAS NMR spectroscopy also promises improved sensitivity in the future [550], so that advances may become achievable on sporadic but important connections [560], also on natural abundance material [553,561].

NMR spectroscopy has thus made fundamental contributions to both early and recent advances in understanding plant cell wall organization [560,562-565], which is of great value in solving the so called "biomass recalcitrance" to degradation for industrial purposes, including in the field of "green bioenergy" [566,567].

2.2.2. Peptidoglycans

NMR spectroscopic studies have also provided important information about bacterial peptidoglycan (PG), the branched glycan-peptide heteropolymer from which bacterial cell walls are composed [496,568]. Chemical structures of PGs have often been known for decades, but classical approaches use radiolabels or digestion and separation steps, which work better on Gram-negative bacteria PG: their Gram-positive counterparts are more difficult to solubilize, densely cross-linked and thus more difficult to analyze. Consistently, most NMR spectroscopy studies on PG have focused on Gram-positive bacteria using solid-state NMR. Several questions remain: the architecture of intact PG tridimensional is still under debate [568,569] and understanding interactions between PG and PG-targeted antibiotics is of vital importance [570-572].

To appreciate the contributions of NMR in the field, it is necessary first to present some elements of PGs' structure (Fig. 11). PG is based around a polymer built from a disaccharide repeated unit, namely a N-acetylglucosamine and a N-acetyl muramic acid, the latter being linked to a 4-5 amino acid stem [573,574]. Gram positive PG chains contain L-Ala, D-Ala, L-Gly, L-Lys, iso-Gln or diaminopimelic acid (DAP), which can be synthesized from L-Asp. Covalent crosslinks between peptide stems are established after integration in the PG layer through peptide bridges. Antibiotics can thus inhibit either the transglycosylases of the carbohydrate backbone, or the transpeptidases that establish crosslinks between the peptidic stems. This can occur through enzyme inhibition or PG stems interaction and sequestration. Antibiotics can also capture lipid II, the precursor of PG, which contains the PG building block tethered to a pyrophosphoryl-undecaprenyl membrane anchor, whose copy-numbers are very limited in cells [575-577].

As early as 1977, Irving and Lapidot showed that the pentaglycyl bridge of *Staphylococcus aureus* PG was in a random coil conformation in intact cells, by using ^{15}N-glycine selective labeling and ^{15}N-detected solution NMR [580]. They used the efficiency of ^{1}H-^{15}N magnetization transfer to characterize cell wall components' mobility. Importantly, they showed that PG mobility was higher in isolated *E. coli* cell-envelope than in whole cells, demonstrating a need for characterization of intact cells [581]. The first atomic-scale information was also obtained on the differentiated modes of action of the antibiotic vancomycin: it reduced the mobility of the surface polymer (teichoic acid) in *Bacillus licheniformis*, and that of the PG C-terminal D-Ala residue in *Micrococcus lysodeikticus* (which lacks teichoic acid) [582]. At that time, although providing only low sensitivity, ^{15}N and its low gyromagnetic ratio were giving access to resolved solution NMR spectra of semi-mobile polymers, yielding distinguishable PG spectral signatures from species to species [583].

As for plant cell walls, the more solid fraction of the PG became observable using CP-MAS solid-state NMR [504,505]. And again as for plant cell walls, isotopic ^{13}C/^{15}N labeling was necessary to assign NMR resonances, identify covalent and spatial proximities between residues, and establish strategies to filter out the bacterial backbone. Such a rationale has been employed from 1983 by Schaefer and colleagues on *Aerococcus viridans*. In this bacterium, PG peptide stems show a lysyl-amide peak at 95 ppm when cross-links exist between lysine N-epsilon and D-alanine carbonyl, while non-bridged stems show a lysyl-amine peak at 5 ppm. By recording CP-MAS spectra on bacteria fed with ^{15}N-lysine, ^{15}N-NMR signals were observed for lysine ^{15}N-epsilon in both free and D-Ala-linked states, which allowed the quantification of cross-linking upon exposure to penicillin [584]. This method was convenient and safe, avoiding extensive purification processes and the use of radiolabeled amino acids. It demonstrated that penicillin causes the production of larger amounts of peptidoglycan but with fewer cross-links [585], and that no C-terminal D-Ala or D-Ala-D-Ala existed in the vicinity of Lys-D-Ala cross-links [586].

Schaefer and his coworkers improved their approach from the early 1990's, by using their recent developments, such as DANTE ^{13}C-^{13}C and REDOR or TEDOR ^{13}C-^{15}N editing filters (see [570,587-591]). This improved both sensitivity and the removal of cellular background signals from natural abundance ^{13}C and ^{15}N [592,593]. Hence, a number of PG cross-links and bridge-links could be analyzed upon amino-acid specific ^{13}C/^{15}N-labeling, which produced ^{13}C-^{13}C and/or ^{13}C-^{15}N covalent bonds associated with specific chemical shifts. The degree of cross-linking between PG peptide stems was measured on isolated cell walls of *Bacillus subtilis* fed with [1-^{13}C]-D-Ala and [1,2-^{13}C-^{15}N]-Asp as a precursor of DAP, revealing changes upon exposure to the antibiotic cephalotin [594-596]. Similar strategies and analysis have been carried out in the 2000's, using various D-Ala, L-Gly, L-Lys ^{13}C or ^{15}N-labeling schemes with *Staphylococcus aureus* and *Enterococcus faecium* to analyze the impact of antibiotics (vancomycin, amphomycin, plusbacin, oritavancin) on cross-links, bridge-links and stems [597-601], to detect PG lysine succinimidation [602], to characterize PG structures of *S. aureus* mutant strains [603,604] and in different growth phases and nutrient media [605].

Moreover, REDOR gave access to internuclear distance measurements [606]. This has been used fruitfully in the years 2000-2010, notably by combining ^{13}C- and/or ^{15}N-amino acid specific labeling and ^{19}F-containing antibiotics. Indeed, ^{13}C-^{19}F, ^{15}N-^{19}F, and even ^{31}P-^{19}F distance measurements became feasible between

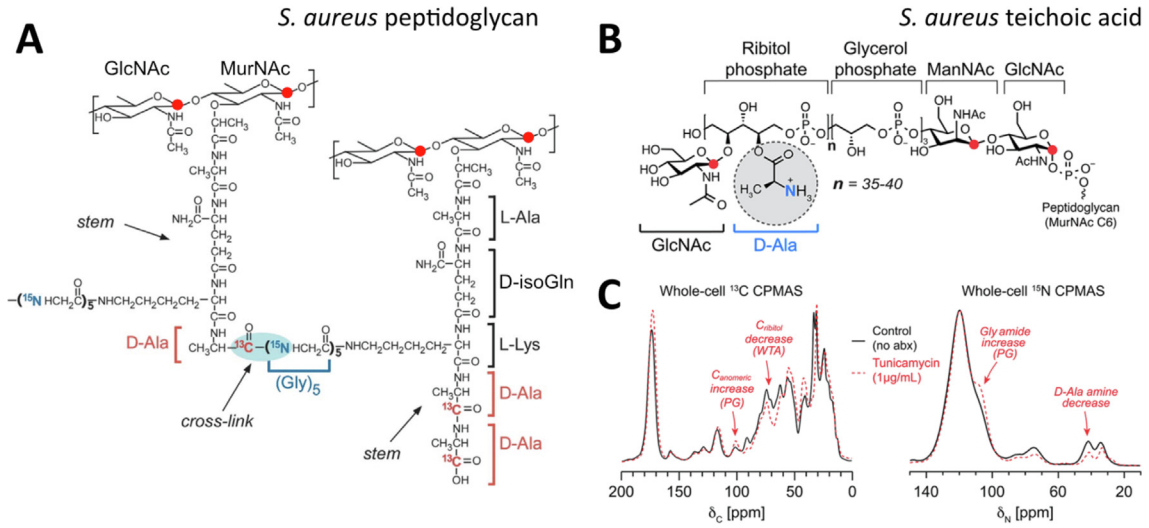

Fig. 11. A) Chemical structure of two PG stems from *S. aureus*, showing isotope labeling obtained from growing cells in a media supplemented with D-[1-^{13}C]Ala and ^{15}N-Gly and with an alanine racemase inhibitor. Other labeling schemes have been used, e.g. ^{15}N- or ^{13}C-Lys, ^{19}F-side chain Lys, ^{15}N-Ala, which permitted dissection of PG structures in various conditions (adapted from Cegelski et al. 2008 [578]). **B)** Chemical structure of TA, composed of polyribitol phosphate chains, whose ^{31}P nuclei permit natural abundance ^{31}P-NMR and ^{31}P-REDOR filters; the scheme shows a possible D-[^{15}N]Ala labeling pattern that has been used in the literature; anomeric carbons are indicated by red dots (adapted from Romaniuk et al. 2018 [579]). **C)** One-dimensional ^{13}C and ^{15}N CPMAS solid-state NMR spectrum of uniformly ^{13}C- or ^{15}N-labeled *S. aureus* cells treated with (red) or without (black) 1 ug/mL tunicamycin. The resolved peaks that permit the quantification of peptidoglycan (PG) and wall teichoic acid (WTA) are shown with arrows (adapted from Romaniuk et al. 2018 [579]).

PG residues and the antibiotics, and between bacterial phospholipids (exploiting the 100% natural abundance of ^{31}P) and the antibiotics. This helped Schaefer and his coworkers to progressively elucidate the interaction modes of ^{19}F-labeled derivates of antibiotics (vancomycin, oritavancin, eremomycin, chloroeremomycin, Plusbacin A3) with *S. aureus* or *E. faecium* PGs [578,600,607-611] (see for example Fig. 12). In complete contrast to a widely accepted belief amongst the community from earlier *in vitro* studies [612-614], vancomycin and oritavancin were never found to form dimers *in situ* according to REDOR analysis [578,579,607,609,611]. Deuteration of the lipid moiety of Plusbacin A3 also permitted ^{2}H-^{13}C and ^{2}H-^{31}P REDOR distance measurements, showing that this lipid side chain was essential for the antibiotic action, but did not insert itself into the bacterial lipid membrane [615].

To finally derive a model of the tridimensional PG architecture, Schaefer and colleagues had to create one more solid-state NMR experiment called CODEX, which was designed for measurement of ^{13}C spin diffusion, giving access to ^{13}C-^{13}C distance information between pentaglycyl bridge and the *S. aureus* PG glycan moiety in isolated intact cell walls [616]. In the 2010's, the introduction of L-[5-^{19}F]-lysine together with use of D-^{13}C-Ala, L-^{13}C-Ala, L-^{15}N-Ala or L-^{13}C-Gly in the culture medium generated PG in which ^{13}C/^{15}N-^{19}F labels were combined so as to facilitate use of REDOR to derive distances in intact cell walls of *S. aureus* and some mutant strains [589,617,618]. These combined studies allowed advanced models of the PG mesh of *S. aureus* to be established [574].

NMR of whole bacterial cells also helped to characterize teichoic acid (TA), another important surface polymer of bacterial cell walls. TA contains D-Ala residues, which had been observed to be quite mobile by ^{15}N-NMR in the late 1970's [582,583]. However, TA D-Ala is sufficiently constrained to allow solid-state cross-polarization and to yield ^{13}C-CP-MAS spectra, but its ^{13}C resonance is severely overlapped with signals of other D-Ala residues in peptidoglycan [598]. Spectral deconvolution permitted comparison of the TA-associated D-Ala content in different species and upon exposure to antibiotics [589,598,615,619,620]. In contrast, ^{15}N-NMR peaks of D-Ala from TA and PG are well separated, and also helped to monitor TA D-Ala in various conditions [589,599,620,621]. Uniform ^{13}C- and ^{15}N- labeling was used recently to evaluate the contents in TA ribitol and D-Ala in intact cells (Fig. 11) [579]. This represents a convenient approach for rapid characterization of antibiotic mechanism. Finally, ^{13}C-^{19}F or ^{19}F-^{31}P REDOR filtering proved the absence of contact between the antibiotics ^{19}F-oritavancin or ^{19}F-Plusbacin A_3 and TA [600,611].

Hence, in their very extensive work on the characterization of PG and the impact of PG-interacting antibiotics, Schaefer and colleagues provided an impressive body of results, but also very significant developments of solid-state NMR approaches. However, to the best of our knowledge, we must note that these NMR experimental advances are not so well integrated into the common toolset for PG analysis [568,572,622]. This is probably due to the sophisticated NMR instruments and the highly advanced expertise that are required. Also, the poor sensitivity of NMR hampers the study of rare, but functionally relevant events that affect PG upon antibiotic exposure, for example.

Such issues may be solved in the future by ^{1}H-detected solid-state NMR, which has been carried out *in vitro* on purified PG sacculi of *B. subtilis* [623], or by DNP-enhancement using intact cells [624]. These two techniques have already led to proposals of structural models for the interaction between two antibiotics (nisin and teixobactin) and the essential, low-copy number lipid II molecule, using bacterial membrane extracts [625,626] (see Section 2.4.2 for more details).

The carbohydrate moieties of PG and cell wall teichoic acids have not been extensively studied by in-cell NMR, to the best of our knowledge. NMR spectroscopy of carbohydrates is not straightforward, because most of the carbohydrate resonances are in crowded regions of the spectra, except those from the anomeric protons and carbons. Appropriate carbohydrate isotopic labeling may help to observe the GlcNAc and MurNAc moieties contained in PG and TA.

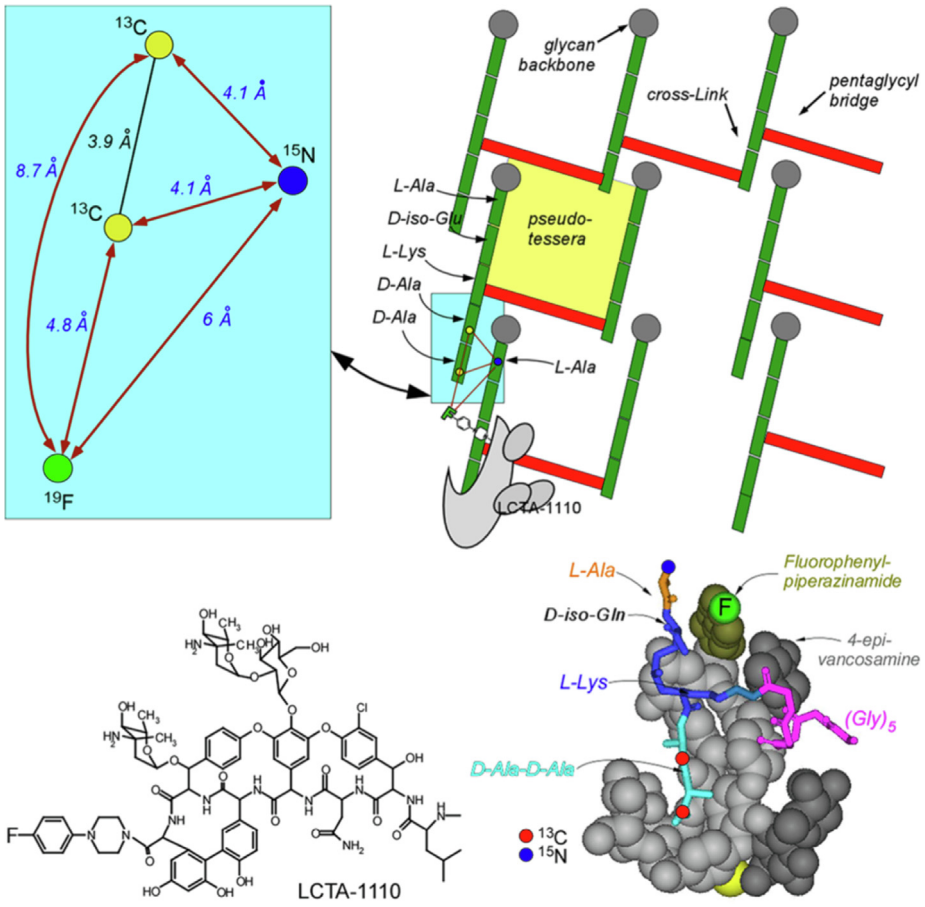

Fig. 12. Structural information obtained from REDOR distance measurements in *S. aureus* whole cells incubated with the ^{19}F-labeled glycopeptide drug LCTA-1110. Top right : Schematic cross-section of the PG tertiary structure of S. aureus (grey balls: GlcNAc-MurNAc glycan backbone; green rectangles: PG stems; red rectangles: PG bridges; LCTA-1110 is represented by a grey cartoon); Top left : ^{13}C-^{15}N, ^{13}C-19F, and ^{15}N-^{19}F measured distances in S. aureus grown in a medium containing D-[1-^{13}C]Ala and L-[^{15}N]Ala; Bottom left: chemical structure of LCTA-1110; Bottom right: Model of the interaction between LCTA-1110 and PG based on measured REDOR distances. Adapted from Kim et al. 2013 [589].

2.2.3. Lipopolysaccharides and beta-glucans

Cell wall polymers of higher flexibility such as bacterial or yeast polysaccharides are also observable by NMR in intact cells. The so-called High-Resolution Magic-Angle Spinning (HR-MAS) NMR technique [627-631] has been instrumental in characterizing polysaccharides *in situ*, allowing their analysis without any solvent extraction or separation steps, during which information could be lost [632,633].

Because of their density in the membrane context, these polysaccharides form a loose meshwork that restricts molecular motion to some extent. Added to the sample heterogeneity between local environments (intracellular, extracellular and membrane), this restricted mobility causes broad NMR signals for surface polysaccharides. This prevents a precise, atomic-scale characterization using classical liquid-state NMR. Surface polysaccharides still conserve high degrees of local mobility, which can generate sharp NMR peaks once the sample is rotated at the so-called magic-angle (54.7°). Restricted motion and sample heterogeneity do cause broadening effects, which are observable and can be assessed in the shape of NMR peaks in non-spinning conditions (see Section 3.2.2. for more extensive explanations). Magic-Angle Spinning (MAS) averages out these effects when spinning rates are faster in Hz than the observed deleterious peak broadening, i.e. a few hundreds of Hz for cell surface polysaccharides. The resulting high-resolution spectra obtained under MAS gave rise to the acronym HR-MAS (see Section 3.3.4. for specific explanations on HR-MAS).

Surface polysaccharides are often produced in high quantities and in rather homogeneous populations by microorganisms, so that their NMR signals surpass those of the other cellular species. ^{1}H-HR-MAS permits the detection and analysis of surface polysaccharides from milligram quantities of live bacteria (~10-50 mg wet weight, ~1 mg dry weight), thus avoiding the need for large scale production and supplementary purification [634]. The HR-MAS NMR analysis of surface polysaccharides in live cells allows observation of the effects of drug exposure, environment, growth phase and gene mutations on microorganism cell walls, while requiring only moderate manipulations of the biological material. HR-MAS requires spinning the samples at kHz frequencies in cylindrical rotors, whose diameters are in the millimeter range. This generates forces that do not affect microorganism viability [635] but can often damage mammalian cells or tissues [636]. We consider HR-MAS NMR studies on mammalian cells further in a later section, which focuses on real-time monitoring of live-cells metabolism (Section 2.3.5.).

^{1}H-HR-MAS has been applied from the late 1990's to verify the integrity of the extracted and purified polysaccharides that were used for "structural characterization" (in the carbohydrate community, this corresponds to the equivalent of protein primary structure determination, i.e. finding the sequence and linkage of

monosaccharide units). We should mention that ^{13}C-HR-MAS has also been used in one publication to study the three-dimensional features of cell wall glucans from *Saccharomyces cerevisiae* [637]. Kenne and coworkers applied ^{1}H-HR-MAS to Gram-negative, opportunistic pathogenic bacteria to establish the structure of their surface-exposed O-specific polysaccharides [638,639]. At the same time, Wieruszeski, Lippens and their coworkers showed that the osmo-regulated cyclic glucans of a plant pathogenic bacterium i) adopted the same three-dimensional arrangement *in vitro* and in live cells and ii) had reduced diffusion in their native crowded environment, i.e. the periplasm [640,641].

The ^{1}H-HR-MAS approach was next applied to the analysis of *Campylobacter jejuni*, an infamous gastrointestinal pathogen: structures of its capsular polysaccharides and lipo-oligosaccharides (LOS) were compared upon gene mutation [642,643], between clonal variants [644,645] and strains [646,647]. ^{1}H-HR-MAS similarly permitted elucidation of the the structures of the surface polysaccharides from Gram-negative [648-651] and Gram-positive bacteria [652], mycobacteria [653], and yeast [654]. These studies were carried out either to detail the function of genes involved in polysaccharide biosynthesis, or simply to verify the absence of degradation during the purification steps used for other analyses. Kinetics of acid incorporation [655], growth-phase and pH-dependent O-acetylation [656,657] were also monitored, which may help to understand the adaptation of bacteria to their environment.

More generally, all these studies have shown that microorganism surface polysaccharides conserve similar three-dimensional structures and a high conformational flexibility when isolated or in the native membrane meshwork. This is an important, fundamental piece of information.

2.2.4. Lipid dynamics in membranes

We address here NMR studies focusing on lipids in cellular membranes. Approaches aiming at measuring transmembrane diffusion are considered in Section 2.1, and measurements of cytoplasmic lipids are mostly treated in Section 2.3.5.

^{1}H-, ^{2}H-, ^{13}C-, ^{19}F- and ^{31}P-NMR spectroscopy was applied to study lipid dynamics in the early 1960's, complementing other spectroscopies already in use (Raman, Infrared, light scattering methods, fluorescence probes, spin label probes for EPR spectroscopy...) [658,659]. Early ^{1}H NMR spectra of erythrocytes, mitochondria and sarcoplasmic reticulum membranes had revealed that only the high mobility choline head group was observable, while signals of the acyl chains were extremely broad in the absence of detergent [660-663]. Hence, lipid dynamics in cellular membranes were first investigated by ^{13}C NMR because of its favorable relaxation characteristics. The first ^{13}C NMR spectra of native membranes by Metcalfe and coworkers in the early 1970's showed very broad signals, either from human erythrocytes or from the small bacterium *Acholeplasma laidlawii* (a species devoid of cell-wall and thus very practical for lipid membrane studies) [664]. The information on lipid dynamics came first from the characterization of membranes among the most fluid membranes, i.e. those of the sarcoplasmic reticulum [665] and the retinal rod outer membranes [666], which contain high proportions of unsaturated acyl chains. These studies reported ^{13}C (natural abundance) T1 values for the acyl chains similar to those measured for purified lipid vesicles, while ^{1}H NMR signals were very broad. Hence, native membranes probably had similar viscosities, but produced more complex environments due to the presence of membrane proteins [659]. Similar conclusions came from ^{13}C NMR studies on the choline head group of less fluid membranes from virions or cultured cells [667,668]. The same ^{13}C signal from choline head groups was also used to monitor the distribution of ^{13}C-labeled phosphatidyl-choline in the inner- and outer- leaflet of sarcoplasmic reticulum samples purified from rat muscles [669,670]; the addition of a shift reagent (here Dy^{3+}, see Section 2.1.2. for further explanation of shift reagents) in the extracellular medium permitted the distinction of choline groups pointing towards the intra- or extra-cellular sides of the membrane.

Hence, ^{13}C T1 relaxation and linewidth analysis was providing scarce and rather qualitative information on cellular lipid membrane dynamics. Moreover, strong dipolar interactions and magnetic susceptibility gradients were producing broad ^{1}H NMR signals, which were also poorly informative. ^{31}P-NMR has been extremely useful for *in vitro* studies on lipid phases, because it yields very different spectra from bilayers, hexagonal, vesicular and micellar phases, without any need for isotopic enrichment [671,672]. It has been much less informative for intact cellular membranes [673-681], for several reasons: i) there is no need to prove they are bilayers; ii) different phosphate ester functions have overlapping resonances; iii) intense signals from cellular phosphate-containing species (ATP, etc..) can obscure the broad signals from membranes.

With the advent in the mid-1970's of pulse schemes (namely the quadrupolar echo) adapted to the measurement of ^{2}H quadrupolar splittings [682], more quantitative measurements of cellular membrane dynamics could be achieved. Indeed, the quadrupolar nature of the ^{2}H nucleus revealed itself to be extremely useful here (Fig. 13) [683,684]: i) the quadrupolar peak splitting is related to the order parameter of the carbon-deuterium bond vector S_{CD}, ii) it is very large, spanning up to dozens of kHz in the case of restricted dynamics, iii) it is usually wider than the ^{2}H linewidth (the low ^{2}H gyromagnetic ratio results in weak dipolar interactions and low sensitivity to field inhomogeneity).

Because of the simplicity of its single membrane and the capacity to produce it at gram scales, the bacterium *A. laidlawii* became an interesting model for ^{2}H NMR investigations. In the early 1970's, perdeuterated or 16-$^{2}D_3$ (tri-deuterated at the end of the acyl chain) palmitate was successfully inserted in *A. laidlawii* membranes by supplementation in the growth medium [689,690]. The end-chain ^{2}H-labeling permitted measurements of its ^{2}H residual quadrupolar splitting in freeze-dried, rehydrated *A. laidlawii* membranes, giving access to the end-chain order parameter [690]. Repeating this experiment with specific ^{2}H-labeling at every position of the acyl chain successively, Stockton and colleagues reported the order parameter through the entire thickness of intact cellular membranes [691]. This revealed a behavior very similar to that observed with single phospholipids in the lamellar liquid crystalline phase at 42 °C. Similar measurements with decreasing temperatures showed the progressive shift of an equilibrium between liquid crystal and gel phases: the two populations exchanged with rates lower than 10^{-4} Hz, and the *A. laidlawii* membrane showed an almost complete motional freezing at 1 °C (micro-millisecond timescale) [688]. The impact of cholesterol insertion on *A. laidlawii* membrane dynamics was also evaluated, as well as the dynamics of saturated fatty acids and those of various fatty acid headgroups incorporated into the same membranes [687,692-695]. *Mycoplasma caprilocum*, which is naturally dependent on fatty acids and cholesterol supply, was also analyzed by ^{2}H-NMR: the intact cells had membrane dynamics similar to those of model lipid membranes, and only those grown under low cholesterol supplementation showed a liquid-crystalline-gel phase transition [696]. All these results were very consistent with those obtained from purified lipids, and thus proved the suitability of *in vitro* approaches in the field [697]. It also emphasized that membrane proteins had little effect on average membrane lipid dynamics.

Similar studies were carried out almost in parallel on *E. coli* in the late 1970's. Deuterated lipids were incorporated in auxotrophic *E. coli* strains defective in certain lipid production steps. The ^{2}H-NMR analysis was essentially performed on membrane vesicles,

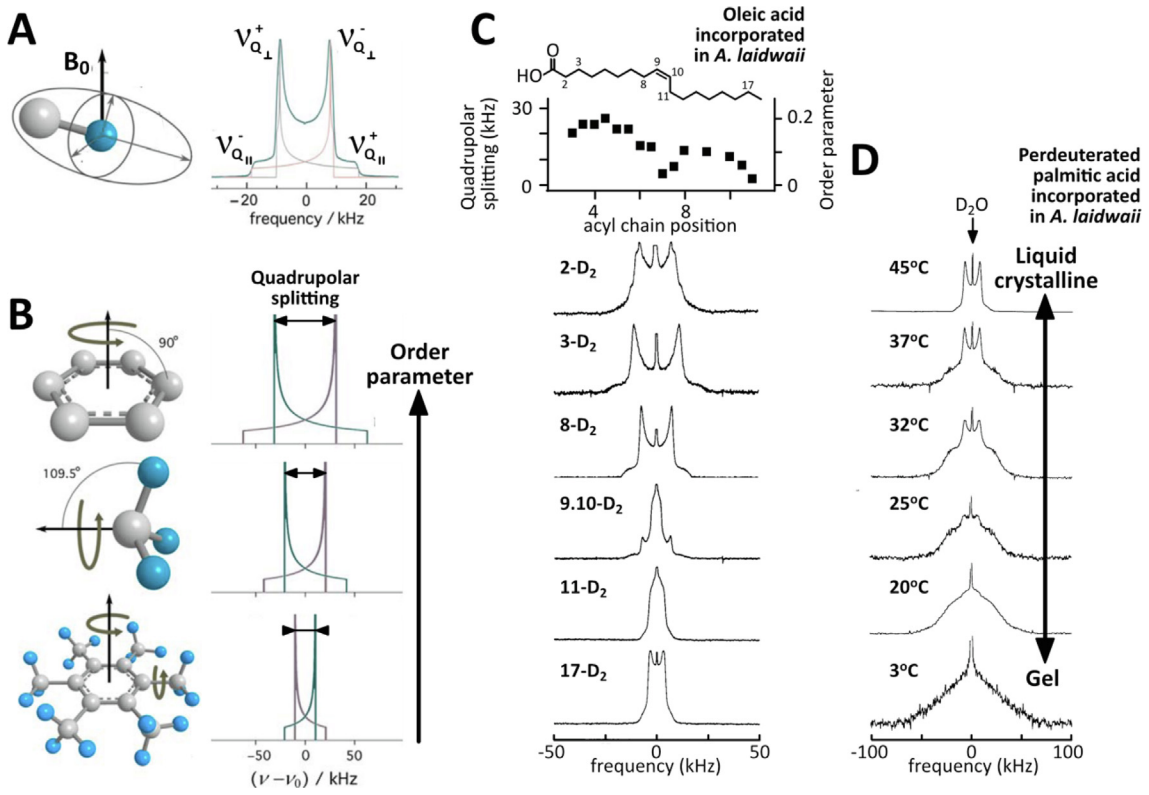

Fig. 13. Principle of ^{2}H-NMR quadrupolar splitting analysis. The chemical bond C-D is represented with carbon as a grey ball and deuterium as a blue ball. Most of the original work described in the main text was carried out following the rationale presented here. However, a new approach taking advantage of Magic-Angle Spinning (MAS) has been proposed in recent years, which offers better sensitivity [685]. **A)** The ^{2}H nucleus has a spin I=1, giving rise to two different energy transitions due to the electric quadrupolar interaction, hence two resonance frequencies ν^+ and ν^-; moreover, these two quadrupole frequencies are dependent on individual spin orientations, and the density of orientation states determines a powder pattern for a non-oriented sample (with the typical "Pake doublet" shape); **B)** The residual quadrupolar splitting $\Delta\nu=\nu^- - \nu^+$ is proportional to the square of the order parameter (adapted from Molugu et al. Chem Rev 2017 [686]); **C)** Oleic acid deuterated at various positions was incorporated in the small bacterium *A. laidlawii* and position-specific quadrupolar splitting of oleyl chains measured in intact membranes at 25 °C (adapted from Rance et al. 1980 [687]); **D)** Perdeuterated palmitic acid was incorporated in *A. laidlawii* and palmitoyl chains observed by ^{2}H-NMR at varying temperatures, showing progressive loss of the powder pattern due to the liquid crystalline phase (adapted from Smith et al. 1979 [688]).

and showed that i) these membranes had a similar dynamic fingerprint to that of model liposomes, although they were 10-20% less ordered probably because membrane proteins slightly "destructure" the liquid-crystalline lipid bilayer [698-701], ii) *E. coli* membranes were >97% in liquid crystalline phase at 37 °C. The inner and outer membranes were also separated in two samples, which revealed that the inner membrane was less ordered and had a 7 °C lower liquid-crystalline-gel transition than the outer one [700,702,703]. In the 1980's, deuterated DPPC was incorporated by incubation with erythrocyte ghost membranes: similar dynamics were observed in these membranes and in pure DPPC vesicles, which also showed no transition to the gel phase down to 5 °C [704]. Brains of rats fed with deuterated choline headgroups were also analyzed by ^{2}H-NMR, revealing similar lipid dynamics in intact tissues to those in model vesicles [705]. Later ^{2}H-NMR studies on intact *E. coli* cells in the 1990's showed that acyl chains in their membranes were indeed slightly less ordered than in model liposomes [680] and that glycerol or trehalose had little effect on these dynamics [681]. More recently, in the late 2000's, similar conclusions were drawn from ^{2}H-NMR studies of intact sea urchin sperm cells incubated with deuterated phospholipids [706].

Since the 2010's, some applications of ^{2}H-NMR have been reported that focused on the effects of antimicrobial agents on bacterial membranes in intact cells. Even at sublethal concentrations, some antimicrobial peptides were shown to cause a decrease of order on the acyl chains of deuterated lipids, which were previously integrated by a lipid-auxotrophic *E. coli* [707]. In contrast, other antimicrobial agents provoked the appearance of a gel phase in intact *E. coli* cells similarly supplemented with deuterated lipids [708]. In this latter study, Marcotte and coworkers managed to integrate deuterated fatty acids from the growth medium into a wild-type *E. coli* strain, where they were incorporated in phospholipids. Magic-Angle Spinning (MAS) was finally used on such a system only in 2015, to the best of our knowledge: ^{2}H-MAS NMR spectra of a cell pellet (about 80 μL) acquired in 10-20 minutes gave access to the order parameters of *E. coli* membranes, with the same precision as without MAS but ten times faster [685]. Warschawski, Marcotte et al. could show that *E. coli* membranes were mostly in a gel phase when grown only with saturated palmitic acid, while the addition of unsaturated oleic acid ensured a fluid phase at every temperature. Deuterated palmitic acid was again incorporated in the Gram-negative *E. coli* and in the Gram-positive *Bacillus subtilis* to compare their reaction to antimicrobial peptides: disordering effects of these peptides occurred at different concentrations on the two bacterial strains [709,710]. The same authors incorporated deuterated palmitic acid in the pathogenic marine *Vibrio splendidus*, and could show that its membrane fluidity varied through the different growth phases, dependent on the saturated/unsaturated lipid content [711].

Altogether, NMR spectroscopy has been instrumental in quantifying the dynamic features of membranes at the atomic scale, and in assessing their validity in intact cells, notably using ^{2}H-NMR

[686,712]. It established fundamental knowledge in the 1970-80's, using methods that required rather long acquisition times and often membrane separation. The recent implementation of deuterated lipid incorporation and of MAS has created new opportunities: the functional monitoring of membranes by NMR becomes faster and more straightforward. This may help in mechanistic studies of membrane binders like antimicrobial agents, for example [713,714].

2.3. Metabolic activity

We will not address metabolomics of body fluids and plants. This is now an immense field in its own right [38-46], which mostly deals with samples extracted from the studied organisms or tissues. Still, a number of developments have focused on measuring metabolome evolution of living biological material in an NMR spectrometer, and the corresponding experimental procedures and technical possibilities are typically in the scope of this review.

Magnetic field inhomogeneities and slow molecular tumbling generally hamper NMR spectroscopy, and these are exactly the conditions met in cells. As shown below, it was soon recognized, in the early 1970's, that ^{13}C- and ^{31}P-NMR were likely to yield analyzable spectra of free metabolites in cells. This was possible because these were fast tumbling species showing slow NMR relaxation and thus sharp NMR signals, even though broadened by sample inhomogeneities and the multiple, transient interactions with cellular species [715-717]. Due to their low cell mobility, macromolecules like proteins [715] or DNA [716] appeared at that time to be intractable, yielding very broad, low intensity resonances. The observation of low gyromagnetic ratios nuclei like ^{15}N represented a possible solution for obtaining narrow linewidths, because they are less susceptible to dipolar line broadening and thus generate slower relaxation. Although providing the highest sensitivity, ^{1}H NMR became useful only later, once specific editing strategies and techniques to narrow ^{1}H signals were available. Every nucleus is thus adapted to the observation of different metabolites and different concentrations or timescales. We discuss these various aspects below.

2.3.1. The early days: studying carbon fluxes using ^{13}C-NMR

In the early 1970's, different groups had progressively established the use of ^{13}C labeling as a powerful method to decipher metabolic pathways and carbon fluxes: cells were grown on natural abundance (98.9% ^{12}C, 1.1% ^{13}C) media supplemented with precursors carrying a ^{13}C atom at a specific position; products of interest were extracted, isolated and analyzed by ^{13}C-NMR spectroscopy, which permitted identification of the ^{13}C-labeled final positions [718,719]. This relied on the scarce ^{13}C natural abundance and the approximation that all detected ^{13}C nuclei found their origins in the supplemented ^{13}C-precusors. It was also possible because the cellular ^{13}C-signal was low enough to generate simple, low background spectra.

Soon after the observation of dissolved $^{13}CO/^{13}CO_2/^{13}CN$ in erythrocytes [720,721], Matwiyoff and colleagues established the feasibility of observing global metabolites using one-dimensional ^{13}C-detected NMR of *Neurospora crassa* grown with ^{13}Cε-Methionine [722], or of *Candida utilis* grown on ^{13}C-labeled acetic acid [715]. In this latter publication, the authors also traced ^{13}C atoms from [1-^{13}C]-glucose, showing the concomitant disappearance of the anomeric ^{13}C-peak and the appearance of the C2 signal of ethanol, followed later by signals of unknown species. Hence, the weak natural abundance of ^{13}C (∼1.1%) made isotopic enrichment necessary for carbon metabolism studies, but it was immediately recognized as an advantageous feature allowing the use of ^{13}C-tracers of metabolic activity: introducing a ^{13}C-labeled compound permitted ^{13}C-detection of the successive metabolic products in a mostly ^{12}C-containing background. Only small, fast-tumbling molecules were NMR observable, even though they showed broader linewidths than *in vitro*. But they were even observable in living animals: in 1981, *in vivo* ^{13}C-detected NMR of the rat abdomen on feeding with [1-^{13}C]-glucose was used to demonstrate its progressive conversion into [1-^{13}C]-glycogen by recording spectra every 30 minutes [723].

Shulman and coworkers took advantage of these capabilities, reporting in 1978 a real time NMR study of the first steps of glycolysis in *E.coli*, observing the progressive ^{13}C transmission from [1-^{13}C]-glucose to fructose biphosphate, lactate, succinate, acetate and amino acids [724]. Less than 5 years later they published similar studies focusing on gluconeogenesis in rat liver cells exposed to [1,3-^{13}C]- and [2-^{13}C]-glycerol [725,726] or to [3-^{13}C]-alanine and [2-^{13}C]-ethanol [727], on *S. cerevisiae* anaerobic glycolysis from [1-^{13}C]- or [6-^{13}C]-glucose [728] or aerobic metabolism of [1-^{13}C]- and [2-^{13}C]-acetate [729], and on the consumption of endogenous [3-4-^{13}C]-trehalose and exogenous [1-^{13}C]-glucose by *Pichia pastoris* spores upon germination [730,731]. To illustrate the variety of organisms and metabolic phenomena that ^{13}C-NMR was able to tackle, in the meantime, Scott and colleagues characterized ^{13}C redistribution in the biosynthesis of the more complex molecules like porphyrinogens or polyketides in living *Rhodobacter sphaeroides* or *Penicillium urticae* [732-734] and glucose catabolism in tsetse fly parasites *Trypanosoma brucei* [735]; Nicolay and his coworkers had monitored acetate metabolism in photosynthetic bacteria depending on light conditions [736,737]; Ashworth and colleagues had traced ^{13}C nuclei incorporation from glycine, serine or glucose into serine, tryptophane and acetate by tobacco suspension plants or bacteria (using devices to ventilate the NMR sample or to pump fermenting agents in and out of the NMR tube from an extra-spectrometer fermentor) [738,739].

Then, London and colleagues found an interesting application in the measurement of oxidized and reduced populations of intracellular electron carriers NAD+/NADH and NADP+/NADPH [476,477]. These metabolites were ^{13}C-labeled via the incorporation of ^{13}C-nicotinate in *E. coli* and *S. cerevisiae*, and their reduced and oxidized states yielded different ^{13}C-NMR signals. These enabled the simultaneous observation of a global redox ratio, but peaks from NAD+ and NADP+ or from NADH and NADPH could not be distinguished, the nicotinamide moiety being too far from the adenine phosphorylation site to result in resolvable shift differences.

Concerning microorganisms, we mention works on amino acid biosynthesis by *Corynebacterium glutamicum*, a bacterium used for industrial production of amino acids [740-742], glucose metabolism of the pathological *S. aureus* [743,744], of the yeast *S. cerevisiae* [745-748], of rumen bacteria [749-751] and of *Lactococcus lactis* [752-754], formaldehyde [755] and acetate [756] utilization by *E. coli*, and acetate, methanol or methylamine utilization by methylotrophic strains [757-760].

The early cellular studies paved the way towards future ^{13}C studies carried out *in vivo* [761 762], which included studies of glucose metabolism of erythrocytes [763,764], acetate and glucose utilization in lymphocytes and breast cancer cells [765,766], the effects of 2-deoxyglucose in cancer cells [767,768], amino acid [769] and succinate [770] metabolism by renal cells, and glucose and glutamine metabolism by hybridomas [771]. After early reports on ethanol and alanine metabolism in perfused mouse livers in the late 1970's [725,772], ^{13}C-MRS studies (i.e. NMR characterization of localized chemical composition and metabolism) included investigations of metabolism of plant seeds, brain, tumors, heart, but were limited by their low sensitivity [773-775]. Hyperpolarization can nowadays overcome these limitations in some cases, as we discuss in a later paragraph.

However, spectroscopists realized in the late 1980's that, for most ^{13}C-labeled precursors, their insertion in intricate metabolic cycles resulted in the progressive scrambling of ^{13}C atoms into numerous, low abundance species (for a thorough discussion, see [776]). Together with the low sensitivity of ^{13}C-NMR and its low spectral resolution due to sample inhomogeneities resulting in broad signals, *in vivo* ^{13}C-NMR was limited in its ability to carry out a fine analysis of metabolic pathways. Moreover, high quantities of ^{13}C-labeled precursors necessary for real time NMR detection impacted cellular metabolism [776]. Among other difficulties, distinguishing NMR signals of intra- and extracellular populations of molecules was also a common concern: unlike those of ^{31}P as we will see below, ^{13}C chemical shifts often depend too weakly on pH or on the other phenomena that can vary between intra- and extra-cellular spaces [776]. Another concrete obstacle was the problem of maintaining cells in steady-state conditions. Indeed, many parameters influencing metabolism become unstable at the high cell density needed to obtain sufficient NMR signal-to-noise, e.g. oxygenation, nutrient levels, pH, osmolarity, (toxic) end products [740,776]. A number of bioreactors inside spectrometers were designed at that time (see Section 3.7.). These permitted continuous monitoring of cell metabolism, notably to characterize the impact of drug-treatment and irradiation on mammalian cancer cell metabolism by ^{13}C- and ^{31}P-NMR [768,777-794], or to study the effects of ethanol and various chemicals on hepatocytes [795,796], as well as metabolism in hybridoma [771,797]. However, in-cell NMR studies of metabolic activities appeared to be limited to cases involving the study of high concentration metabolites. It is striking that all these impediments to live cell ^{13}C-NMR metabolomics were also faced 25 years later by the in-cell structural biology community.

Hence, in combination with gas- and liquid-chromatography mass spectrometry (GC-MS) since the early 1990's, NMR spectroscopy of extracted and isolated materials delivered the main body of atomic scale information on metabolic pathways for the so-called Metabolic Flux Analysis [39,762,798-800]. However, when adapted, specific advantages of real time measurements, like using a single sample and avoiding sample preparation, remained attractive at times to characterize simple metabolic transformations.

2.3.2. ^{31}P-NMR of phospho-species, energy fluxes and cellular localization

Studies of ^{13}C-NMR were early combined with those of ^{31}P-NMR, the latter providing interesting information on cellular metabolic activity [746,801,802]. ^{31}P was considered to be easier to detect by NMR because of its ~100% isotopic abundance, and one-dimensional ^{31}P NMR spectra were reported from red blood cells a few months after the ^{13}C-experiments described above [462]. Direct observation was thus possible of highly abundant molecules such as inorganic phosphate, ATP and diphosphoglycerate (DPG), which are important cellular metabolites. Hence, ^{31}P-NMR showed early promise for monitoring metabolic activities or mechanisms. Large DNA and RNA molecules also contain significant amounts of ^{31}P, but these are mostly undetected by solution NMR because of their slow tumbling, or by solid-state NMR because of their heterogeneity.

^{31}P in phosphate groups often shows large chemical shifts variations with pH, and in the early 1970's DPG signals were proposed as useful pH reporters in erythrocytes [462]. DPG was also quantified in real time using ^{31}P-NMR peak intensities upon inosine and pyruvate supplementation of erythrocytes [803]. Salt concentrations, notably [Mg^{2+}], were later shown to also have an influence on ^{31}P-phosphate pKa and chemical shifts [804,805]. The use of ^{31}P-NMR for reporting on ATP or DPG binding to Mg^{2+} and quantifying cellular free Mg^{2+} concentration is extensively discussed in Section 2.1.6. Suffice to mention here that about 90% of intracellular ATP is found to chelate Mg^{2+} in a fast exchange equilibrium.

Of course, it became apparent that tissue metabolism could be observed via the detection of the ^{31}P NMR signals of cellular phosphate moieties *in vivo*: ^{31}P-NMR studies of rat muscle showing well-resolved signals from phosphocreatine, ATP and inorganic phosphate were reported in 1974 [311]. This prompted ^{31}P-NMR studies on the evolution of inorganic phosphate/ATP/ADP/phospho creatine levels in rat hearts [806,807], rat kidneys [808] and mouse livers [809] subjected to ischemia and frog muscles under fatigue [810-812], completed with intra-tissue pH monitoring using ^{31}P-NMR [812-814]. The stage was thus set for *in vivo* ^{31}P-MRS/MRI, which was developed from the late 1970's [815-818] also on human patients [819,820]: it has contributed important knowledge, notably on metabolism of healthy or diseased organs, under rest or effort, but such studies are out of the scope of this review; dedicated reviews on this field exist [821,822].

In parallel, ^{31}P-NMR on whole cells yielded important advances in the description of intracellular organization. It clarified mechanisms of polyphosphate storage and its use in yeast [823,824], and permitted quantification of phosphate-containing metabolites, including ATP/ADP/NAD and phospholipid precursors (phosphorylcholine and phosphorylethanolamine) in lymphoid, Friend erythroleukemia, and HeLa cells [716,825]. pH Measurements by ^{31}P-NMR also showed multiple intracellular ^{31}P-phosphate NMR peaks, revealing the existence of different intracellular phosphate pools: this permitted distinction between cytosolic and mitochondrial pH in rat liver cells [826], cytosolic and vacuolar pH in maize root tips [827-829], and cytosolic and vacuolar pH and phosphate stocks in various yeast strains [737,824,830,831] including in spores [832]. Similarly, ^{31}P-NMR analysis of intact weeds showed that glyphosate-resistant species can store this herbicide in vacuoles and thus elude its inhibitory capacities [833-835].

Real time pH monitoring also became accessible, and gave rise to reports on i) ATP metabolism upon oxygenation or deoxyglucose supplementation in Ehrlich ascites tumor cells [836], ii) intracellular and extracellular pH under aerobic or anaerobic conditions in *E. coli* [837-840], and iii) light-induced pH variations in photosynthetic bacteria [841,842]. NMR spectrometers gained a reputation of being the most expensive pH meter in the world [461], but the non-invasive nature of the method was certainly appealing. Moreover, complex metabolic studies were also carried out on glycolytic mutant strains of *S. cerevisiae*, by reporting multiple phospho-metabolite levels upon addition of glucose or O_2 [843]. This demonstrated the ability of NMR to report multiple metabolite levels in order to support more system-wide characterizations.

Still more informative ^{31}P-NMR experiments were developed once Shulman and colleagues showed that reaction rates could also be measured between orthophosphate and ATP in *E. coli*: upon saturation of either the resonance of ^{31}Pγ-ATP or of phosphate, they observed peak intensity losses of phosphate or of ^{31}Pγ-ATP, respectively [844]. Hence, it was not only possible to monitor phosphate and ATP levels, but also to measure rates of ATP hydrolysis or synthesis. This "saturation" method, developed in the 1960's [845,846], relies on the selective destruction of magnetization of a chosen resonance, i.e. corresponding to a chosen atom in a chosen species, which thus acts as a tracer of chemical exchange: the saturated atoms transfer their loss of magnetization to the product of the studied chemical reaction, whose NMR resonance intensities are attenuated proportionally to the reaction kinetic rate (Fig. 14). Saturation approaches have later been used in ligand-observed NMR spectroscopy of ligand:protein interactions, as described in Section 2.5 on drug discovery.

Resonance saturation also underlies recent Chemical Exchange Saturation Transfer (CEST) studies for advanced protein conforma-

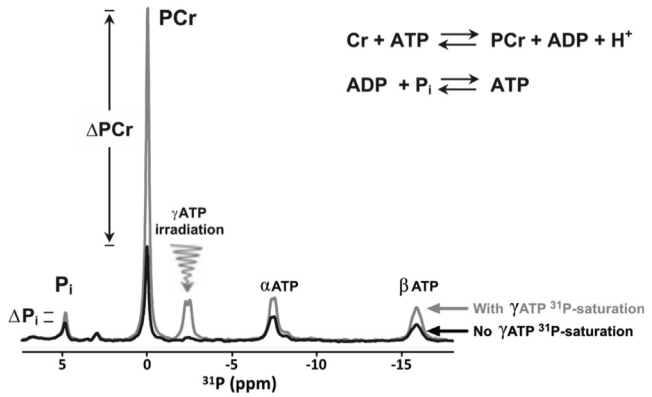

Fig. 14. 1D ^{31}P NMR spectra without (grey) and with (black) saturation of the γ-phosphate of ATP at -2 ppm. ^{31}P signals can be attenuated upon γ-ATP saturation either because i) they are close in space to γ-ATP (i.e. β- and α-ATP), or because ii) they are in chemical exchange with γ-ATP (i.e. phospho-creatine or phosphate). The signal intensities in these peaks provide quantitative information on the kinetic rates of the chemical reactions. Adapted from Befroy et al. 2012 [847].

tional studies, notably on "invisible" minor species [848,849]. In the case of living cells, ^{31}P-NMR saturation transfer was applied in the 1980's to quantify rates of inorganic phosphate or ATP consumption in *E. coli* [850], in human erythrocytes [851], in breast cancer cells [852] and also the fluxes towards glucose-6-phosphate or fructose-1,6-bis-phosphate in aerobic and anaerobic conditions in *S. cerevisiae* [746,853-855]. In parallel, a number of groups used ^{31}P-resonance saturation transfer to measure ATP and phosphocreatine consumption and replenishment, hence measuring creatine or ATPase kinase activity in rabbit [856] and rat hearts [857-862], in frog [863] and cat muscles [864] and in rat brain [865]. These led to *in vivo* measurements and the description of altered metabolism in diseased tissues [821,847], i.e. the MRS/MRI field and the limits of our scope. Shulman and coworkers combined ^{31}P- and ^{13}C-detected NMR to describe ATP and glucose metabolism in an integrative fashion in *E. coli* and rat liver cells, and used NMR saturation transfer to evaluate phosphate transfer to ATP, i.e. ATP synthesis by ATPase in their conditions [801].

Lastly, regular ^{31}P-NMR monitoring of intracellular ATP has shown its usefulness to check the health status of cells in the NMR tube, which in turn helped to establish the benefits of intra-spectrometer bioreactors (see Section 3.7.). As discussed above (Section 2.3.2.), in combination with ^{13}C-NMR, ^{31}P-NMR and bioreactors were used to study the effects of various drugs on mammalian cancer cell metabolism [768,777-794], of ethanol and various chemicals on hepatocytes [795,796], and the metabolism of hybridoma [771,797], and yeast immobilized in gel matrices [866]. More recently, ^{31}P-NMR also provided interesting checks for cellular health during in-cell structural biology studies [867-869].

2.3.3. Nitrogen flux studied by ^{15}N-NMR and ^{14}N-NMR

^{15}N-NMR detection in living cells was explored from the mid-1970's, providing a whole cell pattern for a parasite fungus [870]. In a more extensive study, Lapidot and Irving reported ^{15}N-detected spectra of uniformly ^{15}N-labeled *E. coli*, *S. cerevisiae* and Friend leukemic cells, as well as *S. aureus* labeled with ^{15}N-glycine [580]. They took advantage of the large signal increase generated by ^{1}H-decoupling via the heteronuclear ^{15}N{^{1}H} NOE effect: fast tumbling small molecules show an enhancement ratio of up to -3.93, while slowly tumbling macromolecules show an enhancement ratio of approx. +1 (i.e. close to no effect) [871], and semi-mobile molecules can produce a null signal in these conditions. Lapidot and Irving demonstrated the high flexibility and ^{15}N-NMR detectability of phosphatidylethanolamine, lysine and arginine nitrogens as well as many other unidentified nitrogens in cells, and of glycines in *S. aureus* peptidoglycan. Because they are pH- and viscosity-dependent, related ^{15}N relaxation times and peak linewidth of amino acid signals were also used to probe their local environments, either cytoplasmic or vacuolar [467,872].

Hence, ^{15}N-NMR under ^{1}H-decoupling and NOE enhancement provided clean spectra of high abundance ^{15}N-containing metabolites produced from ^{15}N-labeled precursors such as $^{15}NH_4^+$ or $^{15}NO_3^-$. The rationale used earlier for ^{13}C-NMR of carbon fluxes was applied similarly to nitrogen fluxes: living organisms fed with natural abundance nutrients (99.6% ^{14}N, 0.4% ^{15}N) are suddenly exposed to ^{15}N-labeled precursors; ^{15}N-NMR spectroscopy then reports the integration of ^{15}N atoms in the first metabolic products, the natural abundance background signal being close to zero. Using this ^{15}N-NMR approach, nitrogen metabolism was characterized in live microorganisms such as the fungus *Neurospora crassa* [873,874], *C. glutamicum*, a bacterium used for industrial production of amino acids [875,876], Pseudomonas [758], or cyanobacteria [877], and even once in mammalian cells [878]. From the late 1980's, most ^{15}N-NMR studies on living organisms were concerned with nitrogen assimilation by plants, focusing on symbiotic bacteria [879] or fungi [880-882], algae [883], spruce buds [884] or cell cultures [885], maize root [886-888], duckweed [889], invasive weed [890,891] and even carrot cell suspensions [892,893]. ^{15}N-detected solid-state NMR spectra were also carried out on lyophilized soybean cotyledon or leaves to determine nitrogen fluxes from ammonium, nitrate, N_2, asparagine, glutamine, allantoin or methionine [894-899]. Overall, these studies permitted characterization of the relative contributions of two complementary pathways (glutamine synthetase/glutamate synthase GS/GOGAT, and glutamate dehydrogenase GDH) in nitrogen assimilation, or comparison of NH_4^+ and NO_3^- incorporation rates in various conditions [900,901]. ^{15}N-NMR of cell extracts has found convenient applications to evaluate the impact of various stresses, since it does not require any separation steps [901-903], although it still demands a careful exploitation of the spectroscopic data [904]. ^{15}N-NMR also permitted a few studies of secondary nitrogen metabolism of alkaloid precursors, notably using ^{15}N-tropinone [890,891,900,901,905,906]. It has also provided quantification of the metabolism of the neurotransmitter glutamate in MRS studies of animal brains, which lies outside the scope of this review [907].

Similar limits to those encountered in studies of ^{13}C-NMR carbon fluxes were also met in ^{15}N-NMR metabolite studies: the low sensitivity of NMR compared to mass-spectrometry made it less attractive from the early 1990's [908]. ^{15}N-direct detection is practically feasible only for species found at millimolar concentrations. Moreover, the use of the ^{15}N{^{1}H} NOE to enhance sensitivity coupled to the long T1 relaxation (due to the low ^{15}N gyromagnetic ratio) make it difficult to analyze ^{15}N-NMR spectra quantitatively [904]. It has however some advantages. ^{15}N-detection is feasible at every pH and temperature, in contrast to indirect ^{15}N-filtered ^{1}H-detection, which became popular from the 1980's [908-910]: although it can yield a 10-100 fold better sensitivity theoretically, ^{1}H-indirect detection is impossible for many protons attached to ^{15}N that exchange with water protons at rates above 10-100 Hz under physiological conditions. Long-range, multiple bond magnetic transfers have been designed that partially circumvent this problem, but at the expense of sensitivity [911]. ^{15}N-NMR is also convenient for the straightforward, direct observation of NH_4^+ and NO_3^- *in situ* without extraction. This may seem an unsophisticated NMR application, but it is useful because the methods used for extraction prior to for mass-spectrometry analysis can lead to information losses [908,911].

However, for nitrogen NMR studies focused on quantifying NH_4^+ and NO_3^-, ^{14}N-NMR can be also considered. The quadrupolar nature

of ^{14}N is an obstacle to NMR measurement in most cases, but has less effect on ^{14}N resonances of simple, symmetric, fast tumbling metabolites like NH_4^+ and NO_3^- even inside cells [912]. Close to symmetric nitrogen sites such as those of urea, trimethylamines or betaine may also be observed using ^{14}N-NMR [913]. It does not require any isotope enrichment, because ^{14}N represent 99.6% of nitrogen nuclei at natural abundance, as mentioned earlier. ^{14}N-NMR permits more reliable quantification than ^{15}N-NMR, notably because of the faster ^{14}N T1 relaxation [914,915]. It has been applied to various systems such as mammalian tissues [912,916,917], plant roots and leaves [914,918,919], algae [920], *E. coli* [913], and spruce seedlings [884,885,921,922]. Shift reagents have also been used to distinguish extra-cellular from intracellular ^{14}N-signals [923,924]. These were used, in combination with saturation transfer methods similar to those presented above for ^{31}P-NMR, for measurement of transmembrane fluxes of ammonia in erythrocytes [925]. Moreover, ^{14}N-NMR signal linewidth and peak multiplicity of NH_4^+ is sensitive to pH because of the varying exchange rate of protons with water: the local pH where the detected pools of NH_4^+ are found can be measured [918,921]. The related measurements are less direct than ^{13}C, ^{15}N or ^{31}P chemical shifts characterization of chosen metabolites whose protonation states are pH-dependent [926]. Nevertheless, ^{14}N-NMR permitted quantification of NH_4^+ present in the cytoplasm, or its storage in very acidic vacuoles of maize roots [918] or spruce seedlings [921,922].

2.3.4. Overcoming spectral congestion in ^1H-NMR spectroscopy for higher sensitivity: monitoring cellular species below millimolar concentrations in the timescale of minutes.

Macromolecules and molecules embedded in macroassemblies, such as lipids in cell membranes, contain innumerable NMR-visible protons. Proton resonance frequencies have a narrower dispersion than ^{13}C or ^{15}N nuclei, and species such as water, lipids or macromolecules generate important and broad ^1H-NMR signals that obscure ^1H resonances from metabolites. As far as NMR detection is concerned, the benefits of low natural abundance of ^{13}C cellular contents, or of the sparsity of observable ^{31}P signals do not apply for ^1H species. Hence, although being the highest gyromagnetic ratio nucleus and yielding theoretically the highest NMR signal intensities, ^1H-detected NMR was not the first-choice method in early studies. ^1H NMR necessitated development of signal-filtering strategies before it could become established for the observation of metabolites in living cells and organisms. Various solutions have been found for various applications that we detail below.

A prior requirement for studies on metabolites in live cells is always a robust suppression of the very large NMR signal from water protons. The studies mentioned below used contemporary methods that were developed in parallel. Dedicated reviews exist on this topic [927], which is much less problematic now than it once was (see also [928-930] for live material).

NMR signals from macromolecules were first removed using the so-called spin-echo technique to purge out resonances from slow-tumbling species (see Section 3.3.2. for some brief explanations). In the mid-1970's, Daniels and coworkers used a spin-echo pulse sequence to separate the sharp resonances of adrenaline from the cellular background of adrenal gland slices [931]. The resulting ^1H-detected one-dimensional NMR signal was the first experimental observation able to support the hypothesis of a homogeneous, fluid pool of adrenaline in this native context. The metabolite was selectively observed also because of its high concentration. The sharpest resonances from metabolite species present at millimolar concentrations were then used to study specific aspects of cellular metabolism. Using one-dimensional spin-echo ^1H-NMR, scientists in Oxford started to quantify erythrocyte metabolic activities such as glutathione redox equilibrium, or glucose consumption [932]. They used the same technique to monitor D-Alanine or L-Alanine influx after adding a paramagnetic agent in the external medium to suppress NMR signals from outside erythrocytes [933]. A growing number of workers applied one-dimensional spin-echo ^1H-NMR, either to quantify Zn^{2+} complexation by glutathione in erythrocytes [934], or variations in levels of phosphorylcholines through the cell cycle in Friend Leukemia cells [935], choline levels in erythrocytes [936], the metabolism of malate, fumarate and lactate as a function of NAD+, pyruvate or oxalate concentrations in erythrocytes [937], amino acids levels and glucose consumption in HeLa cells [938], methylglyoxal metabolism and the stability of ergothioneine in erythrocytes [939,940].

An important aspect of spin-echo experiments is the evolution of scalar couplings between protons during the echo time. Within specific ranges of spin-echo durations, scalar couplings cause the inversion of certain proton signals (i.e. the signals become negative) (Fig. 15). Interestingly, if a proton-deuterium exchange occurs for one of the protons involved in the spin-spin coupling, the coupling is effectively removed (^1H-^2H couplings are approx. 6.5 times smaller than the corresponding ^1H-^1H coupling, and the ^2H nuclei are unaffected by ^1H pulses) and the spin-echo does not invert the resonance signs of the neighboring protons anymore. This concept permitted monitoring of the incorporation of deuterated glycine into glutathione [941], of specific enzyme activities that result in H/D exchange between water and pyruvate and lactate [942-944], and of lactate/pyruvate exchange upon supplementing cells with deuterated lactate or pyruvate [945-947], again in erythrocytes.

Unlike ^{12}C nuclei (that have no spin), ^{13}C spins are also scalar-coupled to covalently bonded protons. Integration of ^{13}C nuclei into metabolites can thus be detected in ^1H-detected spectra in multiple ways: i) they cause a peak splitting in ^1H-detected spectra, the two new peaks being separated by the scalar coupling ^1J (^1H-^{13}C)$\sim$100-150 Hz; ii) the signs of these peaks can be also manipulated specifically by ^{13}C 180° pulses during the spin-echo (see Section 3.3.2.). Shulman and coworkers were the first to use this phenomenon to quantify ^{13}C-incorporation from [2-^{13}C]-acetate into glutamate or aspartate by *S. cerevisiae* [948]. A more-advanced ^{13}C-modulated ^1H spin-echo was exploited by Brindle and colleagues to monitor the ^{12}C- and ^{13}C-methyl content of alanine and pyruvate and thus quantify the activity of the alanine aminotransferase in erythrocytes [949]. Foxall and coworkers used and published a similar application of ^1H-^{13}C spin echo difference to report the conversion of [1-^{13}C]-glucose into [2-^{13}C]-ethanol in yeast [950]. They showed that such indirect ^1H-detection of the presence of ^{13}C provided a 22-fold higher sensitivity than direct ^{13}C-detection. This strategy was also employed to detect ^{15}N-incorporation from ammonium or glutamine in cultured mammalian cells, with similar sensitivity benefits [876]. Use of such spin-echo related filters was however abandoned by the majority of the community, and substituted by magnetization transfers allowing ^1H-detected, ^{13}C- or ^{15}N-edited 2D NMR spectroscopy. These spread the signals in a supplementary dimension and are thus likely largely to avoid peak overlaps (see below in Section 2.3.6.)

The combined use of multiple nuclei including ^1H-detection was explored from the early 1980's [946,951,952]. ^1H-detected NMR was soon considered to be complementary to ^{13}C and ^{31}P-NMR in the characterization of living tissue metabolism [761,953,954]. For example, ^1H- and ^{31}P-NMR were combined to measure total creatine and creatine phosphate pools in frog muscles [951], and to report simultaneously pH and lactate levels in guinea pig brain slices using multiple channel NMR-probes [955,956]. In recent years, this complementarity between ^1H- and ^{31}P-NMR was also applied to the simultaneous monitoring of

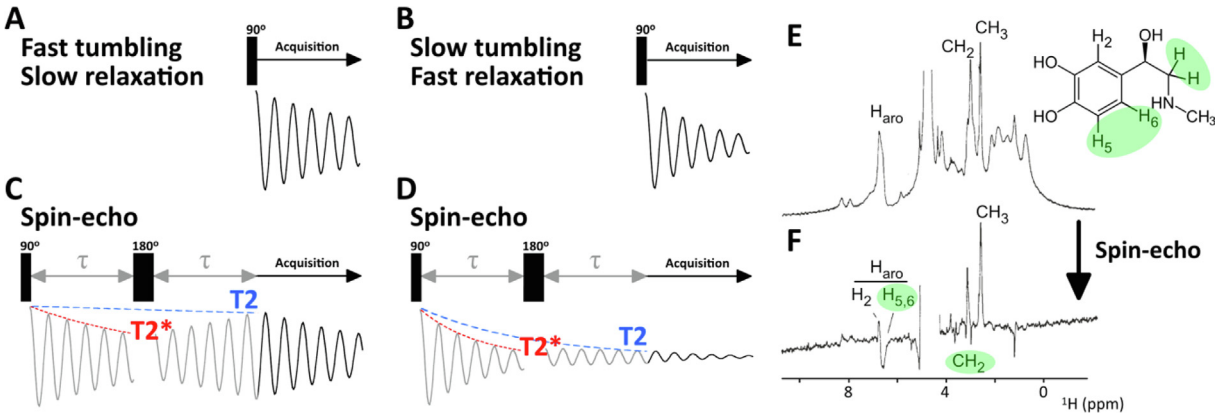

Fig. 15. A spin-echo can filter out signals from slowly tumbling molecules. We show here the theoretical schemes for the time-domain evolution of ^{1}H-signals acquired after a single 90° pulse for A) fast tumbling or B) slow tumbling molecules. The effective transverse relaxation T2* can be dominated by sample inhomogeneities and chemical shift distribution. C) A spin-echo refocuses the magnetization coherence lost due to inhomogeneities, but not that lost because of the intrinsic molecular T2. Hence, spin-echo ^{1}H-spectra show signal intensities modulated by the molecule-specific T2x2τ, which is much attenuated for D) slowly-tumbling molecules. E) One-dimensional ^{1}H-detected spectrum of a bovine adrenaline medulla slice; F) one-dimensional spectrum acquired after (2x 60 ms) a spin-echo of the same slice, revealing signals from adrenaline molecules (found at high concentration in this tissue). Signals from species having short transverse relaxation times T2 vanished. Because scalar couplings can evolve during the spin-echo, signals from CH_2 groups or from protons with a large, vicinal scalar coupling H_5/H_6 are inverted (highlighted in green). These spectra were recorded in 1976 at 270 MHz. Adapted from Daniels et al. [931].

cellular metabolite levels, RNA synthesis or folding and protein interactions [466]. A number of cellular structural biology studies focusing on proteins took the simpler approach of using ^{31}P-NMR to check cellular metabolic states from ATP levels, together with ^{1}H-detected NMR of proteins [867,868].

^{1}H-NMR acquisition can also be performed without background filters when monitoring metabolites supplemented at very high-concentrations, e.g. the metabolism of diluted *E. coli* cell suspension in ~100 mM glucose [957,958]. At such high concentrations, ^{13}C-coupled ^{1}H-doublet signals are also easily observed, which allowed monitoring of ^{13}C-glucose metabolism and the incorporation of carbon by the rumen cellulolytic bacterium *Fibrobacter succinogenes* [959]. We mentioned previously that lipids can often be seen as a problem, because their signals completely obscure parts of ^{1}H NMR spectra. These large signals can become interesting for monitoring the global lipid content of cells, and have been exploited to quantify live microalgae cultures in real time [960,961962,963].

The observation of metabolite consumption is of course possible in the spent medium following culture of any cells, like plant, tumor spheroids [964] or mammalian cells grown to produce therapeutic proteins [965,966]. Extracellular metabolites generally provide sharp NMR signals that are good reporters of intracellular metabolism. A recent study of primary cancer cells permitted examination of their adaptation to hypoxic conditions: about 35 metabolites were identified and about a dozen monitored over 24 hours using samples containing 1.10^{7} to 5.10^{7} cells/mL embedded in agarose [967]. Similarly, a dozen metabolites were monitored in lactic bacteria growing over 24 hours in various glucose and pH conditions in the NMR tube [968]. Using this approach and up-to-date commercial NMR probes, one-dimensional proton spectra can be recorded every 5-10 minutes and provide metabolite quantification with ~10 µM precision for 500 µL sample volumes. Similar results were obtained from primary cancer cells embedded in methylcellulose, which allowed monitoring of extracellular levels of about 10 metabolites over 24 hours [969]. Although presenting practical advantages when compared to classical methods using quenching and extraction, this live-cell metabolomics approach using ^{1}H-NMR requires a careful deconvolution of signals because of progressive peak shifting and broadening [967,968]. The corresponding signals can thus be exploited with confidence only if their intensities surpass those of the other signals with similar chemical shifts, which often means if the quantified species are found in the millimolar range. However, such applications fall in the area of metabolomics studies and are not considered here in greater detail.

2.3.5. HR-MAS ^{1}H-NMR spectroscopy: lipid filtering/editing and metabolome of intact cells, tissues and small living organisms.

Although spin-echo and T2-filters improved the ^{1}H NMR detectability of a number of metabolites, the observed peak linewidths were still too broad to allow analysis of the intracellular metabolome with much accuracy. Magnetic inhomogeneities or restricted motion of mobile species cause line-broadening of NMR signals, preventing deconvolution of signals. Moreover, resonances from lipids are often not completely removed by T2 filters: some intracellular pools of lipids exhibit largely liquid-like behavior and, even though constrained, maintain high mobilities. In general, the metabolites that could be analyzed with this approach were those found at high concentration, that were highly mobile, and producing NMR resonances far from those of lipids. Non-membrane lipids themselves, with their semi-restricted motional regime, were thus "in limbo" as far as accurate in-cell NMR description was concerned.

In an earlier Section (2.2.3.) on cell-surface lipopolysaccharides and glucans, we discussed briefly the deleterious effects of molecular restricted motion and non-homogeneous magnetic susceptibility, especially for ^{1}H NMR observation (see also Sections 3.2.2. for more detailed explanations). These broaden the NMR signals observed using classical liquid-state NMR approaches. However, high degrees of local mobility are often maintained for small molecules like metabolites in non-frozen samples, which can yield sharper peaks if Magic-Angle Spinning (MAS) is applied. Hence, high peak intensities and narrow linewidths (Fig. 16) can be obtained from mobile species, including lipids, contained in cell pellets, excised animal tissues or even small animals, e.g. *C. elegans*, small crustaceans or flies. These have to be loaded in a cylindrical sample container (the "rotor") and spun between 1 and 4 kHz at an angle of 54.7°, with respect to the spectrometer magnetic field B_0.

This approach has been coined as High-Resolution-MAS (HR-MAS) NMR spectroscopy and has the obvious advantage of permitting the analysis of intact, non-processed samples (see Section 3.4.3. for a specific discussion on HR-MAS). It has been applied for more than 20 years in chemistry and food science,

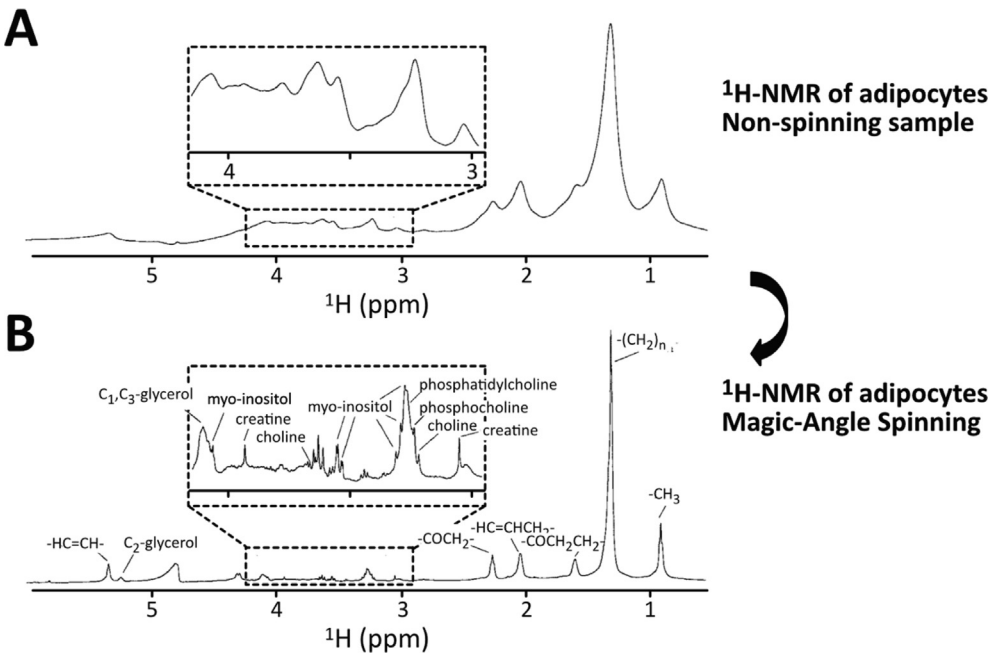

Fig. 16. One-dimensional ^{1}H NMR spectra of cultured adipocytes under **A)** non-spinning conditions, and **B)** Magic-Angle Spinning (MAS) at 3.5 kHz. Both spectra were recorded at 11.7 T (500 MHz) in 42 minutes and twice as many cells were used in the non-spinning conditions. Adapted from Weybright et al. 1998 [987].

but also to characterize the metabolome of intact cells or tissues in conditions such as those we describe below. Recent reviews can be found on this topic [970,971]. This approach is attractive because of its relative convenience: it requires ~5 million cells per measurement, i.e. 15-50 uL or mg of wet pellets, and no time-consuming chemical extraction. It benefits from the sensitivity of ^{1}H NMR and thus permits accurate quantification of metabolites present at ~0.1 mM concentrations [972]. To put this in context, more than 60 metabolites are present at 0.1 mM or above in growing *E. coli* [973]. Investigations on intact cells deliver only relative quantifications of the identified metabolites: they rely on semi-quantitative, comparative measurements of signal intensities in the various conditions tested. Absolute quantification can still be achieved using synthetic signals as an electronic reference [974,975]. The corresponding analysis falls in the category of largely classical metabolomics studies of quenched -although often "intact"- samples, which we do not cover extensively in this review. However, a number of recent developments permitted real-time observation of metabolic fluxes in small animals, for which we made an exception.

The benefits of Magic-Angle Spinning had been shown for drastically narrowing ^{1}H and ^{13}C NMR signals of plant seeds at the end of the 1980's [630,976], and fruit tissues at the beginning of the 1990's [977-979]. The idea was taken up in the 1990's to compare the metabolome of normal and metastatic lymph nodes [980], and for the analysis of other animal soft tissues, e.g. kidneys [981,982], brain [983], adipocyte [984,985] and breast tissues [986]. Correspondingly, at the end of the 1990's, Singer and colleagues had shown that MAS at ~3-4 kHz permitted narrowing down ^{1}H NMR signals linewidth of intracellular lipids and metabolites by a factor ~10 in cultured adipocytes (Fig. 16) [987].

This helped to quantify cellular contents in various lipids from undifferentiated and differentiated adipocytes and to extend this type of characterization to benign and malignant liposarcoma tissues [988,989], and to measure intracellular diffusion coefficients of lipids [987,990]. Similar experiments were carried out more recently on cultured cells (exposed to cytotoxic agents) to derive the diffusion coefficients of intracellular lipids on the millisecond timescale using HR-MAS, in a complementary fashion to fluorescence microscopy measurements on a time scale of seconds [991]. Because intracellular lipids conserve some mobility, ^{1}H HR-MAS NMR gave access to lipid analysis in intact cultured cells for various purposes: to distinguish neuronal and glial cells [992], to monitor phospholipid content in melanoma cells upon exposure to chemicals [993], fatty acid content variations in insulin secreting cells [994] and in mesenchymal stem cells [995]. These quantifications should however not be taken as absolute: increasing MAS spinning rates cause different degrees of ^{1}H NMR signal enhancement in different lipid pools, probably because of variable release of mobility restriction, as shown on glial cells [996]. Similar differences were observed for ^{1}H HR-MAS lipid signals of biopsies from different brain tissues [997].

^{1}H and ^{13}C HR-MAS NMR also proved to be valuable for analyzing the whole-cell metabolic profile of algae in one single experiment [998-1000], which would usually have been carried out from separate water-soluble fractions and lipophilic extracts. Such a convenient profiling method of intact cells by HR-MAS NMR was presented as well suited to the analysis of algal content for nutritional and bio-fuel applications [960,1001-1003] and the identification of marine microorganisms [1004,1005]. Recent approaches favor flow-cell ^{1}H NMR in line with bioreactors to monitor the global lipid content of live microalgae cultures in real-time [960,961], also using benchtop NMR spectrometers [962,963]. These last characterizations do not require MAS and ensure a true non-invasive monitoring, although they provide less detailed information on the nature of the observed lipids.

Improved lipid editing/filtering capacities have been shown by diffusion editing methods: in combination with more classical T2-relaxation filters, they permit isolation of signals from species that present either unrestricted or restricted diffusion, semi-solid behavior and even those from true solid material (like chitin or lipid-protein matrices) if ^{13}C-labeling and -detection are exploited [1006,1007]. This information can be useful to delineate the different pools of molecules, e.g. those that are free, and thus ready to be

incorporated in biosynthesis reactions, as opposed to those that are less mobile, and which are used for energy storage.

In the past decade, ^{1}H HR-MAS NMR has also been used to analyze the metabolome evolution of intact mammalian cultured cells previously exposed to chemicals: human cancer cells responding to chemotherapeutic agents [1008-1014], cultured cells reacting to pathway activators [990,1015,1016] or exposed to nanoparticles [1017], or expressing proteins with oncogenic mutations [1018], and reconstructed human epidermis exposed to skin allergens [1019]. In this last case, we can highlight the use of derivatives of ^{13}C-labeled methanesulfonate, an allergenic reactive agent metabolized into new metabolites, which were quantified using ^{13}C-filtered, ^{1}H-detected HR-MAS NMR [1020,1021]. Recently, HR-MAS has been applied to monitor the metabolic changes occurring within aggregating brain cell cultures, which may be promising for future neurotoxicology investigations according to the original authors [1022].

^{1}H HR-MAS was also used for studying microorganisms, e.g. to monitor the internalization and intracellular processing of a prodrug in mycobacteria [1023,1024], to compare planktonic and biofilm forms of *Pseudomonas aeruginosa* [1025,1026], and to characterize the metabolic consequences of reductase overexpression in the protozoan parasite *Giardia lamblia* [1027]. The metabolic activity of *G. lamblia* at confluency had been previously observed in real-time using HR-MAS at 3 kHz, which did not affect the stability of the trophozoites according to the authors [1028]. In a recent report, mycelia of *Neurospora crassa* were submitted to 6 kHz HR-MAS without apparent sedimentation and cell death, according to the authors, which permitted continuous monitoring of central metabolism pathways in aerobic and anaerobic conditions over 11 hours [474].

We stressed cell survival in the previous paragraph because it is a clear issue in HR-MAS experiments. Classical HR-MAS experiments require spinning rates in the range of 1-5 kHz to avoid the appearance of artefactual signals called "spinning sidebands". Using a standard disposable 4 mm diameter rotor, these spinning rates generate centrifugal acceleration between 8,000 and 100,000 g (gravity of Earth), which affects the viability of most mammalian cells and tissues [67] (see Section 3.3.4.). Certain cells are less sensitive to MAS at kHz rates, like erythrocytes [1029] or the above mentioned microorganisms. Improved pulse sequences and sample preparation protocols have been designed to make HR-MAS NMR feasible at slower MAS rates. Hence, a single lumpfish egg spun at only 400 Hz remained intact and provided NMR spectra showing promising resolution and signal-to-noise ratio for metabolic studies (Fig. 17) [1030]. Advanced pulse sequences permitted recording of highly resolved HR-MAS spectra of mouse and rat tissues using spinning rates down to 40 Hz and even 1 Hz in the early 2000's [1031-1033], but these approaches have so far not proved sufficiently practical for common use [929].

Slow MAS is essential for studies on live pluricellular organisms. These are promising approaches for understanding and evaluating the toxicity of environmental stressors on model animals like water fleas (*Daphnia magna*), fresh water shrimp (*Hyallela azteca*) and *C. elegans*. Continuous monitoring of single individuals or populations is an efficient approach to avoid the blurring impact of metabolic variability before starting the observation: real-time trajectories can greatly improve the interpretation and reduce the number of repeat experiments needed [1034]. Early studies in the 2010's had shown that anesthetized *D. magna* could be maintained alive at 2 kHz for days, giving access to the lipidic profile of juvenile and adult animals carrying eggs or not [1035]. Similarly, low-temperature anesthetized flies *D. melanogaster* were placed in HR-MAS rotors and survived 2 kHz MAS, the aim again being to compare the lipid content of individuals [1036]. Similar conditions were used to obtain a spatial map of high-concentration metabolites of the head, thorax and abdomen of living, anesthetized flies [1037]. However, anesthetized animals are poor models for toxicity assays and spinning generates significant stress. The non-anesthetized fresh-water shrimp *H. azteca* survive about 40 and 6 hours at 0.5 and 2.5 kHz MAS rates, respectively [929,1038]. Above 2.5 kHz, their survival is affected in one hour [1006]. *D. magna* is even more sensitive to MAS and withstands only 24 hours at 50 Hz MAS [1038]. Simpson and coworkers have developed advanced NMR pulse sequences and sample preparation that made it possible to obtain quality spectra of *H. azteca* at these low MAS rates [929,1006,1038-1040]. These notably include labeling of animals by feeding with ^{13}C, thus allowing heteronuclear correlation NMR, which we will describe in the next subsection. The development of slow (300 Hz) micro-HR-MAS systems by Wong and colleagues has even permitted acquisition of promising spectra from one single *C. elegans* worm [1041]. Using the same experimental design, they managed to analyze samples containing only 19 million yeast cells (~250 nL) and to distinguish their metabolome at various stages of growth or under osmotic stress [1042]. These recent low-spinning HR-MAS approaches may thus have interesting applications in the near future to study small organoids or animals.

2.3.6. 2D ^{1}H/^{13}C-correlation NMR of live cells and small animals: metabolites at submillimolar concentrations on time-scales of minutes to hours

In the previous subsections, we presented the capabilities of one-dimensional NMR spectroscopy for monitoring the metabolite content of cells. The approach is always limited by peak resolution: in most cases, overlapping signals means loss of information, even though peak deconvolution can sometimes extract peak intensities from known resonances. As discussed above, although it is the most sensitive approach on paper, ^{1}H-detected NMR provides poorly dispersed and broad peaks in cells. We have seen that HR-MAS can narrow intracellular ^{1}H peaks, but this strategy has its own limits currently, particularly concerning its effects on living material.

Two-dimensional ^{1}H-detected ^{1}H/^{13}C-correlation NMR offers additional spectral dispersion, which is clearly useful to avoid peak overlaps while preserving ^{1}H-detection sensitivity. In the late 1970's, Bodenhausen, Freeman, Ernst and their coworkers proposed pulse sequences correlating ^{1}H to covalently bonded lower gamma nuclei like ^{13}C or ^{15}N [1043-1047]. This not only gave access to ^{13}C or ^{15}N chemical shift measurements with the sensitivity of ^{1}H NMR, but being a two-dimensional technique, it could "disentangl[e] spectra that are complicated by extensive and multiple overlapping" as described by the aforementioned authors [1048]. This principle has been used for classical metabolomics studies of extracts and biofluids, originally under the name 2D ^{1}H-^{13}C correlation spectroscopy [1049]. It is nowadays more often referred to as 2D ^{1}H-^{13}C HSQC or HMQC spectroscopy and their derivatives (see for example [1050,1051]). Like one-dimensional NMR, ^{1}H-^{13}C correlation spectroscopy is quantitative and several hundreds of metabolites have their signals assigned in 2D NMR spectra databases [1007]. It is however a bit more complicated to extract absolute quantities from 2D spectra than from 1D spectra (for a comprehensive discussion, see [1052,1053]).

In the context of classical metabolomics using extracts or biofluids, 2D ^{1}H-^{13}C correlation spectra can be recorded using samples at natural isotopic: the 1.1% of ^{13}C isotope can be sufficient to obtain a reasonable S/N ratio, provided that the sample is stable enough to remain intact during the recording of a large number of scans. When it comes to intact cells, ^{13}C-enriched metabolites are supplemented in the culture media and their processing is monitored similarly to what was achieved using one-dimensional ^{13}C NMR spectroscopy (see subsection 2.3.1): the assigned peaks

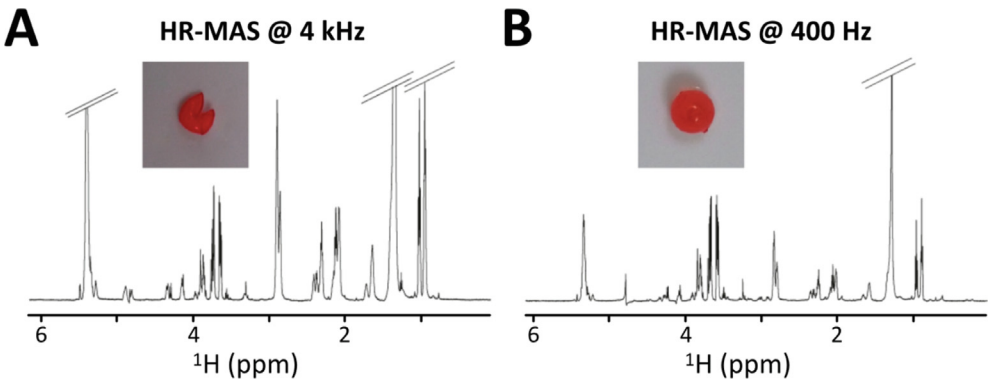

Fig. 17. One-dimensional ^{1}H NMR HR-MAS spectra of a single lumpfish egg (1 mm diameter) recorded at **A)** 4 kHz, or **B)** at 400 Hz, both using the PROJECT T2-filter suppressing the broad signals from macromolecular assemblies. The photographs show the lumpfish egg after MAS at 4 kHz (left) or 400 Hz (right). Both spectra were recorded in 4.5 minutes at 9.4 T (400 MHz). The higher S/N at 4 kHz is due notably to the higher fluidity of the leaked cytosol. Adapted from André et al. 2014 [1030].

are quantified in time-series of spectra, which contains information about the fluxes of the supplemented ^{13}C nuclei. The isotopic filter works as well as for one-dimensional ^{13}C-spectroscopy, but 2D ^{1}H-^{13}C NMR has been reported only since the 2000's, first in combination with HR-MAS [641,974,1015,1020], and then using "classical" solution NMR for metabolic monitoring of live cells or organisms, to the best of our knowledge.

Thus, Park and colleagues have monitored and compared the metabolism of normal and cancer cells in real-time by tracing the levels of alanine, glycine, serine, pyruvate, lactate, acetate, succinate and α-ketoglutarate upon ^{13}C-glucose supplementation [1054]. They were also able to describe the dynamic changes of metabolism after subjecting cancer cells to galloflavin, an inhibitor of lactate dehydrogenase. In a later study, they showed how to measure metabolism in live mitochondria upon ^{13}C-pyruvate supplementation, by monitoring 2D ^{1}H-^{13}C signals from acetate, citrate, succinate, glutamate, acetate, acetyl phosphate and acetyl-CoA [1055]. These measurements were executed on wild-type and p53-KO cells, revealing their fundamental metabolic differences. With intact cells or isolated mitochondria, they recorded 2D ^{1}H-^{13}C spectra every 5 minutes, which generated spectra showing an accuracy for concentration estimated (by the present authors) to be in the range in the range of ~20 μM.

In parallel, Simpson and coworkers studied two algal strains and one cyanobacterium cultivated in presence of $^{13}CO_2$, and established the ability of 2D ^{1}H-^{13}C to identify and quantify 40-50 metabolites in freeze-dried whole cells [1056]. These were actually grown with the purpose of feeding water fleas *D. magna*: once placed in a flow-cell supplying oxygenated water, the living animals provided reasonable quality 2D ^{1}H-^{13}C correlation spectra revealing differences between those fed with algae or cyanobacteria [1057], with natural algal bloom or laboratory control algae [1058], between pregnant and non-pregnant females [1059], or under hypoxic stress [1034]. In a similar fashion, using 2D ^{1}H-^{13}C NMR, Park and colleagues have recently monitored the time-dependent changes of 24 metabolites in living *C. elegans* fed with ^{13}C-labeled *E. coli*: two *C. elegans* strains engineered to knock out two different isotypes of a catalytic subunit of the AMP-activated kinase showed different metabolic reactions to starvation [1060]. We can also mention that Kazimierczuk and his coworkers monitored the metabolism of live *E. coli* exposed, or not, to ampicillin using 2D ^{1}H-^{13}C correlation NMR [1061]. According to Simpson et al., the use of electronic referencing appears to make absolute quantification possible [1051]. Moreover, they have evaluated that a species at 100 μM would yield a signal-to-noise ratio of 10:1 in 2D ^{1}H-^{13}C spectra recorded in about 5 minutes (at 500 MHz using a cryoprobe) [930,1051]. 2D ^{1}H-^{13}C correlation spectra are commonly recorded using ^{1}H-detection because of its higher sensitivity, but ^{13}C-detection avoids problems from any unsuppressed water signal and thus can be complementary in peak detection and assignment: over 60 metabolites have been identified in living *D. magna* using both schemes [1062,1063].

Supplementary filters can be exploited. By selecting only ^{1}H-^{15}N-^{13}CO protons, it is possible to observe very specifically ^{13}C/^{15}N-labeled glutamine supplemented in a natural abundance culture medium and thus to monitor its hydrolysis in live mammalian cells [1064]. Simpson and colleagues have established amino-acid specific 2D ^{1}H-^{13}C pulse sequences to monitor the free amino-acid concentrations [1065]. Hence, they measured their increase in *D. magna* upon exposure to a concentration ramp of bisphenol-A with a 1 minute time-frame allowing a very precise determination of the lowest concentration eliciting a response [1066]. They also introduced ^{12}C-editing methods to monitor specifically the incorporation of ^{12}C-molecules in animals grown under a ^{13}C-labeled diet. They showed in a case study that they could use HR-MAS at 2.5 kHz to follow the conversion of nicotine into cotinine by *H. Azteca*, and the incorporation of ^{12}C nutrients by *D. magna* in their ^{13}C initial metabolome using an advanced strategy selecting signals only from ^{1}H-^{12}C-^{13}C groups [1067]. Finally, they also tested a strategy using ^{2}H-^{13}C labeling of algae, *H. Azteca* and *D. magna* to record 2D ^{2}H-^{13}C correlation spectra: while ^{2}H-detection is intrinsically much less sensitive than ^{1}H-detection, Simpson and colleagues have shown that it can generate useful 2D spectra under 50 Hz HR-MAS of about 20 metabolites when very mobile, without any background issues from signals of water, lipids or macromolecules [1038].

All these approaches are clearly applicable not only for NMR studies of live animals, but also those on live cells and organoids. Although 2D ^{1}H-^{13}C correlation NMR requires ^{13}C-labeling, which can be expensive in some cases, a number of organisms can now commonly be obtained fully or partially ^{2}H-, ^{13}C-, and or ^{15}N-labeled, notably for recombinant expression purposes. A number of culture media depleted in specific amino acids are commercially available for many cell types, and their supplementation with specifically labeled amino-acids can be relatively affordable. These may be applied for NMR in the near future for studies on metabolic and toxicologic responses to inhibitors or pollutants. In a complementary manner to classical quench- and end-point studies, the ability to monitor single samples in a continuous, non-destructive fashion over periods of days is of great interest for understanding biochemical pathways, toxic-mode-of-action or to firmly establish the lowest toxic concentrations.

Low-speed spinning methods have been developed for these applications linked to metabolomics [636,929,972,1030,1068, 1069], but detailed discussion is beyond the scope of this review.

2.3.7. ^{13}C-hyperpolarization for carbon-flux quantification at low-millimolar concentrations and time scales of seconds

As mentioned earlier, the "NMR-visible" ^{13}C isotope has a low natural abundance. Hence, tracing ^{13}C-labeled species by ^{13}C-detected NMR can be a convenient approach to monitor metabolite incorporation and processing in cells that are themselves mostly made of "NMR-invisible" ^{12}C. However, the poor sensitivity of ^{13}C-NMR has been a major limitation. This is mainly due to the low extent of nuclear magnetic polarization at physiological temperatures, about 0.001% (that is to say the lower energy spin state has about 0.001% higher population than the higher) at common commercial magnetic field strengths, namely about 10 T. ^{13}C-hyperpolarization strategies have been proposed to enhance this population difference substantially.

Among such methods, dissolution-DNP (d-DNP) enhanced NMR has been the principal hyperpolarization approach used for achieving real-time monitoring of metabolic reactions in living cells. Pioneering d-DNP studies were reported in the early 2000's [1070,1071], making it possible to achieve 10,000-50,000 fold enhancements in signal, and this spurred a number of applications [1071,1072]. Concise explanations of this technique and others that are closely related are given in Section 3 (see also [1073,1074]), but the outline of a d-DNP experiment will also be described here: ^{13}C-enriched metabolites are hyperpolarized at cryogenic temperatures (~1K) in the presence of polarizing agents carrying free electrons by irradiating with microwaves at appropriate frequencies; importantly, this is usually done in a separate apparatus from the main NMR magnet. The ^{13}C nuclear magnetic polarization achieved can reach 10-50% within an hour. The metabolites are then submitted to fast dilution to quickly thaw the hyperpolarized samples and permit their entry into cells. The half-life of the hyperpolarization typically ranges from 1 to 50 seconds, depending on the metabolite and the conditions, which makes rapid transport to the magnet of the NMR spectrometer an absolute necessity. This also implies the technique is only useful for fast metabolic reactions that can be monitored in a few tens of seconds (Fig. 18).

The reasons that initially made ^{13}C-NMR appealing for MRI and MRS become still stronger if ^{13}C is hyperpolarized: i) ^{13}C-enriched, hyperpolarized molecules generate ^{13}C-NMR signals, which ensure their selective observation; ii) ^{13}C-enriched, hyperpolarized molecules that happen to be substrates of a chemical reaction transmit their ^{13}C-enrichment and hyperpolarization to the reaction products, which also become observable. The immediate proof-of-concept application of d-DNP by Ardenkjaer-Larsen and colleagues was a rat angiography study using hyperpolarized ^{13}C-urea [1076]. Following their previous work on ^{13}C-NMR/MRS, Brindle and colleagues, followed by a growing number of others, showed progressively that d-DNP hyperpolarized ^{13}C-metabolites (notably pyruvate[1077], but also lactate [1078], glucose [1079] or fumarate [1080], bicarbonate as a pH sensor [469] or ascorbic acid as a redox sensor [487]) were exquisite reporters of tumor-specific enzymatic activity for *in vivo* imaging applications [33,1081]. As shown by successful applications in humans, this approach may arguably compete with or be complementary to positron emission tomography (PET) for clinical purposes [1082-1086]. It also has potential for imaging heart or brain metabolism [1084,1087-1090]. Translation to clinical applications requires a number of difficulties to be overcome [1084,1091,1092], which we will not detail here.

With such promise and clinical potential, the d-DNP field and its application to investigations with cells multiplied greatly in the last 10 years. A number of hyperpolarized molecules have been tested, often with use in imaging applications as a motivation. They gave access to real-time monitoring of cellular metabolism in a variety of situations. Among hyperpolarized ^{13}C-metabolites, pyruvate has probably been the most frequently used to characterize mammalian cells: it permits quantification of cancer-related glycolysis through pyruvate to lactate conversion by lactate dehydrogenase (LDH). This requires that cells be maintained in well-defined metabolic states, which led to approaches where cells are encapsulated in polymers, coupled with the use of a perfusion system: this permits cells to be kept in a constant flow of fresh medium while hyperpolarized substrates are injected at defined time points [1093,1094]. These first studies revealed that carboxylate pyruvate/lactate transmembrane transport by MCT1/MCT4 was as important as LDH activity for cancer cell metabolism. Advanced mathematical treatments integrating these parameters were recognized to be necessary for a proper quantification of pyruvate to lactate conversion [1095-1097], unless paramagnetic species like Gd-DO3A were added to quench the extracellular ^{13}C-pyruvate/lactate NMR signals [1098]. Hence, the effects of a PI3K inhibitor on the glycolysis pathway in murine lymphoma cells were attributed to a decrease in LDH expression [1095], while the exposure to a MEK inhibitor caused higher or lower expression of the pyruvate import protein MCT1 in prostate or breast cancer cells, respectively [1099]. Using varying flow rates of medium in the NMR tubes, Kurhanewicz and colleagues evaluated ^{13}C-hyperpolarized lactate efflux, and its importance was underlined by the high expression of lactate exporter MCT4 in metastatic renal carcinoma cells, as compared to non-metastatic ones [1094]. More recently, hyperpolarized ^{13}C-pyruvate influx due to MCT1 and lactate efflux due to MCT4 were shown to have a preeminent role in the oncogenic metabolism of pyruvate, as measured by d-DNP experiments [1100,1101]. Consistently, reduced expression of LDH, MCT1 and MCT4 caused lower pyruvate to lactate conversion rates in mutant IDH1 (isocitrate dehydrogenase 1) glioma cells [1102].

It is interesting to note that in a highly homogeneous field, two close but separated ^{13}C-NMR signals corresponding to extra- and intra-cellular lactate could be distinguished [1103,1104]. Alternative strategies were recently developed to distinguish intra- from extra-cellular hyperpolarized metabolites, which rely on the varying diffusion coefficients between the two environments [1105,1106]. These made it possible to detect pyruvate to lactate conversion together with their extra- and intracellular populations and diffusion rates in cultured cancer cells.

Hyperpolarized ^{13}C-pyruvate d-DNP experiments were combined with more classical metabolomics using ^{1}H-NMR HR-MAS and ^{31}P-NMR, which made possible a distinction between benign and malignant prostate cancer tissues [1107]. Another combination of d-DNP with more standard ^{13}C-NMR metabolomics was proposed, whereby cells were cultured in a medium containing [3-^{13}C]-pyruvate and briefly exposed to hyperpolarized [1-^{13}C]-pyruvate: this allowed quantification of the rapid conversion of [1-^{13}C]-pyruvate into lactate and bicarbonate via the cancer-associated glycolytic metabolism and the slower integration of [3-^{13}C]- or [1-^{13}C]-pyruvate via the more standard Krebs cycle, also in the presence of Akt inhibitors [1108]. To apply hyperpolarized ^{13}C-pyruvate d-DNP experiments to mass-limited samples, Keshari and coworkers implemented a micro-coil apparatus, which made possible the real-time monitoring of pyruvate metabolism in ~10^5 cells in a 1.05 T permanent magnet [1109] or in a 3 T MRI scanner [1110]. This allowed rapid assessment of the cancer-related glycolytic metabolism of various cancer cells upon drug exposure, which should now also be feasible for primary cells, organoids or biopsies.

Although monitoring glucose uptake and degradation would be more logical for quantification of glycolysis in cells, the fast T1 longitudinal relaxation of [U-^{1}H,U-^{13}C]-glucose (~1 second) precluded

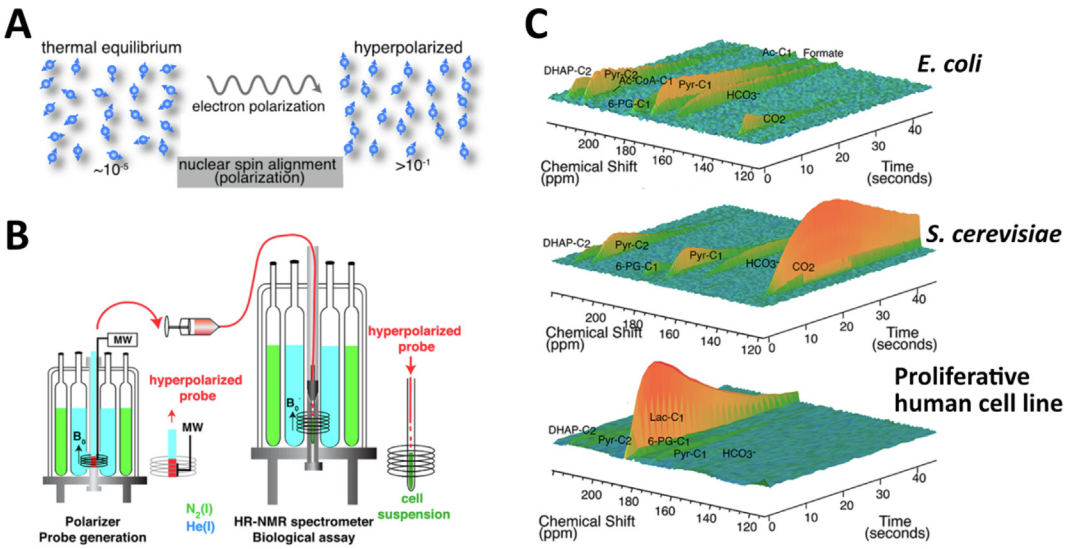

Fig. 18. A) Operating principle of Dynamic Nuclear Polarization (DNP). Current technologies in common use employ intense microwaves to polarize nuclear spins in the presence of polarizing agents (particular molecules containing unpaired electrons, i.e. free radicals) at cryogenic temperatures; **B)** Operating principle of dissolution-DNP: hyperpolarization of nuclear spins is reached at cryogenic temperature under microwave (MW) irradiation; the hyperpolarized substrate is then dissolved in the final liquid sample for analysis (here suspension cells); **C)** Stacked one-dimensional ^{13}C-NMR spectra showing real-time observation of glucose in *E. coli*, *S. cerevisiae* and cultured proliferative human cells: hyperpolarized ^{13}C-labeled glucose is supplemented to the medium at time 0 and time series of 1D ^{13}C-spectra are then recorded. These show the progressive integration of ^{13}C-atoms into various metabolic products, together with a progressive fading of the signal due to T1 relaxation, ending with the loss of the hyperpolarization. (The ^{13}C-glucose signals below 100 ppm are not shown here). Adapted from Lerche et al. 2015 [1075].

such an approach: all hyperpolarization would be lost in just a few seconds. Several groups proposed use of uniformly deuterated ^{13}C-glucose, which slowed this relaxation by a factor of about 10 [1079,1111-1114]. Hence, using d-DNP ^{13}C-NMR, Frydman and coworkers could observe a number of intermediate products of the glycolytic pathways from supplemented hyperpolarized [U-^{2}H,U-^{13}C]glucose, such as dihydroxyacetone phosphate, 3-phosphoglycerate and lactate [1112]. They also revealed the presence of "invisible" intermediate products present at low concentrations: they applied saturation pulses at the NMR frequencies where these products resonate and then measured the resulting variations of signal from the downstream "visible" products that were more abundant. Such a saturation strategy is very similar to those used for ^{31}P-NMR earlier (see above). Because of the multiple intermediate products generated in these carbohydrate pathways, it can be difficult to assign the emerging signals to single species [1112,1115]. Using an approach exploited earlier in standard ^{13}C-NMR experiments [776], the cytosolic NAD+/NADH equilibrium has been measured from the ratio between intracellular ^{13}C-pyruvate and ^{13}C-lactate produced from hyperpolarized ^{13}C-glucose [1113].

Dissolution-DNP experiments have also been used to study microorganism metabolism. Researchers affiliated to the Carlsberg Laboratory directed their investigations towards yeast glycolysis and CO_2/ethanol production: upon feeding *S. cerevisiae* cell suspensions with hyperpolarized (and deuterated) ^{13}C-glucose or fructose, they observed the successive appearance of a dozen intermediate products from central carbon metabolism [1116], its inhibition by sulfite notably via pyruvate-sulfite adducts formation [1117], acetaldehyde accumulation upon acetate exposure [1118] and its impact on the intracellular redox status of the glycolysis pathway [1119]. They also used hyperpolarized ^{13}C-acetate to monitor its influx: because the acetate chemical shift depends on pH, two peaks corresponding to extracellular (low pH) and intracellular (pH∼7) acetate could be observed by NMR in real-time [1118]. They performed similar experiments on *E. coli*, revealing subtle metabolic differences in different growth phases [1120] and strains [1111]. Later studies on hyperpolarized pyruvate metabolism revealed its conversion to acetate in *E. coli* and *S. aureus*, in an opposite fashion to pyruvate metabolism in human cells (see above) [1103]. d-DNP experiments were also carried out on *Trypanosoma brucei* (the sleeping-sickness parasite) to study pyruvate conversion to alanine, and revealed important differences between the form of *T. brucei* found in the insect vector and the form found in the bloodstream of the animal host [1121]. There have also been studies on pyruvate metabolism using d-DNP on motile human sperm [1122] and T lymphocytes [1123].

A number of other hyperpolarized metabolites were used to carry out d-DNP experiments [33,1081,1124,1125], e.g. fumarate to quantify fumarase activity associated with necrosis [1080,1126,1127], ascorbic acid to evaluate intracellular redox potential [487,488], α-ketoglutarate to quantify its conversion to 2-oxoglutarate by the isocitrate dehydrogenase 1 (IDH1) or to glutamate by the branched-chain amino acid transaminase 1 (BCAT1) in glioma cells [1128,1129], arginine to detect its degradation in urea by arginase in myeloid-derived suppressor cells [1130], and glutamine to observe oncogenic glutaminase activity [1131,1132]. A more complete list of hyperpolarized metabolites that have been used, including for *in vivo* applications, can be found in a recent review from Sando and colleagues [1133]. Other nuclei can also be usefully hyperpolarized. ^{13}C-hyperpolarization can be progressively transferred to covalently bound protons after dissolution, which can be useful in cases where ^{13}C-NMR signals from substrates and products overlap [1134]. ^{133}Cs has been shown to yield different peaks in the extracellular medium and in yeast [441] and erythrocytes [442]. Indeed, the $^{133}Cs^{+}$ chemical shift is sensitive to osmolarity, which could make it useful as a cytosolic sensor for this parameter. It was recently used to report cation channel activation in erythrocytes. ^{15}N-labeled compounds have also been tested, such as choline or carnitine, whose slower T1 relaxation (about 5 times slower than that of pyruvate) render

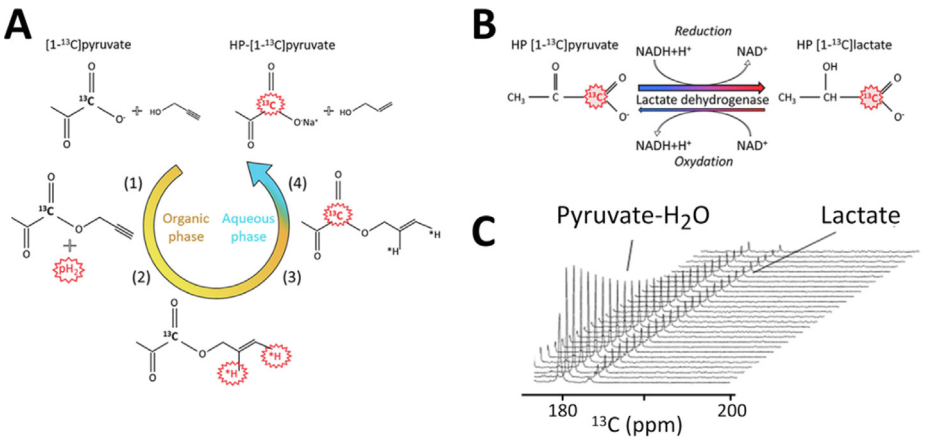

Fig. 19. Operating principle of the current para-hydrogen induced hyperpolarization (PHIP). **A)** (1) a alkyne-containing moiety is attached to the ^{13}C-labeled metabolite of interest, (2) hyperpolarized para-hydrogen reacts with the alkyne function in an organic solvent, (3) the hyperpolarization is transferred to the ^{13}C-nuclei by magnetic field-cycling and (4) the final metabolite of interest is extracted in water; **B)** Anaerobic glycolysis, a hallmark of cancer, is monitored by [1-^{13}C]pyruvate reduction, which leads to [1-^{13}C]lactate; **C)** Stacked one-dimensional ^{13}C-NMR spectra of cancer cells in suspension upon supplementation with hyperpolarized [1-^{13}C]pyruvate. Adapted from Cavallari al. 2019 [1138].

them appealing [1135]. Non-permeating compounds may also be studied using d-DNP combined with an online electroporator placed on the route between the polarizer and the analyzing magnet [1136]. To be more useful, this complicated arrangement would probably require improvements to cell survival upon electroporation, which reached only 50% according to the authors.

Analogously to d-DNP, para-hydrogen induced hyperpolarization (PHIP) is another method recently applied to monitor cellular metabolism in real time. Dihydrogen can be hyperpolarized at cryogenic temperatures (~30-70 K) at low cost compared to DNP. Hyperpolarization transfer to ^{13}C-labeled metabolites requires execution of a suite of chemical reactions on precursors that can be hydrogenated, followed by magnetic field cycling and then extraction into water [1137] (Fig. 19). PHIP permitted characterization of hyperpolarized ^{13}C-pyruvate to lactate conversion [1138,1139] and hyperpolarized ^{13}C-fumarate to malate conversion [1140] in suspensions of cancer cells.

Although one might naively predict polarization enhancements in the order of ~10,000-50,000 fold, in practice d-DNP and PHIP have only been used to study metabolites in the millimolar range, far from the originally expected (sub)micromolar range. We consider this point further in Section 3. d-DNP is however a flexible method, which may theoretically be applied to many metabolites, even though they are not all equally amenable due to their different intrinsic relaxation times. However, d-DNP NMR is far from being a standard method for studying cellular metabolism. Many working on Metabolic Flux Analysis use chromatography-coupled Mass Spectrometry approaches, together with NMR spectroscopy of extracted material from quenched biological samples [39,762,798-800,1141]. d-DNP NMR is surely promising for metabolomics studies of biological extracts and fluids though, as shown by the recent ^{13}C-NMR study at natural ^{13}C-abundance of tomato extracts in less than 30 min per spectrum [1142]. Concerning our focus, i.e. real-time, non-destructive measurements on living cells, d-DNP NMR for metabolic studies offers interesting capabilities: we can imagine for example repeated injections of hyperpolarized material would permit surveying of the metabolic status of single samples over periods of days, provided that bioreactors are used to ensure cell viability. Such "high-end" equipment and expertise are of course not yet commonly available, but are becoming more and more accessible via established networks of NMR facilities.

2.4. Cellular structural biology

High resolution NMR is one of the few methods that allows structure determination at atomic-resolution of biological macromolecules. Compared to X-ray crystallography and cryo-electron microscopy, 3D structures determined by NMR spectroscopy only account for ~10% of all deposited structures in the Protein Data Bank [1143]. Nonetheless, NMR remains a very useful technique, particularly for studying smaller proteins that do not crystallize, as well as relatively weak interactions in solution; it has important capabilities in characterizing the conformational dynamics of many macromolecules (for instance, see [1144-1147]). NMR is thus extremely helpful in understanding the function of folded proteins, but it is indispensable for studying disordered proteins [1148-1158]. NMR is also useful to study cellular processes that occur at slower timescales than those of the internal motions, such as protein maturation events, cofactor binding, and post-translational modifications [1159-1166], all of which can contribute to regulation of protein function. These unique abilities for characterizing proteins at the atomic scale can be applied in complex native environments, notably by using ^{13}C/^{15}N isotope-filters.

Classical structure determination by solution NMR is applicable to relatively small, freely tumbling proteins [1143], while ssNMR is applicable to insoluble samples such as proteins embedded in intact membranes, fibrils, sediments or microcrystalline samples [1167]. Both approaches have been applied to determine the structure of proteins within intact cells or in native membranes, as discussed below. More recently, DNP-assisted ssNMR greatly improved the lower limits of sensitivity [1073,1074,1168-1171]. Currently, this technique necessitates low temperatures to be effective (~100 K or below) and is thus applied to frozen samples. It can provide structural information at atomic-resolution that complements cryo-electron microscopy data [1172,1173].

In-cell NMR has the ability to probe the deep ocean of macromolecular interactions occurring within the cell. These include the classical protein-protein interaction networks, the building blocks of all textbook cellular pathways, but also the complex macromolecular assemblies between proteins and nucleic acids phenomena, and finally the elusive "protein quinary structure", a postulated self-organization of the cellular milieu itself occurring

through weak, diffusive interactions between all cellular components.

Importantly, *in vitro* NMR studies of proteins commonly use high concentrations, approx. 0.1 to 1 mM. So far, in-cell NMR spectra of proteins have been recorded down to ~10 μM at the lowest, which gives access to less accurate structural information than *in vitro* NMR [1174]. However, higher concentrations would not necessarily be advisable: to put things into context, most endogenous proteins show cellular concentrations in the micromolar range, although the distribution is broad, from the picomolar to the millimolar range [1175-1177] (see Section 3.5.).

2.4.1. Solving structures of folded, soluble proteins in cells

^{13}C and ^{15}N isotope labeling, as well as ^{19}F incorporation have been used since the 1970's to permit NMR isotope filtering to suppress the cellular background signals and study cellular walls or metabolites in living cells (see Sections 2.2. and 2.3.) [583,584,668,715]. This concept was later applied to proteins in cells. To the best of our knowledge, the first example reported ^{13}C-histidine labeling and ^{13}C-observation of hemoglobin in erythrocytes from mice fed with ^{13}C-histidine [1178]. Isotope labeling of proteins was not then the standard approach that it has become since, and it took about twenty years before NMR measurements in complex media re-emerged as an interesting possibility. We can cite the ^{1}H-^{15}N NMR spectra of GB1 in crude extracts in the 1990's, and, closer to our topic, the incorporation of 5-fluorotryptophan in yeast by Brindle and colleagues, which gave access to background-free ^{19}F-NMR of enzymes in living cells [1179]. The approach became more popular once, in the early 2000's, Dötsch and colleagues used ^{15}N-labeling of proteins overexpressed and then measured in *E. coli*, demonstrating the feasibility of the technique and the variety of the accessible information [1,1180-1182]. Cells could be grown initially in natural abundance media, and then transferred into ^{15}N-enriched medium before inducing recombinant protein expression. Isotope labeling provided an effective filter to distinguish the protein signals from the cellular background, thus in principle allowing structural studies in complex biomolecular mixtures. This advantage was used to determine the structure of a ^{13}C,^{15}N-labeled protein from NOE-based restraints measured in a crude cell-extract stabilized with protease inhibitors [1183]. Intact cells, however, present several additional challenges. Above all, the 3D NMR experiments that are needed for resonance assignment and NOE-based structure calculation require long acquisition times, which are incompatible with the short lifetime of cells densely packed in the NMR tube. This and other limitations were overcome by Ito, Güntert and their coworkers, who demonstrated in 2009 that NOE-based *de novo* 3D protein structures could be obtained from NMR spectra recorded from intact bacteria [1184]. Despite the huge methodological effort [1185,1186], the in-cell structure of the small metalloprotein TTHA1718 overexpressed in *E. coli* was overall superimposable to that determined *in vitro*, except for small differences in the heavy-metal binding loop attributed to the interaction with metal ions in the bacterial cytosol. These authors further improved their protocols to allow structural determination from lower levels of expressed proteins in bacteria [1187] and in insect cells [1188]. The resulting structures of 5 proteins were mostly superimposable on those determined *in vitro*, and the minor differences observed were again attributed either to the smaller number of distance restraints available from in-cell spectra, or to the interaction of the protein with metal ions or other cofactors in the cytosol (Fig. 20). This is consistent with the minute chemical shift differences observed by others in in-cell NMR spectra of small folded proteins relative to *in vitro* values [1189-1192].

While in-cell NOE-based structure calculation remained a tedious task, an alternative approach to obtain protein structures from simple 2D ^{1}H-^{15}N spectra with the aid of paramagnetic restraints was proposed independently by three groups in 2016 [1193-1195]. In these studies, the small folded GB1 domain or ubiquitin were tagged with lanthanide chelating tags and injected into *Xenopus laevis* oocytes or HeLa cells. The paramagnetic tags gave access to orientation and distance restraints (namely pseudo-contact shifts, PCS, and residual dipolar couplings, RDCs) for structural calculations. Similarly to the NOE-derived structures, the structural model of GB1 obtained in both studies was almost identical to the structure determined *in vitro*, and the minor differences were again attributed to weak interactions with the cellular milieu.

PCSs are also complementary to ^{19}F-labeling, which permits protein structural characterization in cells using 1D ^{19}F-NMR, as shown by Li and his coworkers: i) they characterized *in vitro* the ^{19}F-NMR signature of open and closed conformations of a Tb^{3+}-chelated form of calmodulin containing ^{19}F-tyrosine; ii) they microinjected this labelled protein into *X. laevis* oocytes with or without a binding peptide, and could monitor calmodulin conformations using ^{19}F-NMR [1196].

The structures obtained to date in cellular settings suggest that the tertiary structure of soluble folded proteins is generally unchanged. This observation may be biased by the selected set of studied proteins, i.e. small, stable proteins yielding good quality spectra such as GB1, ubiquitin and, TTHA1718. Therefore, aside of the methodological achievements, it remains to be seen whether it will be worthwhile in future to determine protein structures in cells, if the same structures can be obtained *in vitro* with much less effort. Notably, an important conclusion of these studies is that minor differences in protein conformation or dynamics are often

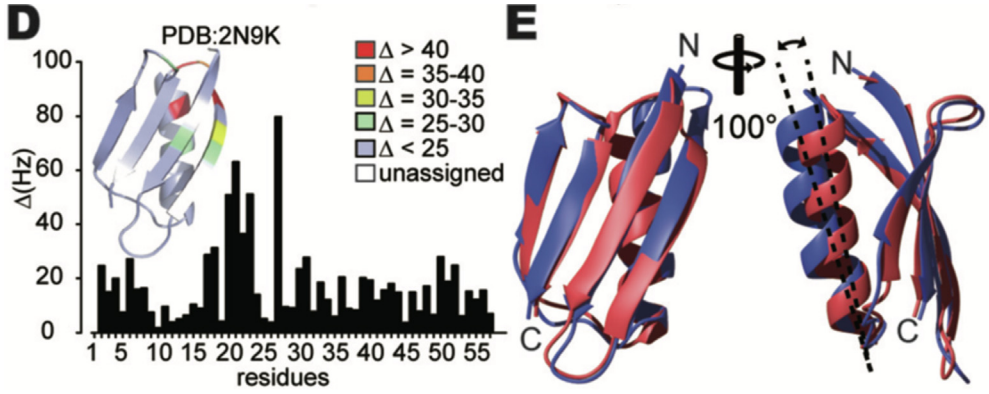

Fig. 20. In-cell NMR structure of the small model protein GB1 in insect cells. Left: backbone amide chemical shift differences between purified and in-cell GB1 at 600 MHz; Right: Overlay of lowest energy structures of purified (red) and in-cell (blue) GB1. Adapted from [1188].

correlated with chemical shift changes in the backbone resonances, meaning that chemical shift perturbation can help in the initial assessment of intracellular conformational changes at the single residue level, without needing a complete structural characterization.

2.4.2. Structural studies of membrane and cytoplasmic proteins using solid-state NMR

All the above approaches based on solution NMR are restricted to macromolecules that i) tumble freely in the cytosol, ii) are not significantly involved in diffuse interactions, iii) are not associated in large complexes, any of which cases would cause severe relaxation broadening of the signals. In parallel, solid-state NMR approaches have been developed that overcome these intrinsic limitations of solution NMR and allow the structural characterization of integral membrane proteins in intact cells or in native membranes, intracellular fibrils and – in frozen samples – soluble proteins inaccessible by solution NMR. DNP-assisted cellular ssNMR approaches have been further developed to overcome the low sensitivity associated with the use of small, fast spinning rotors.

NMR structural characterizations of membrane proteins in native cellular membranes were reported concomitantly by a handful groups in the early 2010's [1197-1200]. Tian and colleagues overexpressed the transmembrane domain (TM) of the human LR11 protein in *E. coli* using uniform ^{13}C,^{15}N. Then, they lysed the bacteria and isolated the bacterial membranes by ultracentrifugation and recorded ^{13}C-^{13}C correlation spectra, which revealed the characteristic chemical shifts of an α-helical conformation similar to that observed in DPC micelles [1198]. Similarly, Miao et al. applied ssNMR to investigate the structure of the M2 proton channel tetramer of influenza A embedded in *E. coli* membranes [1200]. The data obtained by NMR *in situ* was compared to that from the purified channel in reconstituted synthetic bilayer and revealed that, aside from small differences, the conformation of the histidine tetrad in the channel was essentially unperturbed. The same membrane extraction methodology was pursued by the groups of Oschkinat and Reif, but they took advantage of the higher sensitivity offered by the commercial DNP-ssNMR system recently developed at that time, which allowed spectra to be recorded using lower amounts of protein. Notably, they obtained structural information on a small bacterial protein in native membranes using GSTV-amino acid selective ^{13}C/^{15}N-labeling. ^{15}N-edited 3D experiments allowed suppression of the lipid resonances. Here again, the authors could observe resonances at chemical shifts corresponding to α-helical conformations in native membranes.

The Baldus group further extended the above approach to whole bacterial cells [1201,1202]. Renault et al. applied DNP-ssNMR to analyze ^{13}C,^{15}N-labeled whole *E. coli* cells overexpressing the integral outer membrane protein PagL. By comparing the whole cell spectra with those obtained at higher resolution on isolated cell envelopes, they could identify resonances of PagL and other membrane-associated macromolecules (major lipoprotein, lipopolysaccharides, peptidoglycans and phospholipids). Using ssNMR at low temperatures, the same group characterized the major components of the bacterial membrane at even higher resolution in ^{13}C,^{15}N-labeled whole cells and cell envelopes. ^{13}C resonance assignments obtained from purified samples were transferred to the native membranes with the aid of further 2D/3D experiments, allowing conformational analysis from ^{13}C chemical shifts. While lipopolysaccharides and the peptidoglycan layer were rather mobile, PagL adopted the overall rigid fold seen in the crystal structure. However, several loops and the transmembrane segments 1-3 appeared to be sensitive to the effects of the native membrane environment.

Following these seminal works, (DNP-)ssNMR was slowly but increasingly adopted and can now be considered as the NMR technique of choice to investigate structural and dynamic features of proteins embedded in native membranes. When studying proteins in heterogeneous samples such as native membranes, the cryogenic temperatures required for DNP-ssNMR decrease the spectral resolution, due to the fact that flexible proteins are frozen in many different conformations. Despite this limitation, tailored amino acid selective labeling strategies allow assignment of residue pairs and secondary structure analysis, as shown by Kaplan et al. in an exemplary application of DNP-ssNMR to investigate the megadalton-sized bacterial type IV secretion system core complex [1173]. Yamamoto et al. evaluated the suitability of a similar approach, using low-temperature ssNMR and DNP to investigate cytochrome b5, a single-pass membrane protein harboring a large soluble domain, both in intact bacteria and in artificial membranes [1203]. Conversely, Shahid et al. showed that ssNMR at higher, closer-to-physiological temperature still enabled structural and dynamic information of a membrane-anchored domain of YadA, previously overexpressed in the isolated outer membrane of *E. coli* [1204]. In this case too, the transmembrane domain of YadA was found essentially in the same conformation as for the isolated microcrystalline protein, even though the more flexible regions exhibited a more dynamic behavior.

The supramolecular assembly of the KcsA channel was further investigated by Baldus, Weingarth and their colleagues in membranes reconstituted with *E. coli* lipids [1205]. Vissher et al. combined ^{13}C-detected DNP-ssNMR with MD simulations to settle a debate about the opening mechanism of the channel, demonstrating that, in the membrane, channel gating and clustering are correlated phenomena, supporting the notion that the clustered channels can open in a concerted manner *in vivo*. An atomistic explanation of this phenomenon was given based on the observation that the gate opening/closing perturbed the structure of the N-terminal TM helix that contributes to the channel–channel interface and modulates clustering. The mechanism of KcsA gating in a reconstituted lipid bilayer was further elucidated by Jekhmane et al. through ^{1}H-ssNMR and MD simulations [1206]. Consistent with the above, mutations in a residue critical for gate selectivity were shown to cause marked changes in conformational dynamics. With the same approach, Pinto et al. investigated the bacterial β-barrel assembly machinery complex (BAM), a large multiprotein membrane complex required for the insertion of proteins into the outer membrane, in native *E. coli* membranes by ^{13}C- and ^{1}H-detected ssNMR [1207]. Fractional deuteration and amino acid-selective ^{13}C labeling strategies were employed to reduce the spectral complexity and provide structural information on the complex assembly in natural membranes. Overall, the results suggested that the various subdomains of BAM adopt the same folds observed in their detergent-solubilized complex. However, the large size and spectral complexity of the system prevented a detailed analysis at the spectral resolution reached by ssNMR. The complex assembly could be characterized in higher detail in synthetic lipid bilayers by ssNMR and DNP-ssNMR [1208].

The Weingarth group showed that (DNP-)ssNMR can provide precious atomistic insights into the mechanism of action of antibiotics bound to native bacterial membranes. For this purpose, Medeiros-Silva at al. combined high resolution ^{1}H-detected ssNMR in non-freezing conditions [1209] and DNP-enhanced ^{13}C-detected ssNMR in frozen samples to determine the structure of the pore-forming antibiotic nisin bound to its target, the peptidoglycan precursor lipid II, in native membranes from the nisin-sensitive bacterium *Micrococcus flavus* [625]. The lipid II-nisin structure in the membranes was strikingly different from that determined in organic solvents, as the nisin–lipid II pore can form only in the membrane environment. In the pore structure, flexible hinge

regions were identified that allow nisin to adapt to the target membrane, suggesting that they could be mutated to improve nisin activity towards membranes from other pathogens. The same group used (DNP-)ssNMR to further study the mode of action of teixobactins, a recently discovered class of antibiotics highly active against several pathogenic bacteria, in native *Micrococcus flavus* membranes [626]. In that work, Shukla et al. showed that teixobactins form clusters on the membrane surface and solved the structure of the teixobactin-Lipid II complex. By comparing the complex in native membranes with that formed in different synthetic micelles, it was found that the binding affinity is strongly attenuated if membranes are anionic (as is the case for *M. flavus*), suggesting that changes in bacterial membrane composition modulate the efficacy of teixobactins.

Overall, the work by Baldus, Weingarth and other groups showed that ssNMR and DNP-ssNMR approaches can provide unique contributions to the characterization of membrane proteins embedded in native membranes. Furthermore, the insights into protein dynamics obtained by solid-state NMR perfectly complement the high-resolution structural information that nowadays can be obtained by cryo-electron tomography (cryo-ET). In explorative work by Baker et al., Baldus and Grünewald combined ssNMR and cryo-ET in a hybrid approach to investigate the structure and dynamics of *E. coli* YidC, a protein of the inner membrane responsible for inserting other inner membrane proteins into native cell envelopes [1210]. The same sample preparations were analyzed by ssNMR and cryo-ET, thereby allowing the integration of the results in the same structural model without introducing artifacts arising from sample differences. The correct morphology of cell envelope samples was assessed by cryo-EM, while ssNMR revealed conformational differences with respect to YidC reconstituted in micelles. Additionally, a structural model of the ribosome nascent chain in complex with YidC was obtained by cryo-ET, albeit at low resolution due to the low number of molecules. While this method has not been applied further, the recent progress of ssNMR and cryo-ET, in terms of spectral and spatial resolution, suggest that such hybrid strategies will be crucial in the future to provide a complete atomistic description of highly dynamic proteins, which are still challenging for cryo-EM/ET (see Section 4.1.).

The above studies show that samples of bacterial cells or isolated membranes are amenable to ssNMR studies, thanks in part to the adaptability of bacteria to deuteration and to the development of protocols for single-protein overexpression and selective isotope labeling schemes. Clearly, from the sample preparation standpoint, eukaryotic cells are more demanding, as the variety of expression and labeling protocols that is available for bacteria cannot be used. Furthermore, the increased size and complexity of eukaryotic cells imposes additional limitations in terms of increased spectral crowding and decreased concentration of the molecule of interest. Despite these difficulties, Kaplan et al. showed that ssNMR could be successfully applied to investigate natively abundant membrane proteins in plasma membrane vesicles extracted from human cells [1211]. For this purpose, they focused on the human epidermal growth factor receptor (EGFR), which was found to be highly abundant on the plasma membrane of A431 cells. In the purified vesicles, EGFR retained the correct orientation with respect to the asymmetric composition of the native membrane. The dynamics of the extracellular domain of EGFR isolated from isotope-labeled cells were characterized by room-temperature ssNMR and low-temperature DNP-ssNMR, revealing an unexpected conformational flexibility, which was greatly decreased upon binding to the epidermal growth factor. According to the authors, this would imply that a reduction in conformational entropy drives the EGF-dependent activation of EGFR by contributing to the free energy of EGFR dimerization.

Unlike membrane proteins, for which the 'native environment' can be preserved to a good extent by isolating the cellular membranes in which they reside, cytosolic and other intracellular proteins must be analyzed in intact cells to avoid dilution or alteration of the intracellular environment. Compared to isolated membranes, intact cells pose additional problems such as mechanical stability and dilution of the molecule of interest. Signal enhancement by DNP has been suggested to be necessary for obtaining sufficient intensity since the first in-cell ssNMR study by the Dötsch group in 2012 [1212]. In terms of applications, Narasimhan et al. demonstrated recently that intracellular soluble proteins, which would normally be studied by solution NMR, can be characterized at the structural level by DNP-ssNMR in intact human cells [1213]. In that work, an approach relying on cell electroporation for delivering isotope-labeled proteins (previously purified from recombinant bacterial expression) [1214] was chosen. This was applied to wild type ubiquitin, which is notoriously undetectable by conventional in-cell solution NMR due to extensive interactions with other cellular components (see Section 3.2.3.). Intracellular ^{13}C,^{15}N-labeled ubiquitin was selectively observed and shown to be correctly folded. 2D and 3D DNP-ssNMR experiments provided sufficient resolution to assign unambiguously several signals to protein residues, thereby suggesting that this method could pave the way for further structural studies in intact cells.

We expect that further methodological developments in the short term will focus on the optimization of cell sample preparation, and on the application of DNP to biological samples of increasing complexity, approaching that of real tissues. Concerning the latter, the Baldus group reported very recently the first pilot DNP-ssNMR study of isotopically labeled spheroids, which are 3D cell cultures increasingly employed as high-fidelity tumor model systems [1215]. In this latter work, Damman et al. established optimal conditions for *in vitro* spheroid growth and handling for DNP sample preparation. ^{1}H-^{13}C INEPT spectra recorded on uniformly labeled cells showed different metabolic composition compared to that of the same cells cultured on monolayers. In addition, they showed that protein DNP-ssNMR was possible by observing ^{13}C-^{13}C correlations from an isotope-labeled EGFR-bound nanobody, thus opening the way towards structural biology studies in highly organized, tissue-like cell samples.

2.4.3. Disordered proteins: intracellular conformations, dynamics and interactions

The ability of NMR to probe protein conformational dynamics is of strong interest when studying the intracellular behavior of "intrinsically disordered" proteins or regions of proteins (IDPs, IDRs). By definition, these do not adopt a stable 3D structure by themselves, but can adopt ordered conformations upon binding [1149,1216,1217]. It may seem strange now, but the existence of disordered proteins was controversial twenty years ago, with some assuming that the absence of a stable fold was a simple matter of proteins waiting for a partner [1218]. However, the functionality of disordered regions in modulating binding kinetics and affinities of neighboring regions, exerting chaperoning activities, connecting multidomain proteins, transmitting cell signaling through post-translational modifications or triggering phase separation has now become clearer [1153,1219-1226]. NMR has contributed to the exploration of the physical properties of these objects, and, importantly, has allowed atomic-scale experimental observation of the existence of disordered states in cells.

How disordered proteins were affected by macromolecular crowding was one of the first questions that were tackled using in-cell NMR in the early 2000's [1227]. The highly complex intracellular environment can indeed affect the propensity of IDPs to adopt secondary or tertiary structures, to aggregate, or to modulate

their interaction with cellular partners or metal ions [6,1151,1228]. For studying these peculiar proteins, solution NMR at physiological temperatures is the technique of choice: freezing the cells would immobilize every molecule in a different conformation, preventing analysis of the conformational ensemble by ssNMR or single particle cryo-EM in most cases. Furthermore, the dynamic nature of IDPs/IDRs is advantageous for in-cell solution NMR studies: unlike stably folded proteins, where global tumbling dominates the correlation time of every residue, local dynamics at the level of individual residues in an unfolded peptide are mostly independent from each other. Therefore, while any interaction on any surface patch of a folded protein will affect global tumbling and thus cause line-broadening of all residues, only the residues directly involved in a given interaction will be affected in IDPs. This gives access to residue-level mapping of interactions even in the case of signal broadening beyond detection.

This effect was observed by Pielak and colleagues on FlgM, a polypeptide from *Salmonella enterica Typhimurium* that regulates flagellar synthesis [1227]. The bacterial environment caused signal broadening in the FlgM C-terminal half, which was attributed to a shift towards an alpha-helical conformation, that was previously observed *in vitro* [1229]. This conclusion was probably insecure at that time, because intermolecular interactions in cells would have had the same impact on FlgM NMR spectra, as was recognized later by Pielak [1230]. The opposite approach was exploited by the Shekhtman group to investigate the behavior of a prokaryotic ubiquitin-like protein (Pup) in the cellular environment. In *Mycobacterium tuberculosis*, Pup links covalently to substrate proteins and targets them to the proteasome by binding to mycobacterium proteasomal ATPase (Mpa). Maldonado et al. observed that, in the absence of Mpa, the protein remained fully unfolded in bacteria and was free from any other interactions [1231]. Using the so-called STINT-NMR approach employing mono- or dual- overexpression in *E. coli* of a pair of proteins of interest [1232,1233], the authors further investigated the interaction between Pup and Mpa in cells, and observed line broadening within the α-helical region (residues 21–51) and at the C-terminus (52-64), together with chemical shift perturbation in the C-terminal half of the α-helix, providing a mapping on Pup of the Pup:Mpa interaction [1231]. More extensive interaction was observed between Pup and the intact 1.2 MDa proteasome, leading to line broadening of most Pup signals. In later work, Majumder et al. re-analyzed the same interaction using singular value decomposition (SVD, see Section 3), in order to filter out spectral changes that were not directly caused by the Pup:proteasome interaction [1234]. They derived a more accurate set of interacting residues localized in the conserved region of the Pup α-helix, in agreement with X-ray data.

Among IDPs, α-Synuclein (α-Syn) has been by far the most studied. Its hallmark aggregates in Parkinson's patients (α-Syn is the primary component of Lewy Bodies) makes α-Syn a target of high biological and clinical relevance. In addition, α-Syn exhibits excellent stability at high concentrations and low secondary structure propensities *in vitro*. Hence, α-Syn is often used as a gold standard for developing NMR methods devoted to IDPs [396,397,1156,1157,1235-1240]. α-Syn is also found to bind lipid surfaces in cells, where the N-terminal residues 1–100 adopt an α-helical structure in their bound conformation [1241-1243]. In 2011, Bartels et al. reported that α-Syn purified from human cells adopted a tetrameric, α-helical conformation, but this interpretation was soon rejected by most of the community [1244,1245] prompting further investigation of the conformation of α-Syn in the cellular environment. The original hypothesis was said to be corroborated by a surprising interpretation of some α-Syn NMR spectra that supposedly indicated an α-helical conformation, maintained due to a milder purification strategy from the *E. coli* cells used for recombinant expression [1246]. The Selenko group provided more definitive proof that the unfolded monomer is the major conformation of α-Syn both in bacteria and human cells, independently from the N-terminal acetylation. First, Binolfi et al. showed an exact superimposition of the NMR spectra from non-purified α-Syn in bacteria and all those recorded *in vitro* [1247]. This observation has been corroborated independently by multiple groups [1236,1248,1249]. Later, Theillet et al. performed a deeper investigation of the backbone dynamics of α-Syn in human cells by NMR and EPR [1214]. The authors developed a protein electroporation approach to deliver ^{15}N-labeled recombinant α-Syn in a variety of human cell lines, both of non-neuronal and neuronal origin. Once present in the cytosol of these cells, α-Syn was quantitatively N-terminally acetylated in a post-translational fashion, as revealed by the chemical shifts of the N-terminal amino acids. This was in good correspondence with the stoichiometric acetylation of α-Syn previously shown in the human brain [1244,1245]. The whole in-cell NMR spectrum was clearly that of a disordered monomeric α-Syn in all cell lines. Residue-specific ^{15}N NMR relaxation measurements were consistent with the high degree of conformational dynamics observed on IDPs *in vitro*, even though they were slowed down by an intracellular viscosity 1.5-fold higher than that in buffer. The same relaxation rates also indicated interactions with the cytosol, the residue-by-residue analysis revealing that the central region (the aggregation-prone non-amyloid-β component, NAC) was less exposed to the cellular environment than the N- and C-terminal segments. Finally, using Gd^{3+}-loaded DOTA-derived cages linked by a thioester bond at different locations on the proteins, the authors measured intramolecular average distances by NMR and EPR spectroscopy, and could show that α-Syn adopted slightly more compact conformations in the cytosol than in buffer. All these results have been verified independently by Burrmann et al., using similar protocols, i.e. electroporation delivery in cultured human cells of recombinant, purified ^{15}N-labeled α-Syn. They showed complementarily that the intracellular N-terminal interactions established by α-Syn in cells disappeared to a large extent upon silencing of Hsc70 and HSP90 [1250]. This chaperoning had a protective role on α-Syn binding to lipid membranes, notably those of mitochondria, and later α-Syn aggregation in cells.

As previously explained, globular and unfolded regions react very differently to interactions in cells. Globular proteins soon become NMR invisible in the case of multiple cellular interactions or interactions with high molecular weight species, as observed for ubiquitin in *E. coli* [1191]. At the opposite extreme, only the interacting residues disappear in spectra of IDPs, the other segments remaining flexible and NMR visible, as observed with α-Syn [1236,1247-1249]. An interesting effect of this differential line broadening between globular and unfolded regions was reported by the Pielak group: they built a chimera of ubiquitin and α-Syn, and observed the disappearance of the NMR signal from ubiquitin but not from the α-Syn segment of the chimera [1248]. This ability to detect unfolded regions of protein constructs in cells was exploited by Pastore and colleagues [1251]. The authors compared the effect of the bacterial environment on recombinantly expressed bacterial (CyaY) and yeast (Yfh1) orthologs of human frataxin. While the globular domain of both proteins experienced intracellular interactions that caused broadening beyond detection, the unfolded N-terminal tail of Yfh1 was detected, indicating that an important population remained free from any interactions in *E. coli*.

The crowded cellular environment is expected to affect the dynamic behavior of IDRs. Among many implications, this effect may be critical for modulating the function of nucleoporins, which take part in the formation of the eukaryotic nuclear pore complex (NPC), and harbor long IDRs containing FG-rich repeats (FG-Nups)

that are responsible (together with non-FG Nups) for the selective permeability of the NPC towards macromolecules bound to specific transport factors (TFs) [1252,1253]. Hough et al. investigated at the residue-level the conformation and dynamics of two representative fragments of the FG-Nup Nsp1 *in vitro* and in bacteria [1254]. Both fragments were shown by analyzing ^{13}C secondary chemical shifts to remain highly disordered in bacteria. In addition, intracellular ^{15}N T_1 and T_2 relaxation measurements compared to *in vitro* data revealed that the regions adjacent to the FG repeats underwent interactions with the environment, while the spacer regions remained mostly unaffected. The interaction between Nup1 and a TF was further characterized in vitro, revealing a similar pattern of weak transient interactions between the FG repeats and several binding pockets on the TF, and suggesting that these constant interactions with the cellular milieu contribute to stabilizing the disordered state and preventing the aggregation of nucleoporins. Wall and Hough further investigated the conformational dynamics of Nsp1 in yeast cells [1255]. In addition to providing the first example of in-cell NMR in *S. cerevisiae*, the work showed that the bacterial and yeast cytosol interacted with the Nsp1 fragment FSFG-K in a slightly different fashion, reflecting the different composition of the two environments. Specifically, the bacterial milieu preferentially interacted with hydrophobic residues of Nsp1, while the yeast protein was more promiscuous and also interacted with hydrophilic residues.

In general, as seen in the studies cited above, the main source of information when investigating IDPs/IDRs in cells comes from changes in transverse relaxation rates. However, it is not always trivial to determine the underlying physical reasons, as increased apparent relaxation rates can be caused by decreased motions in the ns timescale (due to the interaction with macromolecules) but also by the presence of motions in the μs-ms timescale and/or by increased solvent exchange rates.

2.4.4. Protein maturation: metal binding, post-translational modifications and redox regulation

NMR chemical shifts are excellent reporters of changes in the chemical environment of amino acids such as those due to chemical modifications or non-covalent interactions. This holds true in cells and it allows the investigation of protein maturation events such as post-translational modifications, cofactor binding and redox regulation. These are often associated with changes in tertiary or quaternary structure, including sometimes the unfolded/-folded equilibrium. In this Section, we present some examples of proteins, whose proper folding was shown to depend on metal binding or redox regulation, possibly catalyzed by dedicated chaperones. Protein stability in cells is a more global question, which we treat in a dedicated subsection (2.4.6.).

NMR spectroscopy has been shown to permit the detection and real-time monitoring of protein post-translational modifications (PTMs) [1160,1163-1166,1256-1258]. The power of this approach lies in the ability of heteronuclear NMR to distinguish multiple phosphorylation events at the single-residue level. This method is particularly adapted to the characterization of PTMs on IDPs. Kinetic profiles of each species can be determined, thus providing mechanistic insights [310,1156,1160,1256]: Are residues simultaneously or sequentially phosphorylated? Are the modifications mutually exclusive? In 2008, simultaneous publications from the Selenko and Lippens groups reported the direct in-cell NMR observation of residue-specific phosphorylation in intact *X. laevis* oocytes [1259,1260]. After microinjecting a ^{15}N-labeled peptide derived from the viral SV40 large T antigen regulatory region, Selenko monitored the stepwise modification of SV40 adjacent target sites of casein kinase 2 (CK2) in intact *X. laevis* oocytes and in oocyte extracts using time-resolved ^{1}H-^{15}N-edited NMR. Moreover, upon oocyte maturation induced by a progesterone treatment, Cdk1 became activated and the simultaneous activity of Cdk1 and CK2 on the SV40 peptide was also monitored by real-time NMR. Similarly, Bodart et al. monitored the phosphorylation of the neuronal ^{15}N-labeled Tau protein after injecting it into *X. laevis* oocytes. Using ^{1}H-^{15}N-edited NMR, they detected many phosphorylation sites on the injected Tau in these oocytes, some of which may be due to PKA activity. In contrast, while using the same ^{1}H-^{15}N-edited NMR approach, Zhang, Liu and their colleagues observed that Tau prephosphorylated by MARK2 was dephosphorylated upon delivery in mammalian cells (HEK-293T) [1261]. Pons and colleagues used ^{1}H-^{15}N-edited NMR to observe multiple phosphorylation and dephosphorylation events on the recombinant ^{15}N-labeled "unique domain" of the c-Src protein in intact *X. laevis* oocytes and extracts thereof [1262]: A single phosphorylation was observed in intact oocytes, whereas multiple events were observed after prolonged incubation in oocyte extracts; they also explored the PTMs cross-talks by adding various CDKs and PKA inhibitors in the extracts. Residue-specific methionine oxidation and oxidation repair [1263], acetylation [1214] and proteolysis [1161] have also been detected in live cells. A number of reports used NMR to monitor various PTMs in cell extracts, using the same principle of real-time ^{1}H-^{15}N, ^{1}H-^{13}C or $^{15}N/^{13}C\alpha$-^{13}CO edited NMR, which we will not discuss further here (see for example [20,1156,1256,1264-1269]). ^{31}P-NMR for monitoring phosphorylation has poor sensitivity and resolution in comparison, but can sometimes be useful [1270-1273].

Phosphorylation can also be detected indirectly via spectral changes of a phospho-dependent binding partner. This rationale was used by Burz and Shekhtman to detect the phospho-dependent intracellular interaction between ubiquitin and two proteins containing ubiquitin-binding domains, namely STAM2 (Signal-transducing adaptor molecule) and Hrs (Hepatocyte growth factor regulated substrate): i) they transformed *E. coli* cells with plasmids encoding for STAM2, Hrs, ubiquitin, and the constitutively active tyrosine kinase Fyn, ii) they coexpressed STAM2 or Hrs (or chimera including both) and, optionally, Fyn in a natural abundance medium (99.6% ^{14}N, 0.4% ^{15}N) and later expressed ubiquitin in a ^{15}N-labeled medium (the opposite scenario is also possible, see Section 3.5.4.); iii) they acquired ^{1}H-^{15}N NMR spectra of ubiquitin in the presence of unphospho- or phospho- STAM2 and Hrs (with or without Fyn expression). Chemical shift perturbations in the ubiquitin spectrum upon interaction revealed how the interaction surface is affected by the substrate phosphorylation state, and notably that one of the two binding patches was lost upon STAM2 phosphorylation [1274]. A similarly indirect observation of the consequences of phosphorylation on protein interactions was provided by the Dötsch group [1275]. They investigated the intracellular behavior of the peptidyl-prolyl isomerase Pin1 in *X. laevis* oocytes as a function of its phosphorylation state: while the active, non-phosphorylated form of the WW domain of Pin1 generates very poor in-cell NMR spectra, the PKA-phosphorylated Pin1 or the WW domain in complex with a SMAD3-peptide permitted acquisition of good quality spectra with resolved signals after injection in oocytes. Hence, the authors concluded that in-cell NMR spectra of the active Pin1 suffered from the additive effects of enhanced conformational flexibility and multiple interactions with cellular components.

A change in the cysteine redox state may not be strictly speaking a post-translational modification, but it has similar consequences in terms of changes in chemical environments and thus chemical shifts. Hence, in-cell NMR has found a very interesting application in monitoring protein redox states in live cells, which is hardly achievable with any other technique. Moreover, NMR permits monitoring of the glutathione redox equilibrium in parallel. The equilibrium between the basic two cysteine forms, thiol or disulfide bond, is often accompanied by the proper folding of the

studied protein. In this case, not only do cysteines have different chemical shifts in their two forms, but large chemical shifts are also observed for all the amino acids from the domain folding upon cysteine oxidation. This has been observed using in-cell NMR for Mia40 [1276,1277], Cox17 [1278] and SOD1 [867,1279-1285]. Hence, two sets of resonances, i.e. those from the unfolded and those from the folded conformations, can emerge in the same spectrum, and their relative peak intensities give access to the quantification of the equilibrium. This showed that the intracellular redox potential, measured according to the GSH/GSSG equilibrium, is not strictly linked to the redox states of proteins as measured on Cox17, Mia40 and SOD1 in *E. coli* and human cells [1278], or on thioredoxin in human cells [475]. Chaperones are of course at least partially responsible for this discrepancy between thermodynamics and kinetic regulation. For example, the reduced, unfolded state of Mia40, which must be maintained in the cytosol before being directed to the mitochondria, is favored by an increased expression of the redox-regulating proteins Grx1 or Trx1. Other cysteine reactions can be monitored in cells, like the appearance of sulfinic acid upon H_2O_2 treatment [1286] or the formation of covalent bonds with drugs [1284].

Metal ion binding also affects protein chemical shifts. Similar to the changes associated with cysteine disulfide bonds, metal binding is often necessary for adopting the native, folded conformations, which results in extensive chemical shift perturbations for most amino acids in the domain of interest. Although in-cell NMR studies focused on the chelation of paramagnetic metals by proteins are technically feasible [1287], paramagnetic metals provoke fast NMR relaxation and thus low signal intensities in their vicinity, so that to the best of our knowledge no such studies have been carried out (not counting the in-cell NMR of hemoglobin in erythrocytes, whose NMR signals disappear upon deoxygenation but not because of the chelated metal itself [1288]). Nevertheless, Banci, Luchinat and colleagues provided a very interesting example of the importance of studying metal binding by proteins in cells: the metalloprotein copper, zinc superoxide dismutase (Cu,Zn-SOD or SOD1), whose mutant variants in humans are linked to the onset of familial Amyotrophic Lateral Sclerosis (fALS) [1289]. In order to adopt its mature, enzymatically active conformation, SOD1 must dimerize, bind one Zn^{2+} and one $Cu^{+/2+}$ per protomer and establish an intramolecular disulfide bond [1290]. SOD1 is thus quite complex to study because of these multiple layers of maturation steps. Notably, while SOD1 readily binds two Zn^{2+} per protomer in the absence of copper ions *in vitro*, this does not occur in cells according to in-cell spectra: SOD1 remains in a E-Zn-SOD1^{SH} (one metal-chelating site empty, the other one Zn-loaded) form in cells not supplemented with copper, thanks to the cellular homeostasis of zinc [1279,1280]. The full maturation of SOD1 requires the presence of higher levels of the Copper Chaperone for SOD (CCS), which is necessary for Cu^{+} insertion and is also capable of favoring the intramolecular SOD1 cysteine oxidation [1280]. In-cell NMR also allowed it to be proved that some fALS-linked SOD1 mutations, which do not perturb the structure of the final mature protein *in vitro*, prevented Zn^{2+} binding in cells and caused the formation of unstructured species [1282]. Furthermore, CCS coexpression can stabilize the correct fold of these SOD1 mutants, avoiding the formation of aggregation-prone species, thereby revealing that CCS is active as a molecular chaperone in addition to its known metallochaperone activity [1282,1283]. The same authors have also used in-cell NMR to investigate the binding of Cd^{2+} to intracellular SOD1 [1285], and that of copper and zinc to the putative deglycase protein DJ-1 [1286]: although it readily occurs *in vitro*, no sign of any such metal binding could be detected in cells, according to the absence of any chemical shift perturbations in the in-cell ^{1}H-^{15}N NMR spectra of the two proteins.

Altogether, in-cell NMR offers good capabilities to investigate redox reactions and ion binding, which can be greatly perturbed *in vitro* or upon cell lysis. Hence, in-cell NMR may be quite helpful and complementary in the pharmacological pipeline to study the impact of cellular stress or drug exposure on the proper folding and redox state of some pathogenic protein targets [867].

2.4.5. Nucleic acids

DNA and RNA are difficult polymers to study by NMR because of their large size, their relatively low chemical diversity (as compared to proteins) and the difficulties of producing isotopically labeled samples. Nonetheless, NMR spectroscopy is clearly a key approach for describing a method of choice to describe their dynamic structural ensembles, and has provided invaluable information in the field [1291,1292]. The influences of the intracellular milieu on nucleic acids are many: crowding and ion binding have drastic effects on the adoption of canonical and non-canonical structures [1293,1294].

Early studies took advantage of the 100% natural abundance of the NMR-visible ^{31}P isotope present in nucleic acids in many viruses, which in the early 1980's notably allowed exploration of DNA and RNA dynamics in viruses. ^{31}P has large chemical shift anisotropy values, which produce ~200 ppm wide ^{31}P NMR signals with powder patterns for ^{31}P nuclei of limited mobility. At the opposite extreme, isotropic motion progressively sharpens these signals. This typical broad, powder pattern ^{31}P NMR spectra revealed immobilized nucleic acids in a single-stranded RNA plant virus (Tomato bushy stunt virus, tobacco mosaic virus) [1295,1296] and in the single-stranded DNA (ssDNA) filamentous bacteriophages fd, Pf1 and M13 [1296-1299]. Relative restriction was also reported from other RNA plant viruses (southern bean mosaic virus, beladonna mottle virus, turnip yellow virus, cowpea mosaic virus, alfafa mosaic virus), but internal, low-amplitude motions of the RNA phosphates were detected on the nanosecond timescale, yielding ~20 ppm wide ^{31}P-NMR signals [1300-1304]. Pf1 DNA was found to be well-organized and uniformly oriented, while fd DNA was not [1305]. Precise structural information required ^{15}N- and ^{13}C-labeling of viruses, and their analysis by magic-angle spinning and solid-state NMR. In the late 2000's, ^{15}N-^{31}P distance measurements could be realized for T4 bacteriophage (containing double-stranded DNA) and revealed a B-DNA conformation [1306]. $^{13}C/^{15}N$ chemical shift assignments for T7 bacteriophage were also consistent with a highly ordered B-DNA conformation with a C2'-endo sugar conformation, according to the previously deposited chemical shifts for B-DNA structures [1307]. Since the early 2010's, DNA conformations of ssDNA fd and Pf1 bacteriophages have also been characterized using ^{13}C-chemical shift assignments, which were also consistent with B-DNA, C2'-endo conformations, and an *anti* conformation of the glycosidic bond, but a with a higher tendency for base-pairing in fd [1308-1312]. Important proximities between lysine side chains and DNA phosphate groups were also demonstrated in T4 and fd phages but not in Pf1 [1306,1308-1312].

Nucleic acids structure has also been studied in eukaryotic cells from the late 2000's onwards. Concentrated ^{15}N-labeled DNA oligonucleotides that can form G-quadruplexes were injected into *X. laevis* oocytes and their ^{1}H-^{15}N spectra provided direct proof that G-quadruplex structures were stable in a cellular environment [1313-1315]. Similar experiments were carried out using ^{19}F-NMR on RNA or DNA oligonucleotides containing a fluorinated moiety : ^{19}F chemical shifts were sufficiently sensitive to distinguish the G-quadruplex structures and yielded background-free NMR spectra from frog oocytes [1316-1319]. The first observations of DNA in human cells came only in 2018, using improved pore-forming streptolysin O (SLO) [1320] or electroporation [1321,1322] methods for intracellular delivery. SLO pore sealing

appears to suffer some leakage that makes cells that have been treated in this way more delicate to handle [1320,1323]. These advances have apparently unblocked the situation: in the last three years, there have been NMR studies in mammalian cells, which i) proved the stability of the DNA i-motif [1321,1324], ii) monitored DNA-ligand interactions [1325,1326], iii) showed the stability of a DNA-RNA hybrid G-quadruplex structure [1327], iv) investigated the Z-DNA conformation [1328], or v) detected the binding of a RNA riboswitch aptamer to ligands [1329]. Using DNP-enhanced MAS solid-state NMR on frozen cells, Petzold and colleagues could also observe an antisense oligonucleotide that had previously been electroporated into human cells, and whose phosphorothioate backbone shows peaks at chemical shifts that differ from the natural cellular DNA [1330]. Hence, even though these DNA oligonucleotides are not integrated in the native context of chromatin, their NMR characterization in cells is full of promise. NMR spectroscopy can report RNA chemical modifications at an atomic scale in cell extracts [1331]. Fluorination schemes for nucleic acids are regularly proposed that would facilitate in-cell NMR [1332,1333], also by allowing ^{13}C-^{19}F TROSY NMR of larger objects [1334]. Improved production protocols have emerged [1335] and Covid-19-linked research on ssRNA coronaviruses or on RNA-based vaccines will probably fuel further innovation in the field. Notably, methods to characterize cellular uptake and processing of RNA are needed [1336], among which NMR spectroscopy offers the usual advantages: it can be non-destructive and provides an atomic-scale information.

2.4.6. Protein folding, quinary structure and large assemblies

Cellular environments can affect protein folding in multiple ways. At the outset, we want to stress the fact that folding free energy or folding thermodynamics are meaningful terms only for experiments on isolated systems at equilibrium. Hence, the concept of folding free energy applies usually to an isolated system [comprising a set of purified proteins and buffer] under constant solvent conditions. In living cells, one should rather limit the analysis to the simple concept of folded/unfolded populations.

Macromolecular crowding causes excluded volume effects that can promote folding stabilization, while attractive and repulsive interactions between the crowding agents and a given protein can reinforce or weaken a protein fold [1337-1340]. Hence, a fifth level of protein structure emerges from its interactions with the ensemble of cellular species, which is *bona fide* a structural organization category, a "quinary structure" [1341], in addition to being a driving force of proteins' structural behavior (Fig. 21). In-cell NMR clearly has a role to play in studying this integrative phenomenon.

Early observations had shown that different proteins can establish what could be called different densities of intracellular interactions, as revealed by the variable NMR-detectability of intracellular proteins. In the late 1990's, Brindle and colleagues reported that two yeast enzymes showed NMR spectra consistent with a ~2 times higher viscosity in yeast cells than in buffer, while two other proteins were not NMR visible at all in intact cells, although they became detectable upon cell lysis [1179,1343]. The broadening beyond detection in the latter two cases revealed lower average molecular tumbling rates, which in turn showed that the apparent local viscosity measured for the two NMR-visible enzymes was not universal. This information was obtained by recording ^{19}F-NMR spectra of yeast cells supplemented with 5-fluorotryptophan and overexpressing the proteins of interest. Overall, this revealed differential intracellular motional restrictions. In the early 2010's, several studies attempted to understand this effect. Gierasch and colleagues measured the intracellular ^{1}H-^{15}N TROSY effect on overexpressed GB1 in live *E. coli* to extrapolate an intracellular viscosity, which was only 2-3 times higher than that of aqueous buffers [1191]. ^{19}F-labeling strategies were used by Pielak, Li and colleagues to deconvolute viscosity and cellular interactions in *E. coli* expressing recombinant GB1 and ubiquitin. While GB1 was only weakly involved in cellular interactions, ubiquitin experienced important transient, unspecific binding in the heterologous bacterial cytosol [1344]. Using ^{15}N-edited NMR, Gierasch and colleagues reported the same cellular interactions on small model proteins NmerA and ubiquitin expressed in *E. coli*, and could show that a triple mutant ubiquitin-L8A-I44A-V70A provided much bet-

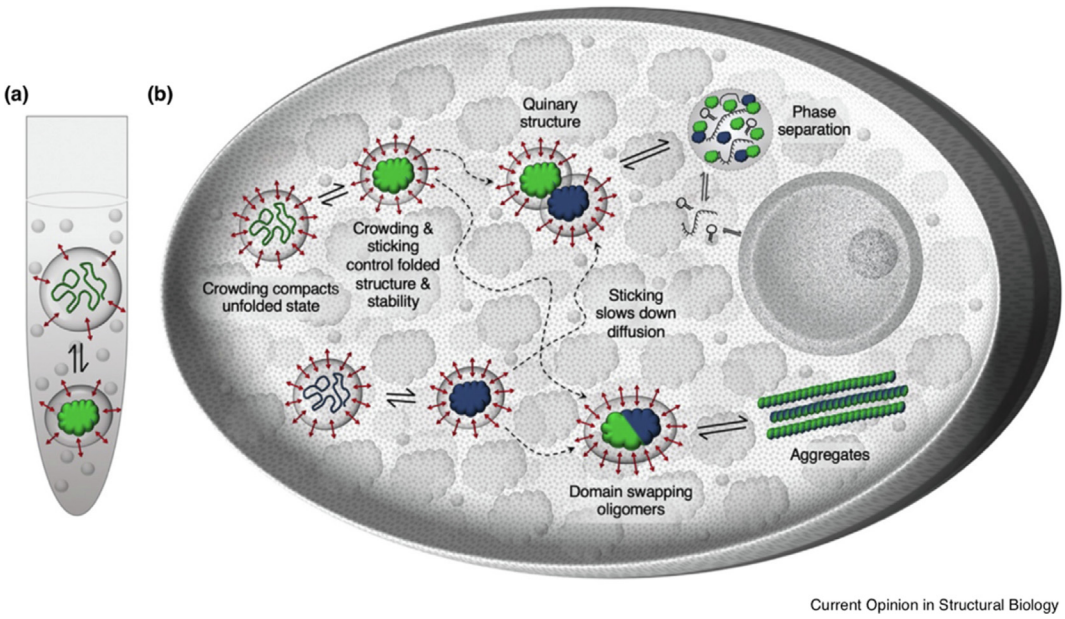

Fig. 21. Representation of the impact of quinary interactions, i.e. the interactions of a protein with its native cellular environment, which are proposed to create a fifth level of protein structure. This scheme represents the possible phenomena specific to the intracellular milieu that may affect protein stability. Unlike purified proteins in aqueous buffers (shown in **a**), high macromolecular concentrations as shown in **b**) can produce crowding, which may favor protein compactness and folding, while both specific and non-specific interactions with other cellular components may either stabilize or destabilize a protein's fold, or provoke phase separation, oligomerization or even aggregation. Adapted from Gopan et al. 2021 [1342].

ter spectra in cell lysates [1191]. Hydrophobic patches at the surface appeared to favor unspecific interactions in cells.

Hence, intermolecular interactions were mainly responsible for a certain motional restriction in cells, which provoked the broadening beyond detection of some globular proteins. The impact of these cellular interactions on protein stability had to be investigated.

Let us first extend the picture by considering also intracellular electrostatic interactions. In parallel, Crowley et al. employed a combination of in-cell NMR spectroscopy and SEC analysis to determine the origin of the diffuse interactions of cytochrome c in bacterial cells, which prevented NMR detection [1345]. By analyzing the SEC elution profile of CytC in crude cell lysates, in the presence of increasing amounts of salt, CytC was shown to interact electrostatically with negatively charged components, through a positively charged Lys/Arg-rich area on the protein surface. With the same approach, the Crowley group showed that electrostatic interactions mediated by the Lys/Arg-rich HIV-1 Tat peptide fused to GB1 induced 'stickiness' in cells and in lysates [1346], and later showed by ^{1}H-^{15}N and ^{19}F in-cell NMR that these electrostatic interactions increased gradually as a function of the length of a poly-Arg tail fused to GB1 [1347], thereby suggesting a general, non-specific interaction with negatively charged cellular components. The Banci group showed that proteins undergo both diffuse and partner-mediated interactions, depending on the composition of the cellular environment. Barbieri et al. analyzed a series of surface mutants of human profilin in the cytosol of bacterial and human cells [1348]. Profilin is a small soluble actin-binding protein that is also involved in several functional interactions with proteins harboring poly-proline regions, and with phosphoinositides. In bacteria, which lack the functional partners of profilin, a freely-tumbling protein could be obtained by mutating just the surface Lys/Arg residues, which were responsible for the diffuse electrostatic interactions, whereas in human cells the free protein was observed only after all three functional interactions were abolished by introducing mutations on specific surface residues. Both Tat-GB1 and profilin also experienced interactions in the bacterial lysate and, remarkably, it was observed that treatment with Mg^{2+} and RNase abolished the interactions, suggesting that a common cause of NMR line broadening was the interaction with bacterial RNA [1346,1348].

In the mid-2010's, Danielsson, Oliveberg and colleagues examined the effects of both hydrophobic and electrostatic quinary interactions on the NMR spectral features in the cytoplasm of *E. coli*. Mu et al. applied in-cell NMR to estimate the intracellular rotational diffusion of three evolutionarily unrelated proteins, bacterial TTHA, human HAH1, and human SOD1 β-barrel [1349]. Surface mutations were introduced on each protein to evaluate the electrostatic dependence of rotational diffusion in cells. While the WT proteins had different rotational diffusion rates, analysis of the mutants revealed that all three proteins showed a common diffusion dependence on net charge density, surface hydrophobicity and electric dipole moment, suggesting that intracellular macromolecular interactions follow a simple set of physicochemical rules. To decode these rules, Leeb et al. analyzed the intracellular T_1 and T_2 relaxation measured for the above set of proteins and charge mutants introduced in the cytoplasm of human cells, and found that they are inconsistent both with a simplistic 'increased viscosity' model [1350] and with simple exchange broadening. Instead, it fits within a theoretical framework where the anomalous T_1 increase and T_2 decrease arise from the formation of transient complexes with intracellular macromolecules, in fast exchange with the free protein. Good agreement with the experimental data was obtained when considering a proteome-like distribution of particle sizes. Fitting of relaxation data with the above model allowed estimation of the fractional population of the bound state of each protein. Proteins with a less negative net charge were found to have a higher bound state fraction, while a plot of the bound population as a function of net charge revealed the 'basal' interaction propensity of each protein, independent of its net charge.

Complementary observations have been reported by the Shekhtman group. When they first applied in-cell NMR to observe a protein overexpressed in *P. pastoris*, they observed that different metabolic states triggered a change in localization of overexpressed yeast ubiquitin [1192]. When methanol was used as the carbon source, ubiquitin was uniformly distributed in the cytosol and was detected by ^{1}H-^{15}N in-cell NMR, whereas when a mixture of dextrose/methanol was used ubiquitin was mainly localized in intracellular vesicles or granules, and was undetectable by in-cell NMR. That finding pointed to a strong connection between cellular metabolism and quinary interactions. The same group further investigated the molecular origins of quinary interactions. Majumder et al. showed that RNAs are an important component of protein quinary interactions both in bacteria and eukaryotic cells by measuring the efficiency of cross-correlated relaxation-induced polarization transfer in ^{1}H-^{15}N CRINEPT-HMQC-TROSY spectra [1351]. This approach allowed an estimation of the average size of the complexes occurring between a set of globular proteins and intracellular components. By comparing the intracellular behavior with proteins alone or in the presence of RNA *in vitro*, the authors concluded that RNA is a key component of quinary interactions. The group further investigated the metabolic dependence of quinary interactions previously observed in yeast [1192] and observed by confocal microscopy an increased colocalization between ubiquitin and RNA when *P. pastoris* was grown in a mixed dextrose/methanol medium, together with a change in the total cellular RNA content and its size distribution [1352]. In later works, Shekhtman and coworkers showed that proteins can interact with ribosomes. DeMott et al. investigated such interactions *in vitro* and in cells and observed that the enzymes adenylate kinase, dihydrofolate reductase and thymidylate synthase could bind intact ribosomes with micromolar affinity, and that such interactions modulated their enzymatic activity [1353]. GFP also interacted with ribosomes, leading to decreased translational diffusion. In later work, the group developed an NMR bioreactor and applied it to monitor in real time the behavior of intracellular thioredoxin in response to cell treatment with antibiotics binding to the small ribosomal subunit [1354]. Treatment with these antibiotics resulted in an increase of quinary interactions between thioredoxin and mRNA, further strengthening the notion that, for some proteins, quinary interactions are strongly modulated by the intracellular content of mRNA, rRNA and by the assembly state of ribosomes. Such interactions could explain the dependence of protein rotational diffusion on the intracellular metabolic state previously observed in yeast by Bertrand et al. when changing growth media [1192]. Consistently, Sugiki et al. observed a marked change in protein rotational diffusion in bacteria when inducing GB1 expression for different times and at different optical densities [1355], suggesting that metabolic changes affect the extent of quinary interactions also in *E. coli*, possibly through a change in RNA and ribosome content. Other hypotheses might also be appropriate, such as the metabolite content, the metabolic state and the capacities of the chaperone ensemble to bind to the folded and unfolded forms of the overexpressed protein, or even to catalyze their proper folding.

What is the impact of all these intracellular interactions on protein stability? The Pielak group has extensively studied the effect of crowding agents on protein folding, and turned to in-cell measurement in the early 2010's. In 2011, they observed that the bacterial cytosol could not force the folding of a protein carrying mutations, destabilizing it by only 1 kcal/mol [1356]. This implied that the stabilizing effect of volume exclusion was compensated by

destabilizing interactions with the crowding agents. To quantify these effects at the residue level, Monteith & Pielak investigated the effects of transient opening of the folded structure in the small model protein GB1 in bacteria, which system is well-suited to H/D exchange measurements by NMR. By placing bacteria overexpressing GB1 in D_2O over periods of hours, and by measuring H-amide peak intensities after quenching the exchange (at low pH/Temp) they could quantify H/D exchange in a residue-specific manner. They analyzed the impact of the cellular milieu on the free energy of fold opening and concluded that GB1 is stabilized in bacteria by about 0.75 kcal/mol, whereas crowding agents *in vitro* may have the opposite effect [1357]. However, after realizing that the intracellular pH was much lower than expected, they concluded in a correction that GB1 was actually destabilized by about 1 kcal/mol [1358]. Using ^{19}F-labeling and ^{19}F-detected NMR, they observed similar destabilization for a GB1 mutant in a later paper [470], and almost no effect on a small SH3 domain [1359], always in *E. coli*. In the next paper, using measurements of H/D exchange in bacteria, they showed that surface mutations of GB1 were more stabilizing in cells than in buffer [1360]. They noticed that this cellular stabilization was comparable to that from a classical protein-protein interaction, thereby putting at the same level functional interactions with specific partners and the non-specific cytosolic interactions. Again using H/D exchange in bacteria placed in D_2O, Pielak and colleagues explored the effect of intracellular pH [470,1361] and observed stronger destabilization of GB1 in acidic conditions. This led them to the conclusion that low pH would cause an accumulation of positive charges on cellular proteins, which, in turn, would exert increased numbers of destabilizing interactions with the negatively charged GB1. Finally, they observed a destabilization of ^{19}F-labeled SH3 in bacteria submitted to osmotic shock, which could be compensated by addition of glycine betaine [1362]. We must acknowledge the fact that there are daunting questions in characterizing quinary interactions of heterologous proteins in variable bacterial environments. It is difficult to know whether the bacterial proteome, the metabolome, chaperone activity, the amount of unfolded cellular species, etc... are constant after the cells have been transferred from H_2O into D_2O for periods of hours. It is still more difficult to think that it is the case in low pH or high salt conditions. All of these conditions might stabilize/destabilize the unfolded/folded states of the protein of interest.

The contribution of electrostatic interactions to folding stability and quinary structure in living cells was also investigated using solution NMR by the Oliveberg group. Danielsson et al. investigated the thermal unfolding of the SOD1 β-barrel, a synthetic model protein showing a simple two-state unfolding equilibrium *in vitro* [1363], which is amenable to intracellular delivery [1364,1365]. By integrating the volume of the crosspeaks corresponding either to the folded or to the unfolded species, the authors compared the temperature dependence of the "folding free energy" of SOD1 β-barrel purified *in vitro*, overexpressed in *E. coli* and delivered by electroporation in human adenocarcinoma cells [1365]. The concept of folding free energy should be taken with caution here, as discussed below at the end of this section. Consistent with what has been observed for other globular proteins in bacteria, SOD1 β-barrel was markedly destabilized in the cytosol of both bacteria and human cells, leading to a decreased melting temperature and, notably, moving both cold and heat unfolding into the physiological regime. Also in this case, the effect was attributed to interactions with cellular components that stabilize the denatured state of the protein. In most organisms, the intracellular environment behaves like a polyanionic system due to the average net-charge of the macromolecules being negative [1366]. Based on this assumption, Sörensen et al. investigated *in vitro* the destabilization of SOD1 β-barrel using polyacetate ions and observed that, similar to what is observed in cells, the apparent SOD1 destabilization originated from favorable interactions between polyacetate and the unfolded state of the protein [1367]. More recently, Iwakawa et al. studied the effect of a negatively charged crowding agent, lysozyme, on SOD1 β-barrel structure and oligomerization. Lysozyme slowed down the protein oligomerization, while NMR analysis of the monomer revealed that the interactions between lysozyme and SOD1 stabilized the latter in alternative excited state [1368].

Overall, we have seen that the intracellular environment can have disruptive effects on the NMR spectrum of a macromolecule. Indeed, the increased viscosity of the cytosol, the interactions with other cellular components and the possible alteration of the folding/unfolding equilibria result in signal broadening. This broadening commonly renders many signals undetectable when studying macromolecules by solution in-cell NMR. We discuss this more thoroughly and provide orders of magnitude concerning protein size, viscosity, multiple interactions and relaxation effects in Section 3.

We want to give a quick cautious note to conclude: varying temperature, pH or salt concentrations can have strong effects on cells, their native contents, and their capacity to maintain homeostasis, and all these can affect the studied protein. As far as in-cell studies are concerned, we recommend care using the term "folding free energy". If they are healthy, living cells are anyway not systems that let their components evolve towards thermodynamic equilibria. Examples have been reported showing that cellular stress or cell growth phase can have an impact on intracellular NMR spectra [1355,1369]. The same comments apply to other methods using thermal profiling followed by mass-spectrometry [1370-1375] or in-cell FRET readouts [1342,1375-1378]. Nonetheless, NMR experiments can reveal crowding and viscosity effects, intracellular interactions and their impact on folding and binding populations. Such knowledge will certainly help refine perceptions of protein structure and therapeutic strategies.

2.5. Cellular drug assays

Drug research pipelines have incorporated NMR spectroscopy fruitfully at several steps of drug development [1379-1381]. Here again, the versatility of NMR permits a broad range of applications, including fragment-based approaches [1382,1383], competition or affinity assays [1384], structure-based design [1385,1386], enzymatic reaction monitoring [1387], metabolic footprinting [40,1388], among others. All these possibilities have also been applied in cells [19,22]. The benefits of studying drug:target interactions directly in cells are evident: the simultaneous assessment of drug membrane permeability, cellular availability, drug:protein binding and eventually dose-dependent binding curves *in situ* is clearly appealing. Moreover, the experiments are not necessarily costly or convoluted, they are even quite simple in some cases as we show below.

More common approaches than in-cell NMR techniques exist to monitor ligand impact on cellular activities. These are discussed in Section 4.

2.5.1. In-cell drug screening through binding

Different strategies have been used to develop in-cell NMR drug screening protocols. We distinguish three categories: observing either the target, the candidate drug compounds, or a reporter of the target activity.

Shekhtman and colleagues have used the selective observation of a ^{15}N-labeled protein target, focusing on the inhibition of heterodimeric protein:protein interactions [1389]. We discuss details of the corresponding protocols for sequential protein expression in Section 3 (subsection "Protein:protein interactions"). The protein

target is observed using a ^{15}N-editing pulse sequence, so that the ^{14}N cellular content is rendered "NMR-invisible". The NMR spectra (usually 2D ^{1}H-^{15}N correlation spectra) or the protein of interest are different in the presence and absence of the interaction with the protein partner. Hence, drug screens have been performed to identify inhibitors of the interactions between i) FKBP and FRB, two components of the mTOR pathway controlling notably T-cell activation [1390], and ii) the mycobacterial ATPase MPa and the ubiquitin-like protein Pup [1391]. The compounds identified later showed inhibiting activities in yeast and mycobacteria. Luchinat, Banci and their coworkers also recently carried out an in-cell screen on human carbonic anhydrases CA1 and CA2 in cultured human HEK293T cells [1392]. The study was facilitated by the fact that CA1/CA2 histidine side chain amide protons yield NMR signal in a remote, usually empty region of ^{1}H-NMR spectra, between 11 and 16 ppm. Drug binding was detected by CA1/CA2-histidine peak shifting in one-dimensional ^{1}H-NMR spectra. In principle, about 100 compounds may be screened per week using such a setup, in combination with the matrix approach employed by Shekhtman. Although it requires prior cell transfection and overexpression of the target protein, this approach permits detection of the binding of a compound to the enzymatic site of a human protein target in a human cellular background. Even better, it can report the dissociation of a compound from its target, revealing possible engagements with off-target cellular entities [1393].

Enzyme activity reporters have been shown to be promising instruments for in-cell NMR drug screening. Breeze, Hu and their coworkers have for example used meropenem, an antibiotic degraded by the New Delhi metallo-β-lactamase subclass 1 (NDM-1), an infamous bacterial drug resistance enzyme. They first established real-time monitoring of meropenem hydrolysis by NDM-1 overexpressed in live *E.coli*: methyl NMR signals of intact and degraded meropenem are not the same (Fig. 22), and can be used as reporters of progress of the reaction using one-dimensional ^{1}H-NMR spectroscopy [1394]. Next, these cells were grown in 96-well plates, exposed to a collection of compounds and NDM-1 inhibition assessed by integrating NMR signals of intact and decomposed meropenem after quenching the reaction [1395]. The authors calculated that their protocol would permit screening of about 10,000 compounds per week. Garau, Dalvit and their coworkers used a similar approach, but this time by recording ^{19}F-NMR one-dimensional spectra of ARN1203, a fluorinated analog of the cannabinoid neurotransmitter anandamine. Its ^{19}F-moiety has different chemical shifts before and after ARN1203 degradation by the fatty acid amide hydrolase (FAAH). The corresponding NMR peaks proved to be valuable probes of FAAH activity *in situ*, as shown using membrane extracts of HeLa cells overexpressing this protein [1396]. HEK293 cells overexpressing FAAH in 24-well plates were later used to screen compounds [1397]. This approach is appealing: it relies on simple, sensitive, background free ^{19}F-NMR spectroscopy [1387,1398] of the supernatant pipetted from the culture plates. Moreover, it allows an approximate cell toxicity assay by using ^{1}H-NMR for the quantification of lactate production [1397].

As shown in subsection 2.3. "Metabolic activities" (see above), a number of molecules probing specific cellular activities using an NMR-readout have been developed. Many of them may be useful instruments for in-cell NMR drug screening. In particular, other cleavable ^{19}F-reporters have been published to detect specific enzyme activities in cells [1399,1400]. MRI ^{19}F-reporters for detecting enzymatic activities have also been developed: they contain a paramagnetic moiety, which destroys the NMR signal of the ^{19}F moiety as long as the reporter is intact; upon cleavage by the enzyme of interest, the two moieties are separated and the ^{19}F NMR signal becomes observable [137,1401,1402]. These have often been tested in cells [1403-1407] and some of them may be used for drug screening. Other ^{19}F-, ^{13}C- or ^{15}N-labeled reporters of kinase activity [1408,1409] or methionine sulfoxide reductase [1410] may also be useful for example.

To the best of our knowledge, ligand-based NMR detection has not been used to achieve drug screening in live cells. The most closely-related study that we found was a Saturation Transfer Difference (STD-NMR) screening study of Rademacher and Peters on norovirus virus-like particles (VLPs, auto-assembled particles made of viral capsid proteins) [1411]. The usual NMR screening methods, like STD-NMR, waterLOGSY, or relaxation weighted spectroscopy detect weak interactions showing affinities in the micro- to milli-molar range and fast association/dissociation [1386,1412]. Hence, they are likely to generate high rates of false positives, even when recording experiments with and without expression of the protein target: weak interactions can be detected with cellular content, which itself is not perfectly reproducible and constant. Nikolaev, Allain and their coworkers have for example detected significant numbers of weak interactions between metabolites (notably those containing aromatic rings) and common *E. coli* proteins [1413,1414]. This implies that the metabolic states should be very similar between cell aliquots to avoid different competition levels between screened drugs and metabolites. These ligand-based NMR

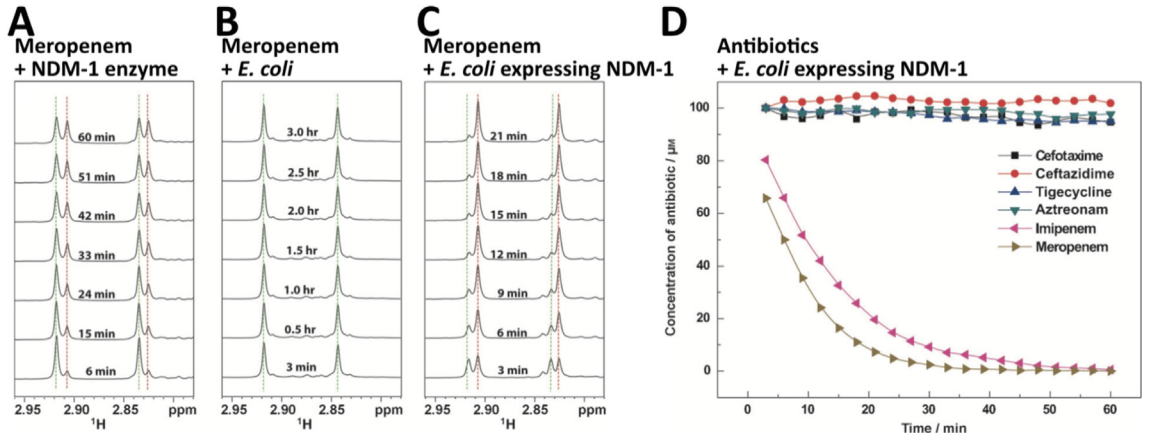

Fig. 22. ^{1}H-NMR analysis of antibiotic degradation by living bacteria: times series of spectra can be recorded, which report notably the evolution of antibiotics in the supernatant in real-time. **A)** One-dimensional ^{1}H spectra showing the progressive hydrolysis of Meropenem by purified NDM-1 drug-resistance enzyme, **B)** in presence of living cells of a standard *E. coli* strain and **C)** in presence of an *E. coli* strain expressing NDM-1. **D)** Time-dependent evolution ^{1}H-NMR signal intensities of various antibiotics in presence of *E. coli* cells expressing NDM-1.

detection methods (STD-NMR, TRNOE, waterLOGSY,..) are thus more adapted to "on-cell NMR" studies, which we detail below.

Other methods using paramagnetic tagging of protein targets [1415,1416] may be better adapted to these kind of assays: they may permit a more specific signal broadening of compounds binding to a defined protein carrying a paramagnetic center. We would not be surprised to see such approaches being developed in the coming years.

2.5.2. Drug modes of action and cell penetrance

The present subsection presents two aspects of drug treatment, which relate to i) the effects of drugs on the overall profiling of cellular composition, and ii) the detection of NMR signals revealing intracellular drug molecules, hence drug penetrance in cells. To some extent, this subsection covers studies that were also presented in Section 2.2.2., which treated the characterization of peptidoglycan and its interaction with antibiotics, and Section 2.3., which focused on monitoring metabolism, sometimes in presence of drugs. Hence, we will not repeat here explanation of the principles of NMR readout used in these studies.

The mechanisms of action of antibiotics have been studied on intact cell walls from the early days of NMR in biology, and on whole cells from the 2000's. Early solution NMR observations had revealed that the peptidoglycan (PG) residue ^{15}N-D-Ala of the Gram-positive *B. licheniformis* became more mobile upon exposure to vancomycin [582]. Lower cross-linking in PG was later observed in the presence of penicillin G or benzylpenicillin, using ^{15}N CPMAS solid state NMR of the isolated cell walls of *A. viridans* labeled with ^{15}N-Lys [584,1417]. Because the PG of *B. subtilis* does not contain any lysine, the incorporation of L-[2-^{13}C-^{15}N]-Asp was used to record ^{15}N-REDOR-filtered ^{13}C-solid state NMR spectra and to evaluate the decrease of PG cross-linking index upon cephalosporin treatment [595,596]. In the 2000's and 2010's, combinations of ^{13}C- and ^{15}N-amino acid supplementation were used to execute isotopic ^{13}C or ^{15}N-REDOR-filters followed by ^{15}N- or ^{13}C-NMR detection, which allowed quantification of PG cross-links on bacterial cells exposed to various antibiotics (notably vancomycin, amphomycin, plusbacin, oritavancin on *S. aureus* and *E. faecium*) (Fig. 23) [578,597-601,610,615,619]. The effects of antibiotics on D-Ala incorporation in the surface teichoic acid polymer have also been scrutinized by solid state NMR of Gram-positive bacteria [589,598,599,615,620,621]. Lately, Cegelski and coworkers have also reported solid-state NMR ^{13}C and ^{15}N spectral signatures of whole bacterial cells at natural abundance, which allow the relative quantification of PG and WTA, thus permitting a rapid evaluation of the mechanism of action of antibiotics [579,1418]. Similar applications may emerge for the analysis of bacterial or fungal extracellular matrices [1419,1420] or mammalian cells, whose whole-cell solid-state NMR spectra show visible changes depending on their metabolic state [1421,1422] or upon protein synthesis inhibition for example [1423]. The level of accuracy on the metabolic state provided by ssNMR is however rather limited and probably less adapted to the characterization of minute metabolic changes in mammalian cells. HR-MAS NMR is more likely to provide useful insights in such situations (see Sections 2.3.5. and 3.3.4.). It has indeed been used to study the effects of cell exposure to various compounds like chemotherapeutic agents [1008-1014] or pathway activators [990,1015,1016]. Unless it is performed at low spinning rate, HR-MAS does affect cell viability and does not permit real-time NMR monitoring of cells upon drug treatment.

The drug mechanisms can also be characterized on a structural level. We described in-cell studies aiming at mapping drug candidate epitopes in Section 2.6. Concerning proven drugs and their tridimensional structures *in situ*, we found mostly reports on antibiotics. Since the 2000's, using similar solid-state REDOR NMR spectroscopy, Schaefer and his coworkers progressively revealed the structural details of drug binding in bacterial cell walls. The presence of ^{19}F nuclei in antibiotic molecules has been helpful, because it allows ^{13}C-^{19}F or ^{15}N-^{19}F REDOR measurements for example. Hence, coupled with ^{13}C- or ^{15}N-amino acid specific

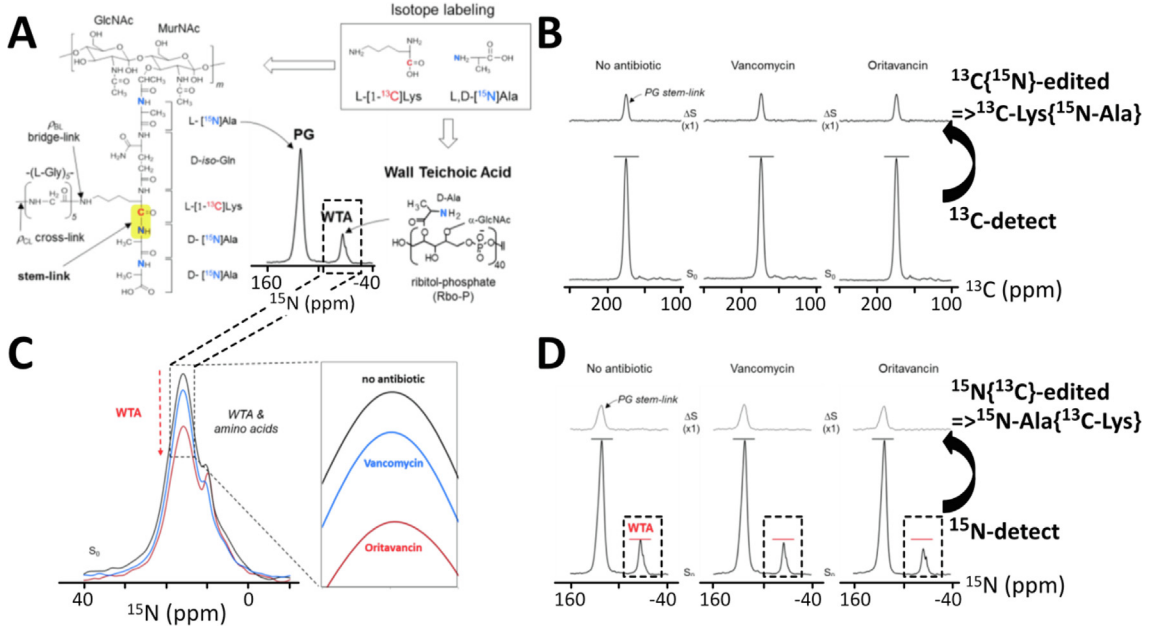

Fig. 23. Example of an application of solid-state NMR (ssNMR) to whole bacterial cells (*S. aureus*) to characterize the effects of antibiotics: here, vancomycin and oritavancin inhibit the incorporation of D-Ala in wall teichoic acid (WTA). **A)** The cells are grown in a medium supplemented with L-[1-^{13}C]Lys and L,D[^{15}N]-Ala, which are incorporated in the peptidoglycan (PG) and wall teichoic acid; only the ^{15}N-NMR signals of constrained species are visible using solid-state NMR techniques. **B)** ^{13}C-ssNMR spectra using REDOR methods showing either (lower) ^{13}C-labeled species, here mostly L-[1-^{13}C]Lys, or (upper) ^{13}C-labeled species bound to ^{15}N-labeled species, i.e. L-[1-^{13}C]Lys-{D[^{15}N]-Ala}. **C)** Close-up view of ^{15}N-NMR spectra of whole *S. aureus* treated either with no antibiotic, with vancomycin or with oritavancin. **D)** ^{15}N-ssNMR spectra obtained using REDOR methods showing either (lower) ^{15}N-labeled species, here mostly [^{15}N]Ala, or (upper) ^{15}N-labeled species bound to ^{13}C-labeled species, i.e. D-[^{15}N]Ala-{L-[1-^{13}C]-Lys}. Adapted from Singh et al. 2017 [621].

labeling, this allows combined isotope editing and internuclear distance measurements for those rare events where antibiotic molecules bind to PG precursors [578,589,597,600,607-609,619,1424]. Other ssNMR studies have been carried out to solve the structures of nisin or teixobactins binding to the bacterial Lipid-II in native membranes, using recently developed ^{1}H-detected ssNMR techniques and equipment (see Section 2.4.2.) [577,625,626].

An important aspect of drug activity is the ability to penetrate cells. In many cases, the process starts with entry of a cell-penetrant pro-drug followed by its intracellular chemical modification to generate the final active compound. NMR spectroscopy has interesting capabilities in this regard, because of its atomic scale resolution combined with real-time measurements. These were explored by Lippens and colleagues in the early 2000's, to monitor the pro-drug ethionamide penetration and activation in mycobacteria using HR-MAS NMR [1023,1024]. We have seen earlier that NMR is very well suited to characterize diffusion coefficients, and Lippens and coworkers used this ability to distinguish intracellular from extracellular molecules by employing diffusion filters within pulse sequences to separate signals. This provided a definitive proof and time-monitoring of the localization of the prodrug. More recently, Luchinat, Banci and their coworkers tracked drug penetrance by observing the NMR signal displacements of a protein target, the human carbonic anhydrase 2 (CA2) [867,1392,1393]. After its overexpression in cultured, transfected cells, this protein provides ^{1}H-NMR signals in empty windows of the spectrum, because of its catalytic histidines, whose side chain imidazoles generate slowly exchanging NH resonances at 11-16 ppm. These resonances shift upon binding to drugs, thus reporting notably drug cell penetrance. This approach may be adapted to a number of protein targets, but it requires of course finding convenient, well-observable NMR signals that report drug-protein binding. Hence, it will probably require finding a specific amino acid isotope labeling adapted for every novel target.

2.6. Epitope mapping, structure-activity relationship

Structure-activity relationship (SAR) studies refer to hit or lead compound optimization, which has been a recognized application of NMR to structural biology for about 25 years [1425-1427]. Extensive details about the typical methods dedicated to SAR by NMR (STD-NMR, TRNOE, waterLOGSY, and others) can be found in these latter citations, and will not be discussed further here; specific examples of applications to cellular samples were discussed in Sections 3.4.2 and 3.4.3.

2.6.1. Virus receptors

We will first mention NMR studies of virus:ligand interactions. We will not take part in the debate of whether viruses are really cells or live organisms, which probably depends very much on the chosen definition of life [1428,1429]. However, virus:ligand NMR investigations are included here, because they represent an important body of work in the development of on-cell NMR studies. NMR spectroscopy can indeed help to map the epitopes of ligands binding surface proteins of viruses. This is of interest because many viruses attach to cellular surface glycans to favor their entry into appropriate host cells, which also often implies the existence of a glycan-cleaving enzyme for the later release of replicated virus particles [1430-1432]. Hence, characterizing these recognition events can help to understand viral infection mechanisms, including possible inter-species or inter-individual transmission, and to design antiviral therapeutics [1433-1437].

In 1992, the first publication that we found in this field reported the use of intact H3N2 influenza virus at 2-4 g/L and the observation of ^{1}H-NMR signals of sialoside oligosaccharides upon titration from 1 to 20 g/L [1438]. Binding affinities in the millimolar range were extracted and the virus preferences for the various surface oligosaccharides were discussed. This approach required high quantities of virus and of glycans and was likely to provide information only on weak affinity interactions. The situation was improved by the exploitation of Saturation-Transfer Difference NMR (STD-NMR) spectroscopy, a concept already exploited in the late 1970s' [1439-1441] that can provide a spectroscopic footprint of binding epitopes (a number of dedicated reviews have been published on this subject, see [1384,1442,1443]). Soon after being recognized as an efficient drug discovery method in the late 1990's [1412], STD-NMR was used to map the epitope of an antiviral compound binding to human rhinovirus particles [1444]. These results were obtained using a virus concentration of 20 nM, i.e. 170 mg/L, and antiviral compounds at 120 μM. Similar STD-NMR studies described glycan preferences of virus-like particles, i.e. assemblies of viral structural proteins that do not contain any viral genetic material. The molecular basis of glycan epitope recognition was described at the atomic-scale for various influenza serotypes [1445-1447], rabbit hemorrhagic disease virus [1448], bovine norovirus [1449], rhesus rotavirus [1450], and human norovirus [1411,1451,1452].

Virus-like particles have also been used to detail the interaction between peptide inhibitors and hepatitis B virus [1453], and between fusion inhibitors and influenza hemagglutinin [1454]. In the last 5 years, investigators reported studies using whole virus particles to understand the adaptation of various influenza serotypes to different glycans and thus different species [1455,1456], to verify the proper binding of fluorescent probes to enteroviruses binding [1457], and to map the epitopes of compounds inhibiting the entry of the enterovirus EV71 [1458].

Recently, Vasile and colleagues published STD-NMR studies using transfected mammalian cell lines stably expressing functional influenza hemagglutinin on their membranes: using 10^{7} cells and avoiding purification steps, they could achieve a rapid epitope mapping of various ligands [1459,1460]. The wealth of structural information from all these STD studies would be difficult to describe fully. The corresponding results may be seen as overlapping with those of mass-spectrometry, glycan arrays or crystallography. However, results from isolated viral receptors can often be unreliable [1461,1462], crystal structures of protein:glycan complexes are often limited to the resolved description of very few glycan residues, and studies on viral particles clearly provide a useful support to the *in vitro* toolbox [1463].

2.6.2. Mammalian membrane proteins

Mammalian cell transfection has also been useful to characterize the binding epitopes of drug candidates targeting membrane proteins by NMR spectroscopy *in situ*. Membrane proteins represent an abundant reservoir of drug targets [1464], but difficulties with their purification and stability for *in vitro* studies often make their study extremely problematic.

In this context, STD-NMR has the capacity to provide ligand mapping without the classical purification steps. Jimenez-Barbero and colleagues published a proof of concept in 2005, where they showed that mannan STD-NMR signals were detected in the presence of K562 cells transfected with the immune system lectin-like receptor DC-SIGN, but not with mock-transfected cells [1465]. This approach was applied to a human Golgi resident nucleotide sugar transporter (called CST) expressed in *Pichia pastoris*: STD signals of CMP-sialic acid were recorded in the presence of Golgi-enriched fractions of cells either expressing CST or not [1466], and, in a subsequent study, expressing CST mutants that affect binding or saturation transfer [1467]. In the absence of 3D structural data, this provided a primary mapping of the interaction both on the ligand and on the membrane-protein. Similar experiments were carried

out on GDP-mannose and the GDP-mannose transporter of *Aspergillus niger* [1468].

The extremely important drug-target family of G-Protein Coupled Receptors (GPCRs) has also been studied by on-cell STD-NMR spectroscopy, confirming *in situ* binding of ligands on i) insect cells expressing and exposing human cannabinoid receptors (the NMR samples containing 5.10^6 cells/mL exposing the receptor at about 100 nM) [1469]; ii) membrane fractions of mammalian cells expressing the human sweet receptor and an inactive mutant [1470,1471], the chemokine receptor CXCR4 [1472], and the thiol odorant receptors MOR244-3 [1473] and OR2T11 [1474] (the NMR samples containing about 10 nM of the relevant GPCRs). These studies often report STD signals even without expression of the receptor, probably because of unspecific interactions of the tested hydrophobic ligands. Spectroscopists have thus used Saturation Transfer Double-Difference (STDD-NMR) by subtracting the STD signals obtained in presence and absence of receptor expression. Naturally, this compromises sensitivity. However, such experiments provided direct evidence of GPCR binding, and led to an epitope mapping. This approach is highly complementary to the more common luciferase GloSensor assays, which report end-point, indirect evaluations of GPCR activation through cAMP production [1472,1474].

Another issue comes from the tendency of adherent mammalian cell lines to aggregate and settle, which often forces the use of suspension cells or membrane fractions. Jimenez-Barbero and colleagues proposed a solution: they introduced 1 million cells in a 4 mm diameter cylindrical sample container, conventionally called a "rotor", and spun them between 1 and 4 kHz using a HR-MAS probe (see Sections 2.2.3. on LPS, 2.3.5. on lipids and 3.4.3. for specific discussion of HR-MAS). This caused cell sedimentation and the formation of a homogeneous layer on the rotor walls, which permitted STDD-NMR measurements for a glucose co-transporter and some ligands [1475].

This sedimentation issue is one of the reasons that pushed spectroscopists to use slow-settling platelets for a number of early on-cell STDD studies. Another convenient aspect when using platelets is their very high content of integrin $\alpha_{IIb}\beta_3$ (1-5.10^4 per cell, about 50% of membrane proteins [1476]), which is required for platelet aggregation. Combined with a low cytoplasmic volume, platelets were thus ideal for early characterizations of ligand binding to intact mammalian cells by NMR (integrin $\alpha_{IIb}\beta_3$ was at a concentration of about 600 nM in the NMR samples) [1476]). Because native ligands of integrins are short peptides containing an RGD motif, resolving their receptor-bound conformations was of considerable interest. Another NMR method known for a long time, named TRNOE, had been developed for such applications: it detects the large negative NOE of slow tumbling species, which reveals a footprint of the bound-ligand conformation (via interatomic distances) even though it is detected on the free ligand population [1412,1477]. Applied to platelets, the measured TRNOE allowed the bound conformations of two cyclic RGD-containing peptides to be solved [1478]. TRNOE spectroscopy was later used to characterize the interaction between RGD-containing peptides and the integrin $\alpha_v\beta_3$ expressed at high levels by certain cancer cell lines (generating nM range concentrations in the NMR samples) [1479-1484], or with the integrin $\alpha_v\beta_1$ [1485,1486]. These studies led to design of RGD-containing peptidomimetics showing improved affinity and specificity for the studied integrins. Recently, STD epitope mapping was carried out for the large protein osteopontin binding to integrins, using mammalian cells entrapped in a methylcellulose hydrogel [1487], which seems to us a promising approach.

In the last 5 years, two remarkable on-cell STD-NMR studies led to the progressive design of high-affinity ligands of the B-cell receptor Siglec-2 [1488] and of CXCR4 [1489]. STD-NMR or TRNOEs also confirmed the binding of some peptides to the vascular endothelial growth factor receptors VEGFRs [1490,1491] or the angiogenesis associated CD13 [1492], and permitted mapping at a residue-scale of the Bombesin peptide interaction with the GPCR Gastrin Releasing Peptide Receptor (GRP-R) [1493].

Finally, another interesting approach was explored by Izadi-Pruneyre and colleagues, aimed at providing direct experimental evidence of drug binding to a putative membrane protein target [1494]. A series of candidate drugs against *Mycobacterium tuberculosis* had been discovered, and the QcrB subunit of the cytochrome bc_1-aa_3 complex had been identified as its target from spontaneous mutant strains. STD-NMR experiments were performed on live bacteria cells, expressing either the wild type or the resistant mutant of the QcrB subunit, exposed to one of these new drugs: i) STD signals from the drug were observed only in the presence of the wild-type QcrB, therefore confirming the identity of the drug target; ii) the relative intensities of the STD signals gave clues about the chemical moieties that were the most engaged in binding pockets. This method is perfectly complementary to the chemical and genetic approaches that led to discovery of the drug series, and thus sets a stronger basis for the future drug developments.

3. In-cell NMR theoretical and practical considerations

3.1. A historical aside: the beginnings of NMR of biological material

In this section, we sketch a brief historical summary of early NMR work on biological tissues and cells. Many initial misinterpretations were resolved only later as the subject progressed. We have included a discussion of these here, in part because we feel they have historical interest, but also because some of the incorrect theories described below were still cited and re-employed by non-specialists after they had been disproved.

3.1.1. Early controversies in NMR studies of water (1950-70's), and what can be learned from them

As early as 1950, Shaw, Palmer and Elsken carried out NMR studies on water in biological material such as apple, potato and maple wood to establish a method for water content quantification [1495]. The NMR signal was measured by low resolution nuclear magnetic absorption at that time, and the authors soon discovered that the correlation between measured intensities and water content was not perfect [1496]. They realized for instance that "soluble solids" such as carbohydrates, proteins or fatty acids were contributing to the NMR signal from apple tissues or in milk, whereas starch in potato tissues made negligible contributions [1497-1500]. Hence, to be accurate, NMR quantification of water required a prior estimation of these soluble species. They noticed however that these solutes were causing broader linewidths for the observed signal, and suggested that characterizing these linewidths might provide a method to investigate the interaction between water and the non-aqueous species [1495-1497]. They also pointed out that T1 relaxation became faster as the viscosity increased in sucrose and gelatin solutions [1499], in agreement with earlier results from Bloembergen, Purcell and Pound [1501]. Faster T1 relaxation had also been reported in various rabbit tissues and in yeast cells by Odeblad and Lindström in 1955 [1502]. These T1 rates would later be connected explicitly to molecular correlation times and the nature of the surrounding spin lattice. Odeblad and Lindström also quantified the water exchange rate in red blood cells by measuring their remaining water ^1H signal after incubation in D_2O. The authors acknowledged however the progressive appearance of deoxygenated hemoglobin, whose paramagnetism would cause faster relaxation times and lower apparent signal strength, as shown earlier independently by Bloch,

Bloembergen et al., and Odeblad et al. [1503-1505]. Hence, in 1956, these first studies had already established the observables and the parameters that would be scrutinized in cellular studies in the decades that followed: signal intensity, linewidth and relaxation times could be related to molecular composition, chemical exchange, viscosity, chemical environment and the effects of paramagnetic species.

The next two decades of NMR research on water in living samples were nevertheless controversial, at least in part because all of these parameters can influence all of these NMR observables. Different interpretations as to what was the dominant parameter causing intensities to be missing could easily emerge and be argued. Hence, the field became involved in two major controversies. The first one has its origin in a model, that in retrospect seems surprising, from Gilbert Ling, who disputed the existence of cellular cation pumps and their function in regulating transmembrane cation concentration gradients: these would have cost too much energy to the cell in his view. Instead, he had proposed since the 1950's an "association-induction hypothesis" leading to the model of a "polarized-oriented multilayer" of structured cellular water and Na^+/K^+ ions in cells [1506-1508]. This sounds strange now that cation pumps are well-established, that venom and drugs targeting them are known, and that several Nobel prizes have been awarded to researchers in the field. In fact, it did already sound awkward to a number of contemporaries, but during the 1960's some experimental results were published that were consistent with this controversial theory [74,1509-1515]. These papers reported line broadening and relaxation rates of the water NMR signal in animal tissues, notably upon muscle or nerve excitation. The results were interpreted in the framework of a two-phase model, with one minor "liquid" population and one major "solid" or "ice-like state" population of water molecules. These interpretations were also supported by other NMR experiments on Na^+ and K^+, but, as discussed in a later section, these latter experiments proved to have an incorrect interpretation of "invisible" signal. Among others, Cope, Hazlewood and Damadian became involved in the debate [1516], which became more complex once Damadian and others reported variations of T1 relaxation rates in tumors and in normal tissues in the 1970's, again in highly influential journals [1517-1520]. Damadian adopted the model of Ling [1517,1521], which provided a framework to describe the loss of water structure as a hallmark of cancer cells, and his findings led him to promote NMR as a method to detect tumors. While his support of the model of Ling proved to be mistaken, Damadian's recognition of the possibility of using relaxation properties to distinguish tumors from healthy tissue encouraged the development of MRI (see [1522] for review). Another positive outcome was that the controversies, which were hotly debated (see [1521]), pushed the community to propose better explanations during the 1970's. To summarize these results briefly, with hindsight the incorrect interpretations proved to arise from i) an inability to detect the early, rapidly relaxing components of NMR signals, which in turn resulted from using materials and equipment that required delays between excitation and acquisition, and/or ii) the use of imperfect models [197,272].

Indeed, physicists working in the field determined several possible mechanisms that would affect T1 and T2 relaxation rates of water. Water T1 relaxation rates in cells and tissues were found to be correlated with water content [1523-1526], which varies, for example, between different organs. Thus, water T1 and T2 appeared to be an ambiguous parameter for diagnosis in the mid-1970's (a good review appears in [1526]). Intracellular T2 relaxation could be interpreted in terms of multiexponential regimes, and accelerated notably i) by chemical exchange between bulk water and water molecules in the hydration layer of macromolecules, ii) by the diffusion of water molecules in magnetic field gradients generated by heterogeneous magnetic susceptibility, iii) by the exchange between intracellular and extracellular media, iv) by the progressive appearance of paramagnetic species due to hemoglobin deoxygenation and the release of reactive oxygen species in tissue samples [73,1527-1534]. The physics of these interactions was not straightforward, and the quantification of their effects remains an active subject for study, notably to achieve a good understanding of Blood Oxygenation Level Dependent (BOLD) MRI (see Section 3.2. and the following references [79,1535-1537]). Fortunately, the introduction of injectable paramagnetic agents contributed substantially to the success of MRI, by strongly affecting water NMR relaxation rates and thus generating simpler T1- or T2-weighted imaging contrast.

3.1.2. The case of quadrupolar nuclei

Quadrupolar nuclei require careful manipulation during NMR experiments. Their fast relaxation is accelerated by dense and heterogeneous cellular environments. We will not discuss the theoretical background to this, which would be well beyond the scope of this review (see for instance [263,1538,1539]). Instead, we present this as a historical discussion, complementary to the previous subsection on water.

We start by discussing the impact that ^{39}K NMR studies made on the understanding of intracellular K^+ dynamics. Similarly to what happened with ^{23}Na, ^{39}K NMR spectroscopy started with the observation by Cope and Damadian in 1970 of limited "NMR-visibility" of the intracellular pool of $^{39}K^+$: only 30-40% of the expected signal could be observed in cells by NMR [269]. In the late 1960's, a fundamental debate on the nature of the cellular solvent took place: this low signal was interpreted as an argument in favor of limited ^{39}K dynamics in cells, and thus in favor of the existence of an organized, semi-crystalline intracellular solvent. The tenacity (see [1521]) of its champions had long-lasting effects on the debate in the literature. This model was however not compatible with diffusion and electrical conductivity measurements [270]. This motivated some NMR spectroscopists to try to better understand and characterize ionic dynamics, which in turn implies trying to better understand and characterize quadrupolar relaxation, since these ions are quadrupolar. As a result, ^{39}K NMR signal intensity and relaxation were thus quantified in multiple systems and correlated with the relaxation theory of quadrupolar nuclei. ^{39}K studies showed that K^+ was freely mobile in vacuoles of pea stem, which are very aqueous in character [193,194]; low percentages of immobilized K^+ were estimated in frog muscle [271] and halobacteria [1540]; 100% ^{39}K signal, i.e. 100% free K^+, was observed in duck erythrocytes, which contain nuclei and mitochondria, and in mammalian erythrocytes, which do not [218].

Theoretical frameworks had been provided as early as 1970, and through the 1970's by multiple groups: in a cellular environment where $^{23}Na^+$ and $^{39}K^+$ interact even very weakly with macromolecular assemblies, their spin 3/2 and quadrupolar nature would result in the appearance of a fast-relaxing component affecting 60% of the total expected NMR signal [196,270,1541-1545]. This fast-relaxing signal could be detected only with advanced equipment. Consistent with this, Shporer and Civan had shown experimentally from 1972 that $^{23}Na^+$ and $^{39}K^+$ showed multiple T2 relaxation components in non-homogeneous samples where these ions could interact transiently, including frog muscles and halobacteria [195,196,271,1540]. Although this framework became consistent and had good predictive power [202,336,1546], the controversy continued during the 1980's, and different groups regularly reported low $^{39}K^+$ intensities equivalent to ~40% of the expected signal in yeast [200], in rat hearts [225,1547], and in *E. coli* [276]. The experimental proofs were broadly agreed only in the 1990's, showing that the observation of the fast and slow components of the intracellular ^{39}K signal required a number of advances in

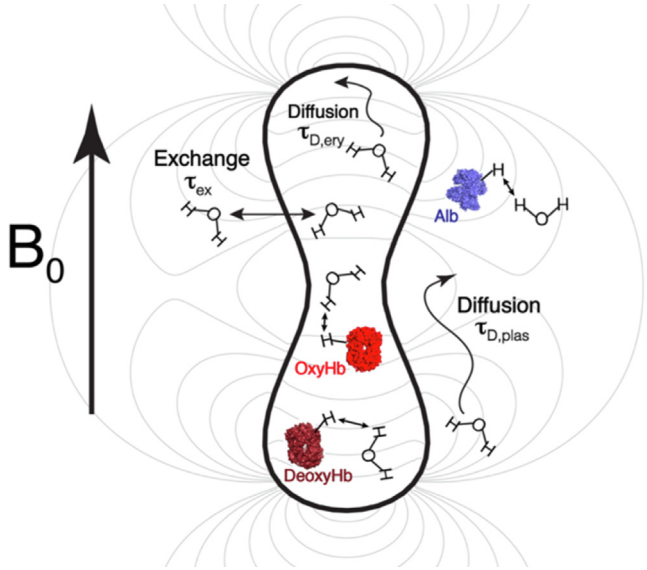

Fig. 24. Schematic representation of an erythrocyte in a B_0 magnetic field, and of the phenomena influencing NMR relaxation of water. The gray lines indicate the magnetic field lines generated by the difference between the magnetic susceptibilities of the intra- and extra-cellular media. These magnetic field gradients are intrinsically lower inside the cells, but cause basal peak broadening. Signal linewidth is also affected by faster relaxation due to i) diffusion of water molecules through magnetic field gradients (the resonance frequency of every molecule varies during acquisition, yielding coherence losses), ii) interactions with diamagnetic proteins (albumin or oxygenated hemoglobin), iii) proximity with paramagnetic compounds (like deoxy-hemoglobin), and iv) exchange between sample compartments (intra- and extra-cellular). All these phenomena can affect every molecule observable by NMR in cellular samples. Adapted from Li & van Zijl 2020 NMR Biomed [1536].

equipment: advanced probes and sensitivity, magnetic field homogeneity, faster electronics to record the NMR signal with the shortest delays after pulses and improved baseline correction so as not to cancel the broad, fast relaxing component of ^{39}K even in the presence of significant baseline roll [272,273]. The different mitochondrial content in tissues, and later the ribosome content in *E. coli* [1548] were established as important contributors to ^{39}K interactions and thus of cellular ^{39}K NMR relaxation.

An interesting note: in cells, both T1 and T2 are bi-exponential, having a fast-relaxing component, while the extracellular ^{39}K is likely to show a mono-exponential slow-relaxing relaxation in absence of transient interactions with macromolecules [278,280,1549]. When this slow component of T1 is known, the extracellular signal can be removed using an inversion-recovery block of the appropriate duration (∼-ln(0.5*T1)). The fast-relaxing component can then be selectively excited and observed as has been shown in some ^{39}K studies [278,280,1549].

3.2. Line-broadening and observability

NMR signals are broadened in living samples. It is worthwhile detailing the sources of this line-broadening if we want to understand how to counteract them. We discuss the main contributions below, i.e. viscosity effects, heterogeneous magnetic susceptibility, compartmental exchange, and multiple interactions (see Fig. 24). These take place in spatial dimensions in the range of 1 to 20 micrometers for prokaryotes to mammalian cells, respectively. For each, the subcellular compartments are at least 10 times smaller. The most studied system has been erythrocytes (red blood cells), which can be schematized as disks of 4 μm radius and 2 μm thickness. Mammalian erythrocytes are enucleated, while avian erythrocytes do have a nucleus and functional mitochondria, which has been useful for comparisons in NMR studies. Larger cells exist, such as frog oocytes that are about 1 millimeter across and also have internal subcellular compartments of exceptional sizes, up to hundreds of micrometers.

In this section, we will try to provide helpful numbers and concepts to understand qualitatively the driving forces of NMR line-broadening in samples containing cells. This is necessary for understanding the current limits of the technique, and thus predicting windows of opportunities in terms of applications, as well as imagining solutions to overcome these limitations.

3.2.1. Intra- and extra-cellular mobilities of molecules

Before evaluating the NMR-related phenomena that affect line-broadening in samples containing living cells, we have to determine an important driving factor, namely intra- and extra-cellular apparent viscosities. This is of course more a matter of concern for solution NMR than solid-state NMR. Another difficulty is to determine the molecular diffusion regimes, at the NMR T2 timescale, i.e. in the timeframe between 1 to 10 milliseconds: are we dealing with free diffusion or restricted molecular motion? In this paragraph, we consider the ideal situation where i) only intermolecular steric repulsion affects intra- and extra-cellular molecular mobilities, and ii) translocation is negligible in comparison to intra- and extra-cellular diffusion. The average membrane permeability for small compounds is indeed low [1550] (Fig. 25). Our assumption is thus somehow realistic in most cases, although it suffers plenty of exceptions: the translocation of various small molecular species is of course accelerated by many dedicated membrane channel proteins.

Water self-diffusion coefficients are about $1.5x10^{-9}$ and $3x10^{-9}$ $m^2.s^{-1}$ at 283 K and 310 K, respectively [1551], while diffusion coefficients of small metabolites in pure water are of the same order of magnitude, e.g. 1.05, 0.91 and 0.67 $x10^{-9}$ $m^2.s^{-1}$ at 298 K for glycine, alanine and glucose, respectively [1552]. If we neglect the fraction of water molecules and metabolites that solvate or interact with macromolecules, small molecules (<1 nm diameter) experience intracellular viscosities about 1.5 times that of pure water [1553]. Hence, in one millisecond the Brownian motion of water and glucose would lead to a three-dimensional mean-square displacement of about 3.5 and 2 micrometers, respectively (11 and 6 μm after 10 ms). We can thus consider that small molecules undergo restricted motions in bacteria, and in mammalian cells too, if we take into account the meshwork of subcellular organelles. It is less evident for the extracellular medium, depending on cell density: a packed cell pellet will exert a certain restriction of the mobility of small molecules, whereas cell at densities below ∼5% v/v may not.

Concerning larger molecules such as proteins, intracellular viscosity depends on molecular weight, but also on the diffusion time scale. Regular size proteins (hydrodynamic radius < 5 nm or molecular weight below 200 kDa) experience local viscosities in mammalian cells of about 1.5 to 5 times that in water, and in *E. coli* about 8 to 30 times that in water [1553]. To give some orders of magnitudes, GFP_1, GFP_3 and GFP_5 (28, 84 and 140 kDa) have immediate diffusion coefficients of 0.09, 0.05 and 0.0035 $x10^{-9}$ $m^2.s^{-1}$ in water, and 0.07, 0.03 and 0.015 $x10^{-9}$ $m^2.s^{-1}$ in cultured human cells, respectively [1554]. These coefficients hold true for a few milliseconds, but, on a timescale of about 100 ms, decrease to 0.03, 0.01 and 0.005 $x10^{-9}$ $m^2.s^{-1}$ in the same cells. Intracellular obstacles such as organelles, cytoskeleton and macromolecules are responsible for such anomalous diffusion. Hence, GFP_1 following a Brownian motion in mammalian cultured cells will show a mean square displacement of about 0.6 μm in 1 ms. In *E. coli*, the same GFP_1 can move about 0.3 μm in 1 ms. The cytosol of *E. coli*

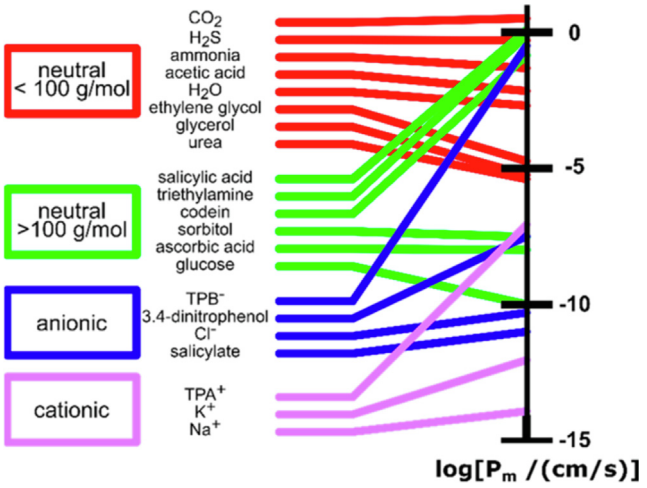

Fig. 25. Indicative, average membrane permeability (P_m, vertical axis) of small substances (listed according to their molecular weight and electric charge) for model lipid bilayers. Straight lines link the substances to their P_m. P_m, corresponds to the membrane permeability in a model of passive membrane diffusion where $J = -P_m \times \Delta c$, with J the transmembrane flux density, and Δc the transmembrane concentration gradient. Adapted from Hannesschlaeger et al. Chem Rev 2019 [1550].

also has an equal impact on non-folded, disordered proteins. Using NMR, Waudby et al. reported interesting numbers for non-folded α-synuclein (radius of gyration ~4 nm [1555]) recombinantly expressed in *E. coli* cells: α-synuclein motion is strongly restricted in the millisecond timescale, its root mean square displacement being constant at about 0.35 μm for any evolution time between 10 and 20 ms, close to the 0.5 μm in width of an *E. coli* cell [104].

Local nanoscale viscosities are similar among cultured mammalian cell lines [1556] and through the cell cycle [1557], except of course for proteins engaged in complexes that vary with the phases of the cell cycle [1558]. Local viscosities are similar in the cytosol and in the nucleus for proteins of average size [1559,1560]. However, important differences have been measured recently at the sub-micrometer scale: a single protein of 28 kDa can show diffusion coefficients of 0.025 $x10^{-9}$ $m^2.s^{-1}$ in the cytosol except in the few hundreds of nanometers close to actin cytoskeleton bundles, where its diffusion drops by a factor two; moreover, its diffusion coefficients in the nucleus were measured to be about 0.02 and 0.007 $x10^{-9}$ $m^2.s^{-1}$ outside and inside nucleoli, respectively [1561]. The same study revealed an intriguing feature: by adding positive net charges to the tracked fluorescent protein, diffusion coefficients dropped progressively to zero. Similar observations have been reported in *E. coli*, where protein-protein and protein-lipid but not protein-nucleic acid interactions play significant roles [1562]. As for small molecules, the apparent extracellular viscosity for proteins is not much affected by the presence of serum or even by the extracellular matrix (ECM) in the case of mammalian multicellular spheroids and tumors: it has been measured recently to be 1.2 to 2 times larger than in pure water for proteins below 200 kDa, depending on the cell line [1563]. However, in this last case, the ECM shows typical correlation lengths of about 20-40 nm that to some extent restrict extracellular protein diffusion.

Altogether, the intracellular and extracellular environment of mammalian cells exert a 1- to 5-fold increase in apparent local viscosity for both small and large molecules. Bacterial cells have more impact on macromolecules, up to 20-30 fold. These reported local viscosities have roughly proportional consequences on translational and rotational diffusion (anomalous effects can appear at the micrometer scale for translational diffusion, and the effects on rotational diffusion are thus theoretically always a bit smaller than the local viscosity measured by translational diffusion) [1553,1564]. We can translate these increases in viscosity into correlation times or apparent molecular weights: the latter would be proportional to viscosity, using the Stokes law and homogeneous spheres as a model for proteins [1565]. Hence, the experimental, apparent viscosities can already be helpful for the NMR spectroscopist: as far as solution NMR is concerned, rapid calculations show that, based on predicted correlation times, folded proteins of over 25 kDa will always be difficult to observe in *E. coli*, while those below 50 kDa in mammalian cells may be within range for producing useful spectra. Once more, this corresponds to the theoretical case of molecules that do not interact with any cellular component.

Finally, organelles and cytoskeleton establish a sub-micrometer meshwork, where small molecules as well as proteins experience somehow an intracellular restricted motion on the NMR T2 timescale of one millisecond. Extracellular metabolites also experience restricted motion in cell pellets. This will be of importance for the next section.

3.2.2. Inhomogeneous magnetic susceptibility

Living material is organized into spatial structures, which causes sample inhomogeneity. This has consequences at different levels, the first being in terms of local magnetic susceptibilities χ_{loc}. Chemical shifts are proportional to the local magnetic susceptibility $B_{loc} \propto \mu_0(1+\chi_{loc})H_0$ (where H_0 the spectrometer magnetic field strength), provided we consider the ideal situation where a molecule does not diffuse during the NMR measurement. Magnetic susceptibilities of cells and subcellular components have been reported, but information about this is relatively scarce in the literature, to the best of our knowledge. We have gathered the experimental numbers that we could find in Table 1.

The most studied cells are erythrocytes (red blood cells), which are mostly filled with hemoglobin at about 5 mM. Hence, erythrocytes show magnetic susceptibility variations due to dia- and paramagnetism of oxygenated and deoxygenated hemoglobin, respectively. Their contribution to NMR signal broadening is difficult to disentangle from those due to intracellular interactions and the chemical environment. The only clear reports -to the best of our knowledge- used variable angle spinning to separate them: magnetic susceptibility differences between the buffer and the cytosol of CO-treated (to generate stable paramagnetic hemoglobin), pelleted erythrocytes (mammalian, i.e. enucleated) generate chemical shift differences of 0.1-0.2 ppm (Fig. 26) [1566-1568] that vary in a linear fashion with the intracellular hemoglobin concentration.

When they do not contain any paramagnetic center, proteins seem to have a common average magnetic susceptibility, which is about 1 ppm more diamagnetic than that of water [1569,1570]. Fatty acids are about 1 ppm less diamagnetic than water, and we can expect similar values for tri-acylglycerides present in intracellular lipid droplets. Cholesterol is also found in lipid droplets, and in contrast is more diamagnetic than water. Among phospholipids, we found experimental information only for dipalmitoyphosphatidylcholine (DPPC), for which susceptibility values surprisingly different from those of fatty acids were reported [1571]. Phospholipids are mainly present in mono- or bilayers such as those in bicelles, whose anisotropy of magnetic susceptibility is on the order of magnitude of 0.5 ppm [1571-1574]. The information on DNA magnetic susceptibility may be interpreted with caution: it appears to depend on the degree of solvation and on the interactions with metals or ammonium groups [1575-1579], to comprise dia- and para-magnetic components over multiple scales and thus to vary with the magnetic field [1580]. In our view, the intracellular magnetic susceptibility of

the cell nucleus is thus quite uncertain. Its measurement has been recently reported by Tao and colleagues in a study that resulted in surprising values, also revealing the cytosol to be paramagnetic [1581]. The authors argue that the cytosol hosts organelles that generate paramagnetic reactive oxygen species such as peroxysomes and mitochondria (whose integrity should probably be verified). These results should be carefully considered: the presence of paramagnetic metal ions in cell culture media and cytosol has been regularly reported by EPR [1582].

Overall, cells and their culture medium represent inhomogeneous samples containing compartments, whose intrinsic magnetic susceptibilities vary in the range of 1 ppm. There is no direct correspondence between local magnetic susceptibility and local chemical shifts: the local magnetic fields are continuous functions of space, and the local susceptibilities have non-negligible impacts on magnetic field gradients on a micrometer scale.

Every local magnetic field generates a local chemical shift. In the case of living samples, the sum of all the local environments generates chemical shift distributions. It is however not straightforward to predict local susceptibility values. Magnetic susceptibility variations cause perturbations of the local magnetic field and Larmor frequency, which is a continuous function of space. Hence, calculating the local chemical shifts in heterogenous samples has long been a matter of concern. Using a model of theoretical round avian erythrocyte cells ($\chi_{nucleus}$=-8.9x10^{-6}, $\chi_{cytoplasm}$=-8.86x10^{-6}, χ_{medium}=-8.82x10^{-6}), Kuchel and colleagues calculated that magnetic field gradients could reach about 2 G/cm (at a spectrometer field of 9.4 T) in the micrometer surrounding the nuclear and plasma membrane, i.e. about 1-2 Hz between molecules at the surface of the nucleus and far away in the cytosol [1594,1595]. The consequences were about 20 times larger for erythrocytes that would contain paramagnetic deoxyhemoglobin ($\chi_{nucleus}$=-8.9x10^{-6} $\chi_{cytoplasm}$=-7.9x10^{-6}, χ_{medium}=-8.82x10^{-6}). Later calculations by Gillis et al. gave about 2-3-fold larger values using more realistic shapes for mammalian paramagnetic erythrocytes (Fig. 27) [1596]. Based on experimental reports, Jensen and Chandra calculated root mean square magnitudes of field inhomogeneity of 0.5 ppm in erythrocyte suspensions and 0.2 ppm in grey matter [1597]. These field variations clearly depend on cell geometry and are half as large for spherical cells [1596,1598]. Given the susceptibility values reported from cells or cell extracts (Table 1), the chemical shift distribution in the cytosol of a round cell is expected to be similar to that in deoxy-erythrocytes, i.e. 0.1-0.2 ppm. This corresponds to the chemical shift distribution due to the presence of nucleus, cytosol and extracellular medium that have susceptibility differences of about 1 ppm.

The variations of local magnetic fields are intrinsically larger outside of the considered compartment, e.g. the nucleus, the internal organelles or the cell. However, the local fields s a few percent (Fig. 27). For large magnetic susceptibility differences between intra- and extra-cellular media (e.g. for paramagnetic deoxygenated erythrocytes), the resulting heterogeneity in magnetic susceptibility can grow until a certain cell density and then progressively decrease for packed cell samples [1536,1599]. Altogether, we can consider that intra- and extra-cellular molecules are equally affected by the resulting chemical shift variations of 0.1-0.2 ppm.

At a more local level, we can also take into account the magnetic susceptibility differences imposed by the sharp transition between aqueous intra- and extra-cellular media and lipids in membranes or droplets. Using a simplistic model of a magnetic dipole moment and its associated magnetic field imposed by a spherical cell, Wind and Hu calculated that chemical shift distributions of lipids (or other molecules) in membranes may be as much as 0.6 ppm due to their variable orientations in the field and the local differences in magnetic susceptibility [636]. Lipid ^{1}H line-widths in cellular samples are usually 0.1-0.2 ppm. A large fraction of these lipids is contained in lipid droplets, which are approximately round objects: spheres generate a homogeneous internal magnetic field, but also local inhomogeneities at their external surface. Frog oocytes show large experimental lipid linewidths of about 0.3 ppm, which may be due to their large asymmetric protein/lipoprotein (yolk) or lipid compartments, but also to the adsorbed microscopic air bubbles that are commonly found on the oocyte surface.

In addition, we can consider the chemical shift averaging that molecular diffusion would cause, which may act to reduce the apparent chemical shift distributions described above. We have seen that metabolites diffuse at rates that would allow them to move micrometers per millisecond, i.e. more than a whole *E. coli* cell length, or a tenth of a mammalian cultured cell. Proteins move

Table 1
Volume magnetic susceptibility at room temperature (SI, dimensionless; divide by 4π for converting to the CGS system); d: density.

Material	$\chi.10^6$ (SI units, dimensionless)	references	Material	$\chi.10^6$ (SI units, dimensionless)	Reference
H_2O	-9.05	[1583]	Deoxygenated erythrocytes	-6.1	[1584]
D_2O	-8.8 (-9.0 in [1585])	[1552]	CO-treated RBC (intracellular diamagnetic hemoglobin ~5 mM ~ 350 g/L)	-9.25/-9.4	[1566,1584]
H_2O+[NaCl]=150 mM (d=1.05 g/mL)	-8.95	Calculated based on [1586]	Hela 12 to 20 mm diameter	-6.45 to -6.5	[1587]
culture medium (mammalian cells, classical medium 199 [1588])	-7.5	[1587]	lymphocyte	-9.1	[1587]
"Pure protein"(d=1.38 g/mL)	-10.5	[1569,1570]	Frog oocyte	-8.7	[1589]
100 g/L BSA in water	-9.1	Calculated based on [1570]	Pellet/yolk (proteins and lipoproteins)	-8.0	[1589]
DNA (d=1.7 g/mL)χ(diamagnetic)	-12.8	[1575,1590]	Cytosolic	-8.8	[1589]
Fatty acids (d=0.85 g/mL)	-8.4	[1552,1591,1592]	Lipid fraction	-8.1	[1589]
Cholesterol	-9.7	[1552]	Phospholipids (DPPC) (d=0.94 g/mL)	-9.4	[1571]
Glycerol	-9.8	[1552]	Glucose	-10.9	[1552]
Oxygenated hemoglobin (diamagnetic)	-9.2	[1584,1587]	Starch granules	-10.9	[1593]
Deoxygenated hemoglobin (paramagnetic)	-5.8 to -6.7	[1537,1584]	CNE-2Z carcinoma cell line human(for d=1 g/mL)	Nucleus: -6.8 Cytosol: 9.9	[1581] Should be interpreted cautiously, in regards to all other reported values

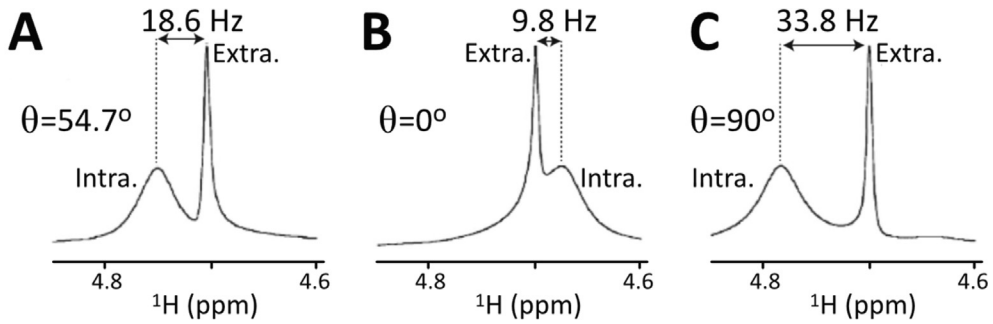

Fig. 26. One-dimensional ^{1}H NMR spectra of an erythrocyte suspension in a rotor spinning at varying angles θ with respect to the spectrometer field: close up views of the water peaks: **A)** Magic-Angle Spinning, which cancels the effects of varying magnetic susceptibilities in the sample, **B)** 0° spinning and **C)** 90° spinning. The labels "Extra." and "Intra." indicate the peaks from water molecules in the supernatant and inside the cells, respectively. The spectrum at the magic-angle reveals the isotropic chemical shifts due to the different chemical environments inside and outside the cells. The difference of magnetic susceptibility between inside and outside the cells is given by $\Delta\chi=2(\Delta\nu_0-\Delta\nu_{90})/\Delta\nu_0$, with $\Delta\nu_0$ and $\Delta\nu_{90}$ the intervals in Hz between the "Intra." and "Extra." peaks when spinning at 0° and 90° with respect to the spectrometer field. Here, $\Delta\chi$ was measured to be -2.18x10^{-7} (SI units, dimensionless). The rotor was spun at 250 Hz, spectra were recorded at 9.4 T (400 MHz). Adapted from Kuchel et al. Prog NMR Spec 2018 [1566].

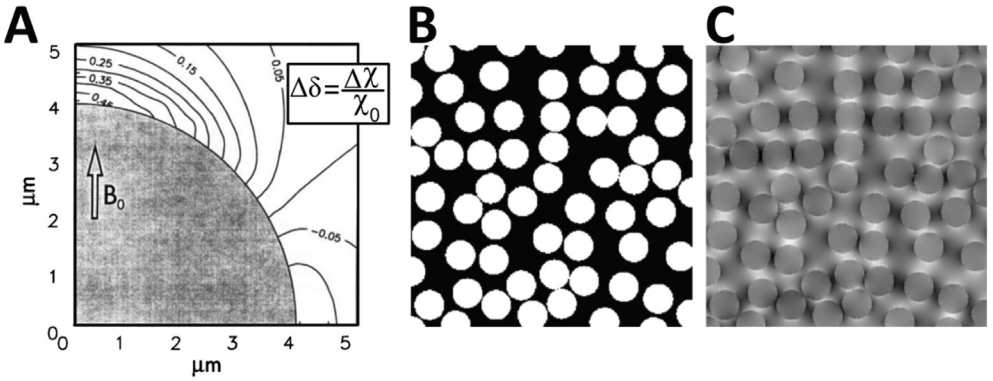

Fig. 27. Schematic representations of **A)** the relative magnetic field variation induced by $\Delta\chi$, the difference of magnetic susceptibility inside and outside an idealized mammalian erythrocyte (4 μm of diameter): if $\Delta\chi$ = 1 ppm, molecules in contact with the erythrocyte membrane can resonate 0.5 ppm away from their remote counterparts (adapted from Gillis et al. 1995 [1596]); **B)** a sample of cells in suspensions (white) with a volume fraction of 0.46, whose intracellular magnetic susceptibility (white) is different from the extracellular medium (black), and **C)** the corresponding magnetic fields (or Larmor frequencies) induced by a field applied vertically, represented using shades of grey. Every intracellular magnetic field is influenced by the presence of neighboring cells and magnetic susceptibility inhomogeneities. Adapted from Novikov and Kiselev 2008 J Magn Reson [1600].

about 0.1-0.5 micrometer per millisecond, which is enough to explore intracellular spaces comprising multiple subcellular compartments. Lipids are on average much less mobile and are thus not considered here. Let us first focus on chemical shifts. Recently, Kiselev and colleagues calculated the frequency shifts of molecules freely diffusing in a medium containing spheroid inclusions: whatever the diffusion rates and cell shapes, chemical shift variations are predicted to be limited to a few hundredths of the difference between magnetic susceptibilities of the solvent and of the inclusions [1601,1602]. We can model cells in their surrounding medium, as well as organelles in the cytosol, in the same way as such diamagnetic inclusions. Hence, as compared to chemical shifts of purified molecules measured in aqueous buffers, we expect chemical shift changes of about 0.1 ppm for both intra- and extracellular molecules in samples containing cells. Again, this discussion applies for a model of extracellular molecules that do not interact with cells, or of intracellular molecules that do not interact with organelle membranes.

As a final point concerning the effects of magnetic susceptibility on NMR line-broadening in cell samples, we must discuss an additional effect that is associated with diffusion in an inhomogeneous field. In the presence of magnetic field gradients, diffusion generates a specific increase in the rate of loss of transverse magnetization [68]. This effect has been fruitfully used for about 50 years to measure diffusion rates by solution NMR spectroscopy. In the context of cellular samples, we face not only the difficulty that magnitudes of the local gradient fields are unknown, but so are the diffusion coefficients and diffusion regimes of the observed molecules. In the case of free diffusion in a steady and linear magnetic field gradient G, the signals attenuate in time (t) proportionally to $\exp(-\gamma^2D^2G^2t^3/12)$, where γ is the gyromagnetic ratio and D is the diffusion coefficient [71]. We have discussed in 3.2.1 the fact that molecular diffusion can be considered to be restricted in the millisecond timescale. This leads to signal attenuation regimes that can be very different from those observed for free diffusion in steady magnetic fields. There is a wealth of literature on NMR measurement of diffusion in heterogeneous media, and the number and sophistication of the physical models in use makes it impossible to present them here in a few lines [69,71,1535,1597,1603-1609]. Rather, we can just keep in mind that diffusion-related transverse signal loss is very dependent on diffusion coefficients and the length and shape of the relevant compartment. Indeed, we did not succeed in finding simple analytical equations in the literature that could be used as simple guides for transverse signal loss in cell samples. The proposed attenuation regimes are quite complex, depending on the starting assumptions, and we would

only be able to provide a long list of possible situations together with impractical equations containing large exponents for every term, given the heterogeneity of magnetic susceptibilities and shapes of cells and subcellular compartments, as well as the variability of cell packing and molecular diffusion coefficients. A phenomenon that is close to this topic is water relaxation in blood, which has been much studied using CMPG sequences and diffusion NMR experiments. The measured diffusion-related ^{1}H relaxation due to susceptibility heterogeneity is dominant from 1.5 T upwards, proportional to $\Delta\chi^2$, γ^2 and B_0^2, and shows dispersion when varying the inter-echo spacing in CPMG experiments because of various exchange mechanisms [933,1536,1584,1596,1597,1599,1603,1610-1612]. Interestingly, if we focus on signal broadening, the diffusion of water molecules in the cellular field gradients has a stronger impact on attenuation of the FID than on CPMG relaxation [1604,1606,1613,1614]. As an extreme example, at a spectrometer field of 300 MHz, the specific FID R2 (1/T2) of intracellular water due to diffusion ranges from ~60 Hz to ~700 Hz for paramagnetic erythrocytes at ~100% and 40% hematocrit (volume percentage of the pelleted cells), respectively [1599]. Fully oxygenated, diamagnetic erythrocytes show diffusion-related water line-broadening below 0.1 ppm. These numbers will hold true for small molecules. As far as macromolecules are concerned, we can mention the fact that, up to 1.2 GHz, α-synuclein linewidth did not increase with the square of the magnetic field in cultured mammalian cells [1615]. This may show that diffusion in cellular samples makes only weak contributions to protein relaxation. Finally, the effects of compartmental exchange between intra- and extra-cellular media are about 5-fold lower for water relaxation in erythrocytes, where water has a lifetime of about 10 ms [1536]. We can expect the effects to be smaller for most metabolites because of their slower exchange kinetics through the plasma membrane.

As a last, speculative point : we should also consider membrane-less organelles produced by liquid-liquid phase separation, which can contain high concentrations of proteins and/or nucleic acids [1616,1617]. These may also be treated as examples of diamagnetic inclusions, although this possibility has not been thoroughly discussed in the literature to the best of our knowledge [1618].

To summarize, according to theoretical calculations on local magnetic field susceptibilities, cellular samples can generate chemical shift distributions, whose width is in the order of 0.1-0.2 ppm for a single molecular species localized either inside or outside cells. These distributions can even be asymmetric if cells are not spherical and molecular diffusion is sufficiently slow (Fig. 28). Larger cells such as oocytes and pluricellular organisms that include large non-spherical portions can provoke larger spreads in the 0.3 ppm range.

3.2.3. Multiple interactions. A warning concerning quantification and referencing.

Interactions with cellular entities are very unpredictable phenomena for any molecule in a cell, yet they are at the core of the in-cell NMR approach, for which the aim is to find information on what happens in the presence of native partners in a native context. They are also possibly the most damaging for NMR investigations, because they can cause signal disappearance. NMR spectroscopists are used to dealing with this possibility *in vitro*, where causes and consequences are well-known: in the case of solution NMR they comprise interactions in the intermediate regime (μs-ms) or with large macromolecular assemblies; in the case of solid-state NMR, multiple interactions and multiple chemical environments or inappropriate conformational dynamics at room temperature. We highlight here some considerations of broad interest.

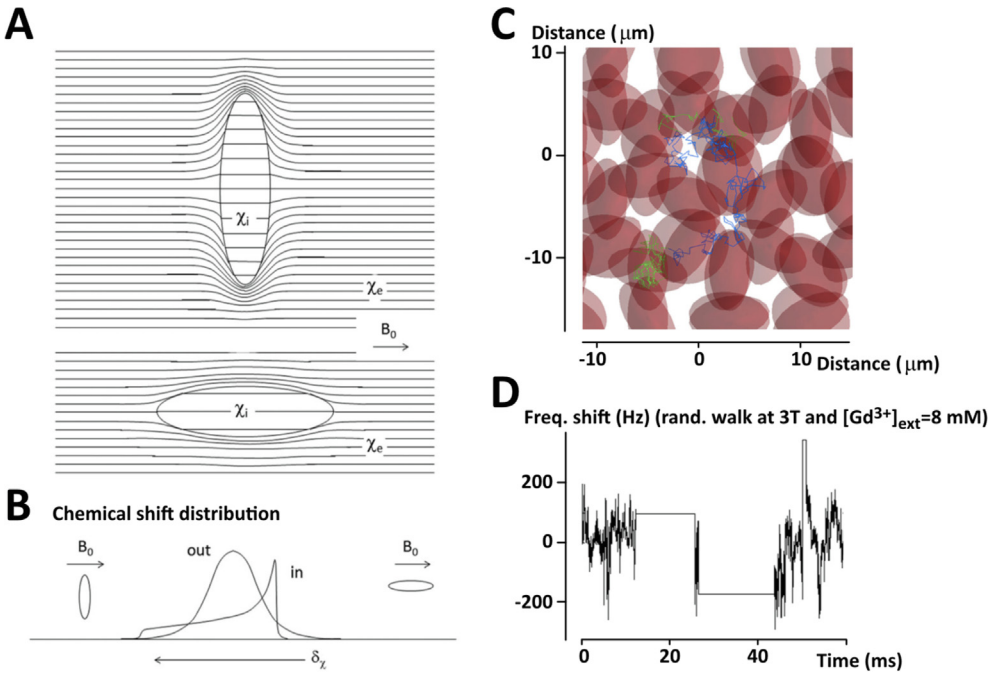

Fig. 28. A) Representation of the magnetic flux induced by ellipsoid cells of homogeneous magnetic susceptibility χ_i in a medium of susceptibility $\chi_e > \chi_i$ and a horizontal magnetic field B_0; **B)** Because randomly oriented cells more often adopt an orientation perpendicular to B_0, the chemical shift distribution of intracellular molecules corresponds to that seen in an NMR powder pattern; **C)** Illustration of the path of a water molecule during a 60 ms long Monte Carlo simulation in a medium where ellipsoid cells (shown semi-transparent red) are randomly oriented and occupy 38% of the volume; through the course of the simulation parts of the pathway shown in blue are extracellular, while the three green sections correspond to cell penetrations; **D)** Calculated frequency shift at every step of the Monte Carlo simulation presented above, using realistic parameters corresponding to diamagnetic erythrocytes at 3T mixed with an external medium containing 8 mM of Gd^{3+}-contrast agent. Adapted from Wilson et al. 2017 [1619].

An important aspect is the lower availability of water for hydrogen-bonding in cells. Cells contain high concentrations of molecules that establish hydrogen bonds with water, e.g. metabolites, proteins or nucleic acids. Hence, water is on average less available for each of these hydrogen bonding events than it would be in dilute systems containing a single solute. Once the effects of magnetic susceptibility on chemical shifts have been removed (using HR-MAS for example), chemical shift differences between intra- and extra-cellular species are reminiscent of those observed between protic and aprotic solvents. This solvent effect makes an important contribution to the NMR split peak effect observed between intra- and extra-cellular populations of small molecules in cell suspensions. It has been extremely well presented by Kuchel and colleagues in a recent review [1568]. All hydrogen bonding metabolites or drugs are affected, notably ^{31}P- or ^{19}F-bearing molecules.

Turning to consideration of the water, protein solvation has consequences on water chemical shift and relaxation. The contribution of water-protein exchange has been measured to be about 0.2 parts-per-billion (ppb) per g/L of protein [1567,1570,1620,1621]. To calculate the effective water frequency in protein solution, this exchange contribution has to be combined with the effects of protein magnetic susceptibility, which is of the opposite sign and about twice as large. These two contributions are very variable among small molecules, and, unfortunately, standard NMR referencing molecules like DSS, TSP, or MDPA interact with proteins at high concentration, which can affect internal chemical shift and quantification referencing [1570,1620,1622]. Although they do not interact with proteins, other referencing molecules, like dioxane, can be affected by the solvent-induced shift presented above [1620]. Considering metabolite quantification, amino acids and important metabolites, e.g. pyruvate or creatine, also interact with proteins [1413,1414,1623]. These interactions depend naturally on the protein, and the binding kinetics vary from slow to fast exchange in the NMR timescale, giving rise to variable changes in signal intensity and chemical shift.

Proteins also have an impact on water relaxation, which is dominated at high field by chemical exchange between protein exchangeable protons, the water molecules from the hydration shell of proteins, and the bulk water molecules [1536,1612,1624-1626]. This exchange shows a strong dispersion at short CPMG inter-echo spacing, and can be modeled in different ways, but we can keep in mind that albumin and diamagnetic hemoglobin have relaxivities of about 10-15 Hz per millimolar of protein (70 Hz/mM for paramagnetic deoxy-hemoglobin) at 500-700 MHz and 310K. These values are naturally very dependent on molecular weight and the folding status of proteins. Nonetheless, one can still extrapolate rough relaxivity values of about 25 Hz at these fields, yielding a water line-broadening value of about 0.1 ppm. This increases with the square of the magnetic field, and is comparable to line-broadenings due to magnetic susceptibility heterogeneity discussed above. The impact of other macromolecular constituents like lipids [1627] or nucleic acids have been less thoroughly characterized, to the best of our knowledge. However, relaxivity effects of glucose and maltose on water can reach 0.1 Hz/mM at 500 MHz, a number that is probably close to those for other carbohydrates [1628-1631]. Glutamate and glutamine also show 0.1 Hz/mM relaxivities (at 400 MHz) [1632]. Overall, these cellular components probably yield water signal line-broadenings of about 0.2-0.4 ppm at high fields. Consequences in terms of water-suppression, cross-relaxation mechanisms and signal intensities of water-exchangeable protons may be non-negligible.

Concerning intracellular interactions and their consequences for proteins and in-cell NMR, we selected below a few striking observations from the literature. The first measurements of protein tumbling features in cells were reported 45 years ago using ^{13}C-histidine labeling of mice (fed with [2-^{13}C]-histidine) and their hemoglobin in erythrocytes [1178]. The intracellular correlation time was consistent with an intracellular viscosity only twice as large as than that of an aqueous buffer. Twenty years later, using 5-fluorotryptophan incorporation and ^{19}F-NMR T1/T2 relaxation measurements, Brindle and colleagues reported similar increases of correlation times for two enzymes overexpressed in yeast [1179]. They noticed however that two other enzymes were not observable in intact cells, whereas they recovered their ^{19}F signals upon cell lysis [1179,1343]. We recall briefly here the strong size-dependency of apparent viscosity experienced by proteins (see Section 3.2.1.). Besides these effects, we meet here the multiple weak interactions that proteins can establish in cells, and their deleterious consequences for NMR signals. The use of ^{19}F-amino acids was later fruitfully exploited by Pielak, Li and their coworkers: T1 and T2 relaxation were very differently affected by the effective local viscosity and transient interactions with other macromolecules [1344]. Hence, by measuring T1 and T2 rates in water-glycerol solutions, diluted *E. coli* extracts and intact *E. coli* cells, they could show that for ubiquitin and GB1 tumbling was similarly affected by a 2-3-fold change in intracellular viscosity, but that ubiquitin was involved in substantial transient interactions in cells while GB1 was almost not. Consequently, the ^{19}F-line-widths of intracellular ubiquitin (8.6 kDa) and GB1 (6.2 kDa) corresponded to those of ~200 kDa and ~50 kDa proteins in buffer, respectively. Similar observations had been previously reported by Gierasch and her coworkers, using an ingenious approach: they measured linewidths of both TROSY and anti-TROSY peaks in ^{1}H-^{15}N spectra, their difference being determined by local dynamics and not by chemical exchange or magnetic field inhomogeneity [1191]. They could show that about 30% of the intracellular GB1 $^{1}H_N$ line-width was due to transient interactions. As a consequence, GB1 yielded good quality NMR spectra in cells, while ubiquitin did not. A triple mutation of hydrophobic amino acids at the surface of ubiquitin (L8A-I44A-V70A) sufficiently reduced the unspecific interactions to result in NMR signal recovery in cell lysate, but not in cells. More generally, hydrophobic residues on protein surfaces, a net-positive charge and also a large dipole moment have been described to negatively affect in-cell NMR signal [1345,1349,1633]. Molecules present in high concentrations, such as ribosomes, may play a role in enhancing transverse relaxation of proteins in cells [1351,1354]. Burmann et al. have shown that for α-synuclein in mammalian cells, chaperone silencing reduced transverse relaxation of the hydrophobic patches involved in loose interactions verified *in vitro*. [1250]. This suggests a more global binding of exposed hydrophobic patches by chaperones. It is well-known by NMR spectroscopists that transient interactions engaging even low populations can cause considerable transverse relaxation. The differential impact of viscosity and transient interactions on ^{1}H-^{15}N T1 and T2 relaxations holds true in cells and may carry information on the size distribution of interacting partners, as proposed recently by Danielsson and colleagues [1350]. Based on their characterization of relevant parameters (namely et charge, surface hydrophobicity and dipolar moment), they also used mutations to greatly improve in-cell NMR spectra of their proteins by removing unspecific transient interactions that spontaneously occur in the cellular environment [1349,1350]. This strategy may be fruitful in the future, even though its use should presumably be limited to specific questions that do not require maintenance of the whole set of native interactions; this, in turn, raises the question of how to know in advance whether the whole set of native interactions is to be maintained. A less-questionable strategy consists in avoiding positively charged peptide tags, which have undesirable effects on intracellular tumbling and on the NMR signal [1190,1347,1561,1562].

3.3. Observation of ions and metabolites

This section mostly focusses on in-cell studies by solution and HR-MAS NMR spectroscopy. We aim to provide information complementary to that presented in the applications Section 2. Because we will be discussing spin-echoes and T2/T1rho filters, we briefly mention the potential sample heating due to the applied RF.

3.3.1. Metal ions

Many metal ions have been used for direct NMR detection in cells: ^{6}Li and ^{7}Li (s=3/2 and s=3/2, natural abundance of 7.6 and 92.4 %, respectively), ^{10}B and ^{11}B (s=3 and s=5/2, n.a. 19.9 and 80.1%, respectively), ^{23}Na (s=5/2, n.a. 100%), ^{27}Al (s=5/2, n.a. 100%), ^{39}K (s=3/2, n.a. 93.3%), ^{85}Rb and ^{87}Rb (s=5/2 and s=3/2, n.a. 72.2 and 27.8%), ^{113}Cd (s=1/2, n.a. 12.2%), ^{133}Cs (s=7/2, n.a. 100%). Unfortunately, for many important metals their only NMR-active isotope has low abundance, which precludes sensitive direct NMR detection: ^{25}Mg (s=5/2 n.a. 10.1%), ^{43}Ca (s=7/2, n.a. 0.14%), ^{57}Fe (n.a. 2.1 %), ^{67}Zn (s=5/2, n.a. 4.1%), ^{77}Se (s=1/2, n.a. 7.6%). Moreover, paramagnetic states prevent direct NMR detection of, e.g., Mn (II), Mn(III), Cu(II), Co(II): ^{55}Mn (s=5/2, n.a. 100%), ^{59}Co (s=7/2, n.a. 100%), ^{63}Cu and ^{65}Cu (s=3/2 and s=3/2, n.a. 69.2 and 30.8%, respectively).

Metal ions often show broad, overlapping signals from outside and inside cells [202]. Membrane-impermeable molecules, so-called "shift reagents", have thus been developed from the early 1980's to generate exploitable chemical shift changes for extracellular nuclei. The rationale for this was presented in Section 2.1.2. These "shift reagents" are commonly chelated lanthanides, notably dysprosium or thulium [131,198,199,201,202,225,242,1634-1636], whose paramagnetic properties yield significant frequency shifts and little signal broadening [133]. These reagents have their "signal-broadening only" counterparts in gadolinium-complexes MRI contrast agents, which can effectively shut off NMR signals in their vicinity [1637]. It was soon realized that some of the "shift reagents" could be unstable [216,238,1638], toxic [239,240,1639], could modify Li^+/Na^+ transport rates and membrane potential in red blood cells [1640,1641], and were dependent on pH or Ca^{2+} concentrations [1638,1641,1642]. Although not perfect, a more harmless Tm-DOTP complex "shift reagent" has been regularly used later for cellular studies [1643,1644]. Advanced versions of "shift reagents" are still being developed for MRI purposes [130].

Most of these NMR-observable isotopes are quadrupolar, making them more challenging for NMR measurements. Interestingly, increases in their relaxation rates can also reveal intracellular interactions in a sensitive fashion (see Sections 2.1.3., 2.1.4, 2.1.5. and 3.1.2.). Double- and Triple-Quantum Filtered experiments allow attenuation of the signals from extracellular quadrupolar nuclei that do not interact with macromolecular assemblies (see Section 2.1.4.).

3.3.2. Spin-echo as an editing strategy

Various versions of spin-echoes have been used in the past to edit certain resonances from cellular samples, and were important in early NMR studies of metabolites. These are now most often substituted by T2/T1rho filters to purge out signals from fast relaxing species, or by ^{13}C/^{15}N-editing pulse blocks such as INEPT to remove signals from non-labeled species. We earlier described a number of studies using spin-echoes in the 1970's-1980's (particularly in Section 2.3.4.), where we described the concept of spin-echo only in brief terms. Here we provide more detailed descriptions.

Spin-echo pulse sequences rely on the following principle: instead of recording ^{1}H-NMR signals immediately after the application of a 90° pulse, one can wait for a few tens of milliseconds, then refocus the spin magnetization (using a 180° pulse), wait for the same amount of time and record the remaining "echoing" signals, those that relax slowly enough to have persisted through the delays (Fig. 15). This purges out the resonances of protons of slow tumbling species from the observable pool of signals, like those of proteins, nucleic acids polymers, and fatty acids from lipid droplets and membranes to some extent. Hence, this spin-echo method provokes a loss of information on slow-tumbling species, while it reveals the available information on fast-tumbling metabolites. Modern variants of this method are called T2- or T1rho-filters.

Scalar couplings can evolve during spin-echoes. This has been exploited notably in the case of ^{1}H-^{1}H and ^{1}H-^{13}C scalar couplings. Indeed, peak inversion can help to assign peaks in ^{1}H-detected spectra, to monitor proton-deuterium exchange or ^{13}C incorporation, as exemplified in Section 2.3.4. Interestingly, ^{13}C metabolic insertion causes the appearance of characteristic splittings in ^{1}H-peaks due to scalar coupling, which coalesce back at the central resonance if ^{13}C-decoupling is applied during acquisition. Hence, it is possible to choose to acquire FIDs after spin echoes that either do or do not allow scalar couplings to evolve, and to combine them by addition or subtraction to select either the ^{13}C- or ^{12}C-containing species in the final ^{1}H-detected spectra, while exploiting ^{1}H sensitivity.

The basic observation of ^{1}H-peak splitting due to ^{13}C incorporation was first exploited in spectra from in living cells by Shulman and his coworkers: by measuring one-dimensional ^{1}H-NMR spectra with or without ^{13}C-decoupling, and subtracting one from the other, they quantified ^{13}C-incorporation from [2-^{13}C]-acetate into glutamate or aspartate by *S. cerevisiae* [948] (Fig. 29). A more sophisticated ^{13}C-modulated ^{1}H spin-echo was exploited by Brindle and colleagues: they combined ^{1}H-coupling and ^{13}C-coupling evolution during spin echoes with ^{13}C-decoupling during acquisition. Addition and subtraction of the FIDs obtained allowed monitoring of the ^{12}C- and ^{13}C-methyl content in the separated spectra. They could quantify ^{12}C- and ^{13}C-labeled alanine and pyruvate in real-time, and thus determine the activity of alanine aminotransferase in erythrocytes [949]. This approach produced spectra in which peak intensities were easier to analyze than those obtained by Shulman previously, by separating the protons bound to ^{13}C from those bound to ^{12}C nuclei into separate spectra.

There is a clear connection to the more standard non-in-cell NMR applications and the vast possibilities of spin-echo derived strategies. A great number of them have been proposed since the 1960's, amongst the most famous being probably the INEPT transfer and BIRD filter for editing ^{13}C/^{15}N-bound protons [1043-1047, 1050,1051,1645,1646], and the TANGO filter for editing ^{12}C-bound protons [1647,1648]. The field would be impossible to cover entirely and is well beyond our scope. The common INEPT has been the most widely used by the in-cell NMR community, but recent applications of BIRD or TANGO on live material show that these can also yield interesting information [1066,1649].

3.3.3. T2, T1-rho filters and other filtering/editing methods for signals from mobile species

As mentioned earlier, spin-echoes are nowadays substituted by T2 or T1-rho filters to relax away the magnetization from slow-tumbling molecules before acquisition, and thus simplify the NMR spectra from complex samples. These filters are notably supposed to suppress scalar coupling evolution of the small molecules of interest, though they do not always do so perfectly. It is recommended to use the improved CPMG scheme proposed by Morris, Bodenhausen and their colleagues, which includes J-refocusing [1650]. Using an adiabatic spinlock offers superior results for the long T2-filters (>400 ms) necessary to remove signals from cellular lipids (they reduce the power deposition and thus sample heating) [1039,1651]. T2-filters can also be combined with diffusion filters

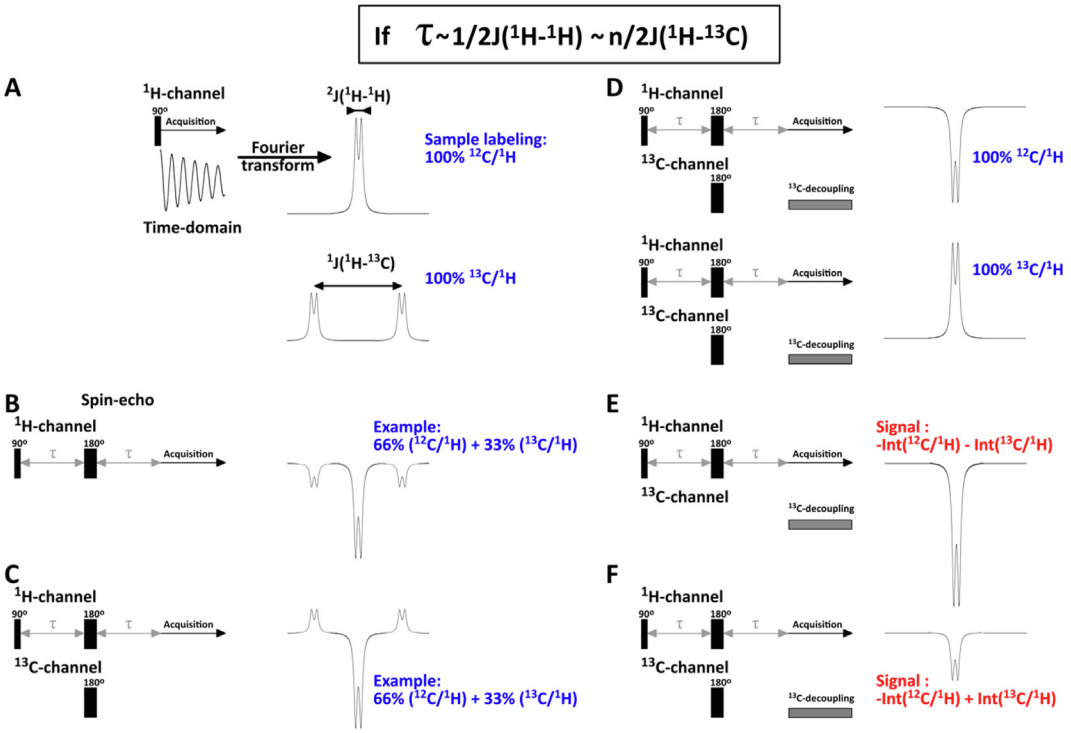

Fig. 29. Spin-echoes and ^{13}C-decoupling allow multiple editing/filtering strategies. **A)** One dimensional ^{1}H-NMR spectra or ^{12}C- or ^{13}C-labeled molecules can be distinguished by the large scalar coupling $^{1}J(^{1}H\text{-}^{13}C)$, which generates typical doublets. However, ^{1}H-spectra are often sufficiently crowded to make analysis of both ^{12}C- and ^{13}C-bound proton signals difficult. **B)** A spin echo with $\tau=1/^{2}J(^{1}H\text{-}^{1}H)$ will invert signals both from ^{12}C- and from ^{13}C-bound protons, whereas **C)** a supplementary 180° pulse on ^{13}C will result in positive signals of ^{13}C-bound protons if $\tau=n/^{1}J(^{1}H\text{-}^{13}C)$. **D)** ^{13}C-decoupling during ^{1}H-acquisition does not affect ^{12}C-bound protons, but causes peak coalescence of ^{13}C-bound proton signals. **E)** Applying ^{13}C-decoupling during acquisition causes overlap and addition of signals from ^{12}C- and ^{13}C-linked protons, but **F)** the addition of a 180° pulse on ^{13}C modulates the sign of ^{13}C-linked protons in the sum. Hence, adding or subtracting spectra **E** and **F** permits monitoring of ^{12}C- or ^{13}C-labeled molecules, respectively.

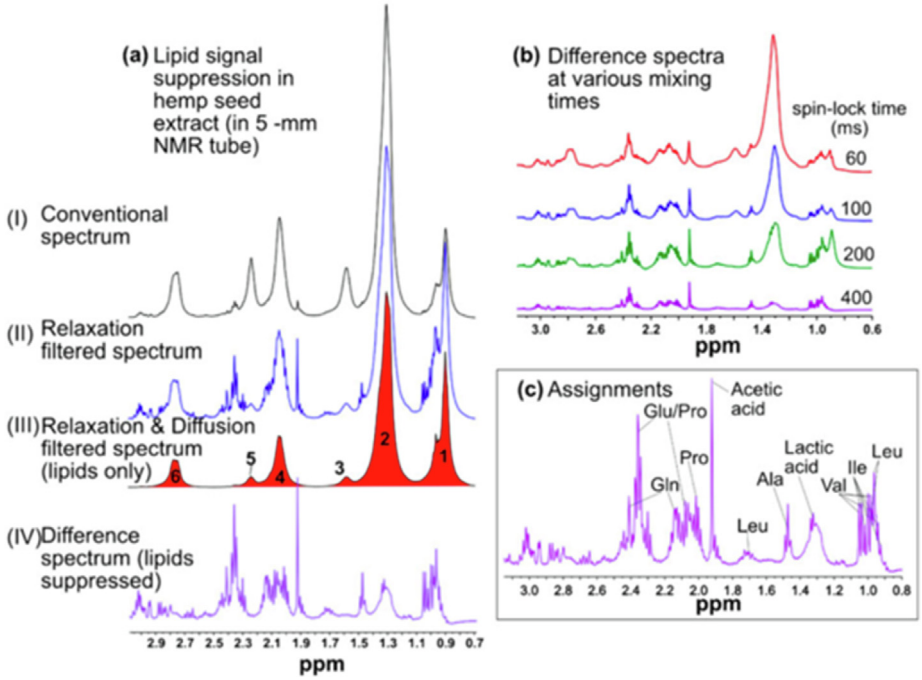

Fig. 30. a) The combined use of relaxation and diffusion filtering methods permits selective observation of different pools of molecules in complex samples (here a hemp seed extract): a short relaxation filter leaves high signal intensities from lipids (ii), which can be edited by a diffusion-filter (iii), the subtraction of (iii) from (ii) providing spectra mostly free of lipid signals (iv); **b)** Long spinlock mixing times are necessary to cancel lipid signals; **c)** the fast-tumbling species conserve high intensities upon the application of relaxation filters. Adapted from Hassan et al. 2019 [1039].

to select signals from molecules with relatively fast correlation times but slow translational diffusion coefficients (e.g. lipids) (Fig. 30) [1006,1039,1056,1651].

Simpson and colleagues have recently proposed using ^{2}H-detected NMR to detect the incorporation of ^{2}H-labeled nutrients in fresh water shrimp and fleas: the quadrupolar nature of ^{2}H ensures that only very mobile ^{2}H-labeled species are observable, but it presupposes the joint use of low-speed HR-MAS [1038]. They also proposed to adapt typical protein NMR pulse schemes to monitor ^{13}C-labeled levels of amino acids in water fleas [1065]: these sequences transfer magnetization through ^{13}C-labeled amino-acid side chains and backbone, using ^{13}C- selective pulses and long magnetization transfers that filter out non-peptidic and large molecules. They also applied a data-processing approach that acts like a relaxation filter: the window function is shifted to suppress early points of the FID (Fig. 31).

Another strategy has sometimes been to record one-dimensional ^{1}H-NMR spectra of similar cell samples, e.g. undifferentiated neuroblastoma/glioma cells and their differentiated counterparts. After normalization of the two spectra according to their global profile intensities, the second spectrum was subtracted from the first: NMR signals from metabolites showing varying levels in the two cell lines, like glutamine and glutamate, could be observed in the difference spectrum [1652]. We did not meet this method very often in the literature, even though a similar approach has been applied recently to remove the cellular background in studies focusing on overexpressed proteins [9,1251,1280].

3.3.4. High-Resolution Magic-Angle Spinning (HR-MAS) to alleviate sample heterogeneity: advantages, drawbacks and late developments

Cells cause intrinsic heterogeneity in magnetic susceptibility (see Section 3.2.2.) and limit the mobility of a number of molecules. Even though cellular samples do not behave like solid matter, they partially lose some of the solution character that facilitates solution NMR. This leads to NMR line-broadening because of dipolar fields due to magnetic susceptibility heterogeneities, and restricted motions increase the negative impacts of dipole–dipole interactions, of chemical shift anisotropy, and of first order quadrupole interactions. All these terms show a dependence on the second-order Legendre polynomial, proportional to $3\cos^2(\theta)-1$, with θ the angle between the field B_0 and the interaction vectors or anisotropy tensors. Magic-Angle Spinning has the capacity to average out these deleterious effects if the rotation rate is faster than the strength of the above mentioned phenomena (Fig. 32) [631,641,1653-1657]. MAS in liquid-like and heterogeneous systems was proposed in the 1970's [627-629,1658-1660], and became progressively more popular in the 1990's under the name HR-MAS to study the mobile fraction in liquid-phase of heterogeneous samples including tissues or living cells

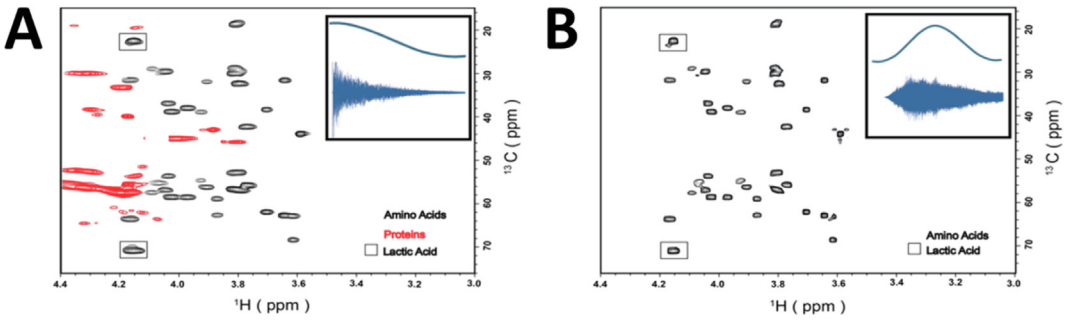

Fig. 31. A shifted sine-squared bell window function can act as a potent relaxation filter. These spectra were obtained from a 2D (H)CbCa(COCa)Ha pulse sequence applied to a ^{13}C-enriched *D. magna* extract. Adapted from Lane et al. 2019 [1065].

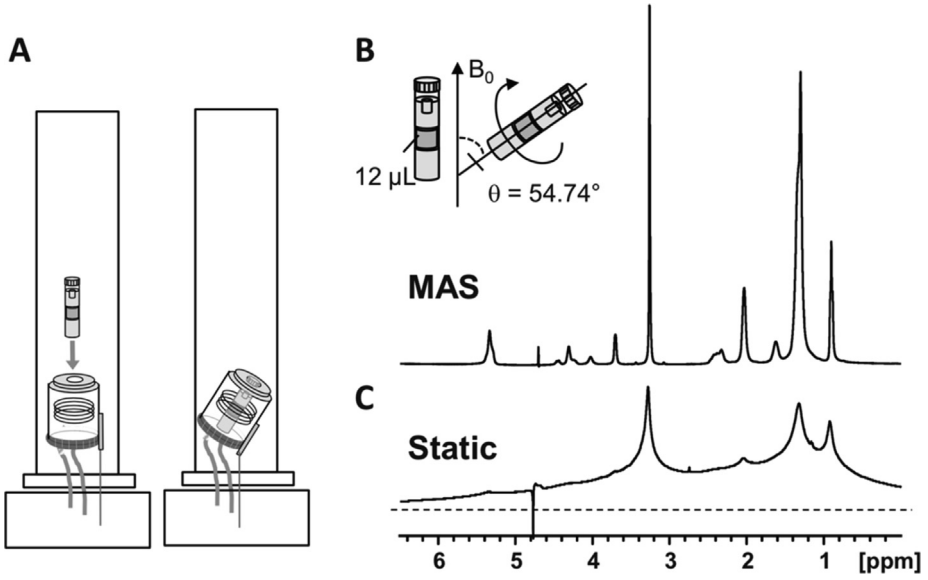

Fig. 32. A) Schematic representation of a MAS probe, where the rotor containing the sample is inserted in a MAS stator; **B)** HR-MAS one-dimensional ^{1}H NMR spectrum of 1,2-dioleoyl-sn-glycero-3-phosphocholine (DOPC) vesicles in D_2O acquired with MAS and **C)** without MAS. Adapted from Vermathen et al. 2017 [970].

[630,636,641,974,1024,1068,1661]. Very good guidelines for sample preparation have been published elsewhere [972,1068,1662].

Carbohydrates and lipids represent a class of molecules that can clearly benefit from the line-narrowing effects of HR-MAS. Carbohydrates are notoriously difficult to study because of the limited dispersion of their NMR signals [1663-1666]. Moreover, in living cells, polysaccharides are often found in the neighborhood of cell membranes where magnetic susceptibility effects due to heterogeneity are particularly strong, and molecular mobility can be severely hampered. Typical examples include bacterial lipopolysaccharides or capsular polysaccharides, or N-glycosylation of eukaryotic membrane proteins. Hence, HR-MAS NMR spectroscopy has been instrumental for their NMR characterization in living cells (see Sections 2.2.3. and 2.3.5. for applications). The available carbohydrate databases will certainly facilitate spectral assignment and glycan studies in cells in the near future [634,1667]. Small molecules such as metabolites can also greatly benefit from HR-MAS, and the applications explored in the metabolomics field have been numerous (see Sections 2.4.5. and 2.4.6.).

There are nonetheless some shortcomings of HR-MAS on living samples. First, cells suffer if subjected to hours-long MAS at rates above ~500 Hz, which packs them tightly on the 4 mm diameter rotor walls and possibly damages their viability. The centrifugal forces generated by MAS are clearly problematic: using disposable 4mm diameter rotors, 1-4 kHz spinning rates translate into forces of 8,000-100,000 g, which rapidly affects the integrity of mammalian cells [67]. These spinning rates are necessary to avoid signal artefacts known as "spinning sidebands". Samples can thus not be recovered after NMR experiments for a continuous survey. These samples are commonly snap-frozen and later thawed just before the NMR acquisition, causing cell damage and lysis that are often not reproducible. Then, ongoing enzymatic activity and metabolome evolution continues to be observed upon cell lysis and during NMR acquisition, so that additional heat-inactivation has recently been proposed for accurate measurements [1668], similar to earlier strategies using microwave irradiation of biopsy samples before analyzing them with HR-MAS [1669]. The delay between harvesting cells and freezing or analysis can also affect reproducibility. All these issues are also met with HR-MAS metabolomic analysis of tissues [972,1622,1670], and have probably hampered its adoption among conventional diagnostic approaches [971,974,1068].

The appealing aspects of HR-MAS have nevertheless motivated improvements in different directions. First, efforts have been made to find pulse sequences and sample preparation protocols that decrease MAS rates without resulting in spinning sidebands. Pulse sequences suitable for slow-spinning rates have been adapted to HR-MAS conditions, and can provide exploitable ^{1}H spectra using MAS rates as low as ~40 Hz (PASS) [1031,1032] and even 1 Hz (PHORMAT) as shown for rat liver tissue [1033]. However, these techniques achieve these outcomes at the expense of NMR ease-of-use and can even cause ~10x sensitivity losses in the case of PHORMAT [636,1671], which probably explains why their use has rarely been reported in the last 20 years, to the best of our knowledge. Techniques have been proposed that recombine spectra obtained at various MAS rates of about 300-700 Hz, which permits localization and removal of spinning sidebands [1672,1673].

In the last 10 years, more attention has been paid to sample preparation: reducing the sample size to a few microliters, shaping it as a sphere, or carefully removing air bubbles from the rotor limits the appearance of spinning sideband artefacts at MAS frequencies of ~400 Hz [1030,1662,1674]. This rules out any renewal of oxygen in the sample. These conditions generate forces of only 1,000 g at which lumpfish eggs, for example, remained intact. Also because of its favorable, spherical shape minimizing the adverse consequences of field heterogeneity, one single egg (~1 mm diameter) provided excellent NMR resolution using HR-MAS at 400 Hz [1030].

At such spinning rates, attention must be paid to J-coupling modulation during spin echoes, which can greatly alter signal quality [1030]. The non-J-modulated spin echo PROJECT [1650] has been usefully adapted in HR-MAS experiments by Caldarelli and Vermathen and their coworkers [1022,1028,1030]. Simpson and colleagues have also proposed the use of a low power adiabatic spin lock to filter out fast-relaxing species [1039], an approach that is further improved by diffusion-filtering [1006,1039]. A proper water suppression scheme is very helpful in clearly removing spinning side-bands, as shown again by Simpson and colleagues [929,1039].

Sakelariou, Wong and colleagues have designed inserts that integrate a rotating coil, enabling analysis of 100-500 nL samples by HR-MAS [1662,1675-1678]. Combined with NMR pulse sequences suitable for low spinning rates, these micro-HR-MAS systems provided a sufficient signal-to-noise ratio for metabolic analysis on a single *C. elegans* worm at a spectrometer field of 1 GHz with 300 Hz MAS [1041,1679,1680].

The development of slow (300 Hz) micro-HR-MAS systems by Wong and colleagues has even permitted analysis of samples containing only ~19 million yeast cells (~250 nL) and enabled their metabolome to be distinguished at various stages of growth or in osmotic stress [1042].

It is also important to emphasize the fact that HR-MAS rotors are hermetically closed before being inserted in the spectrometer, which prevents air exchange and brings about anaerobic conditions. Simpson and colleagues have shown that a "simple" hole drilled in the rotor cap allowed sufficient renewal of oxygen to keep fresh-water shrimps alive in the rotor [1006,1007]. According to the authors, the rotor spinning creates a vortex, which favors air exchange without buffer spilling or rotor instabilities. This rotor cap customization was also used to ensure aerobic conditions in a study on the fungus *N. crassa* [474].

Overall, problems arise from the centrifugal forces exerted on cells in HR-MAS NMR spectroscopy. These are not so problematic for microbial organisms, and novel techniques are being developed to achieve HR-MAS experiments at lower spinning rates. The resulting improved experimental conditions make it possible to study small animals, and, perhaps, organoid metabolism may also be monitored in the future using HR-MAS.

3.3.5. Other solutions to sample heterogeneity, molecular diffusion heterogeneity and sample evolution

We have seen in previous sections that sample heterogeneity causes peak broadening, which greatly hampers NMR analysis. We limit our discussion here to bulk magnetic susceptibility inhomogeneities, because in-cell experiments are usually performed in a constant, locked and shimmed magnetic field. Deleterious effects of such inhomogeneities are particularly problematic for ^{1}H-detected NMR, supposedly the most sensitive and versatile spectroscopy, because of the high gyromagnetic ratio of ^{1}H and its ubiquitous presence in biological samples. As described above, HR-MAS can eliminate some of the negative effects of sample heterogeneity, but it requires high spinning rates that can damage live cells and tissues. Other approaches have been applied to biological samples.

First, when the problem arises from the existence of different intra- and extra-cellular magnetic susceptibilities, it is possible to compensate using paramagnetic, or shift agents. This approach has been used notably in the 1980's to study erythrocytes: these contain high concentrations of hemoglobin, which can be paramagnetic in its deoxygenated form. Extracellular paramagnetic species can be used to match the intracellular magnetic susceptibility [1610,1681,1682]. This ensures lower intracellular

field gradients, and thus slower transverse relaxation times (see 3.2.2.). Whether this approach can be useful for cellular systems other than erythrocytes is questionable, but recent studies reported experimental values of mammalian cells magnetic susceptibility that suggest it may be [1581,1587,1589].

Pulse sequences exist that provide high-resolution spectra in inhomogeneous fields. Interesting research has been achieved using intermolecular zero-, single- or multiple-quantum coherences. In its later forms, this approach relies on establishing long-range dipolar couplings between protons of water and those of solute species [1683,1684]. In a rough simplification, this permits the correlation between local water chemical shifts in the indirect dimension (hence encoding the magnetic susceptibility variations) and local solutes chemical shifts in the direct dimension of 2D spectra. Post-processing treatment of 2D spectra can shear them back to corrected "inhomogeneity-free" spectra (Fig. 33) and yield high-resolution 1D projections. This has been used successfully on very inhomogeneous samples such as fish eggs [1685], grapes [1069], earthworms or water fleas [1686]. It has been combined with a supplementary J-resolved dimension on intact fish or on pig brain tissues [1687-1689]. At its current best, this approach suffers a 90% loss in S/N ratio per unit or time in 1D spectra [1686]. Arguably, a new type of quality criterion may be introduced, which would be the S/N per line-width ratio per unit of time.

Spatially encoded NMR spectroscopy, notably pulse sequences related to the Zanger-Sterk method for obtaining pure shifts, is also capable of removing field inhomogeneities. These rely on slice-by-slice resonance-selective excitation, decoupling and detection along the z-axis, and specific acquisition of chunks of the FID where the J-coupling evolution is negligible. This approach has been very well described recently in a didactic review by Dumez [1690]. To the best of our knowledge, it has been applied recently and only once to a heterogeneous biological sample, namely grape [1691]. This approach also suffers from low S/N and does not address the inhomogeneity in the x-y plane, although spinning the NMR tube can help with this. Above all, such spatially selective strategies cannot cancel the effect of sub-millimeter field inhomogeneities.

Temporal evolution of a living sample is the source of another type of inhomogeneity. This is commonly met when chemical reactions take place (e.g. metabolism, protein post-translational modifications) or when environmental conditions vary (e.g. exposure to chemicals). A classical approach to solve this problem relies on the successive recording of time series of NMR spectra. This implies a prior knowledge of the evolution timeframe to choose an appropriate acquisition time. ULTRAFAST approaches [1690,1692,1693] are rarely expected to be helpful for examining living samples, because the molecules to be detected are often at low concentrations. Time-resolved non-uniform sampling (TR-NUS) has been developed in the last years as a very specific approach to solve the issues related to temporal evolution. This method relies on the following principle: the NMR signal is acquired using a single uninterrupted experiment, during which the increments in the indirect dimension are allowed to vary in a randomized fashion. Sets of data points can be later extracted, which correspond to a limited experimental time window: even though they only partially sample the indirect dimensions, they permit reconstruction of the 2D or 3D spectra using dedicated NUS algorithms [1694]. This approach has been developed notably by Orekhov, Kazimierczuk and colleagues, and applied to characterize protein phosphorylation reactions *in vitro* [1695], bacterial metabolism [1061] and the metabolic response to growing toxin concentrations of water fleas [1066]. TR-NUS offers the appealing possibility to choose the experimental time windows in a post-acquisition fashion, and to use overlapping subsets of data or moving time-windows. The most suitable balance between S/N, resolution and time-frame can thus be found. The available software to process TR-NUS data should help in making this approach popular [1696].

3.3.6. Hyperpolarized metabolites for live-cell studies: 10,000 times more signal, but how many constraints?

Sensitivity is a perennial concern for NMR applications. It is set primarily by poor overall nuclear magnetization under usual experimental conditions, i.e. room temperature and a 1-10 T magnetic field: at equilibrium, it does not reach more than ~0.01% for ^{1}H, the highest γ nucleus. This starting magnetization limits the finally detected signal level. Enhancing nuclear magnetic polarization has been one of the most sought-after goals for NMR spectroscopists. For the purposes of achieving this goal, only "dissolution-Dynamic Polarization Enhancement" (d-DNP) has been consistently used for cellular metabolism studies, although para-Hydrogen induced hyperpolarization (PHIP) shows interesting capabilities too.

We have described applications of d-DNP and PHIP for real-time metabolic studies in live cells in Section 2. Although substantial, these achievements have not yet resulted in d-DNP becoming widely adopted as a regular approach for characterizing metabolism. In the following paragraphs, we highlight some key pieces of information on d-DNP, in an attempt to popularize its capabilities (and shortcomings) for non-specialists. Dedicated experimental designs and NMR pulse sequences have been developed to exploit these dissolved hyperpolarized species, and have been reviewed recently [1697,1698].

To increase the starting equilibrium nuclear magnetization, temperature is a possible parameter to tune that could bring great benefits theoretically: adopting a Boltzmann equilibrium, the useful magnetization of dipolar nuclei like ^{1}H, ^{13}C or ^{15}N is proportional to $\tanh(-\gamma h B_0/2k_B T)$, where γ is the gyromagnetic ratio of the considered nucleus, h and k_B are the Planck and Boltzmann constants respectively, B_0 is the polarizing magnetic field and T is the absolute temperature. Reaching sub-Kelvin temperatures would theoretically allow nuclear polarization to reach over 1% [1699]. Moreover, polarizing agents carrying free electrons can transfer the high electron polarization ($\gamma_{e^-} \sim 660\gamma_{1H}$, $\sim 2600\gamma_{13C}$) to the nuclear spins upon microwave irradiation at appropriate frequencies, a strategy commonly called Dynamic Nuclear Polarization (DNP). This theoretically permits one to reach 10-50% polarization at temperatures below 50 K. DNP-enhanced NMR is a very active field, which has recently gained strong interest and support, but its fundamentals and developments are beyond the scope of this review (see [1073,1074]). For fruitful use in metabolism analysis, it is necessary to implement i) fast dilution as a means to quickly thaw samples hyperpolarized at cryogenic temperatures, and ii) fast transfer to the analyzing magnet. Since the pioneering studies by Ardenkjaer-Larsen and colleagues in the early 2000's [1070], the promising 10,000- to 50,000 fold signal enhancements have been regularly achieved and d-DNP investigations have flourished [1071,1072].

Para-hydrogen induced hyperpolarization (PHIP) has recently been explored as a source of hyperpolarization for metabolism studies on living cells [1138-1140]. It relies on dihydrogen hyperpolarization at ~30-70K, and gives access to high magnetizations at lower cost than d-DNP

PHIP is however much less versatile than d-DNP if we consider the number of metabolites that can be polarized, even though great advances have been achieved showing the possibility to hyperpolarize pyruvate, fumarate, acetate, carbohydrates or amino acids [1700-1707]. Several methods exist to use para-hydrogen hyperpolarization [1708], which we will not discuss here given that there have been only a handful of applications with cells. We expect however that these will multiply in the future, notably

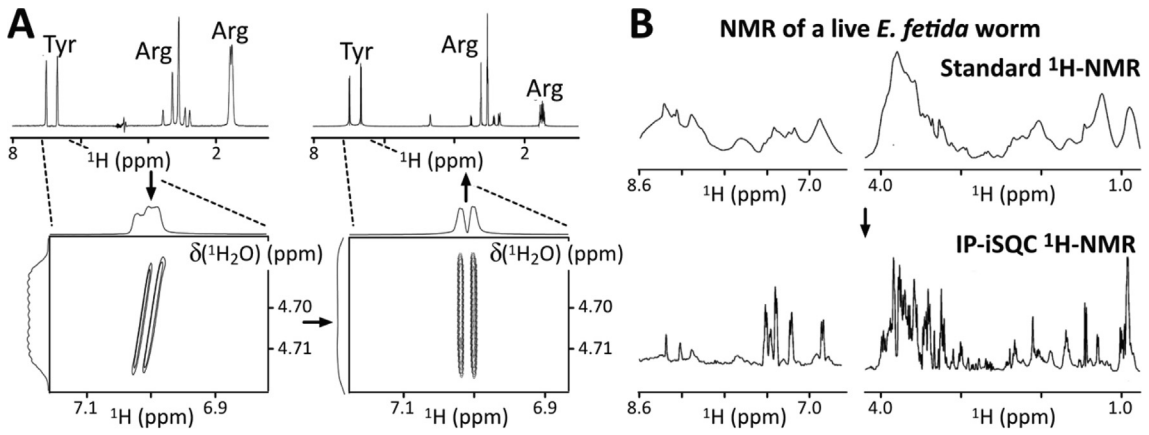

Fig. 33. A) Operating principle of intermolecular single-quantum correlation spectroscopy (iSQC), which correlates solute and water local resonance frequencies resonances and therefore allows a post-acquisition correction yielding an "inhomogeneity-free" final spectrum; ^{1}H-NMR spectra were recorded with a de-shimmed sample containing Tyrosine and Arginine; **B)** ^{1}H-NMR spectra of a live earthworm *E. fetida* recorded with a standard presaturation W5-WATERGATE pulse sequence (*upper panel*), and the IP-iSQC pulse sequence (*lower panel*) [1686]. Adapted from [1686].

thanks to the efforts being spent in improving the biocompatibility and purification of catalysts and products [1707-1710].

D-DNP and PHIP have however been used for real-time monitoring of metabolites that occur only at relatively high concentrations, i.e. in the millimolar range. This is because the technique currently has a number of limitations. First, the initial magnetization cannot be replenished once the experiment starts, whereas monitoring chemical reactions in real-time requires recording of a time-series of NMR spectra. This means a series of spectra can only be obtained by using small flip-angle pulses: a pulse with a flip angle of only ~1-15° leaves more than 95% of the magnetization available for subsequent scans [1072]. However, the cost of using this approach is that the sensitivity of each spectrum is decreased substantially relative to the full intensity for a single spectrum obtained after a 90° pulse.

A still worse problem is that in solution, the T1 relaxation of the studied ^{13}C nuclei ranges from 1 to 50 s for most metabolites at commonly used magnetic field strengths. This means that the hyperpolarization has to be used within minutes of its creation at best, before the global ^{13}C-magnetization has relaxed back to its thermal equilibrium value in the order of ~0.001%. Fortunately, a number of important metabolic reactions are fast enough to meet this constraint. [1-^{13}C]pyruvate is often used because of its "long" hyperpolarization half-life, c.a. ~30 s, compared to about 10 s for [U-^{2}H,U-^{13}C]glucose and just one second for protonated ^{13}C-glucose [1079,1112]. Intracellular ^{13}C-T1 relaxation has even been shown to be about 3 times faster than extracellular for hyperpolarized [1-^{13}C]pyruvate, [1-^{13}C]ketoisocaproate, [1-^{13}C]acetate and [1-^{13}C]butyrate [1711]; moreover, ^{13}C-T1s of such molecules are pH-dependent [1712]. This must be taken into account for the analysis of the reaction kinetics, together with an evaluation of the intra- and extra-cellular pools of observed molecules [1095-11011105,1106].

In complete contrast, DNP hyperpolarization build-up itself takes about an hour (even without including the manipulation time for preparing and properly freezing the DNP mixture). Moreover, it requires expensive polarizers and consumes significant quantities of liquid helium [1071]. Finally, DNP requires mixing the metabolites of interest with polarizing agents carrying unpaired electrons, which themselves greatly enhance T1 relaxation in the frozen state once microwave irradiation stops. Hence, the hyperpolarization vanishes within a few tens of minutes when using classical DNP conditions (glassy frozen solution in presence of "DNP-juice") even in the frozen state [1071,1698,1713,1714].

A number of possible solutions to improve the approach are currently being explored. Many strategies are being developed aiming at storing hyperpolarized metabolites in their frozen state, which would be useful for clinical applications. First, the so-called "brute force hyperpolarization" method has been tested, which relies on i) sustained ^{1}H polarization for ~24 hours at ~1 K and B_0> 10 T, ii) magnetization transfer from ^{1}H to ^{13}C nuclei at low field (B_0 < 0.1 T) to reach a ^{13}C-polarization of about 0.1% and iii) storage at cryogenic temperature (a few hours at T~30 K and B_0~2 T) or dissolution-thawing before acquisition [1699,1715,1716]. In these conditions, carrying out deoxygenation and a slow-freezing annealing have a beneficial impact on hyperpolarization lifetime [1715,1716]. However, it is not clear that it will prove sufficiently competitive with respect to DNP. Second, hyperpolarization can be maintained for hours by improved preparation schemes that introduce enough distance between the polarizing agents (that would otherwise enhance T1 relaxation due to their free electrons) and the metabolite of interest [1713], and it can be further enhanced by storing in a high magnetic field at cryogenic temperature [1717]. Third, radical precursors (notably pyruvate derivatives) have been developed in which unpaired electrons are generated upon UV-irradiation at ~80 K, hence turning them into DNP polarizing agents, but which readopt their non-radical form at ~200 K. Such molecules permit efficient DNP at ~5 K in their radical form, before being quenched at ~200 K, leaving hyperpolarized molecules in a favorable environment for their storage where they have relatively slow T1 relaxation during storage [1714,1718-1721].

Once in the solution state, hyperpolarization should be maintained for as long as possible. Quaternary ^{13}C nuclei are those likely to show the slowest T1 relaxation, because they have only weak dipolar interactions with other ^{13}C nuclei. For the same reason, deuteration of other ^{13}C nuclei drastically lengthens their T1 relaxation times. Importantly, the quadrupolar nature of ^{14}N has a negative impact on T2 relaxation of nitrogen-linked ^{13}C nuclei, which makes ^{15}N-labeling useful as a T2/signal-enhancing strategy [1125,1722]. ^{15}N nuclei themselves can be hyperpolarized and show longer T1 values because of the lower gyromagnetic ratio of ^{15}N than ^{1}H, ^{13}C or ^{14}N, which may makes ^{15}N an interesting nucleus for d-DNP studies [1135]. Hyperpolarization can also be

maintained using so-called "long-lived states" (LLS) for certain molecules, recently reviewed in [1723-1725]; however this topic is out of the scope of this review. Although this approach has allowed spin order lifetimes of minutes to be reached, metabolites of interest have not yet been found that could support LLS for cellular studies at high magnetic fields. The common large chemical shift differences between ^{13}C nuclei prevented the use of LLS as a means of detecting, for example, conversion of pyruvate to lactate [1726]. LLS have been generated mostly on ^{1}H nuclei couples and do not outcompete ^{13}C T1 relaxation times under usual experimental conditions [1702,1725,1727,1728], notably because of the negative impact of dissolved oxygen [1702,1729]. Hence, LLS applications for cellular studies have yet to appear.

Solutions to decrease the cost of d-DNP are being explored, such as the use of a cryogen-free polarizer that would save about 100 L of He per week [1071]. It has been also proposed to analyze simultaneously multiple samples in parallel, or in series, by mixing them with a single split preparation d-DNP hyperpolarized stock [1109,1730]. Altogether, hyperpolarization may hold great promise for studies monitoring real-time metabolism in live-cells, but d-DNP methods are still costly and PHIP approaches remain to be further established. We repeat the attractive ability of NMR to evaluate the metabolic status of cells or of organoids over long periods of time in a non-destructive manner. This would also be of interest as a complement to studies focusing on the intracellular behavior of proteins.

3.4. Observation of ligands

3.4.1. Technical recommendations for ligand observed NMR in presence of cells

The observation of small compounds by NMR can be facilitated by the use of T2/T1rho filters, as described in Sections 3.3.2. and 3.3.3. The removal of background signals arising from macromolecular cellular species is typically achieved using a short T1rho filter [1476] combined with the STD/TRNOE pulse sequences, which has also become normal practice for *in vitro* applications. The large signals from lipids can be removed using long adiabatic spinlock filters, as discussed in Section 3.3.3.

3.4.2. Technical recommendations for STD experiments in presence of cells

We want here to underline some technical aspects of STD experiments on cellular samples. STD-NMR experiments rely on the transfer of magnetization from the target protein to the observed ligand, more precisely on the transfer of magnetization saturation, i.e. null magnetization. Saturation reduces or eliminates signal intensity by driving the spin-state populations towards equality. It is produced by repeated, selective pulses (or alternatively very low-power continuous irradiation) at a ^{1}H-frequency where some protons of the studied protein resonate. Starting from the initially targeted protons, the saturation spreads initially to neighboring protons via the same processes of longitudinal relaxation as drive the NOE; then, via spin-diffusion (which is essentially just a process of many successively repeated NOE transfer steps), it spreads progressively throughout the whole macromolecule, as well as to ligand protons that contact the macromolecule during binding events. This saturation must be applied selectively at a frequency where only protein nuclei resonate to avoid any direct saturation of the ligand, an absolute requirement. Hence, the on-resonance saturation pulses must be applied at a resonance frequency distant enough from the ligand resonances, and simultaneously excite a sufficiently broad resonance window to maximize the saturation of the target protein [1731,1732]. A careful, case-dependent evaluation should probably be carried out systematically. Applying on-resonance pulses at very distant frequencies is feasible on cells, because their very long correlation time and heterogeneous environment cause very broad linewidths. On-resonance saturation at -4 ppm from the closest ligand resonance is very effective for virus like particles for example, as shown by Peters and colleagues [1448]. Saturation spreads rapidly in cellular macromolecules because of fast longitudinal relaxation associated with long correlation times. Two to four seconds-long saturation pulse-trains are usually applied to build a consistent saturation transfer through a maximal accumulation of binding events. However, a clean epitope mapping requires saturation times shorter than the T1 relaxation times of the observed ligand nuclei, otherwise saturation will spread into the rest of the ligand beyond the epitope [1448,1733,1734].

The transfer of saturation from the protein occurs while the ligand is bound, and acts to partially decrease the signal intensities of ligand nuclei that contact the saturated protein. To observe these intensity losses in the saturation spectrum, it is subtracted from a reference spectrum. This reference spectrum is acquired with the same pulse sequence, but the saturation pulses are applied at an "off-resonance" frequency that is sufficiently far removed from the protein spectrum that no protein resonances will be affected at all, even notwithstanding the very broad protein signal linewidths. Peters and colleagues have shown for virus-like particles that even off-resonance ^{1}H irradiation at -80 or +80 ppm (at 500 MHz) still exerted observable saturation for these large objects [1448]. They recommended using an off-resonance saturation frequency of -300 or +300 ppm for STD studies on cellular systems. We will not list all the later publications that reported off-resonance irradiation at only +/-20 or 30 ppm and probably therefore obtained unreliable results, but we note that such issues are not rare.

Another issue is the slow T1-relaxation of cellular species, notably that of surface proteins. Again while studying virus-like particles (estimated correlation time of 75 μs), Peters and Rademacher have shown that interscan delays of 25 seconds were necessary to avoid significant unwanted effects due to residual protein saturation during the off-resonance experiment (in schemes using interleaved on/off experiments) [1735]. This results in a clean epitope mapping, but reduced interscan delays may be more efficient in terms of S/N per unit time, while still delivering STD levels that are sufficiently contrasted to distinguish between ligand protons contacting or not-contacting the studied target.

STD-NMR has often been shown to be more sensitive in D_2O buffers [1731,1736]: these reduce saturation transfers between the protein and bulk water, hence maximizing the transfer of protein saturation directly to the protonated ligand, even though it slows down the longitudinal relaxation and increases the required length of interscan delays. Working in deuterated buffers is acceptable for viruses or isolated membrane fractions, but cells rapidly deteriorate in these conditions and caution is recommended.

Concerning sample preparation, Caffrey and coworkers have shown that serum proteins can establish weak interactions with the observed compounds, which are typically those detected by STD-NMR [1454]. STD pulse sequences in normal use cannot saturate selectively cellular species as opposed to serum species. Advanced saturation schemes using isotope-filtering exist [1737,1738] that would allow a selective saturation of cells, but this would require prior cellular ^{13}C/^{15}N isotopic labeling. One can also consider using ^{13}C/^{15}N labeled antibodies to transfer the magnetization saturation [1739]. Martinek and colleagues have shown that this approach works in cell extracts, but there would likely be a number of complications in the context of living cells. Moreover, it is probable that these strategies would severely complicate the quantitative interpretation of STD results. Of course, the simplest option is the use of serum-free medium during the NMR experiments, which is acceptable for limited measurement times of a few hours.

As mentioned in Section 2, STD-NMR experiments on cells are most often performed in a STD-Difference (STDD) mode: two STD spectra are recorded, for example in the presence of mock-transfected cells (i.e. expressing only native cellular material) and in the presence of cells expressing the protein of interest. This is for two reasons. First, it would not be possible to use the choice of saturation frequency to select between the macromolecule of interest and the cellular background, as all signals of the macromolecule would inevitably be overlapped with signals from the cellular background. Second, saturation is anyway rapidly transmitted to the surrounding cellular species. Hence, compounds that only bind transiently with cellular membranes would show STD signals, but these should not be interpreted as an interaction with the membrane protein of interest. Moreover, a compound can also bind another endogenous receptor and consequently build-up STD signals. Finally, it is also important (and sometimes difficult) to be aware of the potential effects of variations in cellular metabolism and composition: the states of cells during NMR acquisition should still be as similar as possible to avoid any bias (e.g. binding to novel lipids, or phase-separated stalled mRNAs, etc...).

Finally, corrupted results may emerge from experiments using cells that progressively settle towards the base of the NMR tube. An elegant solution for this has been proposed by Jimenez-Barbero and his coworkers, that employs disposable rotor inserts designed for HRMAS [1475]: rotors can be filled with cell suspension and spun at a few kHz, which did not compromise cell viability according to the authors. Cells are thereby homogeneously sedimented on the rotor walls and STD experiments can be carried out. This approach was proposed almost 10 years ago, but we did not find any other later study in which it was used. The recent protocol by Konrat and colleagues may be easier to implement: cells are embedded in methylcellulose hydrogels to maintain a homogeneous dispersion, and settling in the NMR tube does not occur [1487].

3.4.3. On the use and present limits of on-cell NMR and the use of STD/TRNOE

As mentioned in Section 2, in the last 20 years ligand-observed NMR methods (STD-NMR, waterLogsy, T1rho/T2 relaxation) have been have been widely and successfully used for fragment-based drug design *in vitro*. The same has not been true for in-cell studies. Ligand-oriented NMR screening methods are valuable specifically because they detect weak affinity interactions [1386,1412], but these may often be uninterpretable in complex media: abundant metabolites also establish weak interactions [1413,1414], and reliably identifying interesting hits would require highly reproducible metabolic states that current bioreactors can hardly generate.

Instead, in-cell NMR studies using ligand-based NMR detection have been focused on epitope mapping and structure-activity relationships: STD-NMR and TRNOE approaches have been favored due to their ability to deliver atomic-scale information on the interacting moieties of ligands and on their bound conformations. Although other ligand-observed NMR methods, such as waterLOGSY or T1rho relaxation enhancement, would presumably also work in complex media, they have not been extensively used for cellular NMR studies of drugs, probably because they do not provide structural information. However, waterLOGSY and T1rho relaxation enhancement have been shown to offer better sensitivity to binding events [1379,1413,1736,1740]. They may find increased application in the future.

Indeed, we feel that the capabilities of in-cell/on-cell STD/TRNOE/waterLOGSY/T1rho approaches may be exploited more broadly. On paper, their attractions are clear: it would be convenient and useful to observe direct contacts between a ligand and its membrane receptor in a native environment, without having to establish difficult purification and solubilization strategies. Defining standardized protocols for in-cell epitope mapping would promote trust and reproducibility. The use of isolated membrane fractions is likely to give access to simple protocols. However, we feel that avoiding membrane separation would be more convincing for biologists. Generating stable transfected cell lines for every protein target would thus be a prerequisite: it would yield reproducible expression of target proteins in the long term. Moreover, to permit the use of intact cells, experimental designs that avoid cell sedimentation are probably key success factors, as has recently been proposed [1487]. Applying automated procedures developed for background noise removal in metabolomics spectra may also be helpful to simplify the analysis of NMR cellular drug screening [1741,1742].

One reason why these epitope mapping approaches are not that popular for in/on-cell NMR studies may be the nature of the targets chosen to date: almost all publications of cellular experiments based on STD and TRNOE measurements have concerned surface proteins, mostly GPCRs [1469-1474,1489,1493] and integrins [1476,1479-1487] (see Section 2). Ligands of GPCRs commonly have long residence times with off-rates of 1 to 0.01 min^{-1}, as characterized by radioligand assays [1743]. Similar orders of magnitude have been reported for FDA-approved kinase inhibitors *in vitro* [1744]. Unfortunately, STD and TRNOE have the same limits with cells as they do with purified proteins: they can report on

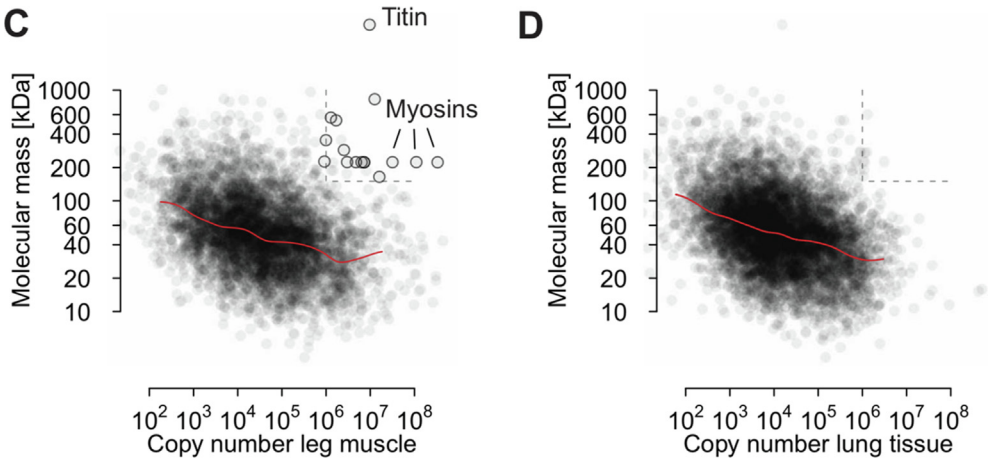

Fig. 34. Distribution of protein-size as a function of protein-copy-number per cell within two tissue types (adapted from Wiesniewski 2014 [1175]). Every dot represents one experimental point from mass-spectrometry quantification. The red line indicates the average protein size for a given copy number per cell. Important differences can be observed between cultured cell lines and the tissues from which they are derived [1176].

interactions showing relatively weak affinities and fast on/off rates (Kd$\sim10^{-7}$-10^{-3} mol/L, $k_{off}\sim10^{2}$-10^{6} s^{-1} [1379,1412]). STD-NMR fragment screening on a solubilized GPCR has been recently proved to be feasible *in vitro* [1745], and, more generally, NMR has made recognized inputs in membrane protein drug research [1746]. Novel NMR approaches will have to be found for sensitive, ligand-observed studies of interactions with slow on- and off-rates, as has been discussed elsewhere [1379]. Such methods would find immediate applications for in- and on-cell studies. Alternatively, detecting ligand:protein interactions by the observation of the protein is a possible solution (see Sections 2.5.1. and 3.5.4.).

3.5. Cellular structural biology

3.5.1. How relevant is the intracellular concentration of the studied species?

If we had to select the single most crucial question concerning in-cell structural biology, that would be the issue of concentration. Conventional NMR structural biology studies use highly purified nucleic acids or proteins at high concentrations, i.e. in the 0.1-1 mM range, orders of magnitude above cellular concentrations. Exceptions exist, such as hemoglobin in erythrocytes (~5 mM). We know the protein copy numbers in many mammalian cells, which are the best characterized cells in this regard. Such cells are about 20 μm across, contain about 200 g/L of proteins (~4% from ribosomal proteins, ~4% from histone proteins) and contain an average of $\sim5.10^{4}$ copies per cell of every single protein species [1175-1177], which corresponds to a concentration of 1 μM. However, the distribution is broad: copy numbers span a wide range of values from 10^{2} to 10^{7} per cell. In addition, all these numbers vary between cell lines and through the cell cycle [1747]. An interesting anti-correlation between protein size and copy number has been reported (Fig. 34). Moreover, many proteins of particular interest show high expression levels, e.g. oncogenes in cancer.

These micromolar concentrations are not generally suitable for acquisition of 3D NMR spectra, but they are compatible with 1D and 2D spectra. However, even when they are packed in wet pellets, cells cannot in practice comprise more than ~20-40% of the volume of an NMR sample, according to our tests (the actual volume of a cell is very difficult to quantify accurately [1175]). This unavoidably reduces the maximum number of molecules from which an NMR signal can be observed, which forces investigators to use unnaturally high intracellular concentrations of the macromolecule(s) of interest, i.e. above 10 μM and often above 100 μM (up to millimolar concentrations for structure determination in cells).

Daunting questions remain moreover concerning protein localization and NMR-detectability. In-cell protein NMR yields averaged signals from all the species that i) tumble sufficiently fast (solution NMR), ii) do not interact with too many partners, each one of these interactions generating a new fractional population in a distinct chemical environment, and thus a supplementary dispersion of the resonances (solution and solid-state NMR) and iii) do not bind their partners with on/off rates in the intermediate exchange timescale (solution NMR). Among other issues, high concentrations of a macromolecule of interest can have saturating effects on the pool of native binding partners: if the total population of binding partners is engaged in interactions with the studied species, supplemented or overexpressed in excess, it can leave a population of molecules free and well-observable by NMR. Hence, situations can be generated where the NMR-detected population is no longer biologically relevant. These aspects should not be forgotten when reaching conclusions for in-cell NMR studies.

Hence, in-cell NMR-assisted structural studies are most often not likely to deliver results directly related to functional biology. Rather, such investigations explore the consequences of the cellular milieux on the structural behavior of macromolecules, which is nonetheless of fundamental importance. It would thus also be unfair to describe them as irrelevant simply because of concentration issues. These concentrations delimit the degree of generalization that can be claimed.

In any event, it is clear that an important goal for improving isotopic labeling schemes and NMR methods should be to help facilitate in-cell NMR studies at lower concentrations.

3.5.2. Sample preparation

Sample preparation for in-cell protein NMR has been reviewed multiple times. We discuss studies focusing on nucleic acids separately (see Section 3.5.6.). Detailed protocols exist for all sorts of samples in prokaryotic or eukaryotic systems, generated from in situ recombinant expression or from protein delivery in cells [4,9,25,1186,1236,1748-1753]. Here, we will simply recommend to check cell viability, protein integrity (by western-blot for example) and protein leakage. Quantifying the intracellular quantity of a protein of interest allows comparison of expected and experimental NMR signal intensities. This requires a good estimation of the signal losses due to $^{1}H/^{13}C/^{15}N$ T2 relaxation during the pulse sequence: these are rather different in a dilute reference sample than they are in the cellular environment. Such quantification is highly relevant for evaluating the percentage of detectable protein. None of these quality controls is individually perfect, but all of them should reinforce each other.

3.5.3. Protein structure determination

In the following, we discuss studies and methods using solution NMR. Although many solid-state NMR studies have reported structural information in cellular environments, these were not used for solving structures.

A normal protein structure determination procedure by NMR starts with the assignment of resonances, which classically requires at least a set of 3-dimensional spectra. Assignment procedures of NOE peaks are most often intertwined with structure calculation within recursive algorithms. This subject is well established from the field of protein NMR and is out of scope for this review. We will only mention that, as far as solution NMR is concerned, NMR assignment will always be hampered in cells, because of faster T2 relaxation (see Section 3.2.) and because 3D spectra necessitate long acquisition times that are not compatible with the lifetime of cellular samples. In this regard, using bioreactors helps to maintain cells viable across extended periods [1188]. Improved strategies have been proposed, notably by Ito and colleagues, to adapt the usual in vitro approaches to the constraints generated by cellular samples. These aim at shortening the acquisition time of 3D spectra by using sampling schemes that reduce the number of increments required [1184-1188,1754]. They also use amino acid specific labeling to decongest the spectra. It is recommended to use 3D pulse sequences that are intrinsically less vulnerable to T2 relaxation losses, such as HNCA, HN(CO)CA, CBCA(CO)NH or NOESY-HSQC.

Another approach relies on the use of lanthanide tags: linking these at multiple selected positions (in separate samples) permits measurement of pseudo-contact shifts (PCS), which provide a very powerful NMR restraint for structure calculation [1755-1757]. Structural models were obtained from tagged proteins delivered in frog oocytes or mammalian cells [1193-1195]. The PCS can be analyzed by the GPS Rosetta algorithm [1758]. This strategy proved to be efficient to solve the structure of small model proteins in cells, using ~50 μM intracellular concentrations. It has been used mostly to obtain backbone restraints, and is probably not likely to provide high resolution structures. Moreover, lanthanide tags can cause protein alignment in the magnetic field, which may be sufficient to measure residual dipolar couplings (RDCs). Although

RDCs have not been as useful as PCSs in the studies mentioned above, some amide ^{1}H-^{15}N RDCs were measured to be as strong as 25 Hz at 600 MHz. They could possibly provide valuable information in future structural/dynamics studies at higher fields. PCSs can provide information up to ~4-5 nm away from the lanthanide tag, while RDCs do not depend on the distance to the tag. As in classical studies on purified proteins, both PCSs and RDCs are of course complementary to NOE-derived structural restraints.

3.5.4. Protein:protein interactions and protein:ligand binding

Questions related to intracellular protein diffusion and multiple, transient interactions with cellular constituents have been discussed in Sections 3.2.1. and 3.2.3.

Strategies to characterize protein:protein interactions by NMR in cells have been developed, notably by Shekhtman and colleagues: *E. coli* cells are i) transformed to carry two plasmids coding for the inducible expression of the two protein partners of interest, ii) grown in Luria Bertani (LB) medium containing a natural abundance isotopic distribution (i.e. 1.1.% of ^{13}C and 0.4% of ^{15}N), iii) transferred into a minimal medium containing $^{15}NH_4^+$ as sole source of nitrogen, in which recombinant expression of the protein target is triggered for a few hours, iv) re-transferred into an LB medium where the recombinant expression of the second protein is triggered [1232,1233,1274]. Hence, the first recombinant protein (but not the second) is ^{15}N-labeled in a mostly ^{14}N cellular background. Long-lived molecules produced during the incubation in the minimal medium are also ^{15}N-labeled, but represent generally a heterogeneous pool of species, whose spectroscopic signature is sufficiently diffuse to not perturb selective NMR observation of the protein of interest. Protein:protein interactions are thus revealed by the ^{15}N-protein signals that shift or disappear upon expression of the second recombinant (^{14}N-labeled) protein. This approach has been used to screen inhibitors or stabilizers in cells, in an attempt to find a complementarity using high-throughput screening approaches [1390,1391].

Luchinat, Banci and their coworkers reported an approach to express and isotope-label target proteins sequentially in mammalian cells [1759]: i) a stable cell line overexpressing a first protein is established and grown on a natural abundance medium; ii) cells are transfected concomitantly with a plasmid encoding for a second protein and silencing siRNA for the first protein; iii) cells are later transferred into a medium supplemented with ^{15}N-labeled amino acids. The precise timing between steps ii and iii is critical to restrict ^{15}N-labeling of the first protein and of the cellular background, while maximizing that of the second protein. A more classical co-transfection and overexpression of two protein partners requires finding the best proportions of the corresponding plasmids and of the transfection reagent. This strategy has been used by Luchinat, Banci and their coworkers, notably to co-transfect and co-overexpress a protein and its chaperones in appropriate proportions [9,1280,1283]. However, this strategy results in an identical isotope-labeling of both proteins.

Protein-observed ligand binding assays have been carried out in cells based on single overexpressed proteins, either in prokaryotic or eukaryotic systems [867,1392,1393,1760,1761]. After overexpression in an isotope-labeling medium, cells can be exposed to the ligand, which provides simultaneously several pieces of information: i) does the ligand bind the protein target in cells and if so with what apparent Kd?; ii) does the ligand penetrate the cells and if so at what rate?; iii) does ligand binding have an impact on the protein target conformation or post-translational-modifications? Naturally, as discussed in Section 3.2.1., the usefulness of the experiment depends on the protein concentration, its cellular localization and its NMR-detectability in cells (is the whole population detected or only a limited proportion?). This approach is nevertheless very promising. It could be further improved by designing experimental procedures i) to obtain valuable NMR spectra using lower and better controlled protein concentrations; ii) to establish reproducible conditions using more standardized bioreactors but also more biologically relevant cell lines.

3.5.5. In-cell solid-state NMR and the road to DNP-enhanced in-cell NMR

Solid-state NMR (ssNMR) using Magic-Angle Spinning (MAS) potentially has a great advantage over solution NMR in that it can acquire signals from proteins immobilized in membranes or in large macromolecular assemblies. As briefly explained in Section 3.3.4., MAS can suppress the effects of magnetic susceptibility inhomogeneities or unfavorable line-broadening due to slow molecular tumbling, which causes large dipole-dipole interactions, chemical shift anisotropy, or first order quadrupolar interactions.

ssNMR has consistently provided useful information on proteins and peptides in native membranes, starting with the work of Schaefer and colleagues on antibacterial peptidoglycan-binding drugs in the 1990's (see Section 2.2.2.). There is currently a growing number of ssNMR studies on transmembrane proteins in native membranes. To the best of our knowledge, only a few solid-state NMR investigations have reported de novo assignment in a native environment (bacterial membranes in most cases) [1173,1199,1752,1762-1764]. The many other ssNMR studies in the literature successfully transferred assignments made *in vitro*, in a similar fashion to what has been seen with in-cell solution NMR. ssNMR requires high MAS frequencies, which would affect cellular viability in physiological conditions (see Section 3.3.4). Frozen samples can preserve cell integrity during the ssNMR measurements, but they also suffer from peak broadening, notably also resulting from freezing heterogeneous ensembles of conformations and interactions with the cellular milieu. These studies often rely on carefully designed amino acid specific labeling to compensate their common poor resolution.

Most of the ssNMR structural characterizations in "native" conditions concern membrane proteins: the cellular membranes represent good 'native environments' and the removal of cytosol increases the proportion of useful sample in the rotor. A number of publications describe the isolation and packing of cellular membranes in ssNMR rotors following various protocols [1173,1197-1200,1203,12041207121012111752]. Until recently, (DNP-) ssNMR studies on membrane proteins in native membranes relied on ^{13}C-detected experiments. In principle, ^{1}H-detected spectroscopy could offer higher sensitivity. However, it requires either MAS above 60 kHz [1765] or extensive deuteration of the sample matrix to suppress dipolar ^{1}H-^{1}H relaxation, which makes it difficult to use this approach for complex biological samples. Medeiros-Silva et al. proposed a novel labeling scheme, namely inverse fractional deuteration, to obtain high resolution ^{1}H-detected ssNMR spectra of the K^+ channel KcsA in liposomes and in native membranes [1209]. This approach improved the detection of water-inaccessible protons and enabled backbone assignment *in vitro* through a 'classical' strategy using triple resonance 3D spectra. These assignments were transferred to signals of the sample *in situ* via 2D ^{1}H-^{15}N spectra, thereby permitting the characterization of as few as 3 nanomoles of TM domain in native membranes; in addition the authors carried out a detailed analysis of its motions *in vitro* through ^{15}N relaxation experiments.

The first application of ssNMR to investigate a soluble protein in intact cells was published by the Dötsch group in 2012, in which Reckel et al. analyzed bacterial cells under freezing conditions using ^{13}C-detected ssNMR [1212]. Bacterial thioredoxin and human FK506-binding protein (FKBP) were chosen because both proteins interact diffusely with the cellular environment: this causes extensive signal broadening at physiological temperatures, and prevents detection by solution NMR. In that work, freezing

temperatures were necessary to preserve cellular integrity. Also, ^{13}C-depleted glucose had to be employed in the culture medium before protein expression, in order to suppress the unwanted signals arising from natural abundance ^{13}C. In their concluding remarks, the authors noted that DNP would likely become an indispensable tool to increase the sensitivity of the method. Since then, DNP-ssNMR has been applied to study proteins in quasi-physiological samples such as cellular lysates and, more recently, directly in intact human cells. Frederick et al. investigated the folding and aggregation of the yeast prion protein NM (i.e. the prion domain of Sup35) in frozen yeast cell lysates using DNP-ssNMR [1172]. When pure NM was added at 1 μM to lysates already containing the prion form of Sup35, it adopted an amyloid form, which was more structured than the amyloid fibrils formed *in vitro*. Deuterated lysates were employed to render the cellular milieu NMR-invisible and to increase polarization efficiency [1170]. Viennet et al. used Bcl-x_L as a model protein to assess the DNP enhancement selectivity in bacterial cell lysates, using a radical-labeled binding partner to selectively enhance the protein signals with respect to the background caused by other labeled cellular components [1766].

The first test of the application of DNP-ssNMR to intact human cells was published by the group of Barnes [1767]. Using biradicals and sterically shielded radicals as polarizing agents, DNP enhancements of ∼50 were obtained at temperatures ranging from 6 to 90 K. A novel fluorophore-containing polarizing agent was introduced, which allowed simultaneous subcellular localization studies through fluorescence microscopy on the same cellular samples. The approach was recently combined with cell sorting through flow-cytometry to investigate the endogenous activation of the HIV virus by correlating GFP expression with increased ^{15}N-amide resonance intensities in highly homogenous cell populations [1768]. The same research group further explored the effects of electron decoupling on cellular DNP-ssNMR spectra, reporting sensitivity improvements at cryogenic temperatures [1769].

A DNP approach to investigate intracellular proteins in frozen human cells was reported recently by Baldus and coworkers [1213]. They delivered isotopically-labeled ubiquitin to cells using electroporation. Then, they proved notably that their DNP polarizing agent diffused within cells using a fluorophore-tagged DNP-biradical: they observed a uniform fluorescence distribution 15 minutes after exposing the cells before filling the rotor with these cells. The preparation of cells for DNP measurement is still not a routine procedure: the mixing of the "DNP-juice", the timing, freezing method, etc.. can all benefit from optimization. The Frederick group has recently addressed these aspects: they reported a detailed workflow for the correct cryopreservation of human cells prior to DNP analysis, which is crucial for preserving high cell integrity and viability [1770].

3.5.6. Nucleic acids

Successful NMR studies of nucleic acids in mammalian cells became frequent only in the last 2-3 years, so that systematic guidelines are difficult to define as yet. Previous studies have been mostly performed in microinjected frog oocytes, and have been reviewed multiple times [4,5,1323,1771]. Using current methods, the concentrations of the nucleic acid of interest can reach ∼15 μM in mammalian cells, and ∼100 μM in oocytes [1322,1329]. Just as for in-cell studies of proteins, checking viability, leakage and localization of the studied nucleic acids is mandatory, especially in cases where they have been delivered into the cells using membrane destabilizing methods.

Detailed protocols exist for sample preparation of phages and NMR analysis of their DNA content [1307,1311,1312,1772]. Such studies benefit from the rather standard and economical ^{13}C/^{15}N labeling procedures of bacteria. It is worth mentioning that supplementing the culture minimal medium with unlabeled amino acids together with ^{13}C-glucose and ^{15}N-ammonium helps to obtain NMR spectra showing almost only ribose signals; supplementing with unlabeled Phe, Tyr Trp, Tyr removes side chain resonances of these residues from ^{13}C/^{15}N-edited spectra, while retaining ^{13}C/^{15}N labeling of DNA bases [1310,1312]. ^{13}C/^{15}N labeling of nucleic acids is extremely helpful to characterize structural ensembles of nucleic acids, which commonly explore different conformations in dynamic equilibria occurring over a broad range of timescales [1291,1292,1294,1773]. Such labelling also helps to define any chemical modifications they may have [1331].

Unfortunately, there is a high financial cost for the methods used to date for preparing ^{13}C/^{15}N labeled nucleic acids, before delivering them in mammalian cells using the published methods, electroporation and pore-forming toxins (electroporation performing better in terms of cell viability and leakage according to the literature [1320,1322,1323,1326,1329]). Hence, the studies have mostly been restricted to observation of ^{1}H-signals from the imino groups, which are largely free of interference from cellular background signals [1321,1324-1326,1329]. ^{19}F-labeled nucleic acids have been also tested recently, which have the advantage that ^{19}F NMR has no cellular background signal, but these molecules could also modify the conformational ensemble being investigated [1326-1328]. In both cases, the stability [1329] and the multiple conformations and/or interactions [1326] of nucleic acids in cells can be a severe obstacle. As discussed for proteins in Section 3.2.3., multiple transient interactions in cells have consequences for the NMR detectability of nucleic acids. Interestingly, Trantirek and colleagues showed recently how G-quadruplexes of similar size can adopt very different structural dynamics, how these fluctuate in presence of G-quadruplex ligands, and how the corresponding NMR spectral fingerprints allow or prevent in-cell NMR studies [1326]; this group has provided some very useful detailed accounts of work in this field. The current in-cell NMR techniques are thus limited in the quality of structural information they can offer and in the number of nucleic acids that can be studied. Even though multidimensional NMR of nucleic acids seems often to be impractical in cells [1329], ^{13}C/^{15}N labeling and NMR-editing of single bases in the nucleic acids of interest might be used in the future to help elucidate conformations or interactions with ligands. Alternatively, monitoring the NMR signals of a ligand can sometimes be sufficiently informative [1329].

3.6. Whole cell analysis

3.6.1. Solid-state NMR analysis of cellular content, molecular proximities and chemical bonds

As mentioned earlier, solid-state NMR coupled to magic-angle spinning permits the detection of the whole set of molecules carrying a specific isotope labeling when edited by a chosen pulse sequence (see Section 3.3.4.). This capability has been extensively exploited by Schaefer and colleagues to characterize a number of connections in bacterial cell walls and to determine the position of some antibiotics in the bacterial cell walls (see Sections 2.2.2. and 2.5.2). It has also been used to quantify the cellular content of certain molecular species upon exposure to chemicals. These techniques are appealing particularly because they do not require prior extraction steps before the NMR analysis.

In the early 1980's, authors used the so-called Double Cross-Polarization (DCP) [1774] from ^{1}H to ^{13}C and then to ^{15}N to enable selective observation of branched ^{15}N-Lys and ^{13}C-D-Ala [584-586]. However, these experiments suffered from weak signal intensities, and moreover were contaminated by signals from cellular components containing ^{15}N at natural abundance (these were removed during processing by spectral subtraction). From the late 1980's, Schaefer and coworkers started i) to remove cellular back-

ground using ^{13}C-^{13}C connectivity filters (DARR), which they demonstrated for the selective observation of [1,2-$^{13}C_2$]-Gly in *Klebsiella pneumoniae* [592] and ii) to improve the sensitivity of ^{13}C-^{15}N proximity filtering using the recently invented REDOR [593] and TEDOR [1775] techniques. The combination of DARR ^{13}C-^{13}C and REDOR ^{13}C-^{15}N or ^{13}C-^{19}F was indeed found to be effective. Importantly, the REDOR approach depends on dipolar couplings, which are distance dependent: distance measurements became possible between ^{13}C and ^{15}N nuclei [606], and later between ^{15}N and ^{31}P (for the analysis of DNA in phages [1306]), or ^{13}C and ^{19}F (for analyzing ^{19}F-containing molecules inserted into cells). Hence, the studies described in Sections 2.2.2. and 2.5.2 rely substantially on REDOR or TEDOR. We thought it would not be appropriate to present them extensively here, instead citing relevant publications [570,587-591].

3.6.2. The case of hyperpolarized ^{129}Xe, a multitask MRI-oriented reporter

Hyperpolarized ^{129}Xe detection represents a peculiar case in the zoo of observable species that have been used for NMR cellular studies. We mentioned ^{129}Xe-based sensors in different sections for various applications. These have been developed for the purpose of designing new sensitive probes for MRI, e.g. to detect cell surface proteins [1776-1779], or to probe pH [1780,1781] and intracellular chemical entities like thiols or ribose [1782,1783], without any fundamental interest for cellular processes themselves. This topic will not be covered further here, but some excellent reviews on ^{129}Xe based sensors have been published [1784,1785].

3.7. The quest for a bioreactor

3.7.1. A re-emerging necessity

Keeping cells healthy in the spectrometer has been a long-term goal in the field. It is necessary for real-time monitoring of metabolic changes or molecular interactions, or to maintain cells in well-defined conditions when long acquisitions are required. We found about 200 reports using or presenting the design of an intra-spectrometer flow-probe bioreactor since the 1970's. The NMR-compatible bioreactor has been re-invented dozens of times, but the individual experimental designs apparently were not widely taken up beyond the labs where they had been developed. Although not fully exhaustive, our statistics show two main periods of activity (Fig. 35). Between the 1970's and the year 2000, a first period started with experiments on perfused animal organs, progressing later to home-made systems for metabolic studies. Since the 2000's, a second period saw in particular the emergence of low-diameter cryoprobes, whose higher intrinsic sensitivity is offset here by their small diameter (< 10 mm), close design and lower flexibility. Those familiar with standardized commercial systems are probably less tolerant of setting up and tuning home-built probes.

Initially, systems to perfuse organs were used in the 1970-80's, mostly to monitor ion equilibria or metabolism in rat or rabbit hearts [277,378,807,812,818,856-859,861,1786-1789], livers [725-727,809,814,1790-1794] and kidneys [808,819], using ^{31}P-, ^{23}Na- ^{13}C- or ^{1}H-detected NMR [1795-1797]. Perfusion systems for NMR spectroscopy of living plants were also proposed [884-886,900,1798]. We will not cover this field further.

In the vast majority of cases, bioreactors were designed in the context of studies on cell metabolism. As discussed in Section 2.3.1., in-cell NMR studies of metabolic activities are more suitable for high concentration metabolites. Hence, NMR spectroscopy of extracted and isolated material became dominant in the study of metabolic pathways in the 1990's, in combination with Gas- and Liquid-Chromatography coupled to Mass Spectrometry [39,762,798-800]. Although they require tedious extraction and calibration procedures, these approaches allow the application of reproducible, systematic protocols. In the 2010's, bioreactors reappeared in the literature as appealing devices for i) in-cell structural biology (see Section 2.4.), ii) metabolism studies using ^{13}C-hyperpolarized metabolites; iii) longitudinal metabolism and toxicology studies on cells (including for online monitoring of external, large-scale reactors), iv) and also on small animals like worms or water fleas [930,1057,1066].

Many NMR-bioreactors were proposed in the 1980-90's for studying cell metabolism. They all involve pumping systems of culture media equilibrated with the appropriate CO_2/O_2 gas ratios. A description of these home-made designs would be quite repetitive and not very informative. Equivalent commercial devices have been proposed in the last ten years, which are compatible with the actual (cryo)probes now present in most laboratories.

3.7.2. Cell immobilization strategies

With regard to the conditions in which cells are maintained in the measurement volume, several options have been explored. First, cells can be kept in suspension in the NMR tube: There has been a long and varied history of many stirring or bubbling devices designed through the years, which avoid settling and clumping and ensure (an)aerobic conditions (see [783,838,841,1802-1819]). These designs are often not compatible with recent, narrow probe designs, where keeping cells inside the active volume of the tube despite the flow of medium has been a long-term challenge. A number of strategies have been proposed.

Flow-probes for suspension cells were initially developed that used dialysis fibers for the circulation of the fresh medium [1820]. Soon afterwards in the mid-1980's, an advanced version of this principle was proposed to provide rapid flow of medium and high O_2 delivery for aerobic cells [1821,1822]. A similar approach involved circulating the fresh fluids through the lumen of hollow fibers, whose polymer porous walls permit nutrient diffusion to the interspace of the fibers, where suspension cells are maintained [771,797,1823]. Adherent cells can also attach on the hollow-fibers walls, either inside [1824] or outside [789,791,797,1823,1825-1830]. Good results have also been obtained with a recent simplified version using a 1 MDa dialysis membrane, in which fresh medium flows continuously [1761]. The most popular approach has been to immobilize cells in beads [1811,1831-1833] or threads made of agarose [167,179,765,777,780-782,786-788,795,796,852,866,867,1354,1801,1834-1850], alginate beads [784,785,790,869,1103,1105,1369,1804-1806,1840,1851-1858], carrageenan gels [1859,1860], or low-temperature melting PNIPAAm-PEG gels [475,868,1861]. Other designs took advantage of improved matrices composed of methylcellulose [1487], poly-L-Lysine containing alginate [1862,1863] or biological material composing extracellular matrices like collagen or Matrigel, which are better adapted to cell proliferation [167,387,785,789,794,1799,1849,1853,1864-1867]. The diameter and composition of gel threads or beads has of course an impact on diffusion of ions [167]. Adherent cells can be grown on micro-carrier polymer beads [167,778,779,792,793,1093,1099,1100,1112,1800,1865,1868-1874], on fibers [1800] or even on polyethylene terephthalate (PET) scaffolds [1875]. Cell spheroids and plant cells or root nodules have convenient characteristics: unlike single bacterial or mammalian cells, they do not require any immobilization to be retained in the NMR tube, and simple perfusion systems can be used [882,964,1876,1877], possibly equipped with loose nets and completed by stirring devices [1878]. Remarkably, insect cells were also maintained viable in suspension at the bottom of the NMR tube while using a low flow rate of culture medium (2 mL/h) [1188].

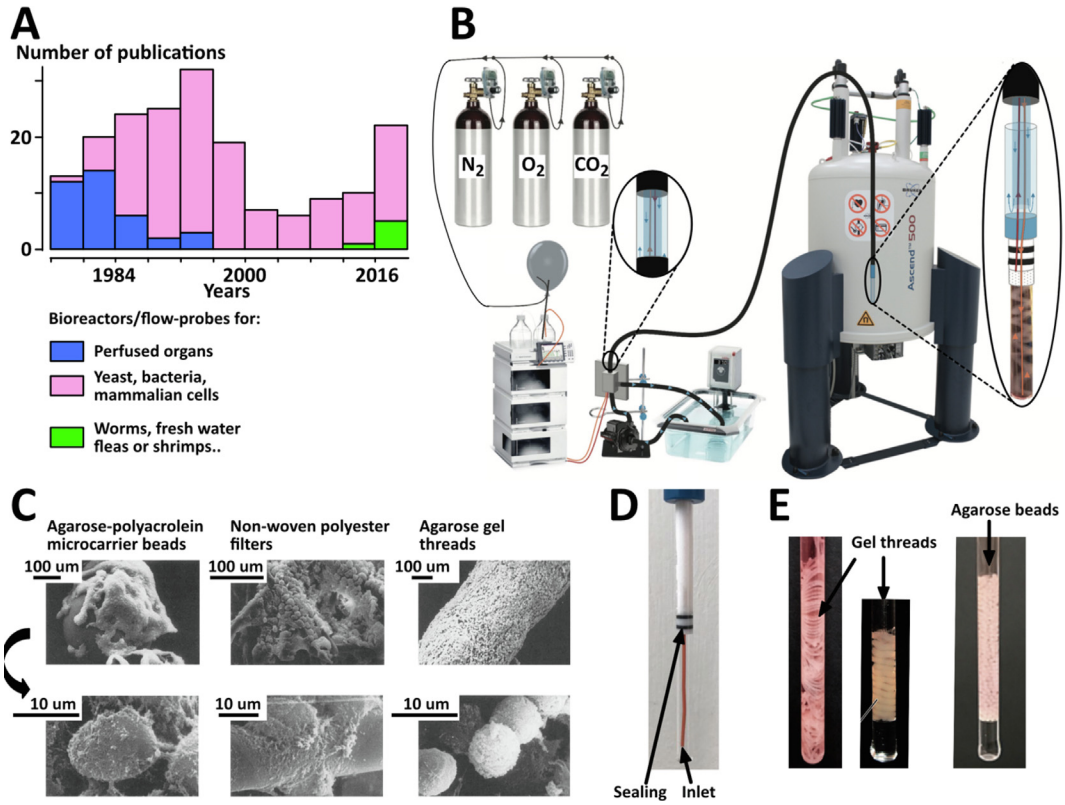

Fig. 35. A) Primary publications of studies (those known to the authors) reporting the design or use of intra-spectrometer bioreactors and flow-probes; **B)** Scheme of a typical NMR bioreactor, using a well-defined gas mixture bubbled into the culture medium, as well as culture medium heating and pumping into the spectrometer using inlet and outlet tubing to deliver fresh nutrients in a NMR tube (typically 5 mm diameter and 0.5 mL for recent probes) (adapted from Hertig et al. 2021 [1799]); **C)** Electron microscopy of anchorage-dependent human breast cancer cells attached to agarose polyacrolein microcarrier beads, polyester or embedded in agarose gel threads (adapted from Neeman et al. 1988 [1800]); **D)** Example of an empty flow unit showing the NMR tube and the inlet tubing (adapted from Luchinat et al. 2020 [867]); **E)** Examples of 5 mm NMR tubes filled with culture medium (its pink color indicates a pH ~7, while it turns yellow when it becomes acidic because of cell metabolism in absence of medium replenishment) and gel threads or agarose beads (adapted from Carvalho et al. 2019 [1801], Kubo et al. 2013 [868], and Inomata et al. 2017 [1369]).

Each of these immobilization methods has advantages and drawbacks. Gel encapsulation is very well suited to studies of suspension cells, while micro-carriers represent an appropriate technique for preserving adherent cell integrity and immediate accessibility of nutrients [167]. Cell density is higher with gel encapsulation methods (up to ~2.10^8 mammalian cells per mL) than with adherent systems (up to ~1.10^7 cells per mL) [768,1864]. Agarose is not electrically charged, while alginate gelification relies on ionic interactions that require Ca^{2+} (or Ba^{2+}) supplementation and low EDTA or phosphate concentrations. Hence, the two gels interfere differently with the diffusion of charged metabolites and O_2 [1840]. The low melting point agarose that is commonly used has a low mechanical strength and large pores; in contrast, alginate beads have a higher mechanical resistance and a finer meshwork [1840]. Alginate has been well characterized as a viable tridimensional culturing system for multiple purposes and cell types [1879,1880]: among others, it produces beads of uniform, tunable size, showing possibly hypoxic cores, which can be very useful, e.g. for radiobiological studies of cancer cells [1879]. Cells may have difficulties multiplying in dense agarose or alginate. In this regard, gels made of components of extracellular matrices such as Matrigel are better mimics of native environments, and allow cells to attach, grow and function in a more satisfactory fashion. They were also reported to interfere less than agarose with ionic diffusion [1849]. Methylcellulose also has superior characteristics to those of agarose, by allowing cells to adhere to its three-dimensional meshwork and ensuring improved cell viability [969,1487]. "Normal" cell growth is also possible on micro-carriers, but attached cells are subject to shear stress. Such stress is absent for cells grown on hollow fibers, but these occupy the largest fraction of the effective volume. Moreover, hollow-fibers require the application of high fluid pressures to exchange nutrients through the fiber walls. Finally, adherent cells that are only able to grow as a monolayer may provide low signal, both with micro-carrier beads and hollow-fibers [1864]. Spheroids can suffer from necrosis at their center [768,964,1876,1878].

3.7.3. Particular problems for consideration

To be effective and notably to achieve sufficient SNR, in-cell NMR often requires high cell densities. This makes nutrient or oxygen diffusion and delivery difficult, although these are essential for maintaining a constant "normal" cell metabolism [1881-1883]. Studies have been reported that attempt to define the best balance between cell density, flow rates and O_2 concentration in the perfused medium [1823,1828,1884,1885]. Non-invasive measurement of dissolved O_2 over time in the bioreactor is accessible, using perfluorocarbons entrapped in the gel matrices, whose T1 relaxation depends on O_2 partial pressure [1799, 1853,1873,1886,1887].

Naturally, cellular composition and metabolic state vary over time. Notably, the compositions of lipids and their glycerol precursors are not the same depending on cell density on carriers or in threads [1800,1839,1864]. It is clearly important to perform control experiments to verify that cells are kept healthy: ^{13}C- and ^{31}P-NMR monitoring of metabolite consumption and ATP levels are good indicators, complementary to cell viability assays [867-869,1105,1761,1888].

Finally, as far as quantification is concerned, it is important to consider the fact that effective T1 relaxation can be affected by the flow rate and the resulting renewal rate of extracellular species: molecules freshly inserted in the tube are not perturbed by previous radiofrequency pulses and therefore provide more signal per mole than molecules that remain within the tube and do not attain their equilibrium magnetization between pulses. For example, the use of a long-T1 species such as inorganic phosphate as a concentration reference was shown to be potentially misleading because its signal intensity was dependent on the flow rate [1889].

3.7.4. Past and recent applications

Bioreactors have been used to characterize cell metabolism in real-time with ^{13}C- and ^{31}P-NMR. A broad variety of studies using NMR-bioreactors have been concerned with the effects of drug-exposure and irradiation on mammalian cancer cell metabolism [768,777-794,1093,1094,1099,1100,1103,1858,1866,1890], the impact of ethanol and chemicals on hepatocytes [795,796], metabolism in hybridoma [771,797] and bacteria [1819,1883,1891-1894], comparisons of the metabolism of cells in suspension or embedded in gels, which has industrial applications for yeast metabolism [1804-1806,1811,1831,1832,1859], and antibody secretion of hybridoma [866]. They also served in the study of intra- extra-cellular $^{23}Na^{+}$ or $^{7}Li^{+}$ fluxes in mammalian cells [167,179,1844,1849]. Real-time monitoring has its advantages, by permitting the longitudinal observation of a single sample without repeated quenching and extraction of solutes. It can provide very well defined kinetics with dense timeframes, thus allowing advanced modeling of metabolism, as shown recently for melanoma cells [1874]. However, it requires the establishment of peculiar arrangements, and more classical metabolomics methods that employ solute extraction and high-resolution NMR and mass-spectrometry are more popular currently.

Hyperpolarization methods hold the promise of providing large sensitivity enhancements (see Sections 2.3.7. and 3.3.6.), and dedicated bioreactors have been proposed since the late 2000's. Cells can be steadily supplied with nutrients and possibly with drugs of interest, and can be exposed at controlled times to hyperpolarized metabolites (mostly ^{13}C-pyruvate). The evolution of their NMR signal and those of their cellular byproducts reveals the metabolic states of the cells. The short half-life of metabolite hyperpolarization limits the application of this approach to fast enzymatic reactions that can be monitored within a few tens of seconds. As was the case in the 1980-90's, ^{13}C-NMR of hyperpolarized metabolites has been studied in bioreactors to establish good references for future MRI/MRS applications [1093,1100,1103,1112,1867,1890], or to examine the effects of various drugs on various cancer cells [1093,1099,1100]. Classical immobilization methods were adopted, using alginate beads [1094,1103,1105,1850,1890] or cell attachment to polymer beads [1093,1099,1100,1112]. Original designs were also proposed: cells were grown on 3D scaffolds through which culture medium and hyperpolarized metabolites were perfused [1895], or embedded in a 3D collagen matrix placed in a 3D-printed bioreactor designed for allowing both NMR spectroscopy and optical Fluorescence Lifetime Imaging Microscopy (FLIM) [1867].

Real-time monitoring of cellular metabolism has also been carried out to characterize the evolution of large, external bioreactors. Continuous "online" monitoring can be achieved by circulating the culture broth through the spectrometer using a bypass tube [739,962,963,1611,1859,1883,1891-1894,1896-1899]: this approach gives access to scale-up studies of potential industrial applications in a non-invasive fashion, and is well suited to use with low-field magnets [962,963,1898,1899]. Using similar designs, circulating the supernatant medium of an external bioreactor into the magnet gives access to indirect monitoring of cell metabolism that can be applied to organoids or microbial biofilms [1813,1900,1901].

Bioreactors are now becoming more mainstream for in-cell structural biology studies. They are clearly necessary to maintain cells in relevant physiological states during the required hours-long acquisition times [867-869,1761,1888]. Evidence exists that the studied proteins can have different folding states or interactions depending on the cellular metabolic state [1355,1369]. Now that early proofs of principle have been realized, which show that observing proteins and nucleic acids in living cells is possible, the field will have to move towards wider adoption of bioreactors in the future.

Overall, it appears that NMR spectroscopists have been very inventive in developing home-made designs to maintain cells in a healthy state in the spectrometer. These designs have a broad variety of applications, from the monitoring of industrial microbial bioreactors to the simple preservation of steady conditions for in-cell structural biology studies. This profusion of systems is a blessing and a curse at the same time. Most of the proposed home-built designs were somehow lost and not transferred from lab to lab, and more standard systems would probably have helped in developing in-cell NMR applications. Commercial solutions proposed recently are derived from devices dedicated to the online-monitoring of external chemical reactors, and are not fully satisfactory when it comes to nutrient delivery. We speculate that solutions will be found to this problem. Online-monitoring of external reactors has a promising future, notably thanks to the recent availability of benchtop, permanent magnets (operating at ~1 T): these are more easily adapted to conditions in the field at reasonable costs, and they should make non-invasive, real-time NMR analysis possible more widely [47,962,963,1899,1901]. Finally, we can hope that the efforts of many groups to miniaturize their designs will succeed and have interesting applications. The integration of micro-fluidics and alternative micro-coil systems may push the capability of NMR to become a non-invasive approach for the characterization of nano- to micro-meter size tissues, egg cells, animals or organoids for therapeutic or toxicologic studies [964,1066,1109,1902-1904].

4. Where next?

NMR spectroscopy is extremely versatile, and the variety of types of information that it has provided from cellular samples is astonishing. The main applications of in-cell NMR have varied through time. The original investigations on cellular water, salts and basic metabolic reactions provided a good basis for clinical developments, notably for MRI, MRS and metabolomics. Unique contributions are regularly delivered by in-cell NMR studies in various fields as shown throughout this review, from the *in-situ* characterization of cell-walls, of protein folding and drug binding, to non-invasive toxicology studies in small living organisms. However, the latest technological developments have oriented modern biological applications towards high-throughput or single-molecule/single-cell analysis, as discussed below. NMR spectroscopy is not a method of choice in this regard and is thus not among the most fashionable methods for cellular analysis currently. The particular capabilities of NMR remain intact, however: the ability to observe multiple nuclei, to provide atomic-scale information in a non-invasive fashion. Hence, even though the designs used in the past for in-cell NMR studies can now appear outdated (using outdated cell strains and culture conditions), we believe a number of strategies may be readapted to more contemporary contexts. This requires identification of complementarity with the most popular current techniques for cellular analysis, the systems that would benefit from non-invasive NMR observa-

tion, the new technologies that would empower the NMR capacities, and those recent NMR developments that may find their use in the analysis of cellular samples.

4.1. Comparison and complementarity with other spectroscopies, spectrometries and microscopies

Many other techniques can provide molecular information from intact cells. Focusing on the fields where NMR can contribute to establishing knowledge on cellular processes, we can distinguish two broad fields: in-cell structural biology, and live-cell enzymatic activities. Although they are likely to evolve rapidly, the specific advantages and drawbacks of other spectroscopies must be considered in order to understand how NMR may be useful, complementary or even unique. We will not give any technical details here, but only mention the present capabilities and applications of the major "in-cell techniques".

4.1.1. In-cell structural biology

We start this section by considering a technique that is particularly closely related to in-cell NMR, namely in-cell EPR. This technique can provide two types of information in particular [1905-1908]: i) the local structural dynamics of a paramagnetic tag on a protein at room temperature, ii) the evaluation of distance distributions between two paramagnetic tags attached on the nucleic acid or protein(s) of interest at cryogenic temperature. In-cell EPR is well-suited to distance measurements in the ~2.5-6 nm range using fairly small amounts of material (down to submicromolar protein concentrations in ~5-10 million cells, as reported recently [1582]), which can be either nucleic acids or proteins, doubly tagged with nitroxides [1909-1914], trityl groups [1915-1917], or Gd^{3+}-based labels [1582,1918-1924]. They yield information on frozen distance distributions measured at cryogenic temperatures, which are commonly reached by using significant quantities of liquid helium. In-cell EPR is an expanding field and may represent an interesting method in the toolbox in the coming years.

Förster Resonance Energy Transfer (FRET)-based methods deliver similar tag-to-tag distance measurements in the ~3-8 nm range, but in this case between two fluorescent labels [1925]. This approach gives access to the subcellular localization of the characterized proteins in single cells, and has been used to study protein thermal stability [1377,1926-1930] and protein:protein interactions [1931,1932]. Single-molecule (or single-particle) FRET (smFRET) approaches allow measurements in live-cells not only of intra- and inter-molecular distance distributions, but also of conformational or binding exchange dynamics [1933-1938], including for membrane proteins [1939]. In combination with Fluorescence Correlation Spectroscopy (FCS), structural dynamics on timescales between ~10 ns and ~1 ms can be observed [1940,1941]. smFRET might soon be effective for in-cell structural modeling [1942] and probably will be an important source of in-cell structural information in the coming years. Similarly to the labels used in EPR, the labels used in such fluorescence studies have sizes in the approximate range 1-2 nm but their flexibility, their potential interference with the studied structural properties, their (photo)stability and the necessity to deliver the labeled proteins in cells (for the non-GFP fluorophores) are current limiting factors [1939,1940,1943].

It is well known that cryogenic electron microscopy (cryo-EM) has become a dominant technique in the field of structural biology during the past several years. In parallel, cryo-electron tomography (cryo-ET) has permitted very considerable advances in the observation of macromolecules *in situ*, i.e. in plunge-frozen cells or even small organisms [1944-1946]. The latest technical developments make it feasible to obtain tomograms of ~100-200-nm-thin cell slices at ~3-4 nm resolution [1945,1947,1948]. At the molecular level, this has already permitted characterization of amyloid aggregates [1949-1951], tubulin- or actin-associated proteins [1952-1954], and membrane protein complexes [1955-1960] at nanometer and subnanometer resolutions using sub-tomogram accumulation and averaging. Recent improvements in data acquisition and computational treatment make cryo-ET capable of reaching resolutions of 3-4 Å [1961-1965], including in cells for ribosomal particles [1965]. Information on "invisible" parts of the complexes can be obtained by complementary analysis from in-cell cross-linking mass-spectrometry [1966]. In-cell cryo-ET structure determination is clearly better suited to large, abundant macromolecular complexes above ~500 kDa like ribosomes and proteasomes, this limit being reportedly set by the cell slices thickness [1945,1964,1967].

The number of reports using the techniques discussed above has grown exponentially in the last 5 years. They have already provided descriptions of fundamental cellular processes and macromolecular assemblies, and provided important data on macromolecular conformational equilibria and dynamics. NMR spectroscopy is certainly not likely to solve intracellular structures of high-molecular weight assemblies, or determine nanometer-scale distances (such measurements are accessible using paramagnetic relaxation enhancement and pseudo-contact shifts, but these are not commonly useable in cells as yet). Nonetheless, NMR has complementary capabilities. Among others, these include: i) solution- and solid-state NMR can deliver atomic-scale information on small and large molecules at the same time; ii) solution NMR can also deliver this atomic-scale information on very flexible regions; iii) solid-state NMR can also deliver this atomic-scale information on the complete ensemble of cellular molecules of interest (targeted and observed via isotopic labeling); iv) solution- and solid-state NMR do not require fluorescent dyes or paramagnetic labels to provide a structural information; v) solution NMR can monitor structural evolution in living cells and in real-time. Ideally, one should keep in mind the actual weak points of NMR (the necessity for high concentrations, the absence of information on subcellular localization and the possibility that only a subpopulation of the molecule of interest gives rise to the signal) and countervail them with one of the potentially complementary techniques cited above.

4.1.2. Live-cell enzymatic activities and drug binding

A tremendous number of biosensors have been designed to report on enzyme activities or molecular interactions/proximities using various bioluminescence and fluorescence phenomena, notably FRET and Bioluminescence Resonance Energy Transfer (BRET) [1968-1971]. It need hardly be said that such light-based approaches are more sensitive and better suited to high-throughput drug screening than is NMR. Moreover, they can often give real-time, spatially resolved information, sometimes even in living animals. Many commercial kits exist requiring minimal equipment for quantifying the cell signaling activities being studied. However, all these methods use either i) competition assays detecting the binding of generic fluorescent probes to the protein of interest [1972,1973], or ii) downstream/secondary reactions triggered by the activity or the proximity of the protein of interest, which can bias the interpretation of the results [1968-1971,1974-1976]. In the context of drug screening, this is of considerable concern because the targeted signaling proteins are often pleiotropic. Consequently, they are prone to generate unreliable downstream outcomes upon activation or inhibition: i) the drug target can have multiple activities and a binding compound may impact only one of these, ii) feedback loops are often activated. Deeper discussions about so-called "biased signaling" have been published elsewhere [1977,1978]. The diversity of reporters is already large, and one can

assume that it will become broader and that multiplexing capabilities will be improved [1979].

High-throughput screening methods using mass-spectrometry (MS) analysis can draw the interaction maps of large compounds libraries at the proteome scale in cells or cell extracts [1980-1982], or identify drug targets even in tissues [1373,1983,1984]. These MS studies do not report direct target binding, but rely on either i) compound functionalization and covalent attachment to their target [1985-1987], or ii) the consequences of drug binding on proteins thermal stabilities or sensitivity to protease treatments [1371]. The thermal stability shifts measured in the presence of ligands are not always sensitive enough to detect weak binders, and such assays are not always able to distinguish between binding to active and unactive forms of the protein target. MS analysis moreover is a destructive method, which does not allow the longitudinal monitoring of a single sample.

In comparison, in-cell NMR drug studies have only low sensitivity and low throughput capabilities, but they deliver direct information on drug:target interactions at the atomic scale: i) The protein target or the screened compounds can be observed directly by NMR, and ii) enzymatic activities can be monitored using the NMR signals of substrates and of their products. In this last case, tailored reporters can be designed to provide NMR exploitable signals, which allows NMR drug:protein studies a great deal of flexibility and adaptability.

4.2. Where to go – what to improve

Prediction is a fool's game, and we do not claim in any way to be able to mentor the community. We thought nevertheless that it would be worthwhile to mention a few directions that we consider to be important and promising for in-cell NMR. We cannot be comprehensive, of course: NMR spectroscopy is far too versatile to guess all its future applications.

4.2.1. Integrating advanced methods

We feel that combining some recent biotechnologies would make in-cell NMR investigations more attractive. We limit our list to a handful of techniques. First, in-cell NMR approaches could be applied to the so-called organoids and organs-on-a-chip, which the literature suggests require supplementary readouts [1988-1992]. A significant proportion of the studies described in the present review have been carried out on living tissues or cultured cells to prepare *in vivo* imaging and metabolic analysis (MRI/MRS) applications. They were often not intended to provide information of great biological relevance, but rather to show the feasibility of such NMR studies on live material. However, many of the approaches described could now find direct applications in longitudinal studies of organoids: NMR spectroscopy is capable of reporting in real time and non-invasively on the organoid's metabolism, drug penetration, its cellular processing or its binding to cellular targets, or its toxic effects, for example. Second, a number of NMR studies on eukaryotic cells would be facilitated by expert handling of the inducible expression or degradation of proteins in eukaryotic cells. That would permit carrying out experiments in cleaner conditions, with and without the nucleic acid or the protein of interest, in closely similar cellular backgrounds. This would be helpful for several types of investigations, from metabolism monitoring, to drug pharmacology, drug binding assays, or protein:protein interactions studies. Among other applications, it could also help in structural biological studies to achieve specific isotope labeling *in situ*: by triggering the expression of the protein of interest concomitantly with the supplementation of the chosen isotopically labeled amino acids, one could limit the NMR signal from the cellular background. Third, integrating genetic code expansion techniques [1993-1995] could permit one to incorporate paramagnetic tags or chemical functions that would provide high NMR sensitivity, and which could help to report on ligand binding or protein conformational changes, as recently exemplified in *in vitro* studies [1996]. CRISPR-Cas9 genome editing techniques may also be useful to control the expression of target proteins, which would be of particular interest for in/on-cell drug binding assays and structural biology. However, for most NMR labs, it would probably be as efficient to rely on the many commercial stable cell lines or the help of dedicated biology labs.

Beyond this, one could think about advanced NMR methods that could profitably be implemented for in-cell studies. Here again, we can only include a few thoughts in a list that is necessarily far from comprehensive. In no particular order: applying pure-shift methods [1646,1649,1690,1691] or implementing post-acquisition data treatment [1741], notably deep-learning analysis [1997,1998], would certainly help to exploit NMR spectra from cellular samples; continuous readout using time-resolved non-uniform sampling could probably become a standard approach, as mentioned in Section 3.3.5. [1061,1066,1694-1696]; recent DNP-agents showing improved persistence in water and signal-enhancement at high magnetic fields will certainly help in/on-cell solid-state NMR approaches [1999-2002]. Methods developed for other spectroscopies might usefully be adapted also. Flash-freezing methods have been developed to improve the vitrification quality of cryo-EM/ET samples and to avoid the dissociation or denaturation of macromolecular complexes [2003,2004]: the slow freezing conditions used in solid-state NMR studies may bias observations and adapting fast freezing techniques may help to capture and analyze the actual cellular state at a precise timepoint. In-cell NMR protein observation will benefit from supplementary schemes of amino acid isotope labeling and combinations thereof, notably to generate NMR spectra with isolated signals and less noise from cellular background [1173,1211,1280,1392,1861] (see also Sections 2.2.2 or 2.5.2 for cell-wall analysis): protocols might be adapted from quantitative proteomics using stable-isotope labeling with amino acids in cell culture (SILAC) [2005-2007]. We can also suggest the future promise of nitrogen-vacancy (NV) centers in diamond and optically detected magnetic resonance: large species with highly restricted motion in cells could favor nano-NMR, but the expertise and the actual experimental designs are not yet sufficiently accessible to allow their application to in-cell studies [2008-2011].

Finally, a few technical aspects should probably be tackled in the future to make in-cell NMR more appealing. First, we already enjoy using commercial cryoprobes with up to five channels (^{1}H, ^{2}H, ^{13}C, ^{15}N, ^{19}F/^{31}P) for studies using samples in conventional 5 mm NMR tubes. As shown in Section 2.1., a broad diversity of nuclei is observable by NMR, and their parallel monitoring would be highly valuable in a number of other situations. Let us imagine a study testing a drug candidate against high blood-pressure on a mini-brain or a mini-heart: biologists would doubtless appreciate a continuous readout of the levels of metabolites (^{1}H and ^{13}C/^{15}N), of ^{31}P-phosphate-containing species and of ^{23}Na or ^{39}K, for example. Hence, we feel that a greater number of RF channels for different nuclei (possibly including tunable broad-band channels) would be highly desirable. Second, solution- and solid-state NMR approaches should be more often combined, which would bring about a more complete representation of the studied systems. Solution NMR can provide information only on fast-tumbling species, but it does so non-invasively in their native state and in real-time; solid-state NMR can report on the complete ensemble of labeled molecules, but only on frozen cells where dynamics cannot be characterized and where conformations and interactions can be influenced by the freezing techniques. Studying in-cell samples might well promote productive collaborations between labs with expertise in solution- and solid-state NMR.

Third, the field should work to establish common standards to validate cell viability and ensure better reproducibility of acquisition conditions. Unfortunately, these requirements will probably necessitate using bioreactors and probes permitting ^{31}P-acquisition to monitor cellular phosphate-containing species, both of which would further stretch budgets. Finally, as explained in Section 3.4.3., NMR spectroscopy has remarkable capabilities in defining weak interactions (Kd$\sim$10^{-7}-10^{-3} mol/L, $k_{off}\sim$10^{2}-10^{6} s^{-1} using STD-NMR or WaterLOGSY for example [1379,1412]), but approved drugs on the market generally show much slower off-rates (1 to 0.01 min^{-1}, see for example [1743,1744]). To be able to participate in the drug research pipeline, it would be desirable to establish in-cell NMR methods that apply to these slower types of binding kinetics.

4.2.2. Specific strengths of NMR that complement other techniques

Once more, the versatility of NMR spectroscopy is too broad to include all the possible subjects that could be tackled on cellular samples. In more concrete terms than in Section 1.2., we want here to put together some of the specific capabilities (and shortcomings) of NMR relevant for in-cell studies.

NMR spectroscopy permits the direct, atomic-scale observation of the studied object itself, rather than of a bound fluorophore or of a reaction product. NMR spectroscopy can report simultaneously on a broad variety of nuclei and of molecules, from ions and metabolites to proteins and membranes, in an isotope-selective fashion. NMR spectroscopy can trace the conformational and chemical environment of nuclei non-invasively and in real-time, and it allows the application of light and of chemical additives.

As far as in-cell studies are concerned, the main drawbacks of NMR are i) its poor sensitivity, ii) its inability to localize the detected species at submicrometer scale, iii) its slow measurement speed and consequent low-throughput. Also, practitioners of NMR spectroscopy require long years of training, and spectroscopists are most often specialized either in small or in large molecules, either in the solution- or in the solid-state.

Altogether, there are particular fields where in-cell NMR can be highly valuable: e.g. the monitoring of redox states, of metal chelation, of light-induced reactions, the characterization of flexible and/or middle-size (1-50 kDa) objects for which cryo-ET is so far "blind", studies where the simultaneous observation of small and large molecular species is required (such as an enzyme and its substrates/products/cofactors, or a ligand and the conformational state of its protein target), the longitudinal monitoring of large panels of metabolites or of protein targets in cells/organs/small animals upon drug exposure, etc. In-cell NMR will inevitably benefit from complementary techniques, especially from microscopies providing information on subcellular localization. By providing experimental evidence on virtually any chosen molecule in live material, in-cell NMR can complement high-throughput methods in the drug research pipeline, in a world where large-scale cell-based or virtual screenings have gained interest and trust (see for example [2012-2015]). Indeed, in-cell NMR delivers information at the atomic scale, which will always be invaluable.

Declaration of Competing Interest

The authors declare that they have no known competing financial interests or personal relationships that could have appeared to influence the work reported in this paper.

Acknowledgements

This work was supported by the CNRS and the CEA-Saclay, and by iNEXT-Discovery, Grant No. 871037, funded by the Horizon 2020 research and innovation programme of the European Commission the French Infrastructure for Integrated Structural Biology (https://frisbi.eu/, grant number ANR-10-INSB-05-01, Acronym FRISBI) and by the French National Research Agency (ANR; research grants ANR-14-ACHN-0015 and ANR-20-CE92-0013), and by the Fondazione Cassa di Risparmio di Firenze (grant CRF2020.1395). We also thank Pierre Barraud and Muriel Delepierre for their helpful reading and comments.

References

[1] Z. Serber, V. Dötsch, In-cell NMR spectroscopy, Biochemistry. 40 (2001) 14317–14323, https://doi.org/10.1021/bi011751w.
[2] S. Reckel, R. Hänsel, F. Lohr, V. Dötsch, In-cell NMR spectroscopy, Prog. Nucl. Magn. Reson. Spectrosc. 51 (2007) 91–101, https://doi.org/10.1016/j.pnmrs.2007.02.002.
[3] A.Y. Maldonado, D.S. Burz, A. Shekhtman, In-cell NMR spectroscopy, Prog. Nucl. Magn. Reson. Spectrosc. 59 (2011) 197–212, https://doi.org/10.1016/j.pnmrs.2010.11.002.
[4] D.I. Freedberg, P. Selenko, Live cell NMR, Annu. Rev. Biophys. 43 (2014) 171–192, https://doi.org/10.1146/annurev-biophys-051013-023136.
[5] R. Hänsel, L.M. Luh, I. Corbeski, L. Trantirek, V. Dötsch, In-Cell NMR and EPR Spectroscopy of Biomacromolecules, Angew. Chem. 53 (2014) 10300–10314, https://doi.org/10.1002/anie.201311320.
[6] F.-X. Theillet, A. Binolfi, T. Frembgen-Kesner, K. Hingorani, M. Sarkar, C. Kyne, C. Li, P.B. Crowley, L. Gierasch, G.J. Pielak, A.H. Elcock, A. Gershenson, P. Selenko, Physicochemical properties of cells and their effects on intrinsically disordered proteins (IDPs), Chem. Rev. 114 (2014) 6661–6714, https://doi.org/10.1021/cr400695p.
[7] A.E. Smith, Z. Zhang, G.J. Pielak, C. Li, NMR studies of protein folding and binding in cells and cell-like environments, Curr. Opin. Struct. Biol. 30 (2015) 7–16, https://doi.org/10.1016/j.sbi.2014.10.004.
[8] Y. Ye, X. Liu, Y. Chen, G. Xu, Q. Wu, Z. Zhang, C. Yao, M. Liu, C. Li, Labeling Strategy and Signal Broadening Mechanism of Protein NMR Spectroscopy in Xenopus laevis Oocytes, Chem. - Eur. J. 21 (2015) 8686–8690, https://doi.org/10.1002/chem.201500279.
[9] L. Barbieri, E. Luchinat, L. Banci, Characterization of proteins by in-cell NMR spectroscopy in cultured mammalian cells, Nat. Protoc. 11 (2016) 1101–1111, https://doi.org/10.1038/nprot.2016.061.
[10] J. Danielsson, M. Oliveberg, Comparing protein behaviour in vitro and in vivo, what does the data really tell us?, Curr. Opin. Struct. Biol. 42 (2017) 129–135, https://doi.org/10.1016/j.sbi.2017.01.002.
[11] E. Luchinat, L. Banci, In-cell NMR: a topical review, IUCrJ. 4 (2017) 108–118, https://doi.org/10.1107/S2052252516020625.
[12] S. Rahman, Y. Byun, M.I. Hassan, J. Kim, V. Kumar, Towards understanding cellular structure biology: In-cell NMR, BBA - Proteins Proteomics. 2017 (1865) 547–557, https://doi.org/10.1016/j.bbapap.2017.02.018.
[13] C. Li, J. Zhao, K. Cheng, Y. Ge, Q. Wu, Y. Ye, G. Xu, Z. Zhang, W. Zheng, X. Zhang, X. Zhou, G. Pielak, M. Liu, Magnetic Resonance Spectroscopy as a Tool for Assessing Macromolecular Structure and Function in Living Cells, Annu. Rev. Anal. Chem. 10 (2017) 157–182, https://doi.org/10.1146/annurev-anchem-061516-045237.
[14] J.M. Plitzko, B. Schuler, P. Selenko, Structural Biology outside the box-inside the cell, Curr. Opin. Struct. Biol. 46 (2017) 110–121, https://doi.org/10.1016/j.sbi.2017.06.007.
[15] G. Lippens, E. Cahoreau, P. Millard, C. Charlier, J. Lopez, X. Hanoulle, J.C. Portais, In-cell NMR: from metabolites to macromolecules, Analyst. 143 (2018) 620–629, https://doi.org/10.1039/C7AN01635B.
[16] E. Luchinat, L. Banci, In-Cell NMR in Human Cells: Direct Protein Expression Allows Structural Studies of Protein Folding and Maturation, Acc. Chem. Res. 51 (2018) 1550–1557, https://doi.org/10.1021/acs.accounts.8b00147.
[17] N. Sciolino, D.S. Burz, A. Shekhtman, In-Cell NMR Spectroscopy of Intrinsically Disordered Proteins, PROTEOMICS. 19 (2019) 1800055–11800016, https://doi.org/10.1002/pmic.201800055.
[18] S.S. Stadmiller, G.J. Pielak, The Expanding Zoo of In-Cell Protein NMR, Biophys. J. 115 (2018) 1628–1629, https://doi.org/10.1016/j.bpj.2018.09.017.
[19] C. Kang, Applications of In-Cell NMR in Structural Biology and Drug Discovery, Int. J. Mol. Sci. 20 (2019), https://doi.org/10.3390/ijms20010139.
[20] A. Kumar, L. Kuhn, J. Balbach, In-Cell NMR: Analysis of Protein-Small Molecule Interactions, Metabolic Processes, and Protein Phosphorylation, Int. J. Mol. Sci. 20 (2019) 378–423, https://doi.org/10.3390/ijms20020378.
[21] T. Sugiki, Y. Lin, Y.-H. Lee, In-cell nuclear magnetic resonance spectroscopy for studying intermolecular interactions, J. Korean Magn. Reson. Soc. 23 (2019) 33–39, https://doi.org/10.6564/JKMRS.2019.23.1.033.
[22] G. Siegal, P. Selenko, Cells, drugs and NMR, J. Magn. Reson. San Diego Calif 1997 306 (2019) 202–212, https://doi.org/10.1016/j.jmr.2019.07.018.
[23] N. Nishida, Y. Ito, I. Shimada, In situ structural biology using in-cell NMR, Biochim. Biophys. Acta Gen. Subj. 1864 (2020), https://doi.org/10.1016/j.bbagen.2019.05.007 129364.
[24] S. Narasimhan, G.E. Folkers, M. Baldus, When Small becomes Too Big: Expanding the Use of In-Cell Solid-State NMR Spectroscopy, ChemPlusChem. 85 (2020) 760–768, https://doi.org/10.1002/cplu.202000167.
[25] In-cell NMR Spectroscopy, Royal Society of Chemistry, Cambridge, 2019. https://doi.org/10.1039/9781788013079..

[26] B.S. Szwergold, NMR spectroscopy of cells, Annu. Rev. Physiol. 54 (1992) 775–798, https://doi.org/10.1146/annurev.ph.54.030192.004015.
[27] P. van Zijl, L. Knutsson, In vivo magnetic resonance imaging and spectroscopy. Technological advances and opportunities for applications continue to abound, J. Magn. Reson. 306 (2019) 55–65, https://doi.org/10.1016/j.jmr.2019.07.034.
[28] J.H. Gilmore, R.C. Knickmeyer, W. Gao, Imaging structural and functional brain development in early childhood, Nat. Rev. Neurosci. 19 (2018) 123–137, https://doi.org/10.1038/nrn.2018.1.
[29] R. Geraldes, O. Ciccarelli, F. Barkhof, N. De Stefano, C. Enzinger, M. Filippi, M. Hofer, F. Paul, P. Preziosa, À. Rovira, G.C. DeLuca, L. Kappos, T. Yousry, F. Fazekas, J. Frederiksen, C. Gasperini, J. Sastre-Garriga, N. Evangelou, J. Palace, MAGNIMS study group, The current role of MRI in differentiating multiple sclerosis from its imaging mimics, Nat. Rev. Neurol. 14 (2018) 199–213, https://doi.org/10.1038/nrneurol.2018.14.
[30] S.B. Eickhoff, B.T.T. Yeo, S. Genon, Imaging-based parcellations of the human brain, Nat. Rev. Neurosci. (2018) 1–15, https://doi.org/10.1038/s41583-018-0071-7.
[31] G. David, S. Mohammadi, A.R. Martin, J. Cohen-Adad, N. Weiskopf, A. Thompson, P. Freund, Traumatic and nontraumatic spinal cord injury: pathological insights from neuroimaging, Nat. Rev. Neurol. 15 (2019) 718–731, https://doi.org/10.1038/s41582-019-0270-5.
[32] A. Stabile, F. Giganti, A.B. Rosenkrantz, S.S. Taneja, G. Villeirs, I.S. Gill, C. Allen, M. Emberton, C.M. Moore, V. Kasivisvanathan, Multiparametric MRI for prostate cancer diagnosis: current status and future directions, Nat. Rev. Urol. 17 (2020) 41–61, https://doi.org/10.1038/s41585-019-0212-4.
[33] R.L. Hesketh, K.M. Brindle, Magnetic resonance imaging of cancer metabolism with hyperpolarized 13C-labeled cell metabolites, Curr. Opin. Chem. Biol. 45 (2018) 187–194, https://doi.org/10.1016/j.cbpa.2018.03.004.
[34] V. Ntziachristos, M.A. Pleitez, S. Aime, K.M. Brindle, Emerging Technologies to Image Tissue Metabolism, Cell Metab. 29 (2019) 518–538, https://doi.org/10.1016/j.cmet.2018.09.004.
[35] L.J. Rich, P. Bagga, N.E. Wilson, M.D. Schnall, J.A. Detre, M. Haris, R. Reddy, 1H magnetic resonance spectroscopy of 2H-to-1H exchange quantifies the dynamics of cellular metabolism in vivo, Nat. Biomed. Eng. 4 (2020) 335–342, https://doi.org/10.1038/s41551-019-0499-8.
[36] A. Mukherjee, H.C. Davis, P. Ramesh, G.J. Lu, M.G. Shapiro, Biomolecular MRI reporters: Evolution of new mechanisms, Prog. Nucl. Magn. Reson. Spectrosc. 102–103 (2017) 32–42, https://doi.org/10.1016/j.pnmrs.2017.05.002.
[37] M.E. Ladd, P. Bachert, M. Meyerspeer, E. Moser, A.M. Nagel, D.G. Norris, S. Schmitter, O. Speck, S. Straub, M. Zaiss, Pros and cons of ultra-high-field MRI/MRS for human application, Prog. Nucl. Magn. Reson. Spectrosc. 109 (2018) 1–50, https://doi.org/10.1016/j.pnmrs.2018.06.001.
[38] D.D. Marshall, R. Powers, Beyond the paradigm: Combining mass spectrometry and nuclear magnetic resonance for metabolomics, Prog. Nucl. Magn. Reson. Spectrosc. 100 (2017) 1–16, https://doi.org/10.1016/j.pnmrs.2017.01.001.
[39] C. Deborde, A. Moing, L. Roch, D. Jacob, D. Rolin, P. Giraudeau, Plant metabolism as studied by NMR spectroscopy, Prog. Nucl. Magn. Reson. Spectrosc. 102–103 (2017) 61–97, https://doi.org/10.1016/j.pnmrs.2017.05.001.
[40] J.R. Everett, NMR-based pharmacometabonomics: A new paradigm for personalised or precision medicine, Prog. Nucl. Magn. Reson. Spectrosc. 102–103 (2017) 1–14, https://doi.org/10.1016/j.pnmrs.2017.04.003.
[41] E. Hatzakis, Nuclear Magnetic Resonance (NMR) Spectroscopy in Food Science: A Comprehensive Review, Compr. Rev. Food Sci. Food Saf. 18 (2019) 189–220, https://doi.org/10.1111/1541-4337.12408.
[42] A.-H. Emwas, R. Roy, R.T. McKay, L. Tenori, E. Saccenti, G.A.N. Gowda, D. Raftery, F. Alahmari, L. Jaremko, M. Jaremko, D.S. Wishart, NMR Spectroscopy for Metabolomics Research, Metabolites. 9 (2019), https://doi.org/10.3390/metabo9070123.
[43] J.R. Everett, E. Holmes, K.A. Veselkov, J.C. Lindon, J.K. Nicholson, A Unified Conceptual Framework for Metabolic Phenotyping in Diagnosis and Prognosis, Trends Pharmacol. Sci. 40 (2019) 763–773, https://doi.org/10.1016/j.tips.2019.08.004.
[44] D. González-Peña, L. Brennan, Recent Advances in the Application of Metabolomics for Nutrition and Health, Annu. Rev. Food Sci. Technol. 10 (2019) 479–519, https://doi.org/10.1146/annurev-food-032818-121715.
[45] D.S. Wishart, Metabolomics for Investigating Physiological and Pathophysiological Processes, Physiol. Rev. 99 (2019) 1819–1875, https://doi.org/10.1152/physrev.00035.2018.
[46] G.A.N. Gowda, D. Raftery, Overview of NMR Spectroscopy-Based Metabolomics: Opportunities and Challenges, in: NMR-Based Metabolomics, Humana, New York, NY, New York, NY, 2019, pp. 3–14, https://doi.org/10.1007/978-1-4939-9690-2_1.
[47] P. Giraudeau, NMR-based metabolomics and fluxomics: developments and future prospects, Analyst. 145 (2020) 2457–2472, https://doi.org/10.1039/d0an00142b.
[48] A. Vignoli, V. Ghini, G. Meoni, C. Licari, P.G. Takis, L. Tenori, P. Turano, C. Luchinat, High-Throughput Metabolomics by 1D NMR, Angew. Chem. Int. Ed Engl. 58 (2019) 968–994, https://doi.org/10.1002/anie.201804736.
[49] M.H. Levitt, Spin Dynamics, John Wiley & Sons Ltd, Chichester, 2008, https://www.wiley.com/en-fr/Spin+Dynamics:+Basics+of+Nuclear+Magnetic+Resonance,+2nd+Edition-p-9780470511176.
[50] C.B. Anfinsen, Principles that govern the folding of protein chains, Science. 181 (1973) 223–230, https://doi.org/10.1126/science.181.4096.223.
[51] M.D. Herbst, J.H. Goldstein, A review of water diffusion measurement by NMR in human red blood cells, Am. J. Physiol.-Cell Physiol. 256 (1989) C1097–C1104, https://doi.org/10.1152/ajpcell.1989.256.5.C1097.
[52] M.L. García-Martín, P. Ballesteros, S. Cerdán, The metabolism of water in cells and tissues as detected by NMR methods, Prog. Nucl. Magn. Reson. Spectrosc. 39 (2001) 41–77. https://doi.org/10.1016/S0079-6565(01)00031-0..
[53] T. Conlon, R. Outhred, Water diffusion permeability of erythrocytes using an NMR technique, Biochim. Biophys. Acta BBA - Biomembr. 288 (1972) 354–361, https://doi.org/10.1016/0005-2736(72)90256-8.
[54] R. Outhred, T. Conlon, The volume dependence of the erythrocyte water diffusion permeability, Biochim. Biophys. Acta BBA - Biomembr. 318 (1973) 446–450, https://doi.org/10.1016/0005-2736(73)90207-1.
[55] M.E. Fabry, M. Eisenstadt, Water exchange between red cells and plasma. Measurement by nuclear magnetic relaxation, Biophys. J. 15 (1975) 1101–1110, https://doi.org/10.1016/S0006-3495(75)85886-3.
[56] D.Y. Chien, R.I. Macey, Diffusional water permeability of red cells Independence on osmolality, Biochim. Biophys. Acta BBA - Biomembr. 464 (1977) 45–52, https://doi.org/10.1016/0005-2736(77)90369-8.
[57] T. Conlon, R. Outhred, The temperature dependence of erythrocyte water diffusion permeability, Biochim. Biophys. Acta BBA - Biomembr. 511 (1978) 408–418, https://doi.org/10.1016/0005-2736(78)90277-8.
[58] M.E. Fabry, M. Eisenstadt, Water exchange across red cell membranes: II. Measurement by nuclear magnetic resonanceT 1, T 2, andT 12 hybrid relaxation. The effects of osmolarity, cell volume, and medium, J. Membr. Biol. 42 (1978) 375–398, https://doi.org/10.1007/BF01870357.
[59] V.V. Morariu, V.I. Pop, O. Popescu, G. Benga, Effects of temperature and pH on the water exchange through erythrocyte membranes: Nuclear magnetic resonance studies, J. Membr. Biol. 62 (1981) 1–5, https://doi.org/10.1007/BF01870194.
[60] G. Benga, V.I. Pop, O. Popescu, M. Ionescu, V. Mihele, Water exchange through erythrocyte membranes: Nuclear magnetic resonance studies on the effects of inhibitors and of chemical modification of human membranes, J. Membr. Biol. 76 (1983) 129–137, https://doi.org/10.1007/BF02000613.
[61] A.M. Serbu, A. Marian, O. Popescu, V.I. Pop, V. Borza, I. Benga, G. Benga, Decreased water permeability of erythrocyte membranes in patients with duchenne muscular dystrophy, Muscle Nerve. 9 (1986) 243–247, https://doi.org/10.1002/mus.880090308.
[62] L.-W.-M. Fung, C. Narasimhan, H.-Z. Lu, M.P. Westerman, Reduced water exchange in sickle cell anemia red cells: a membrane abnormality, Biochim. Biophys. Acta BBA - Biomembr. 982 (1989) 167–172, https://doi.org/10.1016/0005-2736(89)90188-0.
[63] G. Benga, Comparative studies of water permeability of red blood cells from humans and over 30 animal species: an overview of 20 years of collaboration with Philip Kuchel, Eur. Biophys. J. 42 (2012) 33–46, https://doi.org/10.1007/s00249-012-0868-7.
[64] G. Benga, Water transport in red blood cell membranes, Prog. Biophys. Mol. Biol. 51 (1988) 193–245, https://doi.org/10.1016/0079-6107(88)90002-8.
[65] G. Benga, Water exchange through the erythrocyte membrane, Int. Rev. Cytol. 114 (1989) 273–316, https://doi.org/10.1016/s0074-7696(08)60864-5.
[66] V.V. Morariu, M.S. Ionescu, M. Frangopol, R. Grosescu, M. Lupu, P.T. Frangopol, Nuclear magnetic resonance investigation of human erythrocytes in the presence of manganese ions. Evidence for a thermal transition, Biochim. Biophys. Acta BBA - Biomembr. 815 (1985) 189–195, https://doi.org/10.1016/0005-2736(85)90288-3.
[67] S. Aime, E. Bruno, C. Cabella, S. Colombatto, G. Digilio, V. Mainero, HR-MAS of cells: A "cellular water shift" due to water-protein interactions?, Magn. Reson. Med. 54 (2005) 1547–1552, https://doi.org/10.1002/mrm.20707.
[68] H.Y. Carr, E.M. Purcell, Effects of Diffusion on Free Precession in Nuclear Magnetic Resonance Experiments, Phys. Rev. 94 (1954) 630–638, https://doi.org/10.1103/PhysRev.94.630.
[69] A.R. Waldeck, P.W. Kuchel, A.J. Lennon, B.E. Chapman, NMR diffusion measurements to characterise membrane transport and solute binding, Prog. Nucl. Magn. Reson. Spectrosc. 30 (1997) 39–68, https://doi.org/10.1016/S0079-6565(96)01034-5.
[70] F. Stallmach, P. Galvosas, Spin Echo NMR Diffusion Studies, in: Annu. Rep. NMR Spectrosc., Elsevier, 2007: pp. 51–131. https://doi.org/10.1016/S0066-4103(07)61102-8..
[71] D.S. Grebenkov, NMR survey of reflected Brownian motion, Rev. Mod. Phys. 79 (2007) 61.
[72] G. Pagès, V. Gilard, R. Martino, M. Malet-Martino, Pulsed-field gradient nuclear magnetic resonance measurements (PFG NMR) for diffusion ordered spectroscopy (DOSY) mapping, Analyst. 142 (2017) 3771–3796, https://doi.org/10.1039/C7AN01031A.
[73] E.D. Finch, J.F. Harmon, B.H. Muller, Pulsed NMR measurements of the diffusion constant of water in muscle, Arch. Biochem. Biophys. 147 (1971) 299–310, https://doi.org/10.1016/0003-9861(71)90337-7.
[74] D.C. Chang, C.F. Hazlewood, B.L. Nichols, H.E. Rorschach, Spin echo studies on cellular water, Nature. 235 (1972) 170–171, https://doi.org/10.1038/235170a0.
[75] I. Åslund, A. Nowacka, M. Nilsson, D. Topgaard, Filter-exchange PGSE NMR determination of cell membrane permeability, J. Magn. Reson. 200 (2009) 291–295, https://doi.org/10.1016/j.jmr.2009.07.015.
[76] S. Eriksson, K. Elbing, O. Söderman, K. Lindkvist-Petersson, D. Topgaard, S. Lasič, NMR quantification of diffusional exchange in cell suspensions with relaxation rate differences between intra and extracellular compartments,

PLOS ONE. 12 (2017), https://doi.org/10.1371/journal.pone.0177273 e0177273.
[77] N.H. Williamson, R. Ravin, T.X. Cai, D. Benjamini, M. Falgairolle, M.J. O'Donovan, P.J. Basser, Real-time measurement of diffusion exchange rate in biological tissue, J. Magn. Reson. 317 (2020), https://doi.org/10.1016/j.jmr.2020.106782 106782.
[78] M. Šoltésová, H. Elicharová, P. Srb, M. Růžička, L. Janisova, H. Sychrová, J. Lang, Nuclear magnetic resonance investigation of water transport through the plasma membrane of various yeast species, FEMS Microbiol. Lett. 366 (2019) fnz220, https://doi.org/10.1093/femsle/fnz220.
[79] G. Karunanithy, R.J. Wheeler, L.R. Tear, N.J. Farrer, S. Faulkner, A.J. Baldwin, INDIANA: An in-cell diffusion method to characterize the size, abundance and permeability of cells, J. Magn. Reson. 302 (2019) 1–13, https://doi.org/10.1016/j.jmr.2018.12.001.
[80] C.S. Johnson, Diffusion ordered nuclear magnetic resonance spectroscopy: principles and applications, Prog. Nucl. Magn. Reson. Spectrosc. 34 (1999) 203–256, https://doi.org/10.1016/S0079-6565(99)00003-5.
[81] K.I. Momot, P.W. Kuchel, PFG NMR diffusion experiments for complex systems, Concepts Magn. Reson. Part A. 28A (2006) 249–269, https://doi.org/10.1002/cmr.a.20056.
[82] J. Andrasko, Water diffusion permeability of human erythrocytes studied by a pulsed gradient NMR technique, Biochim. Biophys. Acta BBA - Gen. Subj. 428 (1976) 304–311, https://doi.org/10.1016/0304-4165(76)90038-6.
[83] N.V. Lisitza, W.S. Warren, Y.-Q. Song, Study of diffusion in erythrocyte suspension using internal magnetic field inhomogeneity, J. Magn. Reson. 187 (2007) 146–154, https://doi.org/10.1016/j.jmr.2007.04.010.
[84] N.H. Williamson, R. Ravin, D. Benjamini, H. Merkle, M. Falgairolle, M.J. O'Donovan, D. Blivis, D. Ide, T.X. Cai, N.S. Ghorashi, R. Bai, P.J. Basser, Magnetic resonance measurements of cellular and sub-cellular membrane structures in live and fixed neural tissue, ELife. 8 (2019), https://doi.org/10.7554/eLife.51101 e51101.
[85] A. Reginald Waldeck, M. Hossein Nouri-Sorkhabi, D.R. Sullivan, P.W. Kuchel, Effects of cholesterol on transmembrane water diffusion in human erythrocytes measured using pulsed field gradient NMR, Biophys. Chem. 55 (1995) 197–208, https://doi.org/10.1016/0301-4622(95)00007-K.
[86] S.M. Schoberth, N.-K. Bär, R. Krämer, J. Kärger, Pulsed High-Field Gradient in Vivo NMR Spectroscopy to Measure Diffusional Water Permeability in Corynebacterium glutamicum, Anal. Biochem. 279 (2000) 100–105, https://doi.org/10.1006/abio.1999.4450.
[87] D.E. Callahan, S.F. Deamond, D.C. Creasey, T.L. Trapane, S.A. Bruce, P.O.P. Ts'O, L.-S. Kan, NMR studies of intracellular water at 300 MHz:T2-specific relaxation mechanisms in synchronized or EGF-stimulated cells, Magn. Reson. Med. 22 (1991) 68–80. https://doi.org/10.1002/mrm.1910220108..
[88] P. Bogner, A. Miseta, Z. Berente, A. Schwarcz, G. Kotek, I. Repa, Osmotic and diffusive properties of intracellular water in camel erythrocytes: Effect of hemoglobin crowdedness, Cell Biol. Int. 29 (2005) 731–736, https://doi.org/10.1016/j.cellbi.2005.04.008.
[89] K.-J. Suh, Y.-S. Hong, V.D. Skirda, V.I. Volkov, C.-Y.-J. Lee, C.-H. Lee, Water self-diffusion behavior in yeast cells studied by pulsed field gradient NMR, Biophys. Chem. 104 (2003) 121–130, https://doi.org/10.1016/S0301-4622(02)00361-7.
[90] C.-H. Cho, Y.-S. Hong, K. Kang, V.I. Volkov, V. Skirda, C.-Y.-J. Lee, C.-H. Lee, Water self-diffusion in chlorella sp. studied by pulse field gradient NMR, Magn. Reson. Imaging. 21 (2003) 1009–1017, https://doi.org/10.1016/S0730-725X(03)00206-6.
[91] A.I. García-Pérez, E.A. López-Beltrán, P. Klüner, J. Luque, P. Ballesteros, S. Cerdán, Molecular Crowding and Viscosity as Determinants of Translational Diffusion of Metabolites in Subcellular Organelles, Arch. Biochem. Biophys. 362 (1999) 329–338. https://doi.org/10.1006/abbi.1998.1051..
[92] I.A. Avilova, A.V. Smolina, A.I. Kotelnikov, R.A. Kotelnikova, V.V. Loskutov, V.I. Volkov, Self-diffusion of Water and Blood Lipids in Mouse Erythrocytes, Appl. Magn. Reson. 47 (2016) 335–347, https://doi.org/10.1007/s00723-015-0759-z.
[93] D. Shishmarev, K.I. Momot, P.W. Kuchel, Anisotropic diffusion in stretched hydrogels containing erythrocytes: evidence of cell-shape distortion recorded by PGSE NMR spectroscopy: Anisotropic diffusion in stretched RBC-containing gels, Magn. Reson. Chem. 55 (2017) 438–446, https://doi.org/10.1002/mrc.4416.
[94] V.V. Loskutov, V.I. Volkov, I.A. Avilova, A Novel Approach to Interpretation of the Time-Dependent Self-Diffusion Coefficient: Water-Mouse RBCs Suspension Study, Appl. Magn. Reson. 50 (2019) 305–321, https://doi.org/10.1007/s00723-018-1103-1.
[95] P.C. Van Zijl, C.T. Moonen, P. Faustino, J. Pekar, O. Kaplan, J.S. Cohen, Complete separation of intracellular and extracellular information in NMR spectra of perfused cells by diffusion-weighted spectroscopy, Proc. Natl. Acad. Sci. 88 (1991) 3228–3232, https://doi.org/10.1073/pnas.88.8.3228.
[96] L.L. Latour, K. Svoboda, P.P. Mitra, C.H. Sotak, Time-dependent diffusion of water in a biological model system, Proc. Natl. Acad. Sci. 91 (1994) 1229–1233, https://doi.org/10.1073/pnas.91.4.1229.
[97] Y. Roth, A. Ocherashvilli, D. Daniels, J. Ruiz-Cabello, S.E. Maier, A. Orenstein, Y. Mardor, Quantification of water compartmentation in cell suspensions by diffusion-weighted and T2-weighted MRI, Magn. Reson. Imaging. 26 (2008) 88–102, https://doi.org/10.1016/j.mri.2007.04.013.
[98] A. Raffo, R. Gianferri, R. Barbieri, E. Brosio, Ripening of banana fruit monitored by water relaxation and diffusion 1H-NMR measurements, Food Chem. 89 (2005) 149–158, https://doi.org/10.1016/j.foodchem.2004.02.024.
[99] R. Rucińska-Sobkowiak, G. Nowaczyk, M. Krzesłowska, I. Rabęda, S. Jurga, Water status and water diffusion transport in lupine roots exposed to lead, Environ. Exp. Bot. 87 (2013) 100–109, https://doi.org/10.1016/j.envexpbot.2012.09.012.
[100] G.A. Velikanov, T.A. Sibgatullin, L.P. Belova, I.F. Ionenko, Membrane water permeability of maize root cells under two levels of oxidative stress, Protoplasma. 252 (2015) 1263–1273, https://doi.org/10.1007/s00709-015-0758-9.
[101] A.V. Anisimov, N.R. Dautova, M.A. Suslov, Growth function and intercellular water transfer in excised roots, Protoplasma. 256 (2019) 1425–1432, https://doi.org/10.1007/s00709-019-01388-w.
[102] M.A. Suslov, Dynamics of intercellular water transfer in the roots of intact Zea mays L. plants under elevated concentrations of atmospheric CO2, Plant Physiol. Biochem. 151 (2020) 516–525, https://doi.org/10.1016/j.plaphy.2020.04.007.
[103] A. Anisimov, M. Suslov, Estimating the MRI Contrasting Agents Effect on Water Permeability of Plant Cell Membranes Using the 1H NMR Gradient Technique, Appl. Magn. Reson. 52 (2021) 235–246, https://doi.org/10.1007/s00723-021-01313-6.
[104] C.A. Waudby, M.D. Mantle, L.D. Cabrita, L.F. Gladden, C.M. Dobson, J. Christodoulou, Rapid Distinction of Intracellular and Extracellular Proteins Using NMR Diffusion Measurements, J. Am. Chem. Soc. 134 (2012) 11312–11315, https://doi.org/10.1021/ja304912c.
[105] M. Sluyser, C.H. Li, Preparation of a Low Molecular Weight Component with Lactogenic Activity from a Limited Chymotryptic Digest of Ovine Prolactin, Nature. 200 (1963) 1007–1008, https://doi.org/10.1038/2001007a0.
[106] S.H. Koenig, R.D. Brown, Field-cycling relaxometry of protein solutions and tissue: Implications for MRI, Prog. Nucl. Magn. Reson. Spectrosc. 22 (1990) 487–567, https://doi.org/10.1016/0079-6565(90)80008-6.
[107] V.P. Denisov, B. Halle, Protein hydration dynamics in aqueous solution, Faraday Discuss. 103 (1996) 227, https://doi.org/10.1039/fd9960300227.
[108] G. Otting, NMR studies of water bound to biological molecules, Prog. Nucl. Magn. Reson. Spectrosc. 31 (1997) 259–285, https://doi.org/10.1016/S0079-6565(97)00012-5.
[109] D. Laage, T. Elsaesser, J.T. Hynes, Water Dynamics in the Hydration Shells of Biomolecules, Chem. Rev. 117 (2017) 10694–10725, https://doi.org/10.1021/acs.chemrev.6b00765.
[110] K. Venu, V.P. Denisov, B. Halle, Water ^{1}H Magnetic Relaxation Dispersion in Protein Solutions. A Quantitative Assessment of Internal Hydration, Proton Exchange, and Cross-Relaxation, J. Am. Chem. Soc. 119 (1997) 3122–3134, https://doi.org/10.1021/ja963611t.
[111] F.V. Chávez, B. Halle, Molecular basis of water proton relaxation in gels and tissue, Magn. Reson. Med. 56 (2006) 73–81, https://doi.org/10.1002/mrm.20912.
[112] I.P. Gerothanassis, Oxygen-17 NMR spectroscopy: Basic principles and applications (part II), Prog. Nucl. Magn. Reson. Spectrosc. 57 (2010) 1–110, https://doi.org/10.1016/j.pnmrs.2009.12.001.
[113] F. Castiglione, A. Mele, G. Raos, 17O NMR: A "Rare and Sensitivé Probe of Molecular Interactions and Dynamics, Elsevier Ltd. (2015), https://doi.org/10.1016/bs.arnmr.2014.12.004.
[114] M.M. Civan, M. Shporer, 17O Nuclear Magnetic Resonance Spectrum of H217O in Frog Striated Muscle, Biophys. J. 12 (1972) 404–413, https://doi.org/10.1016/S0006-3495(72)86092-2.
[115] M.M. Civan, M. Shporer, Pulsed nuclear magnetic resonance study of 17-O, 2-D, and 1-H of water in frog striated muscle, Biophys. J. 15 (1975) 299–306, https://doi.org/10.1016/S0006-3495(75)85820-6.
[116] M. Shporer, M.M. Civan, NMR study of 17O from H217O in human erythrocytes, Biochim. Biophys. Acta BBA - Gen. Subj. 385 (1975) 81–87, https://doi.org/10.1016/0304-4165(75)90076-8.
[117] M. Shporer, M. Haas, M.M. Civan, Pulsed nuclear magnetic resonance study of 17O from H217O in rat lymphocytes, Biophys. J. 16 (1976) 601–611, https://doi.org/10.1016/S0006-3495(76)85715-3.
[118] E. Baguet, B.E. Chapman, A.M. Torres, P.W. Kuchel, Determination of the Bound Water Fraction in Cells and Protein Solutions Using17O–Water Multiple-Quantum Filtered Relaxation Analysis, J. Magn. Reson. B. 111 (1996) 1–8, https://doi.org/10.1006/jmrb.1996.0053.
[119] S.M. Grieve, B. Wickstead, A.M. Torres, P. Styles, S. Wimperis, P.W. Kuchel, Multiple-quantum filtered 17O and 23Na NMR analysis of mitochondrial suspensions, Biophys. Chem. 73 (1998) 137–143, https://doi.org/10.1016/S0301-4622(98)00155-0.
[120] X. Mao, W. Cui, W.H. Gmeiner, Line shape analyses for water 17O NMR quintet observed in a bacteriophage Pf1 solution at different temperatures, Biophys. Chem. 107 (2004) 255–262, https://doi.org/10.1016/j.bpc.2003.09.007.
[121] E. Persson, B. Halle, Cell water dynamics on multiple time scales, Proc. Natl. Acad. Sci. U. S. A. 105 (2008) 6266–6271, https://doi.org/10.1073/pnas.0709585105.
[122] J. Qvist, E. Persson, C. Mattea, B. Halle, Time scales of water dynamics at biological interfaces: peptides, proteins and cells, Faraday Discuss. 141 (2009) 131–144, https://doi.org/10.1039/B806194G.
[123] E.P. Sunde, P. Setlow, L. Hederstedt, B. Halle, The physical state of water in bacterial spores, Proc. Natl. Acad. Sci. 106 (2009) 19334–19339, https://doi.org/10.1073/pnas.0908712106.
[124] I. Piazza, A. Cupane, E.L. Barbier, C. Rome, N. Collomb, J. Ollivier, M.A. Gonzalez, F. Natali, Dynamical properties of water in living cells, Front. Phys. 13 (2018), https://doi.org/10.1007/s11467-017-0731-5 138301.

[125] M. Jasnin, A. Stadler, M. Tehei, G. Zaccai, Specific cellular water dynamics observed in vivo by neutron scattering and NMR, Phys. Chem. Chem. Phys. 12 (2010) 10154, https://doi.org/10.1039/c0cp01048k.
[126] R. Li, Z. Liu, L. Li, J. Huang, T. Yamada, V.G. Sakai, P. Tan, L. Hong, Anomalous sub-diffusion of water in biosystems: From hydrated protein powders to concentrated protein solution to living cells, Struct. Dyn. 7 (2020), https://doi.org/10.1063/4.0000036 054703.
[127] M. Tros, L. Zheng, J. Hunger, M. Bonn, D. Bonn, G.J. Smits, S. Woutersen, Picosecond orientational dynamics of water in living cells, Nat. Commun. 8 (2017) 904, https://doi.org/10.1038/s41467-017-00858-0.
[128] L. Ronconi, P.J. Sadler, Applications of heteronuclear NMR spectroscopy in biological and medicinal inorganic chemistry, Coord. Chem. Rev. 252 (2008) 2239–2277, https://doi.org/10.1016/j.ccr.2008.01.016.
[129] J. Szklaruk, J.F. Marecek, A.L. Springer, C.S. Springer, Aqueous shift reagents for high-resolution cation NMR spectroscopy. 4. [o-Bis((3-tripolyphosphato) propyloxy)benzene(-)]dysprosate(5-), Inorg. Chem. 29 (1990) 660–667. https://doi.org/10.1021/ic00329a020..
[130] A.C. Harnden, D. Parker, N.J. Rogers, Employing paramagnetic shift for responsive MRI probes, Coord. Chem. Rev. 383 (2019) 30–42, https://doi.org/10.1016/j.ccr.2018.12.012.
[131] A.D. Sherry, C.R. Malloy, F.M.H. Jeffrey, W.P. Cacheris, C.F.G.C. Geraldes, Dy (DOTP)5−: A new, stable 23Na shift reagent, J. Magn. Reson. 1969 (76) (1988) 528–533, https://doi.org/10.1016/0022-2364(88)90354-X.
[132] M.S. Albert, W. Huang, J.H. Lee, J.A. Balschi, C.S. Springer, Aqueous shift reagents for high-resolution cation NMR. VI. Titration curves for in vivo 23Na and 1H2O MRS obtained from rat blood, NMR Biomed. 6 (1993) 7–20, https://doi.org/10.1002/nbm.1940060103.
[133] J.A. Peters, J. Huskens, D.J. Raber, Lanthanide induced shifts and relaxation rate enhancements, Prog. Nucl. Magn. Reson. Spectrosc. 28 (1996) 283–350, https://doi.org/10.1016/0079-6565(95)01026-2.
[134] A. Barandov, B.B. Bartelle, C.G. Williamson, E.S. Loucks, S.J. Lippard, A. Jasanoff, Sensing intracellular calcium ions using a manganese-based MRI contrast agent, Nat. Commun. (2019) 1–9, https://doi.org/10.1038/s41467-019-08558-7.
[135] K.W. MacRenaris, Z. Ma, R.L. Krueger, C.E. Carney, T.J. Meade, Cell-Permeable Esterase-Activated Ca(II)-Sensitive MRI Contrast Agent, Bioconjug. Chem. 27 (2016) 465–473, https://doi.org/10.1021/acs.bioconjchem.5b00561.
[136] S. Ghosh, P. Harvey, J.C. Simon, A. Jasanoff, Probing the brain with molecular fMRI, Curr. Opin. Neurobiol. 50 (2018) 201–210, https://doi.org/10.1016/j.conb.2018.03.009.
[137] Z. Xu, C. Liu, S. Zhao, S. Chen, Y. Zhao, Molecular Sensors for NMR-Based Detection, Chem. Rev. 119 (2019) 195–230, https://doi.org/10.1021/acs.chemrev.8b00202.
[138] C.J. Adams, R. Krueger, T.J. Meade, A Multimodal Ca(II) Responsive Near IR-MR Contrast Agent Exhibiting High Cellular Uptake, ACS Chem. Biol. 15 (2020) 334–341, https://doi.org/10.1021/acschembio.9b00638.
[139] H. Li, T.J. Meade, Molecular Magnetic Resonance Imaging with Gd(III)-Based Contrast Agents: Challenges and Key Advances, J. Am. Chem. Soc. 141 (2019) 17025–17041, https://doi.org/10.1021/jacs.9b09149.
[140] K.P. Malikidogo, H. Martin, C.S. Bonnet, From Zn(II) to Cu(II) Detection by MRI Using Metal-Based Probes: Current Progress and Challenges, Pharmaceuticals. 13 (2020) 436, https://doi.org/10.3390/ph13120436.
[141] G. Wang, G. Angelovski, Highly Potent MRI Contrast Agent Displaying Outstanding Sensitivity to Zinc Ions, Angew. Chem. Int. Ed. 60 (2021) 5734–5738, https://doi.org/10.1002/anie.202014431.
[142] H. Gilboa, B.E. Chapman, P.W. Kuchel, 19F NMR magnetization transfer between 5-FBAPTA and its complexes. An alternative means for measuring free Ca2+ concentration, and detection of complexes with protein in erythrocytes, NMR Biomed. 7 (1994) 330–338, https://doi.org/10.1002/nbm.1940070707.
[143] A. Bar-Shir, A.A. Gilad, K.W.Y. Chan, G. Liu, P.C.M. van Zijl, J.W.M. Bulte, M.T. McMahon, Metal ion sensing using ion chemical exchange saturation transfer 19F magnetic resonance imaging, J. Am. Chem. Soc. 135 (2013) 12164–12167, https://doi.org/10.1021/ja403542g.
[144] G.A. Smith, R.T. Hesketh, J.C. Metcalfe, J. Feeney, P.G. Morris, Intracellular calcium measurements by 19F NMR of fluorine-labeled chelators, Proc. Natl. Acad. Sci. U. S. A. 80 (1983) 7178–7185, https://doi.org/10.1073/pnas.80.23.7178.
[145] E. Murphy, L. Levy, L.R. Berkowitz, E.P. Orringer, S.A. Gabel, R.E. London, Nuclear magnetic resonance measurement of cytosolic free calcium levels in human red blood cells, Am. J. Physiol. 251 (1986) C496–C504, https://doi.org/10.1152/ajpcell.1986.251.4.C496.
[146] P. Bendel, Biomedical applications of 10B and 11B NMR, NMR Biomed. 18 (2005) 74–82, https://doi.org/10.1002/nbm.886.
[147] S. Capuani, P. Porcari, F. Fasano, R. Campanella, B. Maraviglia, 10B-editing 1H-detection and 19F MRI strategies to optimize boron neutron capture therapy, Magn. Reson. Imaging. 26 (2008) 987–993, https://doi.org/10.1016/j.mri.2008.01.040.
[148] M. Kitamura, T. Suzuki, R. Abe, T. Ueno, S. Aoki, 11B NMR Sensing of d-Block Metal Ions in Vitro and in Cells Based on the Carbon-Boron Bond Cleavage of Phenylboronic Acid-Pendant Cyclen (Cyclen = 1,4,7,10-Tetraazacyclododecane), Inorg. Chem. 50 (2011) 11568–11580, https://doi.org/10.1021/ic201507q.
[149] F.S. Coulibaly, A.S. Alnafisah, N.A. Oyler, B.-B.-C. Youan, Direct and Real-Time Quantification Of Bortezomib Release From Alginate Microparticles Using Boron (11B) Nuclear Magnetic Resonance Spectroscopy, Mol. Pharm. 16 (2019) 967–977, https://doi.org/10.1021/acs.molpharmaceut.8b00873.
[150] S.J. Berners-Price, P.W. Kuchel, Reaction of cis- and trans-[PtCl2(NH3)2] with reduced glutathione inside human red blood cells, studied by 1H and 15N-{1H} DEPT NMR, J. Inorg. Biochem. 38 (1990) 327–345, https://doi.org/10.1016/0162-0134(90)80006-J.
[151] M. Becker, R.E. Port, H.J. Zabel, W.J. Zeller, P. Bachert, Monitoring local disposition kinetics of carboplatin in vivo after subcutaneous injection in rats by means of 195Pt NMR, J. Magn. Reson. 133 (1998) 115–122, https://doi.org/10.1006/jmre.1998.1436.
[152] B.M. Still, P.G.A. Kumar, J.R. Aldrich-Wright, W.S. Price, 195Pt NMR—theory and application, Chem Soc Rev. 36 (2007) 665–686, https://doi.org/10.1039/B606190G.
[153] G.S. Malhi, M. Tanious, P. Das, C.M. Coulston, M. Berk, Potential Mechanisms of Action of Lithium in Bipolar Disorder, CNS Drugs. 27 (2013) 135–153, https://doi.org/10.1007/s40263-013-0039-0.
[154] C.A. Lazzara, Y.-H. Kim, Potential application of lithium in Parkinson's and other neurodegenerative diseases, Front. Neurosci. 9 (2015) 157–210, https://doi.org/10.3389/fnins.2015.00403.
[155] W. Ge, E. Jakobsson, Systems Biology Understanding of the Effects of Lithium on Cancer, Front Oncol. 9 (2019) 11–18, https://doi.org/10.3389/fonc.2019.00296.
[156] D. Mota de Freitas, M.M.C.A. Castro, C.F.G.C. Geraldes, Is competition between Li+ and Mg2+ the underlying theme in the proposed mechanisms for the pharmacological action of lithium salts in bipolar disorder?, Acc. Chem. Res. 39 (2006) 283–291, https://doi.org/10.1021/ar030197a.
[157] E. Jakobsson, O. Argüello-Miranda, S.-W. Chiu, Z. Fazal, J. Kruczek, S. Nunez-Corrales, S. Pandit, L. Pritchet, Towards a Unified Understanding of Lithium Action in Basic Biology and its Significance for Applied Biology, J. Membr. Biol. 250 (2017) 587–604, https://doi.org/10.1007/s00232-017-9998-2.
[158] T. Dudev, K. Mazmanian, W.-H. Weng, C. Grauffel, C. Lim, Free and Bound Therapeutic Lithium in Brain Signaling, Acc. Chem. Res. 52 (2019) 2960–2970, https://doi.org/10.1021/acs.accounts.9b00389.
[159] R.A. Komoroski, Biomedical applications of 7Li NMR, NMR Biomed. 18 (2005) 67–73, https://doi.org/10.1002/nbm.914.
[160] J. Andrasko, Measurement of membrane permeability to slowly penetrating molecules by a pulse gradient NMR method, J. Magn. Reson. 1969 (21) (1976) 479–484, https://doi.org/10.1016/0022-2364(76)90053-6.
[161] J.A. Balschi, V.P. Cirillo, C.S. Springer Jr, Direct High-resolution Nuclear Magnetic Resonance Studies of Cation Transport in Vivo: Na+ Transport in Yeast Cells, Biophys. J. 38 (1982) 323–326, https://doi.org/10.1016/S0006-3495(82)84566-9.
[162] M.C. Espanol, D. Mota de Freitas, Lithium-7 NMR studies of lithium transport in human erythrocytes, Inorg. Chem. 26 (1987) 4356–4359, https://doi.org/10.1021/ic00273a016.
[163] F.G. Riddell, A. Patel, M.S. Hughes, Lithium uptake rate and lithium: lithium exchange rate in human erythrocytes at a nearly pharmacologically normal level monitored by 7Li NMR, J. Inorg. Biochem. 39 (1990) 187–192, https://doi.org/10.1016/0162-0134(90)84001-6.
[164] R. Ramasamy, D. Mota de Freitas, V.K. Bansal, E. Dorus, R.J. Labotka, Nuclear magnetic resonance studies of lithium transport in erythrocyte suspensions of hypertensives, Clin. Chim. Acta Int. J. Clin. Chem. 188 (1990) 169–176, https://doi.org/10.1016/0009-8981(90)90161-k.
[165] J. Bramham, A.N. Carter, F.G. Riddell, The uptake of Li+ into human 1321 N1 astrocytomas using 7Li NMR spectroscopy, J. Inorg. Biochem. 61 (1996) 273–284, https://doi.org/10.1016/0162-0134(95)00075-5.
[166] Y. Chi, S. Mo, D. Mota de Freitas, Na(+)-H+ and Na(+)-Li+ exchange are mediated by the same membrane transport protein in human red blood cells: an NMR investigation, Biochemistry. 35 (1996) 12433–12442, https://doi.org/10.1021/bi960814l.
[167] J. Nikolakopoulos, C. Zachariah, D.M. de Freitas, C.F.G.C. Geraldes, Comparison of the use of gel threads and microcarrier beads in Li+ transport studies of human neuroblastoma SH-SY5Y cells, Inorganica Chim. Acta. 251 (1996) 201–205, https://doi.org/10.1016/S0020-1693(96)05273-5.
[168] J. Nikolakopoulos, C. Zachariah, D. Mota de Freitas, E.B. Stubbs, R. Ramasamy, M.C. Castro, C.F. Geraldes, 7Li nuclear magnetic resonance study for the determination of Li+ properties in neuroblastoma SH-SY5Y cells, J. Neurochem. 71 (1998) 1676–1684, https://doi.org/10.1046/j.1471-4159.1998.71041676.x.
[169] V.V. Kupriyanov, B. Xiang, L. Yang, R. Deslauriers, Lithium ion as a probe of Na + channel activity in isolated rat hearts: a multinuclear NMR study, NMR Biomed. 10 (1997) 271–276, https://doi.org/10.1002/(sici)1099-1492(199709)10:6<271::aid-nbm473>3.0.co;2-l.
[170] M.L. Gruwel, B. Kuzio, B. Xiang, R. Deslauriers, V.V. Kupriyanov, Temperature dependence of monovalent cation fluxes in isolated rat hearts: a magnetic resonance study, Biochim. Biophys. Acta. 1415 (1998) 41–55, https://doi.org/10.1016/s0005-2736(98)00177-1.
[171] V.V. Kupriyanov, B. Xiang, B. Kuzio, R. Deslauriers, pH regulation of K(+) efflux from myocytes in isolated rat hearts: (87)Rb, (7)Li, and (31)P NMR studies, Am. J. Physiol. 277 (1999) H279–H289, https://doi.org/10.1152/ajpheart.1999.277.1.H279.
[172] J.W. Pettegrew, J.W. Short, R.D. Woessner, S. Strychor, D.W. McKeag, J. Armstrong, N.J. Minshew, A.J. Rush, The effect of lithium on the membrane molecular dynamics of normal human erythrocytes, Biol. Psychiatry. 22 (1987) 857–871, https://doi.org/10.1016/0006-3223(87)90084-9.

[173] R.P. Gullapalli, R.M. Hawk, R.A. Komoroski, A 7Li NMR study of visibility, spin relaxation, and transport in normal human erythrocytes, Magn. Reson. Med. 20 (1991) 240–252, https://doi.org/10.1002/mrm.1910200207.
[174] Q. Rong, M. Espanol, D. Mota de Freitas, C.F. Geraldes, 7Li NMR relaxation study of Li+ binding in human erythrocytes, Biochemistry. 32 (1993) 13490–13498, https://doi.org/10.1021/bi00212a014.
[175] D. Mota de Freitas, Q. Rong, S. Mo, Reinvestigation of the transmembrane difference in 7Li NMR T1 values in Li(+)-loaded human erythrocyte suspensions, Magn. Reson. Med. 29 (1993) 256–259, https://doi.org/10.1002/mrm.1910290216.
[176] L. Amari, B. Layden, J. Nikolakopoulos, Q. Rong, D.M. de Freitas, G. Baltazar, M. M.C.A. Castro, C.F.G.C. Geraldes, Competition between Li+ and Mg2+ in Neuroblastoma SH-SY5Y Cells: A Fluorescence and 31P NMR Study, Biophys. J. 76 (1999) 2934–2942, https://doi.org/10.1016/S0006-3495(99)77448-5.
[177] C. Srinivasan, N. Minadeo, C.F. Geraldes, D. Mota de Freitas, Competition between Li+ and Mg2+ for red blood cell membrane phospholipids: A 31P, 7Li, and 6Li nuclear magnetic resonance study, Lipids. 34 (1999) 1211–1221, https://doi.org/10.1007/s11745-999-0474-5.
[178] B.T. Layden, A.M. Abukhdeir, N. Williams, C.P. Fonseca, L. Carroll, M.M.C.A. Castro, C.F.G.C. Geraldes, F.B. Bryant, D.M. de Freitas, Effects of Li+ transport and Li+ immobilization on Li+/Mg2+ competition in cells: implications for bipolar disorder, Biochem. Pharmacol. 66 (2003) 1915–1924, https://doi.org/10.1016/j.bcp.2003.07.001.
[179] C.P. Fonseca, L.P. Montezinho, C. Nabais, A.R. Tomé, H. Freitas, C.F.G.C. Geraldes, M.M.C.A. Castro, Effects of Li+ transport and intracellular binding on Li+/Mg2+ competition in bovine chromaffin cells, Biochim. Biophys. Acta BBA - Mol. Cell Res. 1691 (2004) 79–90, https://doi.org/10.1016/j.bbamcr.2003.12.005.
[180] B.T. Layden, A.M. Abukhdeir, C. Malarkey, L.A. Oriti, W. Salah, C. Stigler, C.F.G.C. Geraldes, D. Mota de Freitas, Identification of Li+ binding sites and the effect of Li+ treatment on phospholipid composition in human neuroblastoma cells: a 7Li and 31P NMR study, Biochim. Biophys. Acta BBA - Mol. Basis Dis. 1741 (2005) 339–349, https://doi.org/10.1016/j.bbadis.2005.07.004.
[181] M. Vosahlikova, H. Ujcikova, O. Chernyavskiy, J. Brejchova, L. Roubalova, M. Alda, P. Svoboda, Effect of therapeutic concentration of lithium on live HEK293 cells; increase of Na+/K+-ATPase, change of overall protein composition and alteration of surface layer of plasma membrane, BBA - Gen. Subj. 2017 (1861) 1099–1112, https://doi.org/10.1016/j.bbagen.2017.02.011.
[182] A. Haimovich, A. Goldbourt, How does the mood stabilizer lithium bind ATP, the energy currency of the cell: Insights from solid-state NMR, Biochim. Biophys. Acta Gen. Subj. 1864 (2020), https://doi.org/10.1016/j.bbagen.2019.129456 129456.
[183] A. Haimovich, U. Eliav, A. Goldbourt, Determination of the lithium binding site in inositol monophosphatase, the putative target for lithium therapy, by magic-angle-spinning solid-state NMR, J. Am. Chem. Soc. 134 (2012) 5647–5651, https://doi.org/10.1021/ja211794x.
[184] J. Stout, A.-S. Hanak, L. Chevillard, B. Djemaï, P. Risède, E. Giacomini, J. Poupon, D.A. Barrière, F. Bellivier, B. Mégarbane, F. Boumezbeur, Investigation of lithium distribution in the rat brain ex vivousing lithium-7 magnetic resonance spectroscopy and imaging at 17.2 T, NMR Biomed. 30 (2017) e3770–e3779, https://doi.org/10.1002/nbm.3770.
[185] F.E. Smith, P.E. Thelwall, J. Necus, C.J. Flowers, A.M. Blamire, D.A. Cousins, 3D 7Li magnetic resonance imaging of brain lithium distribution in bipolar disorder, Mol. Psychiatry. (2018) 1–8, https://doi.org/10.1038/s41380-018-0016-6.
[186] K.B. Gagnon, E. Delpire, Sodium Transporters in Human Health and Disease, Front. Physiol. 11 (2021), https://doi.org/10.3389/fphys.2020.588664 588664.
[187] F.W. Cope, Nuclear magnetic resonance evidence for complexing of sodium ions in muscle, Proc. Natl. Acad. Sci. 54 (1965) 225–227, https://doi.org/10.1073/pnas.54.1.225.
[188] F.W. Cope, NMR Evidence for Complexing of Na+ in Muscle, Kidney, and Brain, and by Actomyosin. The Relation of Cellular Complexing of Na+ to Water Structure and to Transport Kinetics, J. Gen. Physiol. 50 (1967) 1353–1375.
[189] C.A. Rotunno, V. Kowalewski, M. Cereijido, Nuclear spin resonance evidence for complexing of sodium in frog skin, Biochim. Biophys. Acta BBA - Biomembr. 135 (1967) 170–173, https://doi.org/10.1016/0005-2736(67)90022-3.
[190] D. Martinez, A.A. Silvidi, R.M. Stokes, Nuclear Magnetic Resonance Studies of Sodium Ions in Isolated Frog Muscle and Liver, Biophys. J. 9 (1969) 1256–1260, https://doi.org/10.1016/S0006-3495(69)86450-7.
[191] J.L. Czeisler, O.G. Fritz Jr, T.J. Swift, Direct Evidence from Nuclear Magnetic Resonance Studies for Bound Sodium in Frog Skeletal Muscle, Biophys. J. 10 (1970) 260–268, https://doi.org/10.1016/S0006-3495(70)86298-1.
[192] F.W. Cope, Spin-echo nuclear magnetic resonance evidence for complexing of sodium ions in muscle, brain, and kidney, Biophys. J. 10 (1970) 843–858, https://doi.org/10.1016/S0006-3495(70)86339-1.
[193] J.A. Magnuson, N.S. Magnuson, NMR studies of sodium and potassium in various biological tissues, Ann. N. Y. Acad. Sci. 204 (1973) 297–309, https://doi.org/10.1111/j.1749-6632.1973.tb30786.x.
[194] J.A. Magnuson, N.S. Magnuson, D.L. Hendrix, N. Higinbotham, Nuclear Magnetic Resonance Studies of Sodium and Potassium in Etiolated Pea Stem, Biophys. J. 13 (1973) 763–771, https://doi.org/10.1016/S0006-3495(73)86022-9.
[195] M. Shporer, M.M. Civan, Nuclear Magnetic Resonance of Sodium-23 Linoleate-Water, Biophys. J. 12 (1972) 114–122, https://doi.org/10.1016/S0006-3495(72)86074-0.
[196] M. Shporer, M.M. Civan, Effects of temperature and field strength on the NMR relaxation times of 23Na in frog striated muscle, Biochim. Biophys. Acta BBA - Gen. Subj. 354 (1974) 291–304, https://doi.org/10.1016/0304-4165(74)90014-2.
[197] M.M. Civan, M. Shporer, Chapter 1 Physical State of Cell Sodium, in: Cell. Mol. Biol. Sodium Transp., Elsevier, 1989: pp. 1–19. https://doi.org/10.1016/S0070-2161(08)60005-2..
[198] M.M. Pike, S.R. Simon, J.A. Balschi, C.S. Springer, High-resolution NMR studies of transmembrane cation transport: use of an aqueous shift reagent for 23Na, Proc. Natl. Acad. Sci. 79 (1982) 810–814, https://doi.org/10.1073/pnas.79.3.810.
[199] R.K. Gupta, P. Gupta, Direct observation of resolved resonances from intra- and extracellular sodium-23 ions in NMR studies of intact cells and tissues using dysprosium(III)tripolyphosphate as paramagnetic shift reagent, J. Magn. Reson. 1969 (47) (1982) 344–350, https://doi.org/10.1016/0022-2364(82)90127-5.
[200] T. Ogino, J.A. den Hollander, R.G. Shulman, 39K, 23Na, and 31P NMR studies of ion transport in Saccharomyces cerevisiae, Proc. Natl. Acad. Sci. 80 (1983) 5185–5189, https://doi.org/10.1073/pnas.80.17.5185.
[201] M.M. Pike, C.S. Springer Jr, Aqueous shift reagents for high-resolution cationic nuclear magnetic resonance, J. Magn. Reson. 1969 (46) (1982) 348–353, https://doi.org/10.1016/0022-2364(82)90153-6.
[202] R.K. Gupta, P. Gupta, R.D. Moore, NMR Studies of Intracellular Metal Ions in Intact Cells and Tissues, Annu. Rev. Biophys. Bioeng. 13 (1984) 221–246, https://doi.org/10.1146/annurev.bb.13.060184.001253.
[203] B.E. Cowan, D.Y. Sze, M.T. Mai, O. Jardetzky, Measurement of the sodium membrane potential by NMR, FEBS Lett. 184 (1985) 130–133, https://doi.org/10.1016/0014-5793(85)80668-2.
[204] H. Nissen, J.P. Jacobsen, M. Hørder, Assessment of the NMR visibility of intraerythrocytic sodium by flame photometric and ion-competitive studies, Magn. Reson. Med. 10 (1989) 388–398, https://doi.org/10.1002/mrm.1910100310.
[205] A.M. Castle, R.M. Macnab, R.G. Shulman, Measurement of intracellular sodium concentration and sodium transport in Escherichia coli by 23Na nuclear magnetic resonance, J. Biol. Chem. 261 (1986) 3288–3294, https://doi.org/10.1016/S0021-9258(17)35780-0.
[206] A.M. Castle, R.M. Macnab, R.G. Shulman, Coupling between the sodium and proton gradients in respiring Escherichia coli cells measured by 23Na and 31P nuclear magnetic resonance, J. Biol. Chem. 261 (1986) 7797–7806, https://doi.org/10.1016/S0021-9258(19)57471-3.
[207] H. Gilboa, M. Kogut, S. Chalamish, R. Regev, Y. Avi-Dor, N.J. Russell, Use of 23Na nuclear magnetic resonance spectroscopy to determine the true intracellular concentration of free sodium in a halophilic eubacterium, J. Bacteriol. 173 (1991) 7021–7023, https://doi.org/10.1128/JB.173.21.7021-7023.1991.
[208] F. Rabaste, G. Dauphin, G. Jeminet, J. Guyot, A.-M. Delort, Phosphate-dependent sodium transport in S. faecalis investigated by 23Na and 31P NMR, Biochem. Biophys. Res. Commun. 181 (1991) 74–79, https://doi.org/10.1016/S0006-291X(05)81383-X.
[209] F. Rabaste, G. Jeminet, G. Dauphin, A.-M. Delort, Conditions modulating the ionic selectivity of transport by monensin examined on Enterococcus hirae (Streptococcus faecalis) by23Na-NMR and K+ atomic absorption, Biochim. Biophys. Acta BBA - Biomembr. 1108 (1992) 177–182, https://doi.org/10.1016/0005-2736(92)90023-F.
[210] F. Rabaste, G. Jeminet, G. Dauphin, A.-M. Delort, Na+ and K+ transport by 4-chlorophenylurethane-monensin in Enterococcus hirae de-energized and energized cells studied by 23Na-NMR and K+ atomic absorption, Biochim. Biophys. Acta BBA - Mol. Cell Res. 1179 (1993) 166–169, https://doi.org/10.1016/0167-4889(93)90138-F.
[211] S. Nagata, K. Adachi, K. Shirai, H. Sano, 23Na NMR spectroscopy of free Na+ in the halotolerant bacterium Brevibacterium sp. and Escherichia coli, Microbiology. 141 (1995) 729–736, https://doi.org/10.1099/13500872-141-3-729.
[212] S. Nagata, K. Adachi, H. Sano, Intracellular Changes in Ions and Organic Solutes in HalotolerantBrevibacterium sp. Strain JCM 6894 after Exposure to Hyperosmotic Shock, Appl. Environ. Microbiol. 64 (1998) 3641–3647, https://doi.org/10.1128/AEM.64.10.3641-3647.1998.
[213] A.-M. Delort, G. Gaudet, E. Forano, 23Na NMR Study of Fibrobacter succinogenes S85: Comparison of Three Chemical Shift Reagents and Calculation of Sodium Concentration Using Ionophores, Anal. Biochem. 306 (2002) 171–180, https://doi.org/10.1006/abio.2002.5685.
[214] K. Górecki, C. Hägerhäll, T. Drakenberg, The Na+ transport in gram-positive bacteria defect in the Mrp antiporter complex measured with 23Na nuclear magnetic resonance, Anal. Biochem. 445 (2014) 80–86, https://doi.org/10.1016/j.ab.2013.10.003.
[215] R.K. Gupta, A.B. Kostellow, G.A. Morrill, NMR studies of intracellular sodium ions in amphibian oocytes, ovulated eggs, and early embryos, J. Biol. Chem. 260 (1985) 9203–9208, https://doi.org/10.1016/S0021-9258(17)39353-5.
[216] J.-B. Martin, G. Klein, M. Satre, 23Na NMR study of intracellular sodium ions in Dictyostelium discoideum amoeba, Arch. Biochem. Biophys. 254 (1987) 559–567, https://doi.org/10.1016/0003-9861(87)90138-X.
[217] M.M. Pike, E.T. Fossel, T.W. Smith, C.S. Springer, High-resolution 23Na-NMR studies of human erythrocytes: use of aqueous shift reagents, Am. J. Physiol. 246 (1984) C528–C536, https://doi.org/10.1152/ajpcell.1984.246.5.C528.

[218] T. Ogino, G.I. Shulman, M.J. Avison, S.R. Gullans, J.A. den Hollander, R.G. Shulman, 23Na and 39K NMR studies of ion transport in human erythrocytes, Proc. Natl. Acad. Sci. 82 (1985) 1099–1103, https://doi.org/10.1073/pnas.82.4.1099.
[219] R. Ouwerkerk, C.J.A.V. Echteld, G.E.J. Staal, G. Rijksen, Erythrocyte Na+/K+ ATPase activity measured with23Na NMR, Magn. Reson. Med. 12 (1989) 164–171, https://doi.org/10.1002/mrm.1910120203.
[220] S.E. Anderson, J.S. Adorante, P.M. Cala, Dynamic NMR measurement of volume regulatory changes in Amphiuma RBC Na+ content, Am. J. Physiol. 254 (1988) C466–C474, https://doi.org/10.1152/ajpcell.1988.254.3.C466.
[221] M. Rochdi, A.M. Delort, J. Guyot, M. Sancelme, G. Dauphin, G. Jeminet, A new Na+ and K+ carrier from chemically modified monensin studied in human erythrocytes by 23Na nuclear magnetic resonance, K+ atomic absorption and H+ potentiometry, Bioelectrochem. Bioenerg. 33 (1994) 83–90, https://doi.org/10.1016/0302-4598(94)87037-3.
[222] M. Rochdi, A.-M. Delort, J. Guyot, M. Sancelme, S. Gibot, J.-G. Gourcy, G. Dauphin, C. Gumila, H. Vial, G. Jeminet, Ionophore Properties of Monensin Derivatives Studied on Human Erythrocytes by ^{23} Na NMR and K^+ and H^+ Potentiometry: Relationship with Antimicrobial and Antimalarial Activities, J. Med. Chem. 39 (1996) 588–595, https://doi.org/10.1021/jm9505829.
[223] M.M. Civan, H. Degani, Y. Margalit, M. Shporer, Observations of 23Na in frog skin by NMR, Am. J. Physiol. 245 (1983) C213–C219, https://doi.org/10.1152/ajpcell.1983.245.3.C213.
[224] S.R. Gullans, M.J. Avison, T. Ogino, G. Giebisch, R.G. Shulman, NMR measurements of intracellular sodium in the rabbit proximal tubule, Am. J. Physiol. 249 (1985) F160–F168, https://doi.org/10.1152/ajprenal.1985.249.1.F160.
[225] M.M. Pike, J.C. Frazer, D.F. Dedrick, J.S. Ingwall, P.D. Allen, C.S. Springer Jr, T.W. Smith, 23Na and 39K nuclear magnetic resonance studies of perfused rat hearts. Discrimination of intra- and extracellular ions using a shift reagent, Biophys. J. 48 (1985) 159–173, https://doi.org/10.1016/S0006-3495(85)83769-3.
[226] Y. Seo, M. Murakami, T. Matsumoto, H. Nishikawa, H. Watari, Applications of aqueous shift reagent, Dy(TTHA), for 23Na NMR studies of exocrine glands. Viabilities of organs perfused with shift reagent, J. Magn. Reson. 1969 72 (1987) 341–346, https://doi.org/10.1016/0022-2364(87)90297-6.
[227] Y. Seo, M. Murakami, T. Matsumoto, H. Nishikawa, H. Watari, Direct measurement of Na influx by 23Na NMR during secretion with acetylcholine in perfused rat mandibular gland, Pflüg. Arch. 409 (1987) 343–348, https://doi.org/10.1007/BF00583787.
[228] M.J. Avison, S.R. Gullans, T. Ogino, G. Giebisch, R.G. Shulman, Measurement of Na+-K+ coupling ratio of Na+-K+-ATPase in rabbit proximal tubules, Am. J. Physiol.-Cell Physiol. 253 (1987) C126–C136, https://doi.org/10.1152/ajpcell.1987.253.1.C126.
[229] D. Powell, D. Burstein, E.T. Fossel, Nuclear magnetic resonance studies of sodium/calcium exchange in frog perfused, beating hearts, Eur. J. Biochem. 193 (1990) 887–889, https://doi.org/10.1111/j.1432-1033.1990.tb19413.x.
[230] E. Murphy, M. Perlman, R.E. London, C. Steenbergen, Amiloride delays the ischemia-induced rise in cytosolic free calcium, Circ. Res. 68 (1991) 1250–1258, https://doi.org/10.1161/01.res.68.5.1250.
[231] H. Naritomi, M. Kanashiro, M. Sasaki, Y. Kuribayashi, T. Sawada, In vivo measurements of intra- and extracellular Na+ and water in the brain and muscle by nuclear magnetic resonance spectroscopy with shift reagent, Biophys. J. 52 (1987) 611–616, https://doi.org/10.1016/S0006-3495(87)83251-4.
[232] S.J. Kohler, N.H. Kolodny, A.C. Celi, T.A. Burr, D. Weinberg, D.J. D'amico, E.S. Gragoudas, In vivo sodium chemical shift imaging, Magn. Reson. Med. 23 (1992) 77–88, https://doi.org/10.1002/mrm.1910230109.
[233] N. Bansal, M.J. Germann, V. Seshan, G.T. Shires III, C.R. Malloy, A.D. Sherry, Thulium 1,4,7,10-tetraazacyclododecane-1,4,7,10-tetrakis(methylene phosphonate) as a sodium-23 shift reagent for the in vivo rat liver, Biochemistry. 32 (1993) 5638–5643.
[234] P.M. Winter, V. Seshan, J.D. Makos, A.D. Sherry, C.R. Malloy, N. Bansal, Quantitation of intracellular [Na^+] in vivo by using $TmDOTP^{5-}$ as an NMR shift reagent and extracellular marker, J. Appl. Physiol. 85 (1998) 1806–1812, https://doi.org/10.1152/jappl.1998.85.5.1806.
[235] P.M. Winter, N. Bansal, TmDOTP5– as a 23Na shift reagent for the subcutaneously implanted 9L gliosarcoma in rats, Magn. Reson. Med. 45 (2001) 436–442, https://doi.org/10.1002/1522-2594(200103)45:3<436::AID-MRM1057>3.0.CO;2-6.
[236] A.-M. Delort, G. Dauphin, J. Guyot, G. Jeminet, Study by NMR of the mode of action of monensin on Streptococcus faecalis de-energized and energized cells, Biochim. Biophys. Acta BBA - Mol. Cell Res. 1013 (1989) 11–20, https://doi.org/10.1016/0167-4889(89)90121-3.
[237] C.S. Springer, Transmembrane Ion Pumping: High Resolution Cation NMR Spectroscopya, Ann. N. Y. Acad. Sci. 508 (1987) 130–148, https://doi.org/10.1111/j.1749-6632.1987.tb32900.x.
[238] N.A. Matwiyoff, C. Gasparovic, R. Wenk, J.D. Wicks, A. Rath, 31P and 23Na NMR studies of the structure and lability of the sodium shift reagent, bis (tripolyphosphate)dysprosium(iii) ([dy(p3O10)]7−) ion, and its decomposition in the presence of rat muscle, Magn. Reson. Med. 3 (1986) 164–168, https://doi.org/10.1002/mrm.1910030125.
[239] Z.H. Endre, J.L. Allis, G.K. Radda, Toxicity of dysprosium shift reagents in the isolated perfused rat kidney, Magn. Reson. Med. 11 (1989) 267–274, https://doi.org/10.1002/mrm.1910110215.
[240] Y. Boulanger, A. Fleser, R. Amarouche, H. Ammann, M. Bergeron, P. Vinay, Monitoring of the effects of dysprosium shift reagents on cell suspensions, NMR Biomed. 5 (1992) 1–10, https://doi.org/10.1002/nbm.1940050103.
[241] B. Gaszner, T. Simor, G. Hild, G.A. Elgavish, The Effects of the NMR Shift-reagents Dy(PPP)2, Dy(TTHA) and Tm(DOTP) on Developed Pressure in Isolated Perfused Rat Hearts. The Role of Shift-reagent Calcium Complexes, J. Mol. Cell. Cardiol. 33 (2001) 1945–1956, https://doi.org/10.1006/jmcc.2001.1459.
[242] S.C. Chu, M.M. Pike, E.T. Fossel, T.W. Smith, J.A. Balschi, C.S. Springer Jr, Aqueous shift reagents for high-resolution cationic nuclear magnetic resonance. III. Dy(TTHA)3−, Tm(TTHA)3−, and Tm(PPP)27−, J. Magn. Reson. 1969. 56 (1984) 33–47. https://doi.org/10.1016/0022-2364(84)90189-6..
[243] J. Pekar, J.S. Leigh, Detection of biexponential relaxation in sodium-23 facilitated by double-quantum filtering, J. Magn. Reson. 1969 (69) (1986) 582–584, https://doi.org/10.1016/0022-2364(86)90180-0.
[244] J. Pekar, P.F. Renshaw, J.S. Leigh, Selective detection of intracellular sodium by coherence-transfer NMR, J. Magn. Reson. 1969 (72) (1987) 159–161, https://doi.org/10.1016/0022-2364(87)90182-X.
[245] W.D. Rooney, T.M. Barbara, C.S. Springer, Two-dimensional double-quantum NMR spectroscopy of isolated spin 3/2 systems: sodium-23 examples, J. Am. Chem. Soc. 110 (1988) 674–681, https://doi.org/10.1021/ja00211a003.
[246] L.A. Jelicks, R.K. Gupta, Double-quantum NMR of sodium ions in cells and tissues. Paramagnetic quenching of extracellular coherence, J. Magn. Reson. 1969 81 (1989) 586–592, https://doi.org/10.1016/0022-2364(89)90097-8.
[247] L.A. Jelicks, R.K. Gupta, Observation of intracellular sodium ions by double-quantum-filtered 23Na NMR with paramagnetic quenching of extracellular coherence by gadolinium tripolyphosphate, J. Magn. Reson. 1969 (83) (1989) 146–151, https://doi.org/10.1016/0022-2364(89)90298-9.
[248] J.L. Allis, A.-M.L. SEYMOUR, G.K. Radda, Absolute quantification of intracellular Na+ using triple-quantum-filtered sodium-23 NMR, J. Magn. Reson. 1969. 93 (1991) 71–76. https://doi.org/10.1016/0022-2364(91)90032-O..
[249] G. Navon, Complete elimination of the extracellular 23Na NMR signal in triple quantum filtered spectra of rat hearts in the presence of shift reagents, Magn. Reson. Med. 30 (1993) 503–506, https://doi.org/10.1002/mrm.1910300415.
[250] L.A. Jelicks, R.K. Gupta, On the extracellular contribution to multiple quantum filtered 23Na NMR of perfused rat heart, Magn. Reson. Med. 29 (1993) 130–133, https://doi.org/10.1002/mrm.1910290124.
[251] T. Knubovets, H. Shinar, U. Eliav, G. Navon, A 23Na Multiple-Quantum-Filtered NMR Study of the Effect of the Cytoskeleton Conformation on the Anisotropic Motion of Sodium Ions in Red Blood Cells, J. Magn. Reson. B. 110 (1996) 16–25, https://doi.org/10.1006/jmrb.1996.0003.
[252] T. Knubovets, H. Shinar, G. Navon, Quantification of the Contribution of Extracellular Sodium to 23Na Multiple-Quantum-Filtered NMR Spectra of Suspensions of Human Red Blood Cells, J. Magn. Reson. 131 (1998) 92–96, https://doi.org/10.1006/jmre.1997.1337.
[253] J.S. Tauskela, E.A. Shoubridge, Response of the 23Na-NMR double-quantum filtered signal to changes in Na+ ion concentration in model biological solutions and human erythrocytes, Biochim. Biophys. Acta BBA - Gen. Subj. 1158 (1993) 155–165, https://doi.org/10.1016/0304-4165(93)90009-W.
[254] J.S. Tauskela, J.M. Dizon, J. Whang, J. Katz, Evaluation of multiple-quantum-filtered 23Na NMR in monitoring intracellular Na content in the isolated perfused rat heart in the absence of a chemical-shift reagent, J. Magn. Reson. 127 (1997) 115–127, https://doi.org/10.1006/jmre.1997.1181.
[255] J.M. Dizon, J.S. Tauskela, D. Wise, D. Burkhoff, P.J. Cannon, J. Katz, Evaluation of triple-quantum-filtered ^{23}Na NMR in monitoring of intracellular na content in the perfused rat heart: Comparison of intra- and extracellular transverse relaxation and spectral amplitudes: Triple-Quantum-Filtered ^{23}Na NMR Spectral in Perfused Rat Heart, Magn. Reson. Med. 35 (1996) 336–345, https://doi.org/10.1002/mrm.1910350311.
[256] P.M. Winter, N. Bansal, Triple-Quantum-Filtered 23Na NMR Spectroscopy of Subcutaneously Implanted 9L Gliosarcoma in the Rat in the Presence of TmDOTP5−, J. Magn. Reson. 152 (2001) 70–78, https://doi.org/10.1006/jmre.2001.2390.
[257] A.M. Babsky, H. Zhang, S.K. Hekmatyar, G.D. Hutchins, N. Bansal, Monitoring chemotherapeutic response in RIF-1 tumors by single-quantum and triple-quantum-filtered 23Na MRI, 1H diffusion-weighted MRI and PET imaging, Magn. Reson. Imaging. 25 (2007) 1015–1023, https://doi.org/10.1016/j.mri.2006.11.004.
[258] A. Babsky, S.K. Hekmatyar, T. Gorski, D.S. Nelson, N. Bansal, Heat-induced changes in intracellular Na +, pH and bioenergetic status in superfused RIF-1 tumour cells determined by 23Na and 31P magnetic resonance spectroscopy, Int. J. Hyperthermia. 21 (2009) 141–158, https://doi.org/10.1080/02656730400023656.
[259] J.R. James, Y. Gao, V.C. Soon, S.M. Topper, A. Babsky, N. Bansal, Controlled radio-frequency hyperthermia using an MR scanner and simultaneous monitoring of temperature and therapy response by ^{1} H, ^{23} Na and ^{31} P magnetic resonance spectroscopy in subcutaneously implanted 9L-gliosarcoma, Int. J. Hyperthermia. 26 (2010) 79–90, https://doi.org/10.3109/02656730903373509.
[260] L. Fleysher, N. Oesingmann, R. Brown, D.K. Sodickson, G.C. Wiggins, M. Inglese, Noninvasive quantification of intracellular sodium in human brain using ultrahigh-field MRI: INTRACELLULAR SODIUM QUANTIFICATION AT 7 T, NMR Biomed. 26 (2013) 9–19, https://doi.org/10.1002/nbm.2813.

[261] C. Mirkes, G. Shajan, J. Bause, K. Buckenmaier, J. Hoffmann, K. Scheffler, Triple-quantum-filtered sodium imaging at 9.4 Tesla, Magn. Reson. Med. 75 (2016) 1278–1289, https://doi.org/10.1002/mrm.25688.
[262] G. Madelin, J.-S. Lee, R.R. Regatte, A. Jerschow, Sodium MRI: methods and applications, Prog. Nucl. Magn. Reson. Spectrosc. 79 (2014) 14–47, https://doi.org/10.1016/j.pnmrs.2014.02.001.
[263] E.G. Sadykhov, Y.A. Pirogov, N.V. Anisimov, M.V. Gulyaev, G.E. Pavlovskaya, T. Meersmann, V.N. Belyaev, D.V. Fomina, Magnetic Resonance Imaging on Sodium Nuclei: Potential Medical Applications of 23Na MRI, Appl. Magn. Reson. 49 (2018) 925–957, https://doi.org/10.1007/s00723-018-1045-7.
[264] K.R. Thulborn, Quantitative sodium MR imaging: A review of its evolving role in medicine, NeuroImage. 168 (2018) 250–268, https://doi.org/10.1016/j.neuroimage.2016.11.056.
[265] O. Zaric, V. Juras, P. Szomolanyi, M. Schreiner, M. Raudner, C. Giraudo, S. Trattnig, Frontiers of Sodium MRI Revisited: From Cartilage to Brain Imaging, J. Magn. Reson. Imaging. (2020), https://doi.org/10.1002/jmri.27326.
[266] V.D. Schepkin, A. Neubauer, A.M. Nagel, T.F. Budinger, Comparison of potassium and sodium binding in vivo and in agarose samples using TQTPPI pulse sequence, J. Magn. Reson. 277 (2017) 162–168, https://doi.org/10.1016/j.jmr.2017.03.003.
[267] A. Neubauer, C. Nies, V.D. Schepkin, R. Hu, M. Malzacher, J. Chacón-Caldera, D. Thiele, E. Gottwald, L.R. Schad, Tracking protein function with sodium multi quantum spectroscopy in a 3D-tissue culture based on microcavity arrays, Sci. Rep. 7 (2017) 3943, https://doi.org/10.1038/s41598-017-04226-2.
[268] D. Kleimaier, V. Schepkin, C. Nies, E. Gottwald, L.R. Schad, Intracellular Sodium Changes in Cancer Cells Using a Microcavity Array-Based Bioreactor System and Sodium Triple-Quantum MR Signal, Processes. 8 (2020) 1267–1320, https://doi.org/10.3390/pr8101267.
[269] F.W. Cope, R. Damadian, Cell potassium by 39K spin echo nuclear magnetic resonance, Nature. 228 (1970) 76–77, https://doi.org/10.1038/228076a0.
[270] H.T. Edzes, H.J.C. Berendsen, The Physical State of Diffusible Ions in Cells, Annu. Rev. Biophys. Bioeng. 4 (1975) 265–285, https://doi.org/10.1146/annurev.bb.04.060175.001405.
[271] M.M. Civan, G.G. McDonald, M. Pring, M. Shporer, Pulsed nuclear magnetic resonance study of 39K in frog striated muscle, Biophys. J. 16 (1976) 1385–1398, https://doi.org/10.1016/S0006-3495(76)85782-7.
[272] S.A. Rashid, W.R. Adam, D.J. Craik, B.P. Shehan, R.M. Wellard, Factors affecting 39K NMR detectability in rat tissue, Magn. Reson. Med. 17 (1991) 213–224, https://doi.org/10.1002/mrm.1910170124.
[273] R.M. Wellard, B.P. Shehan, W.R. Adam, D.J. Craik, NMR measurement of 39K detectability and relaxation constants in rat tissue, Magn. Reson. Med. 29 (1993) 68–76, https://doi.org/10.1002/mrm.1910290113.
[274] P.J. Brophy, M.K. Hayer, F.G. Riddell, Measurement of intracellular potassium ion concentrations by n.m.r, Biochem. J. 210 (1983) 961–963, https://doi.org/10.1042/bj2100961.
[275] P.G. Quirk, I.D. Campbell, 31P and 39K nuclear magnetic resonance spectroscopy studies of halobacterial bioenergetics, Biochim. Biophys. Acta BBA - Bioenerg. 1019 (1990) 81–90, https://doi.org/10.1016/0005-2728(90)90127-P.
[276] B. Richey, D.S. Cayley, M.C. Mossing, C. Kolka, C.F. Anderson, T.C. Farrar, M.T. Record, Variability of the intracellular ionic environment of Escherichia coli. Differences between in vitro and in vivo effects of ion concentrations on protein-DNA interactions and gene expression, J. Biol. Chem. 262 (1987) 7157–7164.
[277] D. Burstein, E.T. Fossel, Nuclear magnetic resonance studies of intracellular ions in perfused frog heart, Am. J. Physiol. 252 (1987) H1138–H1146, https://doi.org/10.1152/ajpheart.1987.252.6.H1138.
[278] S. Kuki, E. Suzuki, H. Watari, H. Takami, H. Matsuda, Y. Kawashima, Potassium-39 nuclear magnetic resonance observation of intracellular potassium without chemical shift reagents during metabolic inhibition in the isolated perfused rat heart, Circ. Res. 67 (1990) 401–405, https://doi.org/10.1161/01.RES.67.2.401.
[279] N.B. Radford, E.E. Babcock, A. Richman, L. Szczepaniak, C.R. Malloy, A.D. Sherry, 39K NMR measurement of intracellular potassium during ischemia in the perfused guinea pig heart, Magn. Reson. Med. 40 (1998) 544–550, https://doi.org/10.1002/mrm.1910400407.
[280] M. Murakami, E. Suzuki, S. Miyamoto, Y. Seo, H. Watari, Direct measurement of K movement by 39K NMR in perfused rat mandibular salivary gland stimulated with acetylcholine, Pflugers Arch. 414 (1989) 385–392, https://doi.org/10.1007/BF00585047.
[281] D.S. Fieno, R.J. Kim, W.G. Rehwald, R.M. Judd, Physiological basis for potassium (39K) magnetic resonance imaging of the heart, Circ. Res. 84 (1999) 913–920, https://doi.org/10.1161/01.res.84.8.913.
[282] R. Umathum, M.B. Rösler, A.M. Nagel, In Vivo 39K MR Imaging of Human Muscle and Brain, Radiology. 269 (2013) 569–576, https://doi.org/10.1148/radiol.13130757.
[283] A.M. Nagel, R. Umathum, M.B. Rösler, M.E. Ladd, I. Litvak, P.L. Gor'kov, W.W. Brey, V.D. Schepkin, 39K and 23Na relaxation times and MRI of rat head at 21.1 T, NMR Biomed. 29 (2016) 759–766. https://doi.org/10.1002/nbm.3528..
[284] I.A. Elabyad, R. Kalayciyan, N.C. Shanbhag, L.R. Schad, First in vivo potassium-39 (^{39}K) MRI at 9.4 T using conventional copper radio frequency surface coil cooled to 77 K, IEEE Trans. Biomed. Eng. 61 (2014) 334–345, https://doi.org/10.1109/TBME.2013.2294277.
[285] S. Ringer, An Investigation regarding the Action of Rubidium and Caesium Salts compared with the Action of Potassium Salts on the Ventricle of the Frog's Heart, J. Physiol. 4 (1884) 370–386, https://doi.org/10.1113/jphysiol.1884.sp000139.
[286] L.A. Beaugé, O. Ortíz, Rubidium, sodium and ouabain interactions on the influx of rubidium in rat red blood cells, J. Physiol. 210 (1970) 519–532, https://doi.org/10.1113/jphysiol.1970.sp009224.
[287] Z.H. Endre, J.L. Allis, P.J. Ratcliffe, G.K. Radda, 87-Rubidium NMR: A novel method of measuring cation flux in intact kidney, Kidney Int. 35 (1989) 1249–1256, https://doi.org/10.1038/ki.1989.117.
[288] J.L. Allis, Z.H. Endre, G.K. Radda, 31P, 87Rb and 23Na studies of the perfused rat kidney, Biochem. Soc. Trans. 17 (1989) 236, https://doi.org/10.1042/bst0170236.
[289] J.L. Allis, C.D. Snaith, A.M. Seymour, G.K. Radda, 87Rb NMR studies of the perfused rat heart, FEBS Lett. 242 (1989) 215–217, https://doi.org/10.1016/0014-5793(89)80472-7.
[290] M.P. Williamson, Measurement of cromakalim-induced 87Rb flux in intact cells by NMR, FEBS Lett. 254 (1989) 171–173, https://doi.org/10.1016/0014-5793(89)81032-4.
[291] J.L. Allis, R.M. Dixon, A.M. Till, G.K. Radda, 87Rb NMR studies for evaluation of K+ fluxes in human erythrocytes, J. Magn. Reson. 1969 (85) (1989) 524–529, https://doi.org/10.1016/0022-2364(89)90242-4.
[292] J.A. Helpern, K.M. Welch, H.R. Halvorson, Rubidium transport in human erythrocyte suspensions monitored by 87Rb NMR with aqueous chemical shift reagents, NMR Biomed. 2 (1989) 47–54, https://doi.org/10.1002/nbm.1940020202.
[293] M.C. Steward, Y. Seo, M. Murakami, H. Watari, NMR relaxation characteristics of rubidium-87 in perfused rat salivary glands, Proc. Biol. Sci. 243 (1991) 115–120, https://doi.org/10.1098/rspb.1991.0019.
[294] P.D. Syme, R.M. Dixon, J.L. Allis, J.K. Aronson, D.G. Grahame-Smith, G.K. Radda, A non-invasive method of measuring concentrations of rubidium in rat skeletal muscle in vivo by 87Rb nuclear magnetic resonance spectroscopy: implications for the measurement of cation transport activity in vivo, Clin. Sci. 78 (1990) 303–309, https://doi.org/10.1042/cs0780303.
[295] J.L. Allis, G.K. Radda, Selective detection of intracellular 87Rb+ by double-quantum filtration, J. Magn. Reson. 1969 (84) (1989) 372–375, https://doi.org/10.1016/0022-2364(89)90382-X.
[296] J.L. Allis, The Application of Cation NMR to Living Systems: 87Rb NMR, in: (Null), Elsevier, 1993: pp. 211–246. https://doi.org/10.1016/S0066-4103(08)60060-5..
[297] J.L. Allis, Z.H. Endre, G.K. Radda, Differentiation between intra- and extracellular components of renal 87Rb nuclear-magnetic-resonance spectra by lineshape analysis, Biochem. Soc. Trans. 16 (1988) 806–807, https://doi.org/10.1042/bst0160806.
[298] F.G. Riddell, T.E. Southon, Contrast reagents for the NMR spectra of the alkali metals, Inorganica Chim. Acta. 136 (1987) 133–137, https://doi.org/10.1016/S0020-1693(00)81144-5.
[299] V.V. Kupriyanov, M.L.H. Gruwel, Rubidium-87 magnetic resonance spectroscopy and imaging for analysis of mammalian K+ transport, NMR Biomed. 18 (2005) 111–124, https://doi.org/10.1002/nbm.892.
[300] V.E. Yushmanov, A. Kharlamov, F.E. Boada, S.C. Jones, Monitoring of brain potassium with rubidium flame photometry and MRI, Magn. Reson. Med. 57 (2007) 494–500, https://doi.org/10.1002/mrm.21155.
[301] V.E. Yushmanov, A. Kharlamov, T.S. Ibrahim, T. Zhao, F.E. Boada, S.C. Jones, K+ dynamics in ischemic rat brain in vivo by 87Rb MRI at 7 T, NMR Biomed. 24 (2011) 778–783, https://doi.org/10.1002/nbm.1652.
[302] A.M.P. Romani, Magnesium Homeostasis in Mammalian Cells, in: L. Banci (Ed.), Met. Cell, Springer Netherlands, Dordrecht, 2013: pp. 69–118. https://doi.org/10.1007/978-94-007-5561-1_4..
[303] A.M.P. Romani, Cellular magnesium homeostasis, Arch. Biochem. Biophys. 512 (2011) 1–23, https://doi.org/10.1016/j.abb.2011.05.010.
[304] S.K. Kolev, P. St, M.A. Petkov, D.V. Rangelov, T.I. Trifonov, G.N.V. Milenov, Interaction of Na +, K +, Mg 2+ and Ca 2+ counter cations with RNA, Metallomics. 10 (2018) 659–678, https://doi.org/10.1039/C8MT00043C.
[305] M. Gebala, S.L. Johnson, G.J. Narlikar, D. Herschlag, Ion counting demonstrates a high electrostatic field generated by the nucleosome, ELife. 8 (2019), https://doi.org/10.7554/eLife.44993 e44993.
[306] A.-A. Farcaș, A. Bende, The influence of monovalent and divalent metal cations on the stability of the DNA-protein interaction in the nucleosome core particle, in, Adv. Quantum Chem., Elsevier (2020) 269–290, https://doi.org/10.1016/bs.aiq.2020.05.001.
[307] R.E. London, Methods for measurement of intracellular magnesium: NMR and fluorescence, Annu. Rev. Physiol. 53 (1991) 241–258, https://doi.org/10.1146/annurev.ph.53.030191.001325.
[308] G.D. Williams, T.J. Mosher, M.B. Smith, Simultaneous Determination of Intracellular Magnesium and pH from the Three 31P NMR Chemical Shifts of ATP, Anal. Biochem. 214 (1993) 458–467, https://doi.org/10.1006/abio.1993.1523.
[309] M. Cohn, T.R. Hughes, Nuclear Magnetic Resonance Spectra of Adenosine Di- and Triphosphate, J. Biol. Chem. 237 (1962) 176–181, https://doi.org/10.1016/S0021-9258(18)81382-5.
[310] M. Julien, C. Bouguechtouli, A. Alik, R. Ghouil, S. Zinn-Justin, F.-X. Theillet, Multiple Site-Specific Phosphorylation of IDPs Monitored by NMR, in: B.B. Kragelund, K. Skriver (Eds.), Intrinsically Disord. Proteins Methods Protoc, Springer, US, New York, NY, 2020, pp. 793–817, https://doi.org/10.1007/978-1-0716-0524-0_41.

[311] D.I. Hoult, S.J. Busby, D.G. Gadian, G.K. Radda, R.E. Richards, P.J. Seeley, Observation of tissue metabolites using 31P nuclear magnetic resonance, Nature. 252 (1974) 285–287, https://doi.org/10.1038/252285a0.
[312] R.K. Gupta, J.L. Benovic, Z.B. Rose, The determination of the free magnesium level in the human red blood cell by 31P NMR, J. Biol. Chem. 253 (1978) 6172–6176.
[313] J.L. Bock, B. Wenz, R.K. Gupta, Changes in intracellular Mg adenosine triphosphate and ionized Mg2+ during blood storage: detection by 31P nuclear magnetic resonance spectroscopy, Blood. 65 (1985) 1526–1530, https://doi.org/10.1182/blood.V65.6.1526.bloodjournal6561526.
[314] A. Petersen, J.P. Jacobsen, M. Hørder, 31P NMR measurements of intracellular pH in erythrocytes: Direct comparison with measurements using freeze-thaw and investigation into the influence of ionic strength and Mg2+, Magn. Reson. Med. 4 (1987) 341–350, https://doi.org/10.1002/mrm.1910040405.
[315] D. Mota de Freitas, L. Amari, C. Srinivasan, Q. Rong, R. Ramasamy, A. Abraha, C.F.G.C. Geraldes, M.K. Boyd, Competition between Li+ and Mg2+ for the phosphate groups in the human erythrocyte membrane and ATP: An NMR and fluorescence study, Biochemistry. 33 (1994) 4101–4110, https://doi.org/10.1021/bi00180a002.
[316] R. Ouwerkerk, C.J.A. van Echteld, G.E.J. Staal, G. Rijksen, Intracellular free magnesium and phosphorylated metabolites in hexokinase- and pyruvate kinase-deficient red cells measured using 31P-NMR spectroscopy, Biochim. Biophys. Acta BBA - Mol. Cell Res. 1010 (1989) 294–303, https://doi.org/10.1016/0167-4889(89)90052-9.
[317] H. Fujise, P. Cruz, N.V. Reo, P.K. Lauf, Relationship between total magnesium concentration and free intracellular magnesium in sheep red blood cells, Biochim. Biophys. Acta BBA - Mol. Cell Res. 1094 (1991) 51–54, https://doi.org/10.1016/0167-4889(91)90025-S.
[318] T.J. Rink, R.Y. Tsien, T. Pozzan, Cytoplasmic pH and free Mg2+ in lymphocytes, J. Cell Biol. 95 (1982) 189–196, https://doi.org/10.1083/jcb.95.1.189.
[319] A. Cittadini, A. Scarpa, Intracellular Mg2+ homeostasis of Ehrlich ascites tumor cells, Arch. Biochem. Biophys. 227 (1983) 202–209, https://doi.org/10.1016/0003-9861(83)90363-6.
[320] S. de Jong, N. Mulder, E. de Vries, G. Robillard, NMR spectroscopy analysis of phosphorus metabolites and the effect of adriamycin on these metabolite levels in an adriamycin-sensitive and -resistant human small cell lung carcinoma cell line, Br. J. Cancer. 63 (1991) 205–212, https://doi.org/10.1038/bjc.1991.50.
[321] M. Merle, I. Pianet, P. Canioni, J. Labouesse, Comparative 31P and 1H NMR studies on rat astrocytes and C6 glioma cells in culture, Biochimie. 74 (1992) 919–930, https://doi.org/10.1016/0300-9084(92)90076-Q.
[322] R.K. Gupta, R.D. Moore, 31P NMR studies of intracellular free Mg2+ in intact frog skeletal muscle, J. Biol. Chem. 255 (1980) 3987–3993, https://doi.org/10.1016/S0021-9258(19)85622-3.
[323] H.J. Vogel, P. Lundberg, S. Fabiansson, H. Rudérus, E. Tornberg, Post-mortem energy metabolism in bovine muscles studied by non-invasive phosphorus-31 nuclear magnetic resonance, Meat Sci. 13 (1985) 1–18, https://doi.org/10.1016/S0309-1740(85)80001-2.
[324] M.J. Kushmerick, P.F. Dillon, R.A. Meyer, T.R. Brown, J.M. Krisanda, H.L. Sweeney, 31P NMR spectroscopy, chemical analysis, and free Mg2+ of rabbit bladder and uterine smooth muscle, J. Biol. Chem. 261 (1986) 14420–14429.
[325] F. Desmoulin, P.J. Cozzone, P. Canioni, Phosphorus-31 nuclear-magnetic-resonance study of phosphorylated metabolites compartmentation, intracellular pH and phosphorylation state during normoxia, hypoxia and ethanol perfusion, in the perfused rat liver, Eur. J. Biochem. 162 (1987) 151–159, https://doi.org/10.1111/j.1432-1033.1987.tb10555.x.
[326] C.T. Burt, H.-M. Cheng, S. Gabel, ATP, ADP, and Magnesium Mixed Solutions: In Vitro 31P NMR Characterization and In Vivo Application to Lens, J. Biochem. (Tokyo). 108 (1990) 441–448. https://doi.org/10.1093/oxfordjournals.jbchem.a123219..
[327] B. Altura, R. Barbour, T. Dowd, F. Wu, B. Altura, R. Gupta, Low extracellular magnesium induces intracellular free Mg deficits, ischemia, depletion of high-energy phosphates and cardiac failure in intact working rat hearts: A 31P-NMR study, Biochim. Biophys. Acta BBA - Mol. Basis Dis. 1182 (1993) 329–332, https://doi.org/10.1016/0925-4439(93)90077-E.
[328] P.M. Matthews, L. Shen, D. Foxall, T.E. Mansour, 31P-NMR studies of metabolite compartmentation in Fasciola hepatica, Biochim. Biophys. Acta BBA - Mol. Cell Res. 845 (1985) 178–188, https://doi.org/10.1016/0167-4889(85)90175-2.
[329] M. Satre, J.-B. Martin, 31P-Nuclear magnetic resonance analysis of the intracellular pH in the slime mold Dictyostelium discoideum, Biochem. Biophys. Res. Commun. 132 (1985) 140–146, https://doi.org/10.1016/0006-291X(85)90999-4.
[330] S.L. Shofer, J.A. Willis, R.S. Tjeerdema, Effects of hypoxia and toxicant exposure on phosphoarginine, intracellular pH, and free Mg2+ in abalone as measured by 31P-NMR, Comp. Biochem. Physiol. A Physiol. 118 (1997) 1183–1191, https://doi.org/10.1016/S0300-9629(97)00061-3.
[331] H.R. Halvorson, A.M. Vande Linde, J.A. Helpern, K.M. Welch, Assessment of magnesium concentrations by 31P NMR in vivo, NMR Biomed. 5 (1992) 53–58, https://doi.org/10.1002/nbm.1940050202.
[332] M. Nelander, J. Weis, L. Bergman, A. Larsson, A.-K. Wikström, J. Wikström, Cerebral Magnesium Levels in Preeclampsia; A Phosphorus Magnetic Resonance Spectroscopy Study, Am. J. Hypertens. 30 (2017) 667–672, https://doi.org/10.1093/ajh/hpx022.
[333] B.M. Altura, A. Gebrewold, A. Zhang, B.T. Altura, R.K. Gupta, Short-term reduction in dietary intake of magnesium causes deficits in brain intracellular free Mg2+ and [H+]i but not high-energy phosphates as observed by in vivo 31P-NMR, Biochim. Biophys. Acta BBA - Mol. Cell Res. 1358 (1997) 1–5, https://doi.org/10.1016/S0167-4889(97)00077-3.
[334] B.M. Altura, R.K. Gupta, Cocaine induces intracellular free Mg deficits, ischemia and stroke as observed by in-vivo 31P-NMR of the brain, Biochim. Biophys. Acta BBA - Biomembr. 1111 (1992) 271–274, https://doi.org/10.1016/0005-2736(92)90320-L.
[335] D. Cameron, A.A. Welch, F. Adelnia, C.M. Bergeron, D.A. Reiter, L.J. Dominguez, N.A. Brennan, K.W. Fishbein, R.G. Spencer, L. Ferrucci, Age and Muscle Function Are More Closely Associated With Intracellular Magnesium, as Assessed by 31P Magnetic Resonance Spectroscopy, Than With Serum Magnesium, Front. Physiol. 10 (2019) 1454, https://doi.org/10.3389/fphys.2019.01454.
[336] C.S. Springer, Measurement of metal cation compartmentalization in tissue by high-resolution metal cation NMR, Annu. Rev. Biophys. Biophys. Chem. 16 (1987) 375–399, https://doi.org/10.1146/annurev.bb.16.060187.002111.
[337] L. Garfinkel, D. Garfinkel, Calculation of free-magnesium concentration in adenosine 5'-triphosphate containing solutions in vitro and in vivo, Biochemistry. 23 (1984) 3547–3552, https://doi.org/10.1021/bi00310a025.
[338] J.A. Helpern, H.R. Halvorson, [16] Measurement of cytosolic magnesium by 31P NMR spectroscopy, in, Methods Neurosci., Elsevier (1995) 319–327, https://doi.org/10.1016/S1043-9471(06)80019-4.
[339] S. Widmaier, T. Hoess, J. Breuer, W.-I. Jung, G.J. Dietze, O. Lutz, Magnesium-Based Temperature Dependence of the ATP Chemical-Shift Separation δαβand Its Relation to Intracellular Free Magnesium, J. Magn. Reson. B. 113 (1996) 16–24, https://doi.org/10.1006/jmrb.1996.0150.
[340] S. Widmaier, W.-I. Jung, M. Bunse, F. van Erckelens, G. Dietze, O. Lutz, Change in Chemical Shift and Splitting of 31P γ-ATP Signal in Human Skeletal Muscle During Exercise and Recovery, NMR Biomed. 9 (1996) 1–7, https://doi.org/10.1002/(SICI)1099-1492(199602)9:1<1::AID-NBM384>3.0.CO;2-8.
[341] S. Nakayama, H. Nomura, L.M. Smith, J.F. Clark, Simultaneous Estimation of Intracellular Free Mg2+ and pH by Use of a New pH-Dependent Dissociation Constant of MgATP, Jpn. J. Physiol. 52 (2002) 323–326, https://doi.org/10.2170/jjphysiol.52.323.
[342] P.J. Mulquiney, P.W. Kuchel, Model of the pH-Dependence of the Concentrations of Complexes Involving Metabolites, Haemoglobin and Magnesium Ions in the Human Erythrocyte, Eur. J. Biochem. 245 (1997) 71–83, https://doi.org/10.1111/j.1432-1033.1997.00071.x.
[343] J.E. Raftos, V.L. Lew, P.W. Flatman, Refinement and evaluation of a model of Mg2+ buffering in human red cells, Eur. J. Biochem. 263 (1999) 635–645, https://doi.org/10.1046/j.1432-1327.1999.00506.x.
[344] J.P. Willcocks, P.J. Mulquiney, J.C. Ellory, R.L. Veech, G.K. Radda, K. Clarke, Simultaneous Determination of Low Free Mg2+ and pH in Human Sickle Cells using 31P NMR Spectroscopy, J. Biol. Chem. 277 (2002) 49911–49920, https://doi.org/10.1074/jbc.M207551200.
[345] K. Clarke, Y. Kashiwaya, M.T. King, D. Gates, C.A. Keon, H.R. Cross, G.K. Radda, R.L. Veech, The β/α Peak Height Ratio of ATP, J. Biol. Chem. 271 (1996) 21142–21150, https://doi.org/10.1074/jbc.271.35.21142.
[346] N.W. Lutz, M. Bernard, Multiparametric quantification of heterogeneity of metal ion concentrations, as demonstrated for [Mg2+] by way of 31P MRS, J. Magn. Reson. 294 (2018) 71–82, https://doi.org/10.1016/j.jmr.2018.06.016.
[347] S. Widmaier, W.-I. Jung, G.J. Dietze, O. Lutz, Potential pitfall in the determination of free [Mg2+] by 31P NMR when using the β/α-ATP peak height ratio method, Magn. Reson. Mater. Phys. Biol. Med. 9 (1999) 1–4.
[348] M.D. Yago, Intracellular magnesium: transport and regulation in epithelial secretory cells, Front. Biosci. 5 (2000) d602–d618, https://doi.org/10.2741/Yago.
[349] M. Liu, X. Yu, M. Li, N. Liao, A. Bi, Y. Jiang, S. Liu, Z. Gong, W. Zeng, Fluorescent probes for the detection of magnesium ions (Mg^{2+}): from design to application, RSC Adv. 8 (2018) 12573–12587, https://doi.org/10.1039/C8RA00946E.
[350] T.S. Lazarou, D. Buccella, Advances in imaging of understudied ions in signaling: A focus on magnesium, Curr. Opin. Chem. Biol. 57 (2020) 27–33, https://doi.org/10.1016/j.cbpa.2020.04.002.
[351] J.L. Bock, G.B. Crull, A. Wishnia, C.S. Springer, 25Mg NMR studies of magnesium binding to erythrocyte constituents, J. Inorg. Biochem. 44 (1991) 79–87, https://doi.org/10.1016/0162-0134(91)84020-a.
[352] W. Xian, J.X. Tang, P.A. Janmey, W.H. Braunlin, The polyelectrolyte behavior of actin filaments: a 25Mg NMR study, Biochemistry. 38 (1999) 7219–7226, https://doi.org/10.1021/bi982301f.
[353] T. Shimizu, M. Hatano, Magnetic resonance studies of trifluoperazine-calmodulin solutions: calcium-43, magnesium-25, zinc-67, and potassium-39 nuclear magnetic resonance, Inorg. Chem. 24 (1985) 2003–2009, https://doi.org/10.1021/ic00207a011.
[354] Y. Ogoma, H. Kobayashi, T. Fujii, Y. Kondo, A. Hachimori, T. Shimizu, M. Hatano, Binding study of metal ions to S100 protein: 43Ca, 25Mg, 67Zn and 39K n.m.r., Int. J. Biol. Macromol. 14 (1992) 279–286. https://doi.org/10.1016/S0141-8130(05)80041-8..
[355] R.S. Ehrlich, R.F. Colman, Cadmium-113 and magnesium-25 NMR study of the divalent metal binding sites of isocitrate dehydrogenases from pig heart, Biochim. Biophys. Acta BBA - Protein Struct. Mol. Enzymol. 1246 (1995) 135–141, https://doi.org/10.1016/0167-4838(94)00192-J.
[356] C. Giorgi, A. Danese, S. Missiroli, S. Patergnani, P. Pinton, Calcium Dynamics as a Machine for Decoding Signals, Trends Cell Biol. 28 (2018) 258–273, https://doi.org/10.1016/j.tcb.2018.01.002.
[357] K.H. Edel, E. Marchadier, C. Brownlee, J. Kudla, A.M. Hetherington, The Evolution of Calcium-Based Signalling in Plants, Curr. Biol. 27 (2017) R667–R679, https://doi.org/10.1016/j.cub.2017.05.020.

[358] H. Bischof, S. Burgstaller, M. Waldeck-Weiermair, T. Rauter, M. Schinagl, J. Ramadani-Muja, W.F. Graier, R. Malli, Live-Cell Imaging of Physiologically Relevant Metal Ions Using Genetically Encoded FRET-Based Probes, Cells. 8 (2019) 492–525, https://doi.org/10.3390/cells8050492.
[359] T. Andersson, T. Drakenberg, S. Forsen, E. Thulin, M. Swaerd, Direct observation of the calcium-43 NMR signals from calcium(2+) bound to proteins, J. Am. Chem. Soc. 104 (1982) 576–580, https://doi.org/10.1021/ja00366a035.
[360] D.L. Bryce, Calcium binding environments probed by 43Ca NMR spectroscopy, Dalton Trans. 39 (2010) 8593–8611, https://doi.org/10.1039/c0dt00416b.
[361] E. Murphy, L.R. Berkowitz, E. Orringer, L. Levy, S.A. Gabel, R.E. London, Cytosolic free calcium levels in sickle red blood cells, Blood. 69 (1987) 1469–1474, https://doi.org/10.1182/blood.V69.5.1469.1469.
[362] N.R. Aiken, J.D. Satterlee, W.R. Galey, Measurement of intracellular Ca2+ in young and old human erythrocytes using 19F-NMR spectroscopy, Biochim. Biophys. Acta BBA - Mol. Cell Res. 1136 (1992) 155–160, https://doi.org/10.1016/0167-4889(92)90251-6.
[363] N.R. Aiken, W.R. Galey, J.D. Satterlee, A peroxidative model of human erythrocyte intracellular Ca2+ changes with in vivo cell aging: measurement by 19F-NMR spectroscopy, Biochim. Biophys. Acta. 1270 (1995) 52–57, https://doi.org/10.1016/0925-4439(94)00071-w.
[364] T.L. Dowd, R.K. Gupta, 19F-NMR study of the effect of lead on intracellular free calcium in human platelets, Biochim. Biophys. Acta. 1092 (1991) 341–346, https://doi.org/10.1016/s0167-4889(97)90010-0.
[365] M.F. Denny, W.D. Atchison, Methylmercury-induced elevations in intrasynaptosomal zinc concentrations: an 19F-NMR study, J. Neurochem. 63 (1994) 383–386, https://doi.org/10.1046/j.1471-4159.1994.63010383.x.
[366] F. Adebodun, J.F.M. Post, 19F NMR studies of changes in membrane potential and intracellular volume during dexamethasone-induced apoptosis in human leukemic cell lines, J. Cell. Physiol. 154 (1993) 199–206, https://doi.org/10.1002/jcp.1041540123.
[367] F.A. Schanne, T.L. Dowd, R.K. Gupta, J.F. Rosen, Lead increases free Ca2+ concentration in cultured osteoblastic bone cells: simultaneous detection of intracellular free Pb2+ by 19F NMR, Proc. Natl. Acad. Sci. 86 (1989) 5133–5135, https://doi.org/10.1073/pnas.86.13.5133.
[368] F.A. Schanne, T.L. Dowd, R.K. Gupta, J.F. Rosen, Effect of lead on parathyroid hormone-induced responses in rat osteoblastic osteosarcoma cells (ROS 17/2.8) using 19F-NMR, Biochim. Biophys. Acta. 1054 (1990) 250–255, https://doi.org/10.1016/0167-4889(90)90249-d.
[369] R.K. Gupta, B.A. Wittenberg, 19F nuclear magnetic resonance studies of free calcium in heart cells, Biophys. J. 65 (1993) 2547–2558, https://doi.org/10.1016/S0006-3495(93)81320-1.
[370] T.L. Dowd, R.K. Gupta, Multinuclear NMR studies of intracellular cations in the prehypertensive rat kidney, Biochim. Biophys. Acta. 1226 (1994) 83–88, https://doi.org/10.1016/0925-4439(94)90062-0.
[371] E. Marban, M. Kitakaze, H. Kusuoka, J.K. Porterfield, D.T. Yue, V.P. Chacko, Intracellular free calcium concentration measured with 19F NMR spectroscopy in intact ferret hearts, Proc. Natl. Acad. Sci. 84 (1987) 6005–6009, https://doi.org/10.1073/pnas.84.16.6005.
[372] E. Marban, M. Kitakaze, V.P. Chacko, M.M. Pike, Ca2+ transients in perfused hearts revealed by gated 19F NMR spectroscopy, Circ. Res. 63 (1988) 673–678, https://doi.org/10.1161/01.res.63.3.673.
[373] D.P. Harding, G.A. Smith, J.C. Metcalfe, P.G. Morris, H.L. Kirschenlohr, Resting and end-diastolic [Ca2+]i measurements in the langendorff-perfused ferret heart loaded with a 19F NMR indicator, Magn. Reson. Med. 29 (1993) 605–615, https://doi.org/10.1002/mrm.1910290505.
[374] H.S. Bachelard, R.S. Badar-Goffer, K.J. Brooks, S.J. Dolin, P.G. Morris, Measurement of free intracellular calcium in the brain by 19F-nuclear magnetic resonance spectroscopy, J. Neurochem. 51 (1988) 1311–1313, https://doi.org/10.1111/j.1471-4159.1988.tb03102.x.
[375] M.T. Espanol, L. Litt, Y. Xu, L.H. Chang, T.L. James, P.R. Weinstein, P.H. Chan, 19F NMR calcium changes, edema and histology in neonatal rat brain slices during glutamate toxicity, Brain Res. 647 (1994) 172–176, https://doi.org/10.1016/0006-8993(94)91414-1.
[376] H. Bachelard, R. Badar-Goffer, P. Morris, N. Thatcher, Magnetic resonance spectroscopy studies on Ca2+, Zn2+ and energy metabolism in superfused brain slices, Biochem. Soc. Trans. 22 (1994) 988–991, https://doi.org/10.1042/bst0220988.
[377] H.L. Kirschenlohr, J.C. Metcalfe, P.G. Morris, G.C. Rodrigo, G.A. Smith, Ca2+ transient, Mg2+, and pH measurements in the cardiac cycle by 19F NMR, Proc. Natl. Acad. Sci. 85 (1988) 9017–9021, https://doi.org/10.1073/pnas.85.23.9017.
[378] J.C. Metcalfe, T.R. Hesketh, G.A. Smith, Free cytosolic Ca2+ measurements with fluorine labelled indicators using 19FNMR, Cell Calcium. 6 (1985) 183–195, https://doi.org/10.1016/0143-4160(85)90043-0.
[379] J. Benters, U. Flögel, T. Schäfer, D. Leibfritz, S. Hechtenberg, D. Beyersmann, Study of the interactions of cadmium and zinc ions with cellular calcium homoeostasis using 19F-NMR spectroscopy., Biochem. J. 322 (Pt 3) (1997) 793–799. https://doi.org/10.1042/bj3220793..
[380] P.W. Kuchel, K. Romanenko, D. Shishmarev, P. Galvosas, C.D. Cox, Enhanced Ca2+ influx in mechanically distorted erythrocytes measured with 19F nuclear magnetic resonance spectroscopy, Sci. Rep. 11 (2021) 3749, https://doi.org/10.1038/s41598-021-83044-z.
[381] H.L. Kirschenlohr, A.A. Grace, S.D. Clarke, Y. Shachar-Hill, J.C. Metcalfe, P.G. Morris, G.A. Smith, Calcium measurements with a new high-affinity n.m.r. indicator in the isolated perfused heart., Biochem. J. 293 (Pt 2) (1993) 407–411. https://doi.org/10.1042/bj2930407..
[382] H.L. Kirschenlohr, A.A. Grace, J.I. Vandenberg, J.C. Metcalfe, G.A. Smith, Estimation of systolic and diastolic free intracellular Ca2+ by titration of Ca2+ buffering in the ferret heart, Biochem. J. 346 (Pt 2) (2000) 385–391.
[383] S.K. Song, R.S. Hotchkiss, J. Neil, P.E. Morris, C.Y. Hsu, J.J. Ackerman, Determination of intracellular calcium in vivo via fluorine-19 nuclear magnetic resonance spectroscopy, Am. J. Physiol. 269 (1995) C318–C322, https://doi.org/10.1152/ajpcell.1995.269.2.C318.
[384] A. Jasanoff, Bloodless fMRI, Trends Neurosci. 30 (2007) 603–610, https://doi.org/10.1016/j.tins.2007.08.002.
[385] E. Mari, P. Berthault, 129Xe NMR-based sensors: biological applications and recent methods, Analyst. 142 (2017) 3298–3308, https://doi.org/10.1039/c7an01088e.
[386] W.H. Li, S.E. fraser, T.J. Meade, A Calcium-Sensitive Magnetic Resonance Imaging Contrast Agent, J. Am. Chem. Soc. 121 (1999) 1413–1414. https://doi.org/10.1021/ja983702l..
[387] G. Angelovski, S. Gottschalk, M. Milošević, J. Engelmann, G.E. Hagberg, P. Kadjane, P. Andjus, N.K. Logothetis, Investigation of a calcium-responsive contrast agent in cellular model systems: feasibility for use as a smart molecular probe in functional MRI, ACS Chem. Neurosci. 5 (2014) 360–369, https://doi.org/10.1021/cn500049n.
[388] S. Okada, B.B. Bartelle, N. Li, V. Breton-Provencher, J.J. Lee, E. Rodriguez, J. Melican, M. Sur, A. Jasanoff, Calcium-dependent molecular fMRI using a magnetic nanosensor, Nat. Nanotechnol. (2018) 1–9, https://doi.org/10.1038/s41565-018-0092-4.
[389] T. Savić, G. Gambino, V.S. Bokharaie, H.R. Noori, N.K. Logothetis, G. Angelovski, Early detection and monitoring of cerebral ischemia using calcium-responsive MRI probes, Proc. Natl. Acad. Sci. U. S. A. 116 (2019) 20666–20671, https://doi.org/10.1073/pnas.1908503116.
[390] S. Sahana, P.K. Bharadwaj, Detection of alkali and alkaline earth metal ions by fluorescence spectroscopy, Inorganica Chim. Acta. 417 (2014) 109–141, https://doi.org/10.1016/j.ica.2014.03.004.
[391] L. Banci, I. Bertini, S. Ciofi-Baffoni, T. Kozyreva, K. Zovo, P. Palumaa, Affinity gradients drive copper to cellular destinations, Nature. 465 (2010) 645–648, https://doi.org/10.1038/nature09018.
[392] J.H. Kaplan, E.B. Maryon, How Mammalian Cells Acquire Copper: An Essential but Potentially Toxic Metal, Biophys. J. 110 (2016) 7–13, https://doi.org/10.1016/j.bpj.2015.11.025.
[393] M.T. Morgan, L.A.H. Nguyen, H.L. Hancock, C.J. Fahrni, Glutathione limits aquacopper(I) to sub-femtomolar concentrations through cooperative assembly of a tetranuclear cluster, J. Biol. Chem. 292 (2017) 21558–21567, https://doi.org/10.1074/jbc.M117.817452.
[394] C. Dennison, S. David, J. Lee, Bacterial copper storage proteins, J. Biol. Chem. 293 (2018) 4616–4627, https://doi.org/10.1074/jbc.TM117.000180.
[395] J.F. Collins, Copper nutrition and biochemistry and human (patho)physiology, in: Adv. Food Nutr. Res., Elsevier, 2021: p. S104345262100005X. https://doi.org/10.1016/bs.afnr.2021.01.005..
[396] F.-X. Theillet, A. Binolfi, S. Liokatis, S. Verzini, P. Selenko, Paramagnetic relaxation enhancement to improve sensitivity of fast NMR methods: application to intrinsically disordered proteins, J. Biomol. NMR. 51 (2011) 487–495, https://doi.org/10.1007/s10858-011-9577-2.
[397] N.A. Oktaviani, M.W. Risør, Y.-H. Lee, R.P. Megens, D.H. de Jong, R. Otten, R.M. Scheek, J.J. Enghild, N.C. Nielsen, T. Ikegami, F.A.A. Mulder, Optimized co-solute paramagnetic relaxation enhancement for the rapid NMR analysis of a highly fibrillogenic peptide, J. Biomol. NMR. 62 (2015) 129–142, https://doi.org/10.1007/s10858-015-9925-8.
[398] L.M.L. Hawk, C.T. Gee, A.K. Urick, H. Hu, W.C.K. Pomerantz, Paramagnetic relaxation enhancement for protein-observed ^{19}F NMR as an enabling approach for efficient fragment screening, RSC Adv. 6 (2016) 95715–95721, https://doi.org/10.1039/C6RA21226C.
[399] V. Kocman, G.M. Di Mauro, G. Veglia, A. Ramamoorthy, Use of paramagnetic systems to speed-up NMR data acquisition and for structural and dynamic studies, Solid State Nucl. Magn. Reson. 102 (2019) 36–46, https://doi.org/10.1016/j.ssnmr.2019.07.002.
[400] F.A.A. Mulder, L. Tenori, C. Luchinat, Fast and Quantitative NMR Metabolite Analysis Afforded by a Paramagnetic Co-Solute, Angew. Chem. Int. Ed. 58 (2019) 15283–15286, https://doi.org/10.1002/anie.201908006.
[401] M. Kolen, W.A. Smith, F.M. Mulder, Accelerating ^{1}H NMR Detection of Aqueous Ammonia, ACS Omega. 6 (2021) 5698–5704, https://doi.org/10.1021/acsomega.0c06130.
[402] T. Kambe, T. Tsuji, A. Hashimoto, N. Itsumura, The Physiological, Biochemical, and Molecular Roles of Zinc Transporters in Zinc Homeostasis and Metabolism, Physiol. Rev. 95 (2015) 749–784, https://doi.org/10.1152/physrev.00035.2014.
[403] W. Maret, Zinc in Cellular Regulation: The Nature and Significance of "Zinc Signals", Int. J. Mol. Sci. 18 (2017) 2285, https://doi.org/10.3390/ijms18112285.
[404] R. Badar-Goffer, P. Morris, N. Thatcher, H. Bachelard, Excitotoxic amino acids cause appearance of magnetic resonance spectroscopy-observable zinc in superfused cortical slices, J. Neurochem. 62 (1994) 2488–2491, https://doi.org/10.1046/j.1471-4159.1994.62062488.x.
[405] A. Bar-Shir, N.N. Yadav, A.A. Gilad, P.C.M. van Zijl, M.T. McMahon, J.W.M. Bulte, Single (19)F probe for simultaneous detection of multiple metal ions using miCEST MRI, J. Am. Chem. Soc. 137 (2015) 78–81, https://doi.org/10.1021/ja511313k.

[406] V.C. Pierre, S.M. Harris, S.L. Pailloux, Comparing Strategies in the Design of Responsive Contrast Agents for Magnetic Resonance Imaging: A Case Study with Copper and Zinc, Acc. Chem. Res. 51 (2018) 342–351, https://doi.org/10.1021/acs.accounts.7b00301.
[407] Y. Yuan, Z. Wei, C. Chu, J. Zhang, X. Song, P. Walczak, J.W.M. Bulte, Development of Zinc-Specific iCEST MRI as an Imaging Biomarker for Prostate Cancer, Angew. Chem. Int. Ed Engl. 58 (2019) 15512–15517, https://doi.org/10.1002/anie.201909429.
[408] J.F. Ma, S. Hiradate, K. Nomoto, T. Iwashita, H. Matsumoto, Internal Detoxification Mechanism of Al in Hydrangea (Identification of Al Form in the Leaves), Plant Physiol. 113 (1997) 1033–1037, https://doi.org/10.1104/pp.113.4.1033.
[409] T. Watanabe, M. Osaki, T. Yoshihara, T. Tadano, Distribution and chemical speciation of aluminum in the Al accumulator plant, Melastoma malabathricum L, Plant Soil. 201 (1998) 165–173, https://doi.org/10.1023/A:1004341415878.
[410] J. Feng Ma, S. Hiradate, H. Matsumoto, High aluminum resistance in buckwheat. Ii. Oxalic acid detoxifies aluminum internally, Plant Physiol. 117 (1998) 753–759, https://doi.org/10.1104/pp.117.3.753.
[411] R. Shen, T. Iwashita, J.F. Ma, Form of Al changes with Al concentration in leaves of buckwheat, J. Exp. Bot. 55 (2004) 131–136, https://doi.org/10.1093/jxb/erh016.
[412] A. Morita, H. Horie, Y. Fujii, S. Takatsu, N. Watanabe, A. Yagi, H. Yokota, Chemical forms of aluminum in xylem sap of tea plants (Camellia sinensis L.), Phytochemistry. 65 (2004) 2775–2780, https://doi.org/10.1016/j.phytochem.2004.08.043.
[413] T. Watanabe, M. Osaki, H. Yano, I.M. Rao, Internal Mechanisms of Plant Adaptation to Aluminum Toxicity and Phosphorus Starvation in Three Tropical Forages, J. Plant Nutr. 29 (2006) 1243–1255, https://doi.org/10.1080/01904160600767484.
[414] A. Morita, O. Yanagisawa, S. Takatsu, S. Maeda, S. Hiradate, Mechanism for the detoxification of aluminum in roots of tea plant (Camellia sinensis (L.) Kuntze), Phytochemistry. 69 (2008) 147–153, https://doi.org/10.1016/j.phytochem.2007.06.007.
[415] T. Ikka, T. Ogawa, D. Li, S. Hiradate, A. Morita, Effect of aluminum on metabolism of organic acids and chemical forms of aluminum in root tips of Eucalyptus camaldulensis Dehnh, Phytochemistry. 94 (2013) 142–147, https://doi.org/10.1016/j.phytochem.2013.06.016.
[416] H. Wang, R.F. Chen, T. Iwashita, R.F. Shen, J.F. Ma, Physiological characterization of aluminum tolerance and accumulation in tartary and wild buckwheat, New Phytol. 205 (2014) 273–279, https://doi.org/10.1111/nph.13011.
[417] G. Xu, Y. Wu, D. Liu, Y. Wang, Y. Zhang, P. Liu, Effects of organic acids on uptake of nutritional elements and Al forms in Brassica napus L. under Al stress as analyzed by 27Al-NMR, Braz. J. Bot. (2015) 1–8, https://doi.org/10.1007/s40415-015-0198-y.
[418] D. Ueno, J.F. Ma, T. Iwashita, F.-J. Zhao, S.P. McGrath, Identification of the form of Cd in the leaves of a superior Cd-accumulating ecotype of Thlaspi caerulescens using 113Cd-NMR, Planta. 221 (2005) 928–936, https://doi.org/10.1007/s00425-005-1491-y.
[419] R. Arkowitz, M. Hoehn-Berlage, K. Gersonde, The effect of cadmium ions on 2,3-bisphosphoglycerate in erythrocytes studied with 31P NMR, FEBS Lett. 217 (1987) 21–24, https://doi.org/10.1016/0014-5793(87)81234-6.
[420] J. Goodman, J.J. Neil, J.J.H. Ackerman, Biomedical applications of 133Cs NMR, NMR Biomed. 18 (2005) 125–134, https://doi.org/10.1002/nbm.909.
[421] A. Burger, I. Lichtscheidl, Stable and radioactive cesium: A review about distribution in the environment, uptake and translocation in plants, plant reactions and plants' potential for bioremediation, Sci. Total Environ. 618 (2018) 1459–1485, https://doi.org/10.1016/j.scitotenv.2017.09.298.
[422] J.D. Halliday, R.E. Richards, R.R. Sharp, Chemical shifts in nuclear resonances of caesium ions in solutions, Proc. R. Soc. Lond. Math. Phys. Sci. 313 (1969) 45–69, https://doi.org/10.1098/rspa.1969.0179.
[423] H.T. Edzes, M. Ginzburg, B.Z. Ginzburg, H.J. Berendsen, The physical state of alkali ions in a Halobacterium: some NMR results, Experientia. 33 (1977) 732–734, https://doi.org/10.1007/BF01944156.
[424] A. Sakhnini, H. Gilboa, Nuclear magnetic resonance studies of cesium-133 in the halophilic halotolerant bacterium Ba1.Chemical shift and transport studies, NMR Biomed. 11 (1998) 80–86, https://doi.org/10.1002/(SICI)1099-1492(199804)11:2<80::AID-NBM505>3.0.CO;2-I.
[425] D.G. Davis, E. Murphy, R.E. London, Uptake of cesium ions by human erythrocytes and perfused rat heart: a cesium-133 NMR study, Biochemistry. 27 (1988) 3547–3551, https://doi.org/10.1021/bi00410a003.
[426] J. Bramham, F.G. Riddell, Cesium uptake studies on human erythrocytes, J. Inorg. Biochem. 53 (1994) 169–176, https://doi.org/10.1016/0162-0134(94)80002-2.
[427] P.A. Schornack, S.K. Song, C.S. Ling, R. Hotchkiss, J.J. Ackerman, Quantification of ion transport in perfused rat heart: 133Cs+ as an NMR active K+ analog, Am. J. Physiol.-Cell Physiol. 272 (1997) C1618–C1634, https://doi.org/10.1152/ajpcell.1997.272.5.C1618.
[428] P.A. Schornack, S.K. Song, R. Hotchkiss, J.J. Ackerman, Inhibition of ion transport in septic rat heart: 133Cs+ as an NMR active K+ analog, Am. J. Physiol.-Cell Physiol. 272 (1997) C1635–C1641, https://doi.org/10.1152/ajpcell.1997.272.5.C1635.
[429] M.L.H. Gruwel, O. Čulić, A. Muhs, J.P. Williams, J. Schrader, Regulation of Endothelial Na+-K+-ATPase Activity by cAMP, Biochem. Biophys. Res. Commun. 242 (1998) 93–97, https://doi.org/10.1006/bbrc.1997.7908.
[430] M.L. Gruwel, J.P. Williams, Short-term regulation of endothelial Na(+)-K(+)-pump activity by cGMP: a 133Cs magnetic resonance study, Mol. Membr. Biol. 15 (1998) 189–192, https://doi.org/10.3109/09687689709044320.
[431] L. Wittenkeller, D. Mota de Freitas, C.F.G.C. Geraldes, A.J.R. Tome, Physical basis for the resolution of intra- and extracellular cesium-133 NMR resonances in cesium(+) loaded human erythrocyte suspensions in the presence and absence of shift reagents, Inorg. Chem. 31 (1992) 1135–1144, https://doi.org/10.1021/ic00033a005.
[432] R.M. Wellard, B.P. Shehan, D.J. Craik, W.R. Adam, Factors affecting 133Cs chemical shifts in erythrocytes from cesium-fed rats, J. Magn. Reson. B. 104 (1994) 276–279, https://doi.org/10.1006/jmrb.1994.1085.
[433] W. Lin, D. Mota de Freitas, Q. Zhang, K.W. Olsen, Nuclear magnetic resonance and oxygen affinity study of cesium binding in human erythrocytes, Arch. Biochem. Biophys. 369 (1999) 78–88, https://doi.org/10.1006/abbi.1999.1285.
[434] B.P. Shehan, R.M. Wellard, W.R. Adam, D.J. Craik, The use of dietary loading of 133Cs as a potassium substitute in NMR studies of tissues, Magn. Reson. Med. 30 (1993) 573–582, https://doi.org/10.1002/mrm.1910300508.
[435] Y. Li, J. Neil, J.H.J. Ackerman, On the use of 133Cs as an NMR active probe of intracellular space in vivo, NMR Biomed. 8 (1995) 183–189, https://doi.org/10.1002/nbm.1940080502.
[436] B.P. Shehan, R.M. Wellard, D.J. Craik, W.R. Adam, 133Cs relaxation times in rat tissues, J. Magn. Reson. B. 107 (1995) 179–185, https://doi.org/10.1006/jmrb.1995.1075.
[437] P.E. Pfeffer, D.B. Rolin, D. Brauer, S.I. Tu, T.F. Kumosinski, In vivo 133Cs-NMR a probe for studying subcellular compartmentation and ion uptake in maize root tissue, Biochim. Biophys. Acta. 1054 (1990) 169–175, https://doi.org/10.1016/0167-4889(90)90238-9.
[438] R.M. Wellard, W.R. Adam, Functional hepatocyte cation compartmentation demonstrated with133Cs NMR, Magn. Reson. Med. 48 (2002) 810–818, https://doi.org/10.1002/mrm.10287.
[439] S.A. Radcliffe, A.J. Miller, R.G. Ratcliffe, Microelectrode and 133Cs nuclear magnetic resonance evidence for variable cytosolic and cytoplasmic nitrate pools in maize root tips, Plant Cell Environ. 28 (2005) 1379–1387, https://doi.org/10.1111/j.1365-3040.2005.01370.x.
[440] P. Le Lay, M.P. Isaure, J.E. Sarry, L. Kuhn, B. Fayard, J.L. Le Bail, O. Bastien, J. Garin, C. Roby, J. Bourguignon, Metabolomic, proteomic and biophysical analyses of Arabidopsis thaliana cells exposed to a caesium stress. Influence of potassium supply, Biochimie. 88 (2006) 1533–1547, https://doi.org/10.1016/j.biochi.2006.03.013.
[441] M. Karlsson, J.H. Ardenkjær-Larsen, M.H. Lerche, Hyperpolarized 133Cs is a sensitive probe for real-time monitoring of biophysical environments, Chem. Commun. 53 (2017) 6625–6628, https://doi.org/10.1039/C7CC02943H.
[442] P.W. Kuchel, M. Karlsson, M.H. Lerche, D. Shishmarev, J.H. Ardenkjaer-Larsen, Rapid zero-trans kinetics of Cs+ exchange in human erythrocytes quantified by dissolution hyperpolarized 133Cs+ NMR spectroscopy, Sci. Rep. 9 (2019) 19726–19812, https://doi.org/10.1038/s41598-019-56250-z.
[443] S.G. Schultz, N.L. Wilson, W. Epstein, Cation Transport in Escherichia coli, J. Gen. Physiol. 46 (1962) 159–166, https://doi.org/10.1085/jgp.46.1.159.
[444] F.G. Riddell, Z. Zhou, NMR visibility of 35Cl− in human erythrocytes, Magn. Reson. Chem. 33 (1995) 66–69, https://doi.org/10.1002/mrc.1260330111.
[445] A.M. Nagel, F. Lehmann-Horn, M.-A. Weber, K. Jurkat-Rott, M.B. Wolf, A. Radbruch, R. Umathum, W. Semmler, In Vivo 35Cl MR Imaging in Humans: A Feasibility Study, Radiology. 271 (2014) 585–595, https://doi.org/10.1148/radiol.13131725.
[446] B.P. Lüscher, L. Vachel, E. Ohana, S. Muallem, Cl ⁻ as a bona fide signaling ion, Am. J. Physiol.-Cell Physiol. 318 (2020) C125–C136, https://doi.org/10.1152/ajpcell.00354.2019.
[447] L. Ding, Y. Lian, Z. Lin, Z. Zhang, X. Wang, Long-Term Quantitatively Imaging Intracellular Chloride Concentration Using a Core-/Shell-Structured Nanosensor and Time-Domain Dual-Lifetime Referencing Method, ACS Sens. 5 (2020) 3971–3978, https://doi.org/10.1021/acssensors.0c01671.
[448] J.A. Magnuson, N.S. Magnuson, A chlorine-35 nuclear magnetic resonance study of dodecyl sulfate binding to bovine serum albumin, J. Am. Chem. Soc. 94 (1972) 5461–5466, https://doi.org/10.1021/ja00770a049.
[449] T.E. Bull, J. Andrasko, E. Chiancone, S. Forsén, Pulsed nuclear magnetic resonance studies on 23Na, 7Li and 35Cl binding to human oxy- and carbon monoxyhaemoglobin, J. Mol. Biol. 73 (1973) 251–259, https://doi.org/10.1016/0022-2836(73)90327-6.
[450] B.M. Rayson, R.K. Gupta, 23Na NMR studies of rat outer medullary kidney tubules, J. Biol. Chem. 260 (1985) 7276–7280, https://doi.org/10.1016/S0021-9258(17)39603-5.
[451] M. Brauer, C.Y. Spread, R.A. Reithmeier, B.D. Sykes, 31P and 35Cl nuclear magnetic resonance measurements of anion transport in human erythrocytes, J. Biol. Chem. 260 (1985) 11643–11650.
[452] D. Hoffman, R.K. Gupta, NMR measurement of intracellular water volume, J. Magn. Reson. 1969 (70) (1986) 481–483, https://doi.org/10.1016/0022-2364(86)90140-X.
[453] D. Hoffman, A.M. Kumar, A. Spitzer, R.K. Gupta, NMR measurement of intracellular water volume in rat kidney proximal tubules, Biochim. Biophys. Acta BBA - Mol. Cell Res. 889 (1986) 355–360, https://doi.org/10.1016/0167-4889(86)90198-9.
[454] G.A. Morrill, A.B. Kostellow, D. Hoffman, R.K. Gupta, NMR Studies of Intracellular Water Use of the Amphibian Oocyte as a Model System, Ann. N. Y. Acad. Sci. 508 (1987) 531–533, https://doi.org/10.1111/j.1749-6632.1987.tb32957.x.

[455] Y. Shachar-Hill, R.G. Shulman, Co2+ as a shift reagent for 35Cl NMR of chloride with vesicles and cells, Biochemistry. 31 (1992) 6272–6278, https://doi.org/10.1021/bi00142a015.
[456] W. Lin, D.M. de Freitas, 35Cl NMR Study of Cl− Distribution and Transport in Human Red Blood Cell Suspensions, Magn. Reson. Chem. 34 (1996) 768–772, https://doi.org/10.1002/(SICI)1097-458X(199610)34:10<768::AID-OMR964>3.0.CO;2-7.
[457] C.F. Diven, F. Wang, A.M. Abukhdeir, W. Salah, B.T. Layden, C.F.G.C. Geraldes, D. Mota de Freitas, Evaluation of [Co(gly) 3] -as a 35Cl -NMR Shift Reagent for Cellular Studies, Inorg. Chem. 42 (2003) 2774–2782, https://doi.org/10.1021/ic0258680.
[458] S. Kirsch, M. Augath, D. Seiffge, L. Schilling, L.R. Schad, In vivo chlorine-35, sodium-23 and proton magnetic resonance imaging of the rat brain, NMR Biomed. 23 (2010) 592–600, https://doi.org/10.1002/nbm.1500.
[459] M.-A. Weber, A.M. Nagel, A.M. Marschar, P. Glemser, K. Jurkat-Rott, M.B. Wolf, M.E. Ladd, H.-P. Schlemmer, H.-U. Kauczor, F. Lehmann-Horn, 7-T ^{35} Cl and ^{23} Na MR Imaging for Detection of Mutation-dependent Alterations in Muscular Edema and Fat Fraction with Sodium and Chloride Concentrations in Muscular Periodic Paralyses, Radiology. 280 (2016) 848–859, https://doi.org/10.1148/radiol.2016151617.
[460] S. Baier, P. Krämer, S. Grudzenski, M. Fatar, S. Kirsch, L.R. Schad, Chlorine and sodium chemical shift imaging during acute stroke in a rat model at 9.4 Tesla, Magn. Reson. Mater. Phys. Biol. Med. 27 (2013) 71–79, https://doi.org/10.1007/s10334-013-0398-z.
[461] P. Lundberg, E. Harmsen, C. Ho, H.J. Vogel, Nuclear magnetic resonance studies of cellular metabolism, Anal. Biochem. 191 (1990) 193–222, https://doi.org/10.1016/0003-2697(90)90210-z.
[462] R.B. Moon, J.H. Richards, Determination of intracellular pH by 31P magnetic resonance, J. Biol. Chem. 248 (1973) 7276–7278.
[463] J.J.H. Ackerman, G.E. Soto, W.M. Spees, Z. Zhu, J.L. Evelhoch, The NMR chemical shift pH measurement revisited: Analysis of error and modeling of a pH dependent reference, Magn. Reson. Med. 36 (1996) 674–683, https://doi.org/10.1002/mrm.1910360505.
[464] T. Li, Y. Liao, X. Jiang, D. Mu, X. Hou, C. Zhang, P. Deng, pH detection in biological samples by 1D and 2D 1H–31P NMR, Talanta. 178 (2018) 538–544, https://doi.org/10.1016/j.talanta.2017.09.085.
[465] N. Cox, R. Kuemmerle, P. Millard, E. Cahoreau, J.-M. François, J.-L. Parrou, G. Lippens, Integrated pH Measurement during Reaction Monitoring with Dual-Reception 1H–31P NMR Spectroscopy, Anal. Chem. 91 (2019) 3959–3963, https://doi.org/10.1021/acs.analchem.8b05147.
[466] Y. Nikolaev, N. Ripin, M. Soste, P. Picotti, D. Iber, F.-H.-T. Allain, Systems NMR: single-sample quantification of RNA, proteins and metabolites for biomolecular network analysis, Nat. Methods. 16 (2019) 743–749, https://doi.org/10.1038/s41592-019-0495-7.
[467] T.L. Legerton, K. Kanamori, R.L. Weiss, J.D. Roberts, Measurements of cytoplasmic and vacuolar pH in Neurospora using nitrogen-15 nuclear magnetic resonance spectroscopy, Biochemistry. 22 (1983) 899–903, https://doi.org/10.1021/bi00273a029.
[468] N. Shimba, Z. Serber, R. Ledwidge, S.M. Miller, C.S. Craik, V. Dötsch, Quantitative Identification of the Protonation State of Histidines in Vitro and in Vivo †, Biochemistry. 42 (2003) 9227–9234, https://doi.org/10.1021/bi0344679.
[469] F.A. Gallagher, M.I. Kettunen, S.E. Day, D.-E. Hu, J.H. Ardenkjaer-Larsen, R. in t Zandt, P.R. Jensen, M. Karlsson, K. Golman, M.H. Lerche, K.M. Brindle, Magnetic resonance imaging of pH in vivo using hyperpolarized 13 C-labelled bicarbonate, Nature. 453 (2008) 940–943. https://doi.org/10.1038/nature07017..
[470] R.D. Cohen, A.J. Guseman, G.J. Pielak, Intracellular pH modulates quinary structure, Protein Sci. Publ. Protein Soc. 24 (2015) 1748–1755, https://doi.org/10.1002/pro.2765.
[471] S. He, R.P. Mason, S. Hunjan, V.D. Mehta, V. Arora, R. Katipally, P.V. Kulkarni, P. P. Antich, Development of novel 19F NMR pH indicators: synthesis and evaluation of a series of fluorinated vitamin B6 analogues, Bioorg. Med. Chem. 6 (1998) 1631–1639, https://doi.org/10.1016/s0968-0896(98)00104-7.
[472] S. Hunjan, R.P. Mason, V.D. Mehta, P.V. Kulkarni, S. Aravind, V. Arora, P.P. Antich, Simultaneous intracellular and extracellular pH measurement in the heart by 19F NMR of 6-fluoropyridoxol, Magn. Reson. Med. 39 (1998) 551–556, https://doi.org/10.1002/mrm.1910390407.
[473] C.K. Rhee, L.A. Levy, R.E. London, Fluorinated o-aminophenol derivatives for measurement of intracellular pH, Bioconjug. Chem. 6 (1995) 77–81, https://doi.org/10.1021/bc00031a008.
[474] M.T. Judge, Y. Wu, F. Tayyari, A. Hattori, J. Glushka, T. Ito, J. Arnold, A.S. Edison, Continuous in vivo Metabolism by NMR, Front. Mol. Biosci. 6 (2019) 26, https://doi.org/10.3389/fmolb.2019.00026.
[475] A. Mochizuki, A. Saso, Q. Zhao, S. Kubo, N. Nishida, I. Shimada, Balanced Regulation of Redox Status of Intracellular Thioredoxin Revealed by in-Cell NMR, J. Am. Chem. Soc. 140 (2018) 3784–3790, https://doi.org/10.1021/jacs.8b00426.
[476] C.J. Unkefer, R.M. Blazer, R.E. London, In vivo determination of the pyridine nucleotide reduction charge by carbon-13 nuclear magnetic resonance spectroscopy, Science. 222 (1983) 62–65, https://doi.org/10.1126/science.6353573.
[477] C.J. Unkefer, R.E. London, In vivo studies of pyridine nucleotide metabolism in Escherichia coli and Saccharomyces cerevisiae by carbon-13 NMR spectroscopy, J. Biol. Chem. 259 (1984) 2311–2320.
[478] S.Y. Rhieu, A.A. Urbas, D.W. Bearden, J.P. Marino, K.A. Lippa, V. Reipa, Probing the intracellular glutathione redox potential by in-cell NMR spectroscopy, Angew. Chem. Int. Ed Engl. 53 (2014) 447–450, https://doi.org/10.1002/anie.201308004.
[479] X. Jin, S. Kang, S. Tanaka, S. Park, Monitoring the Glutathione Redox Reaction in Living Human Cells by Combining Metabolic Labeling with Heteronuclear NMR, Angew. Chem. Int. Ed. 55 (2016) 7939–7942, https://doi.org/10.1002/anie.201601026.
[480] S.Y. Rhieu, A.A. Urbas, K.A. Lippa, V. Reipa, Quantitative measurements of glutathione in yeast cell lysate using 1H NMR, Anal. Bioanal. Chem. 405 (2013) 4963–4968, https://doi.org/10.1007/s00216-013-6858-5.
[481] F.Q. Schafer, G.R. Buettner, Redox environment of the cell as viewed through the redox state of the glutathione disulfide/glutathione couple, Free Radic. Biol. Med. 30 (2001) 1191–1212, https://doi.org/10.1016/S0891-5849(01)00480-4.
[482] M. Deponte, Glutathione catalysis and the reaction mechanisms of glutathione-dependent enzymes, Biochim. Biophys. Acta BBA - Gen. Subj. 2013 (1830) 3217–3266, https://doi.org/10.1016/j.bbagen.2012.09.018.
[483] Y.-M. Go, D.P. Jones, Redox compartmentalization in eukaryotic cells, Biochim. Biophys. Acta BBA - Gen. Subj. 1780 (2008) 1273–1290, https://doi.org/10.1016/j.bbagen.2008.01.011.
[484] N. Couto, J. Wood, J. Barber, The role of glutathione reductase and related enzymes on cellular redox homoeostasis network, Free Radic. Biol. Med. 95 (2016) 27–42, https://doi.org/10.1016/j.freeradbiomed.2016.02.028.
[485] L. Flohé, The fairytale of the GSSG/GSH redox potential, Biochim. Biophys. Acta BBA - Gen. Subj. 2013 (1830) 3139–3142, https://doi.org/10.1016/j.bbagen.2012.10.020.
[486] U. Himmelreich, K.N. Drew, A.S. Serianni, P.W. Kuchel, 13C NMR studies of vitamin C transport and its redox cycling in human erythrocytes, Biochemistry. 37 (1998) 7578–7588, https://doi.org/10.1021/bi970765s.
[487] S.E. Bohndiek, M.I. Kettunen, D.-E. Hu, B.W.C. Kennedy, J. Boren, F.A. Gallagher, K.M. Brindle, Hyperpolarized [1- 13C]-Ascorbic and Dehydroascorbic Acid: Vitamin C as a Probe for Imaging Redox Status in Vivo, J. Am. Chem. Soc. 133 (2011) 11795–11801, https://doi.org/10.1021/ja2045925.
[488] K.N. Timm, D.-E. Hu, M. Williams, A.J. Wright, M.I. Kettunen, B.W.C. Kennedy, T.J. Larkin, P. Dzien, I. Marco-Rius, S.E. Bohndiek, K.M. Brindle, Assessing Oxidative Stress in Tumors by Measuring the Rate of Hyperpolarized [1-13C] Dehydroascorbic Acid Reduction Using 13C Magnetic Resonance Spectroscopy, J. Biol. Chem. 292 (2017) 1737–1748, https://doi.org/10.1074/jbc.M116.761536.
[489] C. Anish, B. Schumann, C.L. Pereira, P.H. Seeberger, Chemical Biology Approaches to Designing Defined Carbohydrate Vaccines, Chem. Biol. 21 (2014) 38–50, https://doi.org/10.1016/j.chembiol.2014.01.002.
[490] R. Mettu, C.-Y. Chen, C.-Y. Wu, Synthetic carbohydrate-based vaccines: challenges and opportunities, J. Biomed. Sci. 27 (2020) 9–22, https://doi.org/10.1186/s12929-019-0591-0.
[491] S. Bontemps-Gallo, J.-M. Lacroix, New insights into the biological role of the osmoregulated periplasmic glucans in pathogenic and symbiotic bacteria, Environ. Microbiol. Rep. 7 (2015) 690–697, https://doi.org/10.1111/1758-2229.12325.
[492] G.B. Whitfield, L.S. Marmont, P.L. Howell, Enzymatic modifications of exopolysaccharides enhance bacterial persistence, Front. Microbiol. 6 (2015) 7350–7421, https://doi.org/10.3389/fmicb.2015.00471.
[493] I. Geoghegan, G. Steinberg, S. Gurr, The Role of the Fungal Cell Wall in the Infection of Plants, Trends Microbiol. 25 (2017) 957–967, https://doi.org/10.1016/j.tim.2017.05.015.
[494] D.A. Dik, J.F. Fisher, S. Mobashery, Cell-Wall Recycling of the Gram-Negative Bacteria and the Nexus to Antibiotic Resistance, Chem. Rev. 118 (2018) 5952–5984, https://doi.org/10.1021/acs.chemrev.8b00277.
[495] R. Kalscheuer, A. Palacios, I. Anso, J. Cifuente, J. Anguita, W.R. Jacobs Jr, M.E. Guerin, R. Prados-Rosales, The Mycobacterium tuberculosis capsule: a cell structure with key implications in pathogenesis, Biochem. J. 476 (2019) 1995–2016, https://doi.org/10.1042/BCJ20190324.
[496] A.J.F. Egan, J. Errington, W. Vollmer, Regulation of peptidoglycan synthesis and remodelling, Nat. Rev. Microbiol. (2020) 1–15, https://doi.org/10.1038/s41579-020-0366-3.
[497] G.P. Rajalekshmy, L. Lekshmi Devi, J. Joseph, M.R. Rekha, An overview on the potential biomedical applications of polysaccharides, Elsevier (2019) 33–94, https://doi.org/10.1016/B978-0-08-102555-0.00002-9.
[498] E. Cho, D. Jeong, Y. Choi, S. Jung, Properties and current applications of bacterial cyclic β-glucans and their derivatives, J. Incl. Phenom. Macrocycl. Chem. 85 (2016) 175–185, https://doi.org/10.1007/s10847-016-0630-3.
[499] J. Liu, X. Wang, H. Pu, S. Liu, J. Kan, C. Jin, Recent advances in endophytic exopolysaccharides: Production, structural characterization, physiological role and biological activity, Carbohydr. Polym. 157 (2017) 1113–1124, https://doi.org/10.1016/j.carbpol.2016.10.084.
[500] B. Zhang, R. Powers, Analysis of bacterial biofilms using NMR-based metabolomics, Future Med. Chem. 4 (2012) 1273–1306, https://doi.org/10.4155/fmc.12.59.
[501] L. Cegelski, Bottom-up and top-down solid-state NMR approaches for bacterial biofilm matrix composition, J. Magn. Reson. 253 (2015) 91–97, https://doi.org/10.1016/j.jmr.2015.01.014.
[502] M.P. Herrling, S. Lackner, H. Nirschl, H. Horn, G. Guthausen, Recent NMR/MRI studies of biofilm structures and dynamics, Elsevier Ltd. (2019), https://doi.org/10.1016/bs.arnmr.2019.02.001.

[503] W. Thongsomboon, D.O. Serra, A. Possling, C. Hadjineophytou, R. Hengge, L. Cegelski, Phosphoethanolamine cellulose: A naturally produced chemically modified cellulose, Science. 359 (2018) 334–338, https://doi.org/10.1126/science.aao4096.
[504] J. Schaefer, E.O. Stejskal, Carbon-13 nuclear magnetic resonance of polymers spinning at the magic angle, J. Am. Chem. Soc. 98 (1976) 1031–1032, https://doi.org/10.1021/ja00420a036.
[505] J. Schaefer, Schaefer, Jacob: A Brief History of the Combination of Cross Polarization and Magic Angle Spinning, EMagRes. 5 (2007) 798–807, https://doi.org/10.1002/9780470034590.emrhp0161.
[506] R.H. Atalla, J.C. Gast, D.W. Sindorf, V.J. Bartuska, G.E. Maciel, Carbon-13 NMR spectra of cellulose polymorphs, J. Am. Chem. Soc. 102 (1980) 3249–3251, https://doi.org/10.1021/ja00529a063.
[507] W.L. Earl, D.L. VanderHart, High resolution, magic angle sampling spinning carbon-13 NMR of solid cellulose I, J. Am. Chem. Soc. 102 (1980) 3251–3252, https://doi.org/10.1021/ja00529a064.
[508] W.L. Earl, D.L. VanderHart, Observations by high-resolution carbon-13 nuclear magnetic resonance of cellulose I related to morphology and crystal structure, Macromolecules. 14 (1981) 570–574, https://doi.org/10.1021/ma50004a023.
[509] W. Kolodziejski, J.S. Frye, G.E. Maciel, Carbon-13 nuclear magnetic resonance spectrometry with cross polarization and magic-angle spinning for analysis of lodgepole pine wood, Anal. Chem. 54 (1982) 1419–1424, https://doi.org/10.1021/ac00245a035.
[510] G.E. Maciel, W.L. Kolodziejski, M.S. Bertran, B.E. Dale, Carbon-13 NMR and order in cellulose, Macromolecules. 15 (1982) 686–687, https://doi.org/10.1021/ma00230a097.
[511] G.J. Leary, K.R. Morgan, R.H. Newman, B. Samuelsson, U. Westermark, A 13C CP/MAS NMR Comparison of Wood Fractions from Spruce, Holzforschung. 40 (1986) 221–224, https://doi.org/10.1515/hfsg.1986.40.4.221.
[512] R.H. Newman, L.M. Davies, P.J. Harris, Solid-State 13C Nuclear Magnetic Resonance Characterization of Cellulose in the Cell Walls of Arabidopsis thaliana Leaves, Plant Physiol. 111 (1996) 475–485, https://doi.org/10.1104/pp.111.2.475.
[513] P. Wormald, K. Wickholm, P.T. Larsson, T. Iversen, Conversions between ordered and disordered cellulose. Effects of mechanical treatment followed by cyclic wetting and drying, Cellulose. 3 (1996) 141–152.
[514] A.N. Fernandes, L.H. Thomas, C.M. Altaner, P. Callow, V.T. Forsyth, D.C. Apperley, C.J. Kennedy, M.C. Jarvis, Nanostructure of cellulose microfibrils in spruce wood, Proc. Natl. Acad. Sci. U. S. A. 108 (2011) E1195–E1203, https://doi.org/10.1073/pnas.1108942108.
[515] V.J. Bartuska, G.E. Maciel, H.I. Bolker, B.I. Fleming, Structural Studies of Lignin Isolation Procedures by 13C NMR, Holzforschung. 34 (1980) 214–217, https://doi.org/10.1515/hfsg.1980.34.6.214.
[516] J. Schaefer, M.D. Sefcik, E.O. Stejskal, R.A. McKay, P.L. Hall, Characterization of the catabolic transformation of lignin in culture by magic-angle carbon-13 nuclear magnetic resonance, Macromolecules. 14 (1981) 557–559, https://doi.org/10.1021/ma50004a020.
[517] T. Mori, E. Chikayama, Y. Tsuboi, N. Ishida, N. Shisa, Y. Noritake, S. Moriya, J. Kikuchi, Exploring the conformational space of amorphous cellulose using NMR chemical shifts, Carbohydr. Polym. 90 (2012) 1197–1203, https://doi.org/10.1016/j.carbpol.2012.06.027.
[518] R.H. Newman, J.A. Hemmingson, Determination of the Degree of Cellulose Crystallinity in Wood by Carbon-13 Nuclear Magnetic Resonance Spectroscopy, Holzforschung. 44 (1990) 351–356, https://doi.org/10.1515/hfsg.1990.44.5.351.
[519] R.H. Newman, Crystalline Forms of Cellulose in Softwoods and Hardwoods, J. Wood Chem. Technol. 14 (1994) 451–466, https://doi.org/10.1080/02773819408003107.
[520] J.F. Haw, G.E. Maciel, H.A. Schroeder, Carbon-13 nuclear magnetic resonance spectrometric study of wood and wood pulping with cross polarization and magic-angle spinning, Anal. Chem. 56 (1984) 1323–1329, https://doi.org/10.1021/ac00272a028.
[521] R. Evans, R.H. Newman, U.C. Roick, I.D. Suckling, A.F.A. Wallis, Changes in Cellulose Crystallinity During Kraft Pulping.Comparison of Infrared, X-ray Diffraction and Solid State NMR Results, Holzforschung. 49 (1995) 498–504, https://doi.org/10.1515/hfsg.1995.49.6.498.
[522] Y.S. Kim, R.H. Newman, Solid State 13C NMR Study of Wood Degraded by the Brown Rot Fungus Gloeophyllum trabeum, Holzforschung. 49 (1995) 109–114, https://doi.org/10.1515/hfsg.1995.49.2.109.
[523] G. Gilardi, L. Abis, A.E.G. Cass, Carbon-13 CP/MAS solid-state NMR and FT-IR spectroscopy of wood cell wall biodegradation, Enzyme Microb. Technol. 17 (1995) 268–275, https://doi.org/10.1016/0141-0229(94)00019-N.
[524] J.A. Hemmingson, R.H. Newman, Changes in molecular ordering associated with alkali treatment and vacuum drying of cellulose, Cellulose. 2 (1995) 71–82.
[525] R. Ibbett, D. Domvoglou, F. Wortmann, K.C. Schuster, Carbon-13 solid state NMR investigation and modeling of the morphological reorganization in regenerated cellulose fibres induced by controlled acid hydrolysis, Cellulose. 17 (2010) 231–243, https://doi.org/10.1007/s10570-010-9397-7.
[526] S.J. Hill, N.M. Kirby, S.T. Mudie, A.M. Hawley, B. Ingham, R.A. Franich, R.H. Newman, Effect of drying and rewetting of wood on cellulose molecular packing, Holzforschung. 64 (2010) 3–7, https://doi.org/10.1515/hf.2010.065.
[527] K. Okushita, E. Chikayama, J. Kikuchi, Solubilization Mechanism and Characterization of the Structural Change of Bacterial Cellulose in Regenerated States through Ionic Liquid Treatment, Biomacromolecules. 13 (2012) 1323–1330, https://doi.org/10.1021/bm300537k.
[528] H. Teramura, K. Sasaki, T. Oshima, S. Aikawa, F. Matsuda, M. Okamoto, T. Shirai, H. Kawaguchi, C. Ogino, M. Yamasaki, J. Kikuchi, A. Kondo, Changes in Lignin and Polysaccharide Components in 13 Cultivars of Rice Straw following Dilute Acid Pretreatment as Studied by Solution-State 2D 1H–13C NMR, PLoS ONE. 10 (2015) e0128417–e128517, https://doi.org/10.1371/journal.pone.0128417.
[529] M. Ghosh, B.P. Prajapati, R.K. Suryawanshi, K.K. Dey, N. Kango, Study of the effect of enzymatic deconstruction on natural cellulose by NMR measurements, Chem. Phys. Lett. 727 (2019) 105–115, https://doi.org/10.1016/j.cplett.2019.04.063.
[530] R.H. Newman, M.-A. Ha, L.D. Melton, Solid-State 13C NMR Investigation of Molecular Ordering in the Cellulose of Apple Cell Walls, J. Agric. Food Chem. 42 (1994) 1402–1406, https://doi.org/10.1021/jf00043a002.
[531] M.C. Jarvis, K.M. Fenwick, D.C. Apperley, Cross-polarisation kinetics and proton NMR relaxation in polymers of Citrus cell walls, Carbohydr. Res. 288 (1996) 1–14, https://doi.org/10.1016/S0008-6215(96)90769-7.
[532] M.-A. Ha, B.W. Evans, M.C. Jarvis, D.C. Apperley, A.M. Kenwright, CP-MAS NMR of highly mobile hydrated biopolymers: Polysaccharides of Allium cell walls, Carbohydr. Res. 288 (1996) 15–23, https://doi.org/10.1016/S0008-6215(96)90771-5.
[533] T.J. Foster, S. Ablett, M.C. McCann, M.J. Gidley, Mobility-resolved 13C-NMR spectroscopy of primary plant cell walls, Biopolymers. 39 (1996) 51–66, https://doi.org/10.1002/(SICI)1097-0282(199607)39:1<51::AID-BIP6>3.0.CO;2-U.
[534] B.G. Smith, P.J. Harris, L.D. Melton, R.H. Newman, The range of mobility of the non-cellulosic polysaccharides is similar in primary cell walls with different polysaccharide compositions, Physiol. Plant. 103 (1998) 233–246, https://doi.org/10.1034/j.1399-3054.1998.1030211.x.
[535] H. Tang, P.S. Belton, A. Ng, P. Ryden, 13C MAS NMR studies of the effects of hydration on the cell walls of potatoes and Chinese water chestnuts, J. Agric. Food Chem. 47 (1999) 510–517, https://doi.org/10.1021/jf980553h.
[536] C. Renard, M. Jarvis, A cross-polarization, magic-angle-spinning, 13C-nuclear-magnetic-resonance study of polysaccharides in sugar beet cell walls, Plant Physiol. 119 (1999) 1315–1322, https://doi.org/10.1104/pp.119.4.1315.
[537] S. Hediger, L. Emsley, M. Fischer, Solid-state NMR characterization of hydration effects on polymer mobility in onion cell-wall material, Carbohydr. Res. 322 (1999) 102–112, https://doi.org/10.1016/S0008-6215(99)00195-0.
[538] M.C. Jarvis, M.C. McCann, Macromolecular biophysics of the plant cell wall: Concepts and methodology, Plant Physiol. Biochem. 38 (2000) 1–13, https://doi.org/10.1016/S0981-9428(00)00172-8.
[539] M. Lahaye, X. Falourd, B. Laillet, S. Le Gall, Cellulose, pectin and water in cell walls determine apple flesh viscoelastic mechanical properties, Carbohydr. Polym. (2019), https://doi.org/10.1016/j.carbpol.2019.115768 115768.
[540] P.L. Irwin, P.E. Pfeffer, W.V. Gerasimowicz, R. Pressey, C.E. Sams, Ripening-related perturbations in apple cell wall nuclear spin dynamics, Phytochemistry. 23 (1984) 2239–2242, https://doi.org/10.1016/S0031-9422(00)80527-0.
[541] T.H. Koh, L.D. Melton, R.H. Newman, Solid-state 13C NMR characterization of cell walls of ripening strawberries, Can. J. Bot. 75 (1997) 1957–1964, https://doi.org/10.1139/b97-908.
[542] R.H. Newman, R.J. Redgwell, Cell wall changes in ripening kiwifruit: 13C solid state NMR characterisation of relatively rigid cell wall polymers, Carbohydr. Polym. 49 (2002) 121–129, https://doi.org/10.1016/S0144-8617(01)00323-X.
[543] C. Rondeau-Mouro, M.-J. Crepeau, M. Lahaye, Application of CP-MAS and liquid-like solid-state NMR experiments for the study of the ripening-associated cell wall changes in tomato, Int. J. Biol. Macromol. 31 (2003) 235–244, https://doi.org/10.1016/s0141-8130(02)00086-7.
[544] T.J. Bootten, P.J. Harris, L.D. Melton, R.H. Newman, Solid-state 13C-NMR spectroscopy shows that the xyloglucans in the primary cell walls of mung bean (Vigna radiata L.) occur in different domains: a new model for xyloglucan-cellulose interactions in the cell wall, J. Exp. Bot. 55 (2004) 571–583, https://doi.org/10.1093/jxb/erh065.
[545] F.H. Larsen, I. Byg, I. Damager, J. Diaz, S.B. Engelsen, P. Ulvskov, Residue specific hydration of primary cell wall potato pectin identified by solid-state 13C single-pulse MAS and CP/MAS NMR spectroscopy, Biomacromolecules. 12 (2011) 1844–1850, https://doi.org/10.1021/bm2001928.
[546] J.K.T. Ng, Z.D. Zujovic, B.G. Smith, J.W. Johnston, R. Schröder, L.D. Melton, Solid-state 13C NMR study of the mobility of polysaccharides in the cell walls of two apple cultivars of different firmness, Carbohydr. Res. 386 (2014) 1–6, https://doi.org/10.1016/j.carres.2013.12.019.
[547] M. Dick-Pérez, Y. Zhang, J. Hayes, A. Salazar, O.A. Zabotina, M. Hong, Structure and interactions of plant cell-wall polysaccharides by two- and three-dimensional magic-angle-spinning solid-state NMR, Biochemistry. 50 (2011) 989–1000, https://doi.org/10.1021/bi101795q.
[548] T. Wang, O. Zabotina, M. Hong, Pectin-cellulose interactions in the Arabidopsis primary cell wall from two-dimensional magic-angle-spinning solid-state nuclear magnetic resonance, Biochemistry. 51 (2012) 9846–9856, https://doi.org/10.1021/bi3015532.
[549] T. Wang, Y.B. Park, D.J. Cosgrove, M. Hong, Cellulose-Pectin Spatial Contacts Are Inherent to Never-Dried Arabidopsis Primary Cell Walls: Evidence from Solid-State Nuclear Magnetic Resonance, Plant Physiol. 168 (2015) 871–884, https://doi.org/10.1104/pp.15.00665.

[550] P. Phyo, M. Hong, Fast MAS 1H–13C correlation NMR for structural investigations of plant cell walls, J. Biomol. NMR. 73 (2019) 661–674, https://doi.org/10.1007/s10858-019-00277-x.
[551] T. Komatsu, J. Kikuchi, Comprehensive Signal Assignment of 13C-Labeled Lignocellulose Using Multidimensional Solution NMR and 13C Chemical Shift Comparison with Solid-State NMR, Anal. Chem. 85 (2013) 8857–8865, https://doi.org/10.1021/ac402197h.
[552] T. Wang, M. Hong, Solid-state NMR investigations of cellulose structure and interactions with matrix polysaccharides in plant primary cell walls, J. Exp. Bot. 67 (2016) 503–514, https://doi.org/10.1093/jxb/erv416.
[553] W. Zhao, L.D. Fernando, A. Kirui, F. Deligey, T. Wang, Solid-state NMR of plant and fungal cell walls: A critical review, Solid State Nucl. Magn. Reson. 107 (2020) 101660–101722, https://doi.org/10.1016/j.ssnmr.2020.101660.
[554] R. Dupree, T.J. Simmons, J.C. Mortimer, D. Patel, D. Iuga, S.P. Brown, P. Dupree, Probing the molecular architecture of Arabidopsis thaliana secondary cell walls using two- and three-dimensional (13)C solid state nuclear magnetic resonance spectroscopy, Biochemistry. 54 (2015) 2335–2345, https://doi.org/10.1021/bi501552k.
[555] T.J. Simmons, J.C. Mortimer, O.D. Bernardinelli, A.-C.P. ouml ppler, S.P. Brown, E.R. deAzevedo, R. Dupree, P. Dupree, Folding of xylan onto cellulose fibrils in plant cell walls revealed by solid-state NMR, Nat. Commun. 7 (2016) 1–9. https://doi.org/10.1038/ncomms13902..
[556] N.J. Grantham, J. Wurman-Rodrich, O.M. Terrett, J.J. Lyczakowski, K. Stott, D. Iuga, T.J. Simmons, M. Durand-Tardif, S.P. Brown, R. Dupree, M. Busse-Wicher, P. Dupree, An even pattern of xylan substitution is critical for interaction with cellulose in plant cell walls, Nat. Plants. (2017) 1–9, https://doi.org/10.1038/s41477-017-0030-8.
[557] O.M. Terrett, J.J. Lyczakowski, L. Yu, D. Iuga, W.T. Franks, S.P. Brown, R. Dupree, P. Dupree, Molecular architecture of softwood revealed by solid-state NMR, Nat. Commun. (2019) 1–11, https://doi.org/10.1038/s41467-019-12979-9.
[558] X. Kang, A. Kirui, M.C.D. Widanage, F. Mentink-Vigier, D.J. Cosgrove, T. Wang, Lignin-polysaccharide interactions in plant secondary cell walls revealed by solid-state NMR, Nat. Commun. (2019) 1–9, https://doi.org/10.1038/s41467-018-08252-0.
[559] T. Wang, Y.B. Park, M.A. Caporini, M. Rosay, L. Zhong, D.J. Cosgrove, M. Hong, Sensitivity-enhanced solid-state NMR detection of expansin's target in plant cell walls, Proc. Natl. Acad. Sci. U. S. A. 110 (2013) 16444–16449, https://doi.org/10.1073/pnas.1316290110.
[560] O.M. Terrett, P. Dupree, Covalent interactions between lignin and hemicelluloses in plant secondary cell walls, Curr. Opin. Biotechnol. 56 (2019) 97–104, https://doi.org/10.1016/j.copbio.2018.10.010.
[561] A. Kirui, Z. Ling, X. Kang, M.C.D. Widanage, F. Mentink-Vigier, A.D. French, T. Wang, Atomic resolution of cotton cellulose structure enabled by dynamic nuclear polarization solid-state NMR, Cellulose. 26 (2018) 329–339, https://doi.org/10.1007/s10570-018-2095-6.
[562] D.J. Cosgrove, Re-constructing our models of cellulose and primary cell wall assembly, Curr. Opin. Plant Biol. 22 (2014) 122–131, https://doi.org/10.1016/j.pbi.2014.11.001.
[563] C. Voiniciuc, M. Pauly, B. Usadel, Monitoring Polysaccharide Dynamics in the Plant Cell Wall, Plant Physiol. 176 (2018) 2590–2600, https://doi.org/10.1104/pp.17.01776.
[564] D.J. Cosgrove, Nanoscale structure, mechanics and growth of epidermal cell walls, Curr. Opin. Plant Biol. 46 (2018) 77–86, https://doi.org/10.1016/j.pbi.2018.07.016.
[565] A. Poulhazan, M.C. Dickwella Widanage, A. Muszyński, A.A. Arnold, D.E. Warschawski, P. Azadi, I. Marcotte, T. Wang, Identification and Quantification of Glycans in Whole Cells: Architecture of Microalgal Polysaccharides Described by Solid-State Nuclear Magnetic Resonance, J. Am. Chem. Soc. 143 (2021) 19374–19388, https://doi.org/10.1021/jacs.1c07429.
[566] M. Foston, R. Samuel, J. He, A.J. Ragauskas, A review of whole cell wall NMR by the direct-dissolution of biomass, Green Chem. 18 (2016) 608–621, https://doi.org/10.1039/C5GC02828K.
[567] L. Petridis, J.C. Smith, Molecular-level driving forces in lignocellulosic biomass deconstruction for bioenergy, Nat. Rev. Chem. (2018) 1–8, https://doi.org/10.1038/s41570-018-0050-6.
[568] S. Porfirio, R.W. Carlson, P. Azadi, Elucidating Peptidoglycan Structure: An Analytical Toolset, Trends Microbiol. 27 (2019) 607–622, https://doi.org/10.1016/j.tim.2019.01.009.
[569] L. Pasquina-Lemonche, J. Burns, R.D. Turner, S. Kumar, R. Tank, N. Mullin, J.S. Wilson, B. Chakrabarti, P.A. Bullough, S.J. Foster, J.K. Hobbs, The architecture of the Gram-positive bacterial cell wall, Nature. 582 (2020) 294–297, https://doi.org/10.1038/s41586-020-2236-6.
[570] J.A.H. Romaniuk, L. Cegelski, Bacterial cell wall composition and the influence of antibiotics by cell-wall and whole-cell NMR, Philos. Trans. R. Soc. Lond. B. Biol. Sci. 370 (2015), https://doi.org/10.1098/rstb.2015.0024.
[571] R.M. Epand, C. Walker, R.F. Epand, N.A. Magarvey, Molecular mechanisms of membrane targeting antibiotics, BBA - Biomembr. 2016 (1858) 980–987, https://doi.org/10.1016/j.bbamem.2015.10.018.
[572] N. Malanovic, K. Lohner, Gram-positive bacterial cell envelopes: The impact on the activity of antimicrobial peptides, BBA - Biomembr. 2016 (1858) 936–946, https://doi.org/10.1016/j.bbamem.2015.11.004.
[573] K.H. Schleifer, O. Kandler, Peptidoglycan types of bacterial cell walls and their taxonomic implications, Bacteriol. Rev. 36 (1972) 407–477.
[574] S.J. Kim, J. Chang, M. Singh, Peptidoglycan architecture of Gram-positive bacteria by solid-state NMR, BBA - Biomembr. 2015 (1848) 350–362, https://doi.org/10.1016/j.bbamem.2014.05.031.
[575] E. Breukink, B. de Kruijff, Lipid II as a target for antibiotics, Nat. Rev. Drug Discov. 5 (2006) 321–323, https://doi.org/10.1038/nrd2004.
[576] S.F. Oppedijk, N.I. Martin, E. Breukink, Hit 'em where it hurts: The growing and structurally diverse family of peptides that target lipid-II, BBA - Biomembr. 2016 (1858) 947–957, https://doi.org/10.1016/j.bbamem.2015.10.024.
[577] J. Medeiros-Silva, S. Jekhmane, E. Breukink, M. Weingarth, Towards the Native Binding Modes of Antibiotics that Target Lipid II, ChemBioChem. 40 (2019) 277–278, https://doi.org/10.1002/cbic.201800796.
[578] L. Cegelski, D. Steuber, A.K. Mehta, D.W. Kulp, P.H. Axelsen, J. Schaefer, Conformational and Quantitative Characterization of Oritavancin-Peptidoglycan Complexes in Whole Cells of Staphylococcus aureus by in Vivo 13C and 15N Labeling, J. Mol. Biol. 357 (2006) 1253–1262, https://doi.org/10.1016/j.jmb.2006.01.040.
[579] J.A.H. Romaniuk, L. Cegelski, Peptidoglycan and Teichoic Acid Levels and Alterations in Staphylococcus aureus by Cell-Wall and Whole-Cell Nuclear Magnetic Resonance, Biochemistry. 57 (2018) 3966–3975, https://doi.org/10.1021/acs.biochem.8b00495.
[580] A. Lapidot, C.S. Irving, Dynamic structure of whole cells probed by nuclear Overhauser enhanced nitrogen-15 nuclear magnetic resonance spectroscopy, Proc. Natl. Acad. Sci. 74 (1977) 1988–1992, https://doi.org/10.1073/pnas.74.5.1988.
[581] C.S. Irving, A. Lapidot, The dynamic structure of the Escherichia coli cell envelope as probed by 15N nuclear magnetic resonance spectroscopy, Biochim. Biophys. Acta BBA - Biomembr. 470 (1977) 251–257, https://doi.org/10.1016/0005-2736(77)90104-3.
[582] C.S. Irving, A. Lapidot, Effects of binding and bactericidal action of vancomycin on Bacillus licheniformis cell wall organization as probed by 15N nuclear magnetic resonance spectroscopy, Antimicrob. Agents Chemother. 14 (1978) 695–703, https://doi.org/10.1128/aac.14.5.695.
[583] A. Lapidot, C.S. Irving, Comparative in vivo nitrogen-15 nuclear magnetic resonance study of the cell wall components of five Gram-positive bacteria, Biochemistry. 18 (1979) 704–714, https://doi.org/10.1021/bi00571a024.
[584] G.S. Jacob, J. Schaefer, G.E. Wilson, Direct measurement of peptidoglycan cross-linking in bacteria by 15N nuclear magnetic resonance, J. Biol. Chem. 258 (1983) 10824–10826.
[585] G.E. Wilson, G.S. Jacob, J. Schaefer, Solid-state 15N NMR studies of the effects of penicillin on cell-wall metabolism of Aerococcus viridans (Gaffkya homari), Biochem. Biophys. Res. Commun. 126 (1985) 1006–1012, https://doi.org/10.1016/0006-291x(85)90285-2.
[586] J. Schaefer, J.R. Garbow, G.S. Jacob, T.M. Forrest, G.E. Wilson, Characterization of peptidoglycan stem lengths by solid-state 13C and 15N NMR, Biochem. Biophys. Res. Commun. 137 (1986) 736–741, https://doi.org/10.1016/0006-291x(86)91140-x.
[587] T. Gullion, Introduction to rotational-echo, double-resonance NMR, Concepts Magn. Reson. 10 (1998) 277–289, https://doi.org/10.1002/(SICI)1099-0534(1998)10:5<277::AID-CMR1>3.0.CO;2-U.
[588] O. Toke, L. Cegelski, J. Schaefer, Peptide antibiotics in action: Investigation of polypeptide chains in insoluble environments by rotational-echo double resonance, Biochim. Biophys. Acta BBA - Biomembr. 1758 (2006) 1314–1329, https://doi.org/10.1016/j.bbamem.2006.02.031.
[589] S.J. Kim, M. Singh, M. Preobrazhenskaya, J. Schaefer, Staphylococcus aureus peptidoglycan stem packing by rotational-echo double resonance NMR spectroscopy, Biochemistry. 52 (2013) 3651–3659, https://doi.org/10.1021/bi4005039.
[590] L. Cegelski, REDOR NMR for drug discovery, Bioorg. Med. Chem. Lett. 23 (2013) 5767–5775, https://doi.org/10.1016/j.bmcl.2013.08.064.
[591] D.M. Rice, J.A.H. Romaniuk, L. Cegelski, Frequency-selective REDOR and spin-diffusion relays in uniformly labeled whole cells, Solid State Nucl. Magn. Reson. 72 (2015) 132–139, https://doi.org/10.1016/j.ssnmr.2015.10.008.
[592] V. Bork, J. Schaefer, Measuring 13C–13C connectivity in spinning solids by selective excitation, J. Magn. Reson. 1969 (78) (1988) 348–354, https://doi.org/10.1016/0022-2364(88)90281-8.
[593] T. Gullion, J. Schaefer, Rotational-echo double-resonance NMR, J. Magn. Reson. 1969 (81) (1989) 196–200, https://doi.org/10.1016/0022-2364(89)90280-1.
[594] T.M. Forrest, G.E. Wilson, Y. Pan, J. Schaefer, Characterization of cross-linking of cell walls of Bacillus subtilis by a combination of magic-angle spinning NMR and gas chromatography-mass spectrometry of both intact and hydrolyzed 13C- and 15N-labeled cell-wall peptidoglycan, J. Biol. Chem. 266 (1991) 24485–24491.
[595] Y. Pan, N.S. Shenouda, G.E. Wilson, J. Schaefer, Cross-links in cell walls of Bacillus subtilis by rotational-echo double-resonance 15N NMR, J. Biol. Chem. 268 (1993) 18692–18695.
[596] N.S. Shenouda, Y. Pan, J. Schaefer, G.E. Wilson, A simple solid-state NMR method for determining peptidoglycan crosslinking in Bacillus subtilis, Biochim. Biophys. Acta. 1289 (1996) 217–220, https://doi.org/10.1016/0304-4165(95)00177-8.
[597] L. Cegelski, S.J. Kim, A.W. Hing, D.R. Studelska, R.D. O'Connor, A.K. Mehta, J. Schaefer, Rotational-Echo Double Resonance Characterization of the Effects of Vancomycin on Cell Wall Synthesis in Staphylococcus aureus†, Biochemistry. 41 (2002) 13053–13058, https://doi.org/10.1021/bi0202326.
[598] G.J. Patti, S.J. Kim, J. Schaefer, Characterization of the Peptidoglycan of Vancomycin-Susceptible Enterococcus faecium †, Biochemistry. 47 (2008) 8378–8385, https://doi.org/10.1021/bi8008032.

[599] M. Singh, J. Chang, L. Coffman, S.J. Kim, Solid-state NMR characterization of amphomycin effects on peptidoglycan and wall teichoic acid biosyntheses in Staphylococcus aureus, Sci. Rep. 6 (2016) 31757–31759, https://doi.org/10.1038/srep31757.
[600] R.D. O'Connor, M. Singh, J. Chang, S.J. Kim, M. VanNieuwenhze, J. Schaefer, Dual Mode of Action for Plusbacin A3 in Staphylococcus aureus, J. Phys. Chem. B. 121 (2017) 1499–1505, https://doi.org/10.1021/acs.jpcb.6b11039.
[601] S.J. Kim, M. Singh, S. Sharif, J. Schaefer, Desleucyl-Oritavancin with a Damaged d-Ala-d-Ala Binding Site Inhibits the Transpeptidation Step of Cell-Wall Biosynthesis in Whole Cells of Staphylococcus aureus, Biochemistry. 56 (2017) 1529–1535, https://doi.org/10.1021/acs.biochem.6b01125.
[602] G.J. Patti, J. Chen, J. Schaefer, M.L. Gross, Characterization of structural variations in the peptidoglycan of vancomycin-susceptible Enterococcus faecium: understanding glycopeptide-antibiotic binding sites using mass spectrometry, J. Am. Soc. Mass Spectrom. 19 (2008) 1467–1475, https://doi.org/10.1016/j.jasms.2008.06.020.
[603] S. Sharif, S.J. Kim, H. Labischinski, J. Schaefer, Characterization of peptidoglycan in fem-deletion mutants of methicillin-resistant Staphylococcus aureus by solid-state NMR, Biochemistry. 48 (2009) 3100–3108, https://doi.org/10.1021/bi801750u.
[604] S. Sharif, S.J. Kim, H. Labischinski, J. Chen, J. Schaefer, Uniformity of Glycyl Bridge Lengths in the Mature Cell Walls of Fem Mutants of Methicillin-Resistant Staphylococcus aureus, J. Bacteriol. 195 (2013) 1421–1427, https://doi.org/10.1128/JB.01471-12.
[605] X. Zhou, L. Cegelski, Nutrient-dependent structural changes in S. aureus peptidoglycan revealed by solid-state NMR spectroscopy, Biochemistry. 51 (2012) 8143–8153, https://doi.org/10.1021/bi3012115.
[606] Y. Pan, T. Gullion, J. Schaefer, Determination of C-N internuclear distances by rotational-echo double-resonance NMR of solids, J. Magn. Reson. 1969 (90) (1990) 330–340.
[607] S.J. Kim, L. Cegelski, D.R. Studelska, R.D. O'Connor, A.K. Mehta, J. Schaefer, Rotational-Echo Double Resonance Characterization of Vancomycin Binding Sites in Staphylococcus aureus†, Biochemistry. 41 (2002) 6967–6977, https://doi.org/10.1021/bi0121407.
[608] S.J. Kim, L. Cegelski, M. Preobrazhenskaya, J. Schaefer, Structures of Staphylococcus aureus Cell-Wall Complexes with Vancomycin, Eremomycin, and Chloroeremomycin Derivatives by 13C{ 19F} and 15N{ 19F} Rotational-Echo Double Resonance †, Biochemistry. 45 (2006) 5235–5250, https://doi.org/10.1021/bi052660s.
[609] S.J. Kim, S. Matsuoka, G.J. Patti, J. Schaefer, Vancomycin Derivative with Damaged D-Ala-D-Ala Binding Cleft Binds to Cross-linked Peptidoglycan in the Cell Wall of Staphylococcus aureus †, Biochemistry. 47 (2008) 3822–3831, https://doi.org/10.1021/bi702232a.
[610] G.J. Patti, S.J. Kim, T.-Y. Yu, E. Dietrich, K.S.E. Tanaka, T.R. Parr Jr, A.R. Far, J. Schaefer, Vancomycin and Oritavancin Have Different Modes of Action in Enterococcus faecium, J. Mol. Biol. 392 (2009) 1178–1191, https://doi.org/10.1016/j.jmb.2009.06.064.
[611] S.J. Kim, K.S.E. Tanaka, E. Dietrich, A. Rafai Far, J. Schaefer, Locations of the Hydrophobic Side Chains of Lipoglycopeptides Bound to the Peptidoglycan of Staphylococcus aureus, Biochemistry. 52 (2013) 3405–3414, https://doi.org/10.1021/bi400054p.
[612] M. Schäfer, T.R. Schneider, G.M. Sheldrick, Crystal structure of vancomycin, Structure. 4 (1996) 1509–1515, https://doi.org/10.1016/s0969-2126(96)00156-6.
[613] G.J. Sharman, A.C. Try, R.J. Dancer, Y.R. Cho, T. Staroske, B. Bardsley, A.J. Maguire, M.A. Cooper, D.P. O'Brie, D.H. Williams, The Roles of Dimerization and Membrane Anchoring in Activity of Glycopeptide Antibiotics against Vancomycin-Resistant Bacteria, J. Am. Chem. Soc. 119 (1997) 12041–12047, https://doi.org/10.1021/ja964477f.
[614] D. Zeng, D. Debabov, T.L. Hartsell, R.J. Cano, S. Adams, J.A. Schuyler, R. McMillan, J.L. Pace, Approved Glycopeptide Antibacterial Drugs: Mechanism of Action and Resistance, Cold Spring Harb. Perspect. Med. 6 (2016), https://doi.org/10.1101/cshperspect.a026989.
[615] S.J. Kim, M. Singh, A. Wohlrab, T.-Y. Yu, G.J. Patti, R.D. O'Connor, M. VanNieuwenhze, J. Schaefer, The isotridecanyl side chain of plusbacin-A3 is essential for the transglycosylase inhibition of peptidoglycan biosynthesis, Biochemistry. 52 (2013) 1973–1979, https://doi.org/10.1021/bi4000222.
[616] S. Sharif, M. Singh, S.J. Kim, J. Schaefer, Staphylococcus aureus peptidoglycan tertiary structure from carbon-13 spin diffusion, J. Am. Chem. Soc. 131 (2009) 7023–7030, https://doi.org/10.1021/ja808971c.
[617] S.J. Kim, M. Singh, S. Sharif, J. Schaefer, Cross-Link Formation and Peptidoglycan Lattice Assembly in the FemA Mutant of Staphylococcus aureus, Biochemistry. 53 (2014) 1420–1427, https://doi.org/10.1021/bi4016742.
[618] M. Singh, S.J. Kim, S. Sharif, M. Preobrazhenskaya, J. Schaefer, REDOR constraints on the peptidoglycan lattice architecture of Staphylococcus aureus and its FemA mutant, BBA - Biomembr. 2015 (1848) 363–368, https://doi.org/10.1016/j.bbamem.2014.05.025.
[619] S.J. Kim, L. Cegelski, D. Stueber, M. Singh, E. Dietrich, K.S.E. Tanaka, T.R. Parr Jr, A.R. Far, J. Schaefer, Oritavancin Exhibits Dual Mode of Action to Inhibit Cell-Wall Biosynthesis in Staphylococcus aureus, J. Mol. Biol. 377 (2008) 281–293, https://doi.org/10.1016/j.jmb.2008.01.031.
[620] H. Yang, M. Singh, S.J. Kim, J. Schaefer, Characterization of the tertiary structure of the peptidoglycan of Enterococcus faecalis, BBA - Biomembr. 2017 (1859) 2171–2180, https://doi.org/10.1016/j.bbamem.2017.08.003.
[621] M. Singh, J. Chang, L. Coffman, S.J. Kim, Hidden Mode of Action of Glycopeptide Antibiotics: Inhibition of Wall Teichoic Acid Biosynthesis, J. Phys. Chem. B. 121 (2017) 3925–3932, https://doi.org/10.1021/acs.jpcb.7b00324.
[622] W. Vollmer, S.J. Seligman, Architecture of peptidoglycan: more data and more models, Trends Microbiol. 18 (2010) 59–66, https://doi.org/10.1016/j.tim.2009.12.004.
[623] C. Bougault, I. Ayala, W. Vollmer, J.-P. Simorre, P. Schanda, Studying intact bacterial peptidoglycan by proton-detected NMR spectroscopy at 100 kHz MAS frequency, J. Struct. Biol. 206 (2019) 66–72, https://doi.org/10.1016/j.jsb.2018.07.009.
[624] H. Takahashi, I. Ayala, M. Bardet, G. De Paëpe, J.-P. Simorre, S. Hediger, Solid-state NMR on bacterial cells: selective cell wall signal enhancement and resolution improvement using dynamic nuclear polarization, J. Am. Chem. Soc. 135 (2013) 5105–5110, https://doi.org/10.1021/ja312501d.
[625] J. Medeiros-Silva, S. Jekhmane, A.L. Paioni, K. Gawarecka, M. Baldus, E. Swiezewska, E. Breukink, M. Weingarth, High-resolution NMR studies of antibiotics in cellular membranes, Nat. Commun. 9 (2018) 3963–4010, https://doi.org/10.1038/s41467-018-06314-x.
[626] R. Shukla, J. Medeiros-Silva, A. Parmar, B.J.A. Vermeulen, S. Das, A.L. Paioni, S. Jekhmane, J. Lorent, A.M.J.J. Bonvin, M. Baldus, M. Lelli, E.J.A. Veldhuizen, E. Breukink, I. Singh, M. Weingarth, Mode of action of teixobactins in cellular membranes, Nat. Commun. (2020) 1–10, https://doi.org/10.1038/s41467-020-16600-2.
[627] D. Doskočilová, D.D. Tao, B. Schneider, Effects of macroscopic spinning upon linewidth of NMR signals of liquid in magnetically inhomogeneous systems, Czechoslov, J. Phys. B. 25 (1975) 202–209, https://doi.org/10.1007/BF01589476.
[628] D. Doskočilová, B. Schneider, J. Jakeš, NMR spectra of systems with restricted motion: Cross-linked polymer gels, J. Magn. Reson. 1969 (29) (1978) 79–90, https://doi.org/10.1016/0022-2364(78)90033-1.
[629] D.H. Burton, R.K. Harris, L.H. Merwin, Magic-angle rotation using a conventional Fourier transform NMR spectrometer, J. Magn. Reson. 1969 (39) (1980) 159–162, https://doi.org/10.1016/0022-2364(80)90167-5.
[630] V. Rutar, M. Kovač, G. Lahajnar, Improved NMR spectra of liquid components in heterogeneous samples, J. Magn. Reson. 1969 (80) (1988) 133–138, https://doi.org/10.1016/0022-2364(88)90065-0.
[631] W.L. Fitch, G. Detre, C.P. Holmes, J.N. Shoolery, P.A. Keifer, High-Resolution 1H NMR in Solid-Phase Organic Synthesis, J. Org. Chem. 59 (1994) 7955–7956, https://doi.org/10.1021/jo00105a006.
[632] J.-M. Wieruszeski, P. Talaga, G. Lippens, Development of a high-resolution magic-angle spinning nuclear magnetic resonance identity assay of the capsular polysaccharide from Haemophilus influenzae type b present in cetavlon precipitate, Anal. Biochem. 338 (2005) 20–25, https://doi.org/10.1016/j.ab.2004.10.038.
[633] W. Li, Multidimensional HRMAS NMR: a platform for in vivo studies using intact bacterial cells, Analyst. 131 (2006) 777–785, https://doi.org/10.1039/b605110c.
[634] W. Li, R.E.B. Lee, R.E. Lee, J. Li, Methods for Acquisition and Assignment of Multidimensional High-Resolution Magic Angle Spinning NMR of Whole Cell Bacteria, Anal. Chem. 77 (2005) 5785–5792, https://doi.org/10.1021/ac050906t.
[635] J.-P. Grivet, A.-M. Delort, NMR for microbiology: In vivo and in situ applications, 54 (2009) 1–53. https://doi.org/10.1016/j.pnmrs.2008.02.001..
[636] R.A. Wind, J.Z. Hu, In vivo and ex vivo high-resolution 1H NMR in biological systems using low-speed magic angle spinning, Prog. Nucl. Magn. Reson. Spectrosc. 49 (2006) 207–259, https://doi.org/10.1016/j.pnmrs.2006.05.003.
[637] E. Krainer, R.E. Stark, F. Naider, K. Alagramam, J.M. Becker, Direct observation of cell wall glucans in whole cells of Saccharomyces cerevisiae by magic-angle spinning 13C-NMR, Biopolymers. 34 (1994) 1627–1635, https://doi.org/10.1002/bip.360341207.
[638] W. Jachymek, T. Niedziela, C. Petersson, C. Lugowski, J. Czaja, L. Kenne, Structures of the O-Specific Polysaccharides from Yokenella regensburgei (Koserella trabulsii) Strains PCM 2476, 2477, 2478, and 2494: High-Resolution Magic-Angle Spinning NMR Investigation of the O-Specific Polysaccharides in Native Lipopolysaccharides and Directly on the Surface of Living Bacteria †, Biochemistry. 38 (1999) 11788–11795, https://doi.org/10.1021/bi990673y.
[639] J. Czaja, W. Jachymek, T. Niedziela, C. Lugowski, E. Aldova, L. Kenne, Structural studies of the O-specific polysaccharide from Plesiomonas shigelloides strain CNCTC 113/92, Eur. J. Biochem. 267 (2000) 1672–1679, https://doi.org/10.1046/j.1432-1327.2000.01161.x.
[640] G. Lippens, J.P. Bohin, Structural Diversity of the Osmoregulated Periplasmic Glucans of Gram-Negative Bacteria by a Combined Genetics and Nuclear Magnetic Resonance Approach., in: M. Pons (Ed.), NMR Supramol. Chem., Springer, Dordrecht, 1999: pp. 191–226. https://doi.org/10.1007/978-94-011-4615-9_13..
[641] J.M. Wieruszeski, A. Bohin, J.P. Bohin, G. Lippens, In Vivo Detection of the Cyclic Osmoregulated Periplasmic Glucan of Ralstonia solanacearum by High-Resolution Magic Angle Spinning NMR, J. Magn. Reson. 151 (2001) 118–123, https://doi.org/10.1006/jmre.2001.2348.
[642] F.S. Michael, C.M. Szymanski, J. Li, K.H. Chan, N.H. Khieu, S. Larocque, W.W. Wakarchuk, J.-R. Brisson, M.A. Monteiro, The structures of the lipooligosaccharide and capsule polysaccharide of Campylobacter jejuni genome sequenced strain NCTC 11168, Eur. J. Biochem. 269 (2002) 5119–5136, https://doi.org/10.1046/j.1432-1033.2002.03201.x.

[643] S. Bernatchez, C.M. Szymanski, N. Ishiyama, J. Li, H.C. Jarrell, P.C. Lau, A.M. Berghuis, N.M. Young, W.W. Wakarchuk, A Single Bifunctional UDP-GlcNAc/Glc 4-Epimerase Supports the Synthesis of Three Cell Surface Glycoconjugates in Campylobacter jejuni, J. Biol. Chem. 280 (2005) 4792–4802, https://doi.org/10.1074/jbc.M407767200.
[644] C.M. Szymanski, F.S. Michael, H.C. Jarrell, J. Li, M. Gilbert, S. Larocque, E. Vinogradov, J.-R. Brisson, Detection of Conserved N-Linked Glycans and Phase-variable Lipooligosaccharides and Capsules from Campylobacter Cells by Mass Spectrometry and High Resolution Magic Angle Spinning NMR Spectroscopy, J. Biol. Chem. 278 (2003) 24509–24520, https://doi.org/10.1074/jbc.M301273200.
[645] J. Kelly, H. Jarrell, L. Millar, L. Tessier, L.M. Fiori, P.C. Lau, B. Allan, C.M. Szymanski, Biosynthesis of the N-Linked Glycan in Campylobacter jejuni and Addition onto Protein through Block Transfer, J. Bacteriol. 188 (2006) 2427–2434, https://doi.org/10.1128/JB.188.7.2427-2434.2006.
[646] D.J. McNally, H.C. Jarrell, J. Li, N.H. Khieu, E. Vinogradov, C.M. Szymanski, J.-R. Brisson, The HS:1 serostrain of Campylobacter jejuni has a complex teichoic acid-like capsular polysaccharide with nonstoichiometric fructofuranose branches and O-methyl phosphoramidate groups, Febs J. 272 (2005) 4407–4422, https://doi.org/10.1111/j.1742-4658.2005.04856.x.
[647] D.J. McNally, M. Lamoureux, J. Li, J. Kelly, J.-R. Brisson, C.M. Szymanski, H.C. Jarrell, HR-MAS NMR studies of 15N-labeled cells confirm the structure of the O-methyl phosphoramidate CPS modification in Campylobacter jejuniand provide insight into its biosynthesis, Can. J. Chem. 84 (2006) 676–684, https://doi.org/10.1139/v06-028.
[648] S.K. Gudlavalleti, C.M. Szymanski, H.C. Jarrell, D.S. Stephens, In vivo determination of Neisseria meningitidis serogroup A capsular polysaccharide by whole cell high-resolution magic angle spinning NMR spectroscopy, Carbohydr. Res. 341 (2006) 557–562, https://doi.org/10.1016/j.carres.2005.11.036.
[649] A. Maciejewska, J. Lukasiewicz, T. Niedziela, Z. Szewczuk, C. Lugowski, Structural analysis of the O-specific polysaccharide isolated from Plesiomonas shigelloides O51 lipopolysaccharide, Carbohydr. Res. 344 (2009) 894–900, https://doi.org/10.1016/j.carres.2009.02.020.
[650] N. Ravenscroft, P. Cescutti, M. Gavini, G. Stefanetti, C.A. MacLennan, L.B. Martin, F. Micoli, Structural analysis of the O-acetylated O-polysaccharide isolated from Salmonella paratyphi A and used for vaccine preparation, Carbohydr. Res. 404 (2015) 108–116, https://doi.org/10.1016/j.carres.2014.12.002.
[651] K. Ucieklak, S. Koj, D. Pawelczyk, T. Niedziela, Structural Masquerade of Plesiomonas shigelloides Strain CNCTC 78/89 O-Antigen—High-Resolution Magic Angle Spinning NMR Reveals the Modified d-galactan I of Klebsiella pneumoniae, Int. J. Mol. Sci. 18 (2017) 2572–2614, https://doi.org/10.3390/ijms18122572.
[652] C.W. Reid, E. Vinogradov, J. Li, H.C. Jarrell, S.M. Logan, J.-R. Brisson, Structural characterization of surface glycans from Clostridium difficile, Carbohydr. Res. 354 (2012) 65–73, https://doi.org/10.1016/j.carres.2012.02.002.
[653] R.E.B. Lee, W. Li, D. Chatterjee, R.E. Lee, Rapid structural characterization of the arabinogalactan and lipoarabinomannan in live mycobacterial cells using 2D and 3D HR-MAS NMR: structural changes in the arabinan due to ethambutol treatment and gene mutation are observed, Glycobiology. 15 (2005) 139–151, https://doi.org/10.1093/glycob/cwh150.
[654] E. Maes, C. Mille, X. Trivelli, G. Janbon, D. Poulain, Y. Guérardel, Molecular Phenotyping of Mannosyltransferases-Deficient Candida albicans Cells by High-Resolution Magic Angle Spinning NMR, J. Biochem. (Tokyo) 145 (2009) 413–419, https://doi.org/10.1093/jb/mvp008.
[655] H.F. Azurmendi, J. Vionnet, L. Wrightson, L.B. Trinh, J. Shiloach, D.I. Freedberg, Extracellular structure of polysialic acid explored by on cell solution NMR, Proc. Natl. Acad. Sci. 104 (2007) 11557–11561, https://doi.org/10.1073/pnas.0704404104.
[656] G. Zandomeneghi, K. Ilg, M. Aebi, B.H. Meier, On-cell MAS NMR: physiological clues from living cells, J. Am. Chem. Soc. 134 (2012) 17513–17519, https://doi.org/10.1021/ja307467p.
[657] K. Ilg, G. Zandomeneghi, G. Rugarabamu, B.H. Meier, M. Aebi, HR-MAS NMR reveals a pH-dependent LPS alteration by de-O-acetylation at abequose in the O-antigen of Salmonella enterica serovar Typhimurium, Carbohydr. Res. 382 (2013) 58–64, https://doi.org/10.1016/j.carres.2013.10.002.
[658] D. Chapman, Phase transitions and fluidity characteristics of lipids and cell membranes, Q. Rev. Biophys. 8 (1975) 185–235, https://doi.org/10.1017/s0033583500001797.
[659] F. Podo, The application of nuclear magnetic resonance spectroscopy to the study of natural and model membranes, Biochimie. 57 (1975) 461–469, https://doi.org/10.1016/S0300-9084(75)80333-6.
[660] D. Chapman, V.B. Kamat, J.D. Gier, S.A. Penkett, Nuclear Magnetic Resonance Spectroscopic Studies of Erythrocyte Membranes, Nature. 213 (1967) 74–75, https://doi.org/10.1038/213074a0.
[661] D. Chapman, V.B. Kamat, J. de Gier, S.A. Penkett, Nuclear magnetic resonance studies of erythrocyte membranes, J. Mol. Biol. 31 (1968) 101–114, https://doi.org/10.1016/0022-2836(68)90058-2.
[662] L.R. Brown, J.H. Bradbury, K. Austin, P.R. Stewart, Comparison of membrane organization in mitochondria from yeast and rat liver by nuclear magnetic resonance spectroscopy, J. Membr. Biol. 24 (1975) 35–54, https://doi.org/10.1007/BF01868614.
[663] D.G. Davis, G. Inesi, T. Gulik-Krzywicki, Lipid molecular motion and enzyme activity in sarcoplasmic reticulum membrane, Biochemistry. 15 (1976) 1271–1276, https://doi.org/10.1021/bi00651a016.
[664] J.C. Metcalfe, N.J.M. Birdsall, A.G. Lee, 13C NMR spectra of acholeplasma membranes containing13C labelled phospholipids, FEBS Lett. 21 (1972) 335–340, https://doi.org/10.1016/0014-5793(72)80196-0.
[665] J.D. Robinson, N.J.M. Birdsall, A.G. Lee, J.C. Metcalfe, Carbon-13 and proton nuclear magnetic resonance relaxation measurements of the lipids of sarcoplasmic reticulum membranes, Biochemistry. 11 (1972) 2903–2909, https://doi.org/10.1021/bi00765a025.
[666] F. Millett, P.A. Hargrave, M.A. Raftery, Natural abundance 13C nuclear magnetic resonance spectra of the lipid in intact bovine retinal rod outer segment membranes, Biochemistry. 12 (1973) 3591–3592, https://doi.org/10.1021/bi00743a002.
[667] W. Stoffel, K. Bister, 13-C nuclear magnetic resonance studies on the lipid organization in enveloped virions (vesicular stomatitis virus), Biochemistry. 14 (1975) 2841–2847, https://doi.org/10.1021/bi00684a008.
[668] R.E. London, C.E. Hildebrand, E.S. Olson, N.A. Matwiyoff, Carbon-13 nuclear magnetic resonance spectroscopy of suspensions of chinese hamster ovary cells specifically enriched with (methyl-13C)choline, Biochemistry. 15 (1976) 5480–5486, https://doi.org/10.1021/bi00670a009.
[669] A.M.H.P. Van Den Besselaar, B. de Kruijff, H. van den Bosch, L.L.M. Van Deenen, Transverse distribution and movement of lysophosphatidylcholine in sarcoplasmic reticulum membranes as determined by 13C NMR and lysophospholipase, Biochim. Biophys. Acta BBA - Biomembr. 555 (1979) 193–199, https://doi.org/10.1016/0005-2736(79)90159-7.
[670] B. de Kruijff, A.M.H.P. Van Den Besselaar, H. van den Bosch, L.L.M. Van Deenen, Inside-outside distribution and diffusion of phosphatidylcholine in rat sarcoplasmic reticulum as determined by 13C NMR and phosphatidylcholine exchange protein, Biochim. Biophys. Acta BBA - Biomembr. 555 (1979) 181–192, https://doi.org/10.1016/0005-2736(79)90158-5.
[671] R.E. Jacobs, E. Oldfield, NMR of membranes, Prog. Nucl. Magn. Reson. Spectrosc. 14 (1980) 113–136, https://doi.org/10.1016/0079-6565(80)80006-9.
[672] A. Watts, P.J.R. Spooner, Phospholipid phase transitions as revealed by NMR, Chem. Phys. Lipids. 57 (1991) 195–211, https://doi.org/10.1016/0009-3084(91)90076-N.
[673] I.C.P. Smith, H.C. Jarrell, Deuterium and phosphorus NMR of microbial membranes, Acc. Chem. Res. 16 (1983) 266–272, https://doi.org/10.1021/ar00092a001.
[674] P.R. Cullis, B. de Kruijff, M.J. Hope, R. Nayar, A. Rietveld, A.J. Verkleij, Structural properties of phospholipids in the rat liver inner mitochondrial membrane. A 31P-NMR study, Biochim. Biophys. Acta BBA - Biomembr. 600 (1980) 625–635, https://doi.org/10.1016/0005-2736(80)90466-6.
[675] B. de Kruijff, A. Reitveld, P.R. Cullis, 31P-NMR studies on membrane phospholipids in microsomes, rat liver slices and intact perfused rat liver, Biochim. Biophys. Acta. 600 (1980) 343–357, https://doi.org/10.1016/0005-2736(80)90438-1.
[676] H. Akutsu, H. Satake, R.M. Franklin, Phosphorus nuclear magnetic resonance studies on the lipid-containing bacteriophage PM2+, Biochemistry. 19 (1980) 5264–5270, https://doi.org/10.1021/bi00564a018.
[677] J. Seelig, L. Tamm, L. Hymel, S. Fleischer, Deuterium and phosphorus nuclear magnetic resonance and fluorescence depolarization studies of functional reconstituted sarcoplasmic reticulum membrane vesicles, Biochemistry. 20 (1981) 3922–3932, https://doi.org/10.1021/bi00516a040.
[678] R. Deslauriers, I. Ekiel, R.A. Byrd, H.C. Jarrell, I.C.P. Smith, A,, 31P-NMR study of structural and functional aspects of phosphate and phosphonate distribution in Tetrahymena, Biochim. Biophys. Acta BBA - Mol. Cell Res. 720 (1982) 329–337, https://doi.org/10.1016/0167-4889(82)90109-4.
[679] J.F. Ellena, R.D. Pates, M.F. Brown, Phosphorus-31 NMR spectra of rod outer segment and sarcoplasmic reticulum membranes show no evidence of immobilized components due to lipid-protein interactions, Biochemistry. 25 (1986) 3742–3748, https://doi.org/10.1021/bi00361a002.
[680] J.A. Killian, C.H.J.P. Fabrie, W. Baart, S. Morein, B. de Kruijff, Effects of temperature variation and phenethyl alcohol addition on acyl chain order and lipid organization in Escherichia coli derived membrane systems. A 2H- and 31P-NMR study, Biochim. Biophys. Acta BBA - Biomembr. 1105 (1992) 253–262. https://doi.org/10.1016/0005-2736(92)90202-W..
[681] C.H.J.P. Fabrie, J.M.W. Smeets, B. de Kruijff, J. de Gier, The cryoprotectant trehalose destabilises the bilayer organisation of Escherichia coli-derived membrane systems at elevated temperatures as determined by 2H and 31P-NMR, Chem. Phys. Lipids. 70 (1994) 133–145, https://doi.org/10.1016/0009-3084(94)90081-7.
[682] J.H. Davis, K.R. Jeffrey, M. Bloom, M.I. Valic, T.P. Higgs, Quadrupolar echo deuteron magnetic resonance spectroscopy in ordered hydrocarbon chains, Chem. Phys. Lett. 42 (1976) 390–394, https://doi.org/10.1016/0009-2614(76)80392-2.
[683] J. Seelig, Deuterium magnetic resonance: theory and application to lipid membranes, Q. Rev. Biophys. 10 (1977) 353–418, https://doi.org/10.1017/S0033583500002948.
[684] J.H. Davis, The description of membrane lipid conformation, order and dynamics by 2H-NMR, Biochim. Biophys. Acta BBA - Rev. Biomembr. 737 (1983) 117–171, https://doi.org/10.1016/0304-4157(83)90015-1.
[685] X.L. Warnet, M. Laadhari, A.A. Arnold, I. Marcotte, D.E. Warschawski, A 2H magic-angle spinning solid-state NMR characterisation of lipid membranes in intact bacteria, Biochim. Biophys. Acta BBA - Biomembr. 2016 (1858) 146–152, https://doi.org/10.1016/j.bbamem.2015.10.020.
[686] T.R. Molugu, S. Lee, M.F. Brown, Concepts and Methods of Solid-State NMR Spectroscopy Applied to Biomembranes, Chem. Rev. 117 (2017) 12087–12132, https://doi.org/10.1021/acs.chemrev.6b00619.

[687] M. Rance, K.R. Jeffrey, A.P. Tulloch, K.W. Butler, I.C.P. Smith, Orientational order of unsaturated lipids in the membranes of Acholeplasma laidlawii as observed by 2H-NMR, Biochim. Biophys. Acta BBA - Biomembr. 600 (1980) 245–262, https://doi.org/10.1016/0005-2736(80)90430-7.
[688] I.C.P. Smith, K.W. Butler, A.P. Tulloch, J.H. Davis, M. Bloom, The properties of gel state lipid in membranes of *acholeplasma laidlawii* as observed by ^{2}H NMR, FEBS Lett. 100 (1979) 57–61, https://doi.org/10.1016/0014-5793(79)81130-8.
[689] E. Oldfield, D. Chapman, W. Derbyshire, Lipid mobility in Acholeplasma membranes using deuteron magnetic resonance, Chem. Phys. Lipids. 9 (1972) 69–81, https://doi.org/10.1016/0009-3084(72)90034-5.
[690] G.W. Stockton, K.G. Johnson, K.W. Butler, C.F. Polnaszek, R. Cyr, I.C.P. Smith, Molecular order in acholeplasma laidlawii membranes as determined by deuterium magnetic resonance of biosynthetically-incorporated specifically-labelled lipids, Biochim. Biophys. Acta BBA - Biomembr. 401 (1975) 535–539, https://doi.org/10.1016/0005-2736(75)90251-5.
[691] G.W. Stockton, K.G. Johnson, K.W. Butler, A.P. Tulloch, Y. Boulanger, I.C.P. Smith, J.H. Davis, M. Bloom, Deuterium NMR study of lipid organisation in Acholeplasma laidlawii membranes, Nature. 269 (1977) 267–268, https://doi.org/10.1038/269267a0.
[692] J.H. Davis, M. Bloom, K.W. Butler, I.C.P. Smith, The temperature dependence of molecular order and the influence of cholesterol in Acholeplasma laidlawii membranes, Biochim. Biophys. Acta BBA - Biomembr. 597 (1980) 477–491, https://doi.org/10.1016/0005-2736(80)90221-7.
[693] M. Rance, K.R. Jeffrey, A.P. Tulloch, K.W. Butler, I.C.P. Smith, Effects of cholesterol on the orientational order of unsaturated lipids in the membranes of Acholeplasma laidlawii: A 2H-NMR study, Biochim. Biophys. Acta BBA - Biomembr. 688 (1982) 191–200, https://doi.org/10.1016/0005-2736(82)90594-6.
[694] H.C. Jarrell, K.W. Butler, R.A. Byrd, R. Deslauriers, I. Ekiel, I.C.P. Smith, A 2H-NMR study of Acholeplasma laidlawii membranes highly enriched in myristic acid, Biochim. Biophys. Acta BBA - Biomembr. 688 (1982) 622–636, https://doi.org/10.1016/0005-2736(82)90373-X.
[695] M. Rance, I.C.P. Smith, H.C. Jarrell, The effect of headgroup class on the conformation of membrane lipids in Acholeplasma Laidlawii: A 2H-NMR study, Chem. Phys. Lipids. 32 (1983) 57–71, https://doi.org/10.1016/0009-3084(83)90070-1.
[696] T.H. Huang, A.J. DeSiervo, Q.X. Yang, Effect of cholesterol and lanosterol on the structure and dynamics of the cell membrane of Mycoplasma capricolum. Deuterium nuclear magnetic resonance study, Biophys. J. 59 (1991) 691–702, https://doi.org/10.1016/S0006-3495(91)82283-4.
[697] R.N. McElhaney, The structure and function of the Acholeplasma laidlawii plasma membrane, Biochim. Biophys. Acta BBA - Rev. Biomembr. 779 (1984) 1–42, https://doi.org/10.1016/0304-4157(84)90002-9.
[698] S.Y. Kang, H.S. Gutowsky, E. Oldfield, Spectroscopic studies of specifically deuterium labeled membrane systems.Nuclear magnetic resonance investigation of protein-lipid interactions in Escherichia coli membranes, Biochemistry. 18 (1979) 3268–3272, https://doi.org/10.1021/bi00582a011.
[699] H.U. Gally, G. Pluschke, P. Overath, J. Seelig, Structure of Escherichia coli membranes.Phospholipid conformation in model membranes and cells as studied by deuterium magnetic resonance, Biochemistry. 18 (1979) 5605–5610, https://doi.org/10.1021/bi00592a013.
[700] H.U. Gally, G. Pluschke, P. Overath, J. Seelig, Structure of Escherichia coli membranes. Fatty acyl chain order parameters of inner and outer membranes and derived liposomes, Biochemistry. 19 (1980) 1638–1643, https://doi.org/10.1021/bi00549a018.
[701] F. Borle, J. Seelig, Structure of Escherichia coli membranes. Deuterium magnetic resonance studies of the phosphoglycerol head group in intact cells and model membranes, Biochemistry. 22 (1983) 5536–5544, https://doi.org/10.1021/bi00293a013.
[702] J.H. Davis, C.P. Nichol, G. Weeks, M. Bloom, Study of the cytoplasmic and outer membranes of Escherichia coli by deuterium magnetic resonance, Biochemistry. 18 (1979) 2103–2112, https://doi.org/10.1021/bi00577a041.
[703] C.P. Nichol, J.H. Davis, G. Weeks, M. Bloom, Quantitative study of the fluidity of Escherichia coli membranes using deuterium magnetic resonance, Biochemistry. 19 (1980) 451–457, https://doi.org/10.1021/bi00544a008.
[704] B. Maraviglia, J.H. Davis, M. Bloom, J. Westerman, K.W.A. Wirtz, Human erythrocyte membranes are fluid down to −5°C, Biochim. Biophys. Acta BBA - Biomembr. 686 (1982) 137–140, https://doi.org/10.1016/0005-2736(82)90160-2.
[705] W. Curatolo, F.B. Jungalwala, B. Sears, L. Tuck, L.J. Neuringer, Deuterium NMR spectroscopy of biosynthetically deuterated mammalian tissues, Biochemistry. 24 (1985) 4360–4364, https://doi.org/10.1021/bi00337a017.
[706] M. Garnier-Lhomme, A. Grélard, R.D. Byrne, C. Loudet, E.J. Dufourc, B. Larijani, Probing the dynamics of intact cells and nuclear envelope precursor membrane vesicles by deuterium solid state NMR spectroscopy, Biochim. Biophys. Acta BBA - Biomembr. 1768 (2007) 2516–2527, https://doi.org/10.1016/j.bbamem.2007.06.004.
[707] J. Pius, M.R. Morrow, V. Booth, ^{2}H Solid-State Nuclear Magnetic Resonance Investigation of Whole *Escherichia coli* Interacting with Antimicrobial Peptide MSI-78, Biochemistry. 51 (2012) 118–125, https://doi.org/10.1021/bi201569t.
[708] C. Tardy-Laporte, A.A. Arnold, B. Genard, R. Gastineau, M. Morançais, J.-L. Mouget, R. Tremblay, I. Marcotte, A 2H solid-state NMR study of the effect of antimicrobial agents on intact Escherichia coli without mutating, BBA - Biomembr. 2013 (1828) 614–622, https://doi.org/10.1016/j.bbamem.2012.09.011.
[709] M. Laadhari, A.A. Arnold, A.E. Gravel, F. Separovic, I. Marcotte, Interaction of the antimicrobial peptides caerin 1.1 and aurein 1.2 with intact bacteria by 2 H solid-state NMR, Biochim. Biophys. Acta BBA - Biomembr. 1858 (2016) 2959–2964, https://doi.org/10.1016/j.bbamem.2016.09.009.
[710] N.P. Santisteban, M.R. Morrow, V. Booth, Effect of AMPs MSI-78 and BP100 on the lipid acyl chains of 2H-labeled intact Gram positive bacteria, Biochim. Biophys. Acta BBA - Biomembr. 1862 (2020), https://doi.org/10.1016/j.bbamem.2020.183199 183199.
[711] Z. Bouhlel, A.A. Arnold, D.E. Warschawski, K. Lemarchand, R. Tremblay, I. Marcotte, Labelling strategy and membrane characterization of marine bacteria Vibrio splendidus by in vivo2H NMR, BBA - Biomembr. 2019 (1861) 871–878, https://doi.org/10.1016/j.bbamem.2019.01.018.
[712] R.L. Smith, E. Oldfield, Dynamic structure of membranes by deuterium NMR, Nature. 225 (1984) 280–288, https://doi.org/10.1126/science.6740310.
[713] X.L. Warnet, A.A. Arnold, I. Marcotte, D.E. Warschawski, In-Cell Solid-State NMR: An Emerging Technique for the Study of Biological Membranes, Biophys. J. 109 (2015) 2461–2466, https://doi.org/10.1016/j.bpj.2015.10.041.
[714] V. Booth, D.E. Warschawski, N.P. Santisteban, M. Laadhari, I. Marcotte, Recent progress on the application of 2H solid-state NMR to probe the interaction of antimicrobial peptides with intact bacteria, BBA - Proteins Proteomics. 2017 (1865) 1500–1511, https://doi.org/10.1016/j.bbapap.2017.07.018.
[715] R.T. Eakin, L.O. Morgan, C.T. Gregg, N.A. Matwiyoff, Carbon-13 nuclear magnetic resonance spectroscopy of living cells and their metabolism of a specifically labeled 13C substrate, FEBS Lett. 28 (1972) 259–264, https://doi.org/10.1016/0014-5793(72)80726-9.
[716] F.E. Evans, N.O. Kaplan, 31P nuclear magnetic resonance studies of HeLa cells, Proc. Natl. Acad. Sci. 74 (1977) 4909–4913, https://doi.org/10.1073/pnas.74.11.4909.
[717] F.E. Evans, 31P nuclear magnetic resonance studies on relaxation parameters and line broadening of intracellular metabolites of HeLa cells, Arch. Biochem. Biophys. 193 (1979) 63–75, https://doi.org/10.1016/0003-9861(79)90009-2.
[718] U. Séquin, A.I. Scott, Carbon-13 as a label in biosynthetic studies, Nature. 186 (1974) 101–107, https://doi.org/10.1126/science.186.4159.101.
[719] A.G. McInnes, J.L.C. Wright, Use of carbon-13 magnetic resonance spectroscopy for biosynthetic investigations, Acc. Chem. Res. 8 (1975) 1–8, https://doi.org/10.1021/ar50093a005.
[720] N.A. Matwiyoff, T.E. Needham, Carbon-13 NMR spectroscopy of red blood cell suspensions, Biochem. Biophys. Res. Commun. 49 (1972) 1158–1164, https://doi.org/10.1016/0006-291x(72)90590-6.
[721] N.A. Matwiyoff, P.J. Vergamini, T.E. Needham, C.T. Gregg, J.A. Volpe, W.S. Caughey, Carbon-13 nuclear magnetic resonance and infrared spectroscopic studies of 13 CO binding to rabbit hemoglobin, J. Am. Chem. Soc. 95 (1973) 4429–4431, https://doi.org/10.1021/ja00794a054.
[722] R.T. Eakin, L.O. Morgan, N.A. Matwiyoff, Carbon-13 nuclear-magnetic-resonance spectroscopy of whole cells and of cytochrome C from Neurospora crass grown with (S-Me-13C)methionine, Biochem. J. 152 (1975) 529–535, https://doi.org/10.1042/bj1520529.
[723] J.R. Alger, L.O. Sillerud, K.L. Behar, R.J. Gillies, R.G. Shulman, R.E. Gordon, D. Shae, P.E. Hanley, In vivo carbon-13 nuclear magnetic resonance studies of mammals, Science. 214 (1981) 660–662, https://doi.org/10.1126/science.7292005.
[724] K. Ugurbil, T.R. Brown, J.A. den Hollander, P. Glynn, R.G. Shulman, High-resolution 13C nuclear magnetic resonance studies of glucose metabolism in Escherichia coli, Proc. Natl. Acad. Sci. 75 (1978) 3742–3746, https://doi.org/10.1073/pnas.75.8.3742.
[725] S.M. Cohen, S. Ogawa, R.G. Shulman, 13C NMR studies of gluconeogenesis in rat liver cells: Utilization of labeled glycerol by cells from euthyroid and hyperthyroid rats, Proc. Natl. Acad. Sci. 76 (1979) 1603–1607, https://doi.org/10.1073/pnas.76.4.1603.
[726] S.M. Cohen, R. Rognstad, R.G. Shulman, J. Katz, A comparison of 13C nuclear magnetic resonance and 14C tracer studies of hepatic metabolism, J. Biol. Chem. 256 (1981) 3428–3432.
[727] S.M. Cohen, P. Glynn, R.G. Shulman, 13C NMR study of gluconeogenesis from labeled alanine in hepatocytes from euthyroid and hyperthyroid rats, Proc. Natl. Acad. Sci. 78 (1981) 60–64, https://doi.org/10.1073/pnas.78.1.60.
[728] J.A. den Hollander, T.R. Brown, K. Ugurbil, R.G. Shulman, 13C nuclear magnetic resonance studies of anaerobic glycolysis in suspensions of yeast cells, Proc. Natl. Acad. Sci. 76 (1979) 6096–6100, https://doi.org/10.1073/pnas.76.12.6096.
[729] J.A. den Hollander, K.L. Behar, R.G. Shulman, 13C NMR study of transamination during acetate utilization by Saccharomyces cerevisiae, Proc. Natl. Acad. Sci. 78 (1981) 2693–2697, https://doi.org/10.1073/pnas.78.5.2693.
[730] J.M. Thevelein, J.A. den Hollander, R.G. Shulman, Changes in the activity and properties of trehalase during early germination of yeast ascospores: Correlation with trehalose breakdown as studied by in vivo13C NMR, Proc. Natl. Acad. Sci. 79 (1982) 3503–3507, https://doi.org/10.1073/pnas.79.11.3503.
[731] J.K. Barton, J.A. den Hollander, J.J. Hopfield, R.G. Shulman, 13C nuclear magnetic resonance study of trehalose mobilization in yeast spores, J. Bacteriol. 151 (1982) 177–185.
[732] A.I. Scott, G. Burton, P.E. Fagerness, Direct observation of porphyrinogen biosynthesis in living cells by 13C n.m.r. spectroscopy, J. Chem. Soc. Chem. Commun. (1979) 199–204, https://doi.org/10.1039/c39790000199.
[733] G. Burton, R.L. Baxter, J.M. Gunn, P.J. Sidebottom, P.E. Fagerness, K. Shishido, J. Y. Lee, A.I. Scott, Direct non-invasive observation of metabolism in living cells by 13C nuclear magnetic resonance spectroscopy, Can. J. Chem. 58 (1980) 1839–1846, https://doi.org/10.1139/v80-289.

[734] G. Burton, P.M. Jordan, N.E. MacKenzie, P.E. Fagerness, A.I. Scott, Control of porphyrin biosynthesis in Rhodopseudomonas spheroides and Propionibacterium shermanii. A direct 13C nuclear-magnetic-resonance spectroscopy study, Biochem. J. 194 (1981) 627–631, https://doi.org/10.1042/bj1940627.
[735] N.E. MacKenzie, J.E. Hall, J.R. Seed, A.I. Scott, Carbon-13 nuclear-magnetic-resonance studies of glucose catabolism by Trypanosoma brucei gambiense, Eur. J. Biochem. 121 (1982) 657–661, https://doi.org/10.1111/j.1432-1033.1982.tb05836.x.
[736] K. Nicolay, K.J. Hellingwerf, R. Kaptein, W.N. Konings, Carbon-13 nuclear magnetic resonance studies of acetate metabolism in intact cells of Rhodopseudomonas sphaeroides, Biochim. Biophys. Acta BBA - Mol. Cell Res. 720 (1982) 250–258, https://doi.org/10.1016/0167-4889(82)90048-9.
[737] K. Nicolay, H. van Gemerden, K.J. Hellingwerf, W.N. Konings, R. Kaptein, In vivo 31P and 13C nuclear magnetic resonance studies of acetate metabolism in Chromatium vinosum, J. Bacteriol. 155 (1983) 634–642.
[738] D.J. Ashworth, I.J. Mettler, Direct observation of glycine metabolism in tobacco suspension cells by carbon-13 NMR spectroscopy, Biochemistry. 23 (1984) 2252–2257, https://doi.org/10.1021/bi00305a025.
[739] D.J. Ashworth, C.S. Chen, Desmond. Mascarenhas, Direct observation of tryptophan biosynthesis in Escherichia coli by carbon-13 nuclear magnetic resonance spectroscopy, Anal. Chem. 58 (1986) 526–532. https://doi.org/10.1021/ac00294a006..
[740] H. Sahm, L. Eggeling, A.A. de Graaf, Pathway Analysis and Metabolic Engineering in Corynebacterium glutamicum, Biol. Chem. 381 (2000) 2145–2212, https://doi.org/10.1515/BC.2000.111.
[741] T.E. Walker, C.H. Han, V.H. Kollman, R.E. London, N.A. Matwiyoff, 13C nuclear magnetic resonance studies of the biosynthesis by Microbacterium ammoniaphilum of L-glutamate selectively enriched with carbon-13, J. Biol. Chem. 257 (1982) 1189–1195.
[742] S. Petersen, A.A. De Graaf, L. Eggeling, M. Möllney, W. Wiechert, H. Sahm, In vivo quantification of parallel and bidirectional fluxes in the anaplerosis of Corynebacterium glutamicum, J. Biol. Chem. 275 (2000) 35932–35941, https://doi.org/10.1074/jbc.M908728199.
[743] F.S. Ezra, D.S. Lucas, R.V. Mustacich, A.F. Russell, Phosphorus-31 and carbon-13 nuclear magnetic resonance studies of anaerobic glucose metabolism and lactate transport in Staphylococcus aureus cells, Biochemistry. 22 (1983) 3841–3849, https://doi.org/10.1021/bi00285a020.
[744] M.T. Ferreira, A.S. Manso, P. Gaspar, M.G. Pinho, A.R. Neves, Effect of Oxygen on Glucose Metabolism: Utilization of Lactate in Staphylococcus Aureus as Revealed by In Vivo NMR Studies, PLoS ONE. 8 (2013) e58277–e58312, https://doi.org/10.1371/journal.pone.0058277.
[745] J.A. den Hollander, K. Ugurbil, R.G. Shulman, 31P and 13C NMR studies of intermediates of aerobic and anaerobic glycolysis in Saccharomyces cerevisiae, Biochemistry. 25 (1986) 212–219, https://doi.org/10.1021/bi00349a030.
[746] S.L. Campbell-Burk, J.A. den Hollander, J.R. Alger, R.G. Shulman, 31P NMR saturation-transfer and 13C NMR kinetic studies of glycolytic regulation during anaerobic and aerobic glycolysis, Biochemistry. 26 (1987) 7493–7500, https://doi.org/10.1021/bi00397a044.
[747] S. Tran-Dinh, M. Hervé, O. Lebourguais, M. Jerome, J. Wietzerbin, Effects of amphotericin B on the glucose metabolism in Saccharomyces cerevisiae cells. Studies by 13C-, 1H-NMR and biochemical methods, Eur. J. Biochem. 197 (1991) 271–279, https://doi.org/10.1111/j.1432-1033.1991.tb15908.x.
[748] S. Tran-Dinh, M. Hervé, J. Wietzerbin, Determination of flux through different metabolite pathways in Saccharomyces cerevisiae by 1H-NMR and 13C-NMR spectroscopy, Eur. J. Biochem. 201 (1991) 715–721, https://doi.org/10.1111/j.1432-1033.1991.tb16333.x.
[749] J.P. Grivet, J. Stevani, G. Hannequart, M. Durand, In vivo 13C NMR studies of glucose catabolism by isolated rumen bacteria, Reprod. Nutr. Dev. 29 (1989) 83–88, https://doi.org/10.1051/rnd:19890106.
[750] J. Stevani, J.P. Grivet, G. Hannequart, M. Durand, Glucose and lactate catabolism by bacteria of the pig large intestine and sheep rumen as assessed by 13C nuclear magnetic resonance, J. Appl. Bacteriol. 71 (1991) 524–530, https://doi.org/10.1111/j.1365-2672.1991.tb03827.x.
[751] J.P. Grivet, M. Durand, J.L. Tholozan, 13C NMR studies of bacterial fermentations, Biochimie. 74 (1992) 897–901, https://doi.org/10.1016/0300-9084(92)90073-n.
[752] A.R. Neves, A. Ramos, C. Shearman, M.J. Gasson, J.S. Almeida, H. Santos, Metabolic characterization of Lactococcus lactis deficient in lactate dehydrogenase using in vivo 13C-NMR, Eur. J. Biochem. 267 (2000) 3859–3868, https://doi.org/10.1046/j.1432-1327.2000.01424.x.
[753] A.R. Neves, R. Ventura, N. Mansour, C. Shearman, M.J. Gasson, C. Maycock, A. Ramos, H. Santos, Is the glycolytic flux in Lactococcus lactis primarily controlled by the redox charge? Kinetics of NAD(+) and NADH pools determined in vivo by 13C NMR, J. Biol. Chem. 277 (2002) 28088–28098, https://doi.org/10.1074/jbc.M202573200.
[754] A.R. Neves, A. Ramos, H. Costa, I.I. van Swam, J. Hugenholtz, M. Kleerebezem, W. de Vos, H. Santos, Effect of Different NADH Oxidase Levels on Glucose Metabolism by Lactococcus lactis: Kinetics of Intracellular Metabolite Pools Determined by In Vivo Nuclear Magnetic Resonance, Appl. Environ. Microbiol. 68 (2002) 6332–6342, https://doi.org/10.1128/AEM.68.12.6332-6342.2002.
[755] B.K. Hunter, K.M. Nicholls, J.K. Sanders, Formaldehyde metabolism by Escherichia coli. In vivo carbon, deuterium, and two-dimensional NMR observations of multiple detoxifying pathways, Biochemistry. 23 (1984) 508–514, https://doi.org/10.1021/bi00298a017.
[756] K. Walsh, D.E. Koshland, Determination of flux through the branch point of two metabolic cycles. The tricarboxylic acid cycle and the glyoxylate shunt, J. Biol. Chem. 259 (1984) 9646–9654.
[757] A. Narbad, M.J.E. Hewlins, A.G. Callely, 13C-NMR Studies of Acetate and Methanol Metabolism by Methylotrophic Pseudomonas Strains, Microbiology. 135 (1989) 1469–1477, https://doi.org/10.1099/00221287-135-6-1469.
[758] J.G. Jones, E. Bellion, In vivo 13C and 15N NMR studies of methylamine metabolism in Pseudomonas species MA, J. Biol. Chem. 266 (1991) 11705–11713.
[759] J.G. Jones, E. Bellion, Methylamine metabolism in Hansenula polymorpha: an in vivo 13C and 31P nuclear magnetic resonance study, J. Bacteriol. 173 (1991) 4959–4969, https://doi.org/10.1128/jb.173.16.4959-4969.1991.
[760] J.G. Jones, E. Bellion, Methanol oxidation and assimilation in Hansenula polymorpha. An analysis by 13C n.m.r. in vivo, Biochem. J. 280 (1991) 475–481, https://doi.org/10.1042/bj2800475.
[761] R.G. Shulman, Contributions of 13C and 1H NMR to physiological control, Ann. N. Y. Acad. Sci. 508 (1987) 10–15, https://doi.org/10.1111/j.1749-6632.1987.tb32890.x.
[762] J. Fernández-García, P. Altea-Manzano, E. Pranzini, S.-M. Fendt, Stable Isotopes for Tracing Mammalian-Cell Metabolism In Vivo, Trends Biochem. Sci. 45 (2020) 185–201, https://doi.org/10.1016/j.tibs.2019.12.002.
[763] N.E. MacKenzie, J. Johnson, G. Burton, G.G. Wagner, A.I. Scott, 13C NMR studies of glycolysis in intra- and extra-erythrocytic Babesia microti, Mol. Biochem. Parasitol. 13 (1984) 13–20, https://doi.org/10.1016/0166-6851(84)90097-5.
[764] A. Ferretti, A. Bozzi, M. Di Vito, F. Podo, R. Strom, 13C and 31P NMR studies of glucose and 2-deoxyglucose metabolism in normal and enzyme-deficient human erythrocytes, Clin. Chim. Acta Int. J. Clin. Chem. 208 (1992) 39–61, https://doi.org/10.1016/0009-8981(92)90021-h.
[765] R.C. Lyon, P.J. Faustino, J.S. Cohen, A perfusion technique for 13C NMR studies of the metabolism of 13C-labeled substrates by mammalian cells, Magn. Reson. Med. 3 (1986) 663–672, https://doi.org/10.1002/mrm.1910030503.
[766] R.C. Lyon, J.S. Cohen, P.J. Faustino, F. Megnin, C.E. Myers, Glucose metabolism in drug-sensitive and drug-resistant human breast cancer cells monitored by magnetic resonance spectroscopy, Cancer Res. 48 (1988) 870–877.
[767] O. Kaplan, G. Navon, R.C. Lyon, P.J. Faustino, E.J. Straka, J.S. Cohen, Effects of 2-deoxyglucose on drug-sensitive and drug-resistant human breast cancer cells: toxicity and magnetic resonance spectroscopy studies of metabolism, Cancer Res. 50 (1990) 544–551.
[768] O. Kaplan, J.S. Cohen, Metabolism of breast cancer cells as revealed by non-invasive magnetic resonance spectroscopy studies, Breast Cancer Res. Treat. 31 (1994) 285–299, https://doi.org/10.1007/BF00666161.
[769] A.W. Jans, D. Leibfritz, A 13C-NMR study on the influxes into the tricarboxylic acid cycle of a renal epithelial cell line, LLC-PK1/Cl4: the metabolism of [2-13C]glycine, L-[3-13C]alanine and L-[3-13C]aspartic acid in renal epithelial cells, Biochim. Biophys. Acta. 970 (1988) 241–250, https://doi.org/10.1016/0167-4889(88)90123-1.
[770] A.W. Jans, R. Willem, A 13C NMR study of the application of [U-13C]succinate for metabolic investigations in rabbit renal proximal convoluted tubular cells, Magn. Reson. Med. 14 (1990) 148–153, https://doi.org/10.1002/mrm.1910140114.
[771] A. Mancuso, S.T. Sharfstein, S.N. Tucker, D.S. Clark, H.W. Blanch, Examination of primary metabolic pathways in a murine hybridoma with carbon-13 nuclear magnetic resonance spectroscopy, Biotechnol. Bioeng. 44 (1994) 563–585, https://doi.org/10.1002/bit.260440504.
[772] S.M. Cohen, R.G. Shulman, 13C n.m.r. studies of gluconeogenesis in rat liver suspensions and perfused mouse livers, Philos. Trans. R. Soc. B Biol. Sci. 289 (1980) 407–411, https://doi.org/10.1098/rstb.1980.0057.
[773] G. Melkus, H. Rolletschek, J. Fuchs, V. Radchuk, E. Grafahrend-Belau, N. Sreenivasulu, T. Rutten, D. Weier, N. Heinzel, F. Schreiber, T. Altmann, P.M. Jakob, L. Borisjuk, Dynamic $^{13}C/^{1}H$ NMR imaging uncovers sugar allocation in the living seed, Plant Biotechnol. J. 9 (2011) 1022–1037, https://doi.org/10.1111/j.1467-7652.2011.00618.x.
[774] J. Valette, B. Tiret, F. Boumezbeur, Experimental strategies for in vivo 13 C NMR spectroscopy, Anal. Biochem. 529 (2017) 216–228, https://doi.org/10.1016/j.ab.2016.08.003.
[775] M. Lai, R. Gruetter, B. Lanz, Progress towards in vivo brain 13C-MRS in mice: Metabolic flux analysis in small tissue volumes, Anal. Biochem. 529 (2017) 229–244, https://doi.org/10.1016/j.ab.2017.01.019.
[776] R.E. London, 13C labeling in studies of metabolic regulation, Prog. Nucl. Magn. Reson. Spectrosc. 20 (1988) 337–383, https://doi.org/10.1016/0079-6565(88)80010-4.
[777] J.S. Cohen, R.C. Lyon, Multinuclear NMR Study of the Metabolism of Drug-Sensitive and Drug-Resistant Human Breast Cancer Cells, Ann. N. Y. Acad. Sci. 508 (1987) 216–228, https://doi.org/10.1111/j.1749-6632.1987.tb32906.x.
[778] M. Neeman, H. Degani, Early estrogen-induced metabolic changes and their inhibition by actinomycin D and cycloheximide in human breast cancer cells: 31P and 13C NMR studies, Proc. Natl. Acad. Sci. 86 (1989) 5585–5589, https://doi.org/10.1073/pnas.86.14.5585.
[779] M. Neeman, H. Eldar, E. Rushkin, H. Degani, Chemotherapy-induced changes in the energetics of human breast cancer cells; 31P- and 13C-NMR studies, Biochim. Biophys. Acta BBA - Mol. Cell Res. 1052 (1990) 255–263, https://doi.org/10.1016/0167-4889(90)90219-4.

[780] K. Berghmans, J. Ruiz-Cabello, H. Simpkins, P.A. Andrews, J.S. Cohen, Increase in the ATP signal after treatment with cisplatin in two different cell lines studied by 31P NMR spectroscopy, Biochem. Biophys. Res. Commun. 183 (1992) 114–120, https://doi.org/10.1016/0006-291X(92)91616-X.
[781] H.M. Sonawat, D. Leibfritz, J. Engel, P. Hilgard, Biotransformation of mafosfamide in P388 mice leukemia cells: Intracellular 31P-NMR studies, Biochim. Biophys. Acta BBA - Mol. Cell Res. 1052 (1990) 36–41, https://doi.org/10.1016/0167-4889(90)90054-H.
[782] F. Commodari, B.C. Sanctuary, W. Feindel, E.A. Shoubridge, Alkalosis monitored by31P NMR in a human glioma cell line exposed to the anti-tumor drug 1, 3-bis (2-chloroethyl)-1-nitrosourea, Magn. Reson. Med. 22 (1991) 394–403, https://doi.org/10.1002/mrm.1910220247.
[783] J.F.M. Post, E. Baum, E.L. Ezell, 13CNMR studies of glucose metabolism in human leukemic CEM-C7 and CEM-C1 cells, Magn. Reson. Med. 23 (1992) 356–366, https://doi.org/10.1002/mrm.1910230215.
[784] C.E. Ng, K.A. Mcgovern, J.P. Wehrle, J.D. Glickson, 31p NMR spectroscopic study of the effects of γ-irradiation on rif-1 tumor cells perfused in vitro, Magn. Reson. Med. 27 (1992) 296–309, https://doi.org/10.1002/mrm.1910270209.
[785] N.R. Aiken, K.A. McGovern, C.E. Ng, J.P. Wehrle, J.D. Glickson, 31P NMR spectroscopic studies of the effects of cyclophosphamide on perfused RIF-1 tumor cells, Magn. Reson. Med. 31 (1994) 241–247, https://doi.org/10.1002/mrm.1910310302.
[786] R.J. Gillies, J.A. Barry, B.D. Ross, In Vitro and in Vivo 13C and 31P NMR analyses of phosphocholine metabolism in rat glioma cells, Magn. Reson. Med. 32 (1994) 310–318, https://doi.org/10.1002/mrm.1910320306.
[787] M.J. Goger, I.S. Login, E.J. Fernandez, C.M. Grisham, 31P NMR investigation of energy metabolism in perifused MMQ cells, Magn. Reson. Med. 32 (1994) 584–591, https://doi.org/10.1002/mrm.1910320507.
[788] J. Ruiz-Cabello, K. Berghmans, O. Kaplan, M.E. Lippman, R. Clarke, J.S. Cohen, Hormone dependence of breast cancer cells and the effects of tamoxifen and estrogen:31P NMR studies, Breast Cancer Res. Treat. 33 (1995) 209–217, https://doi.org/10.1007/BF00665945.
[789] J.-P. Galons, C. Job, R.J. Gillies, Increase of GPC Levels in Cultured Mammalian Cells during Acidosis. A31P MR Spectroscopy Study Using a Continuous Bioreactor System, Magn. Reson. Med. 33 (1995) 422–426, https://doi.org/10.1002/mrm.1910330317.
[790] A. Vivi, M. Tassini, H. Ben-Horin, G. Navon, O. Kaplan, Comparison of action of the anti-neoplastic drug lonidamine on drug-sensitive and drug-resistant human breast cancer cells:31 P and 13C nuclear magnetic resonance studies, Breast Cancer Res. Treat. 43 (1997) 15–25, https://doi.org/10.1023/A:1005781320906.
[791] K.M. Brindle, Investigating the Performance of Intensive Mammalian Cell Bioreactor Systems Using Magnetic Resonance Imaging and Spectroscopy, Biotechnol. Genet. Eng. Rev. 15 (1998) 499–520, https://doi.org/10.1080/02648725.1998.10647967.
[792] K. Glunde, E. Ackerstaff, K. Natarajan, D. Artemov, Z.M. Bhujwalla, Real-time changes in1H and31P NMR spectra of malignant human mammary epithelial cells during treatment with the anti-inflammatory agent indomethacin, Magn. Reson. Med. 48 (2002) 819–825, https://doi.org/10.1002/mrm.10295.
[793] A. Mancuso, N.J. Beardsley, S. Wehrli, S. Pickup, F.M. Matschinsky, J.D. Glickson, Real-time detection of 13C NMR labeling kinetics in perfused EMT6 mouse mammary tumor cells and βHC9 mouse insulinomas, Biotechnol. Bioeng. 87 (2004) 835–848, https://doi.org/10.1002/bit.20191.
[794] A. Mancuso, A. Zhu, N.J. Beardsley, J.D. Glickson, S. Wehrli, S. Pickup, Artificial tumor model suitable for monitoring 31P and 13C NMR spectroscopic changes during chemotherapy-induced apoptosis in human glioma cells, Magn. Reson. Med. 54 (2005) 67–78, https://doi.org/10.1002/mrm.20545.
[795] H. Farghali, L. Rossaro, J.S. Gavaler, D.H. Van Thiel, S.R. Dowd, D.S. Williams, C. Ho, 31P-NMR spectroscopy of perifused rat hepatocytes immobilized in agarose threads: application to chemical-induced hepatotoxicity, Biochim. Biophys. Acta BBA - Mol. Basis Dis. 1139 (1992) 105–114, https://doi.org/10.1016/0925-4439(92)90089-6.
[796] A. Gasbarrini, A.B. Borle, P. Caraceni, A. Colantoni, H. Farghali, F. Trevisani, M. Bernardi, D.H. van Thiel, Effect of ethanol on adenosine triphosphate, cytosolic free calcium, and cell injury in rat hepatocytes: Time course and effect of nutritional status, Dig. Dis. Sci. 41 (1996) 2204–2212, https://doi.org/10.1007/BF02071401.
[797] A. Mancuso, S.T. Sharfstein, E.J. Fernandez, D.S. Clark, H.W. Blanch, Effect of extracellular glutamine concentration on primary and secondary metabolism of a murine hybridoma: An in vivo 13C nuclear magnetic resonance study, Biotechnol. Bioeng. 57 (1998) 172–186, https://doi.org/10.1002/(SICI)1097-0290(19980120)57:2<172::AID-BIT6>3.0.CO;2-K.
[798] T. Szyperski, 13C-NMR, MS and metabolic flux balancing in biotechnology research, Q. Rev. Biophys. 31 (1998) 41–106, https://doi.org/10.1017/s0033583598003412.
[799] T.W.M. Fan, A.N. Lane, Applications of NMR spectroscopy to systems biochemistry, Prog. Nucl. Magn. Reson. Spectrosc. 92–93 (2016) 18–53, https://doi.org/10.1016/j.pnmrs.2016.01.005.
[800] S. Niedenführ, W. Wiechert, K. Nöh, How to measure metabolic fluxes: a taxonomic guide for (13)C fluxomics, Curr. Opin. Biotechnol. 34 (2015) 82–90, https://doi.org/10.1016/j.copbio.2014.12.003.
[801] R.G. Shulman, T.R. Brown, K. Ugurbil, S. Ogawa, S.M. Cohen, J.A. den Hollander, Cellular applications of 31P and 13C nuclear magnetic resonance, Science. 205 (1979) 160–166, https://doi.org/10.1126/science.36664.
[802] P. Styles, C. Grathwohl, F.F. Brown, Simultaneous multinuclear NMR by alternate scan recording of 3P and 13C spectra, J. Magn. Reson. 1969 (35) (1979) 329–336, https://doi.org/10.1016/0022-2364(79)90054-4.
[803] T.O. Henderson, A.J. Costello, A. Omachi, Phosphate metabolism in intact human erythrocytes: determination by phosphorus-31 nuclear magnetic resonance spectroscopy, Proc. Natl. Acad. Sci. 71 (1974) 2487–2490, https://doi.org/10.1073/pnas.71.6.2487.
[804] H.B. Pollard, H. Shindo, C.E. Creutz, C.J. Pazoles, J.S. Cohen, Internal pH and state of ATP in adrenergic chromaffin granules determined by 31P nuclear magnetic resonance spectroscopy, J. Biol. Chem. 254 (1979) 1170–1177.
[805] J.K. Roberts, N. Wade-Jardetzky, O. Jardetzky, Intracellular pH measurements by 31P nuclear magnetic resonance. Influence of factors other than pH on 31P chemical shifts, Biochemistry. 20 (1981) 5389–5394, https://doi.org/10.1021/bi00522a006.
[806] W.E. Jacobus, G.J. TAYLOR, D.P. Hollis, R.L. Nunnally, Phosphorus nuclear magnetic resonance of perfused working rat hearts, Nature. 265 (1977) 756–758. https://doi.org/10.1038/265756a0..
[807] D.P. Hollis, R.L. Nunnally, G.J. Taylor IV, M.L. Weisfeldt, W.E. Jacobus, Phosphorus nuclear magnetic resonance studies of heart physiology, J. Magn. Reson. 1969 (29) (1978) 319–330, https://doi.org/10.1016/0022-2364(78)90156-7.
[808] P.A. Sehr, G.K. Radda, P.J. Bore, R.A. Sells, A model kidney transplant studied by phosphorus nuclear magnetic resonance, Biochem. Biophys. Res. Commun. 77 (1977) 195–202, https://doi.org/10.1016/S0006-291X(77)80182-4.
[809] A.C. McLaughlin, H. Takeda, B. Chance, Rapid ATP assays in perfused mouse liver by 31P NMR, Proc. Natl. Acad. Sci. 76 (1979) 5445–5449, https://doi.org/10.1073/pnas.76.11.5445.
[810] C.T. Burt, T. Glonek, M. Bárány, Analysis of phosphate metabolites, the intracellular pH, and the state of adenosine triphosphate in intact muscle by phosphorus nuclear magnetic resonance, J. Biol. Chem. 251 (1976) 2584–2591.
[811] M.J. Dawson, D.G. Gadian, D.R. Wilkie, Muscular fatigue investigated by phosphorus nuclear magnetic resonance, Nature. 274 (1978) 861–866, https://doi.org/10.1038/274861a0.
[812] P.B. Garlick, G.K. Radda, P.J. Seeley, Studies of acidosis in the ischaemic heart by phosphorus nuclear magnetic resonance, Biochem. J. 184 (1979) 547–554, https://doi.org/10.1042/bj1840547.
[813] C.T. Burt, T. Glonek, M. Bárány, Analysis of living tissue by phosphorus-31 magnetic resonance, Science. 195 (1977) 145–149, https://doi.org/10.1126/science.188132.
[814] R.A. Iles, J.R. Griffiths, A.N. Stevens, D.G. Gadian, R. Porteous, Effects of fructose on the energy metabolism and acid-base status of the perfused starved-rat liver. A 31 phosphorus nuclear magnetic resonance study, Biochem. J. 192 (1980) 191–202, https://doi.org/10.1042/bj1920191.
[815] B. Chance, Y. Nakase, M. Bond, J.S. Leigh, G. McDonald, Detection of 31P nuclear magnetic resonance signals in brain by in vivo and freeze-trapped assays, Proc. Natl. Acad. Sci. 75 (1978) 4925–4929, https://doi.org/10.1073/pnas.75.10.4925.
[816] J.J. Ackerman, T.H. Grove, G.G. Wong, D.G. Gadian, G.K. Radda, Mapping of metabolites in whole animals by 31p nmr using surface coils, Nature. 283 (1980) 167–170, https://doi.org/10.1038/283167a0.
[817] R.E. Gordon, P.E. Hanley, D. Shaw, D.G. Gadian, G.K. Radda, P. Styles, P.J. Bore, L. Chan, Localization of metabolites in animals using 31P topical magnetic resonance, Nature. 287 (1980) 736–738, https://doi.org/10.1038/287736a0.
[818] T.H. Grove, J.J. Ackerman, G.K. Radda, P.J. Bore, Analysis of rat heart in vivo by phosphorus nuclear magnetic resonance, Proc. Natl. Acad. Sci. 77 (1980) 299–302, https://doi.org/10.1073/pnas.77.1.299.
[819] G.K. Radda, J.J.H. Ackerman, P. Bore, P. Sehr, G.G. Wong, B.D. Ross, Y. Green, S. Bartlett, M. Lowry, 31P NMR studies on kidney intracellular pH in acute renal acidosis, Int. J. Biochem. 12 (1980) 277–281, https://doi.org/10.1016/0020-711X(80)90084-1.
[820] G.K. Radda, P.J. Bore, B. Rajagopalan, Clinical aspects of 31P NMR spectroscopy, Br. Med. Bull. 40 (1984) 155–159, https://doi.org/10.1093/oxfordjournals.bmb.a071962.
[821] L. Valkovič, M. Chmelík, M. Krššák, In-vivo 31P-MRS of skeletal muscle and liver: A way for non-invasive assessment of their metabolism, Anal. Biochem. 529 (2017) 193–215, https://doi.org/10.1016/j.ab.2017.01.018.
[822] Y. Liu, Y. Gu, X. Yu, Assessing tissue metabolism by phosphorous-31 magnetic resonance spectroscopy and imaging: a methodology review, Quant. Imaging Med. Surg. 7 (2017) 707–716, https://doi.org/10.21037/qims.2017.11.03.
[823] J.M. Salhany, T. Yamane, R.G. Shulman, S. Ogawa, High resolution 31P nuclear magnetic resonance studies of intact yeast cells, Proc. Natl. Acad. Sci. U. S. A. 72 (1975) 4966–4975, https://doi.org/10.1073/pnas.72.12.4966.
[824] R.J. Gillies, K. Ugurbil, J.A. den Hollander, R.G. Shulman, 31P NMR studies of intracellular pH and phosphate metabolism during cell division cycle of Saccharomyces cerevisiae, Proc. Natl. Acad. Sci. 78 (1981) 2125–2129, https://doi.org/10.1073/pnas.78.4.2125.
[825] G. Navon, R. Navon, R.G. Shulman, T. Yamane, Phosphate metabolites in lymphoid, Friend erythroleukemia, and HeLa cells observed by high-resolution 31P nuclear magnetic resonance, Proc. Natl. Acad. Sci. 75 (1978) 891–895, https://doi.org/10.1073/pnas.75.2.891.
[826] S.M. Cohen, S. Ogawa, H. Rottenberg, P. Glynn, T. Yamane, T.R. Brown, R.G. Shulman, J.R. Williamson, 31P nuclear magnetic resonance studies of isolated rat liver cells, Nature. 273 (1978) 554–556, https://doi.org/10.1038/273554a0.

[827] J.K.M. Roberts, P.M. Ray, N. Wade-Jardetzky, O. Jardetzky, Estimation of cytoplasmic and vacuolar pH in higher plant cells by 31P NMR, Nature. 283 (1980) 870–872, https://doi.org/10.1038/283870a0.
[828] J.K. Roberts, P.M. Ray, N. Wade-Jardetzky, O. Jardetzky, Extent of intracellular pH changes during H(+) extrusion by maize root-tip cells, Planta. 152 (1981) 74–78, https://doi.org/10.1007/BF00384988.
[829] J.K.M. Roberts, D. Wemmer, P.M. Ray, O. Jardetzky, Regulation of Cytoplasmic and Vacuolar pH in Maize Root Tips under Different Experimental Conditions, Plant Physiol. 69 (1982) 1344–1347, https://doi.org/10.1104/pp.69.6.1344.
[830] J.A. den Hollander, K. Ugurbil, T.R. Brown, R.G. Shulman, Phosphorus-31 nuclear magnetic resonance studies of the effect of oxygen upon glycolysis in yeast, Biochemistry. 20 (1981) 5871–5880, https://doi.org/10.1021/bi00523a034.
[831] K. Nicolay, W.A. Scheffers, P.M. Bruinenberg, R. Kaptein, Phosphorus-31 nuclear magnetic resonance studies of intracellular pH, phosphate compartmentation and phosphate transport in yeasts, Arch. Microbiol. 133 (1982) 83–89, https://doi.org/10.1007/BF00413516.
[832] J.K. Barton, J.A. den Hollander, T.M. Lee, A. MacLaughlin, R.G. Shulman, Measurement of the internal pH of yeast spores by 31P nuclear magnetic resonance, Proc. Natl. Acad. Sci. 77 (1980) 2470–2473, https://doi.org/10.1073/pnas.77.5.2470.
[833] X. Ge, D.A. d'Avignon, J.J. Ackerman, R.D. Sammons, Rapid vacuolar sequestration: the horseweed glyphosate resistance mechanism, Pest Manag. Sci. 316 (2010), https://doi.org/10.1002/ps.1911.
[834] X. Ge, D.A. d'Avignon, J.J.H. Ackerman, R.D. Sammons, In vivo ^{31}P-nuclear magnetic resonance studies of glyphosate uptake, vacuolar sequestration, and tonoplast pump activity in glyphosate-resistant horseweed, Plant Physiol. 166 (2014) 1255–1268, https://doi.org/10.1104/pp.114.247197.
[835] D.A. d'Avignon, X. Ge, In vivo NMR investigations of glyphosate influences on plant metabolism, J. Magn. Reson. San Diego Calif 1997 292 (2018) 59–72, https://doi.org/10.1016/j.jmr.2018.03.008.
[836] G. Navon, S. Ogawa, R.G. Shulman, T. Yamane, 31P nuclear magnetic resonance studies of Ehrlich ascites tumor cells, Proc. Natl. Acad. Sci. 74 (1977) 87–91, https://doi.org/10.1073/pnas.74.1.87.
[837] G. Navon, S. Ogawa, R.G. Shulman, T. Yamane, High-resolution 31P nuclear magnetic resonance studies of metabolism in aerobic Escherichia coli cells, Proc. Natl. Acad. Sci. U. S. A. 74 (1977) 888–894, https://doi.org/10.1073/pnas.74.3.888.
[838] S. Ogawa, R.G. Shulman, P. Glynn, T. Yamane, G. Navon, On the measurement of pH in Escherichia coli by 31P nuclear magnetic resonance, Biochim. Biophys. Acta. 502 (1978) 45–50, https://doi.org/10.1016/0005-2728(78)90130-5.
[839] K. Ugurbil, H. Rottenberg, P. Glynn, R.G. Shulman, 31P nuclear magnetic resonance studies of bioenergetics and glycolysis in anaerobic Escherichia coli cells, Proc. Natl. Acad. Sci. 75 (1978) 2244–2248, https://doi.org/10.1073/pnas.75.5.2244.
[840] K. Ugurbil, H. Rottenberg, P. Glynn, R.G. Shulman, Phosphorus-31 nuclear magnetic resonance studies of bioenergetics in wild-type and adenosinetriphosphatase(1-) Escherichia coli cells, Biochemistry. 21 (1982) 1068–1075, https://doi.org/10.1021/bi00534a038.
[841] K. Nicolay, R. Kaptein, K.J. Hellingwerf, W.N. Konings, 31P nuclear magnetic resonance studies of energy transduction in Rhodopseudomonas sphaeroides, Eur. J. Biochem. 116 (1981) 191–197, https://doi.org/10.1111/j.1432-1033.1981.tb05318.x.
[842] K. Nicolay, K.J. Hellingwerf, H. Van Gemerden, R. Kaptein, W.N. Konings, 31P NMR studies of photophosphorylation in intact cells of Chromatium vinosum, FEBS Lett. 138 (1982) 249–254, https://doi.org/10.1016/0014-5793(82)80453-5.
[843] G. Navon, R.G. Shulman, T. Yamane, T.R. Eccleshall, K.B. Lam, J.J. Baronofsky, J. Marmur, Phosphorus-31 nuclear magnetic resonance studies of wild-type and glycolytic pathway mutants of Saccharomyces cerevisiae, Biochemistry. 18 (1979) 4487–4499, https://doi.org/10.1021/bi00588a006.
[844] T.R. Brown, K. Ugurbil, R.G. Shulman, 31P nuclear magnetic resonance measurements of ATPase kinetics in aerobic Escherichia coli cells, Proc. Natl. Acad. Sci. 74 (1977) 5551–5553, https://doi.org/10.1073/pnas.74.12.5551.
[845] S. Forsen, R.A. Hoffman, Study of Moderately Rapid Chemical Exchange Reactions by Means of Nuclear Magnetic Double Resonance, J. Chem. Phys. 39 (1963) 2892–2901, https://doi.org/10.1063/1.1734121.
[846] R.K. Gupta, A.G. Redfield, Double nuclear magnetic resonance observation of electron exchange between ferri- and ferrocytochrome c, Nature. 169 (1970) 1204–1206, https://doi.org/10.1126/science.169.3951.1204.
[847] D.E. Befroy, D.L. Rothman, K.F. Petersen, G.I. Shulman, ^{31}P-magnetization transfer magnetic resonance spectroscopy measurements of in vivo metabolism, Diabetes. 61 (2012) 2669–2678, https://doi.org/10.2337/db12-0558.
[848] N.J. Anthis, G.M. Clore, Visualizing transient dark states by NMR spectroscopy, Q. Rev. Biophys. 48 (2015) 35–116, https://doi.org/10.1017/S0033583514000122.
[849] T.R. Alderson, L.E. Kay, Unveiling invisible protein states with NMR spectroscopy, Curr. Opin. Struct. Biol. 60 (2020) 39–49, https://doi.org/10.1016/j.sbi.2019.10.008.
[850] F. Mitsumori, D. Rees, K.M. Brindle, G.K. Radda, I.D. Campbell, 31P-NMR saturation transfer studies of aerobic Escherichia coli cells, Biochim. Biophys. Acta BBA - Mol. Cell Res. 969 (1988) 185–193, https://doi.org/10.1016/0167-4889(88)90074-2.
[851] R.K. Gupta, Saturation transfer 31P NMR studies of the intact human red blood cell, Biochim. Biophys. Acta BBA - Gen. Subj. 586 (1979) 189–195, https://doi.org/10.1016/0304-4165(79)90417-3.
[852] M. Neeman, E. Rushkin, A.M. Kaye, H. Degani, 31P-NMR studies of phosphate transfer rates in T47D human breast cancer cells, Biochim. Biophys. Acta BBA - Mol. Cell Res. 930 (1987) 179–192, https://doi.org/10.1016/0167-4889(87)90030-9.
[853] J.R. Alger, J.A. den Hollander, R.G. Shulman, In vivo phosphorus-31 nuclear magnetic resonance saturation transfer studies of adenosinetriphosphatase kinetics in Saccharomyces cerevisiae, Biochemistry. 21 (1982) 2957–2963, https://doi.org/10.1021/bi00541a024.
[854] S.L. Campbell-Burk, K.A. Jones, R.G. Shulman, 31P NMR saturation-transfer measurements in Saccharomyces cerevisiae: characterization of phosphate exchange reactions by iodoacetate and antimycin A inhibition, Biochemistry. 26 (1987) 7483–7492, https://doi.org/10.1021/bi00397a043.
[855] J.G. Sheldon, S.P. Williams, A.M. Fulton, K.M. Brindle, 31P NMR magnetization transfer study of the control of ATP turnover in Saccharomyces cerevisiae, Proc. Natl. Acad. Sci. 93 (1996) 6399–6404, https://doi.org/10.1073/pnas.93.13.6399.
[856] R.L. Nunnally, D.P. Hollis, Adenosine triphosphate compartmentation in living hearts: a phosphorus nuclear magnetic resonance saturation transfer study, Biochemistry. 18 (1979) 3642–3646, https://doi.org/10.1021/bi00583a032.
[857] J.J. Ackerman, P.J. Bore, D.G. Gadian, T.H. Grove, G.K. Radda, N.m.r. studies of metabolism in perfused organs, Philos. Trans. R. Soc. B Biol. Sci. 289 (1980) 425–436, https://doi.org/10.1098/rstb.1980.0059.
[858] P.M. Matthews, J.L. Bland, D.G. Gadian, G.K. Radda, A,, 31P-NMR saturation transfer study of the regulation of creatine kinase in the rat heart, Biochim. Biophys. Acta BBA - Mol. Cell Res. 721 (1982) 312–320, https://doi.org/10.1016/0167-4889(82)90084-2.
[859] H. Degani, M. Laughlin, S. Campbell, R.G. Shulman, Kinetics of creatine kinase in heart: a 31P NMR saturation- and inversion-transfer study, Biochemistry. 24 (1985) 5510–5516, https://doi.org/10.1021/bi00341a035.
[860] A.P. Koretsky, V.J. Basus, T.L. James, M.P. Klein, M.W. Weiner, Detection of Exchange Reactions Involving Small Metabolite Pools Using NMR Magnetization Transfer Techniques: Relevance to Subcellular Compartmentation of Creatine Kinase, Magn. Reson. Med. 2 (1985) 586–594, https://doi.org/10.1002/mrm.1910020610.
[861] A.P. Koretsky, S. Wang, M.P. Klein, T.L. James, M.W. Weiner, 31P NMR saturation transfer measurements of phosphorus exchange reactions in rat heart and kidney in situ, Biochemistry. 25 (1986) 77–84, https://doi.org/10.1021/bi00349a012.
[862] K. Ugurbil, M. Petein, R. Maidan, S. Michurski, A.H. From, Measurement of an individual rate constant in the presence of multiple exchanges: application to myocardial creatine kinase reaction, Biochemistry. 25 (1986) 100–107, https://doi.org/10.1021/bi00349a015.
[863] D.G. Gadian, G.K. Radda, T.R. Brown, E.M. Chance, M.J. Dawson, D.R. Wilkie, The activity of creatine kinase in frog skeletal muscle studied by saturation-transfer nuclear magnetic resonance, Biochem. J. 194 (1981) 215–228, https://doi.org/10.1042/bj1940215.
[864] R.A. Meyer, M.J. Kuchmerick, T.R. Brown, Application of 31P-NMR spectroscopy to the study of striated muscle metabolism, Am. J. Physiol. 242 (1982) C1–C11, https://doi.org/10.1152/ajpcell.1982.242.1.C1.
[865] E.A. Shoubridge, R.W. Briggs, G.K. Radda, 31p NMR saturation transfer measurements of the steady state rates of creatine kinase and ATP synthetase in the rat brain, FEBS Lett. 140 (1982) 289–292, https://doi.org/10.1016/0014-5793(82)80916-2.
[866] C. Cadic-Amadeuf, C. Margerin, C. Baquey, B. Dupuy, Modified antibody secretions by embedding hybridoma cell lines in agarose gels, Colloids Surf. B Biointerfaces. 1 (1993) 91–96, https://doi.org/10.1016/0927-7765(93)80039-2.
[867] E. Luchinat, L. Barbieri, T.F. Campbell, L. Banci, Real-Time Quantitative In-Cell NMR: Ligand Binding and Protein Oxidation Monitored in Human Cells Using Multivariate Curve Resolution, Anal. Chem. 92 (2020) 9997–10006, https://doi.org/10.1021/acs.analchem.0c01677.
[868] S. Kubo, N. Nishida, Y. Udagawa, O. Takarada, S. Ogino, I. Shimada, A gel-encapsulated bioreactor system for NMR studies of protein-protein interactions in living mammalian cells, Angew. Chem. Int. Ed Engl. 52 (2013) 1208–1211, https://doi.org/10.1002/anie.201207243.
[869] L. Breindel, D.S. Burz, A. Shekhtman, Active metabolism unmasks functional protein–protein interactions in real time in-cell NMR, Commun. Biol. 3 (2020) 1–9, https://doi.org/10.1038/s42003-020-0976-3.
[870] M. Llinás, K. Wüthrich, W. Schwotzer, W. Von Philipsborn, 15N nuclear magnetic resonance of living cells, Nature. 257 (1975) 817–818, https://doi.org/10.1038/257817a0.
[871] K. Kanamori, J.D. Roberts, Nitrogen-15 NMR studies of biological systems, Acc. Chem. Res. 16 (1983) 35–41, https://doi.org/10.1021/ar00086a001.
[872] K. Kanamori, T.L. Legerton, R.L. Weiss, J.D. Roberts, Nitrogen-15 spin-lattice relaxation times of amino acids in Neurospora crassa as a probe of intracellular environment, Biochemistry. 21 (1982) 4916–4920, https://doi.org/10.1021/bi00263a013.
[873] T.L. Legerton, K. Kanamori, R.L. Weiss, J.D. Roberts, 15N NMR studies of nitrogen metabolism in intact mycelia of Neurospora crassa, Proc. Natl. Acad. Sci. 78 (1981) 1495–1498, https://doi.org/10.1073/pnas.78.3.1495.
[874] K. Kanamori, T.L. Legerton, R.L. Weiss, J.D. Roberts, Effect of the nitrogen source on glutamine and alanine biosynthesis in Neurospora crassa. An in vivo 15N nuclear magnetic resonance study, J. Biol. Chem. 257 (1982) 14168–14172.

[875] N. Haran, Z.E. Kahana, A. Lapidot, In vivo 15N NMR studies of regulation of nitrogen assimilation and amino acid production by Brevibacterium lactofermentum, J. Biol. Chem. 258 (1983) 12929–12933.
[876] M. Tesch, A.A. de Graaf, H. Sahm, In vivo fluxes in the ammonium-assimilatory pathways in corynebacterium glutamicum studied by 15N nuclear magnetic resonance, Appl. Environ. Microbiol. 65 (1999) 1099–1109.
[877] R. Altenburger, S. Abarzua, R. Callies, L.H. Grimme, A. Mayer, D. Leibfritz, Ammonia rhythm in Microcystis firma studied by in vivo 15 N and 31 P NMR spectroscopy, Arch. Microbiol. 156 (1991) 471–476, https://doi.org/10.1007/BF00245394.
[878] J.C. Street, A.M. Delort, P.S. Braddock, K.M. Brindle, A 1H/15N n.m.r. study of nitrogen metabolism in cultured mammalian cells., Biochem. J. 291 (Pt 2) (1993) 485–492. https://doi.org/10.1042/bj2910485..
[879] K. Kanamori, R.L. Weiss, J.D. Roberts, Ammonia assimilation in Bacillus polymyxa. 15N NMR and enzymatic studies, J. Biol. Chem. 262 (1987) 11038–11045.
[880] F. Martin, 15N-NMR studies of nitrogen assimilation and amino acid biosynthesis in the ectomycorrhizal fungus Cenococcum graniforme, FEBS Lett. 182 (1985) 350–354, https://doi.org/10.1016/0014-5793(85)80331-8.
[881] F. Martin, R. Côté, D. Canet, NH4+ assimilation in the ectomycorrhizal basidiomycete Laccaria bicolor (Maire) Orton, a 15N-NMR study, New Phytol. 128 (1994) 479–485, https://doi.org/10.1111/j.1469-8137.1994.tb02994.x.
[882] P. Lundberg, P.-O. Lundquist, Primary metabolism in N2-fixing Alnus incana-Frankia symbiotic root nodules studied with 15N and 31P nuclear magnetic resonance spectroscopy, Planta. 219 (2004) 661–672, https://doi.org/10.1007/s00425-004-1271-0.
[883] A.C. Kuesel, W. Kuhn, J. Sianoudis, L.H. Grimme, D. Leibfritz, A. Mayer, N-15 in vivo NMR spectroscopic investigation of nitrogen deprived cell suspensions of the green alga Chlorella fusca, Arch. Microbiol. 151 (1989) 434–438, https://doi.org/10.1007/BF00416603.
[884] T.A. Thorpe, K. Bagh, A.J. Cutler, D.I. Dunstan, D.D. McIntyre, H.J. Vogel, A 14N and 15N Nuclear Magnetic Resonance Study of Nitrogen Metabolism in Shoot-Forming Cultures of White Spruce (Picea glauca) Buds, Plant Physiol. 91 (1989) 193–202, https://doi.org/10.1104/pp.91.1.193.
[885] R.W. Joy IV, H.J. Vogel, T.A. Thorpe, Inorganic nitrogen metabolism in embryogenic white spruce cultures: A nitrogen 14/15 NMR study, J. Plant Physiol. 151 (1997) 306–315, https://doi.org/10.1016/S0176-1617(97)80257-X.
[886] S. Amancio, H. Santos, Nitrate and Ammonium Assimilation by Roots of Maize (Zea maysL.) Seedlings as Investigated by In Vivo15N-NMR, J. Exp. Bot. 43 (1992) 633–639, https://doi.org/10.1093/jxb/43.5.633.
[887] R.B. Lee, J.V. Purves, R.G. Ratcliffe, L.R. Saker, Nitrogen Assimilation and the Control of Ammonium and Nitrate Absorption by Maize Roots, J. Exp. Bot. 43 (1992) 1385–1396, https://doi.org/10.1093/jxb/43.11.1385.
[888] W. Hartung, R.G. Ratcliffe, Utilization of glycine and serine as nitrogen sources in the roots of Zea mays and Chamaegigas intrepidus, J. Exp. Bot. 53 (2002) 2305–2314, https://doi.org/10.1093/jxb/erf092.
[889] E.-B.-I. Monselise, D. Kost, Different ammonium-ion uptake, metabolism and detoxification efficiencies in two Lemnaceae, Planta. 189 (1993) 167–173, https://doi.org/10.1007/BF00195073.
[890] Y.Y. Ford, G.G. Fox, R. George Ratcliffe, R.J. Robins, In vivo 15N NMR studies of secondary metabolism in transformed root cultures of Datura stramonium and Nicotiana tabacum, Phytochemistry. 36 (1994) 333–339, https://doi.org/10.1016/S0031-9422(00)97071-7.
[891] Y.Y. Ford, R.G. Ratcliffe, R.J. Robins, An in vivo N NMR study of agropine synthesis in transformed root cultures of Nicotiana tabacum, Physiol. Plant. 109 (2000) 123–128, https://doi.org/10.1034/j.1399-3054.2000.100203.x.
[892] A.D. Carroll, G.G. Fox, S. Laurie, R. Phillips, R.G. Ratcliffe, G.R. Stewart, Ammonium Assimilation and the Role of [gamma]-Aminobutyric Acid in pH Homeostasis in Carrot Cell Suspensions, Plant Physiol. 106 (1994) 513–520, https://doi.org/10.1104/pp.106.2.513.
[893] R.W. Joy, D.D. McIntyre, H.J. Vogel, T.A. Thorpe, Stage-specific nitrogen metabolism in developing carrot somatic embryos, Physiol. Plant. 97 (1996) 149–159, https://doi.org/10.1111/j.1399-3054.1996.tb00491.x.
[894] J. Schaefer, E.O. Stejskal, R.A. McKay, Cross-polarization nmr of N-15 labeled soybeans 88 (1979) 274–280, https://doi.org/10.1016/0006-291X(79)91726-1.
[895] T.A. Skokut, J.E. Varner, J. Schaefer, E.O. Stejskal, R.A. McKay, [15N]NMR Determination of Asparagine and Glutamine Nitrogen Utilization for Synthesis of Storage Protein in Developing Cotyledons of Soybean in Culture, Plant Physiol. 69 (1982) 308–316, https://doi.org/10.1104/pp.69.2.308.
[896] J.S. George T Coker III, 15N and 13C NMR Determination of Allantoin Metabolism in Developing Soybean Cotyledons, Plant Physiol. 77 (1985) 129–7. https://doi.org/10.1104/pp.77.1.129..
[897] G.T. Coker, J.R. Garbow, J. Schaefer, 15N and 13C NMR determination of methionine metabolism in developing soybean cotyledons, Plant Physiol. 83 (1987) 698–702, https://doi.org/10.1104/pp.83.3.698.
[898] L. Cegelski, J. Schaefer, Glycine metabolism in intact leaves by in vivo 13C and 15N labeling, J. Biol. Chem. 280 (2005) 39238–39245, https://doi.org/10.1074/jbc.M507053200.
[899] C.E. Norris, S.A. Quideau, S.M. Landhäusser, G.M. Bernard, R.E. Wasylishen, Tracking Stable Isotope Enrichment in Tree Seedlings with Solid-State NMR Spectroscopy, Sci. Rep. 2 (2012) 49–55, https://doi.org/10.1038/srep00719.
[900] B. Schneider, In-vivo nuclear magnetic resonance spectroscopy of low-molecular-weight compounds in plant cells, Planta. 203 (1997) 1–8, https://doi.org/10.1007/s00050158.
[901] F. Mesnard, R.G. Ratcliffe, NMR analysis of plant nitrogen metabolism, Photosynth. Res. 83 (2005) 163–180, https://doi.org/10.1007/s11120-004-2081-8.
[902] E.B.I. Monselise, A.H. Parola, D. Kost, Low-frequency electromagnetic fields induce a stress effect upon higher plants, as evident by the universal stress signal, alanine, Biochem. Biophys. Res. Commun. 302 (2003) 427–434, https://doi.org/10.1016/S0006-291X(03)00194-3.
[903] E.B.I. Monselise, A. Levkovitz, D. Kost, Ultraviolet radiation induces stress in etiolated Landoltia punctata, as evidenced by the presence of alanine, a universal stress signal: a 15N NMR study, Plant Biol. 17 (2014) 101–107, https://doi.org/10.1111/plb.12198.
[904] N. Houyou, C. Pau-Roblot, A. Roscher, 15N relaxation and quantification of 15N-labelled metabolites in cell extracts, Comptes Rendus - Chim. 9 (2006) 520–524, https://doi.org/10.1016/j.crci.2005.06.029.
[905] Y.-Y. Ford, R.G. Ratcliffe, R.J. Robins, In vivo NMR analysis of tropane alkaloid metabolism in transformed root and de-differentiated cultures of Datura stramonium, Phytochemistry. 43 (1996) 115–120, https://doi.org/10.1016/0031-9422(96)00261-0.
[906] Y.Y. Ford, R.G. Ratcliffe, R.J. Robins, In vivo nuclear-magnetic-resonance analysis of polyamine and alkaloid metabolism in transformed root cultures of Datura stramonium L.: evidence for the involvement of putrescine in phytohormone-induced de-differentiation, Planta. 205 (1998) 205–213, https://doi.org/10.1007/s004250050313.
[907] K. Kanamori, In vivo N-15 MRS study of glutamate metabolism in the rat brain, Anal. Biochem. 529 (2017) 179–192, https://doi.org/10.1016/j.ab.2016.08.025.
[908] G.G. Fox, R.G. Ratcliffe, S.A. Robinson, A.P. Slade, G.R. Stewart, Detection of 15N-labeled ammonium. In Vivo, 15N NMR versus mass spectrometry, J. Magn. Reson. 1969 96 (1992) 146–153, https://doi.org/10.1016/0022-2364(92)90295-I.
[909] W. von Philipsborn, R. Müller, 15N-NMR Spectroscopy—New Methods and Applications [New Analytical Methods (28)], Angew. Chem. Int. Ed Engl. 25 (1986) 383–413, https://doi.org/10.1002/anie.198603833.
[910] D. Freeman, N. Sailasuta, S. Sukumar, R.E. Hurd, Proton-Detected 15N NMR-Spectroscopy and Imaging, J. Magn. Reson. B. 102 (1993) 183–192, https://doi.org/10.1006/jmrb.1993.1081.
[911] R. Marek, A. Lycka, E. Kolehmainen, E. Sievanen, J. Tousek, 15N NMR Spectroscopy in Structural Analysis: An Update (2001–2005), Curr. Org. Chem. 11 (2007) 1154–1205, https://doi.org/10.2174/138527207781662519.
[912] R.S. Balaban, M.A. Knepper, Nitrogen-14 nuclear magnetic resonance spectroscopy of mammalian tissues, Am. J. Physiol. 245 (1983) C439–C444, https://doi.org/10.1152/ajpcell.1983.245.5.C439.
[913] B.A. Lewis, S. Cayley, S. Padmanabhan, V.M. Kolb, V. Brushaber, C.F. Anderson, M.T. Record Jr., Natural abundance 14N and 13C NMR of glycine betaine and trehalose as probes of the cytoplasm of Escherichia coli K12, J. Magn. Reson. 1969 (90) (1990) 612–617, https://doi.org/10.1016/0022-2364(90)90071-G.
[914] P.S. Belton, R.B. Lee, R.G. Ratcliffe, A 14N Nuclear Magnetic Resonance Study of Inorganic Nitrogen Métabolism in Barley, Maize and Pea Roots, J. Exp. Bot. 36 (1985) 190–210, https://doi.org/10.1093/jxb/36.2.190.
[915] L.S. Simeral, Determination of Urea, Nitrate, and Ammonium in Aqueous Solution Using Nitrogen-14 Nuclear Magnatic Resonance, Appl. Spectrosc. 51 (1997) 1585–1587, https://doi.org/10.1366/0003702971939145.
[916] O. Lutz, T. Erata, H. Förster, D. Müller, Multinuclear approach to nuclear magnetic resonance investigations in tissue with heteronuclei: 14N, 35Cl, 39K, Naturwissenschaften. 73 (1986) 97–99, https://doi.org/10.1007/BF00365837.
[917] M.P. Gamcsik, I. Constantinidis, J.D. Glickson, In vivo 14N nuclear magnetic resonance spectroscopy of tumors: detection of ammonium and trimethylamine metabolites in the murine radiation induced fibrosarcoma 1, Cancer Res. 51 (1991) 3378–3383.
[918] R.B. Lee, R.G. Ratcliffe, Observations on the subcellular distribution of the ammonium ion in maize root tissue using in-vivo 14 N-nuclear magnetic resonance spectroscopy, Planta. 183 (1991) 359–367, https://doi.org/10.1007/BF00197734.
[919] J. Gerendás, R.G. Ratcliffe, B. Sattelmacher, Relationship between intracellular pH and N metabolism in maize (Zea mays L.) roots, Plant Soil. 155 (156) (1993) 167–170.
[920] P. Lundberg, R.G. Weich, P. Jensén, H.J. Vogel, Phosphorus-31 and Nitrogen-14 NMR Studies of the Uptake of Phosphorus and Nitrogen Compounds in the Marine Macroalgae Ulva lactuca, Plant Physiol. 89 (1989) 1380–1387, https://doi.org/10.1104/pp.89.4.1380.
[921] H. Aarnes, A.B. Eriksen, T.E. Southon, Metabolism of nitrate and ammonium in seedlings of Norway spruce (Picea abies) measured by in vivo 14N and 15N NMR spectroscopy, Physiol. Plant. 94 (1995) 384–390, https://doi.org/10.1111/j.1399-3054.1995.tb00943.x.
[922] H. Aarnes, A. Eriksen, D. Petersen, F. Rise, Accumulation of ammonium in Norway spruce (Picea abies) seedlings measured by in vivo 14N-NMR, J. Exp. Bot. 58 (2007) 929–934, https://doi.org/10.1093/jxb/erl247.
[923] Y. Seo, M. Murakami, Monitoring of intracellular ammonium in perfused rat salivary gland by nitrogen-14 nuclear magnetic resonance spectroscopy, Proc. Biol. Sci. 244 (1991) 191–196, https://doi.org/10.1098/rspb.1991.0069.

[924] Y. Shachar-Hill, P. Pfeffer, R. Ratcliffe, Measuring Nitrate in Plant Cells by in Vivo NMR Using Gd3+ as a Shift Reagent, J. Magn. Reson. B. 111 (1996) 9–14, https://doi.org/10.1006/jmrb.1996.0054.
[925] R.J. Labotka, P. Lundberg, P.W. Kuchel, Ammonia permeability of erythrocyte membrane studied by 14N and 15N saturation transfer NMR spectroscopy, Am. J. Physiol. 268 (1995) C686–C699, https://doi.org/10.1152/ajpcell.1995.268.3.C686.
[926] R.B. Lee, R.G. Ratcliffe, Nuclear magnetic resonance studies of the location and function of plant nutrients in vivo, Plant Soil. 155 (1993) 45–55, https://doi.org/10.1007/BF00024983.
[927] G. Zheng, W.S. Price, Solvent signal suppression in NMR, Prog. Nucl. Magn. Reson. Spectrosc. 56 (2010) 267–288, https://doi.org/10.1016/j.pnmrs.2010.01.001.
[928] B. Lam, A.J. Simpson, Direct 1H NMR spectroscopy of dissolved organic matter in natural waters, Analyst. 133 (2008) 263–269, https://doi.org/10.1039/B713457F.
[929] Y.L. Mobarhan, J. Struppe, B. Fortier-McGill, A.J. Simpson, Effective combined water and sideband suppression for low-speed tissue and in vivo MAS NMR, Anal. Bioanal. Chem. 409 (2017) 5043–5055, https://doi.org/10.1007/s00216-017-0450-3.
[930] R. Soong, Y. Liaghati-Mobarhan, M. Tabatabaei, M. Bastawrous, R.G. Biswas, M. Simpson, A. Simpson, Flow-based in vivo NMR spectroscopy of small aquatic organisms, Magn. Reson. Chem. 58 (2020) 411–426, https://doi.org/10.1002/mrc.4886.
[931] A. Daniels, R.J. Williams, P.E. Wright, Nuclear magnetic resonance studies of the adrenal gland and some other organs, Nature. 261 (1976) 321–323, https://doi.org/10.1038/261321a0.
[932] F.F. Brown, I.D. Campbell, P.W. Kuchel, Human erythrocyte metabolism studies by 1H spin echo NMR, FEBS Lett. 82 (1977) 12–16, https://doi.org/10.1016/0014-5793(77)80875-2.
[933] K.M. Brindle, F.F. Brown, I.D. Campbell, C. Grathwohl, P.W. Kuchel, Application of spin-echo nuclear magnetic resonance to whole-cell systems. Membrane transport, Biochem. J. 180 (1979) 37–44, https://doi.org/10.1042/bj1800037.
[934] D.L. Rabenstein, A.A. Isab, The complexation of zinc in intact human erythrocytes studied by 1H spin-echo NMR, FEBS Lett. 121 (1980) 61–64, https://doi.org/10.1016/0014-5793(80)81267-1.
[935] P.F. Agris, I.D. Campbell, Proton nuclear magnetic resonance of intact Friend leukemia cells: phosphorylcholine increase during differentiation, Nature. 216 (1982) 1325–1327, https://doi.org/10.1126/science.7079765.
[936] B.E. Chapman, G.R. Beilharz, M.J. York, P.W. Kuchel, Endogenous phospholipase and choline release in human erythrocytes: A study using 1H NMR spectroscopy, Biochem. Biophys. Res. Commun. 105 (1982) 1280–1287, https://doi.org/10.1016/0006-291X(82)90925-1.
[937] R.J. Simpson, K.M. Brindle, I.D. Campbell, Spin echo proton NMR studies of the metabolism of malate and fumarate in human erythrocytes, Biochim. Biophys. Acta BBA - Mol. Cell Res. 721 (1982) 191–200, https://doi.org/10.1016/0167-4889(82)90068-4.
[938] J. Reglinski, W.E. Smith, C.J. Suckling, M. Al-Kabban, I.D. Watson, M.J. Stewart, A 1H spin echo NMR study of the HeLa tumour cell, FEBS Lett. 214 (1987) 351–356, https://doi.org/10.1016/0014-5793(87)80086-8.
[939] C. Rae, P.G. Board, P.W. Kuchel, Glyoxalase 2 deficiency in the erythrocytes of a horse: 1H NMR studies of enzyme kinetics and transport of S-lactoylglutathione, Arch. Biochem. Biophys. 291 (1991) 291–299, https://doi.org/10.1016/0003-9861(91)90137-8.
[940] C.D. Rae, K.J. Sweeney, P.W. Kuchel, Stability and nonreactivity of ergothioneine in human erythrocytes studied by 1H NMR, Magn. Reson. Med. 29 (1993) 826–829, https://doi.org/10.1002/mrm.1910290617.
[941] A.A. Isab, D.L. Rabenstein, The incorporation of 2h-labelled glycine into the glutathione of intact human erythrocytes studied by 1h spin-echo fourier transform NMR, FEBS Lett. 106 (1979) 325–329, https://doi.org/10.1016/0014-5793(79)80525-6.
[942] R.J. Simpson, K.M. Brindle, F.F. Brown, I.D. Campbell, D.L. Foxall, Studies of pyruvate-water isotope exchange catalysed by erythrocytes and proteins, Biochem. J. 193 (1981) 401–406, https://doi.org/10.1042/bj1930401.
[943] K.M. Brindle, F.F. Brown, I.D. Campbell, D.L. Foxall, R.J. Simpson, A 1H n.m.r. study of isotope exchange catalysed by glycolytic enzymes in the human erythrocyte, 202 (1982) 589–602. https://doi.org/10.1042/bj2020589..
[944] K.M. Brindle, I.D. Campbell, R.J. Simpson, A 1H n.m.r. study of the kinetic properties expressed by glyceraldehyde phosphate dehydrogenase in the intact human erythrocyte, Biochem. J. 208 (1982) 583–592. https://doi.org/10.1042/bj2080583..
[945] R.J. Simpson, K.M. Brindle, F.F. Brown, I.D. Campbell, D.L. Foxall, A p.m.r. isotope-exchange method for studying the kinetic properties of dehydrogenases in intact cells, Biochem. J. 202 (1982) 573–579, https://doi.org/10.1042/bj2020573.
[946] R.J. Simpson, K.M. Brindle, F.F. Brown, I.D. Campbell, D.L. Foxall, Studies of lactate dehydrogenase in the purified state and in intact erythrocytes, Biochem. J. 202 (1982) 581–587, https://doi.org/10.1042/bj2020581.
[947] K.M. Brindle, I.D. Campbell, R.J. Simpson, A 1H-NMR study of the activity expressed by lactate dehydrogenase in the human erythrocyte, 158 (1986) 299–305. https://doi.org/10.1111/j.1432-1033.1986.tb09751.x..
[948] L.O. Sillerud, J.R. Alger, R.G. Shulman, High-resolution proton NMR studies of intracellular metabolites in yeast using 13C decoupling, J. Magn. Reson. 1969 (45) (1981) 142–150, https://doi.org/10.1016/0022-2364(81)90108-6.
[949] K.M. Brindle, J. Boyd, I.D. Campbell, R. Porteous, N. Soffe, Observation of carbon labelling in cell metabolites using proton spin echo NMR, Biochem. Biophys. Res. Commun. 109 (1982) 864–871, https://doi.org/10.1016/0006-291x(82)92020-4.
[950] D.L. Foxall, J.S. Cohen, R.G. Tschudin, Selective observation of 13C-enriched metabolites by 1H NMR, J. Magn. Reson. 1969 (51) (1983) 330–334, https://doi.org/10.1016/0022-2364(83)90019-7.
[951] K. Yoshizaki, Y. Seo, H. Nishikawa, High-resolution proton magnetic resonance spectra of muscle, Biochim. Biophys. Acta. 678 (1981) 283–291, https://doi.org/10.1016/0304-4165(81)90218-x.
[952] S.T. Oxley, R. Porteous, K.M. Brindle, J. Boyd, I.D. Campbell, A multinuclear NMR study of 2,3-bisphosphoglycerate metabolism in the human erythrocyte, Biochim. Biophys. Acta BBA - Mol. Cell Res. 805 (1984) 19–24, https://doi.org/10.1016/0167-4889(84)90031-4.
[953] J.W. Prichard, R.G. Shulman, NMR spectroscopy of brain metabolism in vivo, Annu. Rev. Neurosci. 9 (1986) 61–85, https://doi.org/10.1146/annurev.ne.09.030186.000425.
[954] K.L. Behar, J.A. den Hollander, M.E. Stromski, T. Ogino, R.G. Shulman, O.A. Petroff, J.W. Prichard, High-resolution 1H nuclear magnetic resonance study of cerebral hypoxia in vivo, Proc. Natl. Acad. Sci. 80 (1983) 4945–4948, https://doi.org/10.1073/pnas.80.16.4945.
[955] T.R. Pirttilä, R.A. Kauppinen, Recovery of intracellular pH in cortical brain slices following anoxia studied by nuclear magnetic resonance spectroscopy: role of lactate removal, extracellular sodium and sodium/hydrogen exchange, NSC. 47 (1992) 155–164, https://doi.org/10.1016/0306-4522(92)90128-o.
[956] T.R. Pirttilä, R.A. Kauppinen, Regulation of intracellular pH in guinea pig cerebral cortex ex vivo studied by 31P and 1H nuclear magnetic resonance spectroscopy: role of extracellular bicarbonate and chloride, J. Neurochem. 62 (1994) 656–664, https://doi.org/10.1046/j.1471-4159.1994.62020656.x.
[957] K.Y. Alam, D.P. Clark, Anaerobic fermentation balance of Escherichia coli as observed by in vivo nuclear magnetic resonance spectroscopy, J. Bacteriol. 171 (1989) 6213–6217, https://doi.org/10.1128/jb.171.11.6213-6217.1989.
[958] L. Brecker, H. Weber, H. Griengl, D.W. Ribbons, In situ proton-NMR analyses of Escherichia coli HB101 fermentations in 1H2O and in D2O, Microbiology. 145 (1999) 3389–3397, https://doi.org/10.1099/00221287-145-12-3389.
[959] G. Gaudet, E. Forano, G. Dauphin, A.M. Delort, Futile cycling of glycogen in Fibrobacter succinogenes as shown by in situ 1H-NMR and 13C-NMR investigation, Eur. J. Biochem. 207 (1992) 155–162, https://doi.org/10.1111/j.1432-1033.1992.tb17032.x.
[960] P.T. Davey, W.C. Hiscox, B.F. Lucker, J.V. O'Fallon, S. Chen, G.L. Helms, Rapid triacylglyceride detection and quantification in live micro-algal cultures via liquid state 1H NMR, Algal Res. 1 (2012) 166–175, https://doi.org/10.1016/j.algal.2012.07.003.
[961] M.S. Bono Jr., R.D. Garcia, D.V. Sri-Jayantha, B.A. Ahner, B.J. Kirby, Measurement of Lipid Accumulation in Chlorella vulgaris via Flow Cytometry and Liquid-State ^{1}H NMR Spectroscopy for Development of an NMR-Traceable Flow Cytometry Protocol, PLOS ONE. 10 (2015), https://doi.org/10.1371/journal.pone.0134846 e0134846.
[962] D. Bouillaud, V. Heredia, T. Castaing-Cordier, D. Drouin, B. Charrier, O. Gonçalves, J. Farjon, P. Giraudeau, Benchtop flow NMR spectroscopy as an online device for the in vivo monitoring of lipid accumulation in microalgae, Algal Res. 43 (2019), https://doi.org/10.1016/j.algal.2019.101624 101624.
[963] D. Bouillaud, D. Drouin, B. Charrier, C. Jacquemmoz, J. Farjon, P. Giraudeau, O. Gonçalves, Using benchtop NMR spectroscopy as an online non-invasive in vivo lipid sensor for microalgae cultivated in photobioreactors, Process Biochem. 93 (2020) 63–68, https://doi.org/10.1016/j.procbio.2020.03.016.
[964] A. Kalfe, A. Telfah, J. Lambert, R. Hergenröder, Looking into Living Cell Systems: Planar Waveguide Microfluidic NMR Detector for in Vitro Metabolomics of Tumor Spheroids, Anal. Chem. 87 (2015) 7402–7410, https://doi.org/10.1021/acs.analchem.5b01603.
[965] S.A. Bradley, A. Ouyang, J. Purdie, T.A. Smitka, T. Wang, A. Kaerner, Fermentanomics: monitoring mammalian cell cultures with NMR spectroscopy, J. Am. Chem. Soc. 132 (2010) 9531–9533, https://doi.org/10.1021/ja101962c.
[966] N. Aranibar, M. Borys, N.A. Mackin, V. Ly, N. Abu-Absi, S. Abu-Absi, M. Niemitz, B. Schilling, Z.J. Li, B. Brock, R.J. Russell II, A. Tymiak, M.D. Reily, NMR-based metabolomics of mammalian cell and tissue cultures, J. Biomol. NMR. 49 (2011) 195–206, https://doi.org/10.1007/s10858-011-9490-8.
[967] K.M. Koczula, C. Ludwig, R. Hayden, L. Cronin, G. Pratt, H. Parry, D. Tennant, M. Drayson, C.M. Bunce, F.L. Khanim, U.L. Günther, Metabolic plasticity in CLL: adaptation to the hypoxic niche, Leukemia. 30 (2016) 65–73, https://doi.org/10.1038/leu.2015.187.
[968] P. Ebrahimi, F.H. Larsen, H.M. Jensen, F.K. Vogensen, S.B. Engelsen, Real-time metabolomic analysis of lactic acid bacteria as monitored by in vitro NMR and chemometrics, Metabolomics. 12 (2016) 1–17, https://doi.org/10.1007/s11306-016-0996-7.
[969] I. Alshamleh, N. Krause, C. Richter, N. Kurrle, H. Serve, U.L. Günther, H. Schwalbe, Real-Time NMR Spectroscopy for Studying Metabolism, Angew. Chem. Int. Ed Engl. 59 (2020) 2304–2308, https://doi.org/10.1002/anie.201912919.
[970] M. Vermathen, G. Diserens, P. Vermathen, J. Furrer, Metabolic Profiling of Cells in Response to Drug Treatment using ^{1}H High-resolution Magic Angle Spinning (HR-MAS) NMR Spectroscopy, Chim. Int. J. Chem. 71 (2017) 124–129, https://doi.org/10.2533/chimia.2017.124.
[971] E. Kaebisch, T.L. Fuss, L.A. Vandergrift, K. Toews, P. Habbel, L.L. Cheng, Applications of high-resolution magic angle spinning MRS in biomedical

studies I-cell line and animal models, NMR Biomed. 30 (2017), https://doi.org/10.1002/nbm.3700 e3700.
[972] O. Beckonert, M. Coen, H.C. Keun, Y. Wang, T.M.D. Ebbels, E. Holmes, J.C. Lindon, J.K. Nicholson, High-resolution magic-angle-spinning NMR spectroscopy for metabolic profiling of intact tissues, Nat. Protoc. 5 (2010) 1019–1032, https://doi.org/10.1038/nprot.2010.45.
[973] B.D. Bennett, E.H. Kimball, M. Gao, R. Osterhout, S.J. Van Dien, J.D. Rabinowitz, Absolute metabolite concentrations and implied enzyme active site occupancy in Escherichia coli, Nat. Chem. Biol. 5 (2009) 593–599, https://doi.org/10.1038/nchembio.186.
[974] B. Sitter, T.F. Bathen, M.-B. Tessem, I.S. Gribbestad, High-resolution magic angle spinning (HR MAS) MR spectroscopy in metabolic characterization of human cancer, Prog. Nucl. Magn. Reson. Spectrosc. 54 (2009) 239–254, https://doi.org/10.1016/j.pnmrs.2008.10.001.
[975] A.A. Crook, R. Powers, Quantitative NMR-Based Biomedical Metabolomics: Current Status and Applications, Molecules. 25 (2020) 5128, https://doi.org/10.3390/molecules25215128.
[976] V. Rutar, Magic angle sample spinning NMR spectroscopy of liquids as a nondestructive method for studies of plant seeds, J. Agric. Food Chem. 37 (1989) 67–70, https://doi.org/10.1021/jf00085a016.
[977] Q.W. Ni, T.M. Eads, Low-speed magic-angle-spinning carbon-13 NMR of fruit tissue, J. Agric. Food Chem. 40 (1992) 1507–1513, https://doi.org/10.1021/jf00021a007.
[978] Q.W. Ni, T.M. Eads, Liquid-phase composition of intact fruit tissue measured by high-resolution proton NMR, J. Agric. Food Chem. 41 (1993) 1026–1034, https://doi.org/10.1021/jf00031a002.
[979] Q.X. Ni, T.M. Eads, Analysis by proton NMR of changes in liquid-phase and solid-phase components during ripening of banana, J. Agric. Food Chem. 41 (1993) 1035–1040, https://doi.org/10.1021/jf00031a003.
[980] L.L. Cheng, C.L. Lean, A. Bogdanova, S.C. Wright, J.L. Ackerman, T.J. Brady, L. Garrido, Enhanced resolution of proton NMR spectra of malignant lymph nodes using magic-angle spinning, Magn. Reson. Med. 36 (1996) 653–658, https://doi.org/10.1002/mrm.1910360502.
[981] D. Moka, R. Vorreuther, H. Schicha, M. Spraul, E. Humpfer, M. Lipinski, P.J.D. Foxall, J.K. Nicholson, J.C. Lindon, Magic Angle Spinning Proton Nuclear Magnetic Resonance Spectroscopic Analysis of Intact Kidney Tissue Samples, Anal. Commun. 34 (1997) 107–109, https://doi.org/10.1039/a701456b.
[982] D. Moka, R. Vorreuther, H. Schicha, M. Spraul, E. Humpfer, M. Lipinski, P.J. Foxall, J.K. Nicholson, J.C. Lindon, Biochemical classification of kidney carcinoma biopsy samples using magic-angle-spinning 1H nuclear magnetic resonance spectroscopy, J. Pharm. Biomed. Anal. 17 (1998) 125–132, https://doi.org/10.1016/s0731-7085(97)00176-3.
[983] L.L. Cheng, M.J. Ma, L. Becerra, T. Ptak, I. Tracey, A. Lackner, R.G. González, Quantitative neuropathology by high resolution magic angle spinning proton magnetic resonance spectroscopy, Proc. Natl. Acad. Sci. 94 (1997) 6408–6413, https://doi.org/10.1073/pnas.94.12.6408.
[984] K.K. Millis, W.E. Maas, D.G. Cory, S. Singer, Gradient, high-resolution, magic-angle spinning nuclear magnetic resonance spectroscopy of human adipocyte tissue, Magn. Reson. Med. 38 (1997) 399–403, https://doi.org/10.1002/mrm.1910380307.
[985] J.-H. Chen, B.M. Enloe, C.D. Fletcher, D.G. Cory, S. Singer, Biochemical Analysis Using High-Resolution Magic Angle Spinning NMR Spectroscopy Distinguishes Lipoma-Like Well-Differentiated Liposarcoma from Normal Fat, J. Am. Chem. Soc. 123 (2001) 9200–9201, https://doi.org/10.1021/ja016182u.
[986] L.L. Cheng, I.W. Chang, B.L. Smith, R.G. González, Evaluating human breast ductal carcinomas with high-resolution magic-angle spinning proton magnetic resonance spectroscopy, J. Magn. Reson. 135 (1998) 194–202, https://doi.org/10.1006/jmre.1998.1578.
[987] P. Weybright, K. Millis, N. Campbell, D.G. Cory, S. Singer, Gradient, high-resolution, magic angle spinning 1H nuclear magnetic resonance spectroscopy of intact cells, Magn. Reson. Med. 39 (1998) 337–345, https://doi.org/10.1002/mrm.1910390302.
[988] K. Millis, P. Weybright, N. Campbell, J.A. Fletcher, C.D. Fletcher, D.G. Cory, S. Singer, Classification of human liposarcoma and lipoma using ex vivo proton NMR spectroscopy, Magn. Reson. Med. 41 (1999) 257–267, https://doi.org/10.1002/(sici)1522-2594(199902)41:2<257::aid-mrm8>3.0.co;2-n.
[989] J.-H. Chen, B.M. Enloe, P. Weybright, N. Campbell, D. Dorfman, C.D. Fletcher, D.G. Cory, S. Singer, Biochemical correlates of thiazolidinedione-induced adipocyte differentiation by high-resolution magic angle spinning NMR spectroscopy, Magn. Reson. Med. 48 (2002) 602–610, https://doi.org/10.1002/mrm.10256.
[990] J.L. Griffin, J.C.M. Pole, J.K. Nicholson, P.L. Carmichael, Cellular environment of metabolites and a metabonomic study of tamoxifen in endometrial cells using gradient high resolution magic angle spinning 1H NMR spectroscopy, Biochim. Biophys. Acta BBA - Gen. Subj. 1619 (2003) 151–158, https://doi.org/10.1016/S0304-4165(02)00475-0.
[991] M. Wylot, D.T.E. Whittaker, S.A.C. Wren, J.H. Bothwell, L. Hughes, J.L. Griffin, Monitoring apoptosis in intact cells by high-resolution magic angle spinning 1H NMR spectroscopy, NMR Biomed. 23 (2021) 620–714, https://doi.org/10.1002/nbm.4456.
[992] J.L. Griffin, M. Bollard, J.K. Nicholson, K. Bhakoo, Spectral profiles of cultured neuronal and glial cells derived from HRMAS1H NMR spectroscopy, NMR Biomed. 15 (2002) 375–384, https://doi.org/10.1002/nbm.792.
[993] D. Morvan, A. Demidem, J. Papon, J.C. Madelmont, Quantitative HRMAS proton total correlation spectroscopy applied to cultured melanoma cells treated by chloroethyl nitrosourea: Demonstration of phospholipid metabolism alterations, Magn. Reson. Med. 49 (2003) 241–248, https://doi.org/10.1002/mrm.10368.
[994] H.K. Nyblom, L.I. Nord, R. Andersson, L. Kenne, P. Bergsten, Glucose-inducedde novo synthesis of fatty acyls causes proportional increases in INS-1E cellular lipids, NMR Biomed. 21 (2008) 357–365, https://doi.org/10.1002/nbm.1197.
[995] C. Shi, X. Wang, S. Wu, Y. Zhu, L.W.K. Chung, H. Mao, HRMAS 1H-NMR measured changes of the metabolite profile as mesenchymal stem cells differentiate to targeted fat cells in vitro: implications for non-invasive monitoring of stem cell differentiation in vivo, J. Tissue Eng. Regen. Med. 2 (2008) 482–490, https://doi.org/10.1002/term.120.
[996] J. Martín-Sitjar, T. Delgado-Goñi, M.E. Cabañas, J. Tzen, C. Arús, Influence of the spinning rate in the HR-MAS pattern of mobile lipids in C6 glioma cells and in artificial oil bodies, Magn. Reson. Mater. Phys. Biol. Med. 25 (2012) 487–496, https://doi.org/10.1007/s10334-012-0327-6.
[997] C. Precht, G. Diserens, A. Oevermann, M. Vermathen, J. Lang, C. Boesch, P. Vermathen, Visibility of lipid resonances in HR-MAS spectra of brain biopsies subject to spinning rate variation, Biochim. Biophys. Acta BBA - Mol. Cell Biol. Lipids. 1851 (2015) 1539–1544, https://doi.org/10.1016/j.bbalip.2015.09.003.
[998] M. Skogen Chauton, T. Røvik Størseth, G. Johnsen, High-resolution magic angle spinning ^{1}H NMR analysis of whole cells of *Thalassiosira pseudonana* (Bacillariophyceae): Broad range analysis of metabolic composition and nutritional value, J. Appl. Phycol. 15 (2003) 533–542, https://doi.org/10.1023/B:JAPH.0000004355.11837.1d.
[999] M.S. Chauton, T.R. Størseth, J. Krane, HIGH-RESOLUTION MAGIC ANGLE SPINNING NMR ANALYSIS OF WHOLE CELLS OF CHAETOCEROS MUELLERI (BACILLARIOPHYCEAE) AND COMPARISON WITH 13C-NMR AND DISTORTIONLESS ENHANCEMENT BY POLARIZATION TRANSFER 13C-NMR ANALYSIS OF LIPOPHILIC EXTRACTS, J. Phycol. 40 (2004) 611–618, https://doi.org/10.1111/j.1529-8817.2004.03134.x.
[1000] T.R. Størseth, K. Hansen, J. Skjermo, J. Krane, Characterization of a beta-D-(1–>3)-glucan from the marine diatom Chaetoceros mülleri by high-resolution magic-angle spinning NMR spectroscopy on whole algal cells, Carbohydr. Res. 339 (2004) 421–424, https://doi.org/10.1016/j.carres.2003.10.021.
[1001] M. Chauton, O. Optun, T. Bathen, Z. Volent, I. Gribbestad, G. Johnsen, HR MAS 1H NMR spectroscopy analysis of marine microalgal whole cells, Mar. Ecol. Prog. Ser. 256 (2003) 57–62, https://doi.org/10.3354/meps256057.
[1002] M.S. Chauton, T. Størseth, HR MAS NMR Spectroscopy of Marine Microalgae, in: Mod. Magn. Reson., Springer International Publishing, Cham, 2018: pp. 1927–1935. https://doi.org/10.1007/978-3-319-28388-3_82..
[1003] N. Merkley, R.T. Syvitski, Profiling whole microalgal cells by high-resolution magic angle spinning (HR-MAS) magnetic resonance spectroscopy, J. Appl. Phycol. 24 (2012) 535–540, https://doi.org/10.1007/s10811-011-9731-y.
[1004] C. Zea Obando, I. Linossier, N. Kervarec, M. Zubia, J. Turquet, F. Faÿ, K. Rehel, Rapid identification of osmolytes in tropical microalgae and cyanobacteria by 1H HR-MAS NMR spectroscopy, Talanta. 153 (2016) 372–380, https://doi.org/10.1016/j.talanta.2016.02.024.
[1005] S. Salaün, N. Kervarec, P. Potin, D. Haras, M. Piotto, S. La Barre, Whole-cell spectroscopy is a convenient tool to assist molecular identification of cultivatable marine bacteria and to investigate their adaptive metabolism, Talanta. 80 (2010) 1758–1770, https://doi.org/10.1016/j.talanta.2009.10.020.
[1006] Y.L. Mobarhan, B. Fortier-McGill, R. Soong, W.E. Maas, M. Fey, M. Monette, H. J. Stronks, S. Schmidt, H. Heumann, W. Norwood, A.J. Simpson, Comprehensive multiphase NMR applied to a living organism, Chem Sci. 7 (2016) 4856–4866, https://doi.org/10.1039/C6SC00329J.
[1007] Y. Liaghati-Mobarhan, R. Soong, D. Lane, A.J. Simpson, In vivo comprehensive multiphase NMR, Magn. Reson. Chem. 58 (2019) 427–444, https://doi.org/10.1002/mrc.4832.
[1008] M. Bayet-Robert, S. Lim, C. Barthomeuf, D. Morvan, Biochemical disorders induced by cytotoxic marine natural products in breast cancer cells as revealed by proton NMR spectroscopy-based metabolomics, Biochem. Pharmacol. 80 (2010) 1170–1179, https://doi.org/10.1016/j.bcp.2010.07.007.
[1009] M. Bayet-Robert, D. Loiseau, P. Rio, A. Demidem, C. Barthomeuf, G. Stepien, D. Morvan, Quantitative two-dimensional HRMAS 1H-NMR spectroscopy-based metabolite profiling of human cancer cell lines and response to chemotherapy, Magn. Reson. Med. 63 (2010) 1172–1183, https://doi.org/10.1002/mrm.22303.
[1010] M. Bayet-Robert, D. Morvan, P. Chollet, C. Barthomeuf, Pharmacometabolomics of docetaxel-treated human MCF7 breast cancer cells provides evidence of varying cellular responses at high and low doses, Breast Cancer Res. Treat. 120 (2010) 613–626, https://doi.org/10.1007/s10549-009-0430-1.
[1011] I. García-Álvarez, L. Garrido, L. Romero-Ramírez, M. Nieto-Sampedro, A. Fernández-Mayoralas, R. Campos-Olivas, The effect of antitumor glycosides on glioma cells and tissues as studied by proton HR-MAS NMR spectroscopy, PLoS ONE. 8 (2013), https://doi.org/10.1371/journal.pone.0078391 e78391.
[1012] T. Mesti, P. Savarin, M.N. Triba, L. Le Moyec, J. Ocvirk, C. Banissi, A.F. Carpentier, Metabolic Impact of Anti-Angiogenic Agents on U87 Glioma Cells, PLoS ONE. 9 (2014), https://doi.org/10.1371/journal.pone.0099198 e99198.
[1013] I. Lamego, I.F. Duarte, M.P.M. Marques, A.M. Gil, Metabolic Markers of MG-63 Osteosarcoma Cell Line Response to Doxorubicin and Methotrexate

Treatment: Comparison to Cisplatin, J. Proteome Res. 13 (2014) 6033–6045, https://doi.org/10.1021/pr500907d.
[1014] M. Vermathen, L.E.H. Paul, G. Diserens, P. Vermathen, J. Furrer, 1H HR-MAS NMR Based Metabolic Profiling of Cells in Response to Treatment with a Hexacationic Ruthenium Metallaprism as Potential Anticancer Drug, PLOS ONE. 10 (2015), https://doi.org/10.1371/journal.pone.0128478 e0128478.
[1015] W. Li, R. Slominski, A.T. Slominski, High-resolution magic angle spinning nuclear magnetic resonance analysis of metabolic changes in melanoma cells after induction of melanogenesis, Anal. Biochem. 386 (2009) 282–284, https://doi.org/10.1016/j.ab.2008.12.017.
[1016] N. Martínez-Martín, A. Blas-García, J.M. Morales, M. Marti-Cabrera, D. Monleon, N. Apostolova, Metabolomics of the effect of AMPK activation by AICAR on human umbilical vein endothelial cells, Int. J. Mol. Med. 29 (2012) 88–94, https://doi.org/10.3892/ijmm.2011.802.
[1017] J. Feng, J. Li, H. Wu, Z. Chen, Metabolic responses of HeLa cells to silica nanoparticles by NMR-based metabolomic analyses, Metabolomics. 9 (2013) 874–886, https://doi.org/10.1007/s11306-013-0499-8.
[1018] B.J. Blaise, C. Lopez, C. Vercherat, A. Lacheretz-Bernigaud, M. Bayet-Robert, L. Rezig, J.-Y. Scoazec, A. Calender, L. Emsley, B. Elena-Herrmann, M. Cordier-Bussat, Metabolic expressivity of human genetic variants: NMR metabotyping of MEN1 pathogenic mutants, J. Pharm. Biomed. Anal. 93 (2014) 118–124, https://doi.org/10.1016/j.jpba.2013.09.029.
[1019] F. Moussallieh, E. Moss, K. Elbayed, G. Lereaux, F. Tourneix, J. Lepoittevin, Modifications induced by chemical skin allergens on the metabolome of reconstructed human epidermis: A pilot high-resolution magic angle spinning nuclear magnetic resonance study, Contact Dermatitis. 82 (2020) 137–146, https://doi.org/10.1111/cod.13415.
[1020] K. Elbayed, V. Berl, C. Debeuckelaere, F.-M. Moussallieh, M. Piotto, I.-J. Namer, J.-P. Lepoittevin, HR-MAS NMR Spectroscopy of Reconstructed Human Epidermis: Potential for the *in Situ* Investigation of the Chemical Interactions between Skin Allergens and Nucleophilic Amino Acids, Chem. Res. Toxicol. 26 (2013) 136–145, https://doi.org/10.1021/tx300428u.
[1021] H. Srour, F.-M. Moussallieh, K. Elbayed, E. Giménez-Arnau, J.-P. Lepoittevin, In Situ Alkylation of Reconstructed Human Epidermis by Methyl Methanesulfonate: A Quantitative HRMAS NMR Chemical Reactivity Mapping, Chem. Res. Toxicol. 33 (2020) 3023–3030, https://doi.org/10.1021/acs.chemrestox.0c00362.
[1022] G. Diserens, M. Vermathen, M.-G. Zurich, P. Vermathen, Longitudinal investigation of the metabolome of 3D aggregating brain cell cultures at different maturation stages by 1H HR-MAS NMR, Anal. Bioanal. Chem. 410 (2018) 6733–6749, https://doi.org/10.1007/s00216-018-1295-0.
[1023] X. Hanoulle, J.-M. Wieruszeski, P. Rousselot-Pailley, I. Landrieu, A.R. Baulard, G. Lippens, Monitoring of the ethionamide pro-drug activation in mycobacteria by 1H high resolution magic angle spinning NMR, Biochem. Biophys. Res. Commun. 331 (2005) 452–458, https://doi.org/10.1016/j.bbrc.2005.03.197.
[1024] X. Hanoulle, J.-M. Wieruszeski, P. Rousselot-Pailley, I. Landrieu, C. Locht, G. Lippens, A.R. Baulard, Selective intracellular accumulation of the major metabolite issued from the activation of the prodrug ethionamide in mycobacteria, J. Antimicrob. Chemother. 58 (2006) 768–772, https://doi.org/10.1093/jac/dkl332.
[1025] E.L. Gjersing, J.L. Herberg, J. Horn, C.M. Schaldach, R.S. Maxwell, NMR Metabolomics of Planktonic and Biofilm Modes of Growth in *Pseudomonas aeruginosa*, Anal. Chem. 79 (2007) 8037–8045, https://doi.org/10.1021/ac070800t.
[1026] V. Righi, C. Constantinou, M. Kesarwani, L.G. Rahme, A.A. Tzika, Effects of a small, volatile bacterial molecule on Pseudomonas aeruginosa bacteria using whole cell high-resolution magic angle spinning nuclear magnetic resonance spectroscopy and genomics, Int. J. Mol. Med. 42 (2018) 2129–2136, https://doi.org/10.3892/ijmm.2018.3760.
[1027] J. Müller, M. Vermathen, D. Leitsch, P. Vermathen, N. Müller, Metabolomic Profiling of Wildtype and Transgenic Giardia lamblia Strains by 1H HR-MAS NMR Spectroscopy, Metabolites. 10 (2020) 53, https://doi.org/10.3390/metabo10020053.
[1028] M. Vermathen, J. Müller, J. Furrer, N. Müller, P. Vermathen, 1H HR-MAS NMR spectroscopy to study the metabolome of the protozoan parasite Giardia lamblia, Talanta. 188 (2018) 429–441, https://doi.org/10.1016/j.talanta.2018.06.006.
[1029] P.W. Kuchel, W.A. Bubb, S. Ramadan, B.E. Chapman, D.J. Philp, M. Coen, J.E. Gready, P.J. Harvey, A.J. McLean, J. Hook, 31P MAS-NMR of human erythrocytes: Independence of cell volume from angular velocity, Magn. Reson. Med. 52 (2004) 663–668, https://doi.org/10.1002/mrm.20139.
[1030] M. André, J.-N. Dumez, L. Rezig, L. Shintu, M. Piotto, S. Caldarelli, Complete protocol for slow-spinning high-resolution magic-angle spinning NMR analysis of fragile tissues, Anal. Chem. 86 (2014) 10749–10754, https://doi.org/10.1021/ac502792u.
[1031] R.A. Wind, J.Z. Hu, D.N. Rommereim, High-resolution 1H NMR spectroscopy in organs and tissues using slow magic angle spinning, Magn. Reson. Med. 46 (2001) 213–218, https://doi.org/10.1002/mrm.1181.
[1032] J.Z. Hu, R.A. Wind, D.N. Rommereim, 1H relaxation times of metabolites in biological samples obtained with nondestructive ex-vivo slow-MAS NMR, Magn. Reson. Chem. 44 (2006) 269–275, https://doi.org/10.1002/mrc.1764.
[1033] J.Z. Hu, D.N. Rommereim, R.A. Wind, High-resolution1H NMR spectroscopy in rat liver using magic angle turning at a 1 Hz spinning rate, Magn. Reson. Med. 47 (2002) 829–836, https://doi.org/10.1002/mrm.10139.
[1034] M. Tabatabaei-Anaraki, M.J. Simpson, A.J. Simpson, Reducing impacts of organism variability in metabolomics via time trajectory in vivo NMR, Magn. Reson. Chem. 56 (2018) 1117–1123, https://doi.org/10.1002/mrc.4759.
[1035] A. Bunescu, J. Garric, B. Vollat, E. Canet-Soulas, D. Graveron-Demilly, F. Fauvelle, In vivo proton HR-MAS NMR metabolic profile of the freshwater cladoceran Daphnia magna, Mol BioSyst. 6 (2010) 121–125, https://doi.org/10.1039/B915417E.
[1036] V. Righi, Y. Apidianakis, N. Psychogios, L.G. Rahme, R.G. Tompkins, A.A. Tzika, In vivo high-resolution magic angle spinning proton NMR spectroscopy of Drosophila melanogaster flies as a model system to investigate mitochondrial dysfunction in Drosophila GST2 mutants, Int. J. Mol. Med. 34 (2014) 327–333, https://doi.org/10.3892/ijmm.2014.1757.
[1037] V. Sarou-Kanian, N. Joudiou, F. Louat, M. Yon, F. Szeremeta, S. Même, D. Massiot, M. Decoville, F. Fayon, J.-C. Beloeil, Metabolite localization in living drosophila using High Resolution Magic Angle Spinning NMR, Sci. Rep. 5 (2015) 79–85, https://doi.org/10.1038/srep09872.
[1038] Y. Liaghati-Mobarhan, R. Soong, W. Bermel, M.J. Simpson, J. Struppe, H. Heumann, S. Schmidt, H. Boenisch, D. Lane, A.J. Simpson, In Vivo Ultraslow MAS 2H/ 13C NMR Emphasizes Metabolites in Dynamic Flux, ACS Omega. 3 (2018) 17023–17035, https://doi.org/10.1021/acsomega.8b02882.
[1039] Q. Hassan, R. Dutta Majumdar, B. Wu, D. Lane, M. Tabatabaei-Anraki, R. Soong, M.J. Simpson, A.J. Simpson, Improvements in lipid suppression for 1H NMR-based metabolomics: Applications to solution-state and HR-MAS NMR in natural and in vivo samples, Magn. Reson. Chem. 57 (2019) 69–81, https://doi.org/10.1002/mrc.4814.
[1040] M.T. Anaraki, D.H. Lysak, K. Downey, F.V.C. Kock, X. You, R.D. Majumdar, A. Barison, L.M. Lião, A.G. Ferreira, V. Decker, B. Goerling, M. Spraul, M. Godejohann, P.A. Helm, S. Kleywegt, K. Jobst, R. Soong, M.J. Simpson, A.J. Simpson, NMR spectroscopy of wastewater: A review, case study, and future potential, Prog. Nucl. Magn. Reson. Spectrosc. 126–127 (2021) 121–180, https://doi.org/10.1016/j.pnmrs.2021.08.001.
[1041] A. Wong, X. Li, L. Molin, F. Solari, B. Elena-Herrmann, D. Sakellariou, µHigh resolution-magic-angle spinning NMR spectroscopy for metabolic phenotyping of Caenorhabditis elegans, Anal. Chem. 86 (2014) 6064–6070, https://doi.org/10.1021/ac501208z.
[1042] A. Wong, C. Boutin, P.M. Aguiar, 1H high resolution magic-angle coil spinning (HR-MACS) µNMR metabolic profiling of whole Saccharomyces cerevisiae cells: a demonstrative study, Front. Chem. 2 (2014) 1–7.
[1043] G. Bodenhausen, R. Freeman, Correlation of proton and carbon-13 nmr spectra by heteronuclear two-dimensional spectroscopy, J. Magn. Reson. 1969 (28) (1977) 471–476, https://doi.org/10.1016/0022-2364(77)90289-X.
[1044] G. Bodenhausen, R. Freeman, Correlation of chemical shifts of protons and carbon-13, J. Am. Chem. Soc. 100 (1978) 320–321, https://doi.org/10.1021/ja00469a073.
[1045] A.A. Maudsley, R.R. Ernst, Indirect detection of magnetic resonance by heteronuclear two-dimensional spectroscopy, Chem. Phys. Lett. 50 (1977) 368–372, https://doi.org/10.1016/0009-2614(77)80345-X.
[1046] G.A. Morris, R. Freeman, Enhancement of nuclear magnetic resonance signals by polarization transfer, J. Am. Chem. Soc. 101 (1979) 760–762, https://doi.org/10.1021/ja00497a058.
[1047] G. Bodenhausen, D.J. Ruben, Natural abundance nitrogen-15 NMR by enhanced heteronuclear spectroscopy, Chem. Phys. Lett. 69 (1980) 185–189, https://doi.org/10.1016/0009-2614(80)80041-8.
[1048] G. Bodenhausen, R. Freeman, R. Niedermeyer, D.L. Turner, Double fourier transformation in high-resolution NMR, J. Magn. Reson. 1969 (26) (1977) 133–164, https://doi.org/10.1016/0022-2364(77)90243-8.
[1049] T. Szyperski, Biosynthetically Directed Fractional 13C-labeling of Proteinogenic Amino Acids. An Efficient Analytical Tool to Investigate Intermediary Metabolism, Eur. J. Biochem. 232 (1995) 433–448, https://doi.org/10.1111/j.1432-1033.1995.tb20829.x.
[1050] P.K. Mandal, A. Majumdar, A comprehensive discussion of HSQC and HMQC pulse sequences, Concepts Magn. Reson. 20A (2004) 1–23, https://doi.org/10.1002/cmr.a.10095.
[1051] D. Lane, T.E. Skinner, N.I. Gershenzon, W. Bermel, R. Soong, R. Dutta Majumdar, Y. Liaghati-Mobarhan, S. Schmidt, H. Heumann, M. Monette, M.J. Simpson, A.J. Simpson, Assessing the potential of quantitative 2D HSQC NMR in 13C enriched living organisms, J. Biomol. NMR. 73 (2019) 31–42, https://doi.org/10.1007/s10858-018-0221-2.
[1052] P. Giraudeau, Quantitative 2D liquid-state NMR, Magn. Reson. Chem. 52 (2014) 259–272, https://doi.org/10.1002/mrc.4068.
[1053] J. Farjon, C. Milande, E. Martineau, S. Akoka, P. Giraudeau, The FAQUIRE Approach: FAst, QUantitative, hIghly Resolved and sEnsitivity Enhanced ^{1}H, ^{13}C Data, Anal. Chem. 90 (2018) 1845–1851, https://doi.org/10.1021/acs.analchem.7b03874.
[1054] H. Wen, Y.J. An, W.J. Xu, K.W. Kang, S. Park, Real-time monitoring of cancer cell metabolism and effects of an anticancer agent using 2D in-cell NMR spectroscopy, Angew. Chem. Int. Ed Engl. 54 (2015) 5374–5377, https://doi.org/10.1002/anie.201410380.
[1055] W.J. Xu, H. Wen, H.S. Kim, Y.-J. Ko, S.-M. Dong, I.-S. Park, J.I. Yook, S. Park, Observation of acetyl phosphate formation in mammalian mitochondria using real-time in-organelle NMR metabolomics, Proc. Natl. Acad. Sci. U. S. A. 115 (2018) 4152–4157, https://doi.org/10.1073/pnas.1720908115.
[1056] M. Akhter, R. Dutta Majumdar, B. Fortier-McGill, R. Soong, Y. Liaghati-Mobarhan, M. Simpson, G. Arhonditsis, S. Schmidt, H. Heumann, A.J. Simpson, Identification of aquatically available carbon from algae through

solution-state NMR of whole 13C-labelled cells, Anal. Bioanal. Chem. 408 (2016) 4357–4370, https://doi.org/10.1007/s00216-016-9534-8.
[1057] R. Soong, E. Nagato, A. Sutrisno, B. Fortier-McGill, M. Akhter, S. Schmidt, H. Heumann, A.J. Simpson, In vivo NMR spectroscopy: toward real time monitoring of environmental stress, Magn. Reson. Chem. 53 (2015) 774–779, https://doi.org/10.1002/mrc.4154.
[1058] M. Tabatabaei-Anaraki, R. Dutta Majumdar, N. Wagner, R. Soong, V. Kovacevic, E.J. Reiner, S.P. Bhavsar, X. Ortiz Almirall, D. Lane, M.J. Simpson, H. Heumann, S. Schmidt, A.J. Simpson, Development and Application of a Low-Volume Flow System for Solution-State in Vivo NMR, Anal. Chem. 90 (2018) 7912–7921, https://doi.org/10.1021/acs.analchem.8b00370.
[1059] R.D. Majumdar, M. Akhter, B. Fortier-McGill, R. Soong, Y. Liaghati-Mobarhan, A.J. Simpson, M. Spraul, S. Schmidt, H. Heumann, In Vivo Solution-State NMR-Based Environmental Metabolomics, EMagRes. 5 (2017) 133–148, https://doi.org/10.1002/9780470034590.emrstm1533.
[1060] T.T.M. Nguyen, Y.J. An, J.W. Cha, Y.-J. Ko, H. Lee, C.H. Chung, S.-M. Jeon, J. Lee, S. Park, Real-Time In-Organism NMR Metabolomics Reveals Different Roles of AMP-Activated Protein Kinase Catalytic Subunits acs.analchem.9b05670 Anal. Chem. (2020), https://doi.org/10.1021/acs.analchem.9b05670.
[1061] R. Dass, K. Grudziaż, T. Ishikawa, M. Nowakowski, R. Dębowska, K. Kazimierczuk, Fast 2D NMR Spectroscopy for In vivo Monitoring of Bacterial Metabolism in Complex Mixtures, Front. Microbiol. 8 (2017) 968–12. https://doi.org/10.3389/fmicb.2017.01306..
[1062] M.T. Anaraki, D.H. Lysak, R. Soong, M.J. Simpson, M. Spraul, W. Bermel, H. Heumann, M. Gundy, H. Boenisch, A.J. Simpson, NMR assignment of the *in vivo* daphnia magna metabolome, Analyst. 145 (2020) 5787–5800, https://doi.org/10.1039/D0AN01280G.
[1063] M. Bastawrous, M. Tabatabaei-Anaraki, R. Soong, W. Bermel, M. Gundy, H. Boenisch, H. Heumann, A.J. Simpson, Inverse or direct detect experiments and probes: Which are "best" for in-vivo NMR research of 13C enriched organisms?, Anal. Chim. Acta. 1138 (2020) 168–180, https://doi.org/10.1016/j.aca.2020.09.065.
[1064] S. Lee, H. Wen, J.W. Cha, S. Park, Specific Detection of Cellular Glutamine Hydrolysis in Live Cells Using HNCO Triple Resonance NMR, ACS Chem. Biol. 11 (2016) 3140–3145, https://doi.org/10.1021/acschembio.6b00493.
[1065] D. Lane, R. Soong, W. Bermel, P. Ning, R. Dutta Majumdar, M. Tabatabaei-Anaraki, H. Heumann, M. Gundy, H. Bönisch, Y. Liaghati-Mobarhan, M.J. Simpson, A.J. Simpson, Selective Amino Acid-Only in Vivo NMR: A Powerful Tool To Follow Stress Processes, ACS Omega. 4 (2019) 9017–9028, https://doi.org/10.1021/acsomega.9b00931.
[1066] D. Lane, W. Bermel, P. Ning, T.-Y. Jeong, R. Martin, R. Soong, B. Wu, M. Tabatabaei-Anaraki, H. Heumann, M. Gundy, H. Boenisch, A. Adamo, G.B. Arhonditsis, A.J. Simpson, Targeting the Lowest Concentration of a Toxin that Induces a Detectable Metabolic Response in living Organisms: Time Resolved In vivo 2D NMR During a Concentration Ramp acs.analchem.0c01370-14 Anal. Chem. (2020), https://doi.org/10.1021/acs.analchem.0c01370.
[1067] A. Jenne, R. Soong, W. Bermel, N. Sharma, A. Masi, M. Tabatabaei-Anaraki, A. Simpson, Focusing on "the important" through targeted NMR experiments: an example of selective 13C–12C bond detection in complex mixtures, Faraday Discuss. 218 (2019) 372–394, https://doi.org/10.1039/C8FD00213D.
[1068] J.C. Lindon, O.P. Beckonert, E. Holmes, J.K. Nicholson, High-resolution magic angle spinning NMR spectroscopy: Application to biomedical studies, Prog. Nucl. Magn. Reson. Spectrosc. 55 (2009) 79–100, https://doi.org/10.1016/j.pnmrs.2008.11.004.
[1069] Y. Huang, S. Cao, Y. Yang, S. Cai, H. Zhan, C. Tan, L. Lin, Z. Zhang, Z. Chen, Ultrahigh-Resolution NMR Spectroscopy for Rapid Chemical and Biological Applications in Inhomogeneous Magnetic Fields, Anal. Chem. 89 (2017) 7115–7122, https://doi.org/10.1021/acs.analchem.7b01036.
[1070] J.H. Ardenkjaer-Larsen, B. Fridlund, A. Gram, G. Hansson, L. Hansson, M.H. Lerche, R. Servin, M. Thaning, K. Golman, Increase in signal-to-noise ratio of >10,000 times in liquid-state NMR, Proc. Natl. Acad. Sci. 100 (2003) 10158–10163, https://doi.org/10.1073/pnas.1733835100.
[1071] A.C. Pinon, A. Capozzi, J.H. Ardenkjaer-Larsen, Hyperpolarization via dissolution dynamic nuclear polarization: new technological and methodological advances, Magn. Reson. Mater. Phys. Biol. Med. 137 (2020) 8428–8519, https://doi.org/10.1007/s10334-020-00894-w.
[1072] S. Jannin, J.-N. Dumez, P. Giraudeau, D. Kurzbach, Application and methodology of dissolution dynamic nuclear polarization in physical, chemical and biological contexts, J. Magn. Reson. 305 (2019) 41–50, https://doi.org/10.1016/j.jmr.2019.06.001.
[1073] A.S.L. Thankamony, J.J. Wittmann, M. Kaushik, B. Corzilius, Dynamic nuclear polarization for sensitivity enhancement in modern solid-state NMR, Prog. Nucl. Magn. Reson. Spectrosc. 102–103 (2017) 120–195, https://doi.org/10.1016/j.pnmrs.2017.06.002.
[1074] B. Plainchont, P. Berruyer, J.-N. Dumez, S. Jannin, P. Giraudeau, Dynamic Nuclear Polarization Opens New Perspectives for NMR Spectroscopy in Analytical Chemistry, Anal. Chem. 90 (2018) 3639–3650, https://doi.org/10.1021/acs.analchem.7b05236.
[1075] M.H. Lerche, P.R. Jensen, M. Karlsson, S. Meier, NMR insights into the inner workings of living cells, Anal. Chem. 87 (2015) 119–132, https://doi.org/10.1021/ac501467x.
[1076] K. Golman, J.H. Ardenkjaer-Larsen, J.S. Petersson, S. Mansson, I. Leunbach, Molecular imaging with endogenous substances, Proc. Natl. Acad. Sci. 100 (2003) 10435–10439, https://doi.org/10.1073/pnas.1733836100.
[1077] S.E. Day, M.I. Kettunen, F.A. Gallagher, D.-E. Hu, M. Lerche, J. Wolber, K. Golman, J.H. Ardenkjaer-Larsen, K.M. Brindle, Detecting tumor response to treatment using hyperpolarized 13C magnetic resonance imaging and spectroscopy, Nat. Med. 13 (2007) 1382–1387, https://doi.org/10.1038/nm1650.
[1078] M.J. Albers, R. Bok, A.P. Chen, C.H. Cunningham, M.L. Zierhut, V.Y. Zhang, S.J. Kohler, J. Tropp, R.E. Hurd, Y.-F. Yen, S.J. Nelson, D.B. Vigneron, J. Kurhanewicz, Hyperpolarized 13C Lactate, Pyruvate, and Alanine: Noninvasive Biomarkers for Prostate Cancer Detection and Grading, Cancer Res. 68 (2008) 8607–8615, https://doi.org/10.1158/0008-5472.CAN-08-0749.
[1079] T.B. Rodrigues, E.M. Serrao, B.W.C. Kennedy, D.-E. Hu, M.I. Kettunen, K.M. Brindle, Magnetic resonance imaging of tumor glycolysis using hyperpolarized 13C-labeled glucose, Nat. Med. 20 (2014) 93–97, https://doi.org/10.1038/nm.3416.
[1080] 9] F.A. Gallagher, M.I. Kettunen, D.-E. Hu, P.R. Jensen, R. in t Zandt, M. Karlsson, A. Gisselsson, S.K. Nelson, T.H. Witney, S.E. Bohndiek, G. Hansson, T. Peitersen, M.H. Lerche, K.M. Brindle, Production of hyperpolarized [1,4-13C2]malate from [1,4-13C2]fumarate is a marker of cell necrosis and treatment response in tumors., Proc. Natl. Acad. Sci. U. S. A. 106 (2009) 19801–19806. https://doi.org/10.1073/pnas.0911447106..
[1081] J. Singh, E.H. Suh, G. Sharma, C. Khemtong, A.D. Sherry, Z. Kovacs, Probing carbohydrate metabolism using hyperpolarized 13C-labeled molecules, NMR Biomed. 32 (2018) 1–23, https://doi.org/10.1002/nbm.4018.
[1082] F.A. Gallagher, S.E. Bohndiek, M.I. Kettunen, D.Y. Lewis, D. Soloviev, K.M. Brindle, Hyperpolarized 13C MRI and PET. In Vivo Tumor Biochemistry, J. Nucl. Med. 52 (2011) 1333–1336, https://doi.org/10.2967/jnumed.110.085258.
[1083] S.J. Nelson, J. Kurhanewicz, D.B. Vigneron, P.E.Z. Larson, A.L. Harzstark, M. Ferrone, M. van Criekinge, J.W. Chang, R. Bok, I. Park, G. Reed, L. Carvajal, E.J. Small, P. Munster, V.K. Weinberg, J.H. Ardenkjaer-Larsen, A.P. Chen, R.E. Hurd, L.-I. Odegardstuen, F.J. Robb, J. Tropp, J.A. Murray, Metabolic imaging of patients with prostate cancer using hyperpolarized [1-^{13}C]pyruvate, Sci. Transl. Med. 5 (2013) 198ra108, https://doi.org/10.1126/scitranslmed.3006070.
[1084] Z.J. Wang, M.A. Ohliger, P.E.Z. Larson, J.W. Gordon, R.A. Bok, J. Slater, J.E. Villanueva-Meyer, C.P. Hess, J. Kurhanewicz, D.B. Vigneron, Hyperpolarized 13C MRI: State of the Art and Future Directions, Radiology. 291 (2019) 273–284, https://doi.org/10.1148/radiol.2019182391.
[1085] 6] F.A. Gallagher, R. Woitek, M.A. McLean, A.B. Gill, R. Manzano Garcia, E. Provenzano, F. Riemer, J. Kaggie, A. Chhabra, S. Ursprung, J.T. Grist, C.J. Daniels, F. Zaccagna, M.-C. Laurent, M. Locke, S. Hilborne, A. Frary, T. Torheim, C. Boursnell, A. Schiller, I. Patterson, R. Slough, B. Carmo, J. Kane, H. Biggs, E. Harrison, S.S. Deen, A. Patterson, T. Lanz, Z. Kingsbury, M. Ross, B. Basu, R. Baird, D.J. Lomas, E. Sala, J. Wason, O.M. Rueda, S.-F. Chin, I.B. Wilkinson, M.J. Graves, J.E. Abraham, F.J. Gilbert, C. Caldas, K.M. Brindle, Imaging breast cancer using hyperpolarized carbon-13 MRI., Proc. Natl. Acad. Sci. U. S. A. 117 (2020) 2092–2098. https://doi.org/10.1073/pnas.1913841117..
[1086] R.L. Hesketh, J. Wang, A.J. Wright, D.Y. Lewis, A.E. Denton, R. Grenfell, J.L. Miller, R. Bielik, M. Gehrung, M. Fala, S. Ros, B. Xie, D.-E. Hu, K.M. Brindle, Magnetic Resonance Imaging Is More Sensitive Than PET for Detecting Treatment-Induced Cell Death-Dependent Changes in Glycolysis, Cancer Res. 79 (2019) 3557–3569, https://doi.org/10.1158/0008-5472.CAN-19-0182.
[1087] S. Siddiqui, S. Kadlecek, M. Pourfathi, Y. Xin, W. Mannherz, H. Hamedani, N. Drachman, K. Ruppert, J. Clapp, R. Rizi, The use of hyperpolarized carbon-13 magnetic resonance for molecular imaging, Adv. Drug Deliv. Rev. 113 (2017) 3–23, https://doi.org/10.1016/j.addr.2016.08.011.
[1088] M. Mishkovsky, A. Comment, Hyperpolarized MRS: New tool to study real-time brain function and metabolism, Anal. Biochem. 529 (2017) 270–277, https://doi.org/10.1016/j.ab.2016.09.020.
[1089] K.N. Timm, J.J. Miller, J.A. Henry, D.J. Tyler, Cardiac applications of hyperpolarised magnetic resonance, Prog. Nucl. Magn. Reson. Spectrosc. 106–107 (2018) 66–87, https://doi.org/10.1016/j.pnmrs.2018.05.002.
[1090] B.T. Chung, H.-Y. Chen, J. Gordon, D. Mammoli, R. Sriram, A.W. Autry, L.M. Le Page, M.M. Chaumeil, P. Shin, J. Slater, C.T. Tan, C. Suszczynski, S. Chang, Y. Li, R.A. Bok, S.M. Ronen, P.E.Z. Larson, J. Kurhanewicz, D.B. Vigneron, First hyperpolarized [2-13C]pyruvate MR studies of human brain metabolism, J. Magn. Reson. 309 (2019), https://doi.org/10.1016/j.jmr.2019.106617 106617.
[1091] J.H. Ardenkjaer-Larsen, Hyperpolarized MR - What's up Doc?, J. Magn. Reson. San Diego Calif 1997 (306) (2019) 124–127, https://doi.org/10.1016/j.jmr.2019.07.017.
[1092] J. Kurhanewicz, D.B. Vigneron, J.H. Ardenkjaer-Larsen, J.A. Bankson, K. Brindle, C.H. Cunningham, F.A. Gallagher, K.R. Keshari, A. Kjaer, C. Laustsen, D.A. Mankoff, M.E. Merritt, S.J. Nelson, J.M. Pauly, P. Lee, S. Ronen, D.J. Tyler, S.S. Rajan, D.M. Spielman, L. Wald, X. Zhang, C.R. Malloy, R. Rizi, Hyperpolarized 13C MRI: Path to Clinical Translation in Oncology, NEO. 21 (2019) 1–16, https://doi.org/10.1016/j.neo.2018.09.006.
[1093] T. Harris, G. Eliyahu, L. Frydman, H. Degani, Kinetics of hyperpolarized 13C1-pyruvate transport and metabolism in living human breast cancer cells, Proc. Natl. Acad. Sci. U. S. A. 106 (2009) 18131–18136, https://doi.org/10.1073/pnas.0909049106.
[1094] K.R. Keshari, R. Sriram, B.L. Koelsch, M. van Criekinge, D.M. Wilson, J. Kurhanewicz, Z.J. Wang, Hyperpolarized 13C-Pyruvate Magnetic Resonance

Reveals Rapid Lactate Export in Metastatic Renal Cell Carcinomas, Cancer Res. 73 (2013) 529–538, https://doi.org/10.1158/0008-5472.CAN-12-3461.
[1095] T.H. Witney, M.I. Kettunen, K.M. Brindle, Kinetic Modeling of Hyperpolarized 13C Label Exchange between Pyruvate and Lactate in Tumor Cells, J. Biol. Chem. 286 (2011) 24572–24580, https://doi.org/10.1074/jbc.M111.237727.
[1096] C. Harrison, C. Yang, A. Jindal, R.J. DeBerardinis, M.A. Hooshyar, M. Merritt, A. Dean Sherry, C.R. Malloy, Comparison of kinetic models for analysis of pyruvate-to-lactate exchange by hyperpolarized ^{13} C NMR: COMPARISON OF MODELS OF LDH EXCHANGE FOR ^{13} C HYPERPOLARIZED PYRUVATE, NMR Biomed. 25 (2012) 1286–1294, https://doi.org/10.1002/nbm.2801.
[1097] R. Balzan, L. Fernandes, L. Pidial, A. Comment, B. Tavitian, P.R. Vasos, Pyruvate cellular uptake and enzymatic conversion probed by dissolution DNP-NMR: the impact of overexpressed membrane transporters, Magn. Reson. Chem. 55 (2017) 579–583, https://doi.org/10.1002/mrc.4553.
[1098] F. Reineri, V. Daniele, E. Cavallari, S. Aime, Assessing the transport rate of hyperpolarized pyruvate and lactate from the intra- to the extracellular space, NMR Biomed. 29 (2016) 1022–1027, https://doi.org/10.1002/nbm.3562.
[1099] A. Lodi, S.M. Woods, S.M. Ronen, Treatment with the MEK inhibitor U0126 induces decreased hyperpolarized pyruvate to lactate conversion in breast, but not prostate, cancer cells: U0126-INDUCED CHANGES IN HYPERPOLARIZED LACTATE, NMR Biomed. 26 (2013) 299–306, https://doi.org/10.1002/nbm.2848.
[1100] M. Radoul, C. Najac, P. Viswanath, J. Mukherjee, M. Kelly, A.M. Gillespie, M. M. Chaumeil, P. Eriksson, R. Delos Santos, R.O. Pieper, S.M. Ronen, HDAC inhibition in glioblastoma monitored by hyperpolarized ^{13} C MRSI, NMR Biomed. 32 (2019), https://doi.org/10.1002/nbm.4044 e4044.
[1101] Y. Rao, S. Gammon, N.M. Zacharias, T. Liu, T. Salzillo, Y. Xi, J. Wang, P. Bhattacharya, D. Piwnica-Worms, Hyperpolarized [1- 13C]pyruvate-to-[1-13C]lactate conversion is rate-limited by monocarboxylate transporter-1 in the plasma membrane, Proc. Natl. Acad. Sci. 117 (2020) 22378–22389, https://doi.org/10.1073/pnas.2003537117.
[1102] M.M. Chaumeil, M. Radoul, C. Najac, P. Eriksson, P. Viswanath, M.D. Blough, C. Chesnelong, H.A. Luchman, J.G. Cairncross, S.M. Ronen, Hyperpolarized 13 C MR imaging detects no lactate production in mutant IDH1 gliomas: Implications for diagnosis and response monitoring, NeuroImage Clin. 12 (2016) 180–189, https://doi.org/10.1016/j.nicl.2016.06.018.
[1103] R. Sriram, M. Van Criekinge, A. Hansen, Z.J. Wang, D.B. Vigneron, D.M. Wilson, K.R. Keshari, J. Kurhanewicz, Real-time measurement of hyperpolarized lactate production and efflux as a biomarker of tumor aggressiveness in an MR compatible 3D cell culture bioreactor: Real Time Measure of HP Lactate Production and Efflux, NMR Biomed. 28 (2015) 1141–1149, https://doi.org/10.1002/nbm.3354.
[1104] V. Breukels, K. C.) F. J. Jansen, F.H.A. van Heijster, A. Capozzi, P.J.M. van Bentum, J.A. Schalken, A. Comment, T.W.J. Scheenen, Direct dynamic measurement of intracellular and extracellular lactate in small-volume cell suspensions with 13C hyperpolarised NMR, NMR Biomed. 28 (2015) 1040–1048. https://doi.org/10.1002/nbm.3341..
[1105] B.L. Koelsch, R. Sriram, K.R. Keshari, C. Leon Swisher, M. Van Criekinge, S. Sukumar, D.B. Vigneron, Z.J. Wang, P.E.Z. Larson, J. Kurhanewicz, Separation of extra- and intracellular metabolites using hyperpolarized 13C diffusion weighted MR, J. Magn. Reson. 270 (2016) 115–123, https://doi.org/10.1016/j.jmr.2016.07.002.
[1106] G. Zhang, S. Ahola, M.H. Lerche, V.-V. Telkki, C. Hilty, Identification of Intracellular and Extracellular Metabolites in Cancer Cells Using 13C Hyperpolarized Ultrafast Laplace NMR, Anal. Chem. 90 (2018) 11131–11137, https://doi.org/10.1021/acs.analchem.8b03096.
[1107] K.R. Keshari, R. Sriram, M. van Criekinge, D.M. Wilson, Z.J. Wang, D.B. Vigneron, D.M. Peehl, J. Kurhanewicz, Metabolic Reprogramming and Validation of Hyperpolarized 13C Lactate as a Prostate Cancer Biomarker Using a Human Prostate Tissue Slice Culture Bioreactor, The Prostate. 73 (2013) 1171–1181, https://doi.org/10.1002/pros.22665.
[1108] C. Yang, C. Harrison, E.S. Jin, D.T. Chuang, A.D. Sherry, C.R. Malloy, M.E. Merritt, R.J. DeBerardinis, Simultaneous Steady-state and Dynamic 13C NMR Can Differentiate Alternative Routes of Pyruvate Metabolism in Living Cancer Cells, J. Biol. Chem. 289 (2014) 6212–6224, https://doi.org/10.1074/jbc.M113.543637.
[1109] S. Jeong, R. Eskandari, S.M. Park, J. Alvarez, S.S. Tee, R. Weissleder, M.G. Kharas, H. Lee, K.R. Keshari, Real-time quantitative analysis of metabolic flux in live cells using a hyperpolarized micromagnetic resonance spectrometer, Sci. Adv. 3 (2017), https://doi.org/10.1126/sciadv.1700341 e1700341.
[1110] H. Lees, M. Millan, F. Ahamed, R. Eskandari, K.L. Granlund, S. Jeong, K.R. Keshari, Multi-sample measurement of hyperpolarized pyruvate-to-lactate flux in melanoma cells, NMR Biomed. 103 (2020) 10435–10510, https://doi.org/10.1002/nbm.4447.
[1111] S. Meier, P.R. Jensen, J.Ø. Duus, Direct observation of metabolic differences in living Escherichia coli strains K-12 and BL21, ChemBioChem. 13 (2012) 308–310, https://doi.org/10.1002/cbic.201100654.
[1112] T. Harris, H. Degani, L. Frydman, Hyperpolarized ^{13} C NMR studies of glucose metabolism in living breast cancer cell cultures: HYPERPOLARIZED ^{13} C GLUCOSE NMR OF LIVING BREAST CANCER CELL METABOLISM, NMR Biomed. 26 (2013) 1831–1843, https://doi.org/10.1002/nbm.3024.
[1113] C.E. Christensen, M. Karlsson, J.R. Winther, P.R. Jensen, M.H. Lerche, Non-invasive In-cell Determination of Free Cytosolic [NAD +]/[NADH] Ratios Using Hyperpolarized Glucose Show Large Variations in Metabolic Phenotypes, J. Biol. Chem. 289 (2014) 2344–2352, https://doi.org/10.1074/jbc.M113.498626.
[1114] K. Kumagai, M. Akakabe, M. Tsuda, M. Tsuda, E. Fukushi, J. Kawabata, T. Abe, K. Ichikawa, Observation of glycolytic metabolites in tumor cell lysate by using hyperpolarization of deuterated glucose, Biol. Pharm. Bull. 37 (2014) 1416–1421, https://doi.org/10.1248/bpb.b14-00156.
[1115] K.N. Timm, J. Hartl, M.A. Keller, D.-E. Hu, M.I. Kettunen, T.B. Rodrigues, M. Ralser, K.M. Brindle, Hyperpolarized [U- ^{2} H, U- ^{13} C]Glucose reports on glycolytic and pentose phosphate pathway activity in EL4 tumors and glycolytic activity in yeast cells: Hyperpolarized [U- ^{2} H, U- ^{13} C]Glucose Metabolism, Magn. Reson. Med. 74 (2015) 1543–1547, https://doi.org/10.1002/mrm.25561.
[1116] S. Meier, M. Karlsson, P.R. Jensen, M.H. Lerche, J.Ø. Duus, Metabolic pathway visualization in living yeast by DNP-NMR, Mol. Biosyst. 7 (2011) 2834–2836, https://doi.org/10.1039/C1MB05202K.
[1117] S. Meier, N. Solodovnikova, P.R. Jensen, J. Wendland, Sulfite action in glycolytic inhibition: in vivo real-time observation by hyperpolarized (13)C NMR spectroscopy, ChemBioChem. 13 (2012) 2265–2269, https://doi.org/10.1002/cbic.201200450.
[1118] P.R. Jensen, M. Karlsson, M.H. Lerche, S. Meier, Real-Time DNP NMR Observations of Acetic Acid Uptake, Intracellular Acidification, and of Consequences for Glycolysis and Alcoholic Fermentation in Yeast, Chem. Weinh. Bergstr. Ger. 19 (2013) 13288–13293, https://doi.org/10.1002/chem.201302429.
[1119] P.R. Jensen, M.R.A. Matos, N. Sonnenschein, S. Meier, Combined In-Cell NMR and Simulation Approach to Probe Redox-Dependent Pathway Control, Anal. Chem. 91 (2019) 5395–5402, https://doi.org/10.1021/acs.analchem.9b00660.
[1120] S. Meier, P.R. Jensen, J.Ø. Duus, Real-time detection of central carbon metabolism in living Escherichia coli and its response to perturbations, FEBS Lett. 585 (2011) 3133–3138, https://doi.org/10.1016/j.febslet.2011.08.049.
[1121] Y. Zhuo, C.D. Cordeiro, S.K. Hekmatyar, R. Docampo, J.H. Prestegard, Dynamic nuclear polarization facilitates monitoring of pyruvate metabolism in Trypanosoma brucei, J. Biol. Chem. 292 (2017) 18161–18168, https://doi.org/10.1074/jbc.M117.807495.
[1122] S. Reynolds, N.F. bt Ismail, S.J. Calvert, A.A. Pacey, M.N.J. Paley, Evidence for Rapid Oxidative Phosphorylation and Lactate Fermentation in Motile Human Sperm by Hyperpolarized 13C Magnetic Resonance Spectroscopy, Sci. Rep. 7 (2017) 23–8. https://doi.org/10.1038/s41598-017-04146-1..
[1123] E. Can, M. Mishkovsky, H.A.I. Yoshihara, N. Kunz, D.-L. Couturier, U. Petrausch, M.-A. Doucey, A. Comment, Noninvasive rapid detection of metabolic adaptation in activated human T lymphocytes by hyperpolarized 13C magnetic resonance, Sci. Rep. 10 (2020) 200–208, https://doi.org/10.1038/s41598-019-57026-1.
[1124] D. Shishmarev, P.W. Kuchel, G. Pagès, A.J. Wright, R.L. Hesketh, F. Kreis, K.M. Brindle, Glyoxalase activity in human erythrocytes and mouse lymphoma, liver and brain probed with hyperpolarized 13C-methylglyoxal, Commun. Biol. (2018) 1–8, https://doi.org/10.1038/s42003-018-0241-1.
[1125] A. Cho, R. Eskandari, K.L. Granlund, K.R. Keshari, Hyperpolarized [6- ^{13} C, ^{15} $_{N}$ 3]-Arginine as a Probe for *in Vivo* Arginase Activity, ACS Chem. Biol. 14 (2019) 665–673, https://doi.org/10.1021/acschembio.8b01044.
[1126] B. Feuerecker, M. Durst, M. Michalik, G. Schneider, D. Saur, M. Menzel, M. Schwaiger, F. Schilling, Hyperpolarized ^{13} C Diffusion MRS of Co-Polarized Pyruvate and Fumarate to Measure Lactate Export and Necrosis, J. Cancer. 8 (2017) 3078–3085, https://doi.org/10.7150/jca.20250.
[1127] D. Shishmarev, A.J. Wright, T.B. Rodrigues, G. Pileio, G. Stevanato, K.M. Brindle, P.W. Kuchel, Sub-minute kinetics of human red cell fumarase: 1 H spin-echo NMR spectroscopy and 13 C rapid-dissolution dynamic nuclear polarization, NMR Biomed. 31 (2018), https://doi.org/10.1002/nbm.3870 e3870.
[1128] M.M. Chaumeil, P.E.Z. Larson, H.A.I. Yoshihara, O.M. Danforth, D.B. Vigneron, S.J. Nelson, R.O. Pieper, J.J. Phillips, S.M. Ronen, Non-invasive in vivo assessment of IDH1 mutational status in glioma, Nat. Commun. 4 (2013) 2429, https://doi.org/10.1038/ncomms3429.
[1129] M.M. Chaumeil, P.E.Z. Larson, S.M. Woods, L. Cai, P. Eriksson, A.E. Robinson, J.M. Lupo, D.B. Vigneron, S.J. Nelson, R.O. Pieper, J.J. Phillips, S.M. Ronen, Hyperpolarized [1- ^{13} C] Glutamate: A Metabolic Imaging Biomarker of IDH1 Mutational Status in Glioma, Cancer Res. 74 (2014) 4247–4257, https://doi.org/10.1158/0008-5472.CAN-14-0680.
[1130] C. Najac, M.M. Chaumeil, G. Kohanbash, C. Guglielmetti, J.W. Gordon, H. Okada, S.M. Ronen, Detection of inflammatory cell function using 13C magnetic resonance spectroscopy of hyperpolarized [6-13C]-arginine, Sci. Rep. 6 (2016) 31397, https://doi.org/10.1038/srep31397.
[1131] C. Cabella, M. Karlsson, C. Canapè, G. Catanzaro, S.C. Serra, L. Miragoli, L. Poggi, F. Uggeri, L. Venturi, P.R. Jensen, M.H. Lerche, F. Tedoldi, In vivo and in vitro liver cancer metabolism observed with hyperpolarized [5-13C] glutamine, J. Magn. Reson. 232 (2013) 45–52, https://doi.org/10.1016/j.jmr.2013.04.010.
[1132] C. Canapè, G. Catanzaro, E. Terreno, M. Karlsson, M.H. Lerche, P.R. Jensen, Probing treatment response of glutaminolytic prostate cancer cells to natural drugs with hyperpolarized [5- 13C]glutamine, Magn. Reson. Med. 73 (2014) 2296–2305, https://doi.org/10.1002/mrm.25360.
[1133] Y. Kondo, H. Nonaka, Y. Takakusagi, S. Sando, Design of Nuclear Magnetic Resonance Molecular Probes for Hyperpolarized Bioimaging anie.201915718 Angew. Chem. Int. Ed. (2021), https://doi.org/10.1002/anie.201915718.

[1134] P. Dzien, A. Fages, G. Jona, K.M. Brindle, M. Schwaiger, L. Frydman, Following Metabolism in Living Microorganisms by Hyperpolarized 1H NMR, J. Am. Chem. Soc. 138 (2016) 12278–12286, https://doi.org/10.1021/jacs.6b07483.
[1135] C. Morze, J.A. Engelbach, G.D. Reed, A.P. Chen, J.D. Quirk, T. Blazey, R. Mahar, C.R. Malloy, J.R. Garbow, M.E. Merritt, 15N-carnitine, a novel endogenous hyperpolarized MRI probe with long signal lifetime, Magn. Reson. Med. 85 (2020) 1814–1820, https://doi.org/10.1002/mrm.28578.
[1136] M. Liu, C. Hilty, Metabolic Measurements of Nonpermeating Compounds in Live Cells Using Hyperpolarized NMR, Anal. Chem. 90 (2018) 1217–1222, https://doi.org/10.1021/acs.analchem.7b03901.
[1137] F. Reineri, T. Boi, S. Aime, ParaHydrogen Induced Polarization of 13C carboxylate resonance in acetate and pyruvate, Nat. Commun. 6 (2015) 5858, https://doi.org/10.1038/ncomms6858.
[1138] E. Cavallari, C. Carrera, S. Aime, F. Reineri, Metabolic Studies of Tumor Cells Using [1- 13C] Pyruvate Hyperpolarized by Means of PHIP-Side Arm Hydrogenation, ChemPhysChem. 20 (2018) 318–325, https://doi.org/10.1002/cphc.201800652.
[1139] E. Cavallari, C. Carrera, G. Di Matteo, O. Bondar, S. Aime, F. Reineri, In-vitro NMR Studies of Prostate Tumor Cell Metabolism by Means of Hyperpolarized [1-13C]Pyruvate Obtained Using the PHIP-SAH Method, Front Oncol. 10 (2020) 10158–10159, https://doi.org/10.3389/fonc.2020.00497.
[1140] J. Eills, E. Cavallari, C. Carrera, D. Budker, S. Aime, F. Reineri, Real-Time Nuclear Magnetic Resonance Detection of Fumarase Activity Using Parahydrogen-Hyperpolarized [1- 13C]Fumarate, J. Am. Chem. Soc. 141 (2019) 20209–20214, https://doi.org/10.1021/jacs.9b10094.
[1141] S. Heux, C. Bergès, P. Millard, J.-C. Portais, F. Létisse, Recent advances in high-throughput 13C-fluxomics, Curr. Opin. Biotechnol. 43 (2017) 104–109, https://doi.org/10.1016/j.copbio.2016.10.010.
[1142] A. Dey, B. Charrier, E. Martineau, C. Deborde, E. Gandriau, A. Moing, D. Jacob, D. Eshchenko, M. Schnell, R. Melzi, D. Kurzbach, M. Ceillier, Q. Chappuis, S.F. Cousin, J.G. Kempf, S. Jannin, J.-N. Dumez, P. Giraudeau, Hyperpolarized NMR Metabolomics at Natural ^{13} C Abundance, Anal. Chem. 92 (2020) 14867–14871, https://doi.org/10.1021/acs.analchem.0c03510.
[1143] K. Takeuchi, K. Baskaran, H. Arthanari, Structure determination using solution NMR: Is it worth the effort?, J. Magn. Reson. 306 (2019) 195–201, https://doi.org/10.1016/j.jmr.2019.07.045.
[1144] A. Dubey, K. Takeuchi, M. Reibarkh, H. Arthanari, The role of NMR in leveraging dynamics and entropy in drug design, J. Biomol. NMR. (2020) 1–20, https://doi.org/10.1007/s10858-020-00335-9.
[1145] S. Imai, T. Yokomizo, Y. Kofuku, Y. Shiraishi, T. Ueda, I. Shimada, Structural equilibrium underlying ligand-dependent activation of β2-adrenoreceptor, Nat. Chem. Biol. 16 (2020) 430–439, https://doi.org/10.1038/s41589-019-0457-5.
[1146] T. Xie, T. Saleh, P. Rossi, C.G. Kalodimos, Conformational states dynamically populated by a kinase determine its function eabc2754-18 Science. 62 (2020), https://doi.org/10.1126/science.abc2754.
[1147] T.R. Alderson, L.E. Kay, NMR spectroscopy captures the essential role of dynamics in regulating biomolecular function, Cell. 184 (2021) 577–595, https://doi.org/10.1016/j.cell.2020.12.034.
[1148] M.R. Jensen, M. Zweckstetter, J. Huang, M. Blackledge, Exploring Free-Energy Landscapes of Intrinsically Disordered Proteins at Atomic Resolution Using NMR Spectroscopy, Chem. Rev. 114 (2014) 6632–6660, https://doi.org/10.1021/cr400688u.
[1149] P.E. Wright, H.J. Dyson, Intrinsically disordered proteins in cellular signalling and regulation, Nat. Struct. Mol. Biol. 16 (2015) 18–29, https://doi.org/10.1038/nrm3920.
[1150] 1] A. Prestel, K. Bugge, L. Staby, R. Hendus-Altenburger, B.B. Kragelund, Chapter Eight - Characterization of Dynamic IDP Complexes by NMR Spectroscopy, in: E. Rhoades (Ed.), Methods Enzymol., Academic Press, 2018: pp. 193–226. https://doi.org/10.1016/bs.mie.2018.08.026..
[1151] S. Milles, N. Salvi, M. Blackledge, M.R. Jensen, Characterization of intrinsically disordered proteins and their dynamic complexes: From in vitro to cell-like environments, Prog. Nucl. Magn. Reson. Spectrosc. 109 (2018) 79–100, https://doi.org/10.1016/j.pnmrs.2018.07.001.
[1152] R. Schneider, M. Blackledge, M.R. Jensen, Elucidating binding mechanisms and dynamics of intrinsically disordered protein complexes using NMR spectroscopy, Curr. Opin. Struct. Biol. 54 (2019) 10–18, https://doi.org/10.1016/j.sbi.2018.09.007.
[1153] H.J. Dyson, P.E. Wright, Perspective: the essential role of NMR in the discovery and characterization of intrinsically disordered proteins, J. Biomol. NMR. 73 (2019) 651–659, https://doi.org/10.1007/s10858-019-00280-2.
[1154] W. Adamski, N. Salvi, D. Maurin, J. Magnat, S. Milles, M.R. Jensen, A. Abyzov, C.J. Moreau, M. Blackledge, A Unified Description of Intrinsically Disordered Protein Dynamics under Physiological Conditions Using NMR Spectroscopy, J. Am. Chem. Soc. 141 (2019) 17817–17829, https://doi.org/10.1021/jacs.9b09002.
[1155] G.-N.-W. Gomes, M. Krzeminski, A. Namini, E.W. Martin, T. Mittag, T. Head-Gordon, J.D. Forman-Kay, C.C. Gradinaru, Conformational Ensembles of an Intrinsically Disordered Protein Consistent with NMR, SAXS, and Single-Molecule FRET, J. Am. Chem. Soc. 142 (2020) 15697–15710, https://doi.org/10.1021/jacs.0c02088.
[1156] A. Alik, C. Bouguechtouli, M. Julien, W. Bermel, R. Ghouil, S. Zinn-Justin, F.-X. Theillet, Sensitivity-Enhanced 13 C-NMR Spectroscopy for Monitoring Multisite Phosphorylation at Physiological Temperature and pH, Angew. Chem. Int. Ed Engl. (2020), https://doi.org/10.1002/anie.202002288.
[1157] A. Bodor, J.D. Haller, C. Bouguechtouli, F.-X. Theillet, L. Nyitray, B. Luy, Power of Pure Shift HαCα Correlations: A Way to Characterize Biomolecules under Physiological Conditions, Anal. Chem. 92 (2020) 12423–12428, https://doi.org/10.1021/acs.analchem.0c02182.
[1158] L.E. Wong, T.H. Kim, D.R. Muhandiram, J.D. Forman-Kay, L.E. Kay, NMR Experiments for Studies of Dilute and Condensed Protein Phases: Application to the Phase-Separating Protein CAPRIN1, J. Am. Chem. Soc. 142 (2020) 2471–2489, https://doi.org/10.1021/jacs.9b12208.
[1159] S. Prabakaran, R.A. Everley, I. Landrieu, J.-M. Wieruszeski, G. Lippens, H. Steen, J. Gunawardena, Comparative analysis of Erk phosphorylation suggests a mixed strategy for measuring phospho-form distributions, Mol. Syst. Biol. 7 (2011) 1–15, https://doi.org/10.1038/msb.2011.15.
[1160] F.-X. Theillet, C. Smet-Nocca, S. Liokatis, R. Thongwichian, J. Kosten, M.-K. Yoon, R.W. Kriwacki, I. Landrieu, G. Lippens, P. Selenko, Cell signaling, post-translational protein modifications and NMR spectroscopy, J. Biomol. NMR. 54 (2012) 217–236, https://doi.org/10.1007/s10858-012-9674-x.
[1161] A. Limatola, C. Eichmann, R.S. Jacob, G. Ben-Nissan, M. Sharon, A. Binolfi, P. Selenko, Time-Resolved NMR Analysis of Proteolytic α-Synuclein Processing in vitro and in cellulo, PROTEOMICS. 18 (2018) 1800056–1800113, https://doi.org/10.1002/pmic.201800056.
[1162] R. Hendus-Altenburger, C.B. Fernandes, K. Bugge, M.B.A. Kunze, W. Boomsma, B.B. Kragelund, Random coil chemical shifts for serine, threonine and tyrosine phosphorylation over a broad pH range, J. Biomol. NMR. 73 (2019) 713–725, https://doi.org/10.1007/s10858-019-00283-z.
[1163] A.C. Conibear, K.J. Rosengren, C.F.W. Becker, H. Kaehlig, Random coil shifts of posttranslationally modified amino acids, J. Biomol. NMR. 73 (2019) 587–599, https://doi.org/10.1007/s10858-019-00270-4.
[1164] A. Kumar, V. Narayanan, A. Sekhar, Characterizing Post-Translational Modifications and Their Effects on Protein Conformation Using NMR Spectroscopy, Biochemistry. 59 (2019) 57–73, https://doi.org/10.1021/acs.biochem.9b00827.
[1165] A. Hinterholzer, V. Stanojlovic, C. Regl, C.G. Huber, C. Cabrele, M. Schubert, Detecting aspartate isomerization and backbone cleavage after aspartate in intact proteins by NMR spectroscopy, J. Biomol. NMR. (2021) 1–12, https://doi.org/10.1007/s10858-020-00356-4.
[1166] A. Hinterholzer, V. Stanojlovic, C. Regl, C.G. Huber, C. Cabrele, M. Schubert, Identification and Quantification of Oxidation Products in Full-Length Biotherapeutic Antibodies by NMR Spectroscopy, Anal. Chem. 92 (2020) 9666–9673, https://doi.org/10.1021/acs.analchem.0c00965.
[1167] B. Reif, S.E. Ashbrook, L. Emsley, M. Hong, Solid-state NMR spectroscopy, Nat. Rev. Methods Primer. 1 (2021) 2, https://doi.org/10.1038/s43586-020-00002-1.
[1168] K. Jaudzems, T. Polenova, G. Pintacuda, H. Oschkinat, A. Lesage, DNP NMR of biomolecular assemblies, J. Struct. Biol. 206 (2019) 90–98, https://doi.org/10.1016/j.jsb.2018.09.011.
[1169] M. Lu, M. Wang, I.V. Sergeyev, C.M. Quinn, J. Struppe, M. Rosay, W. Maas, A. M. Gronenborn, T. Polenova, 19F Dynamic Nuclear Polarization at Fast Magic Angle Spinning for NMR of HIV-1 Capsid Protein Assemblies, J. Am. Chem. Soc. 141 (2019) 5681–5691, https://doi.org/10.1021/jacs.8b09216.
[1170] W.N. Costello, Y. Xiao, K.K. Frederick, DNP-Assisted NMR Investigation of Proteins at Endogenous Levels in Cellular Milieu, Methods Enzymol. 615 (2019) 373–406, https://doi.org/10.1016/bs.mie.2018.08.023.
[1171] A.N. Smith, K. Märker, S. Hediger, G. De Paëpe, Natural Isotopic Abundance 13C and 15N Multidimensional Solid-State NMR Enabled by Dynamic Nuclear Polarization, J. Phys. Chem. Lett. 10 (2019) 4652–4662, https://doi.org/10.1021/acs.jpclett.8b03874.
[1172] K.K. Frederick, V.K. Michaelis, B. Corzilius, T.-C. Ong, A.C. Jacavone, R.G. Griffin, S. Lindquist, Sensitivity-Enhanced NMR Reveals Alterations in Protein Structure by Cellular Milieus, Cell. 163 (2015) 620–628, https://doi.org/10.1016/j.cell.2015.09.024.
[1173] M. Kaplan, A. Cukkemane, G.C.P. van Zundert, S. Narasimhan, M. Daniëls, D. Mance, G. Waksman, A.M.J.J. Bonvin, R. Fronzes, G.E. Folkers, M. Baldus, Probing a cell-embedded megadalton protein complex by DNP-supported solid-state NMR, Nat. Methods. 12 (2015) 649–652, https://doi.org/10.1038/nmeth.3406.
[1174] 5] F.-X. Theillet, In-cell structural biology by NMR: the benefits of the atomic-scale., Chem. Rev. (2022) in press. https://doi.org/10.1021/acs.chemrev.1c00937..
[1175] J.R. Wiśniewski, M.Y. Hein, J. Cox, M. Mann, A "Proteomic Ruler" for Protein Copy Number and Concentration Estimation without Spike-in Standards, Mol. Cell. Proteomics. 13 (2014) 3497–3506, https://doi.org/10.1074/mcp.M113.037309.
[1176] F. Edfors, F. Danielsson, B.M. Hallström, L. Käll, E. Lundberg, F. Pontén, B. Forsström, M. Uhlén, Gene-specific correlation of RNA and protein levels in human cells and tissues, Mol. Syst. Biol. 12 (2016) 883, https://doi.org/10.15252/msb.20167144.
[1177] D. Wang, B. Eraslan, T. Wieland, B. Hallström, T. Hopf, D.P. Zolg, J. Zecha, A. Asplund, L. Li, C. Meng, M. Frejno, T. Schmidt, K. Schnatbaum, M. Wilhelm, F. Ponten, M. Uhlen, J. Gagneur, H. Hahne, B. Kuster, A deep proteome and transcriptome abundance atlas of 29 healthy human tissues, Mol. Syst. Biol. 15 (2019), https://doi.org/10.15252/msb.20188503.
[1178] R.E. London, C.T. Gregg, N.A. Matwiyoff, Nuclear magnetic resonance of rotational mobility of mouse hemoglobin labeled with (2–13C)histidine, Science. 188 (1975) 266–268, https://doi.org/10.1126/science.1118727.

[1179] S.P. Williams, P.M. Haggie, K.M. Brindle, 19F NMR measurements of the rotational mobility of proteins in vivo, Biophys. J. 72 (1997) 490–498, https://doi.org/10.1016/S0006-3495(97)78690-9.
[1180] Z. Serber, A.T. Keatinge-Clay, R. Ledwidge, A.E. Kelly, S.M. Miller, V. Dötsch, High-resolution macromolecular NMR spectroscopy inside living cells, J. Am. Chem. Soc. 123 (2001) 2446–2447, https://doi.org/10.1021/ja0057528.
[1181] Z. Serber, R. Ledwidge, S.M. Miller, V. Dötsch, Evaluation of parameters critical to observing proteins inside living Escherichia coli by in-cell NMR spectroscopy, J. Am. Chem. Soc. 123 (2001) 8895–8901, https://doi.org/10.1021/ja0112846.
[1182] N. Shimba, Z. Serber, R. Ledwidge, S.M. Miller, C.S. Craik, V. Dötsch, Quantitative identification of the protonation state of histidines in vitro and in vivo, Biochemistry. 42 (2003) 9227–9234, https://doi.org/10.1021/bi0344679.
[1183] T. Etezady-Esfarjani, T. Herrmann, R. Horst, K. Wüthrich, Automated Protein NMR Structure Determination in Crude Cell-Extract, J. Biomol. NMR. 34 (2006) 3–11, https://doi.org/10.1007/s10858-005-4519-5.
[1184] D. Sakakibara, A. Sasaki, T. Ikeya, J. Hamatsu, T. Hanashima, M. Mishima, M. Yoshimasu, N. Hayashi, T. Mikawa, M. Wälchli, B.O. Smith, M. Shirakawa, P. Güntert, Y. Ito, Protein structure determination in living cells by in-cell NMR spectroscopy, Nature. 458 (2009) 102–105, https://doi.org/10.1038/nature07814.
[1185] P.N. Reardon, L.D. Spicer, Multidimensional NMR spectroscopy for protein characterization and assignment inside cells, J. Am. Chem. Soc. 127 (2005) 10848–10849, https://doi.org/10.1021/ja053145k.
[1186] T. Ikeya, A. Sasaki, D. Sakakibara, Y. Shigemitsu, J. Hamatsu, T. Hanashima, M. Mishima, M. Yoshimasu, N. Hayashi, T. Mikawa, D. Nietlispach, M. Wälchli, B.O. Smith, M. Shirakawa, P. Güntert, Y. Ito, NMR protein structure determination in living E. coli cells using nonlinear sampling, Nat. Protoc. 5 (2010) 1051–1060, https://doi.org/10.1038/nprot.2010.69.
[1187] T. Ikeya, T. Hanashima, S. Hosoya, M. Shimazaki, S. Ikeda, M. Mishima, P. Güntert, Y. Ito, Improved in-cell structure determination of proteins at near-physiological concentration, Sci. Rep. (2016) 1–11, https://doi.org/10.1038/srep38312.
[1188] T. Tanaka, T. Ikeya, H. Kamoshida, Y. Suemoto, M. Mishima, M. Shirakawa, P. Güntert, Y. Ito, High-Resolution Protein 3D Structure Determination in Living Eukaryotic Cells, Angew. Chem. 58 (2019) 7284–7288, https://doi.org/10.1002/anie.201900840.
[1189] P. Selenko, Z. Serber, B. Gadea, J. Ruderman, G. Wagner, Quantitative NMR analysis of the protein G B1 domain in Xenopus laevis egg extracts and intact oocytes, Proc. Natl. Acad. Sci. 103 (2006) 11904–11909, https://doi.org/10.1073/pnas.0604667103.
[1190] K. Inomata, A. Ohno, H. Tochio, S. Isogai, T. Tenno, I. Nakase, T. Takeuchi, S. Futaki, Y. Ito, H. Hiroaki, M. Shirakawa, High-resolution multi-dimensional NMR spectroscopy of proteins in human cells, Nature. 457 (2009) 106–109, https://doi.org/10.1038/nature07839.
[1191] Q. Wang, A. Zhuravleva, L.M. Gierasch, Exploring weak, transient protein–protein interactions in crowded in vivo environments by in-cell nuclear magnetic resonance spectroscopy, Biochemistry. 50 (2011) 9225–9236, https://doi.org/10.1021/bi201287e.
[1192] K. Bertrand, S. Reverdatto, D.S. Burz, R. Zitomer, A. Shekhtman, Structure of proteins in eukaryotic compartments, J. Am. Chem. Soc. 134 (2012) 12798–12806, https://doi.org/10.1021/ja304809s.
[1193] T. Müntener, D. Häussinger, P. Selenko, F.-X. Theillet, In-Cell Protein Structures from 2D NMR Experiments, J. Phys. Chem. Lett. 7 (2016) 2821–2825, https://doi.org/10.1021/acs.jpclett.6b01074.
[1194] B.-B. Pan, F. Yang, Y. Ye, Q. Wu, C. Li, T. Huber, X.-C. Su, 3D structure determination of a protein in living cells using paramagnetic NMR spectroscopy, Chem Commun. 52 (2016) 10237–10240, https://doi.org/10.1039/C6CC05490K.
[1195] Y. Hikone, G. Hirai, M. Mishima, K. Inomata, T. Ikeya, S. Arai, M. Shirakawa, M. Sodeoka, Y. Ito, A new carbamidemethyl-linked lanthanoid chelating tag for PCS NMR spectroscopy of proteins in living HeLa cells, J. Biomol. NMR. 66 (2016) 99–110, https://doi.org/10.1007/s10858-016-0059-4.
[1196] Y. Ye, X. Liu, G. Xu, M. Liu, C. Li, Direct Observation of Ca2+-Induced Calmodulin Conformational Transitions in Intact Xenopus laevis Oocytes by 19F NMR Spectroscopy, Angew. Chem. 127 (2015) 5418–5420, https://doi.org/10.1002/ange.201500261.
[1197] A.H. Linden, S. Lange, W.T. Franks, U. Akbey, E. Specker, B.-J. van Rossum, H. Oschkinat, Neurotoxin II bound to acetylcholine receptors in native membranes studied by dynamic nuclear polarization NMR, J. Am. Chem. Soc. 133 (2011) 19266–19269, https://doi.org/10.1021/ja206999c.
[1198] R. Fu, X. Wang, C. Li, A.N. Santiago-Miranda, G.J. Pielak, F. Tian, In Situ Structural Characterization of a Recombinant Protein in Native Escherichia coli Membranes with Solid-State Magic-Angle-Spinning NMR, J. Am. Chem. Soc. 133 (2011) 12370–12373, https://doi.org/10.1021/ja204062v.
[1199] T. Jacso, W.T. Franks, H. Rose, U. Fink, J. Broecker, S. Keller, H. Oschkinat, B. Reif, Characterization of membrane proteins in isolated native cellular membranes by dynamic nuclear polarization solid-state NMR spectroscopy without purification and reconstitution, Angew. Chem. Int. Ed Engl. 51 (2012) 432–435, https://doi.org/10.1002/anie.201104987.
[1200] Y. Miao, H. Qin, R. Fu, M. Sharma, T.V. Can, I. Hung, S. Luca, P.L. Gor'kov, W.W. Brey, T.A. Cross, M2 proton channel structural validation from full-length protein samples in synthetic bilayers and E. coli membranes., Angew. Chem. Int. Ed Engl. 51 (2012) 8383–8386. https://doi.org/10.1002/anie.201204666..
[1201] M. Renault, S. Pawsey, M.P. Bos, E.J. Koers, D. Nand, R. Tommassen-van Boxtel, M. Rosay, J. Tommassen, W.E. Maas, M. Baldus, Solid-State NMR Spectroscopy on Cellular Preparations Enhanced by Dynamic Nuclear Polarization, Angew. Chem. 51 (2012) 2998–3001, https://doi.org/10.1002/anie.201105984.
[1202] M. Renault, R. Tommassen-van Boxtel, M.P. Bos, J.A. Post, J. Tommassen, M. Baldus, Cellular solid-state nuclear magnetic resonance spectroscopy, Proc. Natl. Acad. Sci. U. S. A. 109 (2012) 4863–4868, https://doi.org/10.1073/pnas.1116478109.
[1203] K. Yamamoto, M.A. Caporini, S.-C. Im, L. Waskell, A. Ramamoorthy, Cellular solid-state NMR investigation of a membrane protein using dynamic nuclear polarization, Biochim. Biophys. Acta. 1848 (2015) 342–349, https://doi.org/10.1016/j.bbamem.2014.07.008.
[1204] S.A. Shahid, M. Nagaraj, N. Chauhan, T.W. Franks, B. Bardiaux, M. Habeck, M. Orwick-Rydmark, D. Linke, B.-J. van Rossum, Solid-state NMR Study of the YadA Membrane-Anchor Domain in the Bacterial Outer Membrane, Angew. Chem. Int. Ed Engl. 54 (2015) 12602–12606, https://doi.org/10.1002/anie.201505506.
[1205] K.M. Visscher, J. Medeiros-Silva, D. Mance, J.P.G.L.M. Rodrigues, M. Daniëls, A.M.J.J. Bonvin, M. Baldus, M. Weingarth, Supramolecular Organization and Functional Implications of K+ Channel Clusters in Membranes, Angew. Chem. Int. Ed Engl. 56 (2017) 13222–13227, https://doi.org/10.1002/anie.201705723.
[1206] S. Jekhmane, J. Medeiros-Silva, J. Li, F. Kümmerer, C. Müller-Hermes, M. Baldus, B. Roux, M. Weingarth, Shifts in the selectivity filter dynamics cause modal gating in K+ channels, Nat. Commun. (2019) 1–12, https://doi.org/10.1038/s41467-018-07973-6.
[1207] C. Pinto, D. Mance, M. Julien, M. Daniels, M. Weingarth, M. Baldus, Studying assembly of the BAM complex in native membranes by cellular solid-state NMR spectroscopy, J. Struct. Biol. 206 (2019) 1–11, https://doi.org/10.1016/j.jsb.2017.11.015.
[1208] C. Pinto, D. Mance, T. Sinnige, M. Daniëls, M. Weingarth, M. Baldus, Formation of the β-barrel assembly machinery complex in lipid bilayers as seen by solid-state NMR, Nat. Commun. 9 (2018) 4135, https://doi.org/10.1038/s41467-018-06466-w.
[1209] J. Medeiros-Silva, D. Mance, M. Daniëls, S. Jekhmane, K. Houben, M. Baldus, M. Weingarth, 1 H-Detected Solid-State NMR Studies of Water-Inaccessible Proteins In Vitro and In Situ, Angew. Chem. Int. Ed Engl. 55 (2016) 13606–13610, https://doi.org/10.1002/anie.201606594.
[1210] L.A. Baker, T. Sinnige, P. Schellenberger, J. de Keyzer, C.A. Siebert, A.J.M. Driessen, M. Baldus, K. Grünewald, Combined 1H-Detected Solid-State NMR Spectroscopy and Electron Cryotomography to Study Membrane Proteins across Resolutions in Native Environments, Struct. Lond. Engl. 1993 26 (2018) 161–170.e3, https://doi.org/10.1016/j.str.2017.11.011.
[1211] M. Kaplan, S. Narasimhan, C. de Heus, D. Mance, S. van Doorn, K. Houben, D. Popov-Čeleketić, R. Damman, E.A. Katrukha, P. Jain, W.J.C. Geerts, A.J.R. Heck, G.E. Folkers, L.C. Kapitein, S. Lemeer, P.M.P. van Bergen en Henegouwen, M. Baldus, EGFR Dynamics Change during Activation in Native Membranes as Revealed by NMR., Cell. 167 (2016) 1241-1251.e11. https://doi.org/10.1016/j.cell.2016.10.038..
[1212] S. Reckel, J.J. Lopez, F. Löhr, C. Glaubitz, V. Dötsch, In-Cell Solid-State NMR as a Tool to Study Proteins in Large Complexes, ChemBioChem. 13 (2012) 534–537, https://doi.org/10.1002/cbic.201100721.
[1213] S. Narasimhan, S. Scherpe, A. Lucini Paioni, J. van der Zwan, G.E. Folkers, H. Ovaa, M. Baldus, DNP-Supported Solid-State NMR Spectroscopy of Proteins Inside Mammalian Cells, Angew. Chem. 58 (2019) 12969–12973, https://doi.org/10.1002/anie.201903246.
[1214] F.-X. Theillet, A. Binolfi, B. Bekei, A. Martorana, H.M. Rose, M. Stuiver, S. Verzini, D. Lorenz, M. van Rossum, D. Goldfarb, P. Selenko, Structural disorder of monomeric α-synuclein persists in mammalian cells, Nature. 530 (2016) 45–50, https://doi.org/10.1038/nature16531.
[1215] R. Damman, A.L. Paioni, K.T. Xenaki, I.B. Hernández, P.M.P. van Bergen en Henegouwen, M. Baldus, Development of in vitro-grown spheroids as a 3D tumor model system for solid-state NMR spectroscopy, J. Biomol. NMR. 74 (2020) 401–412. https://doi.org/10.1007/s10858-020-00328-8..
[1216] I. Krystkowiak, N.E. Davey, SLiMSearch: a framework for proteome-wide discovery and annotation of functional modules in intrinsically disordered regions, Nucleic Acids Res. 45 (2017) W464–W469, https://doi.org/10.1093/nar/gkx238.
[1217] N.E. Davey, The functional importance of structure in unstructured protein regions, Curr. Opin. Struct. Biol. 56 (2019) 155–163, https://doi.org/10.1016/j.sbi.2019.03.009.
[1218] J. Janin, M.J.E. Sternberg, Protein flexibility, not disorder, is intrinsic to molecular recognition., F1000 Biol Rep. 5 (2013) 2, https://doi.org/10.3410/B5-2.
[1219] M.M. Babu, The contribution of intrinsically disordered regions to protein function, cellular complexity, and human disease, Biochem. Soc. Trans. 44 (2016) 1185–1200, https://doi.org/10.1042/BST20160172.
[1220] S. Alberti, A. Gladfelter, T. Mittag, Considerations and Challenges in Studying Liquid-Liquid Phase Separation and Biomolecular Condensates, Cell. 176 (2019) 419–434, https://doi.org/10.1016/j.cell.2018.12.035.
[1221] A. Boija, I.A. Klein, B.R. Sabari, A. Dall'Agnese, E.L. Coffey, A.V. Zamudio, C.H. Li, K. Shrinivas, J.C. Manteiga, N.M. Hannett, B.J. Abraham, L.K. Afeyan, Y.E. Guo, J.K. Rimel, C.B. Fant, J. Schuijers, T.I. Lee, D.J. Taatjes, R.A. Young, Transcription Factors Activate Genes through the Phase-Separation Capacity

of Their Activation Domains, Cell. (2018) 1–31. https://doi.org/10.1016/j.cell.2018.10.042..
[1222] C.S. Sørensen, A. Jendroszek, M. Kjaergaard, Linker Dependence of Avidity in Multivalent Interactions Between Disordered Proteins, J. Mol. Biol. 431 (2019) 4784–4795, https://doi.org/10.1016/j.jmb.2019.09.001.
[1223] K. Bugge, I. Brakti, C.B. Fernandes, J.E. Dreier, J.E. Lundsgaard, J.G. Olsen, K. Skriver, B.B. Kragelund, Interactions by Disorder – A Matter of Context, Front. Mol. Biosci. 7 (2020) 110, https://doi.org/10.3389/fmolb.2020.00110.
[1224] Q. Huang, M. Li, L. Lai, Z. Liu, Allostery of multidomain proteins with disordered linkers, Curr. Opin. Struct. Biol. 62 (2020) 175–182, https://doi.org/10.1016/j.sbi.2020.01.017.
[1225] D. Piovesan, M. Necci, N. Escobedo, A.M. Monzon, A. Hatos, I. Mičetić, F. Quaglia, L. Paladin, P. Ramasamy, Z. Dosztanyi, W.F. Vranken, N.E. Davey, G. Parisi, M. Fuxreiter, S.C.E. Tosatto, MobiDB: intrinsically disordered proteins in 2021, Nucleic Acids Res. 49 (2021) D361–D367, https://doi.org/10.1093/nar/gkaa1058.
[1226] T. Zarin, B. Strome, G. Peng, I. Pritišanac, J.D. Forman-Kay, A.M. Moses, Identifying molecular features that are associated with biological function of intrinsically disordered protein regions, ELife. 10 (2021), https://doi.org/10.7554/eLife.60220 e60220.
[1227] M.M. Dedmon, C.N. Patel, G.B. Young, G.J. Pielak, FlgM gains structure in living cells, Proc. Natl. Acad. Sci. 99 (2002) 12681–12684, https://doi.org/10.1073/pnas.202331299.
[1228] K. Pauwels, P. Lebrun, P. Tompa, To be disordered or not to be disordered: is that still a question for proteins in the cell?, Cell. Mol. Life Sci. 74 (2017) 3185–3204, https://doi.org/10.1007/s00018-017-2561-6.
[1229] G.W. Daughdrill, L.J. Hanely, F.W. Dahlquist, The C-Terminal Half of the Anti-Sigma Factor FlgM Contains a Dynamic Equilibrium Solution Structure Favoring Helical Conformations, Biochemistry. 37 (1998) 1076–1082, https://doi.org/10.1021/bi971952t.
[1230] A.E. Smith, L.Z. Zhou, G.J. Pielak, Hydrogen exchange of disordered proteins in *Escherichia coli*: NMR Studies of Disorder in Cells, Protein Sci. 24 (2015) 706–713, https://doi.org/10.1002/pro.2643.
[1231] A.Y. Maldonado, D.S. Burz, S. Reverdatto, A. Shekhtman, Fate of Pup inside the Mycobacterium Proteasome Studied by in-Cell NMR, PLoS ONE. 8 (2013) e74576–e74616, https://doi.org/10.1371/journal.pone.0074576.
[1232] D.S. Burz, K. Dutta, D. Cowburn, A. Shekhtman, In-cell NMR for protein-protein interactions (STINT-NMR), Nat. Protoc. 1 (2006) 146–152, https://doi.org/10.1038/nprot.2006.23.
[1233] D.S. Burz, K. Dutta, D. Cowburn, A. Shekhtman, Mapping structural interactions using in-cell NMR spectroscopy (STINT-NMR), Nat. Methods. 3 (2006) 91–93, https://doi.org/10.1038/nmeth851.
[1234] S. Majumder, C.M. DeMott, D.S. Burz, A. Shekhtman, Using Singular Value Decomposition to Characterize Protein-Protein Interactions by In-cell NMR Spectroscopy, ChemBioChem. 15 (2014) 929–933, https://doi.org/10.1002/cbic.201400030.
[1235] S. Kim, K.-P. Wu, J. Baum, Fast hydrogen exchange affects ^{15}N relaxation measurements in intrinsically disordered proteins, J. Biomol. NMR. 55 (2013) 249–256, https://doi.org/10.1007/s10858-013-9706-1.
[1236] I.C. Felli, L. Gonnelli, R. Pierattelli, In-cell 13C NMR spectroscopy for the study of intrinsically disordered proteins, Nat. Protoc. 9 (2014) 2005–2016, https://doi.org/10.1038/nprot.2014.124.
[1237] K. Tamiola, B. Acar, F.A.A. Mulder, Sequence-Specific Random Coil Chemical Shifts of Intrinsically Disordered Proteins, J. Am. Chem. Soc. 132 (2010) 18000–18003, https://doi.org/10.1021/ja105656t.
[1238] K. Tamiola, F.A.A. Mulder, Using NMR chemical shifts to calculate the propensity for structural order and disorder in proteins, Biochem. Soc. Trans. 40 (2012) 1014–1020, https://doi.org/10.1042/BST20120171.
[1239] K. Tamiola, R.M. Scheek, P. van der Meulen, F.A.A. Mulder, pepKalc: scalable and comprehensive calculation of electrostatic interactions in random coil polypeptides, Bioinformatics. 79 (2018) 3260–3268, https://doi.org/10.1093/bioinformatics/bty033.
[1240] J.T. Nielsen, F.A.A. Mulder, POTENCI: prediction of temperature, neighbor and pH-corrected chemical shifts for intrinsically disordered proteins, J. Biomol. NMR. 70 (2018) 141–165, https://doi.org/10.1007/s10858-018-0166-5.
[1241] G. Runwal, R.H. Edwards, The Membrane Interactions of Synuclein: Physiology and Pathology, Annu. Rev. Pathol. Mech. Dis. 16 (2021) 465–485, https://doi.org/10.1146/annurev-pathol-031920-092547.
[1242] R.S. Jacob, C. Eichmann, A. Dema, D. Mercadante, P. Selenko, α-Synuclein plasma membrane localization correlates with cellular phosphatidylinositol polyphosphate levels., ELife. 10 (2021). https://doi.org/10.7554/eLife.61951..
[1243] G. Musteikytė, A.K. Jayaram, C.K. Xu, M. Vendruscolo, G. Krainer, T.P.J. Knowles, Interactions of α-synuclein oligomers with lipid membranes, Biochim. Biophys. Acta BBA - Biomembr. 2021 (1863) 183536–183615, https://doi.org/10.1016/j.bbamem.2020.183536.
[1244] T. Bartels, J.G. Choi, D.J. Selkoe, α-Synuclein occurs physiologically as a helically folded tetramer that resists aggregation, Nature. 477 (2011) 107–110, https://doi.org/10.1038/nature10324.
[1245] J. Burré, S. Vivona, J. Diao, M. Sharma, A.T. Brunger, T.C. Südhof, Properties of native brain α-synuclein, Nature. 498 (2013) E4–E6, https://doi.org/10.1038/nature12125.
[1246] W. Wang, I. Perovic, J. Chittuluru, A. Kaganovich, L.T.T. Nguyen, J. Liao, J.R. Auclair, D. Johnson, A. Landeru, A.K. Simorellis, S. Ju, M.R. Cookson, F.J. Asturias, J.N. Agar, B.N. Webb, C. Kang, D. Ringe, G.A. Petsko, T.C. Pochapsky, Q.Q. Hoang, A soluble -synuclein construct forms a dynamic tetramer, Proc. Natl. Acad. Sci. 108 (2011) 17797–17802, https://doi.org/10.1073/pnas.1113260108.
[1247] A. Binolfi, F.-X. Theillet, P. Selenko, Bacterial in-cell NMR of human α-synuclein: a disordered monomer by nature?, Biochem. Soc. Trans. 40 (2012) 950–954, https://doi.org/10.1042/BST20120096.
[1248] C.O. Barnes, W.B. Monteith, G.J. Pielak, Internal and Global Protein Motion Assessed with a Fusion Construct and In-Cell NMR Spectroscopy, ChemBioChem. 12 (2011) 390–391, https://doi.org/10.1002/cbic.201000610.
[1249] C.A. Waudby, C. Camilloni, A.W.P. Fitzpatrick, L.D. Cabrita, C.M. Dobson, M. Vendruscolo, J. Christodoulou, In-Cell NMR Characterization of the Secondary Structure Populations of a Disordered Conformation of α-Synuclein within E. coli Cells, PLoS ONE. 8 (2013), https://doi.org/10.1371/journal.pone.0072286 e72286.
[1250] B.M. Burmann, J.A. Gerez, I. Matečko-Burmann, S. Campioni, P. Kumari, D. Ghosh, A. Mazur, E.E. Aspholm, D. Šulskis, M. Wawrzyniuk, T. Bock, A. Schmidt, S.G.D. Rüdiger, R. Riek, S. Hiller, Regulation of α-synuclein by chaperones in mammalian cells, Nature. (2019) 1–25, https://doi.org/10.1038/s41586-019-1808-9.
[1251] M. Popovic, D. Sanfelice, C. Pastore, F. Prischi, P.A. Temussi, A. Pastore, Selective observation of the disordered import signal of a globular protein by in-cell NMR: the example of frataxins, Protein Sci. Publ. Protein Soc. 24 (2015) 996–1003, https://doi.org/10.1002/pro.2679.
[1252] S. Milles, D. Mercadante, I.V. Aramburu, M.R. Jensen, N. Banterle, C. Koehler, S. Tyagi, J. Clarke, S.L. Shammas, M. Blackledge, F. Gräter, E.A. Lemke, Plasticity of an Ultrafast Interaction between Nucleoporins and Nuclear Transport Receptors, Cell. 163 (2015) 734–745, https://doi.org/10.1016/j.cell.2015.09.047.
[1253] I.V. Aramburu, E.A. Lemke, Floppy but not sloppy: Interaction mechanism of FG-nucleoporins and nuclear transport receptors, Semin. Cell Dev. Biol. 68 (2017) 34–41, https://doi.org/10.1016/j.semcdb.2017.06.026.
[1254] L.E. Hough, K. Dutta, S. Sparks, D.B. Temel, A. Kamal, J. Tetenbaum-Novatt, M.P. Rout, D. Cowburn, The molecular mechanism of nuclear transport revealed by atomic-scale measurements, ELife. 4 (2015), https://doi.org/10.7554/eLife.10027 e10027.
[1255] K.P. Wall, L.E. Hough, In-Cell NMR within Budding Yeast Reveals Cytoplasmic Masking of Hydrophobic Residues of FG Repeats, Biophys. J. 115 (2018) 1690–1695, https://doi.org/10.1016/j.bpj.2018.08.049.
[1256] F.-X. Theillet, S. Liokatis, J.O. Jost, B. Bekei, H.M. Rose, A. Binolfi, D. Schwarzer, P. Selenko, Site-specific mapping and time-resolved monitoring of lysine methylation by high-resolution NMR spectroscopy, J. Am. Chem. Soc. 134 (2012) 7616–7619, https://doi.org/10.1021/ja301895f.
[1257] M.J. Smith, C.B. Marshall, F.-X. Theillet, A. Binolfi, P. Selenko, M. Ikura, Real-time NMR monitoring of biological activities in complex physiological environments, Curr. Opin. Struct. Biol. 32 (2015) 39–47, https://doi.org/10.1016/j.sbi.2015.02.003.
[1258] N. Altincekic, F. Lohr, J. Meier-Credo, J.D. Langer, M. Hengesbach, C. Richter, H. Schwalbe, Site-Specific Detection of Arginine Methylation in Highly Repetitive Protein Motifs of Low Sequence Complexity by NMR, J. Am. Chem. Soc. 142 (2020) 7647–7654, https://doi.org/10.1021/jacs.0c02308.
[1259] P. Selenko, D.P. Frueh, S.J. Elsaesser, W. Haas, S.P. Gygi, G. Wagner, In situ observation of protein phosphorylation by high-resolution NMR spectroscopy, Nat. Struct. Mol. Biol. 15 (2008) 321–329, https://doi.org/10.1038/nsmb.1395.
[1260] J.-F. Bodart, J.-M. Wieruszeski, L. Amniai, A. Leroy, I. Landrieu, A. Rousseau-Lescuyer, J.-P. Vilain, G. Lippens, NMR observation of Tau in Xenopus oocytes, J. Magn. Reson. 192 (2008) 252–257, https://doi.org/10.1016/j.jmr.2008.03.006.
[1261] S. Zhang, C. Wang, J. Lu, X. Ma, Z. Liu, D. Li, Z. Liu, C. Liu, In-Cell NMR Study of Tau and MARK2 Phosphorylated Tau, Int. J. Mol. Sci. 20 (2019) 90–114, https://doi.org/10.3390/ijms20010090.
[1262] I. Amata, M. Maffei, A. Igea, M. Gay, M. Vilaseca, A.R. Nebreda, M. Pons, Multi-phosphorylation of the Intrinsically Disordered Unique Domain of c-Src Studied by In-Cell and Real-Time NMR Spectroscopy, ChemBioChem. 14 (2013) 1820–1827, https://doi.org/10.1002/cbic.201300139.
[1263] A. Binolfi, A. Limatola, S. Verzini, J. Kosten, F.-X. Theillet, H. May Rose, B. Bekei, M. Stuiver, M. van Rossum, P. Selenko, Intracellular repair of oxidation-damaged α-synuclein fails to target C-terminal modification sites, Nat. Commun. 7 (2016) 10251, https://doi.org/10.1038/ncomms10251.
[1264] A. Dose, S. Liokatis, F.-X. Theillet, P. Selenko, D. Schwarzer, NMR profiling of histone deacetylase and acetyl-transferase activities in real time, ACS Chem. Biol. 6 (2011) 419–424, https://doi.org/10.1021/cb1003866.
[1265] F. Cordier, A. Chaffotte, E. Terrien, C. Prehaud, F.-X. Theillet, M. Delepierre, M. Lafon, H. Buc, N. Wolff, Ordered phosphorylation events in two independent cascades of the PTEN C-tail revealed by NMR, J. Am. Chem. Soc. 134 (2012) 20533–20543, https://doi.org/10.1021/ja310214g.
[1266] H.M. Rose, M. Stuiver, R. Thongwichian, F.-X. Theillet, S.M. Feller, P. Selenko, Quantitative NMR analysis of Erk activity and inhibition by U0126 in a panel of patient-derived colorectal cancer cell lines, Biochim. Biophys. Acta. 1834 (2013) 1396–1401, https://doi.org/10.1016/j.bbapap.2013.01.023.
[1267] W. Borcherds, F.-X. Theillet, A. Katzer, A. Finzel, K.M. Mishall, A.T. Powell, H. Wu, W. Manieri, C. Dieterich, P. Selenko, A. Loewer, G.W. Daughdrill, Disorder and residual helicity alter p53-Mdm2 binding affinity and signaling in cells, Nat. Chem. Biol. (2014) 1–5, https://doi.org/10.1038/nchembio.1668.

[1268] R. Thongwichian, J. Kosten, U. Benary, H.M. Rose, M. Stuiver, F.-X. Theillet, A. Dose, B. Koch, H. Yokoyama, D. Schwarzer, J. Wolf, P. Selenko, A Multiplexed NMR-Reporter Approach to Measure Cellular Kinase and Phosphatase Activities in Real-Time, J. Am. Chem. Soc. 137 (2015) 6468–6471, https://doi.org/10.1021/jacs.5b02987.
[1269] B. Bourgeois, T. Gui, D. Hoogeboom, H.G. Hocking, G. Richter, E. Spreitzer, M. Viertler, K. Richter, T. Madl, B.M.T. Burgering, Multiple regulatory intrinsically disordered motifs control FOXO4 transcription factor binding and function, Cell Rep. 36 (2021), https://doi.org/10.1016/j.celrep.2021.109446 109446.
[1270] E.A. Bienkiewicz, K.J. Lumb, Random-coil chemical shifts of phosphorylated amino acids, J. Biomol. NMR. 15 (1999) 203–206.
[1271] A. Kumar, M. Gopalswamy, C. Wishart, M. Henze, L. Eschen-Lippold, D. Donnelly, J. Balbach, N-Terminal Phosphorylation of Parathyroid Hormone (PTH) Abolishes Its Receptor Activity, ACS Chem. Biol. 9 (2014) 2465–2470, https://doi.org/10.1021/cb5004515.
[1272] A. Kumar, M. Gopalswamy, A. Wolf, D.J. Brockwell, M. Hatzfeld, J. Balbach, Phosphorylation-induced unfolding regulates p19 ^{INK4d} during the human cell cycle, Proc. Natl. Acad. Sci. 115 (2018) 3344–3349, https://doi.org/10.1073/pnas.1719774115.
[1273] B. Huang, Y. Liu, H. Yao, Y. Zhao, NMR-based investigation into protein phosphorylation, Int. J. Biol. Macromol. 145 (2020) 53–63, https://doi.org/10.1016/j.ijbiomac.2019.12.171.
[1274] D.S. Burz, A. Shekhtman, In-cell biochemistry using NMR spectroscopy, PLoS ONE. 3 (2008), https://doi.org/10.1371/journal.pone.0002571 e2571.
[1275] L.M. Luh, R. Hänsel, F. Löhr, D.K. Kirchner, K. Krauskopf, S. Pitzius, B. Schäfer, P. Tufar, I. Corbeski, P. Güntert, V. Dötsch, Molecular Crowding Drives Active Pin1 into Nonspecific Complexes with Endogenous Proteins Prior to Substrate Recognition, J. Am. Chem. Soc. 135 (2013) 13796–13803, https://doi.org/10.1021/ja405244v.
[1276] L. Banci, I. Bertini, C. Cefaro, L. Cenacchi, S. Ciofi-Baffoni, I.C. Felli, A. Gallo, L. Gonnelli, E. Luchinat, D. Sideris, K. Tokatlidis, Molecular chaperone function of Mia40 triggers consecutive induced folding steps of the substrate in mitochondrial protein import, Proc. Natl. Acad. Sci. 107 (2010) 20190–20195, https://doi.org/10.1073/pnas.1010095107.
[1277] L. Banci, L. Barbieri, E. Luchinat, E. Secci, Visualization of Redox-Controlled Protein Fold in Living Cells, Chem. Biol. 20 (2013) 747–752, https://doi.org/10.1016/j.chembiol.2013.05.007.
[1278] E. Mercatelli, L. Barbieri, E. Luchinat, L. Banci, Direct structural evidence of protein redox regulation obtained by in-cell NMR, Biochim. Biophys. Acta BBA - Mol. Cell Res. 1863 (2016) 198–204, https://doi.org/10.1016/j.bbamcr.2015.11.009.
[1279] L. Banci, L. Barbieri, I. Bertini, F. Cantini, E. Luchinat, In-cell NMR in E. coli to Monitor Maturation Steps of hSOD1, PLoS ONE. 6 (2011) e23561–e23568, https://doi.org/10.1371/journal.pone.0023561.
[1280] L. Barbieri, I. Bertini, E. Luchinat, E. Secci, Y. Zhao, L. Banci, A.R. Aricescu, Atomic-resolution monitoring of protein maturation in live human cells by NMR, Nat. Chem. Biol. 9 (2013) 297–299, https://doi.org/10.1038/nchembio.1202.
[1281] L. Barbieri, E. Luchinat, L. Banci, Structural insights of proteins in subcellular compartments: In-mitochondria NMR, Biochim. Biophys. Acta. 1843 (2014) 2492–2496, https://doi.org/10.1016/j.bbamcr.2014.06.009.
[1282] E. Luchinat, L. Barbieri, J.T. Rubino, T. Kozyreva, F. Cantini, L. Banci, In-cell NMR reveals potential precursor of toxic species from SOD1 fALS mutants, Nat. Commun. 5 (2014) 5502, https://doi.org/10.1038/ncomms6502.
[1283] E. Luchinat, L. Barbieri, L. Banci, A molecular chaperone activity of CCS restores the maturation of SOD1 fALS mutants, Sci. Rep. (2017) 1–8, https://doi.org/10.1038/s41598-017-17815-y.
[1284] M.J. Capper, G.S.A. Wright, L. Barbieri, E. Luchinat, E. Mercatelli, L. McAlary, J. J. Yerbury, P.M. O'Neill, S.V. Antonyuk, L. Banci, S.S. Hasnain, The cysteine-reactive small molecule ebselen facilitates effective SOD1 maturation, Nat. Commun. 9 (2018) 1693–1699, https://doi.org/10.1038/s41467-018-04114-x.
[1285] P. Polykretis, F. Cencetti, C. Donati, E. Luchinat, L. Banci, Cadmium effects on superoxide dismutase 1 in human cells revealed by NMR, Redox Biol. 21 (2019), https://doi.org/10.1016/j.redox.2019.101102 101102.
[1286] L. Barbieri, E. Luchinat, L. Banci, Intracellular metal binding and redox behavior of human DJ-1, JBIC J. Biol. Inorg. Chem. 23 (2018) 61–69, https://doi.org/10.1007/s00775-017-1509-5.
[1287] E. Ravera, L. Cerofolini, M. Fragai, G. Parigi, C. Luchinat, Characterization of lanthanoid-binding proteins using NMR spectroscopy, in, Methods Enzymol., Elsevier (2021) 103–137, https://doi.org/10.1016/bs.mie.2021.01.039.
[1288] B.K. Fetler, V. Simplaceanu, C. Ho, 1H-NMR investigation of the oxygenation of hemoglobin in intact human red blood cells, Biophys. J. 68 (1995) 681–693, https://doi.org/10.1016/S0006-3495(95)80229-8.
[1289] D.R. Rosen, T. Siddique, D. Patterson, D.A. Figlewicz, P. Sapp, A. Hentati, D. Donaldson, J. Goto, J.P. O'Regan, H.-X. Deng, Z. Rahmani, A. Krizus, D. McKenna-Yasek, A. Cayabyab, S.M. Gaston, R. Berger, R.E. Tanzi, J.J. Halperin, B. Herzfeldt, R. Van den Bergh, W.-Y. Hung, T. Bird, G. Deng, D.W. Mulder, C. Smyth, N.G. Laing, E. Soriano, M.A. Pericak-Vance, J. Haines, G.A. Rouleau, J.S. Gusella, H.R. Horvitz, R.H. Brown, Mutations in Cu/Zn superoxide dismutase gene are associated with familial amyotrophic lateral sclerosis, Nature. 362 (1993) 59–62, https://doi.org/10.1038/362059a0.
[1290] V.C. Culotta, M. Yang, T.V. O'Halloran, Activation of superoxide dismutases: Putting the metal to the pedal, Biochim. Biophys. Acta BBA - Mol. Cell Res. 1763 (2006) 747–758, https://doi.org/10.1016/j.bbamcr.2006.05.003.
[1291] M. Marušič, J. Schlagnitweit, K. Petzold, RNA Dynamics by NMR Spectroscopy, ChemBioChem. 20 (2019) 2685–2710, https://doi.org/10.1002/cbic.201900072.
[1292] B. Liu, H. Shi, H.M. Al-Hashimi, Developments in solution-state NMR yield broader and deeper views of the dynamic ensembles of nucleic acids, Curr. Opin. Struct. Biol. 70 (2021) 16–25, https://doi.org/10.1016/j.sbi.2021.02.007.
[1293] S. Nakano, D. Miyoshi, N. Sugimoto, Effects of molecular crowding on the structures, interactions, and functions of nucleic acids, Chem. Rev. 114 (2014) 2733–2758, https://doi.org/10.1021/cr400113m.
[1294] S. Takahashi, N. Sugimoto, Stability prediction of canonical and non-canonical structures of nucleic acids in various molecular environments and cells, Chem. Soc. Rev. 49 (2020) 8439–8468, https://doi.org/10.1039/D0CS00594K.
[1295] M.G. Munowitz, C.M. Dobson, R.G. Griffin, S.C. Harrison, On the rigidity of RNA in tomato bushy stunt virus, J. Mol. Biol. 141 (1980) 327–333, https://doi.org/10.1016/0022-2836(80)90185-0.
[1296] P.C. Magusin, M.A. Hemminga, Analysis of 31P nuclear magnetic resonance lineshapes and transversal relaxation of bacteriophage M13 and tobacco mosaic virus, Biophys. J. 64 (1993) 1861–1868, https://doi.org/10.1016/S0006-3495(93)81557-1.
[1297] S.J. Opella, T.A. Cross, J.A. DiVerdi, C.F. Sturm, Nuclear magnetic resonance of the filamentous bacteriophage fd, Biophys. J. 32 (1980) 531–548, https://doi.org/10.1016/S0006-3495(80)84988-5.
[1298] J.A. DiVerdi, S.J. Opella, R.I. Ma, N.R. Kallenbach, N.C. Seeman, 31P NMR of DNA in eukaryotic chromosomal complexes, Biochem. Biophys. Res. Commun. 102 (1981) 885–890, https://doi.org/10.1016/0006-291x(81)91620-x.
[1299] P. Tsang, S.J. Opella, Pf1 virus particle dynamics, Biopolymers. 25 (1986) 1859–1864, https://doi.org/10.1002/bip.360251004.
[1300] D.C. McCain, R. Virudachalam, R.E. Santini, S.S. Abdel-Meguid, J.L. Markley, Phosphorus-31 nuclear magnetic resonance study of internal motion in ribonucleic acid of southern bean mosaic virus, Biochemistry. 21 (1982) 5390–5397, https://doi.org/10.1021/bi00265a002.
[1301] R. Virudachalam, K. Sitaraman, K.L. Heuss, J.L. Markley, P. Argos, Evidence for pH-induced release of RNA from belladonna mottle virus and the stabilizing effect of polyamines and cations, Virology. 130 (1983) 351–359, https://doi.org/10.1016/0042-6822(83)90089-2.
[1302] R. Virudachalam, M. Harrington, J.E. Johnson, J.L. Markley, 1H, 13C, and 31P nuclear magnetic resonance studies of cowpea mosaic virus: Detection and exchange of polyamines and dynamics of the RNA, Virology. 141 (1985) 43–50, https://doi.org/10.1016/0042-6822(85)90181-3.
[1303] R. Virudachalam, P.S. Low, P. Argos, J.L. Markley, Turnip yellow mosaic virus and its capsid have thermal stabilities with opposite ph dependence: studies by differential scanning calorimetry and 31P nuclear magnetic resonance spectroscopy, Virology. 146 (1985) 213–220, https://doi.org/10.1016/0042-6822(85)90005-4.
[1304] J.H. Kan, A.F.M. Cremers, C.A.G. Haasnoot, C.W. Hilbers, The dynamical structure of the RNA in alfalfa mosaic virus studied by 31P-nuclear magnetic resonance, Eur. J. Biochem. 168 (1987) 635–639, https://doi.org/10.1111/j.1432-1033.1987.tb13463.x.
[1305] T.A. Cross, P. Tsang, S.J. Opella, Comparison of protein and deoxyribonucleic acid backbone structures in fd and Pf1 bacteriophages, Biochemistry. 22 (1983) 721–726, https://doi.org/10.1021/bi00273a002.
[1306] T.-Y. Yu, J. Schaefer, REDOR NMR Characterization of DNA Packaging in Bacteriophage T4, J. Mol. Biol. 382 (2008) 1031–1042, https://doi.org/10.1016/j.jmb.2008.07.077.
[1307] G. Abramov, A. Goldbourt, Nucleotide-type chemical shift assignment of the encapsulated 40 kbp dsDNA in intact bacteriophage T7 by MAS solid-state NMR, J. Biomol. NMR. 59 (2014) 219–230, https://doi.org/10.1007/s10858-014-9840-4.
[1308] G. Abramov, O. Morag, A. Goldbourt, Magic-Angle Spinning NMR of a Class I Filamentous Bacteriophage Virus, J. Phys. Chem. B. 115 (2011) 9671–9680, https://doi.org/10.1021/jp2040955.
[1309] I.V. Sergeyev, L.A. Day, A. Goldbourt, A.E. McDermott, Chemical Shifts for the Unusual DNA Structure in Pf1 Bacteriophage from Dynamic-Nuclear-Polarization-Enhanced Solid-State NMR Spectroscopy, J. Am. Chem. Soc. 133 (2011) 20208–20217, https://doi.org/10.1021/ja2043062.
[1310] O. Morag, G. Abramov, A. Goldbourt, Complete Chemical Shift Assignment of the ssDNA in the Filamentous Bacteriophage fd Reports on Its Conformation and on Its Interface with the Capsid Shell, J. Am. Chem. Soc. 136 (2014) 2292–2301, https://doi.org/10.1021/ja412178n.
[1311] G. Abramov, O. Morag, A. Goldbourt, Magic-angle spinning NMR of intact bacteriophages: Insights into the capsid, DNA and their interface, J. Magn. Reson. 253 (2015) 80–90, https://doi.org/10.1016/j.jmr.2015.01.011.
[1312] A. Goldbourt, Structural characterization of bacteriophage viruses by NMR, Prog. Nucl. Magn. Reson. Spectrosc. 114–115 (2019) 192–210, https://doi.org/10.1016/j.pnmrs.2019.06.004.
[1313] R. Hänsel, S. Foldynová-Trantírková, F. Löhr, J. Buck, E. Bongartz, E. Bamberg, H. Schwalbe, V. Dötsch, L. Trantírek, Evaluation of Parameters Critical for Observing Nucleic Acids Inside Living *Xenopus laevis* Oocytes by In-Cell NMR Spectroscopy, J. Am. Chem. Soc. 131 (2009) 15761–15768, https://doi.org/10.1021/ja9052027.
[1314] R. Hänsel, F. Löhr, L. Trantirek, V. Dötsch, High-Resolution Insight into G-Overhang Architecture, J. Am. Chem. Soc. 135 (2013) 2816–2824, https://doi.org/10.1021/ja312403b.

[1315] G.F. Salgado, C. Cazenave, A. Kerkour, J.-L. Mergny, G-quadruplex DNA and ligand interaction in living cells using NMR spectroscopy, Chem. Sci. 6 (2015) 3314–3320, https://doi.org/10.1039/C4SC03853C.
[1316] H.-L. Bao, T. Ishizuka, T. Sakamoto, K. Fujimoto, T. Uechi, N. Kenmochi, Y. Xu, Characterization of human telomere RNA G-quadruplex structures in vitro and in living cells using 19F NMR spectroscopy, Nucleic Acids Res. 45 (2017) 5501–5511, https://doi.org/10.1093/nar/gkx109.
[1317] T. Ishizuka, P.-Y. Zhao, H.-L. Bao, Y. Xu, A multi-functional guanine derivative for studying the DNA G-quadruplex structure, Analyst. 142 (2017) 4083–4088, https://doi.org/10.1039/C7AN00941K.
[1318] H.-L. Bao, Y. Xu, Investigation of higher-order RNA G-quadruplex structures in vitro and in living cells by 19F NMR spectroscopy, Nat. Protoc. 13 (2018) 652–665, https://doi.org/10.1038/nprot.2017.156.
[1319] S. Manna, D. Sarkar, S.G. Srivatsan, A Dual-App Nucleoside Probe Provides Structural Insights into the Human Telomeric Overhang in Live Cells, J. Am. Chem. Soc. 140 (2018) 12622–12633, https://doi.org/10.1021/jacs.8b08436.
[1320] Y. Yamaoki, A. Kiyoishi, M. Miyake, F. Kano, M. Murata, T. Nagata, M. Katahira, The first successful observation of in-cell NMR signals of DNA and RNA in living human cells, Phys. Chem. Chem. Phys. 20 (2018) 2982–2985, https://doi.org/10.1039/C7CP05188C.
[1321] S. Dzatko, M. Krafcikova, R. Hänsel-Hertsch, T. Fessl, R. Fiala, T. Loja, D. Krafcik, J.-L. Mergny, S. Foldynova-Trantirkova, L. Trantirek, Evaluation of the Stability of DNA i-Motifs in the Nuclei of Living Mammalian Cells, Angew. Chem. Int. Ed. 57 (2018) 2165–2169, https://doi.org/10.1002/anie.201712284.
[1322] P. Viskova, D. Krafcik, L. Trantirek, S. Foldynova-Trantirkova, In-Cell NMR Spectroscopy of Nucleic Acids in Human Cells, Curr. Protoc. Nucleic Acid Chem. 76 (2019), https://doi.org/10.1002/cpnc.71 e71.
[1323] I.-C. Giassa, J. Rynes, T. Fessl, S. Foldynova-Trantirkova, L. Trantirek, Advances in the cellular structural biology of nucleic acids, FEBS Lett. 592 (2018) 1997–2011, https://doi.org/10.1002/1873-3468.13054.
[1324] M. Cheng, D. Qiu, L. Tamon, E. Ištvánková, P. Víšková, S. Amrane, A. Guédin, J. Chen, L. Lacroix, H. Ju, L. Trantírek, A.B. Sahakyan, J. Zhou, J. Mergny, Thermal and pH Stabilities of i-DNA: Confronting in vitro Experiments with Models and In-Cell NMR Data, Angew. Chem. Int. Ed. 60 (2021) 10286–10294, https://doi.org/10.1002/anie.202016801.
[1325] M. Krafcikova, S. Dzatko, C. Caron, A. Granzhan, R. Fiala, T. Loja, M.-P. Teulade-Fichou, T. Fessl, R. Hänsel-Hertsch, J.-L. Mergny, S. Foldynova-Trantirkova, L. Trantirek, Monitoring DNA–Ligand Interactions in Living Human Cells Using NMR Spectroscopy, J. Am. Chem. Soc. 141 (2019) 13281–13285, https://doi.org/10.1021/jacs.9b03031.
[1326] D. Krafčík, E. Ištvánková, Š. Džatko, P. Víšková, S. Foldynová-Trantírková, L. Trantírek, Towards Profiling of the G-Quadruplex Targeting Drugs in the Living Human Cells Using NMR Spectroscopy, Int. J. Mol. Sci. 22 (2021) 6042, https://doi.org/10.3390/ijms22116042.
[1327] H.-L. Bao, Y. Xu, Telomeric DNA–RNA-hybrid G-quadruplex exists in environmental conditions of HeLa cells, Chem. Commun. 56 (2020) 6547–6550, https://doi.org/10.1039/D0CC02053B.
[1328] H.-L. Bao, T. Masuzawa, T. Oyoshi, Y., Xu, Oligonucleotides DNA containing 8-trifluoromethyl-2′-deoxyguanosine for observing Z-DNA structure, Nucleic Acids Res. (2020) gkaa505, https://doi.org/10.1093/nar/gkaa505.
[1329] P. Broft, S. Dzatko, M. Krafcikova, A. Wacker, R. Hansel-Hertsch, V. Dötsch, L. Trantirek, H. Schwalbe, In-Cell NMR Spectroscopy of Functional Riboswitch Aptamers in Eukaryotic Cells, Angew. Chem. 15 (2020) 679–710, https://doi.org/10.1002/anie.202007184.
[1330] J. Schlagnitweit, S. Friebe Sandoz, A. Jaworski, I. Guzzetti, F. Aussenac, R.J. Carbajo, E. Chiarparin, A.J. Pell, K. Petzold, Observing an Antisense Drug Complex in Intact Human Cells by in-Cell NMR Spectroscopy, ChemBioChem. 20 (2019) 2474–2478, https://doi.org/10.1002/cbic.201900297.
[1331] P. Barraud, A. Gato, M. Heiss, M. Catala, S. Kellner, C. Tisné, Time-resolved NMR monitoring of tRNA maturation, Nat. Commun. (2019) 1–14, https://doi.org/10.1038/s41467-019-11356-w.
[1332] M. Himmelstoß, K. Erharter, E. Renard, E. Ennifar, C. Kreutz, R. Micura, 2′- *O* -Trifluoromethylated RNA – a powerful modification for RNA chemistry and NMR spectroscopy, Chem. Sci. 11 (2020) 11322–11330, https://doi.org/10.1039/D0SC04520A.
[1333] Q. Li, J. Chen, M. Trajkovski, Y. Zhou, C. Fan, K. Lu, P. Tang, X. Su, J. Plavec, Z. Xi, C. Zhou, 4′-Fluorinated RNA: Synthesis, Structure, and Applications as a Sensitive 19F NMR Probe of RNA Structure and Function, J. Am. Chem. Soc. 142 (2020) 4739–4748, https://doi.org/10.1021/jacs.9b13207.
[1334] F. Nußbaumer, R. Plangger, M. Roeck, C. Kreutz, Aromatic 19 F– 13 C TROSY—[19 F, 13 C]-Pyrimidine Labeling for NMR Spectroscopy of RNA, Angew. Chem. Int. Ed. 59 (2020) 17062–17069, https://doi.org/10.1002/anie.202006577.
[1335] H. Karlsson, L. Baronti, K. Petzold, A robust and versatile method for production and purification of large-scale RNA samples for structural biology, RNA. 26 (2020) 1023–1037, https://doi.org/10.1261/rna.075697.120.
[1336] K. Deprey, N. Batistatou, J.A. Kritzer, A critical analysis of methods used to investigate the cellular uptake and subcellular localization of RNA therapeutics, Nucleic Acids Res. 48 (2020) 7623–7639, https://doi.org/10.1093/nar/gkaa576.
[1337] A.P. Minton, Excluded volume as a determinant of macromolecular structure and reactivity, Biopolymers. 20 (1981) 2093–2120, https://doi.org/10.1002/bip.1981.360201006.
[1338] H.-X. Zhou, G. Rivas, A.P. Minton, Macromolecular Crowding and Confinement: Biochemical, Biophysical, and Potential Physiological Consequences, Annu. Rev. Biophys. 37 (2008) 375–397, https://doi.org/10.1146/annurev.biophys.37.032807.125817.
[1339] M. Sarkar, A.E. Smith, G.J. Pielak, Impact of reconstituted cytosol on protein stability, Proc. Natl. Acad. Sci. 110 (2013) 19342–19347, https://doi.org/10.1073/pnas.1312678110.
[1340] G. Rivas, A.P. Minton, Macromolecular Crowding In Vitro, In Vivo, and In Between, Trends Biochem. Sci. 41 (2016) 970–981, https://doi.org/10.1016/j.tibs.2016.08.013.
[1341] D. Guin, M. Gruebele, Weak Chemical Interactions That Drive Protein Evolution: Crowding, Sticking, and Quinary Structure in Folding and Function, Chem. Rev. 119 (2019) 10691–10717, https://doi.org/10.1021/acs.chemrev.8b00753.
[1342] G. Gopan, M. Gruebele, M. Rickard, In-cell protein landscapes: making the match between theory, simulation and experiment, Curr. Opin. Struct. Biol. 66 (2021) 163–169, https://doi.org/10.1016/j.sbi.2020.10.013.
[1343] P.M. Haggie, K.M. Brindle, Mitochondrial citrate synthase is immobilized in vivo, J. Biol. Chem. 274 (1999) 3941–3945, https://doi.org/10.1074/jbc.274.7.3941.
[1344] Y. Ye, X. Liu, Z. Zhang, Q. Wu, B. Jiang, L. Jiang, X. Zhang, M. Liu, G.J. Pielak, C. Li, 19F NMR Spectroscopy as a Probe of Cytoplasmic Viscosity and Weak Protein Interactions in Living Cells, Chem. - Eur. J. 19 (2013) 12705–12710, https://doi.org/10.1002/chem.201301657.
[1345] P.B. Crowley, E. Chow, T. Papkovskaia, Protein Interactions in the Escherichia coli Cytosol: An Impediment to In-Cell NMR Spectroscopy, ChemBioChem. 12 (2011) 1043–1048, https://doi.org/10.1002/cbic.201100063.
[1346] C. Kyne, B. Ruhle, V.W. Gautier, P.B. Crowley, Specific ion effects on macromolecular interactions in Escherichia coli extracts, Protein Sci. Publ. Protein Soc. 24 (2015) 310–318, https://doi.org/10.1002/pro.2615.
[1347] C. Kyne, P.B. Crowley, Short Arginine Motifs Drive Protein Stickiness in the *Escherichia coli* Cytoplasm, Biochemistry. 56 (2017) 5026–5032, https://doi.org/10.1021/acs.biochem.7b00731.
[1348] L. Barbieri, E. Luchinat, L. Banci, Protein interaction patterns in different cellular environments are revealed by in-cell NMR, Sci. Rep. (2015) 1–9, https://doi.org/10.1038/srep14456.
[1349] X. Mu, S. Choi, L. Lang, D. Mowray, N.V. Dokholyan, J. Danielsson, M. Oliveberg, Physicochemical code for quinary protein interactions in Escherichia coli, Proc. Natl. Acad. Sci. 114 (2017) E4556–E4563, https://doi.org/10.1073/pnas.1621227114.
[1350] S. Leeb, F. Yang, M. Oliveberg, J. Danielsson, Connecting Longitudinal and Transverse Relaxation Rates in Live-Cell NMR, J. Phys. Chem. B. 124 (2020) 10698–10707, https://doi.org/10.1021/acs.jpcb.0c08274.
[1351] S. Majumder, J. Xue, C.M. DeMott, S. Reverdatto, D.S. Burz, A. Shekhtman, Probing Protein Quinary Interactions by In-Cell Nuclear Magnetic Resonance Spectroscopy, Biochemistry. 54 (2015) 2727–2738, https://doi.org/10.1021/acs.biochem.5b00036.
[1352] S. Majumder, C.M. DeMott, S. Reverdatto, D.S. Burz, A. Shekhtman, Total Cellular RNA Modulates Protein Activity, Biochemistry. 55 (2016) 4568–4573, https://doi.org/10.1021/acs.biochem.6b00330.
[1353] C.M. DeMott, S. Majumder, D.S. Burz, S. Reverdatto, A. Shekhtman, Ribosome Mediated Quinary Interactions Modulate In-Cell Protein Activities, Biochemistry. 56 (2017) 4117–4126, https://doi.org/10.1021/acs.biochem.7b00613.
[1354] L. Breindel, C. DeMott, D.S. Burz, A. Shekhtman, Real-Time In-Cell Nuclear Magnetic Resonance: Ribosome-Targeted Antibiotics Modulate Quinary Protein Interactions, Biochemistry. 57 (2018) 540–546, https://doi.org/10.1021/acs.biochem.7b00938.
[1355] T. Sugiki, Y. Yamaguchi, T. Fujiwara, M. Inouye, Y. Ito, C. Kojima, In-cell NMR as a sensitive tool to monitor physiological condition of Escherichia coli, Sci. Rep. 10 (2020) 2466–2468, https://doi.org/10.1038/s41598-020-59076-2.
[1356] A.P. Schlesinger, Y. Wang, X. Tadeo, O. Millet, G.J. Pielak, Macromolecular Crowding Fails To Fold a Globular Protein in Cells, J. Am. Chem. Soc. 133 (2011) 8082–8085, https://doi.org/10.1021/ja201206t.
[1357] W.B. Monteith, G.J. Pielak, Residue level quantification of protein stability in living cells, Proc. Natl. Acad. Sci. U. S. A. 111 (2014) 11335–11340, https://doi.org/10.1073/pnas.1406845111.
[1358] Correction for Monteith and Pielak, Residue level quantification of protein stability in living cells, Proc. Natl. Acad. Sci. 112 (2015) E7031. https://doi.org/10.1073/pnas.1521913112..
[1359] A.E. Smith, L.Z. Zhou, A.H. Gorensek, M. Senske, G.J. Pielak, In-cell thermodynamics and a new role for protein surfaces, Proc. Natl. Acad. Sci. 113 (2016) 1725–1730, https://doi.org/10.1073/pnas.1518620113.
[1360] W.B. Monteith, R.D. Cohen, A.E. Smith, E. Guzman-Cisneros, G.J. Pielak, Quinary structure modulates protein stability in cells, Proc. Natl. Acad. Sci. 112 (2015) 1739–1742, https://doi.org/10.1073/pnas.1417415112.
[1361] R.D. Cohen, G.J. Pielak, Electrostatic Contributions to Protein Quinary Structure, J. Am. Chem. Soc. 138 (2016) 13139–13142, https://doi.org/10.1021/jacs.6b07323.
[1362] S.S. Stadmiller, A.H. Gorensek-Benitez, A.J. Guseman, G.J. Pielak, Osmotic Shock Induced Protein Destabilization in Living Cells and Its Reversal by Glycine Betaine, J. Mol. Biol. 429 (2017) 1155–1161, https://doi.org/10.1016/j.jmb.2017.03.001.
[1363] J. Danielsson, M. Kurnik, L. Lang, M. Oliveberg, Cutting Off Functional Loops from Homodimeric Enzyme Superoxide Dismutase 1 (SOD1) Leaves

Monomeric β-Barrels, J. Biol. Chem. 286 (2011) 33070–33083, https://doi.org/10.1074/jbc.M111.251223.
[1364] J. Danielsson, K. Inomata, S. Murayama, H. Tochio, L. Lang, M. Shirakawa, M. Oliveberg, Pruning the ALS-Associated Protein SOD1 for in-Cell NMR, J. Am. Chem. Soc. 135 (2013) 10266–10269, https://doi.org/10.1021/ja404425r.
[1365] J. Danielsson, X. Mu, L. Lang, H. Wang, A. Binolfi, F.-X. Theillet, B. Bekei, D.T. Logan, P. Selenko, H. Wennerstrom, M. Oliveberg, Thermodynamics of protein destabilization in live cells, Proc. Natl. Acad. Sci. U. S. A. 112 (2015) 12402–12407, https://doi.org/10.1073/pnas.1511308112.
[1366] H. Wennerstrom, E. Vallina Estrada, J. Danielsson, M. Oliveberg, Colloidal stability of the living cell, Proc. Natl. Acad. Sci. U. S. A. 117 (2020) 10113–10121, https://doi.org/10.1073/pnas.1914599117.
[1367] T. Sörensen, S. Leeb, J. Danielsson, M. Oliveberg, Polyanions Cause Protein Destabilization Similar to That in Live Cells, Biochemistry. 60 (2021) 735–746, https://doi.org/10.1021/acs.biochem.0c00889.
[1368] N. Iwakawa, D. Morimoto, E. Walinda, S. Leeb, M. Shirakawa, J. Danielsson, K. Sugase, Transient Diffusive Interactions with a Protein Crowder Affect Aggregation Processes of Superoxide Dismutase 1 β-Barrel, J. Phys. Chem. B. 125 (2021) 2521–2532, https://doi.org/10.1021/acs.jpcb.0c11162.
[1369] K. Inomata, H. Kamoshida, M. Ikari, Y. Ito, T. Kigawa, Impact of cellular health conditions on the protein folding state in mammalian cells, Chem. Commun. 53 (2017) 11245–11248, https://doi.org/10.1039/C7CC06004A.
[1370] N. de Souza, P. Picotti, Mass spectrometry analysis of the structural proteome, Curr. Opin. Struct. Biol. 60 (2020) 57–65, https://doi.org/10.1016/j.sbi.2019.10.006.
[1371] J.X. Huang, J.S. Coukos, R.E. Moellering, Interaction profiling methods to map protein and pathway targets of bioactive ligands, Curr. Opin. Chem. Biol. 54 (2020) 76–84, https://doi.org/10.1016/j.cbpa.2020.02.001.
[1372] A. Mateus, N. Kurzawa, I. Becher, S. Sridharan, D. Helm, F. Stein, A. Typas, M. M. Savitski, Thermal proteome profiling for interrogating protein interactions 2019.2012.2030.–11 Mol. Syst. Biol. 16 (2020), https://doi.org/10.15252/msb.20199232.
[1373] J. Perrin, T. Werner, N. Kurzawa, A. Rutkowska, D.D. Childs, M. Kalxdorf, D. Poeckel, E. Stonehouse, K. Strohmer, B. Heller, D.W. Thomson, J. Krause, I. Becher, H.C. Eberl, J. Vappiani, D.C. Sevin, C.E. Rau, H. Franken, W. Huber, M. Faelth-Savitski, M.M. Savitski, M. Bantscheff, G. Bergamini, Identifying drug targets in tissues and whole blood with thermal-shift profiling, Nat. Biotechnol. (2020) 1–15, https://doi.org/10.1038/s41587-019-0388-4.
[1374] N. Prabhu, L. Dai, P. Nordlund, CETSA in integrated proteomics studies of cellular processes, Curr. Opin. Chem. Biol. 54 (2020) 54–62, https://doi.org/10.1016/j.cbpa.2019.11.004.
[1375] T. Tsukidate, Q. Li, H.C. Hang, Targeted and proteome-wide analysis of metabolite-protein interactions, Curr. Opin. Chem. Biol. 54 (2020) 19–27, https://doi.org/10.1016/j.cbpa.2019.10.008.
[1376] J. Stefaniak, K.V.M. Huber, Importance of Quantifying Drug-Target Engagement in Cells, ACS Med. Chem. Lett. 11 (2020) 403–406, https://doi.org/10.1021/acsmedchemlett.9b00570.
[1377] D. Gnutt, S. Timr, J. Ahlers, B. König, E. Manderfeld, M. Heyden, F. Sterpone, S. Ebbinghaus, Stability Effect of Quinary Interactions Reversed by Single Point Mutations, J. Am. Chem. Soc. 141 (2019) 4660–4669, https://doi.org/10.1021/jacs.8b13025.
[1378] M. Gruebele, G.J. Pielak, Dynamical spectroscopy and microscopy of proteins in cells, Curr. Opin. Struct. Biol. 70 (2021) 1–7, https://doi.org/10.1016/j.sbi.2021.02.001.
[1379] A.D. Gossert, W. Jahnke, NMR in drug discovery: A practical guide to identification and validation of ligands interacting with biological macromolecules, Prog. Nucl. Magn. Reson. Spectrosc. 97 (2016) 82–125, https://doi.org/10.1016/j.pnmrs.2016.09.001.
[1380] A.D. Gossert, Assessing molecular interactions with biophysical methods using the validation cross, Biochem. Soc. Trans. 47 (2019) 63–76, https://doi.org/10.1042/BST20180271.
[1381] H. Hanzawa, T. Shimada, M. Takahashi, H. Takahashi, Revisiting biomolecular NMR spectroscopy for promoting small-molecule drug discovery, J. Biomol. NMR. 138 (2020) 4539–4548, https://doi.org/10.1007/s10858-020-00314-0.
[1382] D.A. Erlanson, B.J. Davis, W. Jahnke, Fragment-Based Drug Discovery: Advancing Fragments in the Absence of Crystal Structures, Cell, Chem. Biol. 26 (2019) 9–15, https://doi.org/10.1016/j.chembiol.2018.10.001.
[1383] J. Osborne, S. Panova, M. Rapti, T. Urushima, H. Jhoti, Fragments: where are we now?, Biochem. Soc. Trans. 48 (2020) 271–280, https://doi.org/10.1042/BST20190694.
[1384] C. Dalvit, A. Parent, F. Vallée, M. Mathieu, A. Rak, Fast NMR Methods for Measuring in the Direct and/or Competition Mode the Dissociation Constants of Chemical Fragments Interacting with a Receptor, ChemMedChem. 14 (2019) 1115–1127, https://doi.org/10.1002/cmdc.201900152.
[1385] M.P. Williamson, Using chemical shift perturbation to characterise ligand binding, Prog. Nucl. Magn. Reson. Spectrosc. 73 (2013) 1–16, https://doi.org/10.1016/j.pnmrs.2013.02.001.
[1386] W. Becker, K.C. Bhattiprolu, N. Gubensäk, K. Zangger, Investigating Protein-Ligand Interactions by Solution Nuclear Magnetic Resonance Spectroscopy, ChemPhysChem. 19 (2018) 895–906, https://doi.org/10.1002/cphc.201701253.
[1387] C. Dalvit, M. Veronesi, A. Vulpetti, Fluorine NMR functional screening: from purified enzymes to human intact living cells, J. Biomol. NMR. 74 (2020) 613–631, https://doi.org/10.1007/s10858-020-00311-3.
[1388] N.J. Waters, CHAPTER 3. High-Resolution NMR-Based Metabolic Profiling in Drug Discovery and Development, in: New Appl. NMR Drug Discov. Dev., Royal Society of Chemistry, Cambridge, 2013: pp. 101–133. https://doi.org/10.1039/9781849737661-00101..
[1389] 1] S. Dansereau, D.S. Burz, A. Shekhtman, Chapter 15. Primary Drug Screening by In-cell NMR Spectroscopy, in: New Appl. NMR Drug Discov. Dev., Royal Society of Chemistry, Cambridge, 2019: pp. 249–271. https://doi.org/10.1039/9781788013079-00249..
[1390] J. Xie, R. Thapa, S. Reverdatto, D.S. Burz, A. Shekhtman, Screening of small molecule interactor library by using in-cell NMR spectroscopy (SMILI-NMR), J. Med. Chem. 52 (2009) 3516–3522, https://doi.org/10.1021/jm9000743.
[1391] C.M. DeMott, R. Girardin, J. Cobbert, S. Reverdatto, D.S. Burz, K. McDonough, A. Shekhtman, Potent Inhibitors of Mycobacterium tuberculosis Growth Identified by Using in-Cell NMR-based Screening, ACS Chem. Biol. 13 (2018) 733–741, https://doi.org/10.1021/acschembio.7b00879.
[1392] E. Luchinat, L. Barbieri, M. Cremonini, A. Nocentini, C.T. Supuran, L. Banci, Drug Screening in Human Cells by NMR Spectroscopy Allows the Early Assessment of Drug Potency, Angew. Chem. 59 (2020) 6535–6539, https://doi.org/10.1002/anie.201913436.
[1393] E. Luchinat, L. Barbieri, M. Cremonini, A. Nocentini, C.T. Supuran, L. Banci, Intracellular Binding/Unbinding Kinetics of Approved Drugs to Carbonic Anhydrase II Observed by in-Cell NMR, ACS Chem. Biol. 15 (2020) 2792–2800, https://doi.org/10.1021/acschembio.0c00590.
[1394] J. Ma, S. McLeod, K. MacCormack, S. Sriram, N. Gao, A.L. Breeze, J. Hu, Real-time monitoring of New Delhi metallo-β-lactamase activity in living bacterial cells by 1H NMR spectroscopy, Angew. Chem. Int. Ed Engl. 53 (2014) 2130–2133, https://doi.org/10.1002/anie.201308636.
[1395] J. Ma, Q. Cao, S.M. McLeod, K. Ferguson, N. Gao, A.L. Breeze, J. Hu, Target-Based Whole-Cell Screening by 1H NMR Spectroscopy, Angew. Chem. 127 (2015) 4846–4849, https://doi.org/10.1002/ange.201410701.
[1396] M. Veronesi, E. Romeo, C. Lambruschini, D. Piomelli, T. Bandiera, R. Scarpelli, G. Garau, C. Dalvit, Fluorine NMR-based screening on cell membrane extracts, ChemMedChem. 9 (2014) 286–289, https://doi.org/10.1002/cmdc.201300438.
[1397] M. Veronesi, F. Giacomina, E. Romeo, B. Castellani, G. Ottonello, C. Lambruschini, G. Garau, R. Scarpelli, T. Bandiera, D. Piomelli, C. Dalvit, Fluorine nuclear magnetic resonance-based assay in living mammalian cells, Anal. Biochem. 495 (2016) 52–59, https://doi.org/10.1016/j.ab.2015.11.015.
[1398] C. Dalvit, A. Vulpetti, Ligand-Based Fluorine NMR Screening: Principles and Applications in Drug Discovery Projects, J. Med. Chem. 62 (2019) 2218–2244, https://doi.org/10.1021/acs.jmedchem.8b01210.
[1399] L. Liu, V.D. Kodibagkar, J. Yu, R.P. Mason, 19F-NMR detection of lacZgene expression viathe enzymic hydrolysis of 2-fluoro-4-nitrophenyl β-D-galactopyranoside in vivoin PC3 prostate tumor xenografts in the mouse 1, FASEB J. 21 (2007) 2014–2019, https://doi.org/10.1096/fj.06-7366lsf.
[1400] J. Yu, V.D. Kodibagkar, L. Liu, R.P. Mason, A 19F-NMR approach using reporter molecule pairs to assess β-galactosidase in human xenograft tumors in vivo, NMR Biomed. 21 (2008) 704–712, https://doi.org/10.1002/nbm.1244.
[1401] S. Mizukami, R. Takikawa, F. Sugihara, Y. Hori, H. Tochio, M. Wälchli, M. Shirakawa, K. Kikuchi, Paramagnetic relaxation-based 19f MRI probe to detect protease activity, J. Am. Chem. Soc. 130 (2008) 794–795, https://doi.org/10.1021/ja077058z.
[1402] M.H. Cho, S.H. Shin, S.H. Park, D.K. Kadayakkara, D. Kim, Y. Choi, Targeted, Stimuli-Responsive, and Theranostic 19F Magnetic Resonance Imaging Probes, Bioconjug. Chem. 30 (2019) 2502–2518, https://doi.org/10.1021/acs.bioconjchem.9b00582.
[1403] S. Mizukami, H. Matsushita, R. Takikawa, F. Sugihara, M. Shirakawa, K. Kikuchi, 19F MRI detection of β-galactosidase activity for imaging of gene expression, Chem Sci. 2 (2011) 1151–1155, https://doi.org/10.1039/c1sc00071c.
[1404] H. Matsushita, S. Mizukami, Y. Mori, F. Sugihara, M. Shirakawa, Y. Yoshioka, K. Kikuchi, 19F MRI Monitoring of Gene Expression in Living Cells through Cell-Surface β-Lactamase Activity, ChemBioChem. 13 (2012) 1579–1583, https://doi.org/10.1002/cbic.201200331.
[1405] K. Matsuo, R. Kamada, K. Mizusawa, H. Imai, Y. Takayama, M. Narazaki, T. Matsuda, Y. Takaoka, I. Hamachi, Specific Detection and Imaging of Enzyme Activity by Signal-Amplifiable Self-Assembling 19F MRI Probes, Chem. - Eur. J. 19 (2013) 12875–12883, https://doi.org/10.1002/chem.201300817.
[1406] X. Yue, Z. Wang, L. Zhu, Y. Wang, C. Qian, Y. Ma, D.O. Kiesewetter, G. Niu, X. Chen, Novel 19F Activatable Probe for the Detection of Matrix Metalloprotease-2 Activity by MRI/MRS, Mol. Pharm. 11 (2014) 4208–4217, https://doi.org/10.1021/mp500443x.
[1407] C. Guo, Y. Zhang, Y. Li, S. Xu, L. Wang, 19F MRI Nanoprobes for the Turn-On Detection of Phospholipase A2 with a Low Background, Anal. Chem. 91 (2019) 8147–8153, https://doi.org/10.1021/acs.analchem.9b00435.
[1408] J. Kosten, A. Binolfi, M. Stuiver, S. Verzini, F.-X. Theillet, B. Bekei, M. van Rossum, P. Selenko, Efficient modification of alpha-synuclein serine 129 by protein kinase CK1 requires phosphorylation of tyrosine 125 as a priming event, ACS Chem. Neurosci. 5 (2014) 1203–1208, https://doi.org/10.1021/cn5002254.
[1409] C.M. Tressler, N.J. Zondlo, Perfluoro-tert-Butyl Hydroxyprolines as Sensitive, Conformationally Responsive Molecular Probes: Detection of Protein Kinase Activity by 19F NMR, ACS Chem. Biol. 15 (2020) 1096–1103, https://doi.org/10.1021/acschembio.0c00131.

[1410] C. Sanchez-Lopez, N. Labadie, V. Lombardo, F. Biglione, B. Manta, R. Jacob, V. Gladyshev, S. Abdelilah-Seyfried, P. Selenko, A. Binolfi, An NMR-based biosensor to measure stereo-specific methionine sulfoxide reductase (MSR) activities in vitro and in vivo chem.202002645-7 Chem. - Eur. J. (2020), https://doi.org/10.1002/chem.202002645.
[1411] C. Rademacher, J. Guiard, P.I. Kitov, B. Fiege, K.P. Dalton, F. Parra, D.R. Bundle, T. Peters, Targeting norovirus infection-multivalent entry inhibitor design based on NMR experiments, Chem. - Eur. J. 17 (2011) 7442–7453, https://doi.org/10.1002/chem.201003432.
[1412] B. Meyer, T. Peters, NMR spectroscopy techniques for screening and identifying ligand binding to protein receptors, Angew. Chem. 42 (2003) 864–890, https://doi.org/10.1002/anie.200390233.
[1413] Y.V. Nikolaev, K. Kochanowski, H. Link, U. Sauer, F.-H.-T. Allain, Systematic Identification of Protein-Metabolite Interactions in Complex Metabolite Mixtures by Ligand-Detected Nuclear Magnetic Resonance Spectroscopy, Biochemistry. 55 (2016) 2590–2600, https://doi.org/10.1021/acs.biochem.5b01291.
[1414] M. Diether, Y. Nikolaev, F.H. Allain, U. Sauer, Systematic mapping of protein-metabolite interactions in central metabolism of Escherichia coli, Mol. Syst. Biol. 15 (2019), https://doi.org/10.15252/msb.20199008 e9008.
[1415] L.F. Pinto, J. Correa, L. Zhao, R. Riguera, E. Fernandez-Megia, Fast NMR Screening of Macromolecular Complexes by a Paramagnetic Spin Relaxation Filter, ACS Omega. 3 (2018) 2974–2983, https://doi.org/10.1021/acsomega.7b02074.
[1416] C.A. Softley, M.J. Bostock, G.M. Popowicz, M. Sattler, Paramagnetic NMR in drug discovery, J. Biomol. NMR. 74 (2020) 287–309, https://doi.org/10.1007/s10858-020-00322-0.
[1417] G.S. Jacob, J. Schaefer, G.E. Wilson, Solid-state 13C and 15N nuclear magnetic resonance studies of alanine metabolism in Aerococcus viridans (Gaffkya homari), J. Biol. Chem. 260 (1985) 2777–2781.
[1418] R. Nygaard, J.A.H. Romaniuk, D.M. Rice, L. Cegelski, Spectral Snapshots of Bacterial Cell-Wall Composition and the Influence of Antibiotics by Whole-Cell NMR, Biophys. J. 108 (2015) 1380–1389, https://doi.org/10.1016/j.bpj.2015.01.037.
[1419] C. Reichhardt, J.A.G. Ferreira, L.-M. Joubert, K.V. Clemons, D.A. Stevens, L. Cegelski, Analysis of the Aspergillus fumigatus Biofilm Extracellular Matrix by Solid-State Nuclear Magnetic Resonance Spectroscopy, Eukaryot. Cell. 14 (2015) 1064–1072, https://doi.org/10.1128/EC.00050-15.
[1420] C. Reichhardt, J.C.N. Fong, F. Yildiz, L. Cegelski, Characterization of the Vibrio cholerae extracellular matrix: A top-down solid-state NMR approach, BBA - Biomembr. 2015 (1848) 378–383, https://doi.org/10.1016/j.bbamem.2014.05.030.
[1421] Y.-J. Chen, X. Huang, N.G. Mahieu, K. Cho, J. Schaefer, G.J. Patti, Differential incorporation of glucose into biomass during Warburg metabolism, Biochemistry. 53 (2014) 4755–4757, https://doi.org/10.1021/bi500763u.
[1422] Y.-J. Chen, N.G. Mahieu, X. Huang, M. Singh, P.A. Crawford, S.L. Johnson, R.W. Gross, J. Schaefer, G.J. Patti, Lactate metabolism is associated with mammalian mitochondria, Nat. Chem. Biol. 12 (2016) 937–943, https://doi.org/10.1038/nchembio.2172.
[1423] S.H. Werby, L. Cegelski, Spectral comparisons of mammalian cells and intact organelles by solid-state NMR, J. Struct. Biol. 206 (2019) 49–54, https://doi.org/10.1016/j.jsb.2018.05.007.
[1424] S.J. Kim, M. Singh, J. Schaefer, Oritavancin binds to isolated protoplast membranes but not intact protoplasts of Staphylococcus aureus, J. Mol. Biol. 391 (2009) 414–425, https://doi.org/10.1016/j.jmb.2009.06.033.
[1425] D.A. Erlanson, S.W. Fesik, R.E. Hubbard, W. Jahnke, H. Jhoti, Twenty years on: the impact of fragments on drug discovery, Nat. Rev. Drug Discov. 15 (2016) 605–619, https://doi.org/10.1038/nrd.2016.109.
[1426] M. Pellecchia, I. Bertini, D. Cowburn, C. Dalvit, E. Giralt, W. Jahnke, T.L. James, S.W. Homans, H. Kessler, C. Luchinat, B. Meyer, H. Oschkinat, J. Peng, H. Schwalbe, G. Siegal, Perspectives on NMR in drug discovery: a technique comes of age, Nat. Rev. Drug Discov. 7 (2008) 738–745, https://doi.org/10.1038/nrd2606.
[1427] J.-P. Renaud, A. Chari, C. Ciferri, W. Liu, H.-W. Rémigy, H. Stark, C. Wiesmann, Cryo-EM in drug discovery: achievements, limitations and prospects, Nat. Rev. Drug Discov. 17 (2018) 471–492, https://doi.org/10.1038/nrd.2018.77.
[1428] D. Moreira, P. López-García, Ten reasons to exclude viruses from the tree of life, Nat. Rev. Microbiol. 7 (2009) 306–311, https://doi.org/10.1038/nrmicro2108.
[1429] E.V. Koonin, P. Starokadomskyy, Are viruses alive? The replicator paradigm sheds decisive light on an old but misguided question, Stud. Hist. Philos. Biol. Biomed. Sci. 59 (2016) 125–134, https://doi.org/10.1016/j.shpsc.2016.02.016.
[1430] J.E. Stencel-Baerenwald, K. Reiss, D.M. Reiter, T. Stehle, T.S. Dermody, The sweet spot: defining virus-sialic acid interactions, Nat. Rev. Microbiol. 12 (2014) 739–749, https://doi.org/10.1038/nrmicro3346.
[1431] L. Stavolone, V. Lionetti, Extracellular Matrix in Plants and Animals: Hooks and Locks for Viruses, Front. Microbiol. 8 (2017) 7921–7928, https://doi.org/10.3389/fmicb.2017.01760.
[1432] M.S. Maginnis, Virus-Receptor Interactions: The Key to Cellular Invasion, J. Mol. Biol. 430 (2018) 2590–2611, https://doi.org/10.1016/j.jmb.2018.06.024.
[1433] D.F. Smith, R.D. Cummings, Investigating virus-glycan interactions using glycan microarrays, Curr. Opin. Virol. 7 (2014) 79–87, https://doi.org/10.1016/j.coviro.2014.05.005.
[1434] R. Raman, K. Tharakaraman, V. Sasisekharan, R. Sasisekharan, Glycan-protein interactions in viral pathogenesis, Curr. Opin. Struct. Biol. 40 (2016) 153–162, https://doi.org/10.1016/j.sbi.2016.10.003.
[1435] B.R. Wasik, K.N. Barnard, C.R. Parrish, Effects of Sialic Acid Modifications on Virus Binding and Infection, Trends Microbiol. 24 (2016) 991–1001, https://doi.org/10.1016/j.tim.2016.07.005.
[1436] S.L. Taylor, M.A. McGuckin, S. Wesselingh, G.B. Rogers, Infection's Sweet Tooth: How Glycans Mediate Infection and Disease Susceptibility, Trends Microbiol. 26 (2018) 92–101, https://doi.org/10.1016/j.tim.2017.09.011.
[1437] L. Unione, A. Gimeno, P. Valverde, I. Calloni, H. Coelho, S. Mirabella, A. Poveda, A. Ardá, J. Jiménez-Barbero, Glycans in Infectious Diseases. A Molecular Recognition Perspective, Curr. Med. Chem. 24 (2017) 1–24, https://doi.org/10.2174/0929867324666170217093702.
[1438] J.E. Hanson, N.K. Sauter, J.J. Skehel, D.C. Wiley, Proton nuclear magnetic resonance studies of the binding of sialosides to intact influenza virus, Virology. 189 (1992) 525–533, https://doi.org/10.1016/0042-6822(92)90576-b.
[1439] R.M. Keller, K. Wüthrich, Assignment of the heme c resonances in the 360 MHz 1H NMR spectra of cytochrome c, Biochim. Biophys. Acta BBA - Protein Struct. 533 (1978) 195–208, https://doi.org/10.1016/0005-2795(78)90564-0.
[1440] P.J. Cayley, J.P. Albrand, J. Feeney, G.C.K. Roberts, E.A. Piper, A.S.V. Burgen, Nuclear magnetic resonance studies of the binding of trimethoprim to dihydrofolate reductase, Biochemistry. 18 (1979) 3886–3895, https://doi.org/10.1021/bi00585a008.
[1441] K. Akasaka, Intermolecular spin diffusion as a method for studying macromolecule-ligand interactions, J. Magn. Reson. 1969 (36) (1979) 135–140, https://doi.org/10.1016/0022-2364(79)90223-3.
[1442] A. Bhunia, S. Bhattacharjya, S. Chatterjee, Applications of saturation transfer difference NMR in biological systems, Drug Discov. Today. 17 (2012) 505–513, https://doi.org/10.1016/j.drudis.2011.12.016.
[1443] J.L. Wagstaff, S.L. Taylor, M.J. Howard, Recent developments and applications of saturation transfer difference nuclear magnetic resonance (STD NMR) spectroscopy, Mol. Biosyst. 9 (2013) 571–577, https://doi.org/10.1039/c2mb25395j.
[1444] A.J. Benie, R. Moser, E. Bäuml, D. Blaas, T. Peters, Virus-ligand interactions: identification and characterization of ligand binding by NMR spectroscopy, J. Am. Chem. Soc. 125 (2003) 14–15, https://doi.org/10.1021/ja027691e.
[1445] T. Haselhorst, J.-M. Garcia, T. Islam, J.C.C. Lai, F.J. Rose, J.M. Nicholls, J.S.M. Peiris, M. von Itzstein, Avian influenza H5-containing virus-like particles (VLPs): host-cell receptor specificity by STD NMR spectroscopy, Angew. Chem. Int. Ed Engl. 47 (2008) 1910–1912, https://doi.org/10.1002/anie.200704872.
[1446] J.C.C. Lai, J.-M. Garcia, J.C. Dyason, R. Böhm, P.D. Madge, F.J. Rose, J.M. Nicholls, J.S.M. Peiris, T. Haselhorst, M. von Itzstein, A secondary sialic acid binding site on influenza virus neuraminidase: fact or fiction?, Angew. Chem. Int. Ed Engl. 51 (2012) 2221–2224, https://doi.org/10.1002/anie.201108245.
[1447] J.-M. Garcia, J.C.C. Lai, T. Haselhorst, K.T. Choy, H.-L. Yen, J.S.M. Peiris, M. von Itzstein, J.M. Nicholls, Investigation of the binding and cleavage characteristics of N1 neuraminidases from avian, seasonal, and pandemic influenza viruses using saturation transfer difference nuclear magnetic resonance, Influenza Other Respir. Viruses. 8 (2014) 235–242, https://doi.org/10.1111/irv.12184.
[1448] C. Rademacher, N.R. Krishna, M. Palcic, F. Parra, T. Peters, NMR experiments reveal the molecular basis of receptor recognition by a calicivirus, J. Am. Chem. Soc. 130 (2008) 3669–3675, https://doi.org/10.1021/ja710854r.
[1449] M. Zakhour, N. Ruvoën-Clouet, A. Charpilienne, B. Langpap, D. Poncet, T. Peters, N. Bovin, J. Le Pendu, The alphaGal epitope of the histo-blood group antigen family is a ligand for bovine norovirus Newbury2 expected to prevent cross-species transmission., PLoS Pathog. 5 (2009) e1000504. https://doi.org/10.1371/journal.ppat.1000504..
[1450] T. Haselhorst, T. Fiebig, J.C. Dyason, F.E. Fleming, H. Blanchard, B.S. Coulson, M. von Itzstein, Recognition of the GM3 ganglioside glycan by Rhesus rotavirus particles, Angew. Chem. Int. Ed Engl. 50 (2011) 1055–1058, https://doi.org/10.1002/anie.201004116.
[1451] B. Fiege, C. Rademacher, J. Cartmell, P.I. Kitov, F. Parra, T. Peters, Molecular details of the recognition of blood group antigens by a human norovirus as determined by STD NMR spectroscopy, Angew. Chem. Int. Ed Engl. 51 (2012) 928–932, https://doi.org/10.1002/anie.201105719.
[1452] B. Fiege, M. Leuthold, F. Parra, K.P. Dalton, P.J. Meloncelli, T.L. Lowary, T. Peters, Epitope mapping of histo blood group antigens bound to norovirus VLPs using STD NMR experiments reveals fine details of molecular recognition, Glycoconj. J. 34 (2017) 679–689, https://doi.org/10.1007/s10719-017-9792-5.
[1453] A. Muhamad, K.L. Ho, M.B.A. Rahman, B.A. Tejo, D. Uhrín, W.S. Tan, Hepatitis B virus peptide inhibitors: solution structures and interactions with the viral capsid, Org. Biomol. Chem. 13 (2015) 7780–7789, https://doi.org/10.1039/c5ob00449g.
[1454] A. Antanasijevic, C. Kingsley, A. Basu, T.L. Bowlin, L. Rong, M. Caffrey, Application of virus-like particles (VLP) to NMR characterization of viral membrane protein interactions, J. Biomol. NMR. 64 (2016) 255–265, https://doi.org/10.1007/s10858-016-0025-1.
[1455] P.S.K. Ng, R. Böhm, L.E. Hartley-Tassell, J.A. Steen, H. Wang, S.W. Lukowski, P. L. Hawthorne, A.E.O. Trezise, P.J. Coloe, S.M. Grimmond, T. Haselhorst, M. von Itzstein, A.W. Paton, J.C. Paton, M.P. Jennings, Ferrets exclusively

synthesize Neu5Ac and express naturally humanized influenza A virus receptors, Nat. Commun. 5 (2014) 5750–5759, https://doi.org/10.1038/ncomms6750.
[1456] J. Mayr, K. Lau, J.C.C. Lai, I.A. Gagarinov, Y. Shi, S. McAtamney, R.W.Y. Chan, J. Nicholls, M. von Itzstein, T. Haselhorst, Unravelling the Role of O-glycans in Influenza A Virus Infection, Sci. Rep. 8 (2018) 16382–16412, https://doi.org/10.1038/s41598-018-34175-3.
[1457] M. Martikainen, K. Salorinne, T. Lahtinen, S. Malola, P. Permi, H. Häkkinen, V. Marjomäki, Hydrophobic pocket targeting probes for enteroviruses, Nanoscale. 7 (2015) 17457–17467, https://doi.org/10.1039/c5nr04139b.
[1458] D.F. Earley, B. Bailly, A. Maggioni, A.R. Kundur, R.J. Thomson, C.-W. Chang, M. von Itzstein, Efficient Blocking of Enterovirus 71 Infection by Heparan Sulfate Analogues Acting as Decoy Receptors, ACS Infect. Dis. 5 (2019) 1708–1717, https://doi.org/10.1021/acsinfecdis.9b00070.
[1459] F. Vasile, M. Panigada, A. Siccardi, D. Potenza, G. Tiana, A Combined NMR-Computational Study of the Interaction between Influenza Virus Hemagglutinin and Sialic Derivatives from Human and Avian Receptors on the Surface of Transfected Cells, Int. J. Mol. Sci. 19 (2018), https://doi.org/10.3390/ijms19051267.
[1460] F. Vasile, F. Gubinelli, M. Panigada, E. Soprana, A. Siccardi, D. Potenza, NMR interaction studies of Neu5Ac-α-(2,6)-Gal-β-(1–4)-GlcNAc with influenza-virus hemagglutinin expressed in transfected human cells, Glycobiology. 28 (2018) 42–49, https://doi.org/10.1093/glycob/cwx092.
[1461] L. Han, E.N. Kitova, M. Tan, X. Jiang, B. Pluvinage, A.B. Boraston, J.S. Klassen, Affinities of human histo-blood group antigens for norovirus capsid protein complexes, Glycobiology. 25 (2015) 170–180, https://doi.org/10.1093/glycob/cwu100.
[1462] E.N. Kitova, L. Han, D.F. Vinals, P.I. Kitov, R. Derda, J.S. Klassen, Influence of labeling on the glycan affinities and specificities of glycan-binding proteins. A case study involving a C-terminal fragment of human galectin-3, Glycobiology. 30 (2019) 49–57, https://doi.org/10.1093/glycob/cwz076.
[1463] S. Taube, Á. Mallagaray, T. Peters, Norovirus, glycans and attachment, Curr. Opin. Virol. 31 (2018) 33–42, https://doi.org/10.1016/j.coviro.2018.04.007.
[1464] R. Santos, O. Ursu, A. Gaulton, A.P. Bento, R.S. Donadi, C.G. Bologa, A. Karlsson, B. Al-Lazikani, A. Hersey, T.I. Oprea, J.P. Overington, A comprehensive map of molecular drug targets, Nat. Rev. Drug Discov. 16 (2017) 19–34, https://doi.org/10.1038/nrd.2016.230.
[1465] S. Mari, D. Serrano-Gómez, F.J. Cañada, A.L. Corbí, J. Jiménez-Barbero, 1D saturation transfer difference NMR experiments on living cells: the DC-SIGN/oligomannose interaction, Angew. Chem. 44 (2005) 296–298, https://doi.org/10.1002/anie.200461574.
[1466] A. Maggioni, M. von Itzstein, J. Tiralongo, T. Haselhorst, Detection of ligand binding to nucleotide sugar transporters by STD NMR spectroscopy, ChemBioChem. 9 (2008) 2784–2786, https://doi.org/10.1002/cbic.200800526.
[1467] A. Maggioni, M. von Itzstein, I.B. Rodríguez Guzmán, A. Ashikov, A.S. Stephens, T. Haselhorst, J. Tiralongo, Characterisation of CMP-sialic acid transporter substrate recognition, ChemBioChem. 14 (2013) 1936–1942, https://doi.org/10.1002/cbic.201300298.
[1468] A. Maggioni, J. Meier, F. Routier, T. Haselhorst, J. Tiralongo, Direct investigation of the Aspergillus GDP-mannose transporter by STD NMR spectroscopy, ChemBioChem. 12 (2011) 2421–2425, https://doi.org/10.1002/cbic.201100483.
[1469] A. Pereira, T.A. Pfeifer, T.A. Grigliatti, R.J. Andersen, Functional cell-based screening and saturation transfer double-difference NMR have identified haplosamate A as a cannabinoid receptor agonist, ACS Chem. Biol. 4 (2009) 139–144, https://doi.org/10.1021/cb800264k.
[1470] F.M. Assadi-Porter, M. Tonelli, E. Maillet, K. Hallenga, O. Benard, M. Max, J.L. Markley, Direct NMR detection of the binding of functional ligands to the human sweet receptor, a heterodimeric family 3 GPCR, J. Am. Chem. Soc. 130 (2008) 7212–7213, https://doi.org/10.1021/ja8016939.
[1471] F.M. Assadi-Porter, M. Tonelli, E.L. Maillet, J.L. Markley, M. Max, Interactions between the human sweet-sensing T1R2-T1R3 receptor and sweeteners detected by saturation transfer difference NMR spectroscopy, Biochim. Biophys. Acta. 1798 (2010) 82–86, https://doi.org/10.1016/j.bbamem.2009.07.021.
[1472] B.D. Cox, A.K. Mehta, J.O. DiRaddo, D.C. Liotta, L.J. Wilson, J.P. Snyder, Structural analysis of CXCR4 - Antagonist interactions using saturation-transfer double-difference NMR, Biochem. Biophys. Res. Commun. 466 (2015) 28–32, https://doi.org/10.1016/j.bbrc.2015.08.084.
[1473] J.L. Burger, K.M. Jeerage, T.J. Bruno, Direct nuclear magnetic resonance observation of odorant binding to mouse odorant receptor MOR244-3, Anal. Biochem. 502 (2016) 64–72, https://doi.org/10.1016/j.ab.2016.03.006.
[1474] S. Li, L. Ahmed, R. Zhang, Y. Pan, H. Matsunami, J.L. Burger, E. Block, V.S. Batista, H. Zhuang, Smelling Sulfur: Copper and Silver Regulate the Response of Human Odorant Receptor OR2T11 to Low-Molecular-Weight Thiols, J. Am. Chem. Soc. 138 (2016) 13281–13288, https://doi.org/10.1021/jacs.6b06983.
[1475] C. Airoldi, S. Giovannardi, B. La Ferla, J. Jiménez-Barbero, F. Nicotra, Saturation transfer difference NMR experiments of membrane proteins in living cells under HR-MAS conditions: the interaction of the SGLT1 co-transporter with its ligands, Chem. - Eur. J. 17 (2011) 13395–13399, https://doi.org/10.1002/chem.201102181.
[1476] B. Claasen, M. Axmann, R. Meinecke, B. Meyer, Direct observation of ligand binding to membrane proteins in living cells by a saturation transfer double difference (STDD) NMR spectroscopy method shows a significantly higher affinity of integrin alpha(IIb)beta3 in native platelets than in liposomes, J. Am. Chem. Soc. 127 (2005) 916–919, https://doi.org/10.1021/ja044434w.
[1477] G.M. Clore, A.M. Gronenborn, Theory and applications of the transferred nuclear overhauser effect to the study of the conformations of small ligands bound to proteins, J. Magn. Reson. 1969 (48) (1982) 402–417, https://doi.org/10.1016/0022-2364(82)90073-7.
[1478] D. Potenza, L. Belvisi, Transferred-NOE NMR experiments on intact human platelets: receptor-bound conformation of RGD-peptide mimics, Org. Biomol. Chem. 6 (2008) 258–262, https://doi.org/10.1039/b713036h.
[1479] S. Mari, C. Invernizzi, A. Spitaleri, L. Alberici, M. Ghitti, C. Bordignon, C. Traversari, G.-P. Rizzardi, G. Musco, 2D TR-NOESY Experiments Interrogate and Rank Ligand-Receptor Interactions in Living Human Cancer Cells, Angew. Chem. 49 (2010) 1071–1074, https://doi.org/10.1002/anie.200905941.
[1480] D. Potenza, F. Vasile, L. Belvisi, M. Civera, E.M.V. Araldi, STD and trNOESY NMR study of receptor-ligand interactions in living cancer cells, ChemBioChem. 12 (2011) 695–699, https://doi.org/10.1002/cbic.201000756.
[1481] I. Guzzetti, M. Civera, F. Vasile, E.M. Araldi, L. Belvisi, C. Gennari, D. Potenza, R. Fanelli, U. Piarulli, Determination of the binding epitope of RGD-peptidomimetics to αvβ3 and α(IIb)β3 integrin-rich intact cells by NMR and computational studies, Org. Biomol. Chem. 11 (2013) 3886–3893, https://doi.org/10.1039/c3ob40540k.
[1482] B. Farina, I. de Paola, L. Russo, D. Capasso, A. Liguoro, A.D. Gatto, M. Saviano, P.V. Pedone, S. Di Gaetano, G. Malgieri, L. Zaccaro, R. Fattorusso, A Combined NMR and Computational Approach to Determine the RGDechi-hCit-αv β3 Integrin Recognition Mode in Isolated Cell Membranes, Chem. - Eur. J. 22 (2016) 681–693, https://doi.org/10.1002/chem.201503126.
[1483] F. Vasile, G. Menchi, E. Lenci, A. Guarna, D. Potenza, A. Trabocchi, Insight to the binding mode of triazole RGD-peptidomimetics to integrin-rich cancer cells by NMR and molecular modeling, Bioorg. Med. Chem. 24 (2016) 989–994, https://doi.org/10.1016/j.bmc.2016.01.023.
[1484] F. Nardelli, C. Paissoni, G. Quilici, A. Gori, C. Traversari, B. Valentinis, A. Sacchi, A. Corti, F. Curnis, M. Ghitti, G. Musco, Succinimide-Based Conjugates Improve IsoDGR Cyclopeptide Affinity to αvβ3 without Promoting Integrin Allosteric Activation, J. Med. Chem. 61 (2018) 7474–7485, https://doi.org/10.1021/acs.jmedchem.8b00745.
[1485] I. Guzzetti, M. Civera, F. Vasile, D. Arosio, C. Tringali, U. Piarulli, C. Gennari, L. Pignataro, L. Belvisi, D. Potenza, Insights into the Binding of Cyclic RGD Peptidomimetics to α5β1 Integrin by using Live-Cell NMR And Computational Studies, ChemistryOpen. 6 (2017) 128–136, https://doi.org/10.1002/open.201600112.
[1486] L. Russo, B. Farina, A. Del Gatto, D. Comegna, S. Di Gaetano, D. Capasso, A. Liguoro, G. Malgieri, M. Saviano, R. Fattorusso, L. Zaccaro, Deciphering RGDechi peptide-α 5β 1integrin interaction mode in isolated cell membranes, Pept. Sci. 110 (2018) e24065–e24114, https://doi.org/10.1002/pep2.24065.
[1487] B. Mateos, M. Sealey Cardona, K. Balazs, J. Konrat, G. Staffler, R. Konrat, NMR Characterization of Surface Receptor Protein Interactions in Live Cells Using Methylcellulose Hydrogels, Angew. Chem. 59 (2020) 3886–3890, https://doi.org/10.1002/anie.201913585.
[1488] P.D. Madge, A. Maggioni, M. Pascolutti, M. Amin, M. Waespy, B. Bellette, R.J. Thomson, S. Kelm, M. von Itzstein, T. Haselhorst, Structural characterisation of high affinity Siglec-2 (CD22) ligands in complex with whole Burkitt's lymphoma (BL) Daudi cells by NMR spectroscopy, Sci. Rep. 6 (2016) 36012–36112, https://doi.org/10.1038/srep36012.
[1489] D. Brancaccio, D. Diana, S. Di Maro, F.S. Di Leva, S. Tomassi, R. Fattorusso, L. Russo, S. Scala, A.M. Trotta, L. Portella, E. Novellino, L. Marinelli, A. Carotenuto, Ligand-Based NMR Study of C-X-C Chemokine Receptor Type 4 (CXCR4)-Ligand Interactions on Living Cancer Cells, J. Med. Chem. 61 (2018) 2910–2923, https://doi.org/10.1021/acs.jmedchem.7b01830.
[1490] D. Diana, A. Russomanno, L. De Rosa, R. Di Stasi, D. Capasso, S. Di Gaetano, A. Romanelli, L. Russo, L.D. D'Andrea, R. Fattorusso, Functional binding surface of a β-hairpin VEGF receptor targeting peptide determined by NMR spectroscopy in living cells, Chem. - Eur. J. 21 (2015) 91–95, https://doi.org/10.1002/chem.201403335.
[1491] R. Di Stasi, D. Diana, D. Capasso, S. Di Gaetano, L. De Rosa, V. Celentano, C. Isernia, R. Fattorusso, L.D. D'Andrea, VEGFR Recognition Interface of a Proangiogenic VEGF-Mimetic Peptide Determined In Vitro and in the Presence of Endothelial Cells by NMR Spectroscopy, Chem. - Eur. J. 24 (2018) 11461–11466, https://doi.org/10.1002/chem.201802117.
[1492] B. Valentinis, S. Porcellini, C. Asperti, M. Cota, D. Zhou, P. Di Matteo, G. Garau, C. Zucchelli, N.R. Avanzi, G.-P. Rizzardi, M. Degano, G. Musco, C. Traversari, Mechanism of Action of the Tumor Vessel Targeting Agent NGR-hTNF: Role of Both NGR Peptide and hTNF in Cell Binding and Signaling, Int. J. Mol. Sci. 20 (2019), https://doi.org/10.3390/ijms20184511.
[1493] A. Palmioli, C. Ceresa, F. Tripodi, B. La Ferla, G. Nicolini, C. Airoldi, On-cell Saturation Transfer Difference NMR study of Bombesin binding to GRP receptor, Bioorganic Chem. (2020), https://doi.org/10.1016/j.bioorg.2020.103861 103861.
[1494] G. Bouvier, C. Simenel, J. Jang, N.P. Kalia, I. Choi, M. Nilges, K. Pethe, N. Izadi-Pruneyre, Target Engagement and Binding Mode of an Antituberculosis Drug to Its Bacterial Target Deciphered in Whole Living Cells by NMR, Biochemistry. 58 (2019) 526–533, https://doi.org/10.1021/acs.biochem.8b00975.

[1495] T.M. Shaw, R.H. Elsken, Nuclear Magnetic Resonance Absorption in Hygroscopic Materials, J. Chem. Phys. 18 (1950) 1113–1114, https://doi.org/10.1063/1.1747875.
[1496] Anonymous, Minutes of the Meeting at Chicago, October 24-27, 1951, Phys. Rev. 85 (1952) 700–737. https://doi.org/10.1103/PhysRev.85.700..
[1497] T.M. Shaw, R.H. Elsken, Investigation of Proton Magnetic Resonance Line Width of Sorbed Water, J. Chem. Phys. 21 (1953) 565–566, https://doi.org/10.1063/1.1698959.
[1498] T.M. Shaw, R.H. Elsken, Determination of Hydrogen in Liquids and Suspensions by Nuclear Magnetic Absorption, Anal. Chem. 27 (1955) 1983–1985.
[1499] K.J. Palmer, R.H. Elsken, Moisture Determination, Determination of Water by Nuclear Magnetic Resonance in Hygroscopic Materials Containing Soluble Solids, J. Agric. Food Chem. 4 (1956) 165–167, https://doi.org/10.1021/jf60060a009.
[1500] T.M. Shaw, R.H. Elsken, Moisture Determination, Determination of Water by Nuclear Magnetic Absorption in Potato and Apple Tissue, J. Agric. Food Chem. 4 (1956) 162–164, https://doi.org/10.1021/jf60060a008.
[1501] N. Bloembergen, E.M. Purcell, R.V. Pound, Nuclear magnetic relaxation, Nature. 160 (1947) 475–476, https://doi.org/10.1038/160475a0.
[1502] E. Odeblad, G. LINDSTROM, Some preliminary observations on the proton magnetic resonance in biologic samples., Acta Radiol. 43 (1955) 469–476. https://doi.org/10.3109/00016925509172514..
[1503] F. Bloch, The Nuclear Induction Experiment, Phys. Rev. 70 (1946) 474–485, https://doi.org/10.1103/PhysRev.70.474.
[1504] N. Bloembergen, E.M. Purcell, R.V. Pound, RELAXATION EFFECTS IN NUCLEAR MAGNETIC RESONANCE ABSORPTION, Phys. Rev. 73 (1948) 679–712, https://doi.org/10.1103/PhysRev.73.679}.
[1505] E. Odeblad, B.N. Bhar, G. Lindstrom, Proton magnetic resonance of human red blood cells in heavy-water exchange experiments, Arch. Biochem. Biophys. 63 (1956) 221–225.
[1506] G.N. Ling, The Interpretation of Selective Ionic Permeability and Cellular Potentials in Terms of the Fixed Charge-Induction Hypothesis, J. Gen. Physiol. 43 (1960) 149–174, https://doi.org/10.1085/jgp.43.5.149.
[1507] G.N. Ling, The Physical State of Water in Living Cell and Model Systems*, Ann. N. Y. Acad. Sci. 125 (1965) 401–417, https://doi.org/10.1111/j.1749-6632.1965.tb45406.x.
[1508] G. Ling, History of the membrane (pump) theory of the living cell from its beginning in mid-19th century to its disproof 45 years ago–though still taught worldwide today as established truth, Physiol. Chem. Phys. Med NMR. 39 (2007) 1–67.
[1509] C.B. Bratton, A.L. Hopkins, J.W. Weinberg, Nuclear Magnetic Resonance Studies of Living Muscle, Science. 147 (1965) 738–739, https://doi.org/10.1126/science.147.3659.738.
[1510] M.V. Sussman, L. Chin, Nuclear magnetic resonance spectrum changes accompanying rigor mortis, Nature. 211 (1966) 414, https://doi.org/10.1038/211414a0.
[1511] G. Chapman, K.A. McLauchlan, Oriented Water in the Sciatic Nerve of Rabbit, Nature. 215 (1967) 391–392, https://doi.org/10.1038/215391a0.
[1512] O.G. Fritz Jr, T.J. Swift, The State of Water in Polarized and Depolarized Frog Nerves, Biophys. J. 7 (1967) 675–687, https://doi.org/10.1016/S0006-3495(67)86616-5.
[1513] O.G. Fritz, A.C. Scott, T.J. Swift, Effects of Local Anaesthetic on the State of Water in Frog Nerves, Nature. 218 (1968) 1051–1053, https://doi.org/10.1038/2181051a0.
[1514] F.W. Cope, Nuclear Magnetic Resonance Evidence using D2O for Structured Water in Muscle and Brain, Biophys. J. 9 (1969) 303–319, https://doi.org/10.1016/S0006-3495(69)86388-5.
[1515] C.F. Hazlewood, B.L. Nichols, N.F. Chamberlain, Evidence for the existence of a minimum of two phases of ordered water in skeletal muscle, Nature. 222 (1969) 747–750, https://doi.org/10.1038/222747a0.
[1516] F.W. Cope, Freeman Cope — cation pumps are thermodynamically impossible, Trends Biochem. Sci. 2 (1977) N225–N227, https://doi.org/10.1016/0968-0004(77)90102-5.
[1517] R. Damadian, Tumor detection by nuclear magnetic resonance, Science. 171 (1971) 1151–1153, https://doi.org/10.1126/science.171.3976.1151.
[1518] H.E. Frey, R.R. Knispel, J. Kruuv, A.R. Sharp, R.T. Thompson, M.M. Pintar, Proton spin-lattice relaxation studies of nonmalignant tissues of tumorous mice, J. Natl. Cancer Inst. 49 (1972) 903–906.
[1519] I.D. Weisman, L.H. Bennett, L.R. Maxwell, M.W. Woods, D. Burk, Recognition of cancer in vivo by nuclear magnetic resonance, Science. 178 (1972) 1288–1290, https://doi.org/10.1126/science.178.4067.1288.
[1520] R. Damadian, K. Zaner, D. Hor, T. DiMaio, Human Tumors Detected by Nuclear Magnetic Resonance, Proc. Natl. Acad. Sci. U. S. A. 71 (1974) 1471–1473, https://doi.org/10.1073/pnas.71.4.1471.
[1521] G. Ungar, Panel Discussion*, Ann. N. Y. Acad. Sci. 204 (1973) 616–631, https://doi.org/10.1111/j.1749-6632.1973.tb30809.x.
[1522] T.F. Budinger, P.C. Lauterbur, Nuclear Magnetic Resonance Technology for Medical Studies, Science. 226 (1984) 288–298, https://doi.org/10.1126/science.6385252.
[1523] W.R. Inch, J.A. McCredie, R.R. Knispel, R.T. Thompson, M.M. Pintar, Water content and proton spin relaxation time for neoplastic and non-neoplastic tissues from mice and humans, J. Natl. Cancer Inst. 52 (1974) 353–356, https://doi.org/10.1093/jnci/52.2.353.
[1524] R.G. Parrish, R.J. Kurland, W.W. Janese, L. Bakay, Proton Relaxation Rates of Water in Brain and Brain Tumors, Science. 183 (1974) 438–439, https://doi.org/10.1126/science.183.4123.438.
[1525] D.G. Taylor, C.F. Bore, A review of the magnetic resonance response of biological tissue and its applicability to the diagnosis of cancer by NMR radiology, J. Comput. Tomogr. 5 (1981) 122–133, https://doi.org/10.1016/0149-936x(81)90026-6.
[1526] P.A. Bottomley, C.J. Hardy, R.E. Argersinger, G. Allen-Moore, A review of 1H nuclear magnetic resonance relaxation in pathology: Are T1and T2diagnostic?, Med. Phys. 14 (1998) 1–37, https://doi.org/10.1118/1.596111.
[1527] J.A. Walter, A.B. Hope, Nuclear magnetic resonance and the state of water in cells, Prog. Biophys. Mol. Biol. 23 (1971) 1–20, https://doi.org/10.1016/0079-6107(71)90015-0.
[1528] R.E. Block, Factors affecting proton magnetic resonance linewidths of water in several rat tissues, FEBS Lett. 34 (1973) 109–112, https://doi.org/10.1016/0014-5793(73)80715-x.
[1529] R.K. Outhred, E.P. George, Water and Ions in Muscles and Model Systems, Biophys. J. 13 (1973) 97–103, https://doi.org/10.1016/S0006-3495(73)85972-7.
[1530] R.T. Thompson, R.R. Knispel, M.M. Pintar, A study of the proton exchange in tissue water by spin relaxation in the rotating frame, Chem. Phys. Lett. 22 (1973) 335–337, https://doi.org/10.1016/0009-2614(73)80106-X.
[1531] J.G. Diegel, M.M. Pintar, Origin of the nonexponentiality of the water proton spin relaxations in tissues, Biophys. J. 15 (1975) 855–860, https://doi.org/10.1016/S0006-3495(75)85861-9.
[1532] R. Cooke, I.D. Kuntz, The Properties of Water in Biological Systems, Annu. Rev. Biophys. Bioeng. 3 (1974) 95–126, https://doi.org/10.1146/annurev.bb.03.060174.000523.
[1533] M.M. Civan, A.M. Achlama, M. Shporer, The relationship between the transverse and longitudinal nuclear magnetic resonance relaxation rates of muscle water, Biophys. J. 21 (1978) 127–136, https://doi.org/10.1016/S0006-3495(78)85513-1.
[1534] R. Mathur-De Vré, The NMR studies of water in biological systems, Prog. Biophys. Mol. Biol. 35 (1980) 103–134. https://doi.org/10.1016/0079-6107(80)90004-8..
[1535] V.G. Kiselev, D.S. Novikov, Transverse NMR relaxation in biological tissues, NeuroImage. 182 (2018) 149–168, https://doi.org/10.1016/j.neuroimage.2018.06.002.
[1536] W. Li, P.C.M. van Zijl, Quantitative theory for the transverse relaxation time of blood water, NMR Biomed. 33 (2020), https://doi.org/10.1002/nbm.4207.
[1537] C. Eldeniz, M.M. Binkley, M. Fields, K. Guilliams, D.K. Ragan, Y. Chen, J. Lee, A. L. Ford, H. An, Bulk volume susceptibility difference between deoxyhemoglobin and oxyhemoglobin for HbA and HbS: A comparative study, Magn. Reson. Med. 85 (2021) 3383–3393, https://doi.org/10.1002/mrm.28668.
[1538] W.D. Rooney, C.S. Springer, A comprehensive approach to the analysis and interpretation of the resonances of spins 3/2 from living systems, NMR Biomed. 4 (1991) 209–226, https://doi.org/10.1002/nbm.1940040502.
[1539] D.E. Woessner, NMR relaxation of spin-3/2 nuclei: Effects of structure, order, and dynamics in aqueous heterogeneous systems, Concepts Magn. Reson. 13 (2001) 294–325, https://doi.org/10.1002/cmr.1015.
[1540] M. Shporer, M.M. Civan, Pulsed nuclear magnetic resonance study of 39K within halobacteria, J. Membr. Biol. 33 (1977) 385–400, https://doi.org/10.1007/BF01869525.
[1541] H.J. Berendsen, H.T. Edzes, The observation and general interpretation of sodium magnetic resonance in biological material, Ann. N. Y. Acad. Sci. 204 (1973) 459–485, https://doi.org/10.1111/j.1749-6632.1973.tb30799.x.
[1542] P.S. Hubbard, Nonexponential Nuclear Magnetic Relaxation by Quadrupole Interactions, J. Chem. Phys. 53 (1970) 985–987, https://doi.org/10.1063/1.1674167.
[1543] T.E. Bull, Nuclear magnetic relaxation of spin- nuclei involved in chemical exchange, J. Magn. Reson. 1969 (8) (1972) 344–353, https://doi.org/10.1016/0022-2364(72)90052-2.
[1544] B. Lindman, Applications of quadrupolar effects in NMR for studies of ion binding in biological and model systems, J. Magn. Reson. 1969 (32) (1978) 39–47, https://doi.org/10.1016/0022-2364(78)90073-2.
[1545] T.E. Bull, S. Forsén, D.L. Turner, Nuclear magnetic relaxation of spin 5/2 and spin 7/2 nuclei including the effects of chemical exchange, J. Chem. Phys. 70 (1979) 3106–3111, https://doi.org/10.1063/1.437799.
[1546] S. Forsén, T. Drakenberg, H. Wennerström, NMR studies of ion binding in biological systems, Q. Rev. Biophys. 19 (1987) 83–114, https://doi.org/10.1017/S0033583500004030.
[1547] D. Burstein, H.I. Litt, E.T. Fossel, NMR characteristics of "visible" intracellular myocardial potassium in perfused rat hearts, Magn. Reson. Med. 9 (1989) 66–78, https://doi.org/10.1002/mrm.1910090109.
[1548] H.J. Guttman, S. Cayley, M. Li, C.F. Anderson, M.T. Record, K(+)-ribosome interactions determine the large enhancements of 39K NMR transverse relaxation rates in the cytoplasm of Escherichia coli K-12, Biochemistry. 34 (1995) 1393–1404, https://doi.org/10.1021/bi00004a034.
[1549] T. Hiraishi, Y. Seo, M. Murakami, H. Watari, Detection of biexponential relaxation in intracellular K in the rat heart by double-quantum 39K NMR, J. Magn. Reson. 1969 (87) (1990) 169–173, https://doi.org/10.1016/0022-2364(90)90096-R.

[1550] C. Hannesschlaeger, A. Horner, P. Pohl, Intrinsic Membrane Permeability to Small Molecules, Chem. Rev. 119 (2019) 5922–5953, https://doi.org/10.1021/acs.chemrev.8b00560.
[1551] M. Holz, S.R. Heil, A. Sacco, Temperature-dependent self-diffusion coefficients of water and six selected molecular liquids for calibration in accurate 1H NMR PFG measurements, Phys. Chem. Chem. Phys. 2 (2000) 4740–4742, https://doi.org/10.1039/b005319h.
[1552] D.R. Lide, CRC Handbook of Chemistry and Physics, 84th Edition., CRC Press, 2003.
[1553] M. Tabaka, T. Kalwarczyk, J. Szymanski, S. Hou, R. Holyst, The effect of macromolecular crowding on mobility of biomolecules, association kinetics, and gene expression in living cells, Front. Phys. 2 (2014), https://doi.org/10.3389/fphy.2014.00054.
[1554] M. Baum, F. Erdel, M. Wachsmuth, K. Rippe, Retrieving the intracellular topology from multi-scale protein mobility mapping in living cells, Nat. Commun. 5 (2014) 4494, https://doi.org/10.1038/ncomms5494.
[1555] J. Li, V.N. Uversky, A.L. Fink, Effect of Familial Parkinson's Disease Point Mutations A30P and A53T on the Structural Properties, Aggregation, and Fibrillation of Human α-Synuclein †, Biochemistry. 40 (2001) 11604–11613, https://doi.org/10.1021/bi010616g.
[1556] T. Kalwarczyk, K. Kwapiszewska, K. Szczepanski, K. Sozanski, J. Szymanski, B. Michalska, P. Patalas-Krawczyk, J. Duszynski, R. Holyst, Apparent Anomalous Diffusion in the Cytoplasm of Human Cells: The Effect of Probes' Polydispersity, J. Phys. Chem. B. 121 (2017) 9831–9837, https://doi.org/10.1021/acs.jpcb.7b07158.
[1557] K. Szczepański, K. Kwapiszewska, R. Hołyst, Stability of cytoplasmic nanoviscosity during cell cycle of HeLa cells synchronized with Aphidicolin, Sci. Rep. 9 (2019) 16486, https://doi.org/10.1038/s41598-019-52758-6.
[1558] M. Wachsmuth, C. Conrad, J. Bulkescher, B. Koch, R. Mahen, M. Isokane, R. Pepperkok, J. Ellenberg, High-throughput fluorescence correlation spectroscopy enables analysis of proteome dynamics in living cells, Nat. Biotechnol. 33 (2015) 384–389, https://doi.org/10.1038/nbt.3146.
[1559] G. Bubak, K. Kwapiszewska, T. Kalwarczyk, K. Bielec, T. Andryszewski, M. Iwan, S. Bubak, R. Hołyst, Quantifying Nanoscale Viscosity and Structures of Living Cells Nucleus from Mobility Measurements, J. Phys. Chem. Lett. 12 (2021) 294–301, https://doi.org/10.1021/acs.jpclett.0c03052.
[1560] W. Wang, Y. Ma, S. Bonaccorsi, V.T. Cong, E. Pandžić, Z. Yang, J. Goyette, F. Lisi, R.D. Tilley, K. Gaus, J.J. Gooding, Investigating Spatial Heterogeneity of Nanoparticles Movement in Live Cells with Pair-Correlation Microscopy and Phasor Analysis, Anal. Chem. 93 (2021) 3803–3812, https://doi.org/10.1021/acs.analchem.0c04285.
[1561] L. Xiang, K. Chen, R. Yan, W. Li, K. Xu, Single-molecule displacement mapping unveils nanoscale heterogeneities in intracellular diffusivity, Nat. Methods. 17 (2020) 524–530, https://doi.org/10.1038/s41592-020-0793-0.
[1562] Y. Ye, Q. Wu, W. Zheng, B. Jiang, G.J. Pielak, M. Liu, C. Li, Positively Charged Tags Impede Protein Mobility in Cells as Quantified by ^{19} F NMR, J. Phys. Chem. B. 123 (2019) 4527–4533, https://doi.org/10.1021/acs.jpcb.9b02162.
[1563] M. Pilz, K. Kwapiszewska, T. Kalwarczyk, G. Bubak, D. Nowis, R. Hołyst, Transport of nanoprobes in multicellular spheroids, Nanoscale. 12 (2020) 19880–19887, https://doi.org/10.1039/D0NR01986K.
[1564] F. Cardarelli, Back to the Future: Genetically Encoded Fluorescent Proteins as Inert Tracers of the Intracellular Environment, Int. J. Mol. Sci. 21 (2020) 4164, https://doi.org/10.3390/ijms21114164.
[1565] J. Cavanagh, W.J. Fairbrother, A.G.P. III, N.J. Skelton, Protein NMR Spectroscopy: Principles and Practice, Elsevier, 1995..
[1566] D.J. Philp, W.A. Bubb, P.W. Kuchel, Chemical shift and magnetic susceptibility contributions to the separation of intracellular and supernatant resonances in variable angle spinning NMR spectra of erythrocyte suspensions, Magn. Reson. Med. 51 (2004) 441–444, https://doi.org/10.1002/mrm.20019.
[1567] T.J. Larkin, W.A. Bubb, P.W. Kuchel, Water chemical shift in 1H NMR of red cells: Effects of pH when transmembrane magnetic susceptibility differences are low, Magn. Reson. Med. 59 (2008) 707–711, https://doi.org/10.1002/mrm.21546.
[1568] P.W. Kuchel, K. Kirk, D. Shishmarev, The NMR "split peak effect" in cell suspensions: Historical perspective, explanation and applications, Prog. Nucl. Magn. Reson. Spectrosc. 104 (2018) 1–11, https://doi.org/10.1016/j.pnmrs.2017.11.002.
[1569] M. Cerdonio, S. Morante, D. Torresani, S. Vitale, A. DeYoung, R.W. Noble, Reexamination of the evidence for paramagnetism in oxy- and carbonmonoxyhemoglobins, Proc. Natl. Acad. Sci. 82 (1985) 102–103, https://doi.org/10.1073/pnas.82.1.102.
[1570] J. Luo, X. He, D.A. d'Avignon, J.J.H. Ackerman, D.A. Yablonskiy, Protein-induced water 1H MR frequency shifts: Contributions from magnetic susceptibility and exchange effects, J. Magn. Reson. 202 (2010) 102–108, https://doi.org/10.1016/j.jmr.2009.10.005.
[1571] Y. Kawamura, I. Sakurai, A. Ikegami, S. Iwayanagi, Magneto-Orientation of Phospholipids, Mol. Cryst. Liq. Cryst. 67 (1981) 77–87, https://doi.org/10.1080/00268948108070877.
[1572] E. Boroske, W. Helfrich, Magnetic anisotropy of egg lecithin membranes, Biophys. J. 24 (1978) 863–868, https://doi.org/10.1016/S0006-3495(78)85425-3.
[1573] A. Diller, C. Loudet, F. Aussenac, G. Raffard, S. Fournier, M. Laguerre, A. Grélard, S.J. Opella, F.M. Marassi, E.J. Dufourc, Bicelles: A natural 'molecular goniometer' for structural, dynamical and topological studies of molecules in membranes, Biochimie. 91 (2009) 744–751, https://doi.org/10.1016/j.biochi.2009.02.003.
[1574] R. Dazzoni, A. Grélard, E. Morvan, A. Bouter, C.J. Applebee, A. Loquet, B. Larijani, E.J. Dufourc, The unprecedented membrane deformation of the human nuclear envelope, in a magnetic field, indicates formation of nuclear membrane invaginations, Sci. Rep. 10 (2020) 5147, https://doi.org/10.1038/s41598-020-61746-0.
[1575] S. Nakamae, M. Cazayous, A. Sacuto, P. Monod, H. Bouchiat, Intrinsic Low Temperature Paramagnetism in B-DNA, Phys. Rev. Lett. 94 (2005), https://doi.org/10.1103/PhysRevLett.94.248102 248102.
[1576] Kwon, Young-Wan, Lee, Chang-Hoon, Do, Eui-Doo, Jin, Jung-Il, Kang, Jun-Sung, Go, Ui-Gwan, Hydration Effect on the Intrinsic Magnetism of Natural Deoxyribonucleic Acid as Studied by EMR Spectroscopy and SQUID Measurements, Bull. Korean Chem. Soc. 29 (2008) 1233–1242. https://doi.org/10.5012/BKCS.2008.29.6.1233..
[1577] K. Mizoguchi, S. Tanaka, T. Ogawa, N. Shiobara, H. Sakamoto, Magnetic study of the electronic states of B -DNA and M -DNA doped with metal ions, Phys. Rev. B. 72 (2005), https://doi.org/10.1103/PhysRevB.72.033106 033106.
[1578] Y.-W. Kwon, D.H. Choi, J.-I. Jin, C.H. Lee, E.K. Koh, J.G. Grote, Comparison of magnetic properties of DNA-cetyltrimethyl ammonium complex with those of natural DNA, Sci. China Chem. 55 (2012) 814–821, https://doi.org/10.1007/s11426-012-4507-z.
[1579] T. Kumeta, H. Sakamoto, K. Mizoguchi, Freeze Dried Zn-DNA: Magnetism Dominated by Water Molecules, J. Phys. Soc. Jpn. 83 (2014), https://doi.org/10.7566/JPSJ.83.084801 084801.
[1580] C. Hoon Lee, Y.-W. Kwon, E.-D. Do, D.-H. Choi, J.-I. Jin, D.-K. Oh, J. Kim, Electron magnetic resonance and SQUID measurement study of natural A -DNA in dry state, Phys. Rev. B. 73 (2006), https://doi.org/10.1103/PhysRevB.73.224417 224417.
[1581] Q. Tao, L. Zhang, X. Han, H. Chen, X. Ji, X. Zhang, Magnetic Susceptibility Difference-Induced Nucleus Positioning in Gradient Ultrahigh Magnetic Field, Biophys. J. 118 (2020) 578–585, https://doi.org/10.1016/j.bpj.2019.12.020.
[1582] S. Kucher, C. Elsner, M. Safonova, S. Maffini, E. Bordignon, In-Cell Double Electron-Electron Resonance at Nanomolar Protein Concentrations, J. Phys. Chem. Lett. 12 (2021) 3679–3684, https://doi.org/10.1021/acs.jpclett.1c00048.
[1583] J.S. Philo, W.M. Fairbank, Temperature dependence of the diamagnetism of water, J. Chem. Phys. 72 (1980) 4429–4433, https://doi.org/10.1063/1.439734.
[1584] W.M. Spees, D.A. Yablonskiy, M.C. Oswood, J.J.H. Ackerman, Water proton MR properties of human blood at 1.5 Tesla: Magnetic susceptibility, T1, T2, T*2, and non-Lorentzian signal behavior, Magn. Reson. Med. 45 (2001) 533–542, https://doi.org/10.1002/mrm.1072.
[1585] Y.V. Ergin, L.I. Kostrova, Magnetic susceptibility of water as a function of temperature, J. Struct. Chem. 11 (1970) 5–8, https://doi.org/10.1007/BF00743897.
[1586] S.-H. Lee, Measurements of the Diamagnetic Susceptibility of NaCl Aqueous Solution, J. Navig. Port Res. 27 (2003) 669–675, https://doi.org/10.5394/KINPR.2003.27.6.669.
[1587] B.E. Kashevskii, S.B. Kashevskii, I.V. Prokhorov, E.N. Aleksandrova, Y.P. Istomin, Magnetophoresis and the magnetic susceptibility of HeLa tumor cells, Biophysics. 51 (2006) 902–907, https://doi.org/10.1134/S0006350906060091.
[1588] J.F. Morgan, M. Elizabeth Campbell, H.J. Morton, The Nutrition of Animal Tissues Cultivated In Vitro. I. A Survey of Natural Materials as Supplements to Synthetic Medium 199, JNCI, J. Natl. Cancer Inst. 16 (1955) 557–567, https://doi.org/10.1093/jnci/16.2.557.
[1589] J.M. Valles Jr, K. Lin, J.M. Denegre, K.L. Mowry, Stable magnetic field gradient levitation of Xenopus laevis: toward low-gravity simulation, Biophys. J. 73 (1997) 1130–1133, https://doi.org/10.1016/S0006-3495(97)78145-1.
[1590] 5] K. Mizoguchi, Physical properties of natural DNA and metal ion inserted M-DNA, in: Nanobiosystems Process. Charact. Appl., International Society for Optics and Photonics, 2008: p. 70400Q. https://doi.org/10.1117/12.801478..
[1591] L.S. Szczepaniak, R.L. Dobbins, D.T. Stein, J.D. McGarry, Bulk magnetic susceptibility effects on the assessment of intra- and extramyocellular lipids in vivo, Magn. Reson. Med. 47 (2002) 607–610, https://doi.org/10.1002/mrm.10086.
[1592] E. Yang, A.A. Kirkham, J. Grenier, R.B. Thompson, Measurement and correction of the bulk magnetic susceptibility effects of fat: application in venous oxygen saturation imaging, Magn. Reson. Med. (2018) mrm.27640, https://doi.org/10.1002/mrm.27640.
[1593] B.E. Kashevskii, S.B. Kashevskii, I.V. Prokhorov, Investigation of the Magnetophoretic Properties of Low-Magnetic Microparticles, J. Eng. Phys. Thermophys. 78 (2005) 449–454, https://doi.org/10.1007/s10891-005-0080-z.
[1594] P.W. Kuchel, B.T. Bulliman, Perturbation of homogeneous magnetic fields by isolated single and confocal spheroids. Implications for NMR spectroscopy of cells, NMR Biomed. 2 (1989) 151–160, https://doi.org/10.1002/nbm.1940020404.
[1595] G.L. Mendz, B.T. Bulliman, N.L. James, P.W. Kuchel, Magnetic Potential and Field Gradients of a Model Cell, J. Theor. Biol. 137 (1989) 55–69, https://doi.org/10.1016/s0022-5193(89)80149-3.
[1596] P. Gillis, S. Petö, F. Moiny, J. Mispelter, C.-A. Cuenod, Proton Transverse Nuclear Magnetic Relaxation in Oxidized Blood: a Numerical Approach,

Magn. Reson. Med. 33 (1995) 93–100, https://doi.org/10.1002/mrm.1910330114.
[1597] J.H. Jensen, R. Chandra, NMR relaxation in tissues with weak magnetic inhomogeneities, Magn. Reson. Med. 44 (2000) 144–156, https://doi.org/10.1002/1522-2594(200007)44:1<144::AID-MRM21>3.0.CO;2-O.
[1598] Z.H. Endre, P.W. Kuchel, B.E. Chapman, Cell volume dependence of 1H spin-echo NMR signals in human erythrocyte suspensions: The influence of in situ field gradients, Biochim. Biophys. Acta BBA - Mol. Cell Res. 803 (1984) 137–144, https://doi.org/10.1016/0167-4889(84)90003-X.
[1599] N.A. Matwiyoff, C. Gasparovic, R. Mazurchuk, G. Matwiyoff, The line shapes of the water proton resonances of red blood cells containing carbonyl hemoglobin, deoxyhemoglobin, and methemoglobin: Implications for the interpretation of proton MRI at fields of 1.5 T and below, Magn. Reson. Imaging. 8 (1990) 295–301, https://doi.org/10.1016/0730-725X(90)90102-8.
[1600] 5] Novikov et Kiselev - 2008 - Transverse NMR relaxation in magnetically heteroge.pdf, (n.d.)..
[1601] A. Ruh, H. Scherer, V.G. Kiselev, The larmor frequency shift in magnetically heterogeneous media depends on their mesoscopic structure: Larmor Frequency Shift in Magnetically Heterogeneous Media, Magn. Reson. Med. 79 (2018) 1101–1110, https://doi.org/10.1002/mrm.26753.
[1602] A. Ruh, V.G. Kiselev, Larmor frequency dependence on structural anisotropy of magnetically heterogeneous media, J. Magn. Reson. 307 (2019), https://doi.org/10.1016/j.jmr.2019.106584 106584.
[1603] S. Majumdar, J.C. Gore, Studies of diffusion in random fields produced by variations in susceptibility, J. Magn. Reson. 1969 (78) (1988) 41–55, https://doi.org/10.1016/0022-2364(88)90155-2.
[1604] A.L. Sukstanskii, D.A. Yablonskiy, Gaussian approximation in the theory of MR signal formation in the presence of structure-specific magnetic field inhomogeneities. Effects of impermeable susceptibility inclusions, J. Magn. Reson. (2004) 12.
[1605] L.R. Buschle, F.T. Kurz, T. Kampf, S.M.F. Triphan, H.-P. Schlemmer, C.H. Ziener, Diffusion-mediated dephasing in the dipole field around a single spherical magnetic object, Magn. Reson. Imaging. 33 (2015) 1126–1145, https://doi.org/10.1016/j.mri.2015.06.001.
[1606] V.G. Kiselev, D.S. Novikov, Transverse NMR Relaxation as a Probe of Mesoscopic Structure, Phys. Rev. Lett. 89 (2002), https://doi.org/10.1103/PhysRevLett.89.278101 278101.
[1607] C.H. Ziener, T. Kampf, Spin dephasing in the Gaussian local phase approximation, J Chem Phys. 17 (2018).
[1608] V. Lisý, J. Tóthová, NMR signals within the generalized Langevin model for fractional Brownian motion, Phys. Stat. Mech. Its Appl. 494 (2018) 200–208, https://doi.org/10.1016/j.physa.2017.12.042.
[1609] J. Emmerich, On the influence of two coexisting species of susceptibility-producing structures on the R2∗ relaxation rate, Magn. Reson. Imaging. 8 (2020).
[1610] F.F. Brown, The effect of compartmental location on the proton T2∗ of small molecules in cell suspensions: A cellular field gradient model, J. Magn. Reson. 1969 (54) (1983) 385–399, https://doi.org/10.1016/0022-2364(83)90319-0.
[1611] C. Gasparovic, N.A. Matwiyoff, The magnetic properties and water dynamics of the red blood cell: A study by proton-NMR lineshape analysis, Magn. Reson. Med. 26 (1992) 274–299, https://doi.org/10.1002/mrm.1910260208.
[1612] 8] K. Grgac, W. Li, A. Huang, Q. Qin, P.C.M. van Zijl, Transverse water relaxation in whole blood and erythrocytes at 3T, 7T, 9.4T, 11.7T and 16.4T; determination of intracellular hemoglobin and extracellular albumin relaxivities, Magn. Reson. Imaging. 38 (2017) 234–249. https://doi.org/10.1016/j.mri.2016.12.012..
[1613] A.L. Sukstanskii, D.A. Yablonskiy, Gaussian approximation in the theory of MR signal formation in the presence of structure-specific magnetic field inhomogeneities, J. Magn. Reson. 163 (2003) 236–247, https://doi.org/10.1016/S1090-7807(03)00131-9.
[1614] 0] A.J.L. Berman, G.B. Pike, Transverse signal decay under the weak field approximation: Theory and validation, (n.d.) 10..
[1615] E. Luchinat, L. Barbieri, M. Cremonini, L. Banci, Protein in-cell NMR spectroscopy at 1.2 GHz, J. Biomol. NMR. (2021), https://doi.org/10.1007/s10858-021-00358-w.
[1616] S. Alberti, A.A. Hyman, Biomolecular condensates at the nexus of cellular stress, protein aggregation disease and ageing, Nat. Rev. Mol. Cell Biol. 22 (2021) 196–213, https://doi.org/10.1038/s41580-020-00326-6.
[1617] D.L.J. Lafontaine, J.A. Riback, R. Bascetin, C.P. Brangwynne, The nucleolus as a multiphase liquid condensate, Nat. Rev. Mol. Cell Biol. 22 (2021) 165–182, https://doi.org/10.1038/s41580-020-0272-6.
[1618] L. Emmanouilidis, L. Esteban-Hofer, F.F. Damberger, T. de Vries, C.K.X. Nguyen, L.F. Ibáñez, S. Mergenthal, E. Klotzsch, M. Yulikov, G. Jeschke, F.-H.-T. Allain, NMR and EPR reveal a compaction of the RNA-binding protein FUS upon droplet formation, Nat. Chem. Biol. 17 (2021) 608–614, https://doi.org/10.1038/s41589-021-00752-3.
[1619] G.J. Wilson, C.S. Springer, S. Bastawrous, J.H. Maki, Human whole blood 1H2O transverse relaxation with gadolinium-based contrast reagents: Magnetic susceptibility and transmembrane water exchange, Magn. Reson. Med. 77 (2017) 2015–2027, https://doi.org/10.1002/mrm.26284.
[1620] T. Leutritz, L. Hilfert, K.-H. Smalla, O. Speck, K. Zhong, Accurate quantification of water–macromolecule exchange induced frequency shift: Effects of reference substance, Magn. Reson. Med. 69 (2013) 263–268, https://doi.org/10.1002/mrm.24223.
[1621] T. Leutritz, L. Hilfert, U. Busse, K.-H. Smalla, O. Speck, K. Zhong, Contribution of iron and protein contents from rat brain subcellular fractions to MR phase imaging, Magn. Reson. Med. 77 (2017) 2028–2039, https://doi.org/10.1002/mrm.26288.
[1622] V. Esteve, B. Martínez-Granados, M.C. Martínez-Bisbal, Pitfalls to be considered on the metabolomic analysis of biological samples by HR-MAS, Front. Chem. 2 (2014). https://doi.org/10.3389/fchem.2014.00033..
[1623] M. Jupin, P.J. Michiels, F.C. Girard, S.S. Wijmenga, Magnetic susceptibility to measure total protein concentration from NMR metabolite spectra: Demonstration on blood plasma, Magn. Reson. Med. 73 (2015) 459–468, https://doi.org/10.1002/mrm.25178.
[1624] J. Zhong, J.C. Gore, I.M. Armitage, Relative contributions of chemical exchange and other relaxation mechanisms in protein solutions and tissues, Magn. Reson. Med. 11 (1989) 295–308, https://doi.org/10.1002/mrm.1910110304.
[1625] V.P. Denisov, B. Halle, Hydrogen Exchange Rates in Proteins from Water ^{1}H Transverse Magnetic Relaxation, J. Am. Chem. Soc. 124 (2002) 10264–10265, https://doi.org/10.1021/ja027101c.
[1626] B.P. Hills, S.F. Takacs, P.S. Belton, The effects of proteins on the proton N.M.R. transverse relaxation time of water, Mol. Phys. 67 (1989) 919–937, https://doi.org/10.1080/00268978900101541.
[1627] K. Shmueli, S.J. Dodd, P. van Gelderen, J.H. Duyn, Investigating lipids as a source of chemical exchange-induced MRI frequency shifts, NMR Biomed. 30 (2017), https://doi.org/10.1002/nbm.3525 e3525.
[1628] D. Fabri, M.A.K. Williams, T.K. Halstead, Water T2 relaxation in sugar solutions, Carbohydr. Res. 340 (2005) 889–905, https://doi.org/10.1016/j.carres.2005.01.034.
[1629] N.N. Yadav, J. Xu, A. Bar-Shir, Q. Qin, K.W.Y. Chan, K. Grgac, W. Li, M.T. McMahon, P.C.M. van Zijl, Natural D-glucose as a biodegradable MRI relaxation agent: Glucose as an MRI Relaxation Agent, Magn. Reson. Med. 72 (2014) 823–828, https://doi.org/10.1002/mrm.25329.
[1630] J.M. Goldenberg, M.D. Pagel, J. Cárdenas-Rodríguez, Characterization of D-maltose as a T_{2} -exchange contrast agent for dynamic contrast-enhanced MRI: T_{2ex} DCE-MRI With D-Maltose, Magn. Reson. Med. 80 (2018) 1158–1164, https://doi.org/10.1002/mrm.27082.
[1631] R. Leforestier, F. Mariette, M. Musse, Impact of chemical exchange on transverse relaxation at low and moderate magnetic field strengths for sugar solutions representative of fruit tissues analyzed by simulation and MRI experiments, J. Magn. Reson. 322 (2021), https://doi.org/10.1016/j.jmr.2020.106872 106872.
[1632] C.G. Joo, S.-H. Yang, Y. Choi, H.-Y. Son, D.-H. Kim, Y.-M. Huh, L-glutamine as a T2 exchange contrast agent, Magn. Reson. Med. 84 (2020) 2055–2062, https://doi.org/10.1002/mrm.28305.
[1633] Y. Ye, Q. Wu, W. Zheng, B. Jiang, G.J. Pielak, M. Liu, C. Li, Positively Charged Tags Impede Protein Mobility in Cells as Quantified by 19F NMR, J. Phys. Chem. B. 123 (2019) 4527–4533, https://doi.org/10.1021/acs.jpcb.9b02162.
[1634] M.M. Pike, D.M. Yarmush, J.A. Balschi, R.E. Lenkinski, C.S. Springer, Aqueous shift reagents for high-resolution cationic nuclear magnetic resonance. 2. Magnesium-25, potassium-39, and sodium-23 resonances shifted by chelidamate complexes of dysprosium(III) and thulium(III), Inorg. Chem. 22 (1983) 2388–2392, https://doi.org/10.1021/ic00159a010.
[1635] D.C. Buster, M.M.C.A. Castro, C.F.G.C. Geraldes, C.R. Malloy, A.D. Sherry, T.C. Siemers, Tm(DOTP)5−: A 23Na+ shift agent for perfused rat hearts, Magn. Reson. Med. 15 (1990) 25–32, https://doi.org/10.1002/mrm.1910150104.
[1636] Y. Boulanger, P. Vinay, M. Desroches, Measurement of a wide range of intracellular sodium concentrations in erythrocytes by 23Na nuclear magnetic resonance, Biophys. J. 47 (1985) 553–561, https://doi.org/10.1016/S0006-3495(85)83950-3.
[1637] P. Caravan, J.J. Ellison, T.J. McMurry, R.B. Lauffer, Gadolinium(III) Chelates as MRI Contrast Agents: Structure, Dynamics, and Applications, Chem. Rev. 99 (1999) 2293–2352, https://doi.org/10.1021/cr980440x.
[1638] R. Ramasamy, M.C. Espanol, K.M. Long, D.M. de Freitas, C.F.G.C. Geraldes, Aqueous shift reagents for 7Li+ NMR transport studies in cells, Inorganica Chim. Acta. 163 (1989) 41–52, https://doi.org/10.1016/S0020-1693(00)87140-6.
[1639] D.Y. Sze, N.L. Corbelletta, S.J. Shochat, O. Jardetzky, Inhibition of lymphocyte stimulation by shift reagents, Magn. Reson. Med. 13 (1990) 14–24, https://doi.org/10.1002/mrm.1910130104.
[1640] D. Mota de Freitas, M.T. Espanol, R. Ramasamy, R.J. Labotka, Comparison of lithium ion transport and distribution in human red blood cells in the presence and absence of dysprosium(III) complexes of triphosphate and triethylenetetraminehexaacetate, Inorg. Chem. 29 (1990) 3972–3979, https://doi.org/10.1021/ic00345a013.
[1641] R. Ramasamy, D. Mota de Freitas, W. Jones, F. Wezeman, R. Labotka, C.F.G.C. Geraldes, Effects of negatively charged shift reagents on red blood cell morphology, lithium ion transport, and membrane potential, Inorg. Chem. 29 (1990) 3979–3985, https://doi.org/10.1021/ic00345a014.
[1642] R. Ramasamy, M.M. Castro, D.M. de Freitas, C.F. Geraldes, Lanthanide complexes of aminophosphonates as shift reagents for 7Li and 23Na NMR studies in biological systems, Biochimie. 74 (1992) 777–783, https://doi.org/10.1016/0300-9084(92)90060-r.
[1643] 2] J. Ren, A. Dean Sherry, 7Li, 6Li, 23Na and 133Cs multinuclear NMR studies of adducts formed with shift reagent, TmDOTP5, Inorganica Chim. Acta. 246 (1996) 331–341. https://doi.org/10.1016/0020-1693(96)05080-3..
[1644] A.D. Sherry, J. Ren, J. Huskens, E. Brücher, É. Tóth, C.F.C.G. Geraldes, M.M.C.A. Castro, W.P. Cacheris, Characterization of Lanthanide(III) DOTP Complexes:

Thermodynamics, Protonation, and Coordination to Alkali Metal Ions, Inorg. Chem. 35 (1996) 4604–4612, https://doi.org/10.1021/ic9600590.
[1645] J.R. Garbow, D.P. Weitekamp, A. Pines, Bilinear rotation decoupling of homonuclear scalar interactions, Chem. Phys. Lett. 93 (1982) 504–509, https://doi.org/10.1016/0009-2614(82)83229-6.
[1646] P. Kiraly, M. Nilsson, G.A. Morris, Practical aspects of real-time pure shift HSQC experiments, Magn. Reson. Chem. 56 (2018) 993–1005, https://doi.org/10.1002/mrc.4704.
[1647] S. Wimperis, R. Freeman, An excitation sequence which discriminates between direct and long-range CH coupling, J. Magn. Reson. 1969 (58) (1984) 348–353, https://doi.org/10.1016/0022-2364(84)90227-0.
[1648] S. Wimperis, R. Freeman, Sequences which discriminate between direct and long-range CH couplings. Compensation for a range of 1JCH values, J. Magn. Reson. 1969 62 (1985) 147–152, https://doi.org/10.1016/0022-2364(85)90308-7.
[1649] P. Veeraiah, K. Brouwers, J.E. Wildberger, V.B. Schrauwen-Hinderling, L. Lindeboom, Application of a BIlinear Rotation Decoupling (BIRD) filter in combination with J-difference editing for indirect ^{13}C measurements in the human liver, Magn. Reson. Med. 84 (2020) 2911–2917, https://doi.org/10.1002/mrm.28394.
[1650] J.A. Aguilar, M. Nilsson, G. Bodenhausen, G.A. Morris, Spin echo NMR spectra without J modulation, Chem. Commun. 48 (2012) 811–813, https://doi.org/10.1039/C1CC16699A.
[1651] G. Diserens, M. Vermathen, C. Precht, N.T. Broskey, C. Boesch, F. Amati, J.-F. Dufour, P. Vermathen, Separation of small metabolites and lipids in spectra from biopsies by diffusion-weighted HR-MAS NMR: a feasibility study, Analyst. 140 (2015) 272–279, https://doi.org/10.1039/C4AN01663G.
[1652] G. Navon, H. Burrows, J.S. Cohen, Differences in metabolite levels upon differentiation of intact neuroblastoma X glioma cells observed by proton NMR spectroscopy, FEBS Lett. 162 (1983) 320–323, https://doi.org/10.1016/0014-5793(83)80780-7.
[1653] R.C. Anderson, M.A. Jarema, M.J. Shapiro, J.P. Stokes, M. Ziliox, Analytical Techniques in Combinatorial Chemistry: MAS CH Correlation in Solvent-Swollen Resin, J. Org. Chem. 60 (1995) 2650–2651, https://doi.org/10.1021/jo00114a003.
[1654] W.E. Maas, F.H. Laukien, D.G. Cory, Gradient, High Resolution, Magic Angle Sample Spinning NMR, J. Am. Chem. Soc. 118 (1996) 13085–13086, https://doi.org/10.1021/ja962227t.
[1655] W.T. Winter, D. Barnhart, HR-MAS: The Other NMR Approach to Polysaccharide Solids, in: Polysacch. Mater. Perform. Des., American Chemical Society, Washington DC, 2009: pp. 261–270. https://doi.org/10.1021/bk-2009-1017.ch015..
[1656] J.-P. Grivet, A.-M. Delort, NMR for microbiology: In vivo and in situ applications, Prog. Nucl. Magn. Reson. Spectrosc. 54 (2009) 1–53, https://doi.org/10.1016/j.pnmrs.2008.02.001.
[1657] H. Farooq, D. Courtier-Murias, R. Soong, W. Bermel, W. Kingery, A. Simpson, HR-MAS NMR Spectroscopy: A Practical Guide for Natural Samples, Curr. Org. Chem. 17 (2013) 3013–3031, https://doi.org/10.2174/13852728113179990126.
[1658] D. Chapman, E. Oldfield, D. Doskočilová, B. Schneider, NMR of gel and liquid crystalline phospholipids spinning at the "magic angle", FEBS Lett. 25 (1972) 261–264, https://doi.org/10.1016/0014-5793(72)80499-x.
[1659] D. Doskočilová, B. Schneider, 1H magic angle rotation NMR in polymer studies, Adv. Colloid Interface Sci. 9 (1978) 63–104, https://doi.org/10.1016/0001-8686(78)80001-3.
[1660] D. Doskočilová, B. Schneider, NMR studies of swollen crosslinked polymer gels, Pure Appl. Chem. 54 (1982) 575–584, https://doi.org/10.1351/pac198254030575.
[1661] N.J. Waters, S. Garrod, R.D. Farrant, J.N. Haselden, S.C. Connor, J. Connelly, J.C. Lindon, E. Holmes, J.K. Nicholson, High-Resolution Magic Angle Spinning 1H NMR Spectroscopy of Intact Liver and Kidney: Optimization of Sample Preparation Procedures and Biochemical Stability of Tissue during Spectral Acquisition, Anal. Biochem. 282 (2000) 16–23, https://doi.org/10.1006/abio.2000.4574.
[1662] Lucas-Torres, Bernard, Huber, Berthault, Nishiyama, Kandiyal, Elena-Herrmann, Molin, Solari, Bouzier-Sore, Wong, General Guidelines for Sample Preparation Strategies in HR-μMAS NMR-based Metabolomics of Microscopic Specimens, Metabolites. 10 (2020) 54. https://doi.org/10.3390/metabo10020054..
[1663] M.D. Battistel, H.F. Azurmendi, B. Yu, D.I. Freedberg, NMR of glycans: shedding new light on old problems, Prog. Nucl. Magn. Reson. Spectrosc. 79 (2014) 48–68, https://doi.org/10.1016/j.pnmrs.2014.01.001.
[1664] D.I. Freedberg, J. Kwon, Solution NMR Structural Studies of Glycans, Isr. J. Chem. 59 (2019) 1039–1058, https://doi.org/10.1002/ijch.201900126.
[1665] C.J. Gray, L.G. Migas, P.E. Barran, K. Pagel, P.H. Seeberger, C.E. Eyers, G.-J. Boons, N.L.B. Pohl, I. Compagnon, G. Widmalm, S.L. Flitsch, Advancing Solutions to the Carbohydrate Sequencing Challenge, J. Am. Chem. Soc. 141 (2019) 14463–14479, https://doi.org/10.1021/jacs.9b06406.
[1666] A. Gimeno, P. Valverde, A. Ardá, J. Jiménez-Barbero, Glycan structures and their interactions with proteins. A NMR view, Curr. Opin. Struct. Biol. 62 (2020) 22–30, https://doi.org/10.1016/j.sbi.2019.11.004.
[1667] X. Kang, W. Zhao, M.C.D. Widanage, A. Kirui, U. Ozdenvar, T. Wang, CCMRD: a solid-state NMR database for complex carbohydrates, J. Biomol. NMR. 74 (2020) 239–245, https://doi.org/10.1007/s10858-020-00304-2.
[1668] G. Diserens, D. Hertig, M. Vermathen, B. Legeza, C.E. Flück, J.M. Nuoffer, P. Vermathen, Metabolic stability of cells for extended metabolomical measurements using NMR. A comparison between lysed and additionally heat inactivated cells, Analyst. 142 (2017) 465–471, https://doi.org/10.1039/C6AN02195F.
[1669] J. Detour, K. Elbayed, M. Piotto, F.M. Moussallieh, A. Nehlig, I.J. Namer, Ultra fast in vivo microwave irradiation for enhanced metabolic stability of brain biopsy samples during HRMAS NMR analysis, J. Neurosci. Methods. 201 (2011) 89–97, https://doi.org/10.1016/j.jneumeth.2011.07.014.
[1670] C.-L. Wu, J.L. Taylor, W. He, A.G. Zepeda, E.F. Halpern, A. Bielecki, R.G. Gonzalez, L.L. Cheng, Proton high-resolution magic angle spinning NMR analysis of fresh and previously frozen tissue of human prostate, Magn. Reson. Med. 50 (2003) 1307–1311, https://doi.org/10.1002/mrm.10645.
[1671] J. Zhi Hu, R.A. Wind, The evaluation of different MAS techniques at low spinning rates in aqueous samples and in the presence of magnetic susceptibility gradients, J. Magn. Reson. 159 (2002) 92–100, https://doi.org/10.1016/s1090-7807(02)00005-8.
[1672] J.L. Taylor, C.-L. Wu, D. Cory, R.G. Gonzalez, A. Bielecki, L.L. Cheng, High-resolution magic angle spinning proton NMR analysis of human prostate tissue with slow spinning rates, Magn. Reson. Med. 50 (2003) 627–632, https://doi.org/10.1002/mrm.10562.
[1673] M.A. Burns, J.L. Taylor, C.-L. Wu, A.G. Zepeda, A. Bielecki, D. Cory, L.L. Cheng, Reduction of spinning sidebands in proton NMR of human prostate tissue with slow high-resolution magic angle spinning, Magn. Reson. Med. 54 (2005) 34–42, https://doi.org/10.1002/mrm.20523.
[1674] M. Renault, L. Shintu, M. Piotto, S. Caldarelli, Slow-spinning low-sideband HR-MAS NMR spectroscopy: delicate analysis of biological samples, Sci. Rep. 3 (2013) 111–115, https://doi.org/10.1038/srep03349.
[1675] D. Sakellariou, G.L. Goff, J.F. Jacquinot, High-resolution, high-sensitivity NMR of nanolitre anisotropic samples by coil spinning, Nature. 447 (2007) 694–697, https://doi.org/10.1038/nature05897.
[1676] A. Wong, B. Jiménez, X. Li, E. Holmes, J.K. Nicholson, J.C. Lindon, D. Sakellariou, Evaluation of High Resolution Magic-Angle Coil Spinning NMR Spectroscopy for Metabolic Profiling of Nanoliter Tissue Biopsies, Anal. Chem. 84 (2012) 3843–3848, https://doi.org/10.1021/ac300153k.
[1677] A. Wong, X. Li, D. Sakellariou, Refined magic-angle coil spinning resonator for nanoliter NMR spectroscopy: enhanced spectral resolution, Anal. Chem. 85 (2013) 2021–2026, https://doi.org/10.1021/ac400188b.
[1678] C. Lucas-Torres, A. Wong, Current Developments in μMAS NMR Analysis for Metabolomics, Metabolites. 9 (2019) 29–112, https://doi.org/10.3390/metabo9020029.
[1679] A. Wong, P.M. Aguiar, D. Sakellariou, Slow magic-angle coil spinning: A high-sensitivity and high-resolution NMR strategy for microscopic biological specimens, Magn. Reson. Med. 63 (2010) 269–274, https://doi.org/10.1002/mrm.22231.
[1680] C. Lucas-Torres, A. Wong, Intact NMR spectroscopy: slow high-resolution magic angle spinning chemical shift imaging, Analyst. 145 (2020) 2520–2524, https://doi.org/10.1039/d0an00118j.
[1681] F.F. Brown, G. Jaroszkiewicz, M. Jaroszkiewicz, An NMR method for studying the intracellular distribution and transport properties of small molecules in cell suspensions: The chicken erythrocyte system, J. Magn. Reson. 1969 (54) (1983) 400–418, https://doi.org/10.1016/0022-2364(83)90320-7.
[1682] M.E. Fabry, R.C. San George, Effect of magnetic susceptibility on nuclear magnetic resonance signals arising from red cells: a warning, Biochemistry. 22 (1983) 4119–4125, https://doi.org/10.1021/bi00286a020.
[1683] W.S. Warren, W. Richter, A.H. Andreotti, B.T. Farmer, Generation of impossible cross-peaks between bulk water and biomolecules in solution NMR, Science. 262 (1993) 2005–2009, https://doi.org/10.1126/science.8266096.
[1684] Z. Chen, S. Cai, Y. Huang, Y. Lin, High-resolution NMR spectroscopy in inhomogeneous fields, Prog. Nucl. Magn. Reson. Spectrosc. 90–91 (2015) 1–31, https://doi.org/10.1016/j.pnmrs.2015.05.003.
[1685] H. Cai, Y. Chen, X. Cui, S. Cai, Z. Chen, High-Resolution 1H NMR Spectroscopy of Fish Muscle, Eggs and Small Whole Fish via Hadamard-Encoded Intermolecular Multiple-Quantum Coherence, PLoS ONE. 9 (2014), https://doi.org/10.1371/journal.pone.0086422 e86422.
[1686] I. Fugariu, W. Bermel, D. Lane, R. Soong, A.J. Simpson, In-Phase Ultra High-Resolution In Vivo NMR, Angew. Chem. 129 (2017) 6421–6425, https://doi.org/10.1002/ange.201701097.
[1687] Y. Huang, S. Cai, Z. Zhang, Z. Chen, High-Resolution Two-Dimensional J-Resolved NMR Spectroscopy for Biological Systems, Biophys. J. 106 (2014) 2061–2070, https://doi.org/10.1016/j.bpj.2014.03.022.
[1688] Y. Huang, Z. Zhang, H. Chen, J. Feng, S. Cai, Z. Chen, A high-resolution 2D J-resolved NMR detection technique for metabolite analyses of biological samples, Sci. Rep. 5 (2015) 8390, https://doi.org/10.1038/srep08390.
[1689] C. Tan, Y. Huang, S. Cai, Z. Chen, High-resolution two-dimensional 1H J-resolved MRS measurements on in vivo samples, J. Magn. Reson. San Diego Calif 1997 300 (2019) 51–60, https://doi.org/10.1016/j.jmr.2019.01.012.
[1690] J.-N. Dumez, Spatial encoding and spatial selection methods in high-resolution NMR spectroscopy, Prog. Nucl. Magn. Reson. Spectrosc. 109 (2018) 101–134, https://doi.org/10.1016/j.pnmrs.2018.08.001.
[1691] H. Zhan, Y. Huang, Z. Chen, High-Resolution Probing of Heterogeneous Samples by Spatially Selective Pure Shift NMR Spectroscopy, J. Phys. Chem. Lett. 10 (2019) 7356–7361, https://doi.org/10.1021/acs.jpclett.9b03092.
[1692] P. Giraudeau, L. Frydman, Ultrafast 2D NMR: An Emerging Tool in Analytical Spectroscopy, Annu. Rev. Anal. Chem. 7 (2014) 129–161, https://doi.org/10.1146/annurev-anchem-071213-020208.

[1693] 4] B. Gouilleux, L. Rouger, P. Giraudeau, Chapter Two - Ultrafast 2D NMR: Methods and Applications, in: G.A. Webb (Ed.), Annu. Rep. NMR Spectrosc., Academic Press, 2018: pp. 75–144. https://doi.org/10.1016/bs.arnmr.2017.08.003..
[1694] D. Gołowicz, P. Kasprzak, V. Orekhov, K. Kazimierczuk, Fast time-resolved NMR with non-uniform sampling, Prog. Nucl. Magn. Reson. Spectrosc. 116 (2020) 40–55, https://doi.org/10.1016/j.pnmrs.2019.09.003.
[1695] M. Mayzel, J. Rosenlöw, L. Isaksson, V.Y. Orekhov, Time-resolved multidimensional NMR with non-uniform sampling, J. Biomol. NMR. 58 (2014) 129–139, https://doi.org/10.1007/s10858-013-9811-1.
[1696] M. Urbańczyk, A. Shchukina, D. Gołowicz, K. Kazimierczuk, TReNDS-Software for reaction monitoring with time-resolved non-uniform sampling: TReNDS - software for reaction monitoring with time-resolved non-uniform sampling, Magn. Reson. Chem. 57 (2019) 4–12, https://doi.org/10.1002/mrc.4796.
[1697] P. Berthault, C. Boutin, C. Martineau-Corcos, G. Carret, Use of dissolved hyperpolarized species in NMR: Practical considerations, Prog. Nucl. Magn. Reson. Spectrosc. 118–119 (2020) 74–90, https://doi.org/10.1016/j.pnmrs.2020.03.002.
[1698] S.J. Elliott, Q. Stern, M. Ceillier, T. El Daraï, S.F. Cousin, O. Cala, S. Jannin, Practical dissolution dynamic nuclear polarization, Prog. Nucl. Magn. Reson. Spectrosc. 126–127 (2021) 59–100, https://doi.org/10.1016/j.pnmrs.2021.04.002.
[1699] M.L. Hirsch, N. Kalechofsky, A. Belzer, M. Rosay, J.G. Kempf, Brute-Force Hyperpolarization for NMR and MRI, J. Am. Chem. Soc. 137 (2015) 8428–8434, https://doi.org/10.1021/jacs.5b01252.
[1700] S. Korchak, S. Mamone, S. Glöggler, Over 50 % ^{1}H and ^{13}C Polarization for Generating Hyperpolarized Metabolites—A *para* -Hydrogen Approach, ChemistryOpen. 7 (2018) 672–676, https://doi.org/10.1002/open.201800086.
[1701] W. Iali, S.S. Roy, B.J. Tickner, F. Ahwal, A.J. Kennerley, S.B. Duckett, Hyperpolarising Pyruvate through Signal Amplification by Reversible Exchange (SABRE), Angew. Chem. Int. Ed. 58 (2019) 10271–10275, https://doi.org/10.1002/anie.201905483.
[1702] B. Ripka, J. Eills, H. Kouřilová, M. Leutzsch, M.H. Levitt, K. Münnemann, Hyperpolarized fumarate *via* parahydrogen, Chem. Commun. 54 (2018) 12246–12249, https://doi.org/10.1039/C8CC06636A.
[1703] L. Kaltschnee, A.P. Jagtap, J. McCormick, S. Wagner, L. Bouchard, M. Utz, C. Griesinger, S. Glöggler, Hyperpolarization of Amino Acids in Water Utilizing Parahydrogen on a Rhodium Nanocatalyst, Chem. – Eur. J. 25 (2019) 11031–11035, https://doi.org/10.1002/chem.201902878.
[1704] S. Korchak, M. Emondts, S. Mamone, B. Blümich, S. Glöggler, Production of highly concentrated and hyperpolarized metabolites within seconds in high and low magnetic fields, Phys. Chem. Chem. Phys. 21 (2019) 22849–22856, https://doi.org/10.1039/C9CP05227E.
[1705] P.M. Richardson, W. Iali, S.S. Roy, P.J. Rayner, M.E. Halse, S.B. Duckett, Rapid 13C NMR hyperpolarization delivered from para-hydrogen enables the low concentration detection and quantification of sugars, Chem Sci. 10 (2019) 10607–10619, https://doi.org/10.1039/C9SC03450A.
[1706] M.E. Gemeinhardt, M.N. Limbach, T.R. Gebhardt, C.W. Eriksson, S.L. Eriksson, J.R. Lindale, E.A. Goodson, W.S. Warren, E.Y. Chekmenev, B.M. Goodson, "Direct" ^{13}C Hyperpolarization of ^{13}C-Acetate by MicroTesla NMR Signal Amplification by Reversible Exchange (SABRE), Angew. Chem. Int. Ed. 59 (2020) 418–423, https://doi.org/10.1002/anie.201910506.
[1707] F. Reineri, E. Cavallari, C. Carrera, S. Aime, Hydrogenative-PHIP polarized metabolites for biological studies, Magn. Reson. Mater. Phys. Biol. Med. 34 (2021) 25–47, https://doi.org/10.1007/s10334-020-00904-x.
[1708] J.-B. Hövener, A.N. Pravdivtsev, B. Kidd, C.R. Bowers, S. Glöggler, K.V. Kovtunov, M. Plaumann, R. Katz-Brull, K. Buckenmaier, A. Jerschow, F. Reineri, T. Theis, R.V. Shchepin, S. Wagner, P. Bhattacharya, N.M. Zacharias, E.Y. Chekmenev, Parahydrogen-Based Hyperpolarization for Biomedicine, Angew. Chem. Int. Ed. 57 (2018) 11140–11162, https://doi.org/10.1002/anie.201711842.
[1709] A. Manoharan, P.J. Rayner, M. Fekete, W. Iali, P. Norcott, V. Hugh Perry, S.B. Duckett, Catalyst-Substrate Effects on Biocompatible SABRE Hyperpolarization, ChemPhysChem. 20 (2019) 285–294, https://doi.org/10.1002/cphc.201800915.
[1710] S. Knecht, J.W. Blanchard, D. Barskiy, E. Cavallari, L. Dagys, E. Van Dyke, M. Tsukanov, B. Bliemel, K. Münnemann, S. Aime, F. Reineri, M.H. Levitt, G. Buntkowsky, A. Pines, P. Blümler, D. Budker, J. Eills, Rapid hyperpolarization and purification of the metabolite fumarate in aqueous solution, Proc. Natl. Acad. Sci. 118 (2021), https://doi.org/10.1073/pnas.2025383118 e2025383118.
[1711] M. Karlsson, P.R. Jensen, J.H. Ardenkjaer-Larsen, M.H. Lerche, Difference between Extra- and Intracellular T1Values of Carboxylic Acids Affects the Quantitative Analysis of Cellular Kinetics by Hyperpolarized NMR, Angew. Chem. 128 (2016) 13765–13768, https://doi.org/10.1002/ange.201607535.
[1712] C. Hundshammer, M. Grashei, A. Greiner, S.J. Glaser, F. Schilling, pH Dependence of *T 1* for ^{1}3 C-Labelled Small Molecules Commonly Used for Hyperpolarized Magnetic Resonance Imaging, ChemPhysChem. 20 (2019) 798–802, https://doi.org/10.1002/cphc.201801098.
[1713] X. Ji, A. Bornet, B. Vuichoud, J. Milani, D. Gajan, A.J. Rossini, L. Emsley, G. Bodenhausen, S. Jannin, Transportable hyperpolarized metabolites, Nat. Commun. 8 (2017) 13975, https://doi.org/10.1038/ncomms13975.
[1714] A. Capozzi, T. Cheng, G. Boero, C. Roussel, A. Comment, Thermal annihilation of photo-induced radicals following dynamic nuclear polarization to produce transportable frozen hyperpolarized 13C-substrates, Nat. Commun. 8 (2017) 15757, https://doi.org/10.1038/ncomms15757.
[1715] M.L. Hirsch, B.A. Smith, M. Mattingly, A.G. Goloshevsky, M. Rosay, J.G. Kempf, Transport and imaging of brute-force 13 C hyperpolarization, J. Magn. Reson. 261 (2015) 87–94, https://doi.org/10.1016/j.jmr.2015.09.017.
[1716] D.T. Peat, M.L. Hirsch, D.G. Gadian, A.J. Horsewill, J.R. Owers-Bradley, J.G. Kempf, Low-field thermal mixing in [1- ^{13} C] pyruvic acid for brute-force hyperpolarization, Phys. Chem. Chem. Phys. 18 (2016) 19173–19182, https://doi.org/10.1039/C6CP02853E.
[1717] P. Niedbalski, Q. Wang, C. Parish, F. Khashami, A. Kiswandhi, L. Lumata, Magnetic-Field-Dependent Lifetimes of Hyperpolarized ^{13} C Spins at Cryogenic Temperature, J. Phys. Chem. B. 122 (2018) 1898–1904, https://doi.org/10.1021/acs.jpcb.8b00630.
[1718] A. Capozzi, M. Karlsson, J.R. Petersen, M.H. Lerche, J.H. Ardenkjaer-Larsen, Liquid-State 13C Polarization of 30% through Photoinduced Nonpersistent Radicals, J. Phys. Chem. C. 122 (2018) 7432–7443, https://doi.org/10.1021/acs.jpcc.8b01482.
[1719] A. Capozzi, S. Patel, C.P. Gunnarsson, I. Marco-Rius, A. Comment, M. Karlsson, M.H. Lerche, O. Ouari, J.H. Ardenkjaer-Larsen, Efficient Hyperpolarization of U- 13C-Glucose Using Narrow-Line UV-Generated Labile Free Radicals, Angew. Chem. 58 (2018) 1334–1339, https://doi.org/10.1002/anie.201810522.
[1720] I. Marco-Rius, T. Cheng, A.P. Gaunt, S. Patel, F. Kreis, A. Capozzi, A.J. Wright, K.M. Brindle, O. Ouari, A. Comment, Photogenerated Radical in Phenylglyoxylic Acid for in Vivo Hyperpolarized ^{13} C MR with Photosensitive Metabolic Substrates, J. Am. Chem. Soc. 140 (2018) 14455–14463, https://doi.org/10.1021/jacs.8b09326.
[1721] S. Patel, A.C. Pinon, M.H. Lerche, M. Karlsson, A. Capozzi, J.H. Ardenkjær-Larsen, UV-Irradiated 2-Keto-(1–13 C)Isocaproic Acid for High-Performance 13 C Hyperpolarized MR, J. Phys. Chem. C. 124 (2020) 23859–23866, https://doi.org/10.1021/acs.jpcc.0c07536.
[1722] A. Cho, R. Eskandari, V.Z. Miloushev, K.R. Keshari, A non-synthetic approach to extending the lifetime of hyperpolarized molecules using D2O solvation, J. Magn. Reson. 295 (2018) 57–62, https://doi.org/10.1016/j.jmr.2018.08.001.
[1723] 5] N. Salvi, Applications of Hyperpolarisation and NMR Long-Lived States in Drug Screening, in: Annu. Rep. NMR Spectrosc., Elsevier, 2019: pp. 1–33. https://doi.org/10.1016/bs.arnmr.2018.08.002..
[1724] J.-N. Dumez, Perspective on long-lived nuclear spin states, Mol. Phys. 118 (2019) e1644382–e1644412, https://doi.org/10.1080/00268976.2019.1644382.
[1725] M.H. Levitt, Long live the singlet state!, J. Magn. Reson. 306 (2019) 69–74, https://doi.org/10.1016/j.jmr.2019.07.029.
[1726] I. Marco-Rius, M.C.D. Tayler, M.I. Kettunen, T.J. Larkin, K.N. Timm, E.M. Serrao, T.B. Rodrigues, G. Pileio, J.H. Ardenkjaer-Larsen, M.H. Levitt, K.M. Brindle, Hyperpolarized singlet lifetimes of pyruvate in human blood and in the mouse, NMR Biomed. 26 (2013) 1696–1704, https://doi.org/10.1002/nbm.3005.
[1727] S. Glöggler, S.J. Elliott, G. Stevanato, R.C.D. Brown, M.H. Levitt, Versatile magnetic resonance singlet tags compatible with biological conditions, RSC Adv. 7 (2017) 34574–34578, https://doi.org/10.1039/C7RA05196D.
[1728] F. Teleanu, C. Tuță, A. Cucoanes, S. Vasilca, P.R. Vasos, Magnetization Lifetimes Prediction and Measurements Using Long-Lived Spin States in Endogenous Molecules, Molecules. 25 (2020) 5495, https://doi.org/10.3390/molecules25235495.
[1729] B. Erriah, S.J. Elliott, Experimental evidence for the role of paramagnetic oxygen concentration on the decay of long-lived nuclear spin order, RSC Adv. 9 (2019) 23418–23424, https://doi.org/10.1039/C9RA03748A.
[1730] J. Lee, M.S. Ramirez, C.M. Walker, Y. Chen, S. Yi, V.C. Sandulache, S.Y. Lai, J.A. Bankson, High-throughput hyperpolarized 13C metabolic investigations using a multi-channel acquisition system, J. Magn. Reson. 260 (2015) 20–27, https://doi.org/10.1016/j.jmr.2015.08.025.
[1731] B. Cutting, S.V. Shelke, Z. Dragic, B. Wagner, H. Gathje, S. Kelm, B. Ernst, Sensitivity enhancement in saturation transfer difference (STD) experiments through optimized excitation schemes, Magn. Reson. Chem. 45 (2007) 720–724, https://doi.org/10.1002/mrc.2033.
[1732] N.B. Ley, M.L. Rowe, R.A. Williamson, M.J. Howard, Optimising selective excitation pulses to maximise saturation transfer difference NMR spectroscopy, RSC Adv. 4 (2014) 7347–7355, https://doi.org/10.1039/c3ra46246c.
[1733] V. Jayalakshmi, N.R. Krishna, Complete relaxation and conformational exchange matrix (CORCEMA) analysis of intermolecular saturation transfer effects in reversibly forming ligand-receptor complexes, J. Magn. Reson. 155 (2002) 106–118, https://doi.org/10.1006/jmre.2001.2499.
[1734] N. Rama Krishna, V. Jayalakshmi, Complete relaxation and conformational exchange matrix analysis of STD-NMR spectra of ligand–receptor complexes, Prog. Nucl. Magn. Reson. Spectrosc. 49 (2006) 1–25, https://doi.org/10.1016/j.pnmrs.2006.03.002.
[1735] C. Rademacher, T. Peters, Molecular recognition of ligands by native viruses and virus-like particles as studied by NMR experiments, Top. Curr. Chem. 273 (2008) 183–202, https://doi.org/10.1007/128_2007_19.
[1736] A. Antanasijevic, B. Ramirez, M. Caffrey, Comparison of the sensitivities of WaterLOGSY and saturation transfer difference NMR experiments, J. Biomol. NMR. 60 (2014) 37–44, https://doi.org/10.1007/s10858-014-9848-9.
[1737] K.E. Kövér, P. Groves, J. Jiménez-Barbero, G. Batta, Molecular recognition and screening using a 15N group selective STD NMR method, J. Am. Chem. Soc. 129 (2007) 11579–11582, https://doi.org/10.1021/ja073291l.

[1738] K.E. Kövér, E. Wéber, T.A. Martinek, É. Monostori, G. Batta, (15)N and (13)C group-selective techniques extend the scope of STD NMR detection of weak host-guest interactions and ligand screening, ChemBioChem. 11 (2010) 2182–2187, https://doi.org/10.1002/cbic.201000317.
[1739] A. Hetényi, Z. Hegedűs, R. Fajka-Boja, É. Monostori, K.E. Kövér, T.A. Martinek, Target-specific NMR detection of protein-ligand interactions with antibody-relayed 15N-group selective STD, J. Biomol. NMR. 66 (2016) 227–232, https://doi.org/10.1007/s10858-016-0076-3.
[1740] A.D. Gossert, C. Henry, M.J.J. Blommers, W. Jahnke, C. Fernández, Time efficient detection of protein–ligand interactions with the polarization optimized PO-WaterLOGSY NMR experiment, J. Biomol. NMR. 43 (2009) 211–217, https://doi.org/10.1007/s10858-009-9303-5.
[1741] P.G. Takis, B. Jimenez, C.J. Sands, E. Chekmeneva, M.R. Lewis, SMolESY: an efficient and quantitative alternative to on-instrument macromolecular 1H-NMR signal suppression, Chem Sci. 11 (2020) 6000–6011, https://doi.org/10.1039/D0SC01421D.
[1742] D. Chen, Z. Wang, D. Guo, V. Orekhov, X. Qu, Review and Prospect: Deep Learning in Nuclear Magnetic Resonance Spectroscopy, Chem. - Eur. J. 15 (2020) 91–112, https://doi.org/10.1002/chem.202000246.
[1743] A. Strasser, H.-J. Wittmann, R. Seifert, Binding Kinetics and Pathways of Ligands to GPCRs, Trends Pharmacol. Sci. 38 (2017) 717–732, https://doi.org/10.1016/j.tips.2017.05.005.
[1744] V. Georgi, F. Schiele, B.-T. Berger, A. Steffen, P.A. Marin Zapata, H. Briem, S. Menz, C. Preusse, J.D. Vasta, M.B. Robers, M. Brands, S. Knapp, A. Fernández-Montalván, Binding Kinetics Survey of the Drugged Kinome, J. Am. Chem. Soc. 140 (2018) 15774–15782, https://doi.org/10.1021/jacs.8b08048.
[1745] S. Igonet, C. Raingeval, E. Cecon, M. Pučić-Baković, G. Lauc, O. Cala, M. Baranowski, J. Pérez, R. Jockers, I. Krimm, A. Jawhari, Enabling STD-NMR fragment screening using stabilized native GPCR: A case study of adenosine receptor, Sci. Rep. 8 (2018) 8142–8214, https://doi.org/10.1038/s41598-018-26113-0.
[1746] H. Yin, A.D. Flynn, Drugging Membrane Protein Interactions, Annu. Rev. Biomed. Eng. 18 (2016) 51–76, https://doi.org/10.1146/annurev-bioeng-092115-025322.
[1747] G.E. Neurohr, A. Amon, Relevance and Regulation of Cell Density, Trends Cell Biol. 30 (2020) 213–225, https://doi.org/10.1016/j.tcb.2019.12.006.
[1748] Z. Serber, P. Selenko, R. Hänsel, S. Reckel, F. Lohr, J.E. Ferrell, G. Wagner, V. Dötsch, Investigating macromolecules inside cultured and injected cells by in-cell NMR spectroscopy, Nat. Protoc. 1 (2006) 2701–2709, https://doi.org/10.1038/nprot.2006.181.
[1749] B. Bekei, H.M. Rose, M. Herzig, A. Dose, D. Schwarzer, P. Selenko, In-Cell NMR in Mammalian Cells: Part 1, Intrinsically Disord, Protein Anal. (2012) 43–54, https://doi.org/10.1007/978-1-61779-927-3_4.
[1750] B. Bekei, H.M. Rose, M. Herzig, P. Selenko, In-Cell NMR in Mammalian Cells: Part 2, Intrinsically Disord, Protein Anal. (2012) 55–66, https://doi.org/10.1007/978-1-61779-927-3_5.
[1751] B. Bekei, H.M. Rose, M. Herzig, H. Stephanowitz, E. Krause, P. Selenko, In-Cell NMR in Mammalian Cells: Part 3, Intrinsically Disord, Protein Anal. (2012) 67–83, https://doi.org/10.1007/978-1-61779-927-3_6.
[1752] S. Narasimhan, C. Pinto, A. Lucini Paioni, J. van der Zwan, G.E. Folkers, M. Baldus, Characterizing proteins in a native bacterial environment using solid-state NMR spectroscopy, Nat. Protoc. 16 (2021) 893–918, https://doi.org/10.1038/s41596-020-00439-4.
[1753] C. Fuccio, E. Luchinat, L. Barbieri, S. Neri, M. Fragai, Algal autolysate medium to label proteins for NMR in mammalian cells, J. Biomol. NMR. 64 (2016) 275–280, https://doi.org/10.1007/s10858-016-0026-0.
[1754] J. Hamatsu, D. O'Donovan, T. Tanaka, T. Shirai, Y. Hourai, T. Mikawa, T. Ikeya, M. Mishima, W. Boucher, B.O. Smith, E.D. Laue, M. Shirakawa, Y. Ito, High-Resolution Heteronuclear Multidimensional NMR of Proteins in Living Insect Cells Using a Baculovirus Protein Expression System, J. Am. Chem. Soc. 135 (2013) 1688–1691, https://doi.org/10.1021/ja310928u.
[1755] C. Nitsche, G. Otting, Pseudocontact shifts in biomolecular NMR using paramagnetic metal tags, Prog. Nucl. Magn. Reson. Spectrosc. 98–99 (2017) 20–49, https://doi.org/10.1016/j.pnmrs.2016.11.001.
[1756] X.-C. Su, J.-L. Chen, Site-Specific Tagging of Proteins with Paramagnetic Ions for Determination of Protein Structures in Solution and in Cells, Acc. Chem. Res. 52 (2019) 1675–1686, https://doi.org/10.1021/acs.accounts.9b00132.
[1757] D. Joss, D. Häussinger, Design and applications of lanthanide chelating tags for pseudocontact shift NMR spectroscopy with biomacromolecules, Prog. Nucl. Magn. Reson. Spectrosc. (2019) 1–29, https://doi.org/10.1016/j.pnmrs.2019.08.002.
[1758] K.B. Pilla, G. Otting, T. Huber, Pseudocontact Shift-Driven Iterative Resampling for 3D Structure Determinations of Large Proteins, J. Mol. Biol. 428 (2016) 522–532, https://doi.org/10.1016/j.jmb.2016.01.007.
[1759] E. Luchinat, E. Secci, F. Cencetti, P. Bruni, Sequential protein expression and selective labeling for in-cell NMR in human cells, Biochim. Biophys. Acta BBA - Gen. Subj. 2016 (1860) 527–533, https://doi.org/10.1016/j.bbagen.2015.12.023.
[1760] F. Arnesano, L. Banci, I. Bertini, I.C. Felli, M. Losacco, G. Natile, Probing the interaction of cisplatin with the human copper chaperone Atox1 by solution and in-cell NMR spectroscopy, J. Am. Chem. Soc. 133 (2011) 18361–18369, https://doi.org/10.1021/ja207346p.
[1761] L. Cerofolini, S. Giuntini, L. Barbieri, M. Pennestri, A. Codina, M. Fragai, L. Banci, E. Luchinat, E. Ravera, Real-Time Insights into Biological Events: In-Cell Processes and Protein-Ligand Interactions, Biophys. J. 116 (2019) 239–247, https://doi.org/10.1016/j.bpj.2018.11.3132.
[1762] X. Ding, R. Fu, F. Tian, De novo resonance assignment of the transmembrane domain of LR11/SorLA in E. coli membranes, J. Magn. Reson. San Diego Calif 1997 (310) (2020), https://doi.org/10.1016/j.jmr.2019.106639 106639.
[1763] S. Narasimhan, S. Scherpe, A. Lucini Paioni, J. van der Zwan, G.E. Folkers, H. Ovaa, M. Baldus, DNP supported solid-state NMR of proteins inside Mammalian Cells, Angew. Chem. (2019) 1–7, https://doi.org/10.1002/anie.201903246.
[1764] S. Chordia, S. Narasimhan, A. Lucini Paioni, M. Baldus, G. Roelfes, In Vivo Assembly of Artificial Metalloenzymes and Application in Whole-Cell Biocatalysis**, Angew. Chem. 10 (2021) e0135467–e135469, https://doi.org/10.1002/anie.202014771.
[1765] J. Stanek, L.B. Andreas, K. Jaudzems, D. Cala, D. Lalli, A. Bertarello, T. Schubeis, I. Akopjana, S. Kotelovica, K. Tars, A. Pica, S. Leone, D. Picone, Z.-Q. Xu, N.E. Dixon, D. Martinez, M. Berbon, N. El Mammeri, A. Noubhani, S. Saupe, B. Habenstein, A. Loquet, G. Pintacuda, NMR Spectroscopic Assignment of Backbone and Side-Chain Protons in Fully Protonated Proteins: Microcrystals, Sedimented Assemblies, and Amyloid Fibrils, Angew. Chem. Int. Ed Engl. 55 (2016) 15504–15509, https://doi.org/10.1002/anie.201607084.
[1766] T. Viennet, A. Viegas, A. Kuepper, S. Arens, V. Gelev, O. Petrov, T.N. Grossmann, H. Heise, M. Etzkorn, Selective Protein Hyperpolarization in Cell Lysates Using Targeted Dynamic Nuclear Polarization, Angew. Chem. Int. Ed Engl. 55 (2016) 10746–10750, https://doi.org/10.1002/anie.201603205.
[1767] B.J. Albert, C. Gao, E.L. Sesti, E.P. Saliba, N. Alaniva, F.J. Scott, S.T. Sigurdsson, A.B. Barnes, Dynamic Nuclear Polarization Nuclear Magnetic Resonance in Human Cells Using Fluorescent Polarizing Agents, Biochemistry. 57 (2018) 4741–4746, https://doi.org/10.1021/acs.biochem.8b00257.
[1768] S.A. Overall, L.E. Price, B.J. Albert, C. Gao, N. Alaniva, P.T. Judge, E.L. Sesti, P.A. Wender, G.B. Kyei, A.B. Barnes, In Situ Detection of Endogenous HIV Activation by Dynamic Nuclear Polarization NMR and Flow Cytometry, Int. J. Mol. Sci. 21 (2020) 4649, https://doi.org/10.3390/ijms21134649.
[1769] P.T. Judge, E.L. Sesti, L.E. Price, B.J. Albert, N. Alaniva, E.P. Saliba, T. Halbritter, S.T. Sigurdsson, G.B. Kyei, A.B. Barnes, Dynamic Nuclear Polarization with Electron Decoupling in Intact Human Cells and Cell Lysates, J. Phys. Chem. B. 124 (2020) 2323–2330, https://doi.org/10.1021/acs.jpcb.9b10494.
[1770] R. Ghosh, J. Kragelj, Y. Xiao, K.K. Frederick, Cryogenic Sample Loading into a Magic Angle Spinning Nuclear Magnetic Resonance Spectrometer that Preserves Cellular Viability, J. Vis. Exp. (2020) 61733, https://doi.org/10.3791/61733.
[1771] M. Krafcikova, R. Hänsel-Hertsch, L. Trantirek, S. Foldynova-Trantirkova, In Cell NMR Spectroscopy: Investigation of G-Quadruplex Structures Inside Living Xenopus laevis Oocytes, in: D. Yang, C. Lin (Eds.), G-Quadruplex Nucleic Acids, Springer, New York, New York, NY, 2019, pp. 397–405, https://doi.org/10.1007/978-1-4939-9666-7_25.
[1772] O. Morag, N.G. Sgourakis, G. Abramov, A. Goldbourt, Filamentous Bacteriophage Viruses: Preparation, Magic-Angle Spinning Solid-State NMR Experiments, and Structure Determination, in: R. Ghose (Ed.), Protein NMR Methods Protoc, Springer, New York, NY, 2018, pp. 67–97, https://doi.org/10.1007/978-1-4939-7386-6_4.
[1773] R.K. Reddy Sannapureddi, M.K. Mohanty, A.K. Gautam, B. Sathyamoorthy, Characterization of DNA G-quadruplex Topologies with NMR Chemical Shifts, J. Phys. Chem. Lett. 11 (2020) 10016–10022, https://doi.org/10.1021/acs.jpclett.0c02969.
[1774] J. Schaefer, R.A. McKay, E.O. Stejskal, Double-cross-polarization NMR of solids, J. Magn. Reson. 1969 (34) (1979) 443–447, https://doi.org/10.1016/0022-2364(79)90022-2.
[1775] A.W. Hing, S. Vega, J. Schaefer, Measurement of Heteronuclear Dipolar Coupling by Transferred-Echo Double-Resonance NMR, J. Magn. Reson. A. 103 (1993) 151–162, https://doi.org/10.1006/jmra.1993.1146.
[1776] H.M. Rose, C. Witte, F. Rossella, S. Klippel, C. Freund, L. Schröder, Development of an antibody-based, modular biosensor for 129Xe NMR molecular imaging of cells at nanomolar concentrations, Proc. Natl. Acad. Sci. U. S. A. 111 (2014) 11697–11702, https://doi.org/10.1073/pnas.1406797111.
[1777] K. Jeong, C. Netirojjanakul, H.K. Munch, J. Sun, J.A. Finbloom, D.E. Wemmer, A. Pines, M.B. Francis, Targeted Molecular Imaging of Cancer Cells Using MS2-Based (129)Xe NMR, Bioconjug. Chem. 27 (2016) 1796–1801, https://doi.org/10.1021/acs.bioconjchem.6b00275.
[1778] G. Ile Milanole, B. Gao, A. Paoletti, G. Pieters, C. Dugave, E. Deutsch, S. Rivera, F. Law, J.-L. Perfettini, E. Mari, E. Léonce, C. Boutin, P. Berthault, H. Volland, F. Fenaille, T. Brotin, B. Rousseau, Bimodal fluorescence/129Xe NMR probe for molecular imaging and biological inhibition of EGFR in Non-Small Cell Lung Cancer, Bioorg. Med. Chem. 25 (2017) 6653–6660. https://doi.org/10.1016/j.bmc.2017.11.002..
[1779] A. Piontek, C. Witte, H. May Rose, M. Eichner, J. Protze, G. Krause, J. Piontek, L. Schröder, A cCPE-based xenon biosensor for magnetic resonance imaging of claudin-expressing cells, Ann. N. Y. Acad. Sci. 1397 (2017) 195–208, https://doi.org/10.1111/nyas.13363.
[1780] B.A. Riggle, Y. Wang, I.J. Dmochowski, A "Smart" ^{128}Xe NMR Biosensor for pH-Dependent Cell Labeling, J. Am. Chem. Soc. 137 (2015) 5542–5548, https://doi.org/10.1021/jacs.5b01938.
[1781] E. Léonce, J.-P. Dognon, D. Pitrat, J.-C. Mulatier, T. Brotin, P. Berthault, Accurate pH Sensing using Hyperpolarized ^{129} Xe NMR Spectroscopy, Chem. - Eur. J. 24 (2018) 6534–6537, https://doi.org/10.1002/chem.201800900.
[1782] Q. Zeng, Q. Guo, Y. Yuan, Y. Yang, B. Zhang, L. Ren, X. Zhang, Q. Luo, M. Liu, L.-S. Bouchard, X. Zhou, Mitochondria Targeted and Intracellular Biothiol

Triggered Hyperpolarized 129Xe Magnetofluorescent Biosensor, Anal. Chem. 89 (2017) 2288–2295, https://doi.org/10.1021/acs.analchem.6b03742.
[1783] S.D. Zemerov, B.W. Roose, K.L. Farenhem, Z. Zhao, M.A. Stringer, A.R. Goldman, D.W. Speicher, I.J. Dmochowski, ^{129} Xe NMR-Protein Sensor Reveals Cellular Ribose Concentration, Anal. Chem. 92 (2020) 12817–12824, https://doi.org/10.1021/acs.analchem.0c00967.
[1784] Y. Wang, I.J. Dmochowski, An Expanded Palette of Xenon-129 NMR Biosensors, Acc. Chem. Res. 49 (2016) 2179–2187, https://doi.org/10.1021/acs.accounts.6b00309.
[1785] J. Jayapaul, L. Schröder, Molecular Sensing with Host Systems for Hyperpolarized 129Xe, Molecules. 25 (2020) 4627, https://doi.org/10.3390/molecules25204627.
[1786] P.B. Garlick, G.K. Radda, P.J. Seeley, B. Chance, Phosphorus NMR studies on perfused heart, Biochem. Biophys. Res. Commun. 74 (1977) 1256–1262, https://doi.org/10.1016/0006-291X(77)91653-9.
[1787] W.E. Jacobus, G.J. Taylor, D.P. Hollis, R.L. Nunnally, Phosphorus nuclear magnetic resonance of perfused working rat hearts, Nature. 265 (1977) 756–758, https://doi.org/10.1038/265756a0.
[1788] C.J. Turner, P.B. Garlick, One- and two-dimensional 31P spin-echo studies of myocardial ATP and phosphocreatine, J. Magn. Reson. 1969 (57) (1984) 221–227, https://doi.org/10.1016/0022-2364(84)90121-5.
[1789] C.R. Malloy, A.D. Sherry, F.M. Jeffrey, Evaluation of carbon flux and substrate selection through alternate pathways involving the citric acid cycle of the heart by 13C NMR spectroscopy, J. Biol. Chem. 263 (1988) 6964–6971.
[1790] S.M. Cohen, R.G. Shulman, A.C. McLaughlin, Effects of ethanol on alanine metabolism in perfused mouse liver studied by 13C NMR, Proc. Natl. Acad. Sci. 76 (1979) 4808–4812, https://doi.org/10.1073/pnas.76.10.4808.
[1791] S.M. Cohen, Application of nuclear magnetic resonance to the study of liver physiology and disease, Hepatol. Baltim. Md. 3 (1983) 738–749, https://doi.org/10.1002/hep.1840030519.
[1792] T. Jue, F. Arias-Mendoza, N.C. Gonnella, G.I. Shulman, R.G. Shulman, A 1H NMR technique for observing metabolite signals in the spectrum of perfused liver, Proc. Natl. Acad. Sci. 82 (1985) 5246–5249, https://doi.org/10.1073/pnas.82.16.5246.
[1793] C.C. Cunningham, Use of Nuclear Magnetic Resonance Spectroscopy to Study the Effects of Ethanol Consumption on Liver Metabolism and Pathology, Alcohol. Clin. Exp. Res. 10 (1986) 246–250, https://doi.org/10.1111/j.1530-0277.1986.tb05084.x.
[1794] I.A. Bailey, D.G. Gadian, P.M. Matthews, G.K. Radda, P.J. Seeley, Studies of metabolism in the isolated, perfused rat heart using 13C NMR, FEBS Lett. 123 (2001) 315–318, https://doi.org/10.1016/0014-5793(81)80317-1.
[1795] A.I. Scott, R.L. Baxter, Applications of 13C NMR to metabolic studies, Annu. Rev. Biophys. Bioeng. 10 (1981) 151–174, https://doi.org/10.1146/annurev.bb.10.060181.001055.
[1796] R.A. Iles, A.N. STEVENS, J.R. Griffiths, NMR Studies of metabolites in living tissue, Prog. Nucl. Magn. Reson. Spectrosc. 15 (1982) 49–200. https://doi.org/10.1016/0079-6565(82)80008-3..
[1797] S.R. Williams, D.G. Gadian, Tissue metabolism studied in vivo by nuclear magnetic resonance, Q. J. Exp. Physiol. Camb. Engl. 71 (1986) 335–360, https://doi.org/10.1113/expphysiol.1986.sp002994.
[1798] T.W.M. Fan, R.M. Higashi, A.N. Lane, Monitoring of hypoxic metabolism in superfused plant tissues by in vivo 1H NMR, Arch. Biochem. Biophys. 251 (1986) 674–687, https://doi.org/10.1016/0003-9861(86)90377-2.
[1799] D. Hertig, S. Maddah, R. Memedovski, S. Kurth, A. Moreno, M. Pennestri, A. Felser, J.-M. Nuoffer, P. Vermathen, Live monitoring of cellular metabolism and mitochondrial respiration in 3D cell culture system using NMR spectroscopy, Analyst. 146 (2021) 4326–4339, https://doi.org/10.1039/D1AN00041A.
[1800] M. Neeman, E. Rushkin, A. Kadouri, H. Degani, Adaptation of culture methods for NMR studies of anchorage-dependent cells, Magn. Reson. Med. 7 (1988) 236–242, https://doi.org/10.1002/mrm.1910070212.
[1801] J. Carvalho, S. Alves, M.M.C.A. Castro, C.F.G.C. Geraldes, J.A. Queiroz, C.P. Fonseca, C. Cruz, Development of a bioreactor system for cytotoxic evaluation of pharmacological compounds in living cells using NMR spectroscopy, J. Pharmacol. Toxicol. Methods. 95 (2019) 70–78, https://doi.org/10.1016/j.vascn.2018.11.004.
[1802] R.S. Balaban, D.G. Gadian, G.K. Radda, G.G. Wong, An NMR probe for the study of aerobic suspensions of cells and organelles, Anal. Biochem. 116 (1981) 450–455, https://doi.org/10.1016/0003-2697(81)90387-0.
[1803] R.M. Bourne, A device for aeration and mixing of cell and organelle suspensions during nuclear magnetic resonance studies, Anal. Biochem. 182 (1989) 151–156, https://doi.org/10.1016/0003-2697(89)90733-1.
[1804] J.L. Galazzo, J.V. Shanks, J.E. Bailey, Comparison of suspended and immobilized yeast metabolism using 31P nuclear magnetic resonance spectroscopy, Biotechnol. Tech. 1 (1987) 1–6, https://doi.org/10.1007/BF00156277.
[1805] J.L. Galazzo, J.E. Bailey, In vivo nuclear magnetic resonance analysis of immobilization effects on glucose metabolism of yeastSaccharomyces cerevisiae, Biotechnol. Bioeng. 33 (1989) 1283–1289, https://doi.org/10.1002/bit.260331009.
[1806] J.L. Galazzo, J.E. Bailey, Growing Saccharomyces cerevisiae in calcium-alginate beads induces cell alterations which accelerate glucose conversion to ethanol, Biotechnol. Bioeng. 36 (1990) 417–426, https://doi.org/10.1002/bit.260360413.
[1807] H. Santos, D.L. Turner, Characterization of the improved sensitivity obtained using a flow method for oxygenating and mixing cell suspensions in NMR, J. Magn. Reson. 1969 (68) (1986) 345–349, https://doi.org/10.1016/0022-2364(86)90251-9.
[1808] H. Ammann, Y. Boulanger, P. Legault, P. Vinay, An incubation system for the NMR study of kidney tubules, Magn. Reson. Med. 12 (1989) 339–347, https://doi.org/10.1002/mrm.1910120306.
[1809] H.J. Williams, Y. Gao, A.I. Scott, Simple devices for sterile aeration and mixing in NMR cell metabolism studies, J. Magn. Reson. 1969 (94) (1991) 405–407, https://doi.org/10.1016/0022-2364(91)90119-E.
[1810] M. Lyngstad, H. Grasdalen, A new NMR airlift bioreactor used in 31P-NMR studies of itaconic acid producing Aspergillus terreus, J. Biochem. Biophys. Methods. 27 (1993) 105–116, https://doi.org/10.1016/0165-022X(93)90054-R.
[1811] E.M. Lohmeier-Vogel, D.D. McIntyre, H.J. Vogel, Phosphorus-31 and carbon-13 nuclear magnetic resonance studies of glucose and xylose metabolism in cell suspensions and agarose-immobilized cultures of Pichia stipitis and Saccharomyces cerevisiae, Appl. Environ. Microbiol. 62 (1996) 2832–2838, https://doi.org/10.1128/aem.62.8.2832-2838.1996.
[1812] A. Hartbrich, G. Schmitz, D. Weuster-Botz, A.A. de Graaf, C. Wandrey, Development and application of a membrane cyclone reactor for in vivo NMR spectroscopy with high microbial cell densities, Biotechnol. Bioeng. 51 (1996) 624–635, https://doi.org/10.1002/(SICI)1097-0290(19960920)51:6<624::AID-BIT2>3.0.CO;2-J.
[1813] P.D. Majors, J.S. McLean, G.E. Pinchuk, J.K. Fredrickson, Y.A. Gorby, K.R. Minard, R.A. Wind, NMR methods for in situ biofilm metabolism studies, J. Microbiol. Methods. 62 (2005) 337–344, https://doi.org/10.1016/j.mimet.2005.04.017.
[1814] M. Zakhartsev, C. Bock, Miniaturized device for agitating a high-density yeast suspension that is suitable for in vivo nuclear magnetic resonance applications, Anal. Biochem. 397 (2010) 244–246, https://doi.org/10.1016/j.ab.2009.10.011.
[1815] M. Ben-Tchavtchavadze, J. Chen, M. Perrier, M. Jolicoeur, A noninvasive technique for the measurement of the energetic state of free-suspension mammalian cells, Biotechnol. Prog. (2009), https://doi.org/10.1002/btpr.333.
[1816] L. Brecker, P. Urdl, W. Schmid, H. Griengl, D.W. Ribbons, Simple device to monitor aerobic biotransformations by in situ 1H-NMR, Biotechnol. Lett. 22 (2000) 1135–1141, https://doi.org/10.1023/A:1005664400918.
[1817] L. Brecker, D.W. Ribbons, Biotransformations monitored in situ by proton nuclear magnetic resonance spectroscopy, Trends Biotechnol. 18 (2000) 197–202, https://doi.org/10.1016/S0167-7799(00)01425-6.
[1818] H. Takesada, K. Ebisawa, H. Toyosaki, E. Suzuki, Y. Kawahara, H. Kojima, T. Tanaka, A convenient NMR method for in situ observation of aerobically cultured cells, J. Biotechnol. 84 (2000) 231–236, https://doi.org/10.1016/S0168-1656(00)00358-8.
[1819] A.R. Neves, A. Ramos, H. Costa, I.I. van Swam, J. Hugenholtz, M. Kleerebezem, W. de Vos, H. Santos, Effect of Different NADH Oxidase Levels on Glucose Metabolism by *Lactococcus lactis* : Kinetics of Intracellular Metabolite Pools Determined by In Vivo Nuclear Magnetic Resonance, Appl. Environ. Microbiol. 68 (2002) 6332–6342, https://doi.org/10.1128/AEM.68.12.6332-6342.2002.
[1820] G.S. Karczmar, A.P. Koretsky, M.J. Bissell, M.P. Klein, M.W. Weiner, A device for maintaining viable cells at high densities for NMR studies, J. Magn. Reson. 1969 (53) (1983) 123–128, https://doi.org/10.1016/0022-2364(83)90080-X.
[1821] Y. Boulanger, P. Vinay, M.T. Phan Viet, R. Guardo, M. Desroches, An Improved Perifusion System for NMR Study of Living Cells, Magn. Reson. Med. 2 (1985) 495–500, https://doi.org/10.1002/mrm.1910020509.
[1822] Y. Boulanger, P. Vinay, Use of dialysis fibers for the study of aerobic cells, Biochem. Cell Biol. 64 (1986) 869–879, https://doi.org/10.1139/o86-116.
[1823] D.D. Drury, B.E. Dale, R.J. Gillies, Oxygen transfer properties of a bioreactor for use within a nuclear magnetic resonance spectrometer, Biotechnol. Bioeng. 32 (1988) 966–974, https://doi.org/10.1002/bit.260320804.
[1824] R. Gonzalez-Mendez, D. Wemmer, G. Hahn, N. Wade-Jardetzky, O. Jardetzky, Continuous-flow NMR culture system for mammalian cells, Biochim. Biophys. Acta BBA - Mol. Cell Res. 720 (1982) 274–280, https://doi.org/10.1016/0167-4889(82)90051-9.
[1825] M.I. Hrovat, C.G. Wade, S.P. Hawkes, A space-efficient assembly for NMR experiments on anchorage-dependent cells, J. Magn. Reson. 1969 (61) (1985) 409–417, https://doi.org/10.1016/0022-2364(85)90181-7.
[1826] M.M. Minichiello, D.M. Albert, N.H. Kolodny, M.-S. Lee, J.L. Craft, A perfusion system developed for31p NMR study of melanoma cells at tissue-like density, Magn. Reson. Med. 10 (1989) 96–107, https://doi.org/10.1002/mrm.1910100109.
[1827] Y.H.H. Lien, H.Z. Zhou, C. Job, J.A. Barry, R.J. Gillies, In vivo 31P NMR study of early cellular responses to hyperosmotic shock in cultured glioma cells, Biochimie. 74 (1992) 931–939, https://doi.org/10.1016/0300-9084(92)90077-R.
[1828] R.J. Gillies, J.-P. Galons, K.A. McGovern, P.G. Scherer, Y.-H. Lien, C. Job, R. Ratcliff, F. Chapa, S. Cerdan, B.E. Dale, Design and application of NMR-compatible bioreactor circuits for extended perfusion of high-density mammalian cell cultures, NMR Biomed. 6 (1993) 95–104, https://doi.org/10.1002/nbm.1940060115.
[1829] R. Callies, M.E. Jackson, K.M. Brindle, Measurements of the Growth and Distribution of Mammalian Cells in a Hollow-Fiber Bioreactor Using Nuclear

Magnetic Resonance Imaging, Bio/Technology. 12 (1994) 75–78, https://doi.org/10.1038/nbt0194-75.
[1830] T.P. Trouard, K.D. Harkins, J.L. Divijak, R.J. Gillies, J.-P. Galons, Ischemia-induced changes of intracellular water diffusion in rat glioma cell cultures, Magn. Reson. Med. 60 (2008) 258–264, https://doi.org/10.1002/mrm.21616.
[1831] E.M. Lohmeier-Vogel, B. Hahn-Hägerdal, H.J. Vogel, Phosphorus-31 and carbon-13 nuclear magnetic resonance study of glucose and xylose metabolism in agarose-immobilized Candida tropicalis, Appl. Environ. Microbiol. 61 (1995) 1420–1425, https://doi.org/10.1128/aem.61.4.1420-1425.1995.
[1832] E.M. Lohmeier-Vogel, C.R. Sopher, H. Lee, Intracellular acidification as a mechanism for the inhibition by acid hydrolysis-derived inhibitors of xylose fermentation by yeasts, J. Ind. Microbiol. Biotechnol. 20 (1998) 75–81, https://doi.org/10.1038/sj.jim.2900484.
[1833] E. Dahan-Grobgeld, Z. Livneh, A.F. Maretzek, S. Polak-Charcon, Z. Eichenbaum, H. Degani, Reversible Induction of ATP Synthesis by DNA Damage and Repair in Escherichia coli, J. Biol. Chem. 273 (1998) 30232–30238, https://doi.org/10.1074/jbc.273.46.30232.
[1834] D.L. Foxall, J.S. Cohen, NMR studies of perfused cells, J. Magn. Reson. 1969 (52) (1983) 346–349, https://doi.org/10.1016/0022-2364(83)90210-X.
[1835] D.L. Foxall, J.S. Cohen, J.B. Mitchell, Continuous perfusion of mammalian cells embedded in agarose gel threads, Exp. Cell Res. 154 (1984) 521–529, https://doi.org/10.1016/0014-4827(84)90176-9.
[1836] R.H. Knop, C.W. Chen, J.B. Mitchell, A. Russo, S. McPherson, J.S. Cohen, Metabolic studies of mammalian cells by 31P-NMR using a continuous perfusion technique, Biochim. Biophys. Acta. 804 (1984) 275–284, https://doi.org/10.1016/0167-4889(84)90130-7.
[1837] R.H. Knop, C.W. Chen, J.B. Mitchell, A. Russo, S. McPherson, J.S. Cohen, Adaptive cellular response to hyperthermia: 31P-NMR studies, Biochim. Biophys. Acta BBA - Mol. Cell Res. 845 (1985) 171–177, https://doi.org/10.1016/0167-4889(85)90174-0.
[1838] W. Egan, M. Barile, S. Rottem, 31P-NMR studies of Mycoplasma gallisepticum cells using a continuous perfusion technique, FEBS Lett. 204 (1986) 373–376, https://doi.org/10.1016/0014-5793(86)80846-8.
[1839] M.V. Miceli, L. Kan, D.A. Newsome, Phosphorus-31 nuclear magnetic resonance spectroscopy of human retinoblastoma cells: correlations with metabolic indices, Biochim. Biophys. Acta BBA - Mol. Cell Res. 970 (1988) 262–269, https://doi.org/10.1016/0167-4889(88)90125-5.
[1840] P. Lundberg, S.J.B. Price, S. Roy, P.W. Kuchel, NMR studies of erythrocytes immobilized in agarose and alginate gels, Magn. Reson. Med. 25 (1992) 273–288, https://doi.org/10.1002/mrm.1910250206.
[1841] O. Kaplan, P. Aebersold, J.S. Cohen, Metabolism of peripheral lymphocytes, interleukin-2-activated lymphocytes and tumor-infiltrating lymphocytes from ^{31} NMR studies, FEBS Lett. 258 (1989) 55–58, https://doi.org/10.1016/0014-5793(89)81614-X.
[1842] F. Mégnin, J.F. Nedelec, J.L. Dimicoli, J.M. Lhoste, 31P and13C NMR Studies of Isolated Perfused Hematopoietic Cells from Leukemic Mice, NMR Biomed. 2 (1989) 27–33, https://doi.org/10.1002/nbm.1940020106.
[1843] F. Seguin, C. Jubault, J.-P. Grivet, A. Le Pape, 31P NMR study of intracellular pH during the respiratory burst of macrophages, Exp. Cell Res. 186 (1990) 188–191, https://doi.org/10.1016/0014-4827(90)90226-Z.
[1844] L.L. Hansen, J. Rasmussen, E. Friche, J.W. Jaroszewski, Method for Determination of Intracellular Sodium in Perfused Cancer Cells by 23Na Nuclear Magnetic Resonance Spectroscopy, Anal. Biochem. 214 (1993) 506–510, https://doi.org/10.1006/abio.1993.1530.
[1845] S.P. Williams, A.M. Fulton, K.M. Brindle, Estimation of the intracellular free ADP concentration by 19F NMR studies of fluorine-labeled yeast phosphoglycerate kinase in vivo, Biochemistry. 32 (1993) 4895–4902, https://doi.org/10.1021/bi00069a026.
[1846] L.L. Hansen, J.W. Jaroszewski, Effect of Gossypol on Cultured TM3 Leydig and TM4 Sertoli Cells: 31P and 23Na NMR Study, NMR Biomed. 9 (1996) 72–78, https://doi.org/10.1002/(SICI)1099-1492(199604)9:2<72::AID-NBM406>3.0.CO;2-3.
[1847] H. Farghali, P. Caraceni, H.L. Rilo, A.B. Borle, A. Gasbarrini, J. Gavaler, D.H. Van Thiel, Biochemical and 31P-NMR spectroscopic evaluation of immobilized perfused rat Sertoli cells, J. Lab. Clin. Med. 128 (1996) 408–416, https://doi.org/10.1016/S0022-2143(96)80013-8.
[1848] M.A.C. Reed, J. Roberts, P. Gierth, Ē. Kupče, U.L. Günther, Quantitative Isotopomer Rates in Real-Time Metabolism of Cells Determined by NMR Methods, ChemBioChem. 20 (2019) 2207–2211, https://doi.org/10.1002/cbic.201900084.
[1849] C.P. Fonseca, L.L. Fonseca, L.P. Montezinho, P.M. Alves, H. Santos, M.M.C.A. Castro, C.F.G.C. Geraldes, 23Na multiple quantum filtered NMR characterisation of Na+ binding and dynamics in animal cells: a comparative study and effect of Na+/Li+ competition, Eur. Biophys. J. 42 (2013) 503–519, https://doi.org/10.1007/s00249-013-0899-8.
[1850] R. Sriram, J. Sun, J. Villanueva-Meyer, C. Mutch, J. De Los Santos, J. Peters, D. E. Korenchan, K. Neumann, M. van Criekinge, J. Kurhanewicz, O. Rosenberg, D. Wilson, M.A. Ohliger, Detection of Bacteria-Specific Metabolism Using Hyperpolarized [2-13C]Pyruvate., ACS Infect. Dis. 4 (2018) 797–805, https://doi.org/10.1021/acsinfecdis.7b00234.
[1851] M. Oren-Shamir, M. Avron, H. Degani, In vivo NMR studies of the alga Dunaliella salina embedded in beads, FEBS Lett. 233 (1988) 124–128, https://doi.org/10.1016/0014-5793(88)81368-1.
[1852] K.S. Narayan, E.A. Moress, J.C. Chatham, P.B. Barker, 31P NMR of mammalian cells encapsulated in alginate gels utilizing a new phosphate-free perfusion medium, NMR Biomed. 3 (1990) 23–26, https://doi.org/10.1002/nbm.1940030104.
[1853] K.A. McGovern, J.S. Schoeniger, J.P. Wehrle, C.E. Ng, J.D. Glickson, Gel-entrapment of perfluorocarbons: A fluorine-19 NMR spectroscopic method for monitoring oxygen concentration in cell perfusion systems, Magn. Reson. Med. 29 (1993) 196–204, https://doi.org/10.1002/mrm.1910290207.
[1854] J.M. Macdonald, J. Kurhanewicz, R. Dahiya, M.T. Espanol, L.-H. Chang, B. Goldberg, T.L. James, P. Narayan, Effect of glucose and confluency on phosphorus metabolites of perfused human prostatic adenocarcinoma cells as determined by31P MRS, Magn. Reson. Med. 29 (1993) 244–248, https://doi.org/10.1002/mrm.1910290213.
[1855] M. Hentschel, S. Mirtsch, A. Jordan, P. Wust, T.h. Vogl, W. Semmler, K.-J. Wolf, R. Felix, Heat response of HT29 cells depends strongly on perfusion—A ^{31} P NMR spectroscopy, HPLC and cell survival analysis, Int. J. Hyperthermia. 13 (1997) 69–82, https://doi.org/10.3109/02656739709056431.
[1856] S.J.A. Hesse, G.J.G. Ruijter, C. Dijkema, J. Visser, Measurement of intracellular (compartmental) pH by 31P NMR in Aspergillus niger, J. Biotechnol. 77 (2000) 5–15, https://doi.org/10.1016/S0168-1656(99)00203-5.
[1857] N.G. Sharaf, C.O. Barnes, L.M. Charlton, G.B. Young, G.J. Pielak, A bioreactor for in-cell protein NMR, J. Magn. Reson. 202 (2010) 140–146, https://doi.org/10.1016/j.jmr.2009.10.008.
[1858] H. Ben-Horin, M. Tassini, A. Vivi, G. Navon, O. Kaplan, Mechanism of Action of the Antineoplastic Drug Lonidamine: 31P and 13C Nuclear Magnetic Resonance Studies, Cancer Res. 55 (1995) 2814–2821.
[1859] M.A. Taipa, J.M.S. Cabral, H. Santos, Comparison of glucose fermentation by suspended and gel-entrapped yeast cells: An in vivo nuclear magnetic resonance study, Biotechnol. Bioeng. 41 (1993) 647–653, https://doi.org/10.1002/bit.260410607.
[1860] W.F.H. Sijbesma, J.S. Almeida, M.A.M. Reis, H. Santos, Uncoupling effect of nitrite during denitrification by Pseudomonas fluorescens: An in vivo 31P-NMR study, Biotechnol. Bioeng. 52 (1996) 176–182, https://doi.org/10.1002/(SICI)1097-0290(19961005)52:1<176::AID-BIT18>3.0.CO;2-M.
[1861] Q. Zhao, R. Fujimiya, S. Kubo, C.B. Marshall, M. Ikura, I. Shimada, N. Nishida, Real-Time In-Cell NMR Reveals the Intracellular Modulation of GTP-Bound Levels of RAS, Cell Rep. 32 (2020), https://doi.org/10.1016/j.celrep.2020.108074 108074.
[1862] I. Constantinidis, A. Sambanis, Towards the development of artificial endocrine tissues:31P NMR spectroscopic studies of immunoisolated, insulin-secreting AtT-20 cells, Biotechnol. Bioeng. 47 (1995) 431–443, https://doi.org/10.1002/bit.260470404.
[1863] 0] A. Sambanis, K.K. Papas, P.C. Flanders, R.C. Long, H. Kang, I. Constantinidis, Towards the development of a bioartificial pancreas: immunoisolation and NMR monitoring of mouse insulinomas, in: B.C. Buckland, J.G. Aunins, T.A. Bibila, W.-S. Hu, D.K. Robinson, W. Zhou (Eds.), Cell Cult. Eng. IV Improv. Hum. Health, Springer Netherlands, Dordrecht, 1995: pp. 351–363. https://doi.org/10.1007/978-94-011-0257-5_38..
[1864] P.F. Daly, R.C. Lyon, E.J. Straka, J.S. Cohen, 31P-NMR spectroscopy of human cancer cells proliferating in a basement membrane gel, FASEB J. 2 (1988) 2596–2604, https://doi.org/10.1096/fasebj.2.10.3384239.
[1865] U. Pilatus, H. Shim, D. Artemov, D. Davis, P.C.M. Van Zijl, J.D. Glickson, Intracellular volume and apparent diffusion constants of perfused cancer cell cultures, as measured by NMR, Magn. Reson. Med. 37 (1997) 825–832, https://doi.org/10.1002/mrm.1910370605.
[1866] J.C. Street, U. Mahmood, D. Ballon, A.A. Alfieri, J.A. Koutcher, 13C and 31P NMR Investigation of Effect of 6-Aminonicotinamide on Metabolism of RIF-1 Tumor Cells in Vitro, J. Biol. Chem. 271 (1996) 4113–4119, https://doi.org/10.1074/jbc.271.8.4113.
[1867] B.L. Cox, S. Erickson-Bhatt, J.M. Szulczewski, J.M. Squirrell, K.D. Ludwig, E.B. Macdonald, R. Swader, S.M. Ponik, K.W. Eliceiri, S.B. Fain, A novel bioreactor for combined magnetic resonance spectroscopy and optical imaging of metabolism in 3D cell cultures, Magn. Reson. Med. 81 (2019) 3379–3391, https://doi.org/10.1002/mrm.27644.
[1868] K. Ugurbil, D.L. Guernsey, T.R. Brown, P. Glynn, N. Tobkes, I.S. Edelman, 31P NMR studies of intact anchorage-dependent mouse embryo fibroblasts, Proc. Natl. Acad. Sci. 78 (1981) 4843–4847, https://doi.org/10.1073/pnas.78.8.4843.
[1869] J.F. Baetselier, J. Marvaldi, J.-P. Galons, P.J. Cozzone, P. Canioni, Growth of a human colonic adenocarcinoma cell line (HT 29) on microcarrier beads: Metabolic studies by 31phosphorus nuclear magnetic resonance spectroscopy, Int. J. Cancer. 39 (1987) 255–260, https://doi.org/10.1002/ijc.2910390222.
[1870] D.M. Ojcius, H. Degani, J. Mispelter, A. Dautry-Varsat, Enhancement of ATP Levels and Glucose Metabolism during an Infection by Chlamydia, J. Biol. Chem. 273 (1998) 7052–7058, https://doi.org/10.1074/jbc.273.12.7052.
[1871] P.E. Thelwall, K.M. Brindle, Analysis of CHO-K1 cell growth in a fixed bed bioreactor using magnetic resonance spectroscopy and imaging, Cytotechnology. 30 (1999) 121–132, https://doi.org/10.1023/A:1008039011960.
[1872] P.E. Thelwall, A.A. Neves, K.M. Brindle, Measurement of bioreactor perfusion using dynamic contrast agent-enhanced magnetic resonance imaging, Biotechnol. Bioeng. 75 (2001) 682–690, https://doi.org/10.1002/bit.10039.
[1873] U. Pilatus, E. Aboagye, D. Artemov, N. Mori, E. Ackerstaff, Z.M. Bhujwalla, Real-time measurements of cellular oxygen consumption, pH, and energy metabolism using nuclear magnetic resonance spectroscopy, Magn. Reson. Med. 45 (2001) 749–755, https://doi.org/10.1002/mrm.1102.

[1874] A.A. Shestov, A. Mancuso, S.-C. Lee, L. Guo, D.S. Nelson, J.C. Roman, P.-G. Henry, D.B. Leeper, I.A. Blair, J.D. Glickson, Bonded Cumomer Analysis of Human Melanoma Metabolism Monitored by 13C NMR Spectroscopy of Perfused Tumor Cells, J. Biol. Chem. 291 (2016) 5157–5171, https://doi.org/10.1074/jbc.M115.701862.
[1875] J.J. Crowe, S.C. Grant, T.M. Logan, T. Ma, A magnetic resonance-compatible perfusion bioreactor system for three-dimensional human mesenchymal stem cell construct development, Chem. Eng. Sci. 66 (2011) 4138–4147, https://doi.org/10.1016/j.ces.2011.05.046.
[1876] P.-S. Lin, M. Blumenstein, R.B. Mikkelsen, R. Schmidt-Ullrich, W.W. Bachovchin, Perfusion of cell spheroids for study by NMR spectroscopy, J. Magn. Reson. 1969 (73) (1987) 399–404, https://doi.org/10.1016/0022-2364(87)90002-3.
[1877] H.J. Vogel, P. Brodelius, H. Lilja, E.M. Lohmeier-Vogel, Nuclear magnetic resonance studies of immobilized cells, Methods Enzymol. 135 (1987) 512–528, https://doi.org/10.1016/0076-6879(87)35107-9.
[1878] J.P. Freyer, N.H. Fink, P.L. Schor, J.R. Coulter, M. Neeman, L.O. Sillerud, A system for viably maintaining a stirred suspension of multicellular spheroids during NMR spectroscopy, NMR Biomed. 3 (1990) 195–205, https://doi.org/10.1002/nbm.1940030502.
[1879] G.H. Read, N. Miura, J.L. Carter, K.T. Kines, K. Yamamoto, N. Devasahayam, J. Y. Cheng, K.A. Camphausen, M.C. Krishna, A.H. Kesarwala, Three-dimensional alginate hydrogels for radiobiological and metabolic studies of cancer cells, Colloids Surf. B Biointerfaces. 171 (2018) 197–204, https://doi.org/10.1016/j.colsurfb.2018.06.018.
[1880] J. Gulli, P. Yunker, F. Rosenzweig, Matrices (re)loaded: Durability, viability, and fermentative capacity of yeast encapsulated in beads of different composition during long-term fed-batch culture, Biotechnol. Prog. 36 (2020), https://doi.org/10.1002/btpr.2925.
[1881] J.V. Shanks, In situ NMR systems, Curr. Issues Mol. Biol. 3 (2001) 15–26.
[1882] 9] M. Milkevitch, E.A. Browning, E.J. Delikatny, Perfused Cells, Tissues and Organs by Magnetic Resonance Spectroscopy, in: EMagRes, American Cancer Society, 2016: pp. 1333–1346. https://doi.org/10.1002/9780470034590.emrstm1426..
[1883] Y. Noguchi, N. Shimba, H. Toyosaki, K. Ebisawa, Y. Kawahara, E. Suzuki, S. Sugimoto, In vivo NMR system for evaluating oxygen-dependent metabolic status in microbial culture, J. Microbiol. Methods. 51 (2002) 73–82, https://doi.org/10.1016/S0167-7012(02)00063-5.
[1884] K. Chen, C.E. Ng, J.L. Zweier, P. Kuppusamy, J.D. Glickson, H.M. Swartz, Measurement of the intracellular concentration of oxygen in a cell perfusion system, Magn. Reson. Med. 31 (1994) 668–672, https://doi.org/10.1002/mrm.1910310613.
[1885] B.K. Melvin, J.V. Shanks, Influence of Aeration on Cytoplasmic pH of Yeast in an NMR Airlift Bioreactor, Biotechnol. Prog. 12 (1996) 257–265, https://doi.org/10.1021/bp9500775.
[1886] P. Parhami, B.M. Fung, Fluorine-19 relaxation study of perfluoro chemicals as oxygen carriers, J. Phys. Chem. 87 (1983) 1928–1931, https://doi.org/10.1021/j100234a020.
[1887] S.N.O. Williams, R.M. Callies, K.M. Brindle, Mapping of oxygen tension and cell distribution in a hollow-fiber bioreactor using magnetic resonance imaging, Biotechnol. Bioeng. 56 (1997) 56–61, https://doi.org/10.1002/(SICI)1097-0290(19971005)56:1<56::AID-BIT6>3.0.CO;2-U.
[1888] N. Nishida, Y. Ito, I. Shimada, In situ structural biology using in-cell NMR, BBA - Gen. Subj. (2019) 1–10, https://doi.org/10.1016/j.bbagen.2019.05.007.
[1889] C.A. Briasco, D.A. Ross, C.R. Robertson, A hollow-fiber reactor design for NMR studies of microbial cells, Biotechnol. Bioeng. 36 (1990) 879–886, https://doi.org/10.1002/bit.260360903.
[1890] K.R. Keshari, J. Kurhanewicz, R.E. Jeffries, D.M. Wilson, B.J. Dewar, M. van Criekinge, M. Zierhut, D.B. Vigneron, J.M. Macdonald, Hyperpolarized 13C spectroscopy and an NMR-compatible bioreactor system for the investigation of real-time cellular metabolism, Magn. Reson. Med. 63 (2010) 322–329, https://doi.org/10.1002/mrm.22225.
[1891] A.R. Neves, A. Ramos, M.C. Nunes, M. Kleerebezem, J. Hugenholtz, W.M. de Vos, J. Almeida, H. Santos, In vivo nuclear magnetic resonance studies of glycolytic kinetics in Lactococcus lactis, Biotechnol. Bioeng. 64 (1999) 200–212, https://doi.org/10.1002/(SICI)1097-0290(19990720)64:2<200::AID-BIT9>3.0.CO;2-K.
[1892] Y. Noguchi, N. Shimba, Y. Kawahara, E. Suzuki, S. Sugimoto, 31P NMR studies of energy metabolism in xanthosine-5'-monophosphate overproducing Corynebacterium ammoniagenes, Eur. J. Biochem. 270 (2003) 2622–2626, https://doi.org/10.1046/j.1432-1033.2003.03635.x.
[1893] Y. Noguchi, The Energetic Conversion Competence of Escherichia coli during Aerobic Respiration Studied by 31P NMR Using a Circulating Fermentation System, J. Biochem. (Tokyo) 136 (2004) 509–515, https://doi.org/10.1093/jb/mvh147.
[1894] R. Chen, J.E. Bailey, Observations of aerobic, growingescherichia coli metabolism using an on-line nuclear magnetic resonance spectroscopy system, Biotechnol. Bioeng. 42 (1993) 215–221, https://doi.org/10.1002/bit.260420209.
[1895] S. Lauritsen, L.B. Bertelsen, P. Daugaard, C. Laustsen, N. Nielsen, J.V. Nygaard, H. Stødkilde-Jørgensen, Bioreactor for quantification of cell metabolism by MR-hyperpolarization, Biomed. Phys. Eng. Express. 1 (2015) 047003–47010, https://doi.org/10.1088/2057-1976/1/4/047003.
[1896] A.A. De Graaf, R.M. Wittig, U. Probst, J. Strohhaecker, S.M. Schoberth, H. Sahm, Continuous-flow NMR bioreactor for in vivo studies of microbial cell suspensions with low biomass concentrations, J. Magn. Reson. 1969 (98) (1992) 654–659, https://doi.org/10.1016/0022-2364(92)90020-8.
[1897] R. Chen, J.E. Bailey, Energetic Effect of Vitreoscilla Hemoglobin Expression in Escherichia coli: An Online 31P NMR and a Saturation Transfer Study, Biotechnol. Prog. 10 (1994) 360–364, https://doi.org/10.1021/bp00028a003.
[1898] D. Kreyenschulte, E. Paciok, L. Regestein, B. Blümich, J. Büchs, Online monitoring of fermentation processes via non-invasive low-field NMR: Online-NMR for Fermentation Processes, Biotechnol. Bioeng. 112 (2015) 1810–1821, https://doi.org/10.1002/bit.25599.
[1899] T. Wang, T. Liu, Z. Wang, X. Tian, Y. Yang, M. Guo, J. Chu, Y. Zhuang, A rapid and accurate quantification method for real-time dynamic analysis of cellular lipids during microalgal fermentation processes in Chlorella prototheocoides with low field nuclear magnetic resonance, J. Microbiol. Methods. 124 (2016) 13–20, https://doi.org/10.1016/j.mimet.2016.03.003.
[1900] D.J. O'Leary, S.P. Hawkes, C.G. Wade, Indirect monitoring of carbon-13 metabolism with NMR: Analysis of perfusate with a closed-loop flow system, Magn. Reson. Med. 5 (1987) 572–577, https://doi.org/10.1002/mrm.1910050608.
[1901] N. Mehendale, F. Jenne, C. Joshi, S. Sharma, S.K. Masakapalli, N. MacKinnon, A Nuclear Magnetic Resonance (NMR) Platform for Real-Time Metabolic Monitoring of Bioprocesses, Molecules. 25 (2020) 4675–4711, https://doi.org/10.3390/molecules25204675.
[1902] M. Grisi, F. Vincent, B. Volpe, R. Guidetti, N. Harris, A. Beck, G. Boero, NMR spectroscopy of single sub-nL ova with inductive ultra-compact single-chip probes, Sci. Rep. 7 (2017) 44670, https://doi.org/10.1038/srep44670.
[1903] J. Eills, W. Hale, M. Sharma, M. Rossetto, M.H. Levitt, M. Utz, High-Resolution Nuclear Magnetic Resonance Spectroscopy with Picomole Sensitivity by Hyperpolarization on a Chip, J. Am. Chem. Soc. 141 (2019) 9955–9963, https://doi.org/10.1021/jacs.9b03507.
[1904] E. Montinaro, M. Grisi, M.C. Letizia, L. Pethö, M.A.M. Gijs, R. Guidetti, J. Michler, J. Brugger, G. Boero, 3D printed microchannels for sub-nL NMR spectroscopy, PLOS ONE. 13 (2018), https://doi.org/10.1371/journal.pone.0192780 e0192780.
[1905] A. Bonucci, O. Ouari, B. Guigliarelli, V. Belle, E. Mileo, In-Cell EPR: Progress towards Structural Studies Inside Cells, ChemBioChem. 21 (2019) 451–460, https://doi.org/10.1002/cbic.201900291.
[1906] B. Joseph, E.A. Jaumann, A. Sikora, K. Barth, T.F. Prisner, D.S. Cafiso, In situ observation of conformational dynamics and protein ligand–substrate interactions in outer-membrane proteins with DEER/PELDOR spectroscopy, Nat. Protoc. 14 (2019) 2344–2369, https://doi.org/10.1038/s41596-019-0182-2.
[1907] D. Goldfarb, Pulse EPR in biological systems – Beyond the expert's courtyard, J. Magn. Reson. 306 (2019) 102–108, https://doi.org/10.1016/j.jmr.2019.07.038.
[1908] F. Torricella, A. Pierro, E. Mileo, V. Belle, A. Bonucci, Nitroxide spin labels and EPR spectroscopy: A powerful association for protein dynamics studies, Biochim. Biophys. Acta BBA - Proteins Proteomics. 1869 (2021), https://doi.org/10.1016/j.bbapap.2021.140653 140653.
[1909] M. Azarkh, O. Okle, P. Eyring, D.R. Dietrich, M. Drescher, Evaluation of spin labels for in-cell EPR by analysis of nitroxide reduction in cell extract of Xenopus laevis oocytes, J. Magn. Reson. 212 (2011) 450–454, https://doi.org/10.1016/j.jmr.2011.07.014.
[1910] J.T. Paletta, M. Pink, B. Foley, S. Rajca, A. Rajca, Synthesis and Reduction Kinetics of Sterically Shielded Pyrrolidine Nitroxides, Org. Lett. 14 (2012) 5322–5325, https://doi.org/10.1021/ol302506f.
[1911] M.J. Lawless, A. Shimshi, T.F. Cunningham, M.N. Kinde, P. Tang, S. Saxena, Analysis of Nitroxide-Based Distance Measurements in Cell Extracts and in Cells by Pulsed ESR Spectroscopy, ChemPhysChem. 18 (2017) 1653–1660, https://doi.org/10.1002/cphc.201700115.
[1912] G. Karthikeyan, A. Bonucci, G. Casano, G. Gerbaud, S. Abel, V. Thomé, L. Kodjabachian, A. Magalon, B. Guigliarelli, V. Belle, O. Ouari, E. Mileo, A Bioresistant Nitroxide Spin Label for In-Cell EPR Spectroscopy. In Vitro and In Oocytes Protein Structural Dynamics Studies, Angew. Chem. Int. Ed. 57 (2018) 1366–1370, https://doi.org/10.1002/anie.201710184.
[1913] H.Y. Juliusson, S.T. Sigurdsson, Reduction Resistant and Rigid Nitroxide Spin-Labels for DNA and RNA, J. Org. Chem. 85 (2020) 4036–4046, https://doi.org/10.1021/acs.joc.9b02988.
[1914] A. Collauto, S. Bülow, D.B. Gophane, S. Saha, L.S. Stelzl, G. Hummer, S.T. Sigurdsson, T.F. Prisner, Compaction of RNA Duplexes in the Cell**, Angew. Chem. Int. Ed. 59 (2020) 23025–23029, https://doi.org/10.1002/anie.202009800.
[1915] J.J. Jassoy, A. Berndhäuser, F. Duthie, S.P. Kühn, G. Hagelueken, O. Schiemann, Versatile Trityl Spin Labels for Nanometer Distance Measurements on Biomolecules In Vitro and within Cells, Angew. Chem. Int. Ed. 56 (2017) 177–181, https://doi.org/10.1002/anie.201609085.
[1916] Y. Yang, B.-B. Pan, X. Tan, F. Yang, Y. Liu, X.-C. Su, D. Goldfarb, In-Cell Trityl-Trityl Distance Measurements on Proteins, J. Phys. Chem. Lett. 11 (2020) 1141–1147, https://doi.org/10.1021/acs.jpclett.9b03208.
[1917] S. Ketter, A. Gopinath, O. Rogozhnikova, D. Trukhin, V.M. Tormyshev, E.G. Bagryanskaya, B. Joseph, In Situ Labeling and Distance Measurements of Membrane Proteins in *E. coli* Using Finland and OX063 Trityl Labels, Chem. – Eur. J. 27 (2021) 2299–2304, https://doi.org/10.1002/chem.202004606.
[1918] A. Feintuch, G. Otting, D. Goldfarb, Gd3+ Spin Labeling for Measuring Distances in Biomacromolecules, in, Methods Enzymol., Elsevier (2015) 415–457, https://doi.org/10.1016/bs.mie.2015.07.006.

[1919] Y. Yang, F. Yang, Y.-J. Gong, J.-L. Chen, D. Goldfarb, X.-C. Su, A. Reactive, Rigid Gd ^{III} Labeling Tag for In-Cell EPR Distance Measurements in Proteins, Angew. Chem. Int. Ed. 56 (2017) 2914–2918, https://doi.org/10.1002/anie.201611051.
[1920] Y. Yang, F. Yang, X.-Y. Li, X.-C. Su, D. Goldfarb, In-Cell EPR Distance Measurements on Ubiquitin Labeled with a Rigid PyMTA-Gd(III) Tag, J. Phys. Chem. B. 123 (2019) 1050–1059, https://doi.org/10.1021/acs.jpcb.8b11442.
[1921] M. Azarkh, A. Bieber, M. Qi, J.W.A. Fischer, M. Yulikov, A. Godt, M. Drescher, Gd(III)–Gd(III) Relaxation-Induced Dipolar Modulation Enhancement for In-Cell Electron Paramagnetic Resonance Distance Determination, J. Phys. Chem. Lett. 10 (2019) 1477–1481, https://doi.org/10.1021/acs.jpclett.9b00340.
[1922] S. Kucher, S. Korneev, J.P. Klare, D. Klose, H.-J. Steinhoff, *In cell* Gd $^{3+}$ -based site-directed spin labeling and EPR spectroscopy of eGFP, Phys. Chem. Chem. Phys. 22 (2020) 13358–13362, https://doi.org/10.1039/D0CP01930E.
[1923] Y. Yang, S.-N. Chen, F. Yang, X.-Y. Li, A. Feintuch, X.-C. Su, D. Goldfarb, In-cell destabilization of a homodimeric protein complex detected by DEER spectroscopy, Proc. Natl. Acad. Sci. 117 (2020) 20566–20575, https://doi.org/10.1073/pnas.2005779117.
[1924] Q. Miao, E. Zurlo, D. Bruin, J.A.J. Wondergem, M. Timmer, A. Blok, D. Heinrich, M. Overhand, M. Huber, M. Ubbink, A Two-Armed Probe for In-Cell DEER Measurements on Proteins**, Chem. – Eur. J. 26 (2020) 17128–17133, https://doi.org/10.1002/chem.202002743.
[1925] E. Lerner, T. Cordes, A. Ingargiola, Y. Alhadid, S. Chung, X. Michalet, S. Weiss, Toward dynamic structural biology: Two decades of single-molecule Förster resonance energy transfer, Science. 359 (2018) eaan1133, https://doi.org/10.1126/science.aan1133.
[1926] S. Ebbinghaus, A. Dhar, J.D. McDonald, M. Gruebele, Protein folding stability and dynamics imaged in a living cell, Nat. Methods. 7 (2010) 319–323, https://doi.org/10.1038/nmeth.1435.
[1927] A.J. Wirth, M. Platkov, M. Gruebele, Temporal Variation of a Protein Folding Energy Landscape in the Cell, J. Am. Chem. Soc. 135 (2013) 19215–19221, https://doi.org/10.1021/ja4087165.
[1928] B. Liu, C. Åberg, F.J. van Eerden, S.J. Marrink, B. Poolman, A.J. Boersma, Design and Properties of Genetically Encoded Probes for Sensing Macromolecular Crowding, Biophys. J. 112 (2017) 1929–1939, https://doi.org/10.1016/j.bpj.2017.04.004.
[1929] R. Feng, M. Gruebele, C.M. Davis, Quantifying protein dynamics and stability in a living organism, Nat. Commun. 10 (2019) 1179, https://doi.org/10.1038/s41467-019-09088-y.
[1930] S.N. Mouton, D.J. Thaller, M.M. Crane, I.L. Rempel, O.T. Terpstra, A. Steen, M. Kaeberlein, C.P. Lusk, A.J. Boersma, L.M. Veenhoff, A physicochemical perspective of aging from single-cell analysis of pH, macromolecular and organellar crowding in yeast, ELife. 9 (2020) 959–1023, https://doi.org/10.7554/eLife.54707.
[1931] S. Sukenik, P. Ren, M. Gruebele, Weak protein–protein interactions in live cells are quantified by cell-volume modulation, Proc. Natl. Acad. Sci. (2017) 201700818, https://doi.org/10.1073/pnas.1700818114.
[1932] C.M. Davis, M. Gruebele, Cellular Sticking Can Strongly Reduce Complex Binding by Speeding Dissociation, J. Phys. Chem. B. 125 (2021) 3815–3823, https://doi.org/10.1021/acs.jpcb.1c00950.
[1933] I. König, A. Zarrine-Afsar, M. Aznauryan, A. Soranno, B. Wunderlich, F. Dingfelder, J.C. Stüber, A. Plückthun, D. Nettels, B. Schuler, Single-molecule spectroscopy of protein conformational dynamics in live eukaryotic cells, Nat. Methods. 12 (2015) 773–779, https://doi.org/10.1038/nmeth.3475.
[1934] A. Borgia, M.B. Borgia, K. Bugge, V.M. Kissling, P.O. Heidarsson, C.B. Fernandes, A. Sottini, A. Soranno, K.J. Buholzer, D. Nettels, B.B. Kragelund, R.B. Best, B. Schuler, Extreme disorder in an ultrahigh-affinity protein complex, Nature. 555 (2018) 61–66, https://doi.org/10.1038/nature25762.
[1935] K. Okamoto, M. Hiroshima, Y. Sako, Single-molecule fluorescence-based analysis of protein conformation, interaction, and oligomerization in cellular systems, Biophys. Rev. 10 (2018) 317–326, https://doi.org/10.1007/s12551-017-0366-3.
[1936] K. Okamoto, K. Hibino, Y. Sako, In-cell single-molecule FRET measurements reveal three conformational state changes in RAF protein, Biochim. Biophys. Acta BBA - Gen. Subj. 1864 (2020), https://doi.org/10.1016/j.bbagen.2019.04.022 129358.
[1937] I. König, A. Soranno, D. Nettels, B. Schuler, Impact of In-Cell and In-Vitro Crowding on the Conformations and Dynamics of an Intrinsically Disordered Protein, Angew. Chem. Int. Ed. 60 (2021) 10724–10729, https://doi.org/10.1002/anie.202016804.
[1938] S. Basak, N. Sakia, L. Dougherty, Z. Guo, F. Wu, F. Mindlin, J.W. Lary, J.L. Cole, F. Ding, M.E. Bowen, Probing Interdomain Linkers and Protein Supertertiary Structure In Vitro and in Live Cells with Fluorescent Protein Resonance Energy Transfer, J. Mol. Biol. 433 (2021), https://doi.org/10.1016/j.jmb.2020.166793 166793.
[1939] W.B. Asher, P. Geggier, M.D. Holsey, G.T. Gilmore, A.K. Pati, J. Meszaros, D.S. Terry, S. Mathiasen, M.J. Kaliszewski, M.D. McCauley, A. Govindaraju, Z. Zhou, K.G. Harikumar, K. Jaqaman, L.J. Miller, A.W. Smith, S.C. Blanchard, J.A. Javitch, Single-molecule FRET imaging of GPCR dimers in living cells, Nat. Methods. 18 (2021) 397–405, https://doi.org/10.1038/s41592-021-01081-y.
[1940] E. Lerner, A. Barth, J. Hendrix, B. Ambrose, V. Birkedal, S.C. Blanchard, R. Börner, H. Sung Chung, T. Cordes, T.D. Craggs, A.A. Deniz, J. Diao, J. Fei, R.L. Gonzalez, I.V. Gopich, T. Ha, C.A. Hanke, G. Haran, N.S. Hatzakis, S. Hohng, S.-C. Hong, T. Hugel, A. Ingargiola, C. Joo, A.N. Kapanidis, H.D. Kim, T. Laurence, N.K. Lee, T.-H. Lee, E.A. Lemke, E. Margeat, J. Michaelis, X. Michalet, S. Myong, D. Nettels, T.-O. Peulen, E. Ploetz, Y. Razvag, N.C. Robb, B. Schuler, H. Soleimaninejad, C. Tang, R. Vafabakhsh, D.C. Lamb, C.A. Seidel, S. Weiss, FRET-based dynamic structural biology: Challenges, perspectives and an appeal for open-science practices, ELife. 10 (2021), https://doi.org/10.7554/eLife.60416 e60416.
[1941] B. Schuler, Perspective: Chain dynamics of unfolded and intrinsically disordered proteins from nanosecond fluorescence correlation spectroscopy combined with single-molecule FRET, J. Chem. Phys. 149 (2018), https://doi.org/10.1063/1.5037683 010901.
[1942] R.B. Quast, E. Margeat, Single-molecule FRET on its way to structural biology in live cells, Nat. Methods. 18 (2021) 344–345, https://doi.org/10.1038/s41592-021-01084-9.
[1943] C. Sánchez-Rico, L. Voith von Voithenberg, L. Warner, D.C. Lamb, M. Sattler, Effects of Fluorophore Attachment on Protein Conformation and Dynamics Studied by spFRET and NMR Spectroscopy, Chem. - Eur. J. 23 (2017) 14267–14277, https://doi.org/10.1002/chem.201702423.
[1944] M. Schaffer, S. Pfeffer, J. Mahamid, S. Kleindiek, T. Laugks, S. Albert, B.D. Engel, A. Rummel, A.J. Smith, W. Baumeister, J.M. Plitzko, A cryo-FIB lift-out technique enables molecular-resolution cryo-ET within native Caenorhabditis elegans tissue, Nat. Methods. 16 (2019) 757–762, https://doi.org/10.1038/s41592-019-0497-5.
[1945] M. Turk, W. Baumeister, The promise and the challenges of cryo-electron tomography, FEBS Lett. 594 (2020) 3243–3261, https://doi.org/10.1002/1873-3468.13948.
[1946] D. Castaño-Díez, G. Zanetti, In situ structure determination by subtomogram averaging, Curr. Opin. Struct. Biol. 58 (2019) 68–75, https://doi.org/10.1016/j.sbi.2019.05.011.
[1947] J.L. Vilas, J. Oton, C. Messaoudi, R. Melero, P. Conesa, E. Ramirez-Aportela, J. Mota, M. Martinez, A. Jimenez, R. Marabini, J.M. Carazo, J. Vargas, C.O.S. Sorzano, Measurement of local resolution in electron tomography, J. Struct. Biol. X. 4 (2020), https://doi.org/10.1016/j.yjsbx.2019.100016 100016.
[1948] F.R. Wagner, R. Watanabe, R. Schampers, D. Singh, H. Persoon, M. Schaffer, P. Fruhstorfer, J. Plitzko, E. Villa, Preparing samples from whole cells using focused-ion-beam milling for cryo-electron tomography, Nat. Protoc. (2020) 1–32, https://doi.org/10.1038/s41596-020-0320-x.
[1949] Q. Guo, C. Lehmer, A. Martínez-Sánchez, T. Rudack, F. Beck, H. Hartmann, M. Pérez-Berlanga, F. Frottin, M.S. Hipp, F.U. Hartl, D. Edbauer, W. Baumeister, R. Fernández-Busnadiego, In Situ Structure of Neuronal C9orf72 Poly-GA Aggregates Reveals Proteasome Recruitment, Cell. 172 (2018) 696–705.e12, https://doi.org/10.1016/j.cell.2017.12.030.
[1950] F.J.B. Bäuerlein, R. Fernández-Busnadiego, W. Baumeister, Investigating the Structure of Neurotoxic Protein Aggregates Inside Cells, Trends Cell Biol. 30 (2020) 951–966, https://doi.org/10.1016/j.tcb.2020.08.007.
[1951] V.A. Trinkaus, I. Riera-Tur, A. Martínez-Sánchez, F.J.B. Bäuerlein, Q. Guo, T. Arzberger, W. Baumeister, I. Dudanova, M.S. Hipp, F.U. Hartl, R. Fernández-Busnadiego, In situ architecture of neuronal α-Synuclein inclusions, Nat. Commun. 12 (2021) 2110, https://doi.org/10.1038/s41467-021-22108-0.
[1952] R. Watanabe, R. Buschauer, J. Böhning, M. Audagnotto, K. Lasker, T.-W. Lu, D. Boassa, S. Taylor, E. Villa, The In Situ Structure of Parkinson's Disease-Linked LRRK2, Cell. 182 (2020) 1508–1518.e16, https://doi.org/10.1016/j.cell.2020.08.004.
[1953] F. Fäßler, G. Dimchev, V.-V. Hodirnau, W. Wan, F.K.M. Schur, Cryo-electron tomography structure of Arp2/3 complex in cells reveals new insights into the branch junction, Nat. Commun. 11 (2020) 6437, https://doi.org/10.1038/s41467-020-20286-x.
[1954] L. Burbaum, J. Schneider, S. Scholze, R.T. Böttcher, W. Baumeister, P. Schwille, J.M. Plitzko, M. Jasnin, Molecular-scale visualization of sarcomere contraction within native cardiomyocytes, Nat. Commun. 12 (2021) 4086, https://doi.org/10.1038/s41467-021-24049-0.
[1955] Y.S. Bykov, M. Schaffer, S.O. Dodonova, S. Albert, J.M. Plitzko, W. Baumeister, B.D. Engel, J.A. Briggs, The structure of the COPI coat determined within the cell, ELife. 6 (2017), https://doi.org/10.7554/eLife.32493 e32493.
[1956] C. Rapisarda, Y. Cherrak, R. Kooger, V. Schmidt, R. Pellarin, L. Logger, E. Cascales, M. Pilhofer, E. Durand, R. Fronzes, *In situ* and high-resolution cryo-EM structure of a bacterial type VI secretion system membrane complex, EMBO J. 38 (2019), https://doi.org/10.15252/embj.2018100886.
[1957] X. Shi, M. Chen, Z. Yu, J.M. Bell, H. Wang, I. Forrester, H. Villarreal, J. Jakana, D. Du, B.F. Luisi, S.J. Ludtke, Z. Wang, In situ structure and assembly of the multidrug efflux pump AcrAB-TolC, Nat. Commun. 10 (2019) 2635, https://doi.org/10.1038/s41467-019-10512-6.
[1958] D. Ghosal, K.W. Kim, H. Zheng, M. Kaplan, H.K. Truchan, A.E. Lopez, I.E. McIntire, J.P. Vogel, N.P. Cianciotto, G.J. Jensen, In vivo structure of the Legionella type II secretion system by electron cryotomography, Nat. Microbiol. 4 (2019) 2101–2108, https://doi.org/10.1038/s41564-019-0603-6.
[1959] M. Allegretti, C.E. Zimmerli, V. Rantos, F. Wilfling, P. Ronchi, H.K.H. Fung, C.-W. Lee, W. Hagen, B. Turoňová, K. Karius, M. Börmel, X. Zhang, C.W. Müller, Y. Schwab, J. Mahamid, B. Pfander, J. Kosinski, M. Beck, In-cell architecture of the nuclear pore and snapshots of its turnover, Nature. 586 (2020) 796–800, https://doi.org/10.1038/s41586-020-2670-5.
[1960] A. von Kügelgen, H. Tang, G.G. Hardy, D. Kureisaite-Ciziene, Y.V. Brun, P.J. Stansfeld, C.V. Robinson, T.A.M. Bharat, In Situ Structure of an Intact Lipopolysaccharide-Bound Bacterial Surface Layer, Cell. 180 (2020) 348–358.e15, https://doi.org/10.1016/j.cell.2019.12.006.
[1961] B. Turoňová, F.K.M. Schur, W. Wan, J.A.G. Briggs, Efficient 3D-CTF correction for cryo-electron tomography using NovaCTF improves subtomogram

averaging resolution to 3.4 Å, J. Struct. Biol. 199 (2017) 187–195, https://doi.org/10.1016/j.jsb.2017.07.007.
[1962] B. Turoňová, W.J.H. Hagen, M. Obr, S. Mosalaganti, J.W. Beugelink, C.E. Zimmerli, H.-G. Kräusslich, M. Beck, Benchmarking tomographic acquisition schemes for high-resolution structural biology, Nat. Commun. 11 (2020) 876, https://doi.org/10.1038/s41467-020-14535-2.
[1963] J. Bouvette, H.-F. Liu, X. Du, Y. Zhou, A.P. Sikkema, J. da Fonseca Rezende e Mello, B.P. Klemm, R. Huang, R.M. Schaaper, M.J. Borgnia, A. Bartesaghi, Beam image-shift accelerated data acquisition for near-atomic resolution single-particle cryo-electron tomography, Nat. Commun. 12 (2021) 1957. https://doi.org/10.1038/s41467-021-22251-8..
[1964] B.A. Lucas, B.A. Himes, L. Xue, T. Grant, J. Mahamid, N. Grigorieff, Locating macromolecular assemblies in cells by 2D template matching with cisTEM, ELife. 10 (2021), https://doi.org/10.7554/eLife.68946 e68946.
[1965] D. Tegunov, L. Xue, C. Dienemann, P. Cramer, J. Mahamid, Multi-particle cryo-EM refinement with M visualizes ribosome-antibiotic complex at 3.5 Å in cells, Nat. Methods. 18 (2021) 186–193, https://doi.org/10.1038/s41592-020-01054-7.
[1966] F.J. O'Reilly, L. Xue, A. Graziadei, L. Sinn, S. Lenz, D. Tegunov, C. Blötz, N. Singh, W.J.H. Hagen, P. Cramer, J. Stülke, J. Mahamid, J. Rappsilber, In-cell architecture of an actively transcribing-translating expressome, Science. 369 (2020) 554–557, https://doi.org/10.1126/science.abb3758.
[1967] E. Pyle, G. Zanetti, Current data processing strategies for cryo-electron tomography and subtomogram averaging, Biochem. J. 478 (2021) 1827–1845, https://doi.org/10.1042/BCJ20200715.
[1968] E.C. Greenwald, S. Mehta, J. Zhang, Genetically Encoded Fluorescent Biosensors Illuminate the Spatiotemporal Regulation of Signaling Networks, Chem. Rev. 118 (2018) 11707–11794, https://doi.org/10.1021/acs.chemrev.8b00333.
[1969] N.C. Dale, E.K.M. Johnstone, C.W. White, K.D.G. Pfleger, NanoBRET: The Bright Future of Proximity-Based Assays, Front. Bioeng. Biotechnol. 7 (2019) 56, https://doi.org/10.3389/fbioe.2019.00056.
[1970] H. Singh, K. Tiwari, R. Tiwari, S.K. Pramanik, A. Das, Small Molecule as Fluorescent Probes for Monitoring Intracellular Enzymatic Transformations, Chem. Rev. 119 (2019) 11718–11760, https://doi.org/10.1021/acs.chemrev.9b00379.
[1971] F. Broch, A. Gautier, Illuminating Cellular Biochemistry: Fluorogenic Chemogenetic Biosensors for Biological Imaging, ChemPlusChem. 85 (2020) 1487–1497, https://doi.org/10.1002/cplu.202000413.
[1972] J.D. Vasta, C.R. Corona, J. Wilkinson, C.A. Zimprich, J.R. Hartnett, M.R. Ingold, K. Zimmerman, T. Machleidt, T.A. Kirkland, K.G. Huwiler, R.F. Ohana, M. Slater, P. Otto, M. Cong, C.I. Wells, B.-T. Berger, T. Hanke, C. Glas, K. Ding, D. H. Drewry, K.V.M. Huber, T.M. Willson, S. Knapp, S. Müller, P.L. Meisenheimer, F. Fan, K.V. Wood, M.B. Robers, Quantitative, Wide-Spectrum Kinase Profiling in Live Cells for Assessing the Effect of Cellular ATP on Target Engagement, Cell Chem. Biol. 25 (2018) 206–214.e11, https://doi.org/10.1016/j.chembiol.2017.10.010.
[1973] L. Deng, X. Huang, J. Ren, In Situ Study of the Drug-Target Protein Interaction in Single Living Cells by Combining Fluorescence Correlation Spectroscopy with Affinity Probes, Anal. Chem. 92 (2020) 7020–7027, https://doi.org/10.1021/acs.analchem.0c00263.
[1974] R.H.J. Olsen, J.F. DiBerto, J.G. English, A.M. Glaudin, B.E. Krumm, S.T. Slocum, T. Che, A.C. Gavin, J.D. McCorvy, B.L. Roth, R.T. Strachan, Trupath,, an open-source biosensor platform for interrogating the GPCR transducerome, Nat. Chem. Biol. (2020) 1–13, https://doi.org/10.1038/s41589-020-0535-8.
[1975] X. Zhou, S. Mehta, J. Zhang, Genetically Encodable Fluorescent and Bioluminescent Biosensors Light Up Signaling Networks, Trends Biochem. Sci. 45 (2020) 889–905, https://doi.org/10.1016/j.tibs.2020.06.001.
[1976] A. Bondar, J. Lazar, Optical sensors of heterotrimeric G protein signaling, FEBS J. 288 (2021) 2570–2584, https://doi.org/10.1111/febs.15655.
[1977] J.S. Smith, R.J. Lefkowitz, S. Rajagopal, Biased signalling: from simple switches to allosteric microprocessors, Nat. Rev. Drug Discov. 17 (2018) 243–260, https://doi.org/10.1038/nrd.2017.229.
[1978] T. Kenakin, Biased Receptor Signaling in Drug Discovery, Pharmacol. Rev. 71 (2019) 267–315, https://doi.org/10.1124/pr.118.016790.
[1979] Y. Nasu, Y. Shen, L. Kramer, R.E. Campbell, Structure- and mechanism-guided design of single fluorescent protein-based biosensors, Nat. Chem. Biol. 17 (2021) 509–518, https://doi.org/10.1038/s41589-020-00718-x.
[1980] D. Martinez Molina, P. Nordlund, The Cellular Thermal Shift Assay: A Novel Biophysical Assay for In Situ Drug Target Engagement and Mechanistic Biomarker Studies, Annu. Rev. Pharmacol. Toxicol. 56 (2016) 141–161, https://doi.org/10.1146/annurev-pharmtox-010715-103715.
[1981] S. Klaeger, S. Heinzlmeir, M. Wilhelm, H. Polzer, B. Vick, P.-A. Koenig, M. Reinecke, B. Ruprecht, S. Petzoldt, C. Meng, J. Zecha, K. Reiter, H. Qiao, D. Helm, H. Koch, M. Schoof, G. Canevari, E. Casale, S.R. Depaolini, A. Feuchtinger, Z. Wu, T. Schmidt, L. Rueckert, W. Becker, J. Huenges, A.-K. Garz, B.-O. Gohlke, D.P. Zolg, G. Kayser, T. Vooder, R. Preissner, H. Hahne, N. Tõnisson, K. Kramer, K. Götze, F. Bassermann, J. Schlegl, H.-C. Ehrlich, S. Aiche, A. Walch, P.A. Greif, S. Schneider, E.R. Felder, J. Ruland, G. Médard, I. Jeremias, K. Spiekermann, B. Kuster, The target landscape of clinical kinase drugs, Science. 358 (2017) eaan4368, https://doi.org/10.1126/science.aan4368.
[1982] A. Herholt, S. Galinski, P.E. Geyer, M.J. Rossner, M.C. Wehr, Multiparametric Assays for Accelerating Early Drug Discovery, Trends Pharmacol. Sci. 41 (2020) 318–335, https://doi.org/10.1016/j.tips.2020.02.005.
[1983] F.B.M. Reinhard, D. Eberhard, T. Werner, H. Franken, D. Childs, C. Doce, M.F. Savitski, W. Huber, M. Bantscheff, M.M. Savitski, G. Drewes, Thermal proteome profiling monitors ligand interactions with cellular membrane proteins, Nat. Methods. 12 (2015) 1129–1131, https://doi.org/10.1038/nmeth.3652.
[1984] H. Park, J. Ha, S.B. Park, Label-free target identification in drug discovery via phenotypic screening, Curr. Opin. Chem. Biol. 50 (2019) 66–72, https://doi.org/10.1016/j.cbpa.2019.02.006.
[1985] C.G. Parker, A. Galmozzi, Y. Wang, B.E. Correia, K. Sasaki, C.M. Joslyn, A.S. Kim, C.L. Cavallaro, R.M. Lawrence, S.R. Johnson, I. Narvaiza, E. Saez, B.F. Cravatt, Ligand and Target Discovery by Fragment-Based Screening in Human Cells, Cell. 168 (2017) 527–541.e29, https://doi.org/10.1016/j.cell.2016.12.029.
[1986] Y. Wang, M.M. Dix, G. Bianco, J.R. Remsberg, H.-Y. Lee, M. Kalocsay, S.P. Gygi, S. Forli, G. Vite, R.M. Lawrence, C.G. Parker, B.F. Cravatt, Expedited mapping of the ligandable proteome using fully functionalized enantiomeric probe pairs, Nat. Chem. (2019) 1–14, https://doi.org/10.1038/s41557-019-0351-5.
[1987] C.G. Parker, M.R. Pratt, Click Chemistry in Proteomic Investigations, Cell. 180 (2020) 605–632, https://doi.org/10.1016/j.cell.2020.01.025.
[1988] G. Rossi, A. Manfrin, M.P. Lutolf, Progress and potential in organoid research, Nat. Rev. Genet. 19 (2018) 671–687, https://doi.org/10.1038/s41576-018-0051-9.
[1989] J. Kim, B.-K. Koo, J.A. Knoblich, Human organoids: model systems for human biology and medicine, Nat. Rev. Mol. Cell Biol. 21 (2020) 571–584, https://doi.org/10.1038/s41580-020-0259-3.
[1990] M. Hofer, M.P. Lutolf, Engineering organoids, Nat. Rev. Mater. 6 (2021) 402–420, https://doi.org/10.1038/s41578-021-00279-y.
[1991] C. Ma, Y. Peng, H. Li, W. Chen, Organ-on-a-Chip: A New Paradigm for Drug Development, Trends Pharmacol. Sci. 42 (2021) 119–133, https://doi.org/10.1016/j.tips.2020.11.009.
[1992] Y. Zhu, K. Mandal, A.L. Hernandez, S. Kawakita, W. Huang, P. Bandaru, S. Ahadian, H.-J. Kim, V. Jucaud, M.R. Dokmeci, A. Khademhosseini, State of the art in integrated biosensors for organ-on-a-chip applications, Curr. Opin. Biomed. Eng. 19 (2021), https://doi.org/10.1016/j.cobme.2021.100309 100309.
[1993] K. Krauskopf, K. Lang, Increasing the chemical space of proteins in living cells via genetic code expansion, Curr. Opin. Chem. Biol. 58 (2020) 112–120, https://doi.org/10.1016/j.cbpa.2020.07.012.
[1994] M. Manandhar, E. Chun, F.E. Romesberg, Genetic Code Expansion: Inception, Development, Commercialization, J. Am. Chem. Soc. 143 (2021) 4859–4878, https://doi.org/10.1021/jacs.0c11938.
[1995] M.L.W.J. Smeenk, J. Agramunt, K.M. Bonger, Recent developments in bioorthogonal chemistry and the orthogonality within, Curr. Opin. Chem. Biol. 60 (2021) 79–88, https://doi.org/10.1016/j.cbpa.2020.09.002.
[1996] E.H. Abdelkader, H. Qianzhu, Y.J. Tan, L.A. Adams, T. Huber, G. Otting, Genetic Encoding of N6-(((Trimethylsilyl)methoxy)carbonyl)- l-lysine for NMR Studies of Protein-Protein and Protein-Ligand Interactions, J. Am. Chem. Soc. 143 (2021) 1133–1143, https://doi.org/10.1021/jacs.0c11971.
[1997] D. Chen, Z. Wang, D. Guo, V. Orekhov, X. Qu, Review and Prospect: Deep Learning in Nuclear Magnetic Resonance Spectroscopy, Chem. – Eur. J. 26 (2020) 10391–10401, https://doi.org/10.1002/chem.202000246.
[1998] P. Sen, S. Lamichhane, V.B. Mathema, A. McGlinchey, A.M. Dickens, S. Khoomrung, M. Orešič, Deep learning meets metabolomics: a methodological perspective, Brief. Bioinform. 22 (2021) 1531–1542, https://doi.org/10.1093/bib/bbaa204.
[1999] P. Berruyer, S. Björgvinsdóttir, A. Bertarello, G. Stevanato, Y. Rao, G. Karthikeyan, G. Casano, O. Ouari, M. Lelli, C. Reiter, F. Engelke, L. Emsley, Dynamic Nuclear Polarization Enhancement of 200 at 21.15 T Enabled by 65 kHz Magic Angle Spinning, J. Phys. Chem. Lett. 11 (2020) 8386–8391, https://doi.org/10.1021/acs.jpclett.0c02493.
[2000] A. Lund, G. Casano, G. Menzildjian, M. Kaushik, G. Stevanato, M. Yulikov, R. Jabbour, D. Wisser, M. Renom-Carrasco, C. Thieuleux, F. Bernada, H. Karoui, D. Siri, M. Rosay, I.V. Sergeyev, D. Gajan, M. Lelli, L. Emsley, O. Ouari, A. Lesage, TinyPols: a family of water-soluble binitroxides tailored for dynamic nuclear polarization enhanced NMR spectroscopy at 18.8 and 21.1 T, Chem Sci. 11 (2020) 2810–2818, https://doi.org/10.1039/C9SC05384K.
[2001] S. Mandal, S.T. Sigurdsson, Water-soluble BDPA radicals with improved persistence, Chem. Commun. 56 (2020) 13121–13124, https://doi.org/10.1039/D0CC04920D.
[2002] Xinyi. Cai, A. Lucini Paioni, A. Adler, R. Yao, W. Zhang, D. Beriashvili, A. Safeer, A. Gurinov, A. Rockenbauer, Y. Song, M. Baldus, Y. Liu, Highly Efficient Trityl-Nitroxide Biradicals for Biomolecular High-Field Dynamic Nuclear Polarization, Chem. – Eur. J. (2021) chem.202102253. https://doi.org/10.1002/chem.202102253..
[2003] D.P. Klebl, M.S.C. Gravett, D. Kontziampasis, D.J. Wright, R.S. Bon, D.C.F. Monteiro, M. Trebbin, F. Sobott, H.D. White, M.C. Darrow, R.F. Thompson, S. P. Muench, Need for Speed: Examining Protein Behavior during CryoEM Grid Preparation at Different Timescales, Struct. Des. 28 (2020) 1238–1248.e4, https://doi.org/10.1016/j.str.2020.07.018.
[2004] G. Weissenberger, R.J.M. Henderikx, P.J. Peters, Understanding the invisible hands of sample preparation for cryo-EM, Nat. Methods. 18 (2021) 463–471, https://doi.org/10.1038/s41592-021-01130-6.
[2005] Y. Zhang, H. Wei, D. Xie, D. Calambur, A. Douglas, M. Gao, F. Marsilio, W.J. Metzler, N. Szapiel, P. Zhang, M.R. Witmer, L. Mueller, D. Hedin, An improved protocol for amino acid type-selective isotope labeling in insect

cells, J. Biomol. NMR. 68 (2017) 237–247, https://doi.org/10.1007/s10858-017-0117-6.
[2006] X. Chen, S. Wei, Y. Ji, X. Guo, F. Yang, Quantitative proteomics using SILAC: Principles, applications, and developments, PROTEOMICS. 15 (2015) 3175–3192, https://doi.org/10.1002/pmic.201500108.
[2007] 0] M. Sastry, C.A. Bewley, P.D. Kwong, Effective Isotope Labeling of Proteins in a Mammalian Expression System, Elsevier Inc., 2015. https://doi.org/10.1016/bs.mie.2015.09.021..
[2008] D.R. Glenn, D.B. Bucher, J. Lee, M.D. Lukin, H. Park, R.L. Walsworth, High-resolution magnetic resonance spectroscopy using a solid-state spin sensor, Nature. 555 (2018) 351–354, https://doi.org/10.1038/nature25781.
[2009] D. Cohen, R. Nigmatullin, M. Eldar, A. Retzker, Confined Nano-NMR Spectroscopy Using NV Centers, Adv. Quantum Technol. (2020) 2000019–2000029, https://doi.org/10.1002/qute.202000019.
[2010] D.B. Bucher, Principles of Nano- and Microscale NMR-Spectroscopy with NV-Diamond Sensors, 8 (2019) 8..
[2011] T. Zhang, G. Pramanik, K. Zhang, M. Gulka, L. Wang, J. Jing, F. Xu, Z. Li, Q. Wei, P. Cigler, Z. Chu, Toward Quantitative Bio-sensing with Nitrogen-Vacancy Center in Diamond, ACS Sens. 6 (2021) 2077–2107, https://doi.org/10.1021/acssensors.1c00415.
[2012] S.N. Chandrasekaran, H. Ceulemans, J.D. Boyd, A.E. Carpenter, Image-based profiling for drug discovery: due for a machine-learning upgrade?, Nat. Rev. Drug Discov. 20 (2021) 145–159, https://doi.org/10.1038/s41573-020-00117-w.
[2013] A. Pratapa, M. Doron, J.C. Caicedo, Image-based cell phenotyping with deep learning, Curr. Opin. Chem. Biol. 65 (2021) 9–17, https://doi.org/10.1016/j.cbpa.2021.04.001.
[2014] C. Gorgulla, A. Boeszoermenyi, Z.-F. Wang, P.D. Fischer, P.W. Coote, K.M. Padmanabha Das, Y.S. Malets, D.S. Radchenko, Y.S. Moroz, D.A. Scott, K. Fackeldey, M. Hoffmann, I. Iavniuk, G. Wagner, H. Arthanari, An open-source drug discovery platform enables ultra-large virtual screens, Nature. 580 (2020) 663–668, https://doi.org/10.1038/s41586-020-2117-z.
[2015] G. Ghislat, T. Rahman, P.J. Ballester, Recent progress on the prospective application of machine learning to structure-based virtual screening, Curr. Opin. Chem. Biol. 65 (2021) 28–34, https://doi.org/10.1016/j.cbpa.2021.04.009.